GUT MICROBIAL RESPONSE TO HOST METABOLIC PHENOTYPES

EDITED BY: Jie Yin, Yong Su and Hui Han

PUBLISHED IN: Frontiers in Nutrition

frontiers Research Topics

ISSN 1664-8714
ISBN 978-2-88974-496-1
DOI 10.3389/978-2-88974-496-1

About Frontiers

Frontiers is more than just an open-access publisher of scholarly articles: it is a pioneering approach to the world of academia, radically improving the way scholarly research is managed. The grand vision of Frontiers is a world where all people have an equal opportunity to seek, share and generate knowledge. Frontiers provides immediate and permanent online open access to all its publications, but this alone is not enough to realize our grand goals.

Frontiers Journal Series

The Frontiers Journal Series is a multi-tier and interdisciplinary set of open-access, online journals, promising a paradigm shift from the current review, selection and dissemination processes in academic publishing. All Frontiers journals are driven by researchers for researchers; therefore, they constitute a service to the scholarly community. At the same time, the Frontiers Journal Series operates on a revolutionary invention, the tiered publishing system, initially addressing specific communities of scholars, and gradually climbing up to broader public understanding, thus serving the interests of the lay society, too.

Dedication to Quality

Each Frontiers article is a landmark of the highest quality, thanks to genuinely collaborative interactions between authors and review editors, who include some of the world's best academicians. Research must be certified by peers before entering a stream of knowledge that may eventually reach the public - and shape society; therefore, Frontiers only applies the most rigorous and unbiased reviews.
Frontiers revolutionizes research publishing by freely delivering the most outstanding research, evaluated with no bias from both the academic and social point of view. By applying the most advanced information technologies, Frontiers is catapulting scholarly publishing into a new generation.

What are Frontiers Research Topics?

Frontiers Research Topics are very popular trademarks of the Frontiers Journals Series: they are collections of at least ten articles, all centered on a particular subject. With their unique mix of varied contributions from Original Research to Review Articles, Frontiers Research Topics unify the most influential researchers, the latest key findings and historical advances in a hot research area! Find out more on how to host your own Frontiers Research Topic or contribute to one as an author by contacting the Frontiers Editorial Office: frontiersin.org/about/contact

GUT MICROBIAL RESPONSE TO HOST METABOLIC PHENOTYPES

Topic Editors:
Jie Yin, Hunan Agricultural University, China
Yong Su, Nanjing Agricultural University, China
Hui Han, Chinese Academy of Sciences (CAS), China

Citation: Yin, J., Su, Y., Han, H., eds. (2022). Gut Microbial Response to Host Metabolic Phenotypes. Lausanne: Frontiers Media SA.
doi: 10.3389/978-2-88974-496-1

Table of Contents

EDITORIAL
published: 13 January 2022
doi: 10.3389/fnut.2021.817501

Editorial: Gut Microbial Response to Host Metabolic Phenotypes

Jie Yin[1], Yong Su[2]* and Hui Han[3]*

[1] College of Animal Science and Technology, Hunan Agricultural University, Changsha, China, [2] College of Animal Science and Technology, Nanjing Agricultural University, Nanjing, China, [3] State Key Laboratory of Animal Nutrition, Institute of Animal Science, Chinese Academy of Agricultural Sciences, Beijing, China

Keywords: gut microbiota, metabolism, disease, probiotics, diets

Editorial on the Research Topic

Gut Microbial Response to Host Metabolic Phenotypes

It is increasingly apparent that gut microbiota perform functions crucial to the host, such as regulating host physiology and influencing host health (1–3). Using fecal bacteria transplantation technology, Wu et al. found that fecal microbiota from obese Jinhua pigs and lean Landrace pigs exert different lipid metabolic phenotypes. Zheng et al. also witnessed gut microbial alterations in high fat diet-fed mice, with a high ratio of Firmicutes to Bacteroidetes and abundance of *Allobaculum*. Although this Research Topic failed to receive any papers about the role of gut microbiota in amino acid metabolism, nucleic acid metabolism, and carbohydrate metabolism, other reports have confirmed these functions (4, 5).

Currently, the gut microbiota is attracting much interest due to its role in maintaining host health and its association with all aspects of health and diseases. In this Research Topic, gut microbial disorders are screened in persistent atrial fibrillation patients (Xu et al.) renal cell carcinoma metastasis patients (Dai et al.), and a spinal cord injury animal model (Rong et al.). Xu et al. thoroughly discussed the taxonomic and functional characteristics of the gastrointestinal microbiota and demonstrated the profound relationship between gastrointestinal microbiota and metabolic disorders in ruminants. Together, these results further confirmed the role of gut microbiota in disease occurrence and development and manipulation of gut microbiota might, therefore, be considered a potential target for treating diseases.

Indeed, various disease treatment measures include gut microbial improvement, such as dietary probiotics (6). For example, Zhang et al. reported that dietary *Lactobacillus acidophilus* ATCC 4356 improved gut microbiota distribution and alleviated renal ischemia–reperfusion injury. Similarly, beneficial effects of *Lactobacillus* have been identified in lumbar disc herniation (Wang et al.), hypercholesterolemic golden hamsters (Yang et al.), asthma, and *Clostridium perfringens* infection (Wang et al.). In animal production, the gut is generally disturbed by weaning stress, dietary toxins, and pathogen infections, thus dietary probiotics have been widely introduced to maintain a healthy gut and guarantee higher production performance (7). *Lactococcus lactis*, in this Research Topic, has been identified to improve gut function in piglets (Yu et al.). However, probiotics are not limited to *Lactobacillus*, some species of *Bifidobacterium*, *Escherichia coli*, *Enterococcus*, and *Saccharomyces* have long been used as probiotics to alleviate various diseases by changing gut microbiota compositions.

Gut microbiota diversity and compositions are highly associated with dietary fluctuations. Thus, dietary manipulation has also been used to target gut microbiota to regulate host physiology and metabolism. In this Research Topic, Qian et al. found that dietary dried citrus peel (Chenpi) improved gut microbiota compositions in high fat diet-fed mice. Li et al. concluded that maternal fiber nutrition during pregnancy regulated the health of offspring, and the response of the maternal

OPEN ACCESS

Edited and reviewed by:
Christophe Lacroix,
ETH Zürich, Switzerland

***Correspondence:**
Yong Su
yong.su@njau.edu.cn
Hui Han
hanhui16@mails.ucas.ac.cn

Specialty section:
This article was submitted to Nutrition and Microbes, a section of the journal Frontiers in Nutrition

Received: 18 November 2021
Accepted: 13 December 2021
Published: 13 January 2022

Citation:
Yin J, Su Y and Han H (2022) Editorial: Gut Microbial Response to Host Metabolic Phenotypes. Front. Nutr. 8:817501. doi: 10.3389/fnut.2021.817501

intestinal microbes played an important role in intervening in the phenotype of sows and neonatal piglets. Dietary protein and amino acids are the main factors shaping gut microbiota (8), Fu et al. also reported a role of tryptophan in gut microbiota. Besides, vitamin K2 (Liu et al.), β-carotene (Yuan et al.), olive fruit extracts (Wang et al.), bovine lactoferrin (Wang et al.), and β-sitosterol (Yu et al.) have been reported to shape gut microbiota compositions in this Research Topic.

How does gut microbiota affect host physiology and metabolism? Hou et al. showed that the gut–liver FXR–FGF19 axis is involved in *Lactobacillus delbrueckii*-promoted ileal bile acid deconjugation. In our previous studies, we found that gut microbiota-derived metabolites are highly associated with host metabolic reprograming (9–12). Furthermore, bacterial microRNA, bacteriocin, and microbiota sensing pathways have also been identified to be involved in the relationship between gut microbiota and host metabolism (13, 14). However, with the focus on the detailed mechanism by which gut microbiota influence host metabolism, much still needs to be elucidated.

In summary, papers from the current Research Topic screened the gut microbiota dysbiosis in various diseases and reported the beneficial roles of dietary probiotics and other active components in the improvement of gut microbiota. Despite the progress made in understanding the relationship between gut microbiota and host metabolism, there are a number of prominent research avenues that remain to be explored. For example, what are the molecular and physiological links between the gut microbiota and host metabolism at the epigenetic, transcriptome, and proteome levels? Gut microbiota is changed in various pathologic conditions and microbial biomarkers need to be screened in specific metabolic diseases. Additionally, dietary manipulation is widely used to maintain a healthy gut microbiota composition, and the interaction between diets, gut microbiota, and host metabolism will be an important area of future research.

AUTHOR CONTRIBUTIONS

All authors listed have made a substantial, direct, and intellectual contribution to the work and approved it for publication.

FUNDING

This study was supported by the National Natural Science Foundation of China (32172761) and the Young Elite Scientists Sponsorship Program by CAST (2019-2021QNRC001).

ACKNOWLEDGMENTS

We would like to thank all authors for their papers and the reviewers for the painstaking care taken in helping improve the clarity of the manuscript.

REFERENCES

1. Yin J, Li YY, Han H, Ma J, Liu G, Wu X, et al. Administration of exogenous melatonin improves the diurnal rhythms of the gut microbiota in mice fed a high-fat diet. *mSystems.* (2020) 5:e00002-20. doi: 10.1128/mSystems.00002-20
2. Tian M, Chen JM, Liu JX, Chen F, Guan WT, Zhang HS. Dietary fiber and microbiota interaction regulates sow metabolism and reproductive performance. *Anim Nutr.* (2020) 6:397–403. doi: 10.1016/j.aninu.2020.10.001
3. Ma J, Zheng YM, Tang WJ, Yan WX, Nie HF, Fang J, et al. Dietary polyphenols in lipid metabolism: a role of gut microbiome. *Anim Nutr.* (2020) 6:404–9. doi: 10.1016/j.aninu.2020.08.002
4. Agus A, Planchais J, Sokol H. Gut microbiota regulation of tryptophan metabolism in health and disease. *Cell Host Microbe.* (2018) 23:716–24. doi: 10.1016/j.chom.2018.05.003
5. Fan Y, Pedersen O. Gut microbiota in human metabolic health and disease. *Nat Rev Microbiol.* (2021) 19:55–71. doi: 10.1038/s41579-020-0433-9
6. Azad MAK, Gao J, Ma J, Li TJ, Tan B, Huang XG, et al. Opportunities of prebiotics for the intestinal health of monogastric animals. *Anim Nutr.* (2020) 6:379–88. doi: 10.1016/j.aninu.2020.08.001
7. Azad MAK, Sarker M, Li T, Yin J. Probiotic species in the modulation of gut microbiota: an overview. *Biomed Res Int.* (2018) 2018:9478630. doi: 10.1155/2018/9478630
8. Yin J, Ma J, Li YY, Ma XK, Chen JS, Zhang HH, et al. Branched-chain amino acids, especially of leucine and valine, mediate the protein restricted response in a piglet model. *Food Funct.* (2020) 11:1304–11. doi: 10.1039/C9FO01757G
9. Yin J, Li YY, Han H, Chen S, Gao J, Liu G, et al. Melatonin reprogramming of gut microbiota improves lipid dysmetabolism in high-fat diet-fed mice. *J Pineal Res.* (2018) 65:e12524. doi: 10.1111/jpi.12524
10. Duan YH, Zhong YZ, Xiao H, Zheng CB, Song B, Wang WL, et al. Gut microbiota mediates the protective effects of dietary beta-hydroxy-beta-methylbutyrate (HMB) against obesity induced by high-fat diets. *Faseb J.* (2019) 33:10019–33. doi: 10.1096/fj.201900665RR
11. Han H, Yi B, Zhong R, Wang M, Zhang S, Ma J, et al. From gut microbiota to host appetite: gut microbiota-derived metabolites as key regulators. *Microbiome.* (2021) 9:162. doi: 10.1186/s40168-021-01093-y
12. Han H, Jiang Y, Wang M, Melaku M, Liu L, Zhao Y, et al. Intestinal dysbiosis in nonalcoholic fatty liver disease (NAFLD): focusing on the gut-liver axis. *Crit Rev Food Sci Nutr.* (2021) 18:1–18. doi: 10.1080/10408398.2021.1966738
13. Nicholson JK, Holmes E, Kinross J, Burcelin R, Gibson G, Jia W, et al. Host-gut microbiota metabolic interactions. *Science.* (2012) 336:1262–7. doi: 10.1126/science.1223813
14. Visconti A, Le Roy CI, Rosa F, Rossi N, Martin TC, Mohney RP, et al. Interplay between the human gut microbiome and host metabolism. *Nat Commun.* (2019) 10:4505. doi: 10.1038/s41467-019-12476-z

Conflict of Interest: The authors declare that the research was conducted in the absence of any commercial or financial relationships that could be construed as a potential conflict of interest.

frontiers in Nutrition

ORIGINAL RESEARCH
published: 11 December 2020
doi: 10.3389/fnut.2020.617676

Lactobacillus delbrueckii Interfere With Bile Acid Enterohepatic Circulation to Regulate Cholesterol Metabolism of Growing–Finishing Pigs via Its Bile Salt Hydrolase Activity

Gaifeng Hou[1,2], *Wei Peng*[1,2], *Liangkai Wei*[1,2], *Rui Li*[1,2,3]*, *Yong Yuan*[1,2], *Xingguo Huang*[1,2]* and *Yulong Yin*[1,2,3]

[1] College of Animal Science and Technology, Hunan Agricultural University, Changsha, China, [2] Hunan Co-Innovation Center of Animal Production Safety, Changsha, China, [3] Key Laboratory of Agro-ecological Processes in Subtropical Region, Scientific Observing and Experimental Station of Animal Nutrition and Feed Science in South-Central, Ministry of Agriculture, Hunan Provincial Engineering Research Center for Healthy Livestock and Poultry Production, Institute of Subtropical Agriculture, Chinese Academy of Sciences, Changsha, China

OPEN ACCESS

Edited by:
Yong Su,
Nanjing Agricultural University, China

Reviewed by:
Shunfen Zhang,
Chinese Academy of Agricultural Sciences, China
Bao Yi,
Chinese Academy of Agricultural Sciences (CAAS), China

***Correspondence:**
Rui Li
lirui181000@163.com
Xingguo Huang
huangxi8379@aliyun.com

Specialty section:
This article was submitted to Nutrition and Microbes, a section of the journal Frontiers in Nutrition

Received: *15 October 2020*
Accepted: *16 November 2020*
Published: *11 December 2020*

Citation:
Hou G, Peng W, Wei L, Li R, Yuan Y, Huang X and Yin Y (2020) Lactobacillus delbrueckii Interfere With Bile Acid Enterohepatic Circulation to Regulate Cholesterol Metabolism of Growing–Finishing Pigs via Its Bile Salt Hydrolase Activity. Front. Nutr. 7:617676. doi: 10.3389/fnut.2020.617676

Microbiota-targeted therapies for hypercholesterolemia get more and more attention and are recognized as an effective strategy for preventing and treating cardiovascular disease. The experiment was conducted to investigate the cholesterol-lowering mechanism of *Lactobacillus delbrueckii* in a pig model. Twelve barrows (38.70 ± 5.33 kg) were randomly allocated to two groups and fed corn–soybean meal diets with either 0% (Con) or 0.1% *Lactobacillus delbrueckii* (Con + LD) for 28 days. *L. delbrueckii*–fed pigs had lower serum contents of total cholesterol (TC), total bile acids (TBAs), and triglyceride, but higher fecal TC and TBA excretion. *L. delbrueckii* treatment increased ileal *Lactobacillus* abundance and bile acid (BA) deconjugation and affected serum and hepatic BA composition. Dietary *L. delbrueckii* downregulated the gene expression of ileal apical sodium-dependent bile acid transporter (*ASBT*) and ileal bile acid binding protein (*IBABP*), and hepatic farnesoid X receptor (*FXR*), fibroblast growth factor (*FGF19*), and small heterodimer partner (*SHP*), but upregulated hepatic high-density lipoprotein receptor (*HDLR*), low-density lipoprotein receptor (*LDLR*), sterol regulatory element binding protein-2 (*SREBP-2*), and cholesterol-7α hydroxylase (*CYP7A1*) expression. Our results provided *in vivo* evidence that *L. delbrueckii* promote ileal BA deconjugation with subsequent fecal TC and TBA extraction by modifying ileal microbiota composition and induce hepatic BA neosynthesis via regulating gut–liver FXR–FGF19 axis.

Keywords: ***Lactobacillus delbrueckii,*** **ileal microbiota, cholesterol, bile acids, enterohepatic circulation, pigs**

INTRODUCTION

Cholesterol is an indispensable fundamental building block for all cell membranes, but long-term high level of blood cholesterol may induce hypercholesterolemia-associated cardiovascular diseases (CVDs), a major contributing factor of adult deaths worldwide (1, 2). It is reported that a 1% reduction in blood cholesterol translates to a 2% decrease in heart disease risk (3, 4). Blood cholesterol level is determined by dietary fat and cholesterol intake and the body's cholesterol biosynthesis and excretion (5). Endogenous synthetic cholesterol accounts for nearly 70%, whereas the remaining 30% amount is mainly derived from animal products (6). Pork products are rich in cholesterol ranging from 57 mg/100 g in loin to 116 mg/100 g in dewlap (7). In China, pork is the most popular animal meat, and its production and consumption contribute about 50% of global pork output ranking first in the world (8). Therefore, clarification of underlying mechanisms of cholesterol metabolism in pigs and development of low cholesterol pork products has a promising potential of scientific researches and consumer markets.

Cholesterol is a precursor to bile acid (BA) biosynthesis. Approximately 30% to 40% of cholesterol is converted into primary BAs in liver via two pathways, with CYP7A1 as the rate-limiting enzyme in the classic pathway and CYP7B1 as an important enzyme in the alternative pathway (9, 10). Synthesized primary BAs are conjugated either with taurine or glycine and temporarily stored in the gallbladder. Upon cholecystokinin stimulation, often as a result of a meal, BAs are released into the duodenum via the bile duct. About 95% of BAs are reabsorbed all along the intestine, especially in the distal ileum, via passive diffusion and carrier-mediated transports entering enterohepatic cycle to maintain the BA pool homeostasis (11, 12). In each cycle, nearly 4% BAs are excreted along with feces, which is offset by the hepatic *de novo* synthesis of BAs from cholesterol (12). Obviously, the conversion of cholesterol to the BAs is the major route for cholesterol excretion, and the increased fecal BA excretion favors the conversion from cholesterol to BAs and reduces its release into the systemic circulation (13).

The hypocholesterolemic effect of *Lactobacillus* or its related products are reported extensively in animals and clinical researches (4, 12, 14, 15). Several proposed potential cholesterol-lowering mechanisms of *Lactobacillus* products chiefly cover cholesterol assimilation, cholesterol conversion to coprostanol, BSH activity, production of short fatty acids, and regulation of key enzyme in cholesterol metabolism (3, 12). However, the majority of explanations were based on *in vitro* test or high-fat or cholesterol animal models, and there was no adequate supporting evidence from normal subjects to validate these assumptions. Interestingly, our prior work confirmed that dietary *Lactobacillus delbrueckii* [1.01×10^9 colony-forming units (CFU)/g] lowered serum TC and triglyceride (TG) and increased the fecal TC and total BA (TBA) excretion of fatten pigs in commercial condition; unfortunately, we did not explore the further mechanism (16).

Given that the close relationship between cholesterol and BA metabolism, we supposed that *L. delbrueckii* with BSH activity affected the enterohepatic circulation of BA, which contributed to the reduced serum TC in a pig model. Therefore, we investigated the BSH activity of *L. delbrueckii* through plate assay and gene identification and also evaluated the effects of *L. delbrueckii on* intestinal microbiota, BA and cholesterol metabolism, and tissue lipids of growing–finishing pigs.

MATERIALS AND METHODS

All protocols and procedures involved in the experiment were approved by the Animal Ethics Committee of Hunan Agricultural University (Changsha, China). *L. delbrueckii* was provided by the microbiology functional laboratory of the College of Animal Science and Technology in the Hunan Agricultural University (Changsha, China). The strain was activated and sent to the PERFLY-BIO (Changsha, China) for large-scale production, and the viable count of final products reached 5×10^{11} CFU/g.

Animals and Experimental Design

Twelve Landrace × Yorkshire crossbred barrows with an average initial body weight of 38.70 ± 5.33 kg were randomly allocated to two groups, and each group had six pigs individually housed in the metabolism cage. Pigs were fed with corn–soybean meal diets (basal diets, Con) or basal diets containing 0.1% *L. delbrueckii* preparation (5×10^{10} CFU/g, Con + LD) for 28 days. The basal diets (**Table 1**) were formulated to meet the nutritional requirement of 50- to 75-kg pigs recommended by the NRC 2012 (17). All pigs were fed twice each day (8:00 A.M. and 3:00 P.M.) and had free access to water. The body weight of each pig was weighed at the beginning and end of the experiment, and the daily feed consumption per pig was recorded during the experimental period. Fecal samples were collected, freeze-dried, and stored at −20°C for total cholesterol (TC) and TBA detection. On day 29, the jugular vein blood samples were collected from the fasting pigs before slaughter using electrical stunning. Serum was obtained, aliquoted, and stored at −20°C for lipid analysis and BA profiles quantification. Digesta (in ileum) and tissues (in ileum, liver, longissimus dorsi, subcutaneous fat, and leaf lard) were quickly removed, snap-frozen in the liquid nitrogen, and stored at −80°C for microbiota composition, BA quantification, gene mRNA expression, lipid profile, and enzyme activity measurements.

Qualitative Determination of BSH Activity

Qualitative BSH activity of *L. delbrueckii* was measured according to the method introduced by Jayashree et al. (18) and Guo et al. (19) with a minor modification. Briefly, five sterile paper discs (8-mm diameter) were placed on an MRS agar plate containing 2 g/L taurodeoxycholate and glycodeoxycholate, 2 g/L sodium thioglycolate and 0.37 g/L $CaCl_2$, and 100 µL *L. delbrueckii* solution (1 g bacterial power was diluted with 9 mL of sterile water to get final concentrations of 1.5×10^{10} CFU/mL) were added to the paper discs immediately. The plates were incubated at 37°C for 72 h. The BA precipitates (i.e., opaque granular white colonies with silvery shine) around the discs were considered as BSH activity.

Genomic DNA of the *L. delbrueckii* was extracted using the TIANamp Stool DNA kit [Tiangen Biotech (Beijing) Co., Ltd,

TABLE 1 | Diet composition and nutritional levels of basal diets (air-dry basis, %).

Ingredients	Contents
Corn	66.76
Wheat middling	4.00
Wheat bran	6.00
Soybean meal (43% crude protein)	18.00
Soybean oil	1.00
L-Lysine	0.24
Premix[a]	4.00
Total	100.00
Calculated nutritional levels	
Digestible energy (DE, kcal/kg)	3,413.79
Crude protein	14.82
Standardized ileal digestible lysine (SID Lys)	0.85
Calcium	0.60
Total phosphorus	0.55

[a] *The premix provided the following per kg of diet:VA2 512 IU, VD3 1 200 IU, VE 34 IU, VK3 1.5 mg, VB12 17.6 μg, lactoflavin 2.0.5 mg, pantothenic acid 6.8 mg, niacin 20.3 mg, choline chloride 351, Mn 10 mg, Fe 50 mg, Zn 50 mg, Cu 20 mg, I 0.3 mg, Se 0.3 mg.*

China]. According to the report by Jayashree et al. (18), two primers (**Table 2**) for BSH1 and BSH2 were used to amplify the corresponding target gene, and the polymerase chain reaction (PCR) product sizes were 927 and 978 bp, respectively. The PCR reactions were carried out in 25-μL reaction system in a TaKaRa PCR Thermal Cycler. The PCR conditions were 5 min at 94°C for the initial denaturation followed by 35 cycles of denaturation at 94°C for 30 s, 1 min at 52°C for annealing, 1 min at 72°C for extension, and 5 min at 72°C for the final extension.

Determination of Serum and Tissue Lipids

Fasting blood of pigs were collected and placed at room temperature for 30 min, and the serum were separated by centrifugation (3,000 revolutions/min for 10 min at 4°C). Serum concentrations of TG, glucose (GLU), TBA, TC, high-density lipoprotein cholesterol (HDL-C), and high-density lipoprotein cholesterol (LDL-C) were measured by the BS 200 automatic blood biochemical analyzer (Mindray) with corresponding kits.

The total protein contents (g protein/L) in tissues were quantified using a BCA protein assay reagent kits (Nanjing Jiancheng Bioengineering Institute, Nanjing, China). About 100 mg of liver, longissimus dorsi, subcutaneous fat, or leaf lard was homogenized with 1 mL of chloroform/methannol solution (2:1, vol/vol), respectively. The homogenate were centrifuged at 3,000 revolutions/min for 10 min at 4°C to extract tissue lipids. The contents of TC (mmol/g · protein), TG (mmol/g · protein), and TBA (μmol/g · protein) in the selected tissue were measured by corresponding commercial kits (Nanjing Jianchen Bioengineering Institute, Jiangsu, China).

Measurement of Hepatic Enzyme Activity Using ELISA Kits

Hepatic total protein contents (g protein/L) were measured as described above, and the concentrations of hepatic 3-hydroxy-3-methyl glutaryl coenzyme A reductase (HMGR, U/g · protein) and cholesterol-7α hydroxylase (CYP7A1, U/g · protein) were measured following the instruction of corresponding commercial ELISA Kits (Jiangsu Yutong Biological Technology Co., Ltd., Jiangsu).

TABLE 2 | Primers used in the study.

Items	Gene	Sequence (5′-3′)
BSH gene	*BSH1*	F: GCCACCATGGTAATGTGCACGGCCGTTTCC
		R: CGATGGATCCTTAGGGTACTTGCGATAGG
	BSH2	F:ACCCATGGGTATGTGCACGAGCATCAACGTCA
		R: AAGGATCCGTTCAATTTCACCGGCGCCCAA
BA receptor and signaling	*FXR*	F: GGTCCTCGTAGAATTCACAA
		R: TGAACGGAGAAACATAGCTT
	FGF19	AGTACTCGGATGAGGACTGTGCTT
		AGAGACGGGCAGATGGTGTTTCTT
	SHP	F: GCCTACCTGAAAGGGACCAT
		R: CAACGGGTGTCAAGCCTTTA
BA transport	*ASBT*	F: TACGCGGTATACAGGAAATGGTA
		R: TTTGCCTTTTGGAATGATGACT
	IBABP	F: GTGAACAGCCCCAACTACCACCA
		R: TCGTAGCTCACGCCTCCGAC
BA biosynthesis	*CYP7A1*	F: GAAAGAGAGACCACATCTCGG
		R: GAATGGTGTTGGCTTGCGAT
	CYP27A1	F: ACTGAAGACCGCGATGAAAC
		R: CAAAGGCGAATCAGGAAGGG
Cholesterol biosynthesis and transport	*SREBP-2*	F: GATGGGCAGCAGAGTTCC
		R: ACAGCAGCAGGTCACAGGT
	HMGR	F: ATGGCATGACTCCAGTGGTACGTT
		R: GCAAATCTGCTGGTGCTGTCGAAT
	HDLR	F: CACTATGCCCAGTACGTGCTC
		R: CCTGAATGGCCTCCTTATCCTT
	LDLR	F: TTCTTCACCAACCGCCACGAG
		R: CTCAGTGTCCAGAGCGACC
Housekeeping gene	*GAPDH*	F: ATGGTGAAGGTCGGAGTGAAC
		R: CTCGCTCCTGGAAGATGGT

BSH, bile salt hydrolase; FXR, farnesoid X receptor; FGF19, fibroblast growth factor; SHP, small heterodimer partner; ASBT, apical sodium-dependent bile acid transporter; IBABP, ileal bile acid binding protein; CYP7A1, Cholesterol-7α hydroxylase; CYP27A1, cholesterol-27α hydroxylase; SREBP-2, sterol regulatory element binding protein-2; HMGR, 3-hydroxy-3-methyl glutaryl coenzyme A reductase; HDLR, high-density lipoprotein receptor; LDLR, low-density lipoprotein receptor.

Fecal TC and TBA Excretion

Fecal lipids were extracted as described above for TC analysis. Fecal TBA was extracted according to the method by De Smet et al. (5). Briefly, 1 g frozen fecal sample was dissolved in 40 mL methanol. After 4-min sonication and 1-h shock, the mixture was centrifuged at 10,000 *g* for 10 min to collect the supernatants. Total TC (mmol/L) and TBA (μmol/L) concentrations in the supernatants were determined using a commercial kit purchased from the Nanjing Jianchen Bioengineering Institute.

At last, fecal TC and TBA contents (mg/g) were obtained by formula conversion.

BA Profile Analysis

Metabolite Extraction

About 30 mg of solid samples (ileal digesta or hepatic tissue) were homogenized in 100 μL of precooled ultrapure water, vortexed with 5,000 μL of iced methanol and 10 μL of internal standard solution (for liquid sample, 100 μL serum was directly vortexed with 500 μL of iced methanol and 10 μL of internal standard solution), incubated at −20°C for 20 min for depositing protein, and centrifuged at 14,000 relative centrifugal force (rcf)/min for 15 min at 4°C. The supernatants were vacuum dried for subsequent analysis.

Ultraperformance Liquid Chromatography–Mass Spectrometry (UPLC-MS) Analysis

BA profiles were analyzed with a Waters ACQUITY UPLC I-Class coupled with a 5500 QTRAP mass spectrometer with an ESI source (Waters, Milford, MA). Briefly, the samples above were resolved in 1:1 (vol/vol) methanol solution and centrifuged at 14,000 rcf/min for 15 min at 4°C to obtain supernatants. The supernatants were separated using an ACQUITY UPLC BEH C18 chromatographic column (1.7 μm, 100 × 2.1 mm) (Waters, Milford, MA), and column temperature reached 50°C. The injection volume was 2 μL. A mobile phase system included Solvent A (0.1% FA solution) and Solvent B (methanol), in a gradient system at a flow rate of 0.3 mL/min. The mobile phase B was linearly changed as follows: from 60 to 65% (0–6 min), 65 to 80% (6–13 min), 65 to 80% (6–13 min), 80 to 90% (13–13.5 min), and stabilization at 90% (13.5–15 min). The mass spectrometer was used in Multiple Reaction Monitoring function in the ESI-negative mode to achieve information of tested ion pairs. The operating parameters were as follows: source temperature 550°C; ion source gas1 55 psi; ion source gas1 55 psi; curtain gas 40 psi; and IonSapary voltage floating −4,500 V. UPLC-MS raw data were analyzed using Multiquant™ software (v. 2.1) to obtain calibration equations and the quantitative concentrations of each BA.

Ileal Microbiota Analysis

Microbiota composition was analyzed according to our previous study (20, 21). Briefly, the ileal digesta were collected, frozen in liquid nitrogen, and stored at −80°C for further analysis. Total DNA was extracted and purified from digesta samples ($n = 5$ pigs/group) using TIANamp Stool DNA kit [Tiangen Biotech (Beijing) Co., Ltd, China]. DNA quality and quantity were evaluated by gel electrophoresis and a NanoDrop ND-1000 spectrophotometer (Thermo Fisher Scientific, USA), respectively. Ten acceptable DNA samples were delivered to Novogene (Beijing) for 16S rDNA sequencing.

The V3–V4 hypervariable region of the bacterial 16S rDNA gene was amplified with the barcoded universal primers (341F-806R). Purified amplicons were sequenced on the Illumina HiSeq platform (Illumina, USA) according to the standard procedures in Novogene (Beijing). Sequences with 97% similarity were assigned to the same operational taxonomic units (OTUs). An OTU table was further generated to record the abundance of each OTU in each sample, and a profiling histogram was made using R software (v. 3.1.1) to represent the relative abundance of taxonomic groups from phylum to species. A Venn diagram was generated to visualize the occurrence of shared and unique OTUs among groups.

Real-Time PCR

Total RNA of ileal or hepatic tissue was isolated and reversed transcribed to cDNA as previously described (20, 21). The two-step qRT-PCR reactions were performed in triplicate on 96-well plates using a 7500 Real-time PCR system (Applied Biosystems, Foster, CA) with the SYBR Premix Ex Taq™ (TaKaRa Biotechnology (Dalian), China). The primer sequences (**Table 2**) of farnesoid X receptor (*FXR*), fibroblast growth factor (*FGF19*), *SHP*, *ASBT*, *IBABP*, *CYP7A1*, cholesterol-27α hydroxylase (*CYP27A1*), sterol regulatory element binding protein-2 (*SREBP-2*), *HMGR*, high-density lipoprotein receptor (*HDLR*), low-density lipoprotein receptor (*LDLR*) and *GAPDH* were synthesized by the Sangon Biotech (Shanghai, China). Target gene expression was calculated by the $2^{-\Delta\Delta t}$ method relative to *GAPDH* gene amplification.

Statistical Analysis

All results were expressed as mean ± SD. Statistical analyses, except for microbiota data, were conducted by the two-tailed unpaired Student *t*-test of SPSS 17.0 (SPSS Inc., Chicago, IL, USA), with individual pig as an experimental unit. The Kruskal test was used for *post hoc* comparison of taxonomy. For all tests, $P < 0.05$ was considered as significant difference, while $0.05 < P < 0.10$ as a tendency.

RESULTS

Qualitative Identification of BSH Activity

After incubation for 12 h, non-obvious BA precipitates appeared around the discs in the plate (**Figure 1A**); however, the opaque granular white colonies with silvery shine were observed after 72-h incubation (**Figure 1B**). PCR amplification of two designated genes showed that the BSH2 gene was identified, not BSH1, on the genome sequence of *L. delbrueckii* (**Figure 1C**).

Serum Lipid Profiles

Serum TC, TBA, and TG contents in *L. delbrueckii*–fed pigs were found to be lower than the pigs in the Con group ($P < 0.05$; **Figures 2A,C,D**). *L. delbrueckii* treatment tended to reduce the concentration of serum LDL-C ($P = 0.075$) and elevate serum HDL-C ($P = 0.093$) level (**Figure 2A**). No significant changes in serum GLU and HDL-C/LDL-C contents were observed between two groups ($P > 0.05$, **Figures 2B,E**).

Alterations in BA Profiles of Serum, Ileal Digesta, and Liver

Compared with the Con group, lower serum levels of CDCA, HCA, GCA, GCDCA, GHDCA, TUDCA, THDCA, primary

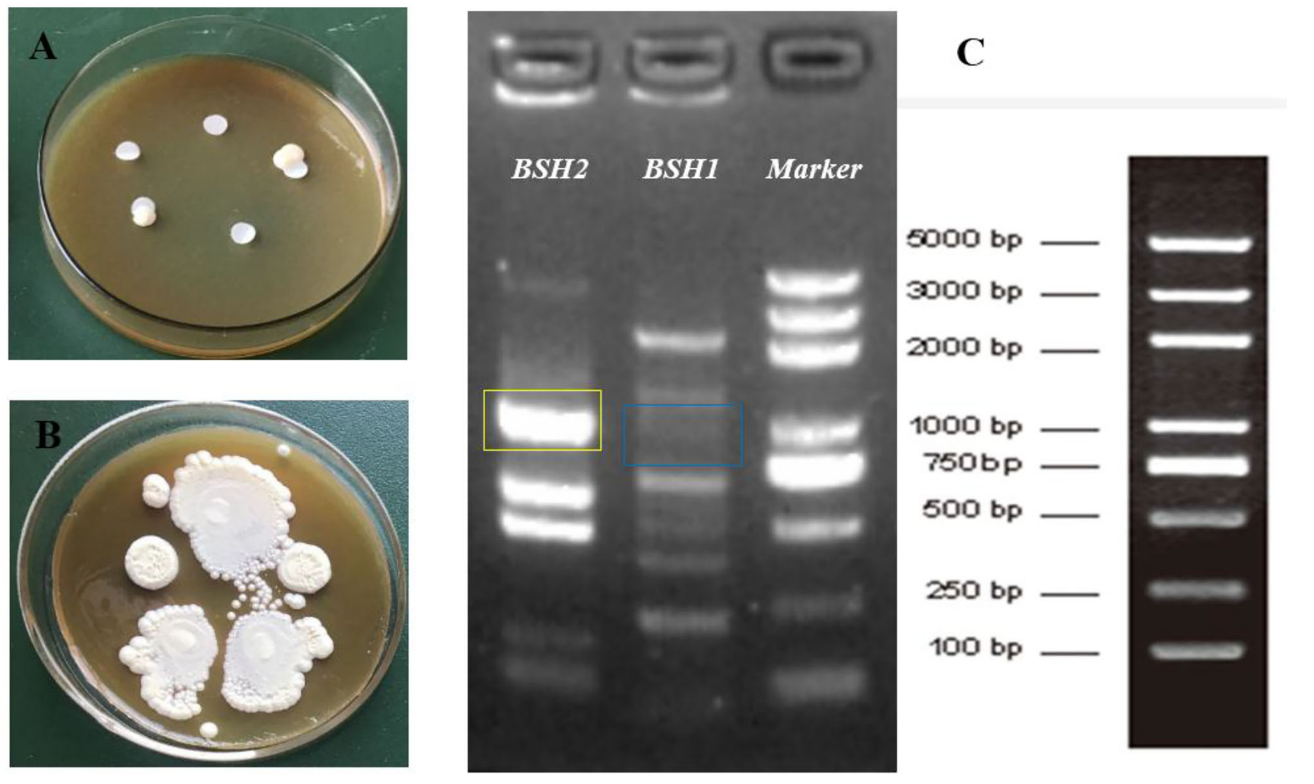

FIGURE 1 | Identification of bile salt hydrolase (BSH) activity in *Lactobacillus delbrueckii*. Incubation on MRS plate containing bile salts for 12 h **(A)** and 72 h **(B)**, respectively. Amplification of BSH genes in *L. delbrueckii* **(C)** and target band sites for *BSH1* and *BSH2* gene were marked with blue and yellow box, respectively.

BA, secondary BA, unconjugated BA, and total BA were found in the Con-LD group ($P < 0.05$, **Figure 3A**). Dietary addition of *L. delbrueckii* increased the ileal concentrations of CA and unconjugated BA ($P = 0.085$), but reduced GCDCA and GLCA ($P < 0.05$, **Figure 3B**). Hepatic concentrations of DCA ($P = 0.052$), HDCA, TCDCA, TUDCA, THDCA, and secondary BA ($P = 0.094$) in *L. delbrueckii*–fed pigs were decreased compared to the pigs in the Con group ($P < 0.05$, **Figure 3C**).

Ileal Bacteria Composition

The Venn picture presented 546 shared OTUs between two groups, and there were 219 and 153 unique OTUs in the Con and Con + LD group, respectively (**Figure 4A**). The bacterial population was dominated by Firmicutes and Proteobacteria, with minor populations such as Actinobacteria and Bacteroidetes (**Figure 4B**). Administration of *L. delbrueckii* increased the abundance of Actinobacteria ($P = 0.071$), Spirochaetes ($P = 0.070$), and Kiritimatiellaeota ($P = 0.029$) and reduced the abundance of Melainabacteria ($P = 0.091$) and Elusimicrobia ($P = 0.029$). Down to the genus level, the higher abundance of *Lactobacillus* ($P = 0.002$) and lower abundance of *Clostridiales* ($P = 0.031$), *Ruminococcaceae* ($P = 0.061$), *Enterococcus* ($P = 0.035$), *Streptococcus* ($P = 0.052$), and *Rothia* ($P = 0.049$) were found (**Figure 4C** and **Supplementary Table 1**).

BA and Cholesterol Transport, Biosynthesis, and Excretion

Administration of *L. delbrueckii* downregulated the gene expression of ileal FGF19 ($P = 0.089$), ASBT, and IBABP and enhanced fecal TC and TBA excretion ($P < 0.05$, **Figures 5A,B**). Hepatic gene expressions of FXR, FGF19, and SHP were reduced, but HDLR, LDLR, SREBP-2, and CYP7A1 were increased in the Con + LD group ($P < 0.05$, **Figure 5C**). Hepatic CYP7A1 activity tended to be greater in the *L. delbrueckii*–fed pigs than those in the Con group ($P = 0.062$, **Figure 5D**). No changes were found in hepatic concentrations of TC, TG, and TBA between two groups ($P > 0.05$, **Figures 5E,F**).

Tissue TG and TC Deposition

The concentrations of TG and TC in the longissimus dorsi, subcutaneous fat, and leaf lard had no differences between two groups ($P > 0.05$, **Figure 6**).

DISCUSSION

Fluctuation of blood lipids parameters can reflect the body's lipid metabolism and health status; chronically high serum TC and LDL-C levels are strongly associated with the increased risks of CVD (22, 23). TC and TG are the main components of blood lipids; lowering their concentrations can prevent hyperlipemia. Considerable researches have confirmed that

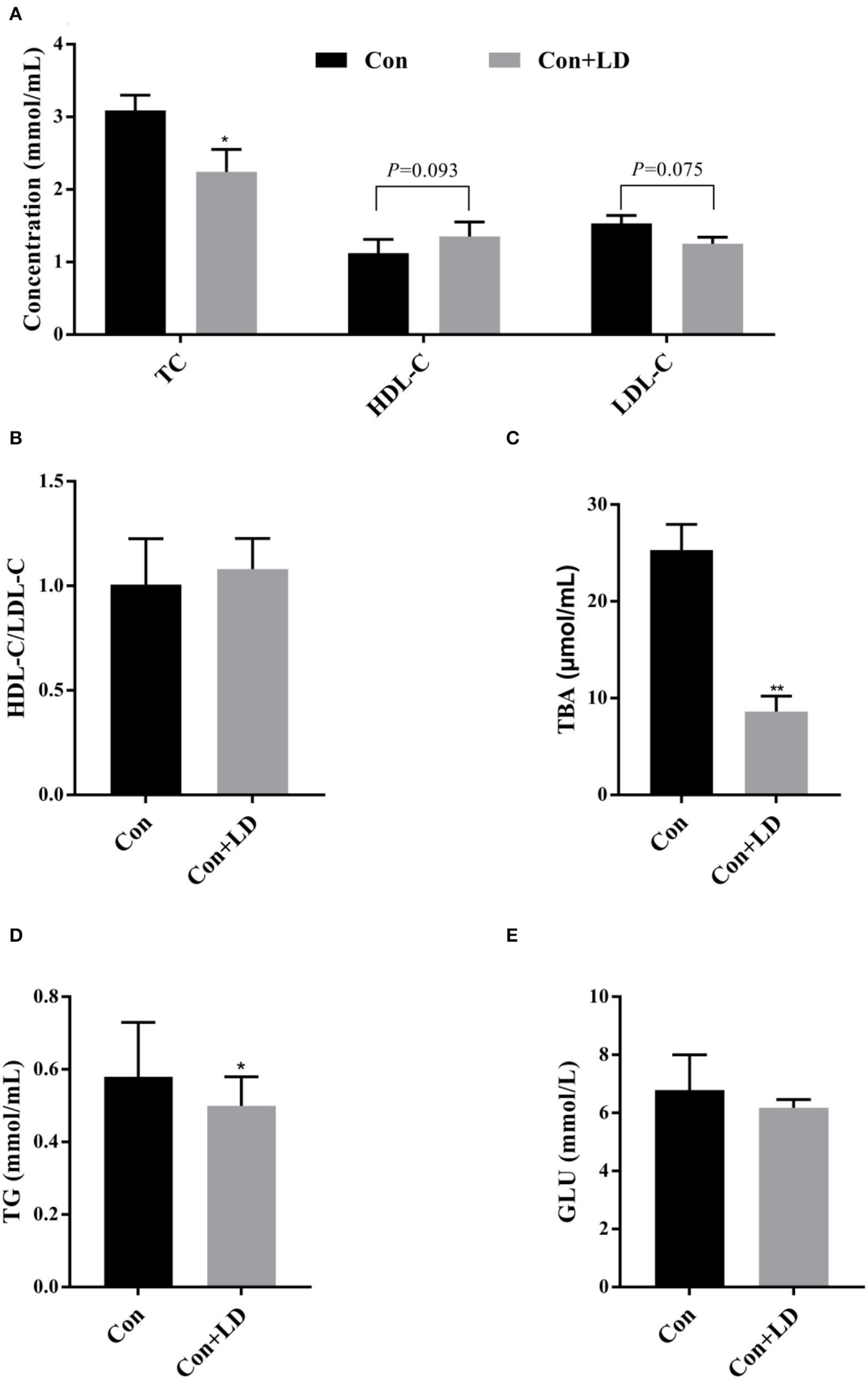

FIGURE 2 | Effects of *Lactobacillus delbrueckii* on serum levels of TC, HDL-C, and LDL-C **(A)**; ratio of HDL-C/LDL-C **(B)**; TBA **(C)**; TG **(D)**; and GLU **(E)** in growing–finishing pig (*$P < 0.05$; **$P < 0.01$).

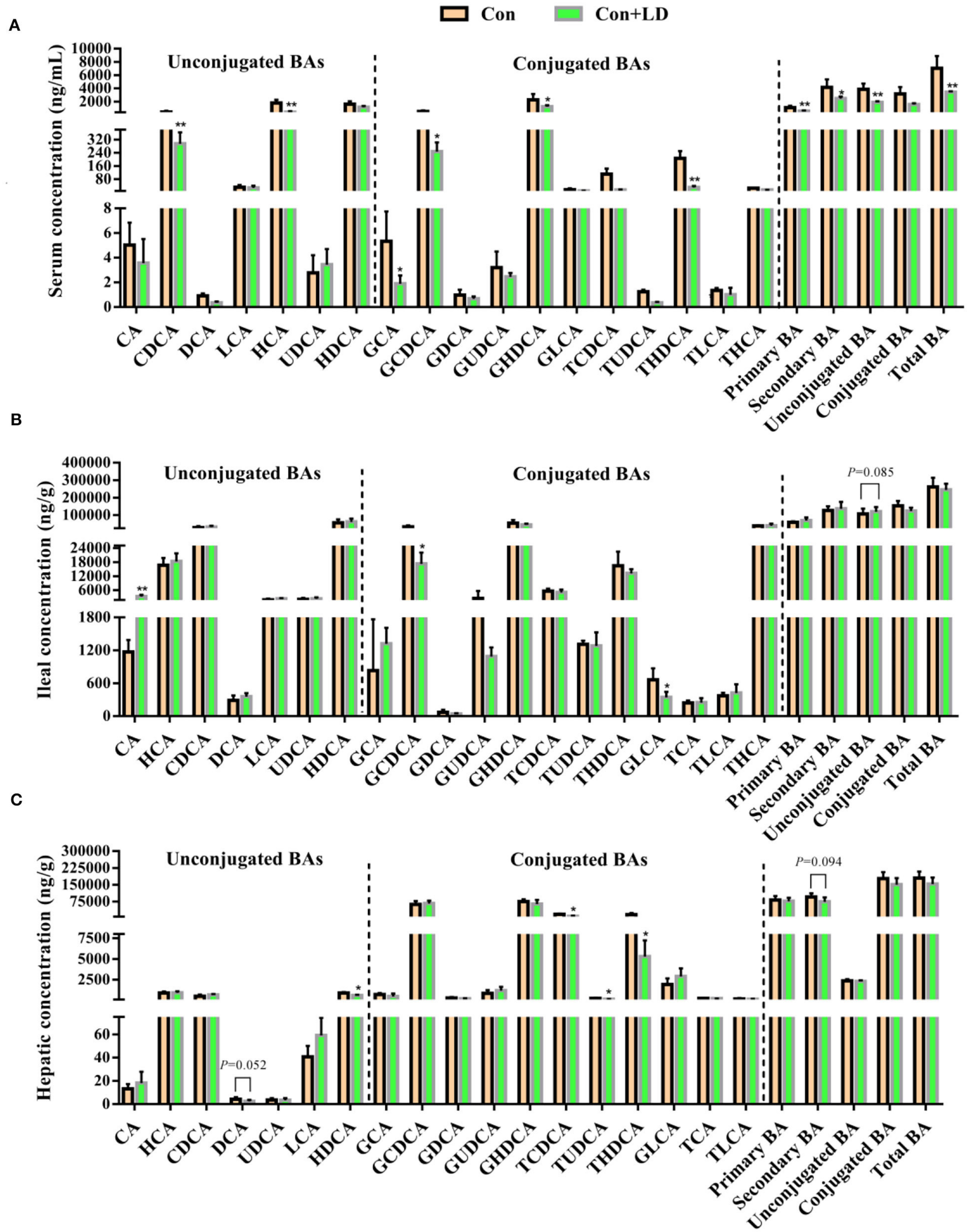

FIGURE 3 | Bile acids profile in the serum **(A)**, ileal digesta **(B)**, and liver **(C)** of growing–finishing pigs (*$P < 0.05$; **$P < 0.01$).

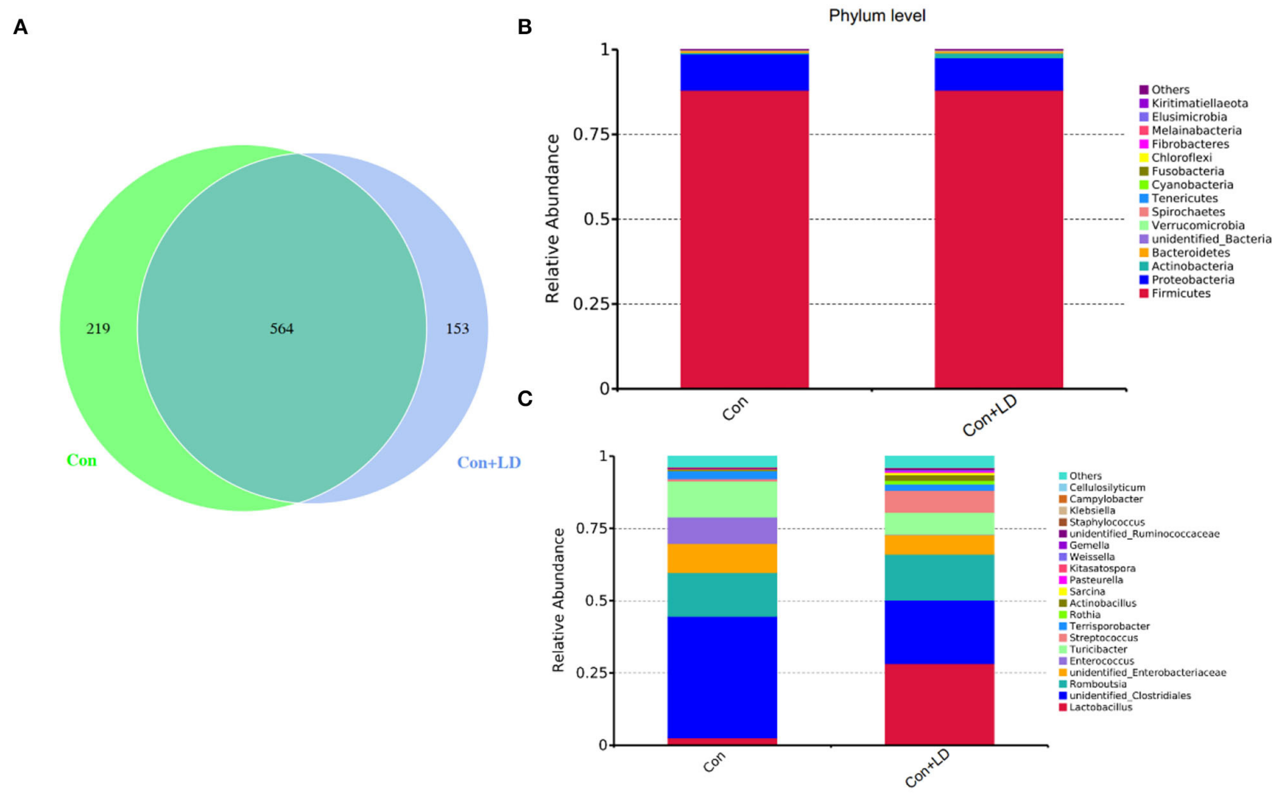

FIGURE 4 | Ileal bacterial composition of growing–finishing pigs. Venn picture showed shared or unique OTUs between two groups **(A)**. Relative abundance of ileal microbiota at the phylum **(B)** or genus **(C)** level.

consumption of *Lactobacillus* products reduced concentrations of serum cholesterol and improved lipid profiles (24–26). In the current study, dietary addition of *L. delbrueckii* decreased serum levels of TC, LDL-C, and TG of pigs. Our findings were again the proof of our previous reports (16) and also offered another evidence for cholesterol-lowering role of lactic acid bacteria in normal subject. The hypocholesterolemic effect of *L. delbrueckii* might provide a potential dietary manipulation way to prevent and improve hyperlipidemia.

Probiotics with BSH activity is hypothesized to be an important character in lowering serum cholesterol, which might be tightly related to the BSH genes on their genome (1, 4, 12, 22, 27). BSH activity has been characterized in *Lactobacillus*, *Bifidobacterium*, *Clostridium*, *Enterococcus*, and *Bacteroides* (12). *L. delbrueckii* tested in this study possessed the BSH2 gene identified by PCR amplification and exhibited a good BSH activity on the modified agar plate, demonstrating the strain was capable of bile salts deconjugation. BSH enzyme or activity is specific to the microbiota and is not present in eukaryotic cells, which is regarded as a crucial probiotic marker that help organisms resist toxic bile salt environment in the digestive tract and also an important colonization factor for gut bacteria (12, 28). *Lactobacillus* with BSH activity contribute to their survival and colonization in the gastrointestinal tract and exert a beneficial effect on host by regulating cholesterol and BA enterohepatic circulation (1, 4, 15, 29). Our results suggest that *L. delbrueckii* might own a good ability of intestinal survival and colonization and play a key role in regulating cholesterol and BA metabolism.

Intestinal microbiota and BA metabolism are mutually linked, enteric bacterial enzymes shape BA pool size and composition by mediating deconjugation and 7α-dehydroxylation of primary BAs (27). Liver cells synthesize primary BAs from cholesterol, mainly consisting of CA and CDCA in human, CA, α-/β-MCA in rodent and CA, HCA, and CDCA in pigs, and these BAs were conjugated with either glycine (G-BAs) or taurine (T-BAs) via their N-acyl amidate to increased solubility before secretion into intestine (30). Bile salt deconjugation is carried out by BSH, expressed in *Lactobacillus*, *Bifidobacterium*, *Clostridium*, and *Bacteroides* (9, 31). The genus *Lactobacillus* and its BSH activity could result in deconjugation of conjugated BAs (32). The conjugated BAs are very soluble, and most of them are reabsorbed in the ileum into enterohepatic circulation. In our study, *L. delbrueckii* administration obviously increased the ileal *Lactobacillus* abundance, indicating that ileal bacterial BA deconjugation might enhance. Interestingly, we found ileal concentrations of GCDCA, GLCA, and unconjugated BAs were decreased in the Con + LD group. Bacterial deconjugation of T-BA or G-BA can reduce serum cholesterol levels via amplifying the formation of new bile salts needed to replace those that

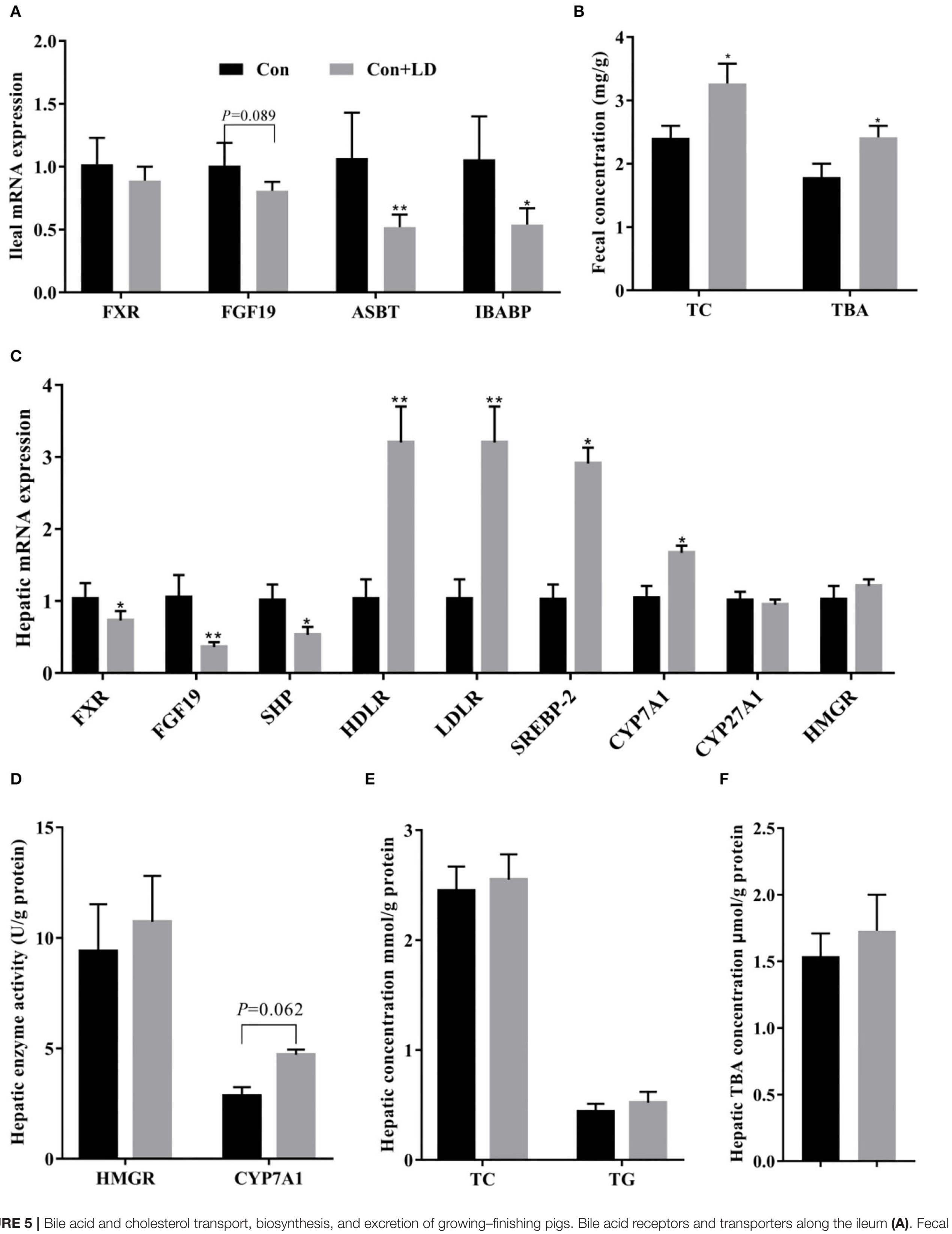

FIGURE 5 | Bile acid and cholesterol transport, biosynthesis, and excretion of growing–finishing pigs. Bile acid receptors and transporters along the ileum **(A)**. Fecal TC and TBA excretion **(B)**. Bile acid metabolism-related genes in the liver **(C)**. Hepatic enzyme activity related to cholesterol and bile acid synthesis **(D)**. Hepatic TC and TG **(E)** and TBA **(F)** concentrations (*$P < 0.05$; **$P < 0.01$).

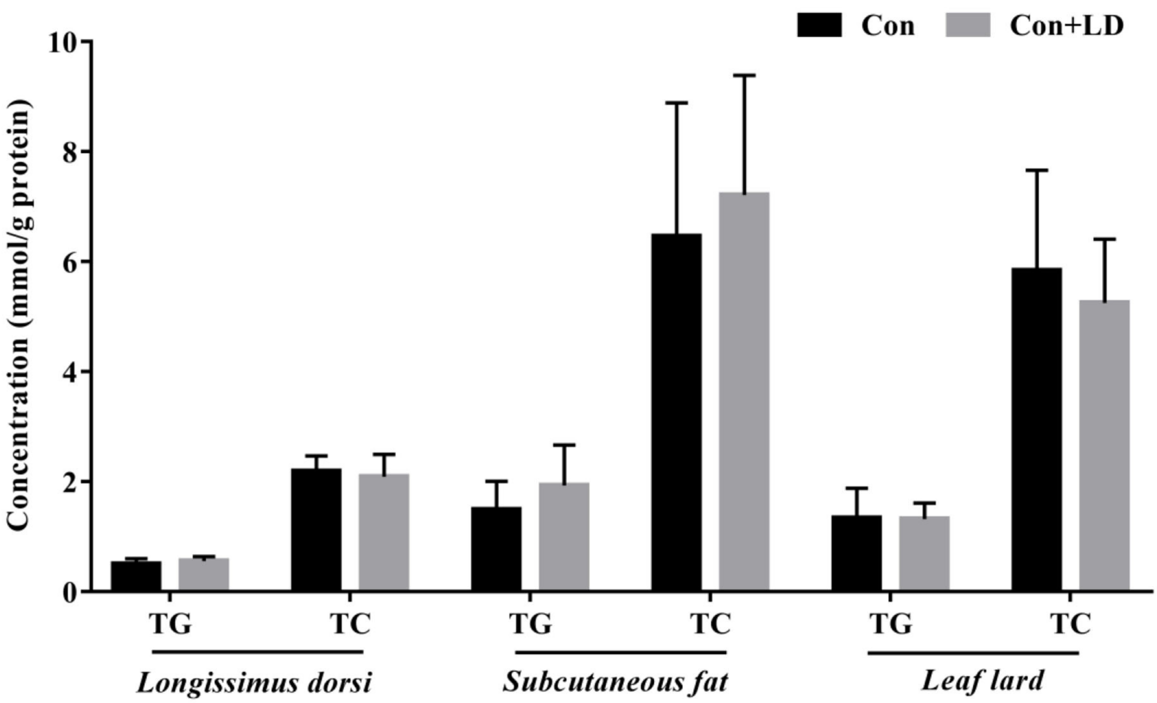

FIGURE 6 | Concentrations of TG and TC in the selected tissues of growing–finishing pigs.

have escaped enterohepatic cycle (26). Therefore, the potential mechanism of cholesterol reduction in *L. delbrueckii* might be the conversion of bile salt to free BA by improving ileal *Lactobacillus* abundance with BSH activity and interfered with BAs enterohepatic circulation.

In the intestine, bile salts play an important role in emulsifying lipids. Ileum is confirmed as the major site for BA reabsorption, and the highest expression of BA transporters and FGF19 was observed along the intestinal segment (10). Intestinal BA transporters play a vital role on the BA reabsorption process. ASBT and IBABP are important BA transporters engaging in BA active or passive transport. ASBT imports luminal BAs to the enterocytes where the BAs bind to IBABP and are transferred to the basement surface and then enter into portal vein with the help of MRP3 and OSTα/OSTβ transporters in the basolateral membrane (10). In the present study, ileal expression of *ASBT* and *IBABP* in *L. delbrueckii*–treated pigs was markedly downregulated, indicating that less ileal BAs were reabsorbed after *L. delbrueckii* consumption.

The liver is the center of the synthesis and metabolism of cholesterol and BAs. Cholesterol *de novo* synthesis begins with acetyl-CoA, and HMGR is the rate-limiting enzyme responsible for catalyzing the conversion of HMG-CoA into mevalonic acid. Our results showed that administration of *L. delbrueckii* did not affect HMGR activity and mRNA expression, but upregulated hepatic *SREBP2*, *LDLR*, and *HDLR* expression. SREBP2 is a key nuclear transcription factor for regulating *LDLR* and *HMGR* target genes in charge of extrahepatic cholesterol uptake and endogenous cholesterol biosynthesis (33). Hepatic HDLR and LDLR are responsible for combining blood HDL-C and LDL-C to remove cholesterol, respectively. HDL-C carries cholesterol from peripheral tissues to liver; conversely, LDL-C transports hepatic cholesterol to peripheral tissues. Our observations implied *L. delbrueckii* treatment had no influence on hepatic cholesterol synthesis, but it might change its metabolism via hepatic clearance. The conversion of cholesterol to BAs is the main way to eliminate hepatic cholesterol, and CYP7A1 is the rate-limiting enzymes in the pathway (4). In the present study, hepatic *CYP7A1* expression was increased, and CYP7A1 activity also tended to rise in the Con + LD group, indicating that dietary *L. delbrueckii* might lower cholesterol via enhancing BAs biosynthesis.

Hepatic BA synthesis is negatively regulated by FXR signaling and FGF19 signaling (34). Ileal FXR activation contributes to FGF19 production, and then FGF19 translocates to the liver via hepatic portal vein where it binds to the FGFR4/β-Klotho complex and inhibits *CYP7A1* expression (9, 15). CYP7A1 is the rate-limiting enzyme in classic pathway for hepatic BA synthesis. Our results showed that ileal *FGF19* expression and hepatic *FXR* and *FGF19* expression were downregulated, but *CYP7A1* expression and CYP7A1 activity were increased by *L. delbrueckii* treatment, suggesting that this strain increased the conversion of cholesterol to BAs in the liver via suppressing FXR–FGF19 signaling and improving CYP7A1 activity. Additionally, reduction of hepatic FXR and SHP expression could also explain the increased CYP7A1 activity, because hepatic FXR stimulation resulted in SHP expression upregulation to inhabit CYP7A1 and CYP8B1 activity (3).

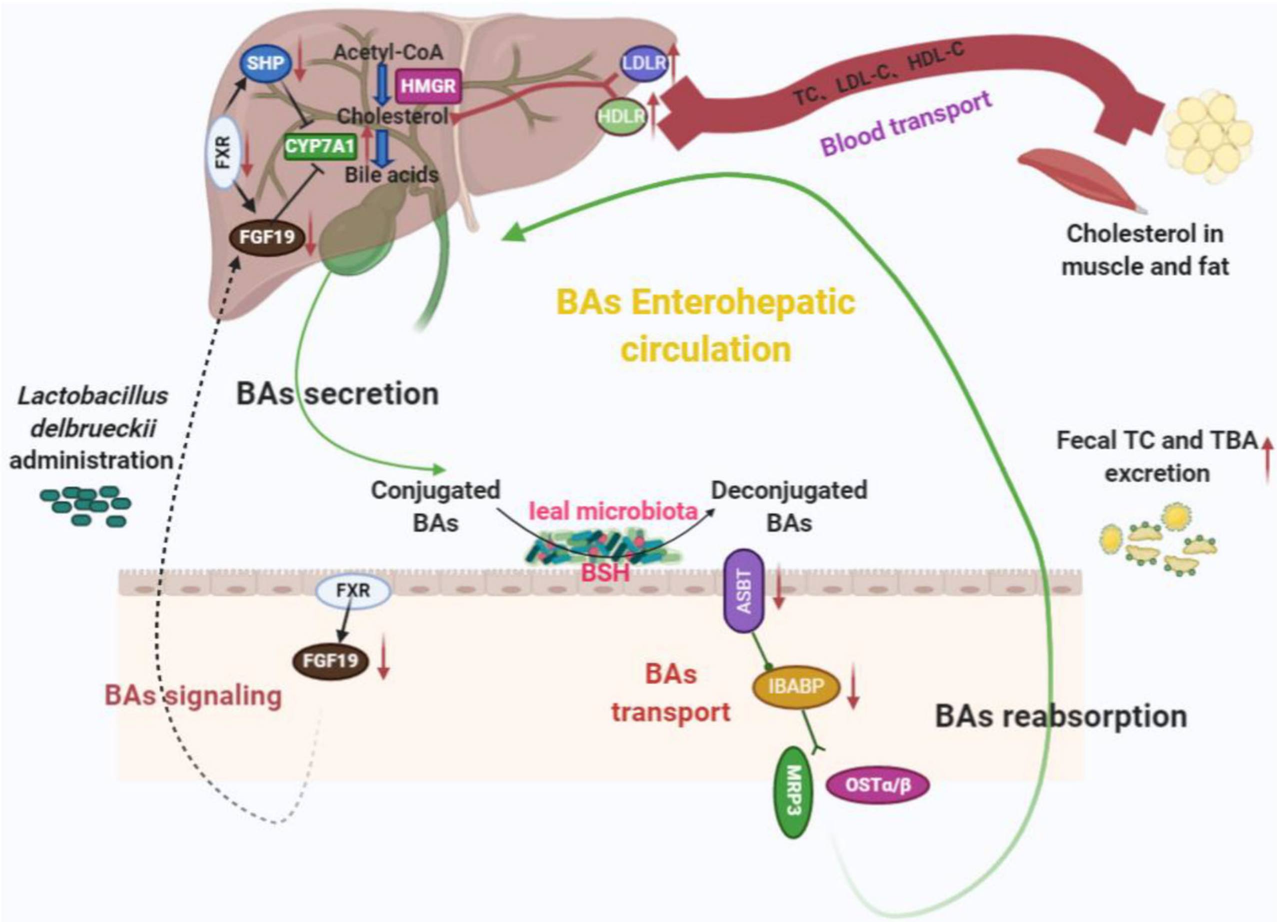

FIGURE 7 | Potential cholesterol-lowering mechanisms of *Lactobacillus delbrueckii*–fed pigs. Ileal microbiota modification (mainly increased ileal *Lactobacillus* abundance) with *L. delbrueckii* administration led to bile salts deconjugation by BSH activity and facilitated fecal TBA and TC excretion. Meanwhile, less deconjugated BAs are reabsorbed into enterohepatic circulation and downregulate BA transporter expression (*ASBT* and *IBABP*) and promote BA synthesis via increasing the conversion of cholesterol to BA with the help of CYP7A1, a rate-limiting enzyme, in the liver. Additionally, ileal BA deconjugation by microbiota alteration affects BA signaling (FXR–FGF19 axis) to regulated BA synthesis. Enhancement of BA synthesis using circulating cholesterol (blood transport) to restore the bile acid pool.

The homeostasis of BAs pool is maintained by enterohepatic cycle. Quantitative determination of BAs profiles via UPLC-MS analysis could reflect the enterohepatic circulation of BAs (35, 36). In our study, we observed great changes in BA composition of serum, ileal digesta, and liver, which might ascribe ileal microbiota modification with *L. delbrueckii*. Deconjugation of ileal bile salts causes less BAs to enter portal vein and return to liver, and unabsorbed BAs flow into hindgut and are excreted along with feces. Fecal BA excretion is almost equal to the hepatic synthesized BAs under the normal physiological condition (4, 37). Enhancement of BA synthesis using circulating cholesterol to restore the BA pool is an important manner for reduction of serum cholesterol (38, 39). In our study, dietary *L. delbrueckii* accelerated fecal TC and TBA output of pigs, which was closely associated to the decrease in serum TC and LDL-C. Reduction of serum cholesterol might lower cholesterol deposition in tissues; however, we found no alterations in TG and TC contents in longissimus dorsi, subcutaneous fat, and leaf lard, which implied that short-term *L. delbrueckii* treatment could not change tissue cholesterol deposition of growing–finishing pigs.

CONCLUSIONS

Ileal microbiota modification induced by *L. delbrueckii* enhances BA deconjugation and fecal excretion in growing–finishing pigs. These events involved changes in ileal BA reabsorption, repression of the enterohepatic FXR–FGF19 axis, and increased hepatic BA neosynthesis (**Figure 7**).

DATA AVAILABILITY STATEMENT

The datasets presented in this study can be found in online repositories. The name of the repository and accession number are SRA and PRJNA670289, respectively.

ETHICS STATEMENT

The animal study was reviewed and approved by the Animal Ethics Committee of Hunan Agricultural University. Written informed consent was obtained from the owners for the participation of their animals in this study.

AUTHOR CONTRIBUTIONS

GH, RL, and XH design the experiment. GH, RL, YY, and LW conducted the animal experiments. GH and RL wrote and revised the manuscript. XH, RL, and YY offered the experimental reagents and materials. GH, RL, and WP did experimental analysis, collected, and analyzed the data. GH and RL preparedthe figures and edited the manuscript. All authors reviewed the manuscript.

FUNDING

This research was supported by the National Natural Science Foundation of China (Grant nos. 31772617 and 31802074), the Hunan Excellent Post-doctoral Innovative Talents Project (Grant no. 2020RC2063), the Hunan postgraduate research and innovation project (Grant nos. CX2017B346 and CX2018B399), and the School-enterprise cooperation project (E0490205 and E0490207).

ACKNOWLEDGMENTS

We would like to thank the hardwork of all the project participants.

SUPPLEMENTARY MATERIAL

The Supplementary Material for this article can be found online at: https://www.frontiersin.org/articles/10.3389/fnut.2020.617676/full#supplementary-material

REFERENCES

1. Oner O, Aslim B, Aydas SB. Mechanisms of cholesterol-lowering effects of lactobacilli and bifidobacteria strains as potential probiotics with their bsh gene analysis. *J Mol Microb Biotech.* (2014) 24:12–8. doi: 10.1159/000354316
2. Thushara RM, Gangadaran S, Solati Z, Moghadasian MH. Cardiovascular benefits of probiotics: a review of experimental and clinical studies. *Food Funct.* (2016) 7:632–42. doi: 10.1039/C5FO01190F
3. Ishimwe N, Daliri EB, Lee BH, Fang F, Du GC. The perspective on cholesterol-lowering mechanisms of probiotics. *Mol Nutr Food Res.* (2015) 59:94–105. doi: 10.1002/mnfr.201400548
4. Wang G, Huang W, Xia YJ, Xiong Z, Ai L. Cholesterol-lowering potentials of *Lactobacillus* strain overexpression of bile salt hydrolase on high cholesterol diet-induced hypercholesterolemic mice. *Food Funct.* (2019) 10:1684–95. doi: 10.1039/C8FO02181C
5. De Smet I, De Boever P, Verstraete W. Cholesterol lowering in pigs through enhanced bacterial bile salt hydrolase activity. *Brit J Nutr.* (1998) 79:185–94. doi: 10.1079/BJN19980030
6. Chiu CW, Kao TH, Chen BH. An improved analytical method for determination of cholesterol oxidation products in meat and animal fat by QuEChERS coupled with gas chromatography-mass spectrometry. *J Agric Food Chem.* (2018) 66:3561–71. doi: 10.1021/acs.jafc.8b00250
7. Dorado M, Gomez EMM, Jimenez-Colmenero F, Masoud TA. Cholesterol and fat contents of Spanish commercial pork cuts. *Meat Sci.* (1999) 51:321–3. doi: 10.1016/S0309-1740(98)00126-0
8. He YN, Yang XG, Xia J, Zhao LY, Yang YX. Consumption of meat and dairy products in China: a review. *Proc Nutr Soc.* (2016) 75:385–91. doi: 10.1017/S0029665116000641
9. Sun LL, Pang YY, Wang XM, Wu Q, Liu HY, Liu B, et al. Ablation of gut microbiota alleviates obesity-induced hepatic steatosis and glucose intolerance by modulating bile acid metabolism in hamsters. *Acta Pharm Sin B.* (2019) 9:702–10. doi: 10.1016/j.apsb.2019.02.004
10. Fang V, Zhang L, Meng Q, Wu W, Lee YK, Xie J, et al. Effects of dietary pectin on the profile and transport of intestinal bile acids in young pigs. *J Anim Sci.* (2018) 96:4743–54. doi: 10.1093/jas/sky327
11. Lepercq P, Relano P, Cayuela C, Juste C. Bifidobacterium animalis strain DN-173 010 hydrolyses bile salts in the gastrointestinal tract of pigs. *Scand J Gastroentero.* (2004) 39:1266–71. doi: 10.1080/00365520410003515
12. Jones ML, Tomaro-Duchesneau C, Martoni CJ, Prakash S. Cholesterol lowering with bile salt hydrolase-active probiotic bacteria, mechanism of action, clinical evidence, and future direction for heart health applications. *Expert Opin Biol Ther.* (2013) 13:631–42. doi: 10.1517/14712598.2013.758706
13. Fang W, Wen XB, Meng QS, Wu WD, Everaert N, Xie JJ, et al. Alteration in bile acids profile in large white pigs during chronic heat exposure. *J Therm Biol.* (2019) 84:375–83. doi: 10.1016/j.jtherbio.2019.07.027
14. Guo CF, Zhang S, Yuan YH, Li JY, Yue TL. Bile salt hydrolase and S-layer protein are the key factors affecting the hypocholesterolemic activity of *Lactobacillus* casei-fermented milk in hamsters. *Mol Nutr Food Res.* (2018) 62:e1800728. doi: 10.1002/mnfr.201800728
15. Yao L, Seaton SC, Ndousse-Fetter S, Adhikari AA, DiBenedetto N, Mina AI, et al. A selective gut bacterial bile salt hydrolase alters host metabolism. *Elife.* (2018) 7:e37182. doi: 10.7554/eLife.37182
16. Li R, Hou GH, Wei LK, Peng W, Pan J, Huang XG. Effects of Lactobacillus delbrueckii on serum biochemical parameters, related genes mRNA expression of cholesterol metabolism and fat deposition in finishing pigs. *Chinese J Anim Nutri.* (2017) *Chin J Anim Nutr*. (2017) 29:3184–92. doi: 10.3969/j.issn.1006-267x.2017.09.027
17. NRC. *Nutrient Requirements of Swine*. 11th Edn. Washington, DC: Natl. Acad. Press (2012).
18. Jayashree S, Pooja S, Pushpanathan M, Rajendhran J, Gunasekaran P. Identification and characterization of bile salt hydrolase genes from the genome of *Lactobacillus* fermentum MTCC 8711. *Appl Biochem Biotechnol.* (2014) 174:855–66. doi: 10.1007/s12010-014-1118-5
19. Guo XH, Kim JM, Nam HM, Park SY, Kim JM. Screening lactic acid bacteria from swine origins for multistrain probiotics based on *in vitro* functional properties. *Anaerobe.* (2010) 16:321–6. doi: 10.1016/j.anaerobe.2010.03.006
20. Li R, Chang L, Hou GF, Song ZH, Fan ZY, He X, et al. Colonic microbiota and metabolites response to different dietary protein sources in a piglet model. *Front Nutr*. (2019) 6:151. doi: 10.3389/fnut.2019.00151
21. Li R, Hou GF, Jiang XD, Song ZH, Fan ZY, Hou DX, et al. Different dietary protein sources in low protein diets regulate colonic microbiota and barrier function in a piglet model. *Food Funct*. (2019) 10:6417–28. doi: 10.1039/C9FO01154D
22. Choi SB, Lew LC, Yeo SK, Nair Parvathy S, Liong MT. Probiotics and the BSH-related cholesterol lowering mechanism: a Jekyll and Hyde scenario. *Crit Rev Biotechnol.* (2015) 35:392–401.
23. Xie N, Cui Y, Yin YN, Zhao X, Yang JW, Wang ZG, et al. Effects of two Lactobacillus strains on lipid metabolism and intestinal microflora in rats fed a high-cholesterol diet. *BMC Complem Altern Med.* (2011) 11:53. doi: 10.1186/1472-6882-11-53
24. Ding WR, Shi C, Chen M, Zhou JW, Long RJ, Guo XS. Screening for lactic acid bacteria in traditional fermented Tibetan yak milk and evaluating their probiotic and cholesterol-lowering potentials in rats fed a high-cholesterol diet. *J Funct Foods.* (2017) 32:324–32. doi: 10.1016/j.jff.2017.03.021

25. Li C, Nie SP, Ding Q, Zhu KX, Wang ZJ, Xiong T, et al. Cholesterol-lowering effect of Lactobacillus plantarum NCU116 in a hyperlipidaemic rat model. *J Funct Foods.* (2014) 8:340–7. doi: 10.1016/j.jff.2014.03.031
26. Wang CY, Wu SC, Ng CC, Shyu YT. Effect of *Lactobacillus*-fermented adlay-based milk on lipid metabolism of hamsters fed cholesterol-enriched diet. *Food Res Int.* (2010) 43:819–24. doi: 10.1016/j.foodres.2009.11.020
27. Degirolamo C, Rainaldi S, Bovenga F, Murzilli S, Moschetta A. Microbiota modification with probiotics induces hepatic bile acid synthesis via downregulation of the Fxr-Fgf15 axis in mice. *Cell Rep.* (2014) 7:12–8. doi: 10.1016/j.celrep.2014.02.032
28. Singh TP, Malik RK, Katkamwar SG, Kaur G. Hypocholesterolemic effects of *Lactobacillus reuteri* LR6 in rats fed on high-cholesterol diet. *Int J Food Sci Nutr.* (2015) 66:71–5. doi: 10.3109/09637486.2014.953450
29. Alonso L, Fontecha J, Cuesta P. Combined effect of *Lactobacillus acidophilus* and β-cyclodextrin on serum cholesterol in pigs. *Br J Nutr.* (2016) 115:1–5. doi: 10.1017/S0007114515003736
30. Wang P, Lin S, Wu D, Fang ZF. Recent progress in nutrition physiology role and metabolism regulation of bile acids. *Chinese J Anim Nutri.* (2019) 31:49–58. doi: 10.3969/j.issn.1006-267x.2019.05.005
31. Han K, Bose S, Wang JH, Lim SK, Chin YW, Kim YM, et al. *In vivo* therapeutic effect of combination treatment with metformin and *Scutellaria baicalensis* on maintaining bile acid homeostasis. *PLoS ONE.* (2017) 12:e0182467. doi: 10.1371/journal.pone.0182467
32. Tian Y, Cai J, Gui W, Nichols RG, Koo I, Zhang J, et al. Berberine directly affects the gut microbiota to promote intestinal farnesoid X receptor activation. *Drug Metab Dispos.* (2019) 47:86–93. doi: 10.1124/dmd.118.083691
33. Luo J, Yang HY, Song BL. Mechanisms and regulation of cholesterol homeostasis. *Nat Rev Mol Cell Bio.* (2020) 21:225–45. doi: 10.1038/s41580-019-0190-7
34. Kim B, Park KY, Ji Y, Park S, Holzapfel W, Hyun CK. Protective effects of *Lactobacillus rhamnosus* GG against dyslipidemia in high-fat diet-induced obese mice. *Biochem Biophys Res Commun.* (2016) 473:530–6. doi: 10.1016/j.bbrc.2016.03.107
35. Li Y, Ma J, Yao K, Su W, Tan B, Wu X, et al. Circadian rhythms and obesity: Timekeeping governs lipid metabolism. *J Pineal Res.* (2020) 69:e12682. doi: 10.1111/jpi.12682
36. Yin J, Li YY, Han H, Ma J, Liu G, Wu X, et al. Administration of exogenous melatonin improves the diurnal rhythms of the gut microbiota in mice fed a high-fat diet. *mSystems.* (2020) 5:e00002–20. doi: 10.1128/mSystems.00002-20
37. Guo CF, Li JY. Hypocholesterolaemic action of *Lactobacillus casei* F0822 in rats fed a cholesterol-enriched diet. *Int Dairy J.* (2013) 32:144–9. doi: 10.1016/j.idairyj.2013.04.001
38. Thandapilly SJ, Ndou SP, Yanan W, Nyachoti CM, Ames NP. Barley β-glucan increases fecal bile acid excretion and short chain fatty acid levels in mildly hypercholesterolemic individuals. *Food Funct.* (2018) 9:3092–6. doi: 10.1039/C8FO00157J
39. Yin J, Li YY, Han H, Chen S, Gao J, Liu G, et al. Melatonin reprogramming of gut microbiota improves lipid dysmetabolism in high-fat diet-fed mice. *J Pineal Res.* (2018) 65:e12524. doi: 10.1111/jpi.12524

Conflict of Interest: The authors declare that the research was conducted in the absence of any commercial or financial relationships that could be construed as a potential conflict of interest.

frontiers in Nutrition

ORIGINAL RESEARCH
published: 14 December 2020
doi: 10.3389/fnut.2020.612875

Modulation of Gut Microbiota and Oxidative Status by β-Carotene in Late Pregnant Sows

Xupeng Yuan[1,2], Jiahao Yan[1], Ruizhi Hu[1], Yanli Li[1], Ying Wang[1], Hui Chen[1], De-Xing Hou[3], Jianhua He[1]* and Shusong Wu[1]*

[1] College of Animal Science and Technology, Hunan Agricultural University, Changsha, China, [2] Hunan Xinguang'an Agricultural Husbandry Co., Ltd., Changsha, China, [3] Department of Food Science and Biotechnology, Faculty of Agriculture, Kagoshima University, Kagoshima, Japan

OPEN ACCESS

Edited by:
Hui Han,
Chinese Academy of Sciences (CAS), China

Reviewed by:
Hongkui Wei,
Huazhong Agricultural University, China
Shengyu Xu,
Sichuan Agricultural University, China

***Correspondence:**
Jianhua He
jianhuahy@hunau.net
Shusong Wu
wush688@hunau.edu.cn

Specialty section:
This article was submitted to Nutrition and Microbes, a section of the journal Frontiers in Nutrition

Received: 01 October 2020
Accepted: 20 November 2020
Published: 14 December 2020

Citation:
Yuan X, Yan J, Hu R, Li Y, Wang Y, Chen H, Hou D-X, He J and Wu S (2020) Modulation of Gut Microbiota and Oxidative Status by β-Carotene in Late Pregnant Sows. Front. Nutr. 7:612875. doi: 10.3389/fnut.2020.612875

Recent evidences suggest that gut microbiota plays an important role in regulating physiological and metabolic activities of pregnant sows, and β-carotene has a potentially positive effect on reproduction, but the impact of β-carotene on gut microbiota in pregnant sows remains unknown. This study aimed to explore the effect and mechanisms of β-carotene on the reproductive performance of sows from the aspect of gut microbiota. A total of 48 hybrid pregnant sows (Landrace × Yorkshire) with similar parity were randomly allocated into three groups ($n = 16$) and fed with a basal diet or a diet containing 30 or 90 mg/kg of β-carotene from day 90 of gestation until parturition. Dietary supplementation of 30 or 90 mg/kg β-carotene increased the number of live birth to 11.82 ± 1.54 and 12.29 ± 2.09, respectively, while the control group was 11.00 ± 1.41 ($P = 0.201$). Moreover, β-carotene increased significantly the serum nitric oxide (NO) level and glutathione peroxidase (GSH-Px) activity ($P < 0.05$). Characterization of fecal microbiota revealed that 90 mg/kg β-carotene increased the diversity of the gut flora ($P < 0.05$). In particular, β-carotene decreased the relative abundance of Firmicutes including *Lachnospiraceae* AC2044 group, *Lachnospiraceae* NK4B4 group and *Ruminococcaceae* UCG-008, but enriched Proteobacteria including *Bilophila* and *Sutterella*, and Actinobacteria including *Corynebacterium* and *Corynebacterium* 1 which are related to NO synthesis. These data demonstrated that dietary supplementation of β-carotene may increase antioxidant enzyme activity and NO, an important vasodilator to promote the neonatal blood circulation, through regulating gut microbiota in sows.

Keywords: β-carotene, nitric oxide, antioxidant, gut microbiota, pregnant sows

INTRODUCTION

Beta-(β-)carotene is a widely distributed phytochromes (1), and is generally considered as a precursor of vitamin A (2, 3). It belongs to the fat-soluble substance which is incorporated into chylomicrons and absorbed in the intestine through passive diffusion (4). When ingested into the intestine, β-carotene is partially transformed into vitamin A, and the remaining β-carotene is passed by blood circulation to target organs such as the liver, ovary, adipose tissue and adrenal gland (5). Around 17–45% of β-carotene can be absorbed into the circulatory system (1). The importance of vitamin A in female reproductive health has been well-documented (6). Previous studies have found a high concentration of β-carotene in the luteum, and the lack of β-carotene results in delayed ovulation, luteal phase defect, and increased risk of ovarian cyst (1, 7). Moreover, the secretion of pregnancy hormones is linked to serum β-carotene concentrations, indicating that β-carotene can play an important role in reproduction (8, 9).

Multiple studies have shown that low-level inflammation, progressive oxidative stress, and metabolic disorders occur during the perinatal period. During pregnancy, the rapid cell proliferation of the uterus and the placenta, growth of the fetus, and childbirth will progressively increase the reactive oxygen species (ROS) and decrease the antioxidant capacity of the body (10). The pro-inflammatory interleukins (ILs) such as IL-6 can be substantially increased in maternal serum as pregnancy progresses (11). Furthermore, insulin resistance during pregnancy will decrease glucose utilization, while excessive energy intake and obesity during pregnancy will exacerbate maternal inflammation and oxidants stress, thereby triggering insulin resistance and having adverse effects on pregnancy (12). Recent studies have shown that significant change in the gut microbiota during different periods of pregnancy can affect the physiological state and metabolic process of host, indicating that gut microbiota plays a vital role during pregnancy (13, 14). In modern pig farming industry, constipation occurs frequently in pregnant sows due to intestinal disorder, which is largely determined by the dysfunction of gut microbiota. β-carotene has been considered as a potent inhibitor of oxidative stress and inflammation both *in vitro* and *in vivo* (15, 16), and it can suppress the expression of proinflammatory cytokines such as IL-1β and IL-6 to alleviate inflammation and oxidative stress induced by ischemia injury (17). However, it is not clear whether β-carotene exerts biological functions by modulating the gut microbiota.

Therefore, this study aimed to investigate the effect of β-carotene on the reproductive performance of sows, and challenged to clarify the potential mechanisms from the aspect of gut microbiota.

MATERIALS AND METHODS

Experimental Design and Diets

The animal model and experimental procedures used in this experiment were approved by the Hunan Agricultural University Institutional Animal Care and Use Committee (No. 201903). A total of 48 hybrid pregnant sows (Landrace × Yorkshire), with similar parity (3–7 fetuses) were used in this study. The experimental animals which kept in gestation stalls with fully slatted floors measuring under environment temperature and had free access to water, were randomly allocated into three treatments ($n = 16$). Based on previous studies, sows in the treatments were fed with a basal diet (control group, CTL), a diet containing 30 mg/kg of β-carotene (β-carotene low dose group, CAR-L), or a diet containing 90 mg/kg of β-carotene (β-carotene high dose group, CAR-H), respectively, based on previous studies (8, 18). The sows were fed at 6:00 a.m., 12:00 p.m., and 6:00 p.m. with ∼3.2 kg of feed/sow/day. The experiment started on day 90 of gestation and continued until delivery. The composition of the basal diet, which meets the nutritional requirements of pigs according to NRC (2012), was shown in **Supplementary Table 1**.

Reproductive Performance Markers

The number of live birth, litter weight at parturition and average weight of piglets born alive were measured within 24 h after farrowing.

Sample Collections

At the day of parturition, blood samples (5 mL) were collected from the marginal auricular vein into anticoagulant-free vacuum tubes and centrifuged on 1,500 × g for 10 min after standing at room temperature for 30 min to get the serum. Fecal samples (around 2 g from each sow) were collected from the innermost of feces into sterile tubes after defecation in the morning, and snap-frozen in liquid nitrogen before storage at −80°C for further DNA extraction.

Measurement of Serum Biochemical Indices

Total antioxidant capacity (T-AOC), total superoxide dismutase (T-SOD) activity, glutathione peroxidase (GSH-Px) activity, the level of thiobarbituric acid reactive substances (TBARS), and the nitric oxide (NO) level were determined in serum by using respective assay kits (Nanjing Jiancheng Bioengineering Institute, Nanjing, China) according to the manufacturer's instructions as described previously (19). The levels of glucose (GLU, 0.06–27.8 mmol/L), total protein (TP, 1.74–100 g/L), total cholesterol (TC, 0.09–25.85 mmol/L), triglycerides (TG, 0.05–11.3 mmol/L), high-density lipoproteins (HDL-c, 0.065–3.8 mmol/L), low-density lipoprotein cholesterol (LDL-c, 0.2–12 mmol/L), immunoglobulin G (IgG, 0.25–35 g/L) and immunoglobulin M (IgM, 0.25–5.00 g/L) were measured with respective kits from Mindray Medical International Ltd., China by using an automated biochemical analyser BS-200 (Mindray, China).

Characterization of Gut Microbiota

Fecal microbiota was characterized by 16S rRNA gene sequencing. Briefly, total DNA was extracted from fecal samples (six random samples from each group) by using a DNA Isolation Kit (MoBio Laboratories, Carlsbad, CA, USA) following the manufacturer's manual. Purity and quality of the genomic DNA were checked on 0.8% agarose gels. The V3–4 hypervariable region of the bacterial 16S rRNA gene was amplified with the primers 338F (5′-ACTCCTACGGGAGGC AGCA-3′) and 806R (5′-GGACTACHVGGGTWTCTAAT-3′). For each sample, 10-digit barcode sequence was added to the 5′ end of the forward and reverse primers (provided by Allwegene Technology Inc., Beijing, China). The PCR was carried out on a Mastercycler Gradient (Eppendorf, Germany) using 25 μL reaction volumes, containing 12.5 μL KAPA 2G Robust Hot Start Ready Mix, 1 μL Forward Primer (5 μmol/L), 1 μL Reverse Primer (5 μmol/L), 5 μL DNA (total template quantity is 30 ng), and 5.5 μL H_2O. Cycling parameters were 95°C for 5 min, followed by 28 cycles of 95°C for 45 s, 55°C for 50 s, and 72°C for 45 s with a final extension at 72°C for 10 min. Three PCR

TABLE 1 | The effect of β-carotene on the reproductive performance of sows.

Item	CTL	CAR-L	CAR-H	*P*-value
Total born number	11.82 ± 1.72	12.55 ± 1.37	13.17 ± 2.29	0.233
The number of live birth	11.00 ± 1.41	11.82 ± 1.54	12.29 ± 2.09	0.201
Litter weight at parturition, kg	16.16 ± 3.72	17.26 ± 4.07	17.13 ± 2.97	0.729
Average weight of piglets born alive, kg	1.42 ± 0.19	1.46 ± 0.27	1.41 ± 0.21	0.844
Stillborn piglets number	9	8	9	-

CTL, a basal diet; CAR-L, a basal diet containing 30 mg/kg β-carotene; CAR-H, a basal diet containing 90 mg/kg β-carotene. Data were shown as means ± SD (n = 16).

products per sample were pooled to mitigate reaction-level PCR biases. The PCR products were purified using a QIAquick Gel Extraction Kit (QIAGEN, Germany), and quantified using Real Time PCR, and sequenced on Miseq platform at Allwegene Technology Inc., Beijing, China. After the run, image analysis, base calling and error estimation were performed using Illumina Analysis Pipeline Version 2.6. The raw data were first screened and sequences were removed from consideration if they were shorter than 200 bp, had a low quality score (≤20), contained ambiguous bases or did not exactly match to primer sequences and barcode tags. Qualified reads were separated using the sample-specific barcode sequences and trimmed with Illumina Analysis Pipeline Version 2.6. And then the dataset was analyzed using QIIME (Version 1.8.0). The sequences were clustered into operational taxonomic units (OTUs) at a similarity level of 97%, to generate rarefaction curves and to calculate the richness and diversity index. The Ribosomal Database Project (RDP) Classifier tool was used to classify all sequences into different taxonomic groups.

Statistical Analysis

Results were expressed as means ± SD. The significant differences between groups were analyzed by one-way analysis of variance tests, followed by Fisher's least significant difference (LSD) and Duncan's multiple range tests with the SPSS statistical program (SPSS19, IBM Corp., Armonk, NY, USA). A probability of $P < 0.05$ was considered significant.

RESULTS

The Influence of β-Carotene on the Reproductive Performance of Sows

As shown in **Table 1**, the number of live birth was increased to 11.82 ± 1.54 and 12.29 ± 2.09 in CAR-L (30 mg/kg β-carotene) group and CAR-H (90 mg/kg β-carotene) group respectively, while the CTL group was 11.00 ± 1.41, although there had no statistical significance ($P = 0.201$). The litter weight at parturition showed a similar trend with the number of live birth, and the average weight of piglets born alive kept no change.

The Effect of β-Carotene on Serum Biochemical Markers in Sows

As progressive oxidative stress plays a negative role during the perinatal period, the oxidative stress markers including T-AOC, TBARS, GSH-Px, and T-SOD were measured in the serum of sows. As shown in **Figure 1**, the activity of GSH-Px (C) was increased significantly ($P < 0.05$) in both CAR-L (85.99 ± 4.75 U/mL) and CAR-H (86.8 ± 1.67 U/mL) group, as compared with CTL group (77.94 ± 4.54 U/mL). However, no significant differences were observed in the levels of T-AOC (A), MDA (B), and T-SOD (D) among the three groups ($P > 0.05$).

Nitric oxide (NO) is a signaling molecule involved in oxidative stress and inflammation, and also considered as an important vasodilator to promote the neonatal blood circulation (14). Thus, NO was further measured in serum, and the results showed that the level of NO was increased to 188.33 ± 37.13 μmol and 186.95 ± 30.06 μmol in CAR-L and CAR-H group respectively, which were significantly ($P < 0.05$) higher than that in CTL group (149.54 ± 17.12 μmol) (**Figure 1E**).

In addition, indicators of immune response and glucolipid metabolism were also measured in serum due to their important roles in pregnancy. However, β-carotene had no significant effects on serum levels of immunoglobulins (IgM & IgG), lipids (Tc, Tg, HDL-c & LDL-c), Glu, and Tp (**Supplementary Table 2**).

Modulation of Gut Microbiota by β-Carotene

To gain an insight into the effect of β-carotene on gut microbiota, the composition and relative abundance of fecal microbiota was characterized by using high throughput 16S rRNA gene sequencing. As shown in **Figure 2**, supplementation of β-carotene dose-dependently increased the Shannon index (A) of the microbiota, and a significant difference was observed between CTL and CAR-H group ($P < 0.05$). Further analysis on the relative abundance of bacterial phyla showed that the microbial community was dominated by Firmicutes, Bacteroidetes, Proteobacteria, Spirochaetae, and Euryarchaeota, which account for 97% of total microbes, and supplementation of β-carotene increased the relative abundance of Proteobacteria.

At the genus level, a total number of 299 microbial genera were analyzed, and nine genera were found to be significantly different among the three groups. As shown in **Figure 3**, β-carotene decreased the relative abundances of *Lachnospiraceae AC2044 group* (A), *Lachnospiraceae NK4B4 group* (B), and *Ruminococcaceae UCG-008* (C), which belong to the phylum of Firmicutes. Meanwhile, β-carotene reduced the relative abundance of *Prevotellaceae UCG-001* (D), a genera belong to the phylum of Bacteroidete. On the other hand, β-carotene increased the relative abundance of *Sedimentibacter* (E) belonging to the phylum of Firmicutes, *Bilophila* (F) and *Sutterella* (G) belonging to the phylum of Proteobacteria, as well as *Corynebacterium 1* (H) and *Corynebacterium* (I) belonging to the phylum of Actinobacteria. Based on the results of gut microbiota and serum biochemical markers, the correlation between GSH-Px, NO and the changed microbial genera were further analyzed. The results showed that *Corynebacterium 1* and *Corynebacterium*

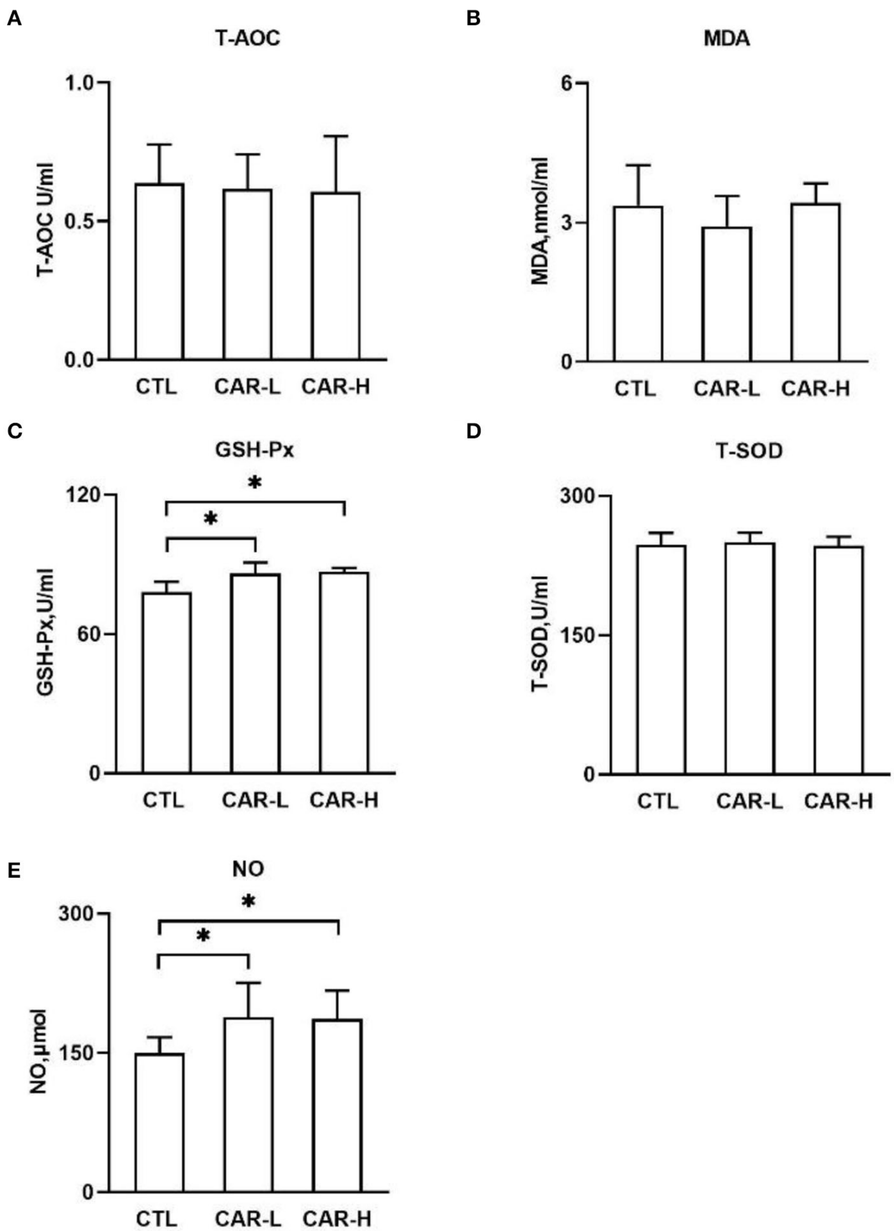

FIGURE 1 | The effect of β-carotene on serum levels of antioxidant indicators and NO. Serum levels of T-AOC **(A)**, TBARS **(B)**, GSH-Px **(C)**, T-SOD **(D)**, and NO **(E)** were determined by using respective kits. CTL, a basal diet; CAR-L, a basal diet containing 30 mg/kg β-carotene; CAR-H, a basal diet containing 90 mg/kg β-carotene. Data were shown as means ± SD ($n = 16$), $^*P < 0.05$.

were positively correlated ($P < 0.01$) with the NO level, while *Prevotellaceae UCG-001 and Lachnospiraceae AC2044 group* were negatively correlated ($P < 0.01$) with the GSH-Px level (J).

DISCUSSION

It has been reported that injection or dietary supplementation of β-carotene during early gestation can enhance embryo survival, litter size and litter weight of piglets (9, 20, 21), but less information on its impact in late pregnancy has been obtained. However, in this study, dietary supplementation of β-carotene at late stage of pregnancy showed limited effect on the number of live birth and litter weight at parturition. During late pregnancy, maternal metabolism will be increased to adapt the nutritional requirements of fetal growth and placenta metabolism, which usually manifested by the increase in TG, TC, HDL-c and LDL-c levels (22–24). However, supplementation of β-carotene had no

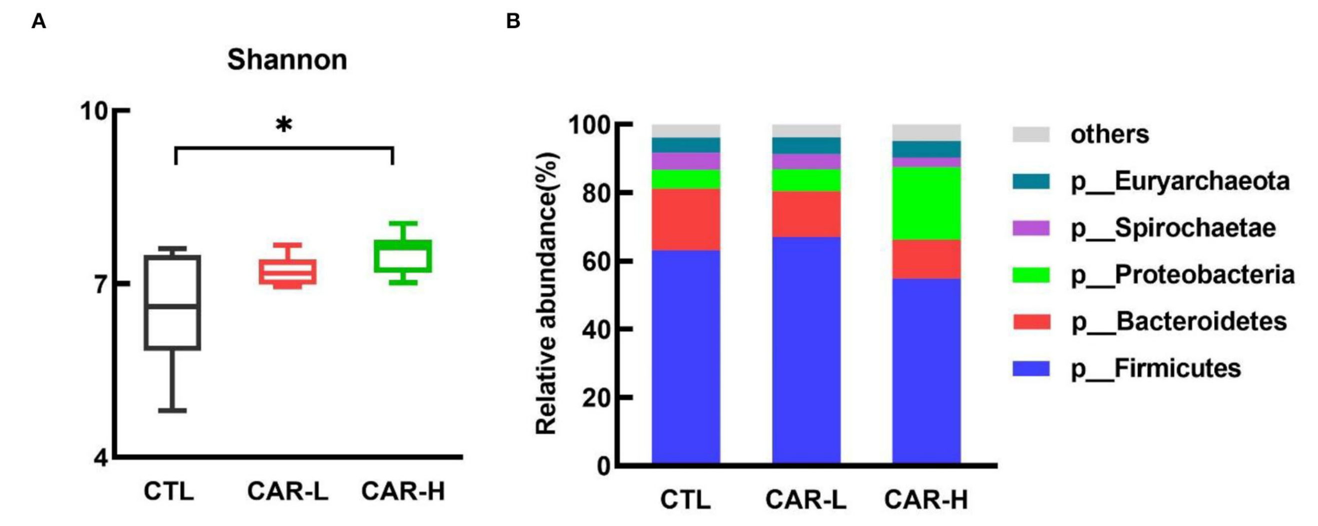

FIGURE 2 | The effect of β-carotene on fecal microbial community. The effect of β-carotene on the Shannon index **(A)** and the relative abundances of microbial phyla **(B)** were analyzed by 16S rRNA gene sequencing. CTL, a basal diet; CAR-L, a basal diet containing 30 mg/kg β-carotene; CAR-H, a basal diet containing 90 mg/kg β-carotene. Data were shown as means ± SD ($n = 6$), $^*P < 0.05$.

significant effect on the serum levels of lipids (TC, TG, HDL-c, and LDL-c) and immunoglobulins (IgM & IgG) in sows, which suggesting that β-carotene has limited effects on lipid metabolism and immunoglobulin production. Oxidative stress has a negative effect on oocyte maturation, ovulation, implantation and blastocyst formation (25). In the perinatal period of mammals, fetal growth, lactation and increased metabolism can induce the production of progressive ROS, and negatively impact sow reproductive performance including reduces litter size, survival ratio of piglets and the ability for lactation (10, 22). Our results revealed that β-carotene significantly increased the activity of GSH-Px, an antioxidant enzyme against ROS. The findings were consistent with a previous cell model analysis in which β-carotene increased Nrf2 expression (2). Moreover, adequate uterine blood flow throughout gestation is reported to be essential for placental and fetal growth, especially in the late phase of pregnancy (26), as the increased blood flow velocity in placenta can enhance fetus to uptake nutrients absorption (10, 26). As a signaling molecule that conveys information between cells, NO is considered to be an important vasodilator to promote the neonatal blood circulation (27). Thus, serum NO levels in the sow serum were further tested, and the findings showed that β-carotene substantially increased NO levels, implying that β-carotene has a possible beneficial effect on uterine and placenta blood circulation.

Gut microbiota plays an essential role in the regulation of nutrient utilization and metabolism (28), and the microbial diversity can be used as a biomarker to reflect health and metabolic capacity of animals (14). A previous study has also pointed out that gut microbiota is closely related to the reproductive performance of sows (13). The intestinal microbial composition changes significantly during pregnancy, and α-diversity will gradually increase throughout the lactation period (29). Furthermore, the structure of intestinal flora differ at different stages of pregnancy, and enrichment of α-diversity can enhance metabolic capacity and increase the flux of nutrients to the fetus for growth and development (30). Clarke et al. (14) revealed that people with rapid metabolism show a higher α-diversity of gut microbiota. In this study, β-carotene increased the Shannon index, which suggested that it may enhance the metabolic capacity and promote fetal development. Further analysis at the genus level revealed that β-carotene mainly down-regulated the relative abundance of genera *Lachnospiraceae AC2044 group*, *Lachnospiraceae NK4B4 group*, and *Ruminococcaceae UCG-008* belonging to the phylum of Firmicutes, as well as *Prevotellaceae UCG-001* belonging to the phylum of Bacteroidete. On the other hand, β-carotene enriched *Sutterella* and *Bilophila* belonging to the phylum of Proteobacteria, *Corynebacterium 1* and *Corynebacterium* belonging to the phylum of Actinobacteria, as well as *Sedimentibacter* belonging to the phylum of Firmicutes. *Lachnospiraceae* and *Ruminococcaceae* are closely related to the production of butyrate (31, 32). *Prevotellaceae UCG-001* belongs to the family of *Prevotellace* showed a positive correlation with the expression of inflammatory factors in our recent study (33). *Sutterella* is positively correlated with neutral detergent fiber (NDF) digestibility (34), and *Bilophila* has a positive correlation with obesity-related markers (18), while *Sedimentibacter* can secrete cellulase enzyme to digest cellulose into glucose (19, 34). Our results revealed that *Corynebacterium 1 and Corynebacterium* were positively correlated with NO level, while *Prevotellaceae UCG-001 and Lachnospiraceae AC2044 group* were negatively correlated with GSH-Px level. Other studies have also shown that *Corynebacterium* can induce the expression of NO synthase in a number of tissues in mice, and the decrease in blood pressure induced by *Corynebacterium* is associated with the induction of NO synthase (35). This can partially explain the increased NO level induced by β-carotene in this study. A recent study has also indicated that the abundance

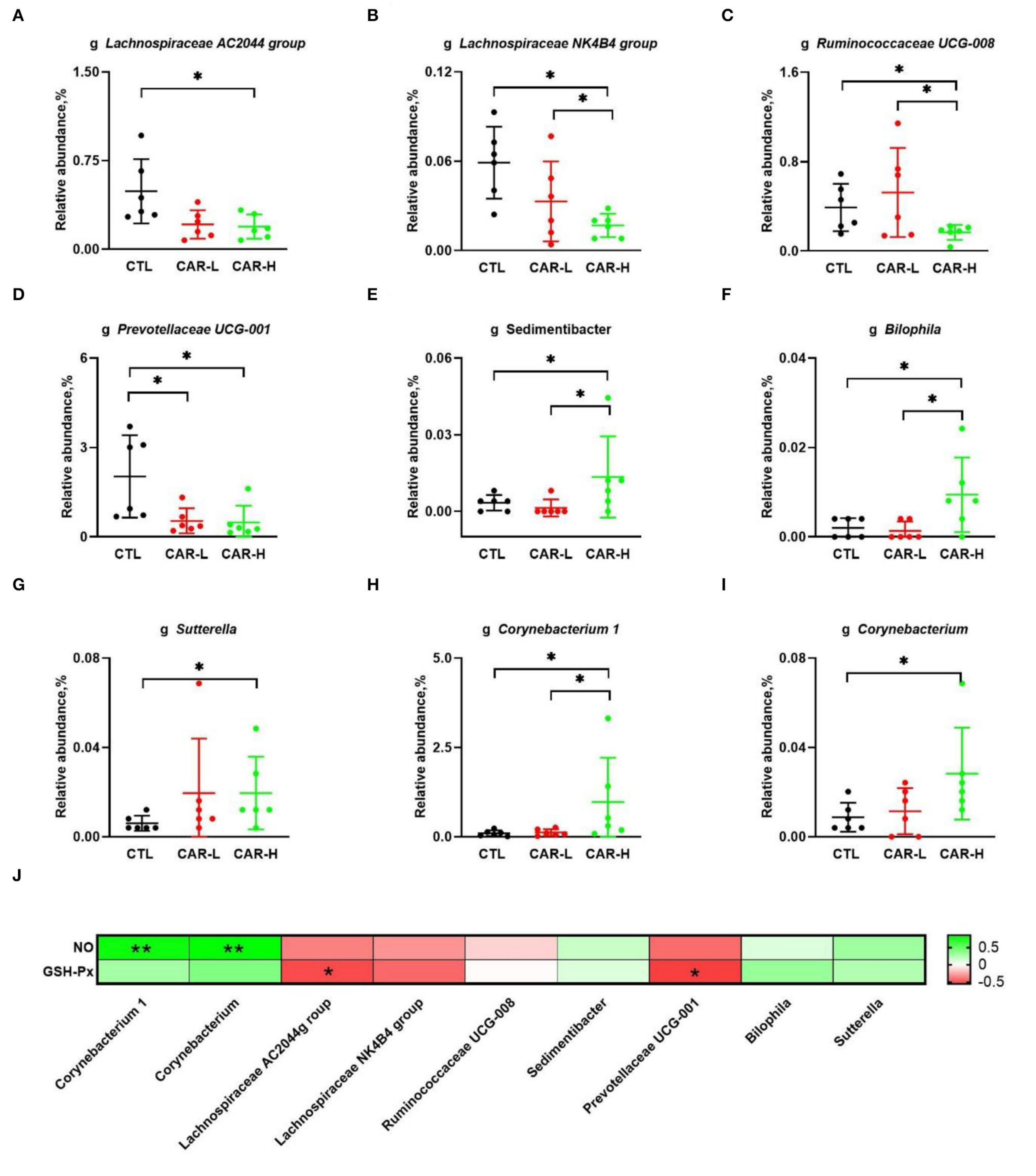

FIGURE 3 | Modulation of fecal microbiota by β-carotene at the genus level. The relative abundance of microbial genera including *Lachnospiraceae* AC2044 group **(A)**, *Lachnospiraceae* NK4B4 group **(B)**, *Ruminococcaceae* UCG-008 **(C)**, *Prevotellaceae UGC-001* **(D)**, *Sedimentibacter* **(E)**, *Bilophila* **(F)**, *Sutterella* **(G)**, *Corynebacterium* 1 **(H)**, and *Corynebacterium* **(I)** in each group were characterized by 16S rRNA gene sequencing, and the correlation between NO, GSH-Px and the changed gut microbiota **(J)** were analyzed by Spearman's correlation analysis. The intensity of the colors represent the degree of association (red, negative correlation; green, positive correlation). Significant correlations were marked by $^*P < 0.05$, $^{**}P < 0.01$. CTL, a basal diet; CAR-L, a basal diet containing 30 mg/kg β-carotene; CAR-H, a basal diet containing 90 mg/kg β-carotene. Data were shown as means ± SD ($n = 6$), $^*P < 0.05$.

of *Corynebacterium* is increased with reproductive performance (36). Therefore, β-carotene potentially enhanced NO production by up-regulating the relative abundance of *Corynebacterium*, although more direct evidences are need.

CONCLUSIONS

In conclusion, dietary supplementation of β-carotene showed limited effect on the reproductive performance of sows but increased the activity of GSH-Px and NO production. Analysis on fecal microbiota revealed that β-carotene may increase the diversity of the microbial flora with enriched *Bilophila*, *Sutterella*, *Sedimentibacter*, *Corynebacterium 1* and *Corynebacterium* which related to the synthesis of NO, an important vasodilator that can promote the neonatal blood circulation.

DATA AVAILABILITY STATEMENT

The raw data supporting the conclusions of this article will be made available by the authors, without undue reservation.

ETHICS STATEMENT

The animal study was reviewed and approved by Hunan Agricultural University Institutional Animal Care and Use Committee.

AUTHOR CONTRIBUTIONS

XY and JY were the primary investigator in this study. RH, YL, and YW participated in the animal experiments. HC participated in sample analysis. D-XH revised the manuscript. SW and JH designed this study and wrote the manuscript as corresponding author. The authors read and approved the final manuscript.

FUNDING

This work was partially supported by the funds from the National Natural Science Foundation of China (31772819 and 31972600), Hunan Provincial Natural Science Foundation for Distinguished Young Scholars (2019JJ30012), and Scientific Research Fund of Hunan Provincial Education Department (18B098).

ACKNOWLEDGMENTS

We thanked Dr. Muhammed Adebayo Arowolo for the language editing.

SUPPLEMENTARY MATERIAL

The Supplementary Material for this article can be found online at: https://www.frontiersin.org/articles/10.3389/fnut.2020.612875/full#supplementary-material

REFERENCES

1. von Lintig J. Colors with functions: elucidating the biochemical and molecular basis of carotenoid metabolism. *Annu Rev Nutr*. 30:35–56 doi: 10.1146/annurev-nutr-080508-141027
2. Bonet ML, Canas JA, Ribot J, Palou A. Carotenoids and their conversion products in the control of adipocyte function, adiposity and obesity. *Arch Biochem Biophys*. (2015) 572:112–25. doi: 10.1016/j.abb.2015.02.022
3. Grune T, Lietz G, Palou A, Ross AC, Stahl W, Tang GW, et al. Beta-carotene is an important vitamin a source for human. *J Nutr*. (2010) 140:2268–85. doi: 10.3945/jn.109.119024
4. Weber D, Grune T. The contribution of beta-carotene to vitamin A supply of humans. *Mol Nutr Food Res*. (2012) 56:251–8. doi: 10.1002/mnfr.201100230
5. Shapiro SS, Mott DJ, Machlin LJ. Kinetic characteristics of β-carotene uptake and depletion in rat tissue. *J Nutr*. (1984) 114:1924–33.
6. Paik J, Haenisch M, Muller CH, Goldstein AS, Arnold S, Isoherranen N, et al. Inhibition of retinoic acid biosynthesis by the bisdichloroacetyldiamine WIN 18,446 markedly suppresses spermatogenesis and alters retinoid metabolism in mice. *J Biol Chem*. (2014) 289:15104–17. doi: 10.1074/jbc.M113.540211
7. Kawashima C, Nagashima S, Sawada K, Schweigert FJ, Miyamoto A, Kida K. Effect of beta-carotene supply during close-up dry period on the onset of first postpartum luteal activity in dairy cows. *Reprod Domest Anim*. (2010) 45:282–7. doi: 10.1111/j.1439-0531.2009.01558.x
8. Talavera F, Chew BP. Comparative role of retinol, retinoic acid and beta-carotene on progesterone secretion by pig corpus luteum *in vitro*. *J Reprod Infertil*. (1988) 82:611–5. doi: 10.1530/jrf.0.0820611
9. Chew B, Rasmussen H, Pubols MH, Preston RL. Effects of vitamin and B-carotene on plasma progesterone and uterine secretions in gilts. *Theriogenology*. (1982) 18:643–54. doi: 10.1016/0093-691X(82)90030-9
10. Burton GJ. Oxygen, the Janus gas; its effects on human placental development and function. *J Anat*. (2009) 215:27–35. doi: 10.1111/j.1469-7580.2008.00978.x
11. Palm M, Axelsson O, Wernroth L, Larsson A, Basu S. Involvement of inflammation in normal pregnancy. *Acta Obstet Gynecol Scand*. (2013) 92:601–5. doi: 10.1111/aogs.12093
12. Chen ZH, Watanabe RM, Stram DO, Buchanan TA, Xiang AH. High calorie intake is associated with worsening insulin resistance and beta-cell function in hispanic women after gestational diabetes mellitus. *Diabetes Care*. (2014) 37:3294–300. doi: 10.2337/dc14-1433
13. Shao YR, Zhou J, Xiong X, Zou LJ, Kong XF, Tan B, et al. Differences in gut microbial and serum biochemical indices between sows with different productive capacities during perinatal period. *Front Microbiol*. (2020) 10:3047. doi: 10.3389/fmicb.2019.03047
14. Clarke SF, Murphy EF, O'Sullivan O, Lucey AJ, Humphreys M, Hogan A, et al. Exercise and associated dietary extremes impact on gut microbial diversity. *Gut*. (2014) 63:1913–20. doi: 10.1136/gutjnl-2013-306541
15. Zhou LH, Ouyang L, Lin SZ, Chen S, Liu YJ, Zhou W, et al. Protective role of beta-carotene against oxidative stress and neuroinflammation in a rat model of spinal cord injury. *Int Immunopharmacol*. (2018) 61:92–9. doi: 10.1016/j.intimp.2018.05.022
16. Lee S-J, Bai S-K, Lee K-S, Namkoong S, Na H-J, Ha K-S, et al. Astaxanthin inhibits nitric oxide production and inflammatory gene expression by suppressing I(kappa)B kinase-dependent NF-kappaB activation. *Molecules Cells*. (2003) 16:97–105.
17. Karamese SA, Toktay E, Unal D, Selli J, Karamese M, Malkoc I. The protective effects of beta-carotene against ischemia/reperfusion injury in rat ovarian tissue. *Acta Histochem*. (2015) 117:790–7. doi: 10.1016/j.acthis.2015.07.006
18. Hou D, Zhao Q, Yousaf L, Khan J, Xue Y, Shen Q. Consumption of mung bean (*Vigna radiata* L.) attenuates obesity, ameliorates lipid metabolic disorders and modifies the gut microbiota composition in mice fed a high-fat diet. *J Funct Foods*. (2020) 64:103687. doi: 10.1016/j.jff.2019.103687
19. Kanokratana P, Wongwilaiwalin S, Mhuantong W, Tangphatsornruang S, Eurwilaichitr L, Champreda V. Characterization of cellulolytic microbial

consortium enriched on Napier grass using metagenomic approaches. *J Biosci Bioeng*. (2018) 125:439–47. doi: 10.1016/j.jbiosc.2017.10.014
20. Krammer G, Aurich J. Effect of intramuscularly administered beta-carotene on reproductive performance in sows. *Berliner Munchener Tierarztl Wochenschr*. (2010) 123:496–9. doi: 10.2376/0005-9366-123-496
21. Lindemann MD, Brendemuhl JH, Chiba LI, Darroch CS, Dove CR, Estienne MJ, et al. A regional evaluation of injections of high levels of vitamin A on reproductive performance of sows. *J Anim Sci*. (2008) 86:333–8. doi: 10.2527/jas.2007-0153
22. Burton GJ, Jauniaux E, Charnock-Jones DS. The influence of the intrauterine environment on human placental development. *Int J Dev Biol*. (2010) 54:303–11. doi: 10.1387/ijdb.082764gb
23. Zhao Y, Flowers WL, Saraiva A, Yeum KJ, Kim SW. Effect of social ranks and gestation housing systems on oxidative stress status, reproductive performance, and immune status of sows. *J Anim Sci*. (2013) 91:5848–58. doi: 10.2527/jas.2013-6388
24. Tanghe S, Missotten J, Raes K, De Smet S. The effect of different concentrations of linseed oil or fish oil in the maternal diet on the fatty acid composition and oxidative status of sows and piglets. *J Anim Physiol Anim Nutr*. (2015) 99:938–49. doi: 10.1111/jpn.12243
25. Kim SW, Weaver AC, Shen YB, Zhao Y. Improving efficiency of sow productivity: nutrition and health. *J Anim Sci Biotechnol*. (2013) 4:26. doi: 10.1186/2049-1891-4-26
26. Shao XM, López-Valdés HE, Liang J, Feldman JL. Inhaled nicotine equivalent to cigarette smoking disrupts systemic and uterine hemodynamics and induces cardiac arrhythmia in pregnant rats. *Sci Rep*. (2017) 7:16974. doi: 10.1038/s41598-017-17301-5
27. Angelis D, Savani R, Chalak L. Nitric oxide and the brain. Part 1: mechanisms of regulation, transport and effects on the developing brain. *Pediatr Res*. (2020). doi: 10.1038/s41390-020-1017-0. [Epub ahead of print].
28. Tremaroli V, Backhed F. Functional interactions between the gut microbiota and host metabolism. *Nature*. (2012) 489:242–9. doi: 10.1038/nature11552
29. Ji YJ, Li H, Xie PF, Li ZH, Li HW, Yin YL, et al. Stages of pregnancy and weaning influence the gut microbiota diversity and function in sows. *J Appl Microbiol*. (2019) 127:867–79. doi: 10.1111/jam.14344
30. Koren O, Goodrich JK, Cullender TC, Spor A, Laitinen K, Backhed HK, et al. Host remodeling of the gut microbiome and metabolic changes during pregnancy. *Cell*. (2012) 150:470–80. doi: 10.1016/j.cell.2012.07.008
31. Chen R, Wu P, Cai Z, Fang Y, Zhou H, Lasanajak Y, et al. Puerariae Lobatae Radix with chuanxiong Rhizoma for treatment of cerebral ischemic stroke by remodeling gut microbiota to regulate the brain-gut barriers. *J Nutr Biochem*. (2019) 65:101–14. doi: 10.1016/j.jnutbio.2018.12.004
32. Hu R, Zeng F, Wu L, Wan X, Chen Y, Zhang J, et al. Fermented carrot juice attenuates type 2 diabetes by mediating gut microbiota in rats. *Food Funct*. (2019) 10:2935–46. doi: 10.1039/C9FO00475K
33. Hu RZ, He ZY, Liu M, Tan JJ, Zhang HF, Hou DX, et al. Dietary protocatechuic acid ameliorates inflammation and up-regulates intestinal tight junction proteins by modulating gut microbiota in LPS-challenged piglets. *J Anim Sci Biotechnol*. (2020) 11:12. doi: 10.1186/s40104-020-00492-9
34. Niu Q, Li P, Hao S, Kim SW, Du T, Hua J, et al. Characteristics of gut microbiota in sows and their relationship with apparent nutrient digestibility. *Int J Mol Sci*. (2019) 20:870. doi: 10.3390/ijms20040870
35. Rees DD, Cunha FQ, Assreuy J, Herman AG, Moncada S. Sequential induction of nitric oxide synthase by *Corynebacterium parvum* in different organs of the mouse. *Br J Pharmacol*. (1995) 114:689–93. doi: 10.1111/j.1476-5381.1995.tb17193.x
36. Elokil AA, Magdy M, Melak S, Ishfaq H, Bhuiyan A, Cui L, et al. Faecal microbiome sequences in relation to the egg-laying performance of hens using amplicon-based metagenomic association analysis. *Animal*. (2020) 14:706–15. doi: 10.1017/S1751731119002428

Conflict of Interest: XY was employed by Hunan Xinguang'an Agricultural Husbandry Co., Ltd., and the sows for experiment were provided by this company.

The remaining authors declare that the research was conducted in the absence of any commercial or financial relationships that could be construed as a potential conflict of interest.

frontiers in Nutrition

ORIGINAL RESEARCH
published: 24 February 2021
doi: 10.3389/fnut.2021.639467

Network and 16S rRNA Sequencing-Combined Approach Provides Insightal Evidence of Vitamin K_2 for Salt-Sensitive Hypertension

Tian-hao Liu[1†], Ming-hao Chen[2†], Wan-qing Tu[1†], Qiu-er Liang[1], Wen-cong Tao[1], Zhen Jin[1], Ya Xiao[1] and Li-guo Chen[1*]*

[1] College of Chinese medicine, Jinan University, Guangzhou, China, [2] College of medicine, Jinan University, Guangzhou, China

Edited by:
Yong Su,
Nanjing Agricultural University, China

Reviewed by:
Zhoujin Tan,
Hunan University of Chinese Medicine, China
Fang Xiang,
South China Agricultural University, China

***Correspondence:**
Ya Xiao
xiaoya0527@126.com
Li-guo Chen
tchenly@jnu.edu.cn

[†] These authors have contributed equally to this work

Specialty section:
This article was submitted to Nutrition and Microbes, a section of the journal Frontiers in Nutrition

Received: 09 December 2020
Accepted: 20 January 2021
Published: 24 February 2021

Citation:
Liu T-h, Chen M-h, Tu W-q, Liang Q-e, Tao W-c, Jin Z, Xiao Y and Chen L-g (2021) Network and 16S rRNA Sequencing-Combined Approach Provides Insightal Evidence of Vitamin K_2 for Salt-Sensitive Hypertension. Front. Nutr. 8:639467. doi: 10.3389/fnut.2021.639467

Vitamin K_2 (VK2), found to act to treat hypertension, has been widely used in the food and pharmaceutical industries nowadays. However, the potential targets and molecular mechanisms of VK2 for salt-sensitive hypertension have not been fully investigated. Therefore, the study aimed to investigate the potential molecular mechanisms of VK2 for salt-sensitive hypertension using network pharmacology and 16S rRNA sequencing strategy. The network pharmacology-based findings from KEGG enrichment analysis revealed that VK2-treated salt-sensitive hypertension was mechanically associated with the complement and coagulation cascades, calcium signaling pathway, renin–angiotensin system, etc. A total of 29 different bacteria in an animal experiment after VK2 supplementation were screened and functionally enriched using PICRUSt2. Additionally, 10 signaling pathways were identified in which the renin–angiotensin system was found to be the potential molecular mechanisms with the greatest change in multiple and statistical significance. Moreover, the results of the renin–angiotensin system-related protein expression exhibited VK2-inhibited renin–angiotensin system in salt-induced hypertensive mice, which significantly verified the previous biological and functional prediction analysis. Finally, spearman correlation analysis showed the different bacteria such as *Dubosiella*, *Ileibacterium*, etc., had a positive or negative correlation with renin–angiotensin system-related proteins in salt-induced mice. In conclusion, the potential molecular mechanisms of VK2 for salt-sensitive hypertension may be beneficially achieved by the specific inhibition of the renin–angiotensin system, contributing to the development for a new preventive strategy of salt-sensitive hypertension.

Keywords: network, gut bacteria, vitamin K_2, salt-sensitive hypertension, mice

INTRODUCTION

Salt-sensitive hypertension refers to low renin type hypertension caused by relatively high salt intake for a long time (1). High salt intake can increase blood pressure and cause damage to target organs such as the heart, brain, and kidneys, while its pathological mechanism is that high salt intake leads to genetic sodium transport disorder, leading to abnormal sodium excretion and tendencies of kidney sodium retention (2). It is found that high-salt diet has a great impact on people's health, and about a larger number of people die of cardiovascular diseases in the world every year due to excessive salt intake (1). Even salt-sensitive hypertension has a high prevalence and serious harm, which has caused huge economic burden to society, families, and individuals (1, 2). Therefore, it is of great significance to study the effective drugs for the treatment of salt-sensitive hypertension.

Recent studies have confirmed that salt intake in human body is related to gut bacteria, which in turn affects blood pressure (3, 4). As the most complex micro ecosystem of the human body, gut bacteria affect human health from many aspects, such as digestion, nutrition absorption, energy supply, fat metabolism, immune regulation, drug metabolism, and toxicity (5, 6). It was found that dietary sodium reduction increases circulating short-chain fatty acids, which are associated with decreased blood pressures, supporting that dietary sodium may influence the gut microbiome (4). In addition to its effect on blood pressure, salt can even act as an independent risk factor for target organ damage (3). Studies have shown that after 4 weeks of high-salt diet, the composition and function of fecal bacteria in mice were changed, resulting in imbalance in the proportion of regulatory T cells and pro-inflammatory helper T cells (Treg/Th17) (3).

Vitamin K_2 (VK2) is a fat-soluble vitamin, mainly produced by bacterial synthesis. Studies have shown that VK2 mainly acts on extrahepatic tissues such as bone, brain, blood vessels, pancreas, kidneys, and lungs to activate K-dependent proteins such as osteocalcin and matrix Gla protein. It has become a focus of research in recent years and has been widely used in the food and pharmaceutical industries. Bentley et al. (7) briefly illustrated VK2 biosynthesis pathway related to bacteria in 1971. Ponziani et al. (8) found that gut bacteria was the main source of VK2 in humans and small intestinal bacterial overgrowth (SIBO) was associated with altered VK2 metabolism. Moreover, a higher intake of vitamin K_2 produced by gut bacteria was associated with lower risk of coronary heart disease (CHD) (9). A meta-analysis showed that VK2 supplementation might prove to be of benefit as a long-term strategy to improve vascular health and reduce cardiovascular risk (9). In addition, Vissers et al. (10) found that a high intake of VK2 was significantly associated with a reduced risk of peripheral arterial disease, including hypertensive participants. It has been shown that the synergistic effect of VK2 and angiotensin-converting enzyme inhibitor (11, 12). All in all, it has been reported that VK2 is related to cardiovascular diseases, even hypertension. However, the molecular mechanism of its pharmacology has not been fully investigated.

Network pharmacology is based on the principle of system biology to explain the process of disease, and further use the holistic view of network structure to understand the mechanisms of drug and disease. In recent years, as a hot method, it has been widely used in the analysis of drug mechanism (13, 14). From the perspective of network pharmacology, the potential targets and mechanisms of VK2 on salt-sensitive hypertension were studied by using various database resources. Then the mice were supplemented with VK2 through animal experiment, the gut bacteria of mice was detected by 16S rRNA and functionally enriched using PICRUSt2. Finally, the common signaling pathway-related proteins in mice were detected to further verify the signaling pathways before the validation of clinical samples.

Abbreviations: ANOVA, one-way analysis of variance; CHD, coronary heart disease; VK2, Vitamin K_2; OTUs, operational taxonomic units.

METHODS

Screening Targets of Vitamin K_2-Treated Salt-Sensitive Hypertension

The structure file of VK2 was downloaded in the PubChem database (https://pubchem.ncbi.nlm.nih.gov, searched on June 22, 2020) by searching for the keyword as "vitamin K_2." The targets of VK2 were obtained by SwissTargetPrediction (http://www.swisstargetprediction.ch, searched on June 22, 2020) and DRAR-CPI (https://cpi.bio-x.cn/drar/, searched on June 22, 2020) using the structure file of VK2. Then the target library of VK2 was constructed using WPS Office software 2019. Salt-sensitive hypertension related therapeutic targets were obtained using the GeneCards database (https://www.genecards.org, searched on June 22, 2020) and Omim database (https://omim.org, searched on June 22, 2020). The "salt-sensitive hypertension" was used to act as searching keyword. Then, the names of target proteins were transformed into the corresponding gene symbols by the UniProt database (https://www.uniprot.org, searched on June 23, 2020).

Screening of Targets of Vitamin K_2-Treated Salt-Sensitive Hypertension and the Construction of the Interrelated Network

The common targets library between putative targets of VK2 and the known therapeutic targets on salt-sensitive hypertension were amalgamated. Then the PPI network was integrated and conducted using the String database (https://string-db.org) according to the common targets.

Analysis of Functional Processes and Molecular Pathways of Vitamin K_2-Treated Salt-Sensitive Hypertension

The KEGG pathway enrichment analysis of common targets was carried out using clusterProfiler package which was used as a software package for pathway enrichment analysis and visualization in the R language (version 3.6.1). The screening condition was set as $p < 0.001$.

Network Construction of Vitamin K_2-Targets-Pathways-Disease Network

The network construction of VK2-targets-pathways-disease network was conducted using Cytoscape_v3.7.1. The detailed methods were described in previous reports (13, 14).

Animals and Experimental Protocols

Eighteen 8-week-old male C57BL/6J mice were purchased from the experimental animal center of Guangzhou University of traditional Chinese medicine and raised in the animal center of Jinan University. All mice were naturally reared in a barrier environment with 12/12 h light cycle, 20–24°C and 40–60% humidity. This animal experiment was approved by the experimental animal ethics committee of Jinan University, which conforms to the principles of animal protection, animal welfare, and ethics, and the relevant provisions of national experimental animal welfare ethics. All mice were randomly divided into three groups: normal group (ND), high salt model group (HS), high salt diet plus VK2 supplementation group (HS_VK2), six mice per group. ND group was fed with a natural diet (containing 0.5% NaCl); HS group was fed with a high salt diet (containing 8% NaCl); HS_VK2 group was fed with high salt diet (containing 8% NaCl and additional 0.025% VK2) for 4 weeks. Finally, the mice were injected with 3% pentobarbital sodium to avoid suffering pain. After the necks were removed and sacrificed, the colon contents of the mice were quickly collected in sterile 1.5-ml EP tubes and stored at −80°C for testing.

Monitoring of Blood Pressure

The systolic blood pressure of all mice before and after the experiment was monitored by tail artery manometry and took the average value using the blood pressure analysis program (BP2000, USA) according to the operation instructions. The temperature of the mouse platform was set to 37°C in advance and test 15 times in each round.

Transmission Electronic Microscope Examination

The mouse aortic tissue was fixed in 2.5% glutaraldehyde at 4°C for 2–4 h under the condition of minimizing the mechanical injury such as traction, contusion, and extrusion. Then, the mouse aortic tissue was fixed and rinsed three times, 15 min each time, using 0.1 M phosphate buffer Pb (pH7.4). After dehydration and infiltration, the aortic tissue of mice was cut into 60–80 nm ultrathin sections. These sections were stained with uranium and lead (2% uranium acetate saturated alcohol solution, lead citrate, each staining for 15 min), and further observed under the TEM (HT7700; Hitachi; Tokyo, Japan), while three images were collected and analyzed from each group.

Microbial Analysis

DNA Extraction and PCR Amplification

Four mice were randomly selected from each group and DNA was extracted from fecal samples using the E.Z.N.A.® soil DNA Kit (Omega Bio-tek, Norcross, GA, U.S.) according to the manufacturer's protocols. The final DNA concentration and purification were determined by NanoDrop 2000 UV-vis spectrophotometer (Thermo Scientific, Wilmington, USA), and DNA quality was checked by 1% agarose gel electrophoresis. The V3–V4 hypervariable regions of the bacteria 16S rRNA gene were amplified with primers 338F (5′-ACTCCTACGGGAGGCAGCAG-3′) and 806R (5′-GGACTACHVGGGTWTCTAAT-3′) by thermocycler PCR system (GeneAmp 9700, ABI, USA). The resulted PCR products were extracted from a 2% agarose gel and further purified using the AxyPrep DNA Gel Extraction Kit (Axygen Biosciences, Union City, CA, USA) and quantified using QuantiFluor™-ST (Promega, USA) according to the manufacturer's protocol. The detailed methods were described in previous reports (14).

Illumina MiSeq Sequencing

Purified amplicons were pooled in equimolar and paired-end sequenced (2 × 300) on an Illumina MiSeq platform (Illumina, San Diego, USA) according to the standard protocols by Majorbio Bio-Pharm Technology Co., Ltd. (Shanghai, China).

Processing of Sequencing Data

Operational taxonomic units (OTUs) were clustered with 97% similarity using UPARSE (version 7.1 http://drive5.com/uparse/) and each 16S rRNA gene sequence was analyzed using a confidence threshold of 70% in RDP Classifier algorithm (http://rdp.cme.msu.edu/) against the Silva (SSU123) 16S rRNA database. PICRUSt2 was used to predict microbial functions according to the normalized OTU tables (15).

Measurements of Renin–Angiotensin System-Related Protein Expression by Western Blotting

Three mice were randomly selected from each group and the proteins in their aortic tissues were detected through Western blotting. Ren antibody (abcam, ab212197), ACE (abcam, ab254222), AT1R (abcam, ab124734), and AT2R (abcam, ab227851) antibodies were used in the current study. According to the kit instructions, the total proteins were obtained by conventional tissue. Thus, PAGE separation was conducted after equivalent sampling. PAGE separins used 10% separating and 5% stacking gel. All proteins separated by PAGE were transferred to PVDF membranes with primary and secondary antibodies added. Moreover, the proteins were exposed, developed, and fixed. GAPDH was used as an internal control. Quantity One 4.0 software was used to analyze the imaging map and the ratios of Ren, ACE, AT1R, and AT2R proteins in each group were calculated.

Statistical Analysis

Statistical analysis on the gut microbiota was performed using R package (MathSoft, Inc., United States). All other data are presented as mean ± standard error of mean (SEM). Statistical analysis was performed using Student *t*-test or one-way analysis of variance (ANOVA) through GraphPad Prism 5 (San Diego, CA, USA). $p < 0.05$ was considered as statistically significant.

RESULTS

Screening Target Information and PPI Network of Vitamin K_2 on Salt-Sensitive Hypertension

The molecular formula of VK2 was $C_{31}H_{40}O_2$, and the molecule structure was shown as **Figure 1A**. A total of 195 reported pharmacological targets related to VK2 were obtained from the databases (**Supplementary Table 1**). A total of 493 salt-sensitive hypertension related targets were obtained from the databases (**Supplementary Table 2**). Combining the common targets of

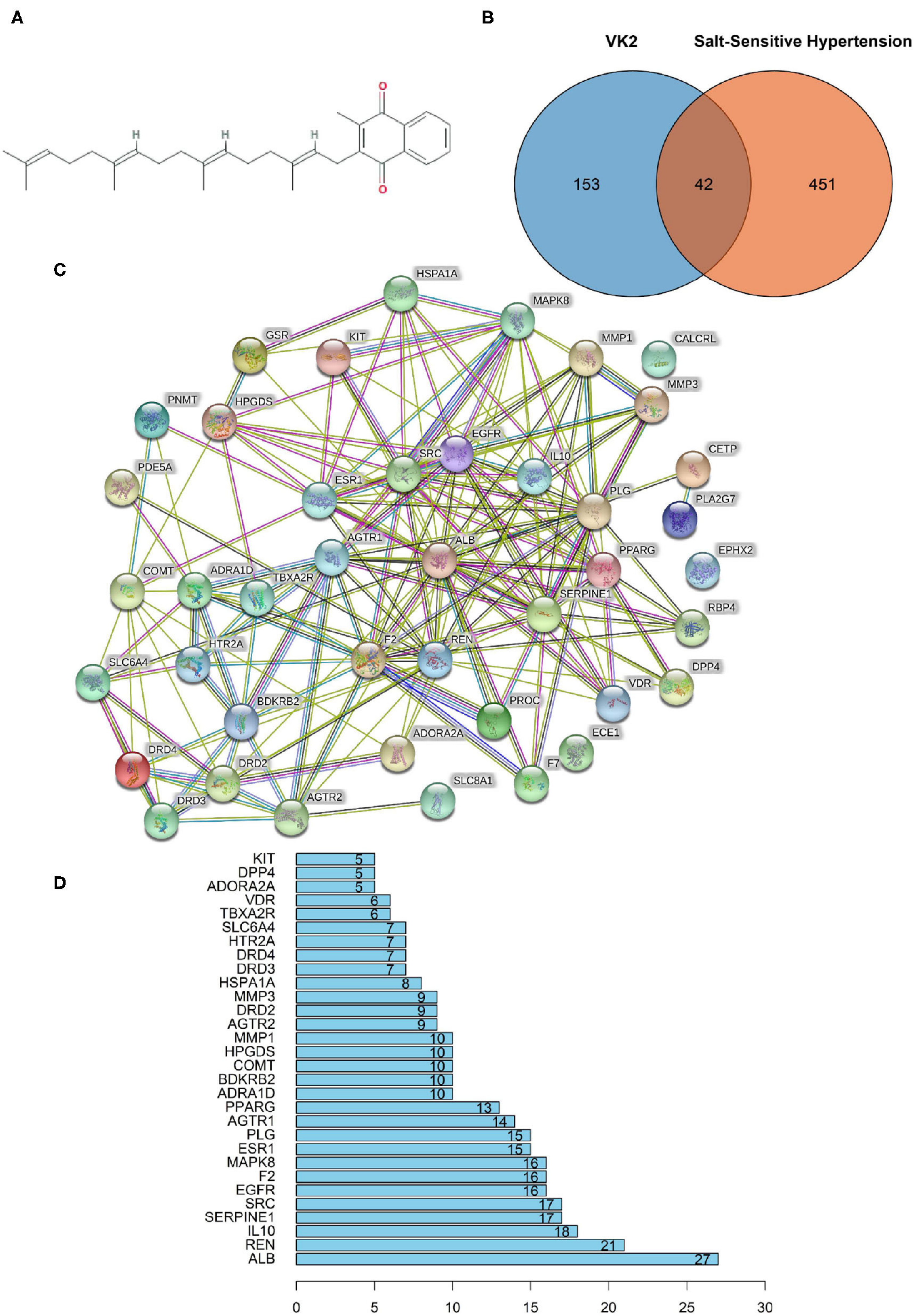

FIGURE 1 | Network pharmacology revealed the target characteristics of Vitamin K_2 (VK2) for salt-sensitive hypertension. **(A)** Molecule formula of VK2. **(B)** Venn diagram of common targets of VK2 for salt-sensitive hypertension. **(C)** The protein-protein interaction (PPI) network based on targets of VK2 for salt-sensitive hypertension. Nodes represent different proteins. Edges represent protein-protein associations, the line thickness indicates the strength of data support. **(D)** The top 10 core genes of VK2 for salt-sensitive hypertension.

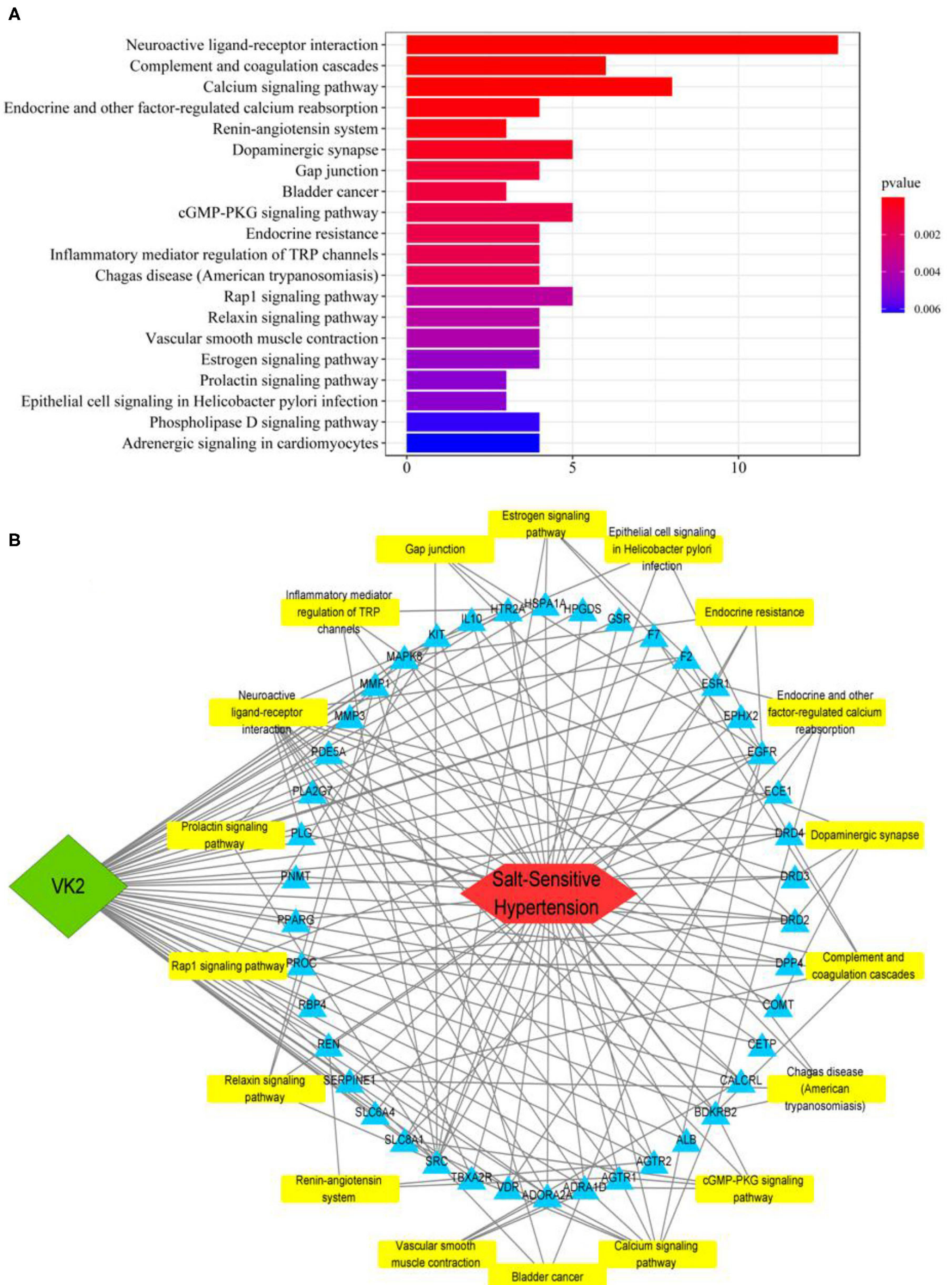

FIGURE 2 | KEGG pathway enrichment of core targets and construction of an integrative network. **(A)** The bar diagram of KEGG pathway enrichment. **(B)** The integrative network of VK2 for salt-sensitive hypertension through the network pharmacology-based findings.

VK2 and salt-sensitive hypertension, 42 targets were screened to be the targets of VK2-treated salt-sensitive hypertension (**Figure 1B**; **Supplementary Table 3**). The function-related PPI network was conducted using the STRING database and shown in **Figure 1C**. The network containing 42 nodes and 185 edges, had significantly more interactions ($p < 1.0 \times e^{-16}$). Additionally, the top 10 core genes were screened as ALB, REN, IL10, SERPINE1, SRC, EGFR, F2, MAPK8, ESR1, and PLG (**Figure 1D**; **Supplementary Table 4**).

KEGG Pathway Enrichment of Core Targets and Construction of an Integrative Network

The KEGG pathway enrichment involved in predicted targets is systematically elucidated based on the KEGG pathway database. In the current study, KEGG pathway enrichment was performed according to the common 42 genes, and the top 20 enrichment data were plotted as a bar diagram (**Figure 2A**; **Supplementary Table 5**). The KEGG pathway enrichment mainly involved in neuroactive ligand-receptor interaction, complement and coagulation cascades, calcium signaling pathway, endocrine, and other factor-regulated calcium reabsorption, and renin–angiotensin system, etc. The integrative network of VK2 for salt-sensitive hypertension through the network pharmacology-based findings was conducted and shown in **Figure 2B**.

Vitamin K_2 Supplementation Protected Blood Pressure and Aortic Vessels in High Salt-Induced Mice

Vascular endothelial cells maintain the normal flow of blood and act as a barrier between blood and tissue fluid, whose injury is related to the occurrence of hypertension (16, 17).

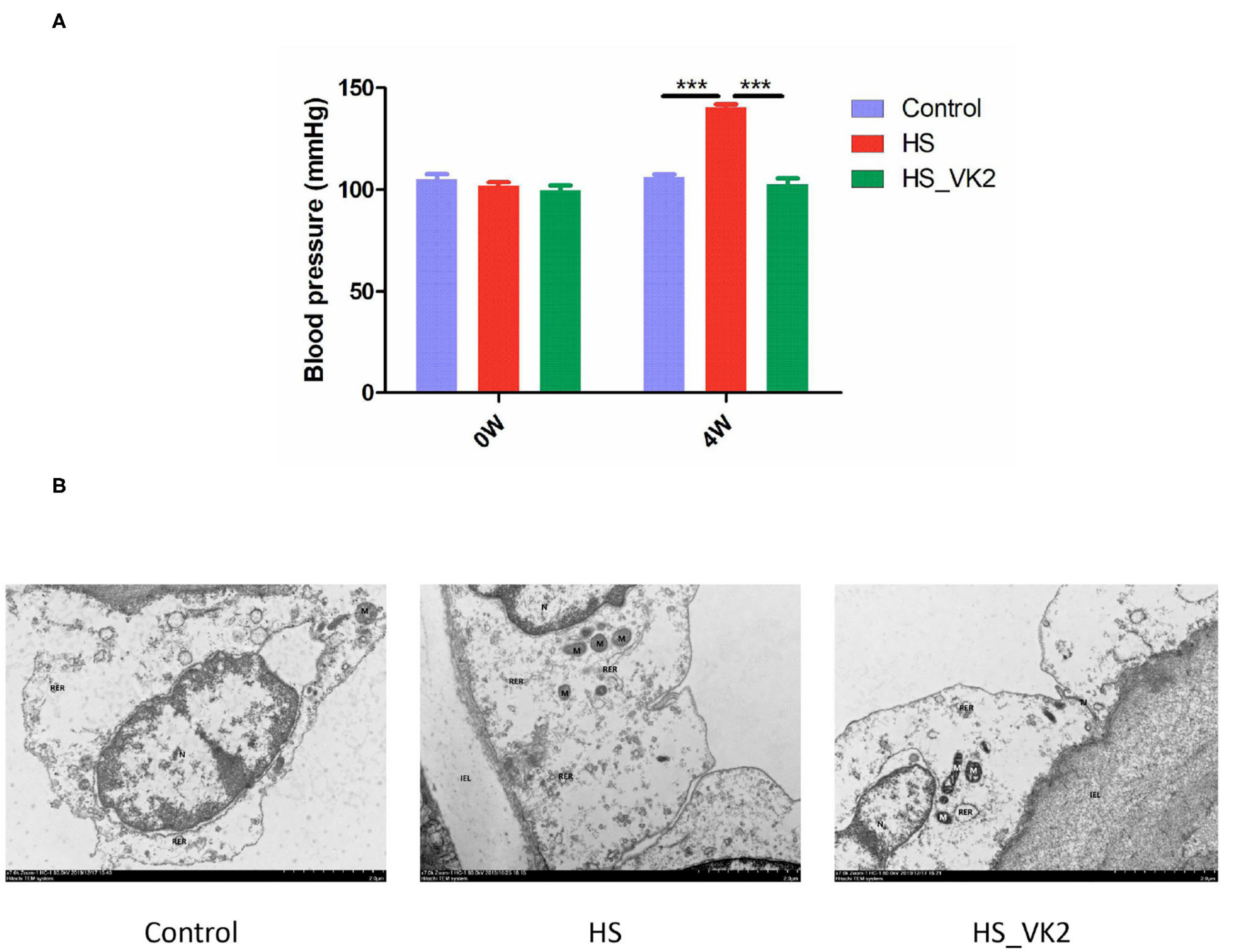

FIGURE 3 | VK2 supplementation protected blood pressure and aortic vessels in salt-induced mice. **(A)** Blood pressure (mmHg). **(B)** The ultrastructural changes of aortic vessels observed by Transmission Electronic Microscope (TEM). Internal elastic lamina (IEL), nucleus (N), mitochondrion (M), rough endoplasmic reticulum (RER), tight junction (TJ), autophagy (AP). Data are presented as mean ± standard error of mean (SEM). ***$p < 0.001$, $n = 6$; statistical comparisons were performed using Student t-test or one-way analysis of variance (ANOVA).

Therefore, the blood pressure and the ultrastructural changes of aortic vessels were observed in animal experiment. The results of animal experiment showed that significantly increased blood pressure was found in the HS group compared with the control group, whereas a significantly decreased blood pressure was found after VK2 supplementation compared with the HS group (**Figure 3A**). Moreover, the results of ultrastructural changes of aortic vessels are shown in **Figure 3B**. Compared with the control group, the vascular endothelial cells showed obvious edema, the intracellular matrix became lighter, the electron density of large area decreased, the internal elastic membrane appeared obvious local fracture; the nucleus showed irregular shape, local depression, heterochromatin edge set; the number of mitochondria decreased, swelling, mitochondrial cristae became shorter, and disappeared; and the rough endoplasmic reticulum showed obvious expansion and degranulation (**Figure 3B**). After VK2 supplementation, the results showed that the edema of vascular endothelial cells was alleviated; the electron density of intracellular matrix was low and the transparency was reduced; the internal elastic membrane was not obviously broken; the damage of cell structure such as nucleus, mitochondria, and rough endoplasmic reticulum was alleviated (**Figure 3B**).

General Bacterial Structural Characteristics After Vitamin K_2 Supplementation in High Salt-Induced Mice

In order to further verify the potential mechanism of VK2 resistance to salt-sensitive hypertension, we supplemented VK2 to intervene in high-salt induced mice, and detected the characteristics of gut bacteria by 16S rRNA analysis (**Figure 4A**) The results showed that there were 690 total OTUs in the control group, 771 total OTUs in the HS group, 663 total OTUs in VK2_HS group, and 530 common OTUs in the three groups (**Figure 4B**). Among them, there were 585 common OTUs in the control group and HS group, 59 personalized OTUs in the control group and 138 personalized OTUs in the HS group, which indicated that OTUs of high salt diet were higher than those of normal diet. There were 667 common OTUs in the HS group and VK2_ HS group, 39 personalized OTUs in the VK2_HS group, 139 personalized OTUs in the HS group, which indicated that VK2 supplementation reduced OTUs in the gut bacteria of mice fed with high salt diet.

Furthermore, phyla level results showed that the proportions of dominant phyla Firmicutes, Bacteroidetes, and Proteobacteria in the control group were 41.26, 40.06, and 5.823%, whereas 43.32, 36, and 4.899% were in the HS group, and 49.99, 34.89, and 4.665% were in the VK2-HS group, respectively, (**Figure 4C**; **Supplementary Table 6**). In addition, 20 dominant genera were found in bacteria (**Figure 4D**; **Supplementary Table 7**). For instance, the relative abundances of *norank_f__Muribaculaceae*, *Lactobacillus*, *Lachnospiraceae_NK4A136_group*, *Helicobacter* in the control group were 34.49, 11, 10.54%, and 6.87; 29.07, 15.60, 5.83, and 5.24% were in the HS group; and 27.29, 2.17, 12.16, and 2.33% were in the VK2_HS group. All these findings revealed that there were differences in bacterial composition and structure after VK2 supplementation.

Screening of Different Bacteria After Vitamin K_2 Supplementation in High Salt-Induced Mice

Similarities of the bacterial composition and structure after VK2 supplementation among groups were compared using ANOSIM and PLS-DA based on Bray–Curtiss (18). The results distance box plot showed that there were significant differences in the bacterial composition and structure (**Figure 5A**; $r = 0.2639$; $p = 0.025$) among different groups. Moreover, there was an obvious tendency for separating the bacterial profiles on genus level after VK2 supplementation (**Figure 5B**), and a great difference in the individual samples was found in the HS group, but little difference in the individual samples after VK2 supplementation (**Figure 5B**), which promulgated a positive action on genera after VK2 supplementation. Additionally, a total of 29 different bacteria after VK2 supplementation were screened among the three groups (**Figure 5C**; **Supplementary Table 8**).

Verification of Functional Prediction Based on the Different Bacteria in High Salt-Induced Mice

To identify signaling pathways found through the previous network of VK2-treated salt-sensitive hypertension, functional analysis was performed using PICRUSt2 after VK2 supplementation. A total of 10 common signaling pathways were enriched and identified. As shown in **Figure 5A**, compared with the control group, decreased relative abundance was found in the signaling pathways in epithelial cell signaling in *Helicobacter pylori* infection, estrogen signaling pathway, and prolactin signaling pathway in the HS group; increased relative abundance was found in the renin–angiotensin system, cGMP-PKG signaling pathway, dopaminergic synapse, endocrine, and other factor-regulated calcium reabsorption, inflammatory mediator regulation of TRP channels, vascular smooth muscle contraction, and calcium signaling pathway in the HS group. Increased relative abundance was found in the signaling pathways in epithelial cell signaling in *Helicobacter pylori* infection, estrogen signaling pathway, and prolactin signaling pathway after VK2 supplementation; decreased relative abundance was found in the renin–angiotensin system, cGMP-PKG signaling pathway, dopaminergic synapse, endocrine, and other factor-regulated calcium reabsorption, inflammatory mediator regulation of TRP channels, vascular smooth muscle contraction, and calcium signaling pathway after VK2 supplementation (**Figure 6A**). Moreover, there was a greatest change multiple and statistical significance of the relative abundance in renin-angiotensin system ($p < 0.05$). Also, the mapper of the renin–angiotensin system is shown in **Figure 6B** combined with the findings in the previous network of VK2-treated salt-sensitive hypertension. All these results further revealed the fact that renin-angiotensin system was the potential mechanisms of VK2-treated salt-sensitive hypertension.

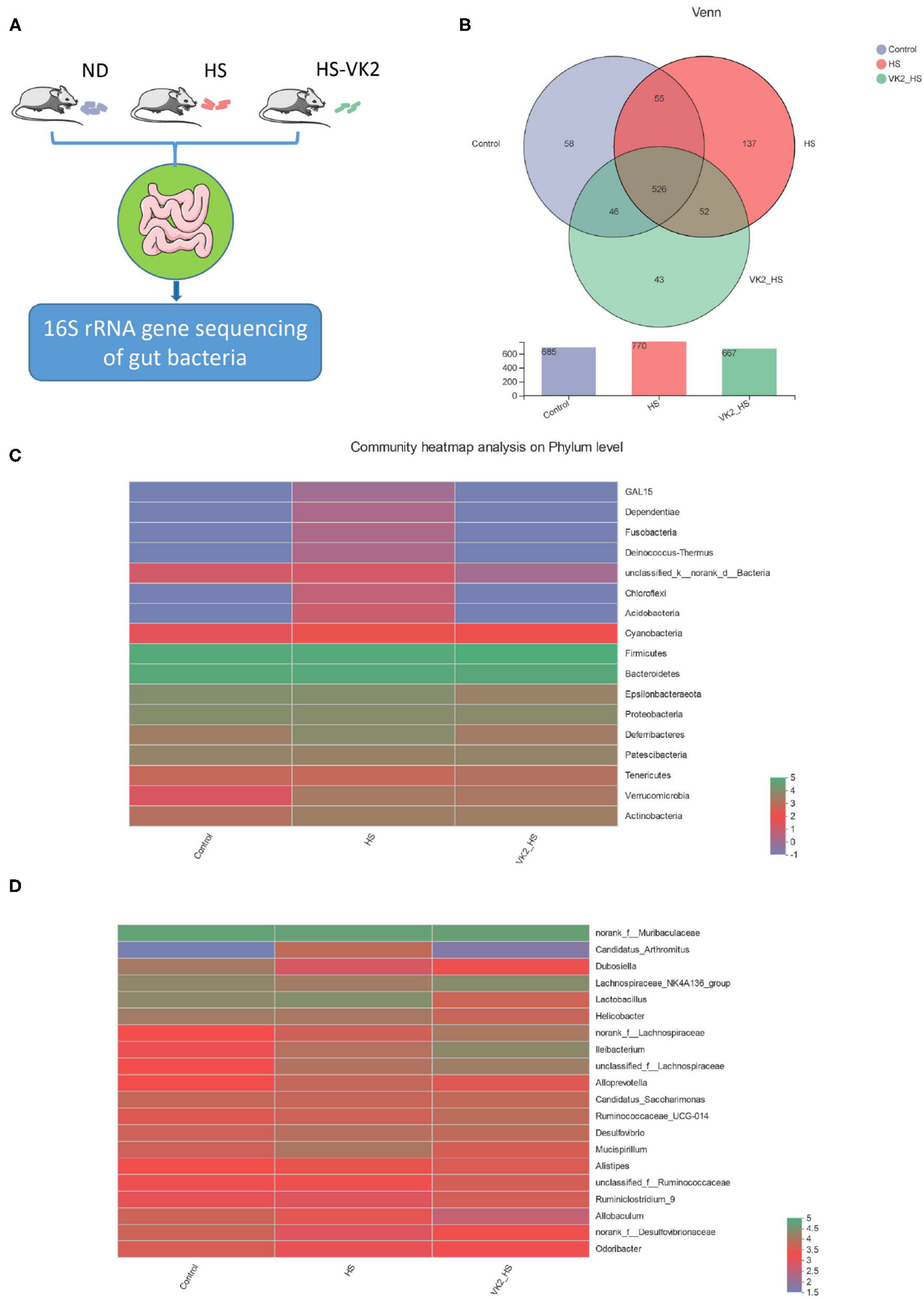

FIGURE 4 | General bacterial structural characteristics after VK2 supplementation ($n = 4$). **(A)** The process of animal experimental verification. **(B)** The operational taxonomic units (OTUs) changes after VK2 supplementation. **(C)** Community heatmap analysis on phylum level after VK2 supplementation. **(D)** Community heatmap analysis on genus level after VK2 supplementation. Color represents relative abundance.

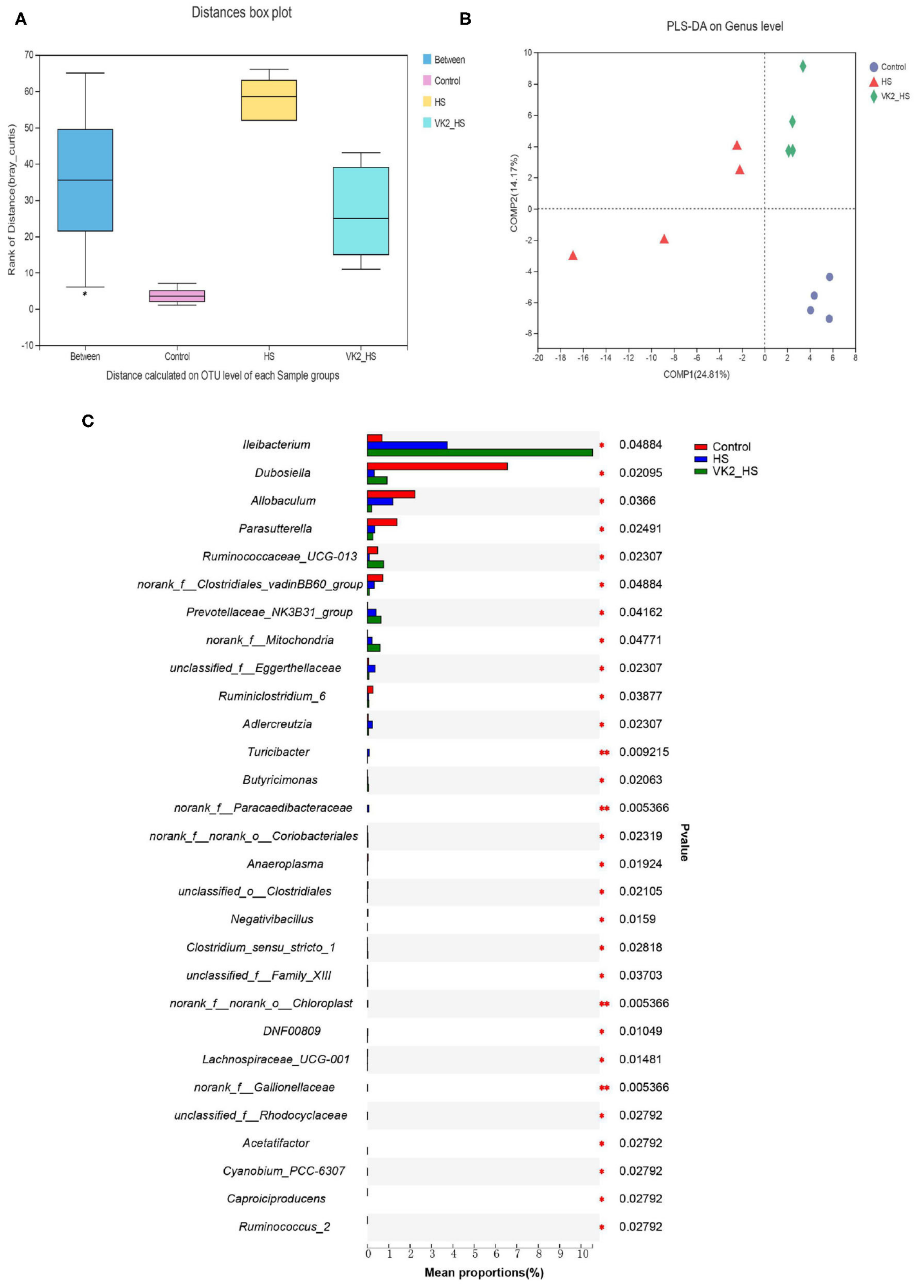

FIGURE 5 | Screening of different bacteria after VK2 supplementation. **(A)** Distance calculated on OTU level. **(B)** PLS-DA. **(C)** Differential bacteria on genus level. $^{*}p < 0.05$ and $^{**}p < 0.01$, $n = 4$. Statistical comparisons were performed using one-way analysis of variance (ANOVA).

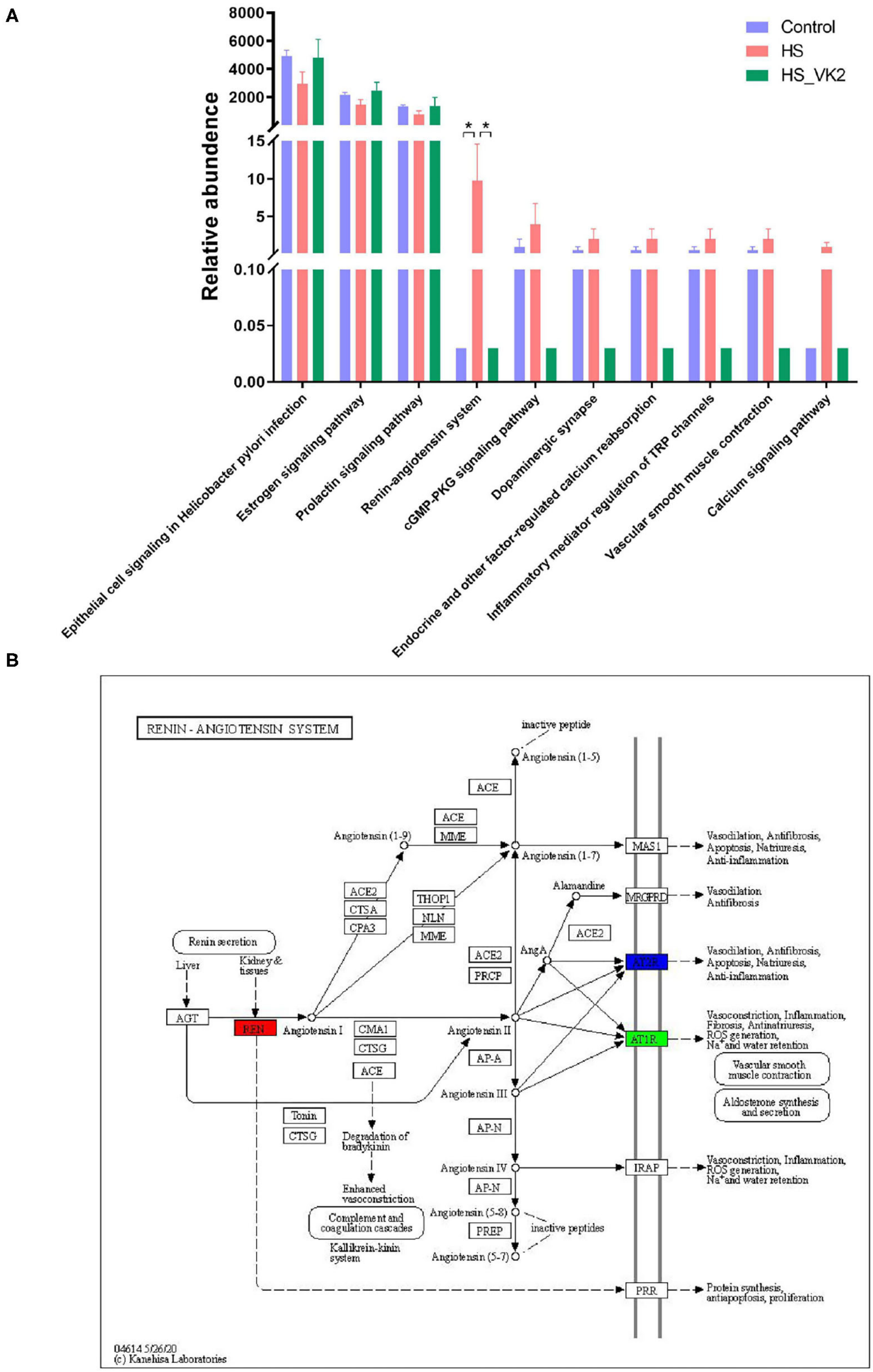

FIGURE 6 | Verification of functional prediction based on the different bacteria. **(A)** Functional enrichment of PICRUSt2 based on the different bacteria. Data are presented as mean ± standard error of mean (SEM); $^*p < 0.05$, $n = 4$; statistical comparisons were performed using Student t-test or one-way analysis of variance (ANOVA). **(B)** The mapper of Renin-angiotensin system.

Vitamin K_2 Supplementation Inhibited Renin–Angiotensin System-Related Protein Expression in High Salt-Induced Mice

To further verify the effect of VK2 on the renin–angiotensin system, the renin–angiotensin system-related proteins expression (including REN, ACE, AT1R, and AT2R) in salt-induced mice were conducted. Significantly increased REN, ACE, AT1R, and AT2R proteins expression were found in the HS group compared with the control group. Moreover, significantly decreased REN, ACE, AT1R, and AT2R proteins expression were found after VK2 supplementation (**Figures 7A–E**). Obviously, the changes in the renin–angiotensin system-related proteins expression exhibited VK2 inhibited renin-angiotensin system-related proteins expression in salt-induced hypertensive mice, which was statistically significantly consistent with the previous biological and functional prediction analysis.

Microbial Correlation

To reveal the relationship between differential bacteria and functional proteins in renin-angiotensin system-related proteins, Spearman correlation analysis of the renin–angiotensin system-related proteins and gut microbiota were performed. The results of spearman correlation analysis indicated that the 20 different bacteria such as *Dubosiella*, *Ileibacterium*, etc., had a positive or negative correlation with REN, ACE, AT1R, and AT2R in salt-induced mice (**Figure 8**).

DISCUSSION

Salt-sensitive hypertension is an important type of essential hypertension, which is a response to high salt intake. Modern studies have suggested that gut bacteria act as a participant and a target role for treatment in salt-sensitive hypertension (3, 4). Human studies have confirmed that VK2 is related to the prevention and treatment of cardiovascular diseases, and has revealed its curative effect on hypertension (9, 10, 19). However, these results lack more scientific evidence and molecular mechanisms. Therefore, this study focused on the molecular mechanisms of VK2 in the treatment of salt-sensitive hypertension, combined with network pharmacology and 16S rRNA sequencing strategy. In the current study, a total of 42 predictive targets of VK2-treated salt-sensitive hypertension were screened and identified accordingly. Moreover, the top 10 core genes of VK2 treated-salt-sensitive hypertension were screened as ALB, REN, IL10, SERPINE1, SRC, EGFR, F2, MAPK8, ESR1, and PLG. The network pharmacology-based findings from KEGG enrichment analysis revealed that VK2 treated salt-sensitive hypertension were mechanically associated with the neuroactive ligand-receptor interaction, complement and coagulation cascades, calcium signaling pathway, endocrine and other factor-regulated calcium reabsorption and renin-angiotensin system, etc. Additionally, a total of 29 different bacteria in animal experiment after VK2 supplementation were screened and functionally enriched using PICRUSt2. Ten common signaling pathways were identified in which the renin-angiotensin system was found to be the potential molecular mechanisms with the greatest change multiple and statistical significance. Finally, the renin-angiotensin system-related proteins expression exhibited that VK2 inhibited renin-angiotensin system in salt-induced mice, which was statistically, significantly consistent with the previous biological and functional prediction analysis.

On the basis of understanding the interaction network of "drug-target-disease," the intervention and influence of drugs on the complex pathological network were observed through network analysis, and the interaction relationship between each node of the network was observed intuitively and clearly by using large-scale data integration, which provided a new platform for the mechanism target research of complex diseases (13, 14). The results of network pharmacology research showed that the core targets of VK2 in the treatment of salt-sensitive hypertension included as ALB, REN, IL10, SERPINE1, SRC, EGFR, F2, MAPK8, ESR1, and PLG. The findings of KEGG function enrichment showed that VK2-treated salt-sensitive hypertension was mechanically associated with the neuroactive ligand–receptor interaction, complement and coagulation cascades, calcium signaling pathway, endocrine, and other factor-regulated calcium reabsorption, renin–angiotensin system, etc. Therefore, the network pharmacology-based findings showed the potential molecular mechanisms of VK2-treated salt-sensitive hypertension.

Gut bacteria play an important role in the digestion and absorption of nutrients in food and are considered as therapeutic targets of many diseases and drugs (30, 31). It has become a hot research method in modern pharmacology to study the molecular mechanisms of drug treating diseases by focusing on gut bacteria (20, 21). In order to further verify the potential mechanisms of VK2 for salt-sensitive hypertension, we supplemented VK2 to intervene high-salt induced mice, and detected the characteristics of gut bacteria by 16S rRNA analysis. Some studies have shown that high-salt diet (8% NaCl) for 4 weeks can cause hypertension in mice (22, 23). The results of animal experiment showed that VK2 supplementation protected blood pressure and aortic vessels in salt-induced mice. Meanwhile, the results of the animal experiment showed VK2 supplementation reduced OTUs in gut bacteria of mice fed with a high-salt diet. The results revealed that there were differences in bacterial composition and structure after VK2 supplementation. Moreover, a total of 29 different bacteria were screened after VK2 supplementation including *Ileibacterium*, *Dubosiella*, *Allobaculum*, *Parasutterella*, *Ruminococcaceae_UCG-013*, etc. To identify signaling pathways found through the previous network of VK2-treated salt-sensitive hypertension, functional analysis was performed using PICRUSt2 after VK2 supplementation. The results showed that the signaling pathways of epithelial cell signaling in *Helicobacter pylori* infection, estrogen signaling pathway, and prolactin signaling pathway, renin–angiotensin system, cGMP-PKG signaling pathway, dopaminergic synapse, endocrine, and other factor-regulated calcium reabsorption, inflammatory mediator regulation of TRP channels, vascular smooth muscle contraction, and calcium signaling pathway were also found in the animal experiment after VK2 supplementation. Meanwhile, the greatest change multiple and

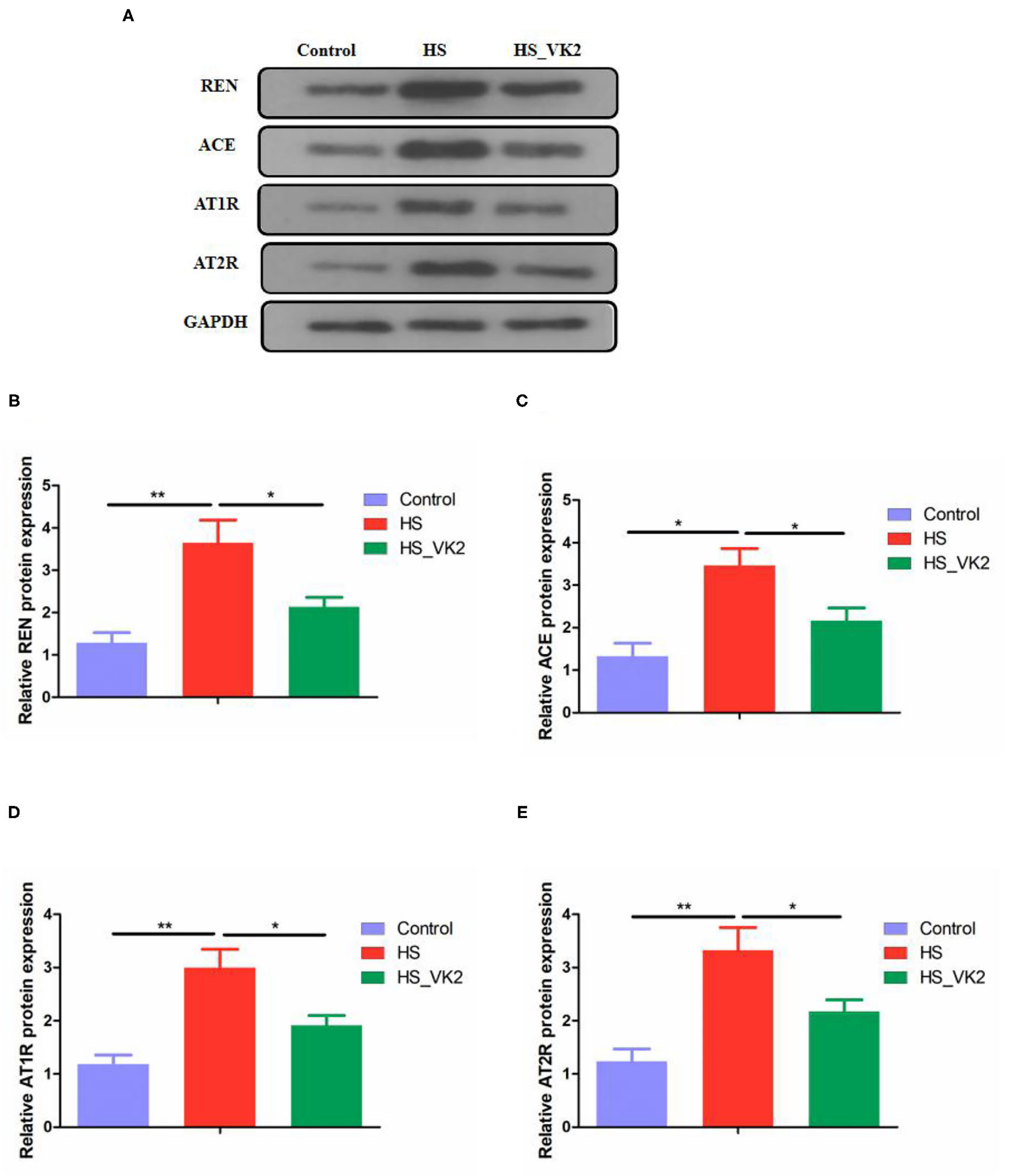

FIGURE 7 | VK2 inhibited renin-angiotensin system-related proteins expression in high salt-induced mice **(A–E)**. Data are presented as mean ± standard error of mean (SEM); $^*p < 0.05$ and $^{**}p < 0.01$, $n = 3$; statistical comparisons were performed using Student t-test or one-way analysis of variance (ANOVA).

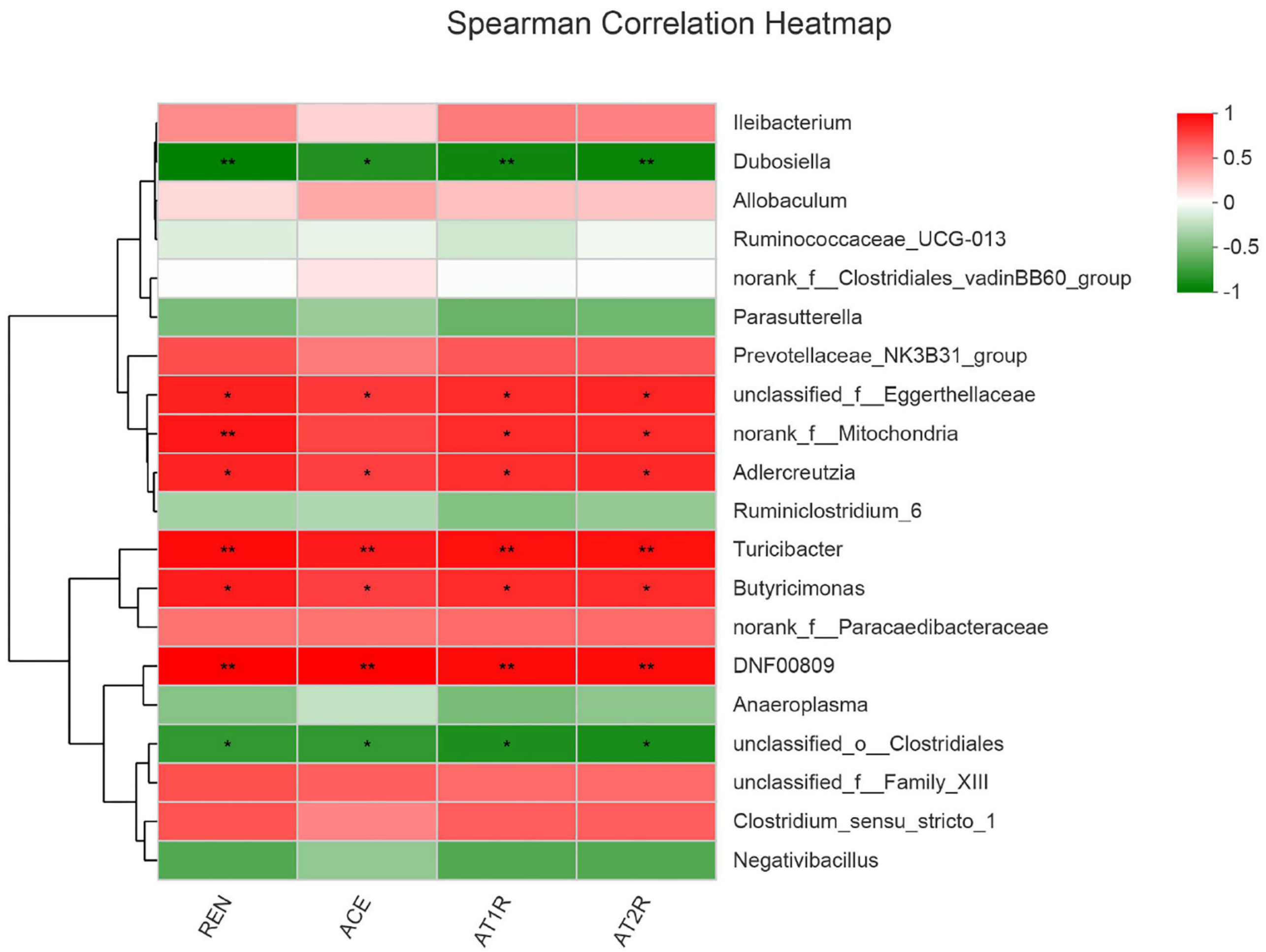

FIGURE 8 | Microbial correlation with renin-angiotensin system-related proteins. Red represents positive correlation, whereas blue represents negative correlation; the darker the color, the stronger the correlation. $0.01 < {}^{*}p \leq 0.05$, $0.001 < {}^{**}p \leq 0.01$.

statistical significance, which verified that the renin–angiotensin system was the potential mechanism of VK2 for salt-sensitive hypertension was found in the relative abundance of the renin–angiotensin system.

The renin–angiotensin system is considered as a peptidergic system with endocrine characteristics, with regard to the regulation of the blood pressure and hydro-electrolytic balance (24, 25). In the classical renin–angiotensin system, the renin cleaves its substrate angiotensinogen (Agt) forming the decapeptide angiotensin I (Ang I) that is in turn cleaved by the angiotensin-converting enzyme (ACE) to produce the angiotensin II (Ang II), which can affect the AT1R and AT2R, key players of this system (24, 25). In fact, it has been revealed that there are associations between insufficiency of fat-soluble vitamins and cardiovascular diseases (26). For example, long-term lack of vitamin D can lead to overactivation of the renin–angiotensin system, which is one of the mechanisms of blood pressure regulation (27, 28). In order to reveal the relationship between differential bacteria and functional proteins in the renin–angiotensin system-related proteins (including REN, ACE, AT1R, and AT2R), Spearman correlation analysis were conducted. The different bacteria, such as *Dubosiella*, *Ileibacterium*, etc., had a positive or negative correlation with REN, ACE, AT1R, and AT2R in salt-induced mice. It was showed that *Dubosiella* may have a role in inhibiting renin–angiotensin system including proteins (including REN, ACE, AT1R, and AT2R), whereas *Ileibacterium* may have a positive role. *Dubosiella newyorkensis* (belonging to genus *Dubosiella*), is related to many disease such as obesity, diabetes, abnormal lipid metabolism, etc., which was even used as a patented probiotic for many diseases (29). However, there are no other differential bacteria and diseases reported. The positive or negative correlation between the differential bacteria and functional proteins in renin–angiotensin system-related proteins (including REN, ACE, AT1R, and AT2R) reveal that the gut microbiota play an essential role in regulating blood pressure and the potential molecular mechanisms. These evidences show the relationship between differential bacteria and functional proteins, providing new research fields.

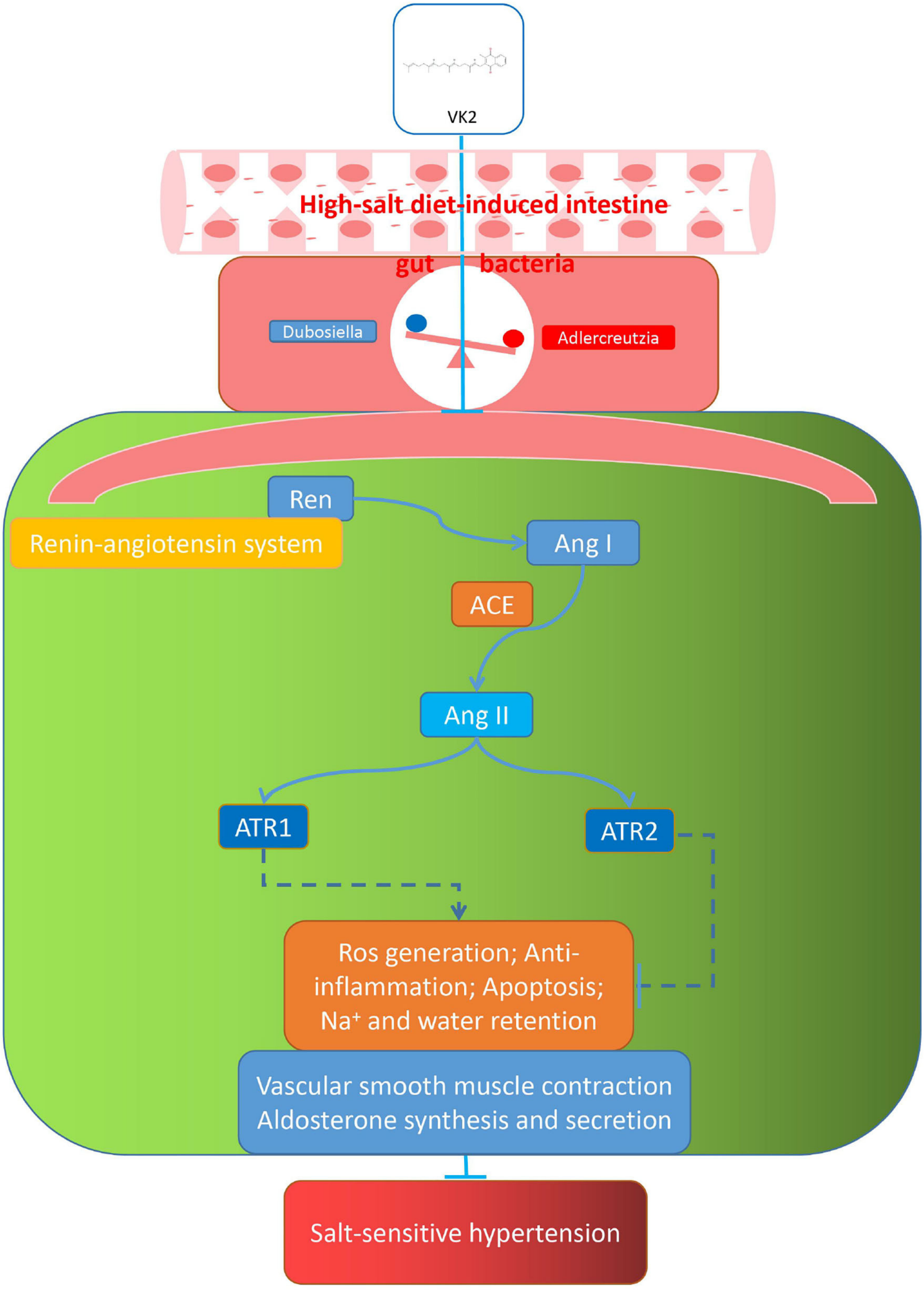

FIGURE 9 | Representative cartoon with the possible mechanisms of VK2 for salt-sensitive hypertension.

The current study showed VK2-treated salt-sensitive hypertension by the specific inhibiting the renin–angiotensin system. Additionally, the renin–angiotensin system-related protein expression (including REN, ACE, AT1R, and AT2R) exhibited that VK2 inhibited the renin–angiotensin system-related protein expression in salt-induced hypertensive mice, which significantly verified the previous biological and functional prediction analysis. Accordingly, the representative cartoon with the potential mechanisms of VK2 for salt-sensitive hypertension is shown in **Figure 9**. However, such an integrated pharmacology and gut bacteria-based analysis further explored the potential mechanismic role of VK2 for salt-sensitive hypertension. More studies using clinical samples still need to be better investigated in the future. Obviously, the current study contributes to the development for a new preventive strategy of salt-sensitive hypertension as far as it is concerned.

CONCLUSION

In the current bioinformatics and animal experiment verification used network and 16S rRNA sequencing-combined approach, the potential molecular mechanisms of VK2 related to salt-sensitive hypertension may be beneficially achieved by the specific inhibition of the renin–angiotensin system, contributing to provide the scientific evidence for the effective treatment of salt-sensitive hypertension.

DATA AVAILABILITY STATEMENT

The data presented in the study are deposited in the (NCBI SRA) repository, accession number (PRJNA690768).

ETHICS STATEMENT

The animal study was reviewed and approved by the experimental animal ethics committee of Jinan University. Written informed consent was obtained from the owners for the participation of their animals in this study.

AUTHOR CONTRIBUTIONS

T-hL, M-hC, YX, and L-gC conceived and designed this study, analyzed the data, and wrote and revised the manuscript. W-qT, W-cT, ZJ, and Q-eL were responsible for the performance of animal experiments.

FUNDING

This study was supported by the National Natural Sciences Foundation of China (81673848 and 82074307), the Science and Technical Plan of Guangzhou, Guangdong, China (201707010100, 201804010213), the Natural Sciences Foundation of Guangdong Province (2017A030313658), the Administration of Traditional Medicine of Guangdong Province (20181068).

SUPPLEMENTARY MATERIAL

The Supplementary Material for this article can be found online at: https://www.frontiersin.org/articles/10.3389/fnut.2021.639467/full#supplementary-material

REFERENCES

1. Pilic L, Pedlar CR, Mavrommatis Y. Salt-sensitive hypertension: mechanisms and effects of dietary and other lifestyle factors. *Nutr Rev.* (2016) 74:645–58. doi: 10.1093/nutrit/nuw028
2. Titze J, Luft FC. Speculations on salt and the genesis of arterial hypertension. *Kidney Int.* (2017) 91:1324–35. doi: 10.1016/j.kint.2017.034
3. Wilck N, Matus MG, Kearney SM, Olesen SW, Forslund K, Bartolomaeus H, et al. Salt-responsive gut commensal modulates TH17 axis and disease. *Nature.* (2017) 551:585–9. doi: 10.1038/nature24628
4. Chen L, He FJ, Dong Y, Huang Y, Wang C, Harshfield GA, et al. Modest sodium reduction increases circulating short-chain fatty acids in untreated hypertensives. *Hypertension.* (2020) 76:73–9. doi: 10.1161/HYPERTENSIONAHA.120.14800
5. Valdes AM, Walter J, Segal E, Spector TD. Role of the gut microbiota in nutrition and health. *BMJ.* (2018) 361:k2179. doi: 10.1136/bmj.k2179
6. Canfora EE, Meex R, Venema K, Blaak EE. Gut microbial metabolites in obesity, NAFLD and T2DM. *Nat Rev Endocrinol.* (2019) 15:261–73. doi: 10.1038/s41574-019-0156-z
7. Bentley R, Campbell IM, Robins DJ, Kelsey M. Biosynthesis of bacterial menaquinones (vitamins K_2). *Biochemistry*. (1971) 10:3069.
8. Ponziani FR, Pompili M, Di Stasio E, Zocco MA, Gasbarrini A, Flore R. Subclinical atherosclerosis is linked to small intestinal bacterial overgrowthvia vitamin K_2-dependent mechanisms. *World J Gastroenterol.* (2017) 23:1241. doi: 10.3748/wjg.v23.i7.1241
9. Haugsgjerd TR, Egeland GM, Nygård OK, Vinknes KJ, Sulo G, Lysne V, et al. Association of dietary vitamin K and risk of coronary heart disease in middle-age adults: the Hordaland Health Study Cohort. *BMJ Open*. (2020) 10:e35953. doi: 10.1136/bmjopen-2019-035953
10. Vissers LET, Dalmeijer GW, Boer JMA, Verschuren WMM, van der Schouw YT, Beulens JWJ. The relationship between vitamin K and peripheral arterial disease. *Atherosclerosis*. (2016) 252:15–20. doi: 10.1016/j.atherosclerosis.2016.07.915
11. Yoshiji H, Noguchi R, Yamazaki M, Ikenaka Y, Sawai M, Ishikawa M, et al. Combined treatment of vitamin K_2 and angiotensin-converting enzyme inhibitor ameliorates hepatic dysplastic nodule in a patient with liver cirrhosis. *World J Gastroenterol.* (2007) 13:3259–61. doi: 10.3748/wjg.v13.i23.3259
12. Yoshiji H, Noguchi R, Toyohara M, Ikenaka Y, Kitade M, Kaji K, et al. Combination of vitamin K_2 and angiotensin-converting enzyme inhibitor ameliorates cumulative recurrence of hepatocellular carcinoma. *J Hepatol*. (2009) 51:315–21. doi: 10.1016/j.jhep.2009.04.011
13. Liu M, Song H, Tian X, Liu Y, Liu D, Hou Z, et al. Recombinant cellular repressor of e1a-stimulated genes protects against renal fibrosis in dahl salt-sensitive rats. *Am J Nephrol.* (2020) 51:401–10. doi: 10.1159/000506411
14. Liu T, Zhang C, Din AU, Li N, Wang Q, Yu J, et al. Bacterial association and comparison between lung and intestine in rats. *Biosci Rep.* (2020) 40:BSR20191570. doi: 10.1042/BSR20191570
15. Douglas GM, Maffei VJ, Zaneveld JR, Yurgel SN, Brown JR, Taylor CM, et al. PICRUSt2 for prediction of metagenome functions. *Nat Biotechnol.* (2020) 38:685–8. doi: 10.1038/s41587-020-0548-6
16. Kandasamy M, Anusuyadevi M, Aigner KM, Unger MS, Kniewallner KM, Sousa DMBD, et al. TGF-β signaling: a therapeutic target to reinstate

regenerative plasticity in vascular dementia? *Aging Dis.* (2020) 11:828. doi: 10.14336/AD.2020.0222
17. Rao KNS, Shen X, Pardue S, Krzywanski DM. Nicotinamide nucleotide transhydrogenase (NNT) regulates mitochondrial ROS and endothelial dysfunction in response to angiotensin II. *Redox Biol.* (2020) 36:101650. doi: 10.1016/j.redox.2020.101650
18. Li T, Long M, Li H, Gatesoupe F, Zhang X, Zhang Q, et al. Multi-omics analysis reveals a correlation between the host phylogeny, gut microbiota and metabolite profiles in cyprinid fishes. *Front Microbiol.* (2017) 8:454. doi: 10.3389/fmicb.2017.00454
19. Lees JS, Chapman FA, Witham MD, Jardine AG, Mark PB. Vitamin K status, supplementation and vascular disease: a systematic review and meta-analysis. *Heart*. (2018) 105:938–45. doi: 10.1136/heartjnl-2018-313955
20. Liu T, Zhang X, Han N, Liu Y, Wu Y, Li X, et al. Regulation effect of a chinese herbal formula on flora and mucosal immune secretory immunoglobulin A in rats. *Evid Based Complem Altern Med.* (2018) 2018:1–9. doi: 10.1155/2018/4821821
21. Xu Z, Liu T, Zhou Q, Chen J, Yuan J, Yang Z. Roles of Chinese medicine and gut microbiota in chronic constipation. *Evid Based Complem Altern Med.* (2019) 2019:1–11. doi: 10.1155/2019/9372563
22. Xiao L, Itani HA, Do Carmo LS, Carver LS, Breyer RM, Harrison DG. Central EP3 (E Prostanoid 3) receptors mediate salt-sensitive hypertension and immune activation. *Hypertension*. (2019) 74:1507–15. doi: 10.1161/HYPERTENSIONAHA.119.13850
23. Wang S, Liu J, Cai H, Liu K, He Y, Liu S, et al. High salt diet elevates the mean arterial pressure of SLC14α1 gene depletion mice. *Life Sci.* (2020) 254:117751. doi: 10.1016/j.lfs.2020.117751
24. Arendse LB, Danser AHJ, Poglitsch M, Touyz RM, Burnett JC, Llorens-Cortes C, et al. Novel therapeutic approaches targeting the renin-angiotensin system and associated peptides in hypertension and heart failure. *Pharm Rev.* (2019) 71:539–70. doi: 10.1124/pr.118.017129
25. Gheblawi M, Wang K, Viveiros A, Nguyen Q, Zhong J, Turner AJ, et al. Angiotensin-converting enzyme 2: SARS-CoV-2 receptor and regulator of the renin-angiotensin system. *Circ Res.* (2020) 126:1456–74. doi: 10.1161/CIRCRESAHA.120.317015
26. Tsugawa, N. (2015). Cardiovascular diseases and fat soluble vitamins: Vitamin D and Vitamin K. *J Nutr Sci Vitaminol.* 61(Suppl):S170–S172. doi: 10.3177/jnsv.61.S170
27. Rostand SG. Vitamin D, blood pressure, and African Americans: toward a unifying hypothesis. *Clin J Am Soc Nephrol.* (2010) 5:1697–703. doi: 10.2215/CJN.02960410
28. Vaidya A, Williams JS. The relationship between vitamin D and the renin-angiotensin system in the pathophysiology of hypertension, kidney disease, and diabetes. *Metab Clin Exp.* (2012) 61:450–8. doi: 10.1016/j.metabol.2011.09.007
29. Cox LM, Blaser M. *Probiotic Compositions for Improving Metabolism and Immunity in (US) Patent Application 15/786, 483*. Justia Patents. New York, NY: New York University (2018).
30. Van Treuren W, Dodd D. Microbial contribution to the human metabolome: implications for health and disease. *Ann Rev Pathol.* (2020) 15:345–69. doi: 10.1146/annurev-pathol-020117-043559
31. Weersma RK, Zhernakova A, Fu J. Interaction between drugs and the gut microbiome. *Gut.* (2020) 69:1510–9. doi: 10.1136/gutjnl-2019-320204

Conflict of Interest: The authors declare that the research was conducted in the absence of any commercial or financial relationships that could be construed as a potential conflict of interest.

frontiers in Nutrition

ORIGINAL RESEARCH
published: 06 April 2021
doi: 10.3389/fnut.2021.645099

Check for updates

Olive Fruit Extracts Supplement Improve Antioxidant Capacity *via* Altering Colonic Microbiota Composition in Mice

Mengyu Wang[1], Shunfen Zhang[1], Ruqing Zhong[1], Fan Wan[1,2], Liang Chen[1], Lei Liu[1], Bao Yi[1]* and Hongfu Zhang[1]

[1] *State Key Laboratory of Animal Nutrition, Institute of Animal Science, Chinese Academy of Agricultural Sciences, Beijing, China,* [2] *College of Pastoral Agriculture Science and Technology, Lanzhou University, Lanzhou, China*

Oxidative stress, one of the most common biological dysfunctions, is usually associated with pathological conditions and multiple diseases in humans and animals. Chinese olive fruit (*Canarium album* L.) extracts (OE) are natural plant extracts rich in polyphenols (such as hydroxytyrosol, HT) and with antioxidant, anti-hyperlipidemia, and anti-inflammatory potentials. This study was conducted to investigate the antioxidant capacity of OE supplementation and its related molecular mechanism in mice. Mice (25.46 ± 1.65 g) were treated with 100 mg/kg body weight (BW) OE or saline solution for 4 weeks, and then the antioxidant and anti-inflammatory capacities of mice were examined. The results showed that OE supplement significantly increased the serum antioxidative enzyme activities of total antioxidant activity (T-AOC), superoxide dismutase (SOD), glutathione peroxidase (GSH-Px), and catalase and decreased the serum malondialdehyde (MDA) level, indicating that OE treatment enhanced the antioxidant capacity in mice. qPCR results showed that the transcriptional expression of antioxidant *SOD1*, *CAT*, *Gpx1*, and *Gpx2* were significantly down-regulated in the small intestine (jejunum and ileum) after OE administration. Meanwhile, OE treatment significantly decreased the T-AOC and increased the MDA level in the small intestine. Furthermore, OE administration dramatically reduced the mRNA expression of pro-inflammatory cytokines (TNF-α and IL-1β), which confirmed its antioxidant and anti-inflammatory capacities with OE administration. Using amplicon sequencing technology, 16S rRNA sequencing results showed that OE supplement significantly increased the colonic *Firmicutes*/*Bacteroidetes* ratio, which also had a negative correlation with the serum MDA level and positively correlated with serum GSH-Px activity through Pearson correlation analysis. Besides that, *Alloprevotella* was negatively correlated with serum T-AOC. *Colidextribacter* was positively correlated with serum MDA and negatively correlated with serum T-AOC, SOD, and GSH-Px levels. In summary, this study showed that treatment with 100 mg/kg BW polyphenol-rich OE could alter colonic microbiota community, which was strongly associated with improved antioxidant capacity in mice.

Keywords: olive extracts, antioxidant capacity, gut microbiota, oxidative stress, anti-inflammatory capacity, hydroxytyrosol

OPEN ACCESS

Edited by:
Yong Su,
Nanjing Agricultural University, China

Reviewed by:
Jianping Wang,
Sichuan Agricultural University, China
Ruizhi Hu,
Hunan Agricultural University, China

Correspondence:
Bao Yi
yibao@caas.cn

Specialty section:
This article was submitted to Nutrition and Microbes, a section of the journal Frontiers in Nutrition

Received: *22 December 2020*
Accepted: *03 March 2021*
Published: *06 April 2021*

Citation:
Wang M, Zhang S, Zhong R, Wan F, Chen L, Liu L, Yi B and Zhang H (2021) Olive Fruit Extracts Supplement Improve Antioxidant Capacity via Altering Colonic Microbiota Composition in Mice. Front. Nutr. 8:645099. doi: 10.3389/fnut.2021.645099

INTRODUCTION

Oxidative stress is regarded as a result of the imbalance of oxidants and antioxidants, which can cause damage to important cellular macromolecules, such as DNA, lipid, and protein, and, in turn, lead to toxicity, chronic inflammation, and diseases, acting as a serious threat to animal and human health (1–3). In animal husbandry, oxidative stress is commonly considered to be associated with various pathological conditions and can severely damage productivity and livestock product quality and even lead to death (4, 5). Similarly, oxidative stress is also an important factor for the progression of human diseases and body disorders, including metabolic diseases and inflammation-related diseases, such as inflammatory bowel disease and diabetes (6–8). Moreover, the overproduction of reactive oxygen species and reactive nitrogen species during oxidative stress can cause inflammatory responses by activating the related signal transduction pathways (9, 10).

Polyphenols are natural compounds present in plants with numerous biological activities, which have been proposed to be useful as adjuvant therapy for their potential antioxidant effect, associated with the anti-inflammatory activity (11). Olive extracts, as one of the important natural plant extracts, have been extensively explored for their potential antioxidant properties (12, 13). The main bioactive component of olive extracts are polyphenols, which are thought to be responsible for their wide range of biological activities. Increasing evidence has indicated that olive extracts rich in polyphenolic compounds have powerful antioxidant and anti-inflammatory effects in mammalian cells, rats, and humans (14–17). Administration of olive oils high in phenolic compounds decreased malondialdehyde (MDA) levels in urine and increased plasma glutathione peroxidase (GSH-Px) activity in a dose-dependent manner in men (18). Olive leaf extract could enhance antioxidation capacity in the liver of aged mice by inducing a decrease in the MDA level and an increase in glutathione (GSH) level (19). Olive pomace extracts supplement followed with increased total antioxidant activity (T-AOC) was shown in the study of A. De Bruno et al. (20). In addition, some studies have shown that olive extracts have anti-bacterial and anti-inflammation effects (21–23). It is well-established that these beneficial health properties of olive extracts are related to one of the polyphenolic compounds named hydroxytyrosol (HT) (24–26). Studies in mammalian cells have demonstrated that HT can exert potential effects against oxidative stress and inflammation (24, 27). Further mechanism research showed that HT alleviated oxidative stress by decreasing the production of oxygen species (24). Thus, olive extracts enriched with various polyphenols (especially HT) may be an effective prevention against disorders related to oxidative stress.

Concerning the metabolism of olive extracts, particularly the olive bioactive component polyphenols, growing evidence has demonstrated that only small amounts of ingested polyphenols can be absorbed in the small intestine and enter the systemic circulation (28, 29). Most remaining polyphenols reach into the large intestine, where they can be metabolized by gut microbiota (28, 29). The colonic microbiota, therefore, plays a key role in the metabolism of polyphenols. A study showed that olive administration could alleviate hypercholesterolemia by reducing the relative abundance of *Lactobacilli* and *Ruminococcus* in the human gut microbiota (30). Extra virgin olive oil supplementation increased the gut microbiota diversity and decreased the relative abundance of *Firmicutes* in mice (31). In addition, another study showed that olive leaf extract can counteract the ecological disorders associated with obesity by altering the colonic microbial community in mice (32). These studies have suggested that olive oil and olive leaf phenolic compounds can induce changes in gut microbial composition and alter its metabolism in mice and humans with metabolic diseases.

However, whether oral administration of Chinese olive fruit (*Canarium album* L.) extracts (OE) could improve colonic microbiota and whether colonic microbiota is a remarkable mechanism further involved in antioxidant and anti-inflammatory effects of OE remain to be elucidated. We here, therefore, investigated the effects of OE on the levels of antioxidant indicators, the expressions of antioxidant enzymes and inflammatory cytokines in the intestine, and the colonic microbiota composition to explore its underlying molecular mechanism.

MATERIALS AND METHODS

Reagents, Mice, and Ethics

The OE was purchased from Shanghai Huahan Biotechnology Co., Ltd. (Shanghai, China), and it was composed of 10 wt% HT as checked by high-performance liquid chromatography. Specifically, an Acquity UPLC BEH C18 (1.7 µm, 2.1 × 50 mm) column was used. The binary mobile phase consists of two different formic acid solutions running in a linear gradient, and detection is carried out with UV–vis at 278 nm. Quantification was performed by the external standard method with tyrosol and HT reference standards. Then, the concentrations of these compounds were calculated using the response factor of HT reference standard. Three-week-old female ICR mice were purchased from Peking University Health Science Center (Beijing, China). The mice were maintained in a 12-h light/dark cycle, with free access to diet and water. All procedures used in this experiment were approved by the Experimental Animal Welfare and Ethical Committee of the Institute of Animal Science, Chinese Academy of Agricultural Sciences (no. IAS2020-86).

Mice Experiment and Sampling

After 1-week acclimatization, the mice (25.46 ± 1.65 g) were divided into two groups ($n = 12$ per group). The OE supplement (OE) group was treated with 100 mg/kg body weight OE (prepared fresh in distilled water before gavage), and the control (Con) mice received the same volume of distilled water every day *via* oral gavage. Body weight and feed intake of the mice were measured weekly. At the end of day 28, blood samples were collected by orbital blooding, and then the mice were killed by cervical dislocation. The jejunum and ileum tissues were quickly removed and frozen in liquid nitrogen for further analysis. For histopathology examinations, part of the jejunum and ileum were cut and fixed in 4% paraformaldehyde. Colonic digesta were collected for 16S rRNA sequencing and short-chain fatty acid analysis.

Serum Oxidant and Antioxidant Marker Analyses

Serum was obtained by centrifugation at 1,000 *g* for 15 min under 4°C and stored in aliquots at −80°C. The activities of total antioxidant capacity (T-AOC), glutathione peroxidase (GSH-Px), catalase (CAT), and superoxide dismutase (SOD) and the level of malondialdehyde (MDA) and inflammatory cytokines (TNF-α, IL-1β, IL-6, and IFN-γ) were measured with corresponding assay kits (Nanjing Jiancheng Bioengineering Institute, Nanjing, China) following the manufacturers' instructions.

Intestinal Morphology Examination

Proximal jejunum and distal ileum sections were used for histologic examination. They were fixed with 4% paraformaldehyde–phosphate-buffered saline overnight, then dehydrated, and embedded in paraffin blocks. After that, a section of 5 μm was cut and mounted on slides. The sections were further deparaffinized and hydrated and then stained with hematoxylin-eosin (H&E) for microscopy. Microphotographs were taken with a DM300 microscope (Leica, Germany). Villus length and crypt depth were performed using Image J software. A minimum of 20 well-orientated villi and associated crypts from at least seven different fields per animal were measured.

RNA Extraction and Quantitative Real-Time Polymerase Chain Reaction Analysis

Total RNAs from jejunum and ileum samples were isolated using Trizol (Invitrogen, USA) reagent and then treated with DNase I (Invitrogen, USA) according to the instruction of the manufacturer. The concentration of each RNA sample was quantified using NanoDrop 2000 (Nanodrop Technologies, USA). Before reverse transcription, possible contaminations from genomic DNA were eliminated using a PrimeScript RT reagent kit (Takara, Japan). cDNA was synthesized using PrimeScript Enzyme Mix 1, RT Primer Mix, and 5× PrimerScript Buffer 2 (Takara, Dalian, China). Reverse transcription was conducted at 37°C for 15 min and 85°C for 5 s. Gene-specific prime sequences (**Table 1**) were designed using Primer 5.0 software and synthesized by Sangon Biotech Co., Ltd (Shanghai, China). Real-time PCR was performed according to the manufacturer's instructions. Briefly, 1 μl cDNA template was added to a total volume of 10 μl containing 5 μl KAPA SYBR FAST qPCR Master Mix Universal, 0.4 μl PCR forward primer, 0.4 μl PCR reverse primer, 0.2 μl ROX low, and 3 μl PCR-grade water (Kapa Biosystems, Beijing, China). We used the following protocol: (i) enzyme activation (3 min at 95°C), (ii) an amplification and quantification program consisting 40 of repeated cycles (3 s at 95°C and 34 s at 60°C), and (iii) a melting curve program (15 s at 95°C, 1 min at 60°C, and 15 s at 95°C). Relative expression was calculated between the control group and treatment group by $2^{-\Delta\Delta Ct}$ method, where $\Delta C_t = C_t$ (Target)–C_t (β-actin). β-actin was chosen as a housekeeping gene to normalize target gene transcript level.

TABLE 1 | Primers used for qPCR assay.

Gene	Accession no.	Sequence (5′-3′)
β-actin	NM_007393.5	F: TGTCCACCTTCCAGCAGATGT R: GCTCAGTAACAGTCCGCCTAGAA
SOD1	NM_011434.2	F: GTGAACCAGTTGTGTTGTC R: ATCACACGATCTTCAATGGA
CAT	NM_009804.2	F: TCAGGTGCGGACATTCTA R: ATTGCGTTCTTAGGCTTCT
GPx1	NM_001329527.1	F: ATCAGTTCGGACACCAGA R: TTCACTTCGCACTTCTCAA
GPx2	NM_030677.2	F: GTGGCGTCACTCTGAGGAACA R: CAGTTCTCCTGATGTCCGAACTG
TNF-α	NM_013693.3	F: CATCTTCTCAAAATTCGAGTGACAA R: TGGGAGTAGACAAGGTACAACCC
IL-1β	NM_008361.4	F: TTCAGGCAGGCAGTATCA R: CCAGCAGGTTATCATCATCA

F, forward; R, reverse.

Bacterial 16S rRNA Gene Sequencing and Analysis

Total genome DNA from colonic digesta was extracted using QIAamp DNA Stool Mini Kit (Qiagen, Germany); then, DNA concentration and purity was monitored on 1% agarose gels. The V3–V4 region of the bacterial 16S ribosomal RNA gene was amplified using a specific primer (338F, 5′-ACTCCTACGGGAGGCAGCAG-3′; 806R, 5′-GGACTACHVGGGTWTCTAAT-3′). Amplicons were detected using 2% agarose gel electrophoresis and purified using the AxyPrep DNA gel extraction kit (Axygen Bioscience, CA, USA) according to the manufacturer's instructions. After having been quantified and purified, the amplicons were sequenced using Illumina MiSeq platform (Illumina, San Diego, CA, USA) at Majorbio Bio-Pharm Technology Co., Ltd. (Shanghai, China) according to standard protocols. The raw reads were deposited into the NCBI Sequence Read Archive database (Accession Number: PRJNA681369). The sequences were analyzed and assigned to operational taxonomic units (OTUs; 97% identity). Alpha diversity was analyzed using QIIME (Version 1.7.0), which included the calculation of ACE, Chao 1, Shannon, and Simpson indices. Beta diversity was estimated by computing the unweighted Unifrac distance and visualized using principal coordinates analysis (PCoA).

Short-Chain Fatty Acid Analysis

For short-chain fatty acid (SCFA) analysis, frozen colonic digesta samples (100 mg) were weighed into 1.5-ml centrifuge tubes and mixed with 1 ml ddH_2O, homogenized, and centrifuged at 10,000 rpm for 10 min under 4°C. A mixture of the supernatant fluid and 25% metaphosphoric acid solution (0.9 and 0.1 ml, respectively) was vortexed for 1 min and centrifuged at 1,000 rpm for 10 min under 4°C after letting it stand in a 1.5-ml centrifuge tube at 4°C for over 2 h. The supernatant portion was then filtered through a 0.45-μm polysulfone filter and analyzed using Agilent 6890 gas chromatography (Agilent Tecnologies, Inc., Palo Alto, CA, USA).

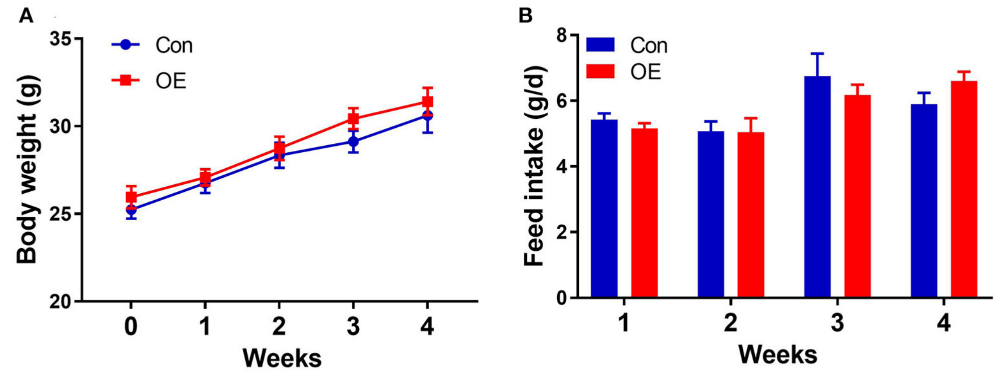

FIGURE 1 | Effects of olive fruit (*Canarium album* L.) extracts on body weight and feed intake. **(A)** Body weight. **(B)** Average daily feed intake. Data were expressed as mean ± SEM.

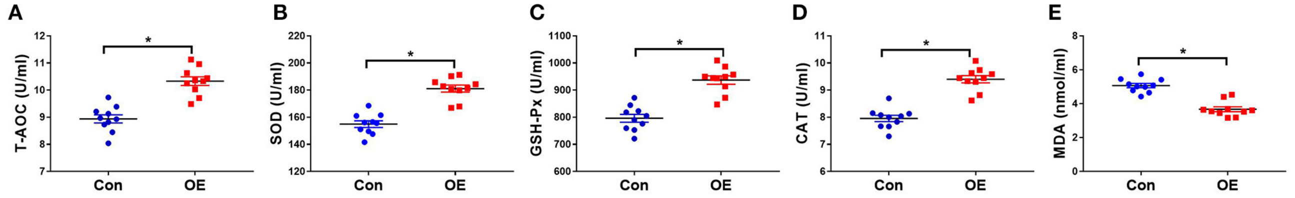

FIGURE 2 | Effects of olive fruit (*Canarium album* L.) extracts on the serum antioxidant indicators. **(A)** T-AOC, **(B)** SOD, **(C)** GSH-Px, **(D)** CAT, **(E)** MDA. Data were expressed as mean ± SEM. **P* < 0.05.

Statistical Analysis

All statistical analyses were performed by using Student's *t*-test (SPSS 21 software). Pearson correlation analysis between the *Firmicutes*/*Bacteroidetes* ratio and serum antioxidant indicators (T-AOC, SOD, GSH-Px, CAT, and MDA) was carried out using GraphPad Prism 7.0. Data are expressed as mean ± SEM. P-value < 0.05 was considered significant.

RESULTS

Effects of OE Supplement on Body Weight and Feed Intake

Oral administration with OE for 4 weeks had no significant effects on the body weight ($P > 0.05$) and average daily feed intake in mice compared with the mice in the Con group ($P > 0.05$; **Figure 1**).

OE Supplement Enhanced the Serum Antioxidant Capacity in Mice

The activities of oxidant–antioxidant enzyme and MDA levels are sensitive indicators for oxidative stress. To determine whether OE affects antioxidant capacity, serum oxidant–antioxidant enzyme activities of T-AOC, SOD, GSH-Px, CAT, and MDA levels were analyzed using test kits. **Figure 2** shows that OE treatment significantly increased the T-AOC ($P < 0.05$), increased the activities of SOD ($P < 0.05$), GSH-Px ($P < 0.05$), and CAT ($P < 0.05$), and decreased the level of MDA ($P < 0.05$).

Effects of OE Supplement on Intestinal Morphology

Intestinal morphology was examined with H&E staining. The villus height, crypt depth, and villus height/crypt depth ratio were measured (**Figure 3**). In the jejunum, treatment with OE had no significant effects on the villus height, crypt depth, and villus height/crypt depth ratio in mice ($P > 0.05$; **Figure 3B**). In the ileum, the villus height and crypt depth had no significant difference between the two groups ($P > 0.05$; **Figure 3C**). However, the villus height/crypt depth ratio was significantly higher in the OE group than in the Con group ($P < 0.05$; **Figure 3C**).

OE Altered Small Intestinal Antioxidant Capacity

Next, we analyzed the mRNA expression of genes associated with antioxidant capacity in the ileum and jejunum, including *SOD1*, *Gpx1*, *Gpx2*, and *CAT* to examine the molecular mechanism of OE administration in enhancing antioxidant capacity. In the jejunum, compared with the Con group, OE treatment significantly down-regulated the mRNA expression of *SOD1*, *CAT*, *Gpx1*, and *Gpx2* ($P < 0.05$; **Figure 4A**). Similarly, in the ileum, the mRNA expression of *SOD1*, *CAT*, and *Gpx2* was markedly lower in the OE group than in the Con group ($P < 0.05$; **Figure 4B**). Besides that, the results showed that, in the ileum and jejunum, the MDA level was significantly higher ($P < 0.05$), while the T-AOC was significantly lower in the OE group compared with that in the Con group ($P < 0.05$; **Figures 4C–F**).

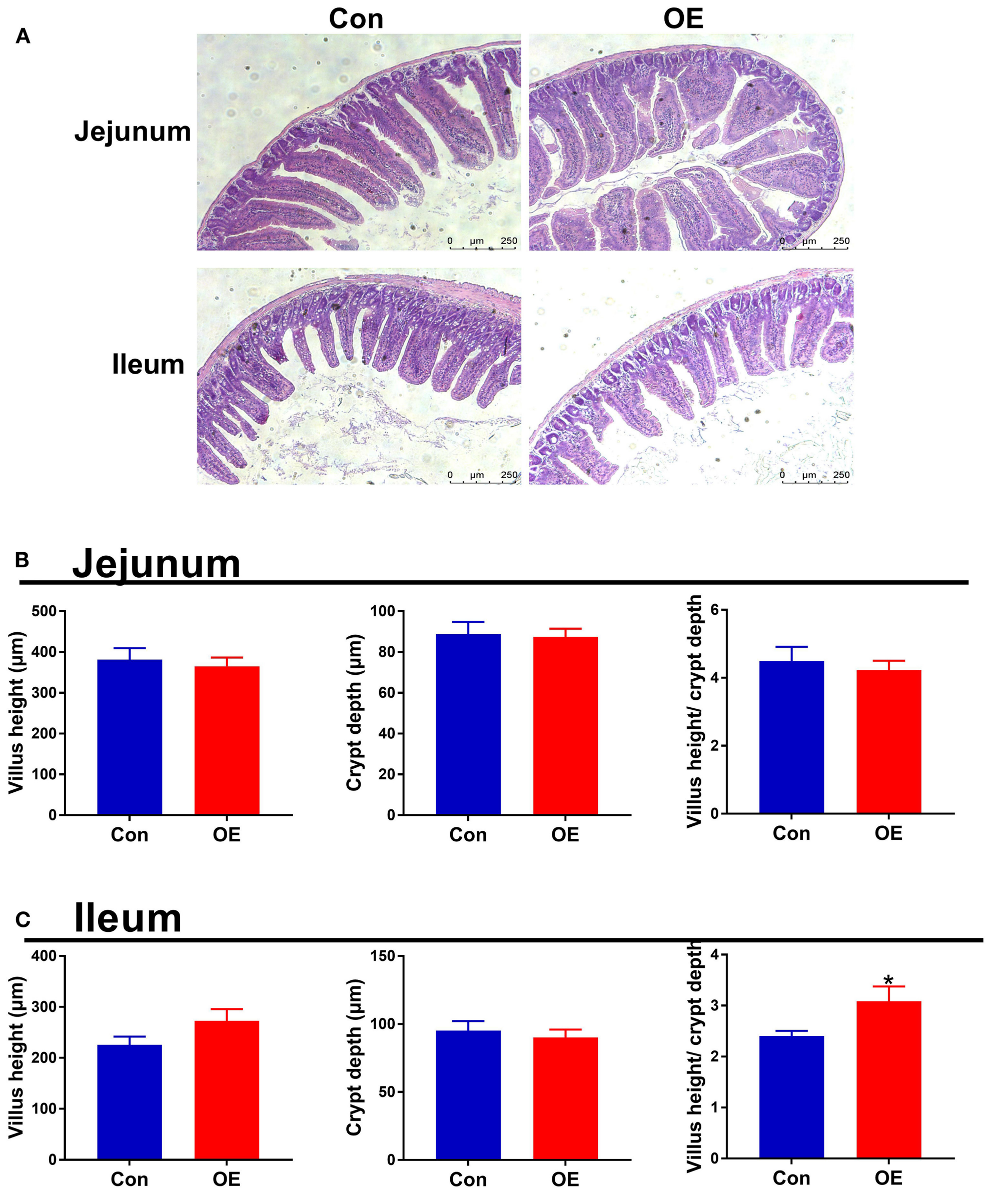

FIGURE 3 | Effects of olive fruit (*Canarium album* L.) extracts on jejunal and ileal morphology. **(A)** Representative images of H&E staining in the jejunum and ileum. **(B)** Jejunal villus height, crypt depth, villus height/crypt depth. **(C)** Ileal villus height, crypt depth, villus height/crypt depth. Data were expressed as mean ± SEM. *$P < 0.05$.

OE Supplement Altered the Expression and Levels of Pro-inflammatory Cytokines in the Small Intestine

Oxidative stress is often involved in inducing inflammatory responses. Thus, the anti-inflammatory capacity of OE was also tested by analyzing the mRNA expression of pro-inflammatory cytokines (TNF-α and IL-1β) in the intestine. The results showed that, in the jejunum, oral administration of OE markedly down-regulated the mRNA levels of TNF-α and IL-1β ($P < 0.05$; **Figure 5A**). OE administration showed a likely significant decrease in IL-1β mRNA expression in the ileum compared with the Con group ($P < 0.05$; **Figure 5B**). However, the ELISA results showed that, in the jejunum and ileum, the pro-inflammatory cytokine (IL-6, IL-1β, TNF-α, and IFN-γ) levels were significantly higher in the OE group than in the Con group ($P < 0.05$; **Figures 5C,D**).

OE Supplement Altered the Composition of Colonic Microbiota Community

To study the effect of OE supplementation on large intestinal microbiota composition, the colonic chyme microflora was analyzed by sequencing V3 + V4 regions of 16S rRNA genes.

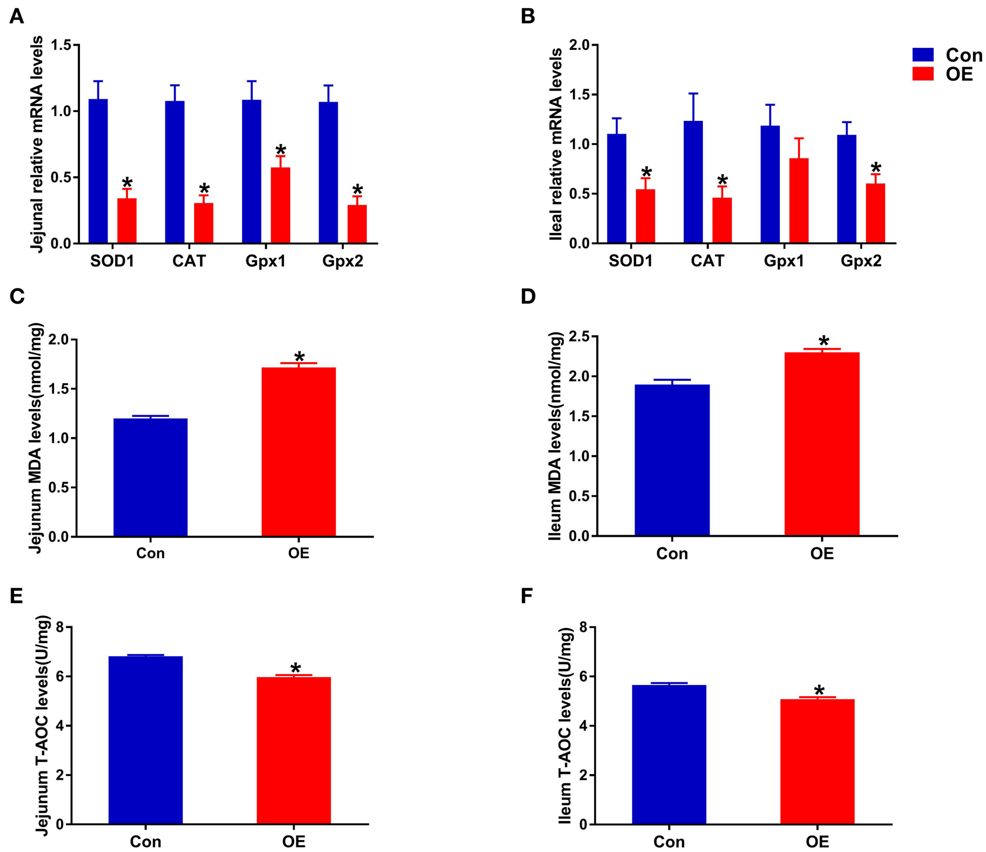

FIGURE 4 | Effects of olive fruit (*Canarium album* L.) extracts on the jejunal and ileal antioxidant capacities. **(A)** Jejunum mRNA expression levels of antioxidant enzymes. **(B)** Ileum mRNA expression levels of antioxidant enzymes. **(C)** Jejunum MDA levels. **(D)** Ileum MDA levels. **(E)** Jejunum T-AOC levels. **(F)** Ileum T-AOC levels. Data were expressed as mean ± SEM. *$P < 0.05$.

After removing the low-quality sequences, a total of 1,184,959 clean tags were clustered into OTUs based on 97% identity. The dilution curves showed that the end of the curve tends to be flat, indicating that the amount and depth of high-throughput sequencing data is reliable (**Figure 6A**). To identify the microbial α-diversity, ACE and Chao 1 indexes were examined for the community richness, and Shannon and Simpson were examined for the community diversity. As shown in **Figure 6B**, OE treatment significantly decreased the Shannon index ($P < 0.05$), while it had a little effect on the ACE, Chao 1, and Simpson indexes compared to the Con group. The Venn diagram shows that there are 464 common OTUs between the Con and OE groups. Meantime, the Con and OE groups contained individual 50 and 101 OTUs, respectively (**Figure 6C**). To further understand the microbial composition between the Con and OE groups, we evaluated β-diversity using PCoA based on unweighted Unifrac. The results showed that the microbial community structure in the OE group significantly differed from that in the control group (**Figure 6C**).

The overall microbial composition in the Con and OE groups differed at the phylum and genus levels. Linear discriminant analysis effect size (LEfSe) analysis was performed to evaluate the differentially expressed bacteria. Of note is the fact that *Staphylococcales* and *Bacillaceae* were shown to be enriched in the OE treatment group (**Figures 7A,B**). The relative abundance results showed that, at the phylum level, OE supplement notably enhanced the *Firmicutes/Bacteroidetes* ratio ($P < 0.05$), while it did not affect the relative abundance of *Firmicutes* and *Bacteroidetes*, respectively ($P > 0.05$; **Figure 7C**). At the genus level, OE tended to decrease the relative abundance of *Candidatus_Arthromitus*, but the difference was not significant ($P > 0.05$). However, the relative abundance of *unclassified_f_Lachnospiraceae* was significantly lower in the OE group than that in the control group ($P < 0.05$; **Figure 7D**).

The Association Analysis Between OE Supplement-Induced Alterations in Colonic Microbiota and Serum Antioxidant Capacity

To investigate whether the alteration in gut microbiota is associated with the antioxidant effects of OE, we performed a correlation analysis using the *Firmicutes/Bacteroidetes* ratio and serum antioxidant indicators (T-AOC, SOD, GSH-Px, CAT, and MDA). As shown in **Figure 8**, there was a negative correlation between the *Firmicutes/Bacteroidetes* ratio and the

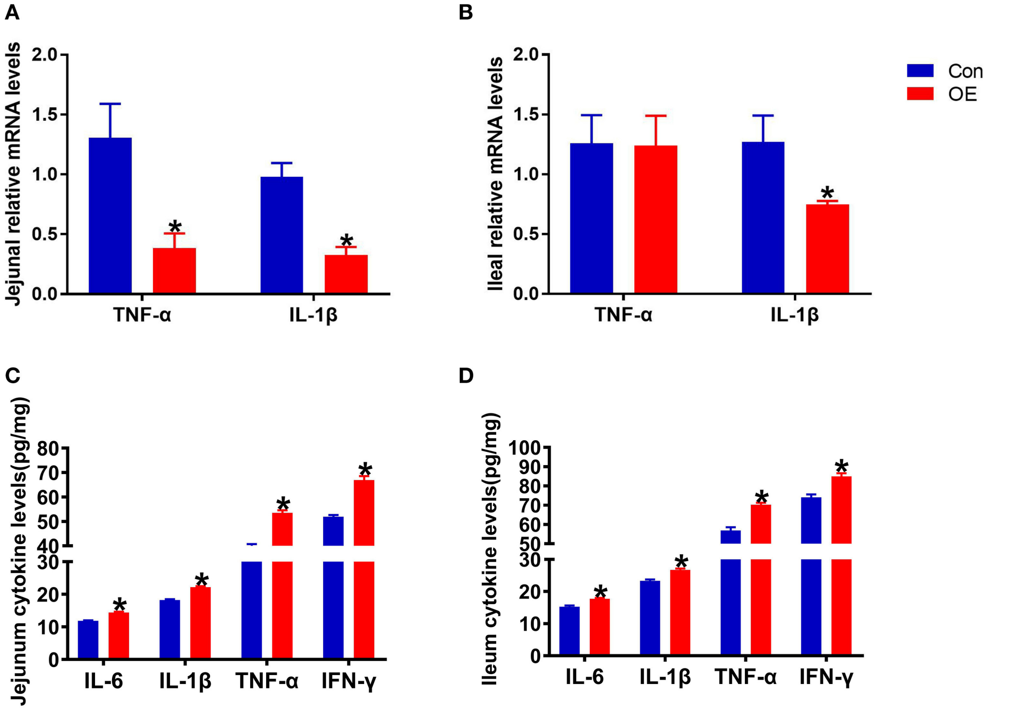

FIGURE 5 | Effects of olive fruit (*Canarium album* L.) extracts on the jejunal and ileal pro-inflammatory cytokines. **(A)** Jejunal relative mRNA levels of cytokines. **(B)** Ileal relative mRNA levels of cytokines. **(C)** Jejunal cytokine levels. **(D)** Ileal cytokine levels. Data were expressed as mean ± SEM. $^*P < 0.05$.

level of serum MDA ($P < 0.05$; **Figure 8E**) as well as a positive correlation between the *Firmicutes/Bacteroidetes* ratio and the activity of serum GSH-Px ($P < 0.05$; **Figure 8C**). Moreover, there was a positive correlation trend between the *Firmicutes/Bacteroidetes* ratio and the activities of serum T-AOC ($0.05 < P < 0.1$), SOD ($0.05 < P < 0.1$), and CAT ($0.05 < P < 0.1$; **Figures 8A,B,D**). In addition, heat map revealed the correlation between the gut microbial population at the genus level and the serum antioxidant indicators (T-AOC, SOD, GSH-Px, CAT, and MDA). The data showed that the relative abundance of *Colidextribacter* was positively correlated with serum MDA level and negatively correlated with serum T-AOC, SOD, and GSH-Px levels ($P < 0.05$; **Figure 9**). The relative abundance of *Alloprevotella* was found to be likely markedly negatively correlated with the serum T-AOC ($P < 0.05$; **Figure 9**).

OE Supplementation Had No Effects on Colonic SCFAs

Since the supplement of OE altered colonic microbiota composition and structure and SCFAs as the metabolites of microbiota, we investigated the SCFA content in the colon. The results showed that oral administration of OE had no significant effect on the levels of SCFAs, including acetic acid, propionic acid, and butyrate, in the colon ($P > 0.05$; **Figure 10**).

DISCUSSION

Studies being conducted both in animal models and humans have revealed the significant role of oxidative stress in the pathogenesis of various diseases, including neurodegenerative and metabolic diseases and cancer (3, 33–35). Emerging evidence has highlighted the beneficial bioactivity of olive fruit, pomace, leaf extracts, and olive oils because of the many bioactive polyphenolic compounds, which have various health-promoting potentials including antioxidant, anti-inflammation, and anti-bacteria (36–38). In this study, we have demonstrated that oral administration of OE was able to enhance the antioxidative capacity as well as the anti-inflammatory activity in mice, which may be associated with the changes of gut microbiota induced by OE treatment.

Investigations have shown that olive extracts contain polyphenols which exhibit powerful antioxidant and anti-inflammatory effects on humans and animals (39, 40). For instance, numerous evidence has demonstrated that olive extracts can ameliorate oxidative stress and inflammation in different cells, such as colon cancer cells (41), kidney cells (42, 43), and renal cells (44). In addition, oral administration of olive extracts could alleviate the lipopolysaccharide (LPS)-induced oxidative stress and inflammatory responses as shown by attenuating the decreased levels of brain GSH and increased levels of brain MDA and serum TNF-α in mice (12). Similarly, in this study, we found that oral administration of OE increased the serum T-AOC and the activities of antioxidant enzymes, including SOD, GSH-Px, and CAT, and decreased the MDA levels in mice. SOD, GSH-Px, and CAT are generally regarded as the primary antioxidant enzyme defense system in animals and humans (45). SOD can catalyze superoxide into oxygen and hydrogen peroxide (45). CAT

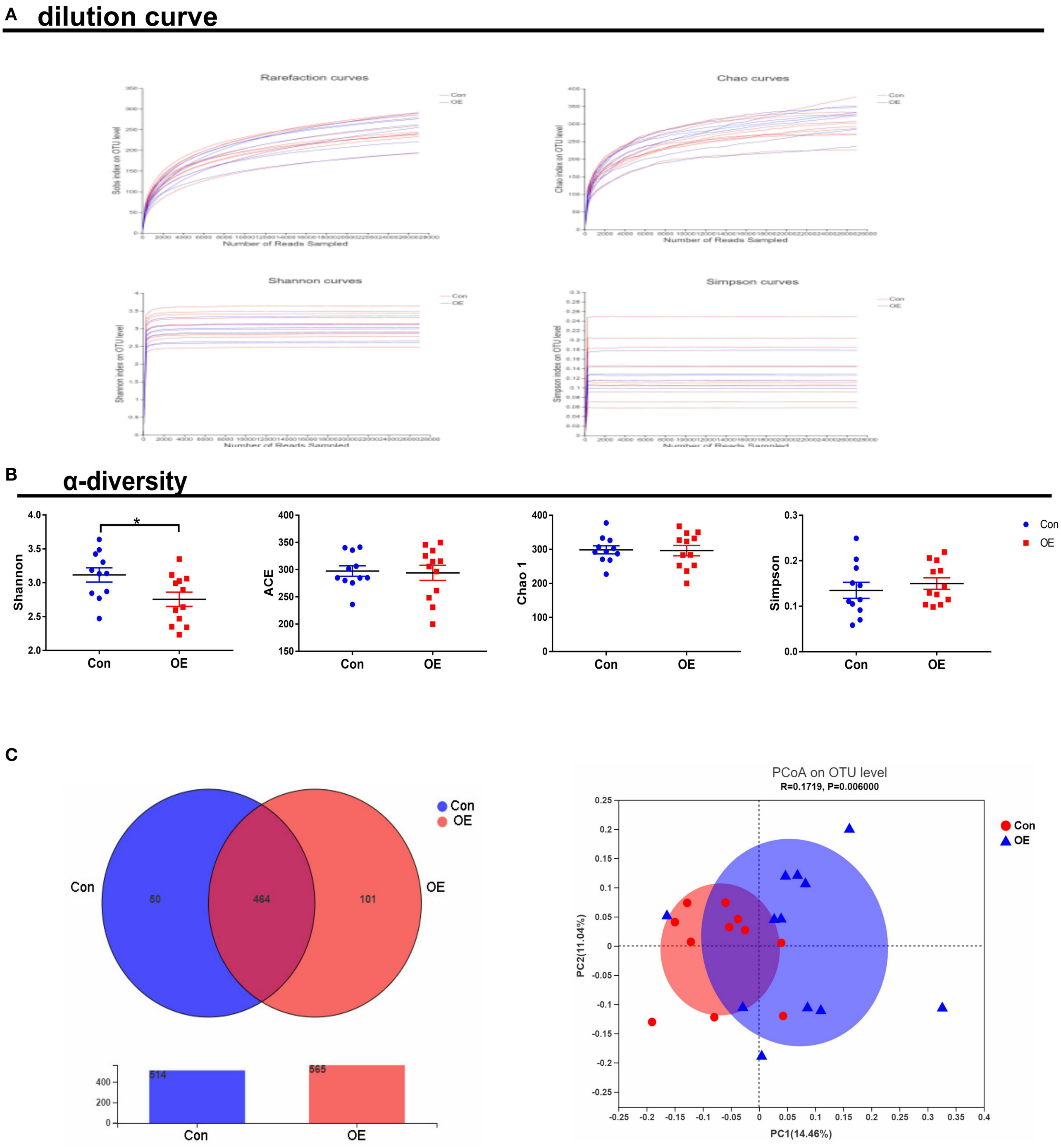

FIGURE 6 | Effects of olive fruit (*Canarium album* L.) extracts on the colonic microbial diversity. **(A)** Dilution curve. **(B)** α-diversity. **(C)** Venn diagram. Data were expressed as mean ± SEM.

has the ability to scavenge hydrogen peroxide into oxygen and water (45). GSH-Px can catalyze hydrogen peroxide into water (46). MDA is one of the products of lipid peroxidation, and it is an important indicator of oxidative stress status in the body (47). These results of serum indicators suggested that OE supplement could enhance the antioxidant ability in mice.

The intestine, a vital organ responsible for nutrient digestion and absorption and a major site of host immunity, is highly susceptible to oxidative stress, which leads to gut dysfunction and body disorders (2, 11, 48, 49). It is well-documented that dietary polyphenols can be absorbed in the small intestine (50) and exhibit antioxidant effects by scavenging oxidant chemical species as well as altering the levels and activities of antioxidant

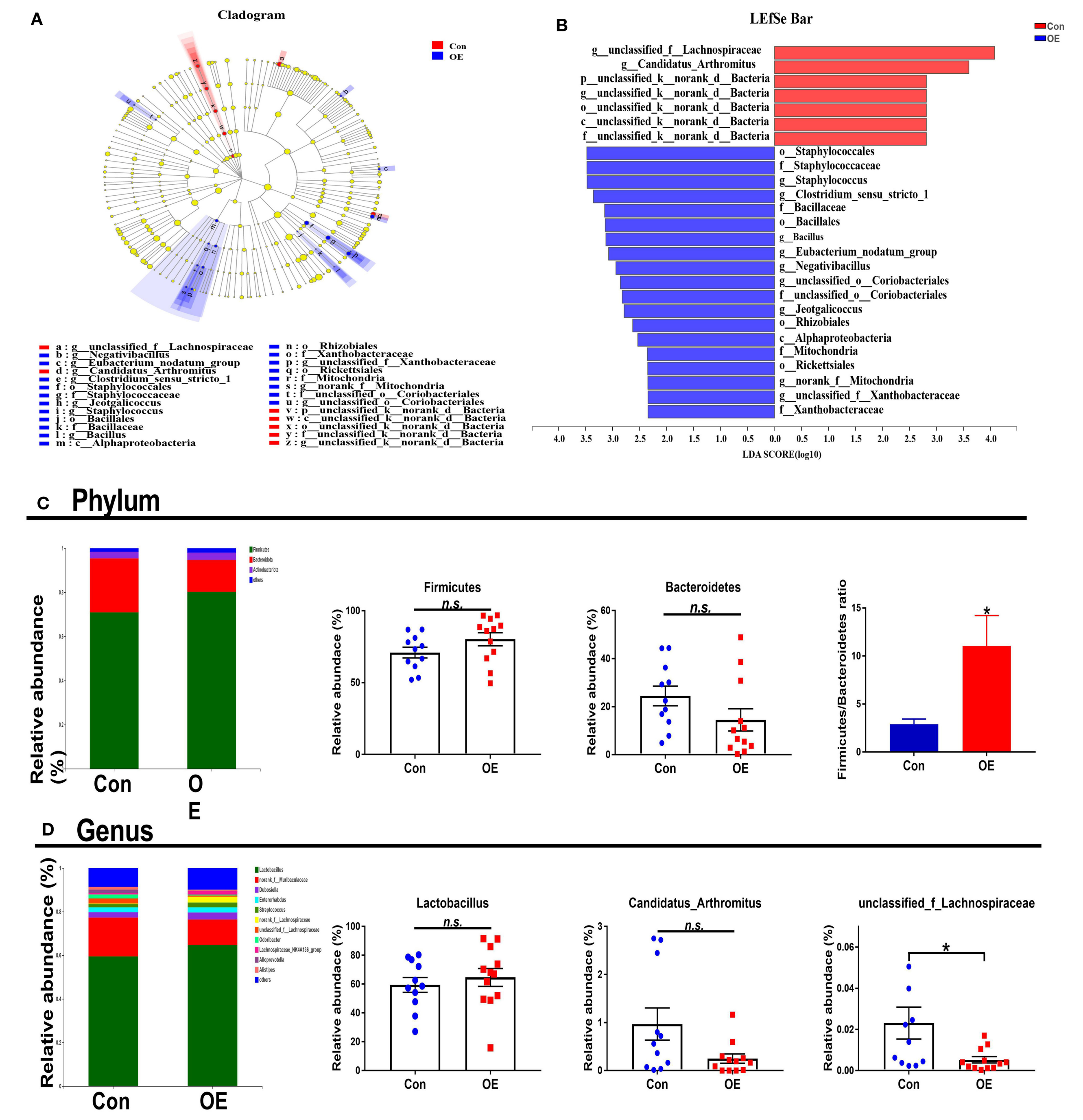

FIGURE 7 | Effects of olive fruit (*Canarium album* L.) extracts on the colonic microbial composition. **(A,B)** LEfSe analysis. **(C)** Phylum level. **(D)** Genus level. Data were expressed as mean ± SEM. *$P < 0.05$; n.s., not statistically significant.

enzymes (11). On the other hand, polyphenolic compounds are commonly recognized as xenobiotics by the enterocytes, which will induce stress (51). Thus, we investigated the effects of OE on oxidative stress in the small intestine of mice. Based on the activities of serum antioxidation enzymes, we then detected the transcript levels of Nrf2-associated antioxidant enzymes in the intestine, including *Sod*, *Cat*, and *Gpx* (52). In mice with severe oxidative stress status, previous studies have shown that extracts from olive oil and olive leaf ameliorated oxidative stress by up-regulating the Nrf2/ARE antioxidant signaling pathways (53, 54). Nrf2, a transcription factor, is activated and translocated to the nucleus during oxidative stress and enhances the expressions of Nrf2-related antioxidant enzymes (55). Interestingly, in this study, the qPCR results showed that OE treatment decreased jejunal and ileal *Sod*, *Cat*, *Gpx1*, and *Gpx2* expressions. Consistently, our study also indicated that OE

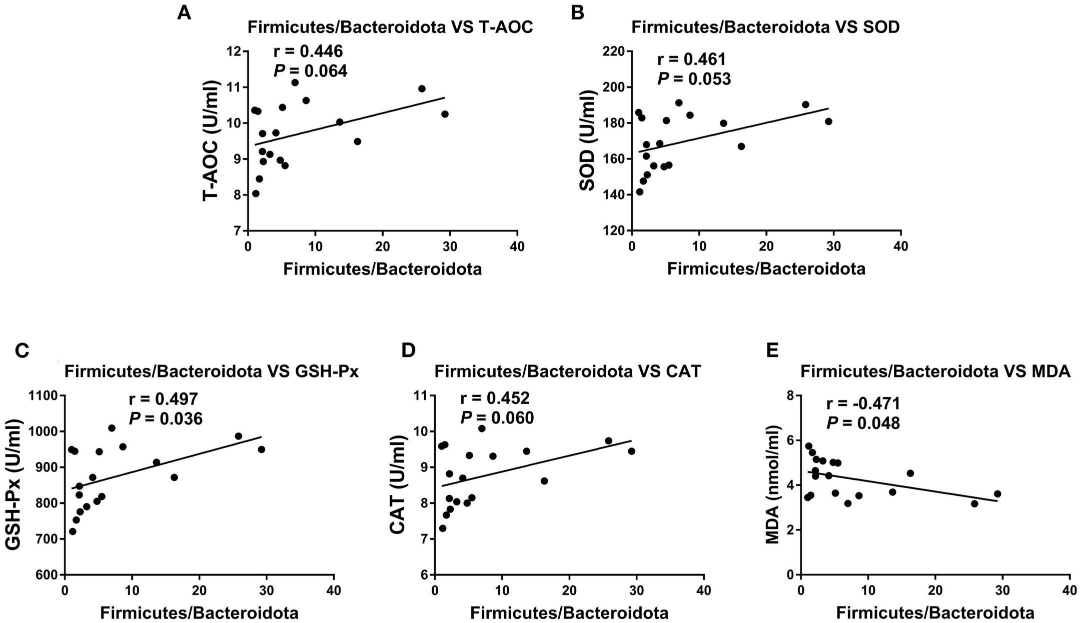

FIGURE 8 | Pearson correlation analyses between the colonic *Firmicutes/Bacteroidetes* ratio and serum antioxidant indicators and liver and kidney mRNA expression levels of TNF-α and IL-1β. **(A)** Correlation analyses between the *Firmicutes/Bacteroidetes* ratio and serum T-AOC. **(B)** Correlation analyses between the *Firmicutes/Bacteroidetes* ratio and serum SOD. **(C)** Correlation analyses between the *Firmicutes/Bacteroidetes* ratio and serum GSH-Px. **(D)** Correlation analyses between the *Firmicutes/Bacteroidetes* ratio and serum CAT. **(E)** Correlation analyses between the *Firmicutes/Bacteroidetes* ratio and serum MDA.

treatment increased the MDA concentration and decreased T-AOC in the jejunum and ileum. We speculated that this may be because OE acted as a xenobiotic, which can induce mild stress in the small intestine of mice (51). However, this slight oxidative stress had no negative effect on the small intestine, which was confirmed by the intestinal morphology without change after OE treatment.

In the meantime, amounts of inflammation-related transcription factors were activated under oxidative stress state, which will initiate the inflammatory process and lead to the increased production of pro-inflammatory cytokines (11). TNF-α and IL-1β are usually considered to be the two key regulators of pro-inflammatory response, which are involved in promoting inflammation and causing tissue damage (56). A previous study has demonstrated that olive extracts had anti-IL-1β activity in humans (57). An *in vitro* study also found that polyphenol-rich olive extracts decreased the mRNA expression of pro-inflammatory cytokines (58). Consistently, in this study, we also found that OE treatment decreased the mRNA expressions of TNF-α and IL-1β in the jejunum and ileum. However, interestingly, we found that the levels of inflammatory cytokines in the small intestine (jejunum and ileum) were all significantly increased, which may be caused by the OE-induced mild oxidative stress. Furthermore, we suggested that the absorption of OE in the small intestine caused down-regulation in mRNA expression of pro-inflammatory cytokines (TNF-α and IL-1β) to play anti-inflammatory activity. Based on the above-mentioned data, we speculated that OE tends to enhance the anti-inflammatory capacity by down-regulating the expressions of pro-inflammatory cytokines.

According to emerging evidence, the majority of dietary polyphenols (including HT) are metabolized by the colonic microbiota (59–61). Meanwhile, *in vivo* studies showed that both olive extracts with complex composition and individual phenolic compounds purified from olive extracts had the ability to modulate bacterial growth and reproduction in the intestine (21, 22). However, little is known about the effects of OE administration on the gut microbiota and whether the gut microbiota associates with the antioxidant and anti-inflammatory effects of OE in mice. Therefore, we analyzed the diversity of the colonic microbial community in OE-treated mice. The results showed that oral administration of OE supplement decreased the Shannon index, suggesting that OE lowered the α-diversity of colonic microbiota, which might be due to the anti-bacterial effects of OE. Additionally, LEfSe results showed that *Staphylococcales* are enriched in the OE group, suggesting that the increased *Staphylococcales* after OE treatment may be one of the reasons for the enhanced antioxidant capacity. Consistently, another study reported that *Staphylococcales* can reduce endogenous and exogenous oxidative stress (62). Besides that, at the phylum level, OE treatment increased the *Firmicutes/Bacteroidetes* ratio. As the main metabolites of colonic microbiota, the increased *Firmicutes/Bacteroidetes* ratio did not change the composition of SCFAs significantly in this study, which is in agreement with the previous study (63). To further examine whether OE-induced microbial alteration associates with its antioxidant effects, we conduct correlation analyses between the *Firmicutes/Bacteroidetes* ratio and serum antioxidant enzyme activities and MDA level by Pearson correlation analysis. Surprisingly, the results showed that the

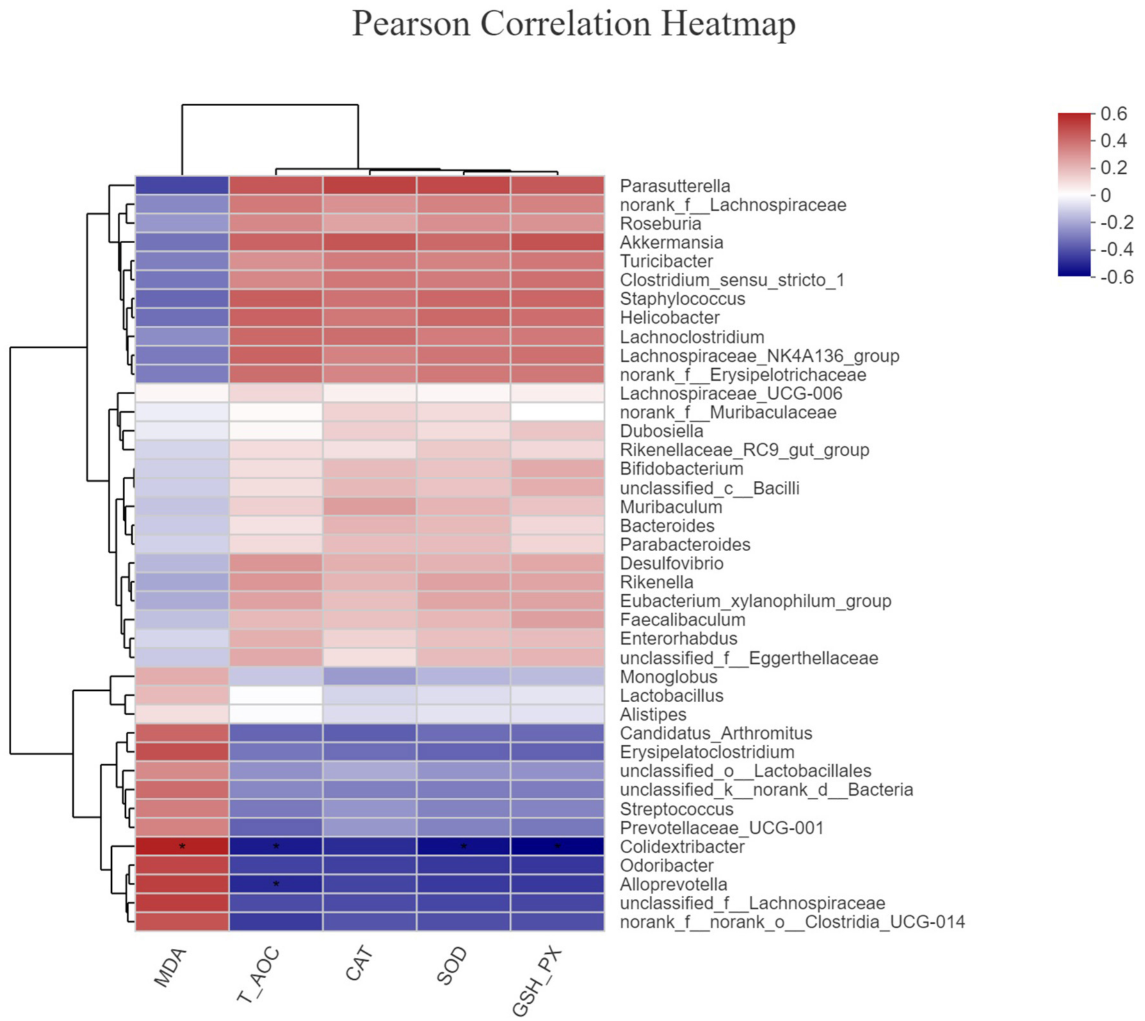

FIGURE 9 | The correlation between the gut microbial population at the genus level and the serum antioxidant indicators. $^*P < 0.05$.

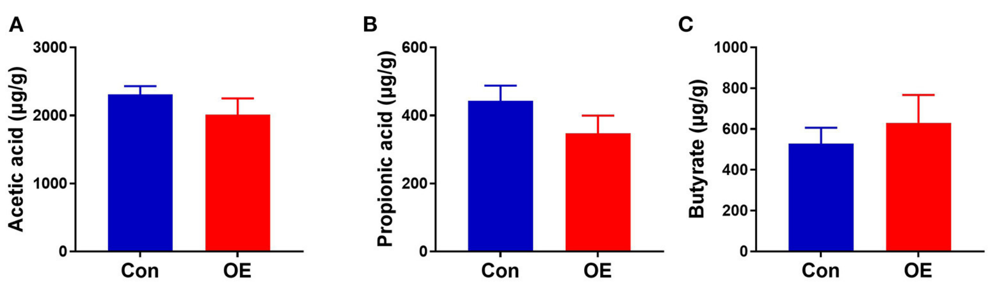

FIGURE 10 | Effects of olive fruit (*Canarium album* L.) extracts on the colonic short-chain fatty acid concentration. **(A)** Acetic acid. **(B)** Propionic acid. **(C)** Butyrate. Data were expressed as mean ± SEM.

Firmicutes/*Bacteroidetes* ratio was negatively correlated with the serum MDA content and positively correlated with the serum GSH-Px activity. In piglets and sows, studies have indicated that oxidative stress has a direct correlation with gut microbiota (64–67). This information in our study contributed to the new understanding of the OE-enhanced antioxidant capacity, at least in part, due to alterations in the gut microbiota in mice. In addition, *Firmicutes* are considered to be involved in maintaining intestinal barrier integrity, which plays a key role in modulating host inflammation (68). Meanwhile, bacteria in phylum *Bacteroidetes* have the ability to release LPS, which then leads to higher inflammatory responses (69). So, a decreased

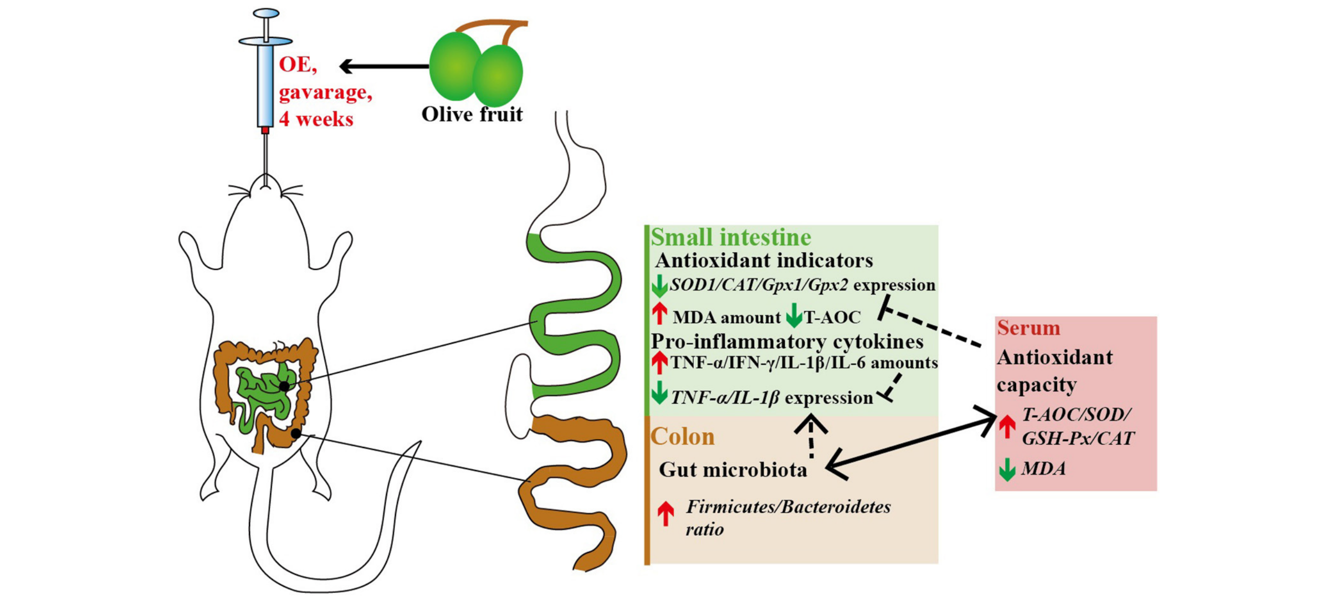

FIGURE 11 | Antioxidant and anti-inflammatory effects of olive fruit (*Canarium album* L.) extracts administration in mice: a possible mechanism.

proportion of *Bacteroidetes* may be related to lower inflammatory factors, which is consistent with our results. In humans, healthy adults who are more resistant to pathogens have a higher *Firmicutes*/*Bacteroidetes* ratio than infants and the elderly (70). Similarly, in piglets, a higher *Firmicutes*/*Bacteroidetes* ratio is associated with enhanced oxidative response and lower inflammation and infection risk (71–73). Therefore, it appears reasonable to speculate that OE administration exhibits antioxidant and anti-inflammatory effects closely associated with the increased *Firmicutes*/*Bacteroidetes* ratio in the colon of mice. At the genus level, *Alloprevotella* was highly negatively correlated with serum T-AOC. Similarly, Zhang et al. showed that OE can ameliorate oxidative stress and reduce the relative abundance of fecal *Alloprevotella* in LPS-challenged piglets (74), suggesting that *Alloprevotella* may play a role in enhancing antioxidant capacity. In addition, we also found that *Colidextribacter* is highly correlated with the levels of MDA, T-AOC, SOD, and GSH-Px in serum, which however needs further investigation.

Although OE contains various polyphenols, current evidence indicates that the beneficial health properties of OE are mainly related to HT, which needs more and further investigation (24–26). As summarized in **Figure 11**, in conclusion, our data provide a new insight that oral treatment with OE can improve the antioxidant capacity by enhancing the circulating activities of antioxidant enzymes, and the most important is that the improved antioxidant capacity is connected to the increased colonic *Firmicutes*/*Bacteroidetes* ratio as well as the change of *Alloprevotella* and *Colidextribacter* in mice.

DATA AVAILABILITY STATEMENT

The data used to support the findings of this study are available from the corresponding author upon request. Sequencing raw data on colonic microbiota of mice were deposited into the NCBI Sequence Read Archive (SRA) database (PRJNA681369).

ETHICS STATEMENT

The studies involving human participants were reviewed and approved by Experimental Animal Welfare and Ethical Committee of the Institute of Animal Science, Chinese Academy of Agricultural Sciences. The patients/participants provided their written informed consent to participate in this study. The animal study was reviewed and approved by Experimental Animal Welfare and Ethical Committee of the Institute of Animal Science, Chinese Academy of Agricultural Sciences. Written informed consent was obtained from the owners for the participation of their animals in this study.

AUTHOR CONTRIBUTIONS

MW and SZ conducted the study. MW, RZ, SZ, and FW helped to perform the experiment. MW, LC, and RZ helped to write the paper. BY and HZ designed the experiment and revised the manuscript. All authors contributed to the article and approved the submitted version.

FUNDING

This study was supported by the Major Scientific Research Tasks for Scientific and Technological Innovation Projects of the Chinese Academy of Agricultural Sciences (CAAS-ZDRW202006-02), National Natural Science Foundation of China (31702119), National Key Research and Development Program of China (2016YFD0500501), and China Agriculture Research System (CARS-41).

REFERENCES

1. Fuccelli R, Fabiani R, Rosignoli P. Hydroxytyrosol exerts anti-inflammatory and anti-oxidant activities in a mouse model of systemic inflammation. *Molecules*. (2018) 23:3212. doi: 10.3390/molecules23123212
2. Yin J, Liu M, Ren W, Duan J, Yang G, Zhao Y, et al. Effects of dietary supplementation with glutamate and aspartate on diquat-induced oxidative stress in piglets. *PLoS ONE*. (2015) 10:e0122893. doi: 10.1371/journal.pone.0122893
3. Matyas C, Haskó G, Liaudet L, Trojnar E, Pacher P. Interplay of cardiovascular mediators, oxidative stress and inflammation in liver disease and its complications. *Nat Rev Cardiol*. (2021) 18:117–35. doi: 10.1038/s41569-020-0433-5
4. He Y, Sang Z, Zhuo Y, Wang X, Guo Z, He L, et al. Transport stress induces pig jejunum tissue oxidative damage and results in autophagy/mitophagy activation. *J Anim Physiol Anim Nutr (Berl)*. (2019) 103:1521–9. doi: 10.1111/jpn.13161
5. Lykkesfeldt J, Svendsen O. Oxidants and antioxidants in disease: oxidative stress in farm animals. *Vet J*. (2007) 173:502–11. doi: 10.1016/j.tvjl.2006.06.005
6. Forrester SJ, Kikuchi DS, Hernandes MS, Xu Q, Griendling KK. Reactive oxygen species in metabolic and inflammatory signaling. *Circ Res*. (2018) 122:877–902. doi: 10.1161/circresaha.117.311401
7. Rojo de la Vega M, Chapman E, Zhang DD. NRF2 and the hallmarks of cancer. *Cancer Cell*. (2018) 34:21–43. doi: 10.1016/j.ccell.2018.03.022
8. Nguyen M, Wong YC, Ysselstein D, Severino A, Krainc D. Synaptic, mitochondrial, and lysosomal dysfunction in Parkinson's disease. *Trends Neurosci*. (2019) 42:140–9. doi: 10.1016/j.tins.2018.11.001
9. Milic M, Frustaci A, Del Bufalo A, Sánchez-Alarcón J, Valencia-Quintana R, Russo P, et al. DNA damage in non-communicable diseases: a clinical and epidemiological perspective. *Mutat Res*. (2015) 776:118–27. doi: 10.1016/j.mrfmmm.2014.11.009
10. Mishra V, Banga J, Silveyra P. Oxidative stress and cellular pathways of asthma and inflammation: therapeutic strategies and pharmacological targets. *Pharmacol Ther*. (2018) 181:169–82. doi: 10.1016/j.pharmthera.2017.08.011
11. Hussain T, Tan B, Yin Y, Blachier F, Tossou MC, Rahu N. Oxidative stress and inflammation: what polyphenols can do for us? *Oxid Med Cell Longevity*. (2016) 2016:7432797. doi: 10.1155/2016/7432797
12. Gupta A, Vij G, Chopra K. Possible role of oxidative stress and immunological activation in mouse model of chronic fatigue syndrome and its attenuation by olive extract. *J Neuroimmunol*. (2010) 226:3–7. doi: 10.1016/j.jneuroim.2010.05.021
13. Yeh YT, Cho YY, Hsieh SC, Chiang AN. Chinese olive extract ameliorates hepatic lipid accumulation *in vitro* and *in vivo* by regulating lipid metabolism. *Sci Rep*. (2018) 8:1057. doi: 10.1038/s41598-018-19553-1
14. Erol Ö, Arda N, Erdem G. Phenols of virgin olive oil protects nuclear DNA against oxidative damage in HeLa cells. *Food Chem Toxicol*. (2012) 50:3475–9. doi: 10.1016/j.fct.2012.07.048
15. Maalej A, Mahmoudi A, Bouallagui Z, Fki I, Marrekchi R, Sayadi S. Olive phenolic compounds attenuate deltamethrin-induced liver and kidney toxicity through regulating oxidative stress, inflammation and apoptosis. *Food Chem Toxicol*. (2017) 106:455–65. doi: 10.1016/j.fct.2017.06.010
16. Hermans N, Van der Auwera A, Breynaert A, Verlaet A, De Bruyne T, Van Gaal L, et al. A red yeast rice-olive extract supplement reduces biomarkers of oxidative stress, OxLDL and Lp-PLA(2), in subjects with metabolic syndrome: a randomised, double-blind, placebo-controlled trial. *Trials*. (2017) 18:302. doi: 10.1186/s13063-017-2058-5
17. Flamminii F, Di Mattia CD, Difonzo G, Neri L, Faieta M, Caponio F, et al. From by-product to food ingredient: evaluation of compositional and technological properties of olive-leaf phenolic extracts. *J Sci Food Agric*. (2019) 99:6620–7. doi: 10.1002/jsfa.9949
18. Weinbrenner T, Fitó M, de la Torre R, Saez GT, Rijken P, Tormos C, et al. Olive oils high in phenolic compounds modulate oxidative/antioxidative status in men. *J Nutr*. (2004) 134:2314–21. doi: 10.1093/jn/134.9.2314
19. Çoban J, Öztezcan S, Dogru-Abbasoglu S, Bingül I, Yeşil-Mizrak K, Uysal M. Olive leaf extract decreases age-induced oxidative stress in major organs of aged rats. *Geriatr Gerontol Int*. (2014) 14:996–1002. doi: 10.1111/ggi.12192
20. De Bruno A, Romeo R, Fedele FL, Sicari A, Piscopo A, Poiana M. Antioxidant activity shown by olive pomace extracts. *J Environ Sci Health B*. (2018) 53:526–33. doi: 10.1080/03601234.2018.1462928
21. Kishikawa A, Ashour A, Zhu Q, Yasuda M, Ishikawa H, Shimizu K. Multiple biological effects of olive oil by-products such as leaves, stems, flowers, olive milled waste, fruit pulp, and seeds of the olive plant on skin. *Phytother Res*. (2015) 29:877–86. doi: 10.1002/ptr.5326
22. Gilling DH, Ravishankar S, Bright KR. Antimicrobial efficacy of plant essential oils and extracts against *Escherichia coli*. *J Environ Sci Health A Tox Hazard Subst Environ Eng*. (2019) 54:608–16. doi: 10.1080/10934529.2019.1574153
23. Almayouf MA, El-Khadragy MF, Awad MA, Al-Olayan EM. The effects of silver nanoparticles biosynthesized using fig and olive extracts on cutaneous leishmaniasis induced inflammation in female Balb/c Mice. *Biosci Rep*. (2020) 40:BSR20202672. doi: 10.1042/BSR20202672
24. Basiricò L, Morera P, Dipasquale D, Bernini R, Santi L, Romani A, et al. (-)-Epigallocatechin-3-gallate and hydroxytyrosol improved antioxidative and anti-inflammatory responses in bovine mammary epithelial cells. *Animal*. (2019) 13:2847–56. doi: 10.1017/s1751731119001356
25. Yonezawa Y, Miyashita T, Nejishima H, Takeda Y, Imai K, Ogawa H. Anti-inflammatory effects of olive-derived hydroxytyrosol on lipopolysaccharide-induced inflammation in RAW264.7 cells. *J Vet Med Sci*. (2018) 80:1801–7. doi: 10.1292/jvms.18-0250
26. Fonollá J, Maldonado-Lobón JA, Luque R, Rodríguez C, Bañuelos Ó, López-Larramendi JL, et al. Effects of a combination of extracts from olive fruit and almonds skin on oxidative and inflammation markers in hypercholesterolemic subjects: a randomized controlled trial. *J Med Food*. (2020). doi: 10.1089/jmf.2020.0088. [Epub ahead of print].
27. Scoditti E, Carpi S, Massaro M, Pellegrino M, Polini B, Carluccio MA, et al. Hydroxytyrosol modulates adipocyte gene and miRNA expression under inflammatory condition. *Nutrients*. (2019) 11:2493. doi: 10.3390/nu11102493
28. Cardona F, Andrés-Lacueva C, Tulipani S, Tinahones FJ, Queipo-Ortuño MI. Benefits of polyphenols on gut microbiota and implications in human health. *J Nutr Biochem*. (2013) 24:1415–22. doi: 10.1016/j.jnutbio.2013.05.001
29. Santhakumar AB, Battino M, Alvarez-Suarez JM. Dietary polyphenols: structures, bioavailability and protective effects against atherosclerosis. *Food Chem Toxicol*. (2018) 113:49–65. doi: 10.1016/j.fct.2018.01.022
30. Conterno L, Martinelli F, Tamburini M, Fava F, Mancini A, Sordo M, et al. Measuring the impact of olive pomace enriched biscuits on the gut microbiota and its metabolic activity in mildly hypercholesterolaemic subjects. *Eur J Nutr*. (2019) 58:63–81. doi: 10.1007/s00394-017-1572-2
31. Millman J, Okamoto S, Kimura A, Uema T, Higa M, Yonamine M, et al. Metabolically and immunologically beneficial impact of extra virgin olive and flaxseed oils on composition of gut microbiota in mice. *Eur J Nutr*. (2020) 59:2411–25. doi: 10.1007/s00394-019-02088-0
32. Vezza T, Rodríguez-Nogales A, Algieri F, Garrido-Mesa J, Romero M, Sánchez M, et al. The metabolic and vascular protective effects of olive (*Olea europaea* L.) leaf extract in diet-induced obesity in mice are related to the amelioration of gut microbiota dysbiosis and to its immunomodulatory properties. *Pharmacol Res*. (2019) 150:104487. doi: 10.1016/j.phrs.2019.104487
33. Kahroba H, Ramezani B, Maadi H, Sadeghi MR, Jaberie H, Ramezani F. The role of Nrf2 in neural stem/progenitors cells: from maintaining stemness and self-renewal to promoting differentiation capability and facilitating therapeutic application in neurodegenerative disease. *Ageing Res Rev*. (2020) 65:101211. doi: 10.1016/j.arr.2020.101211
34. Stern M, McNew JA. A transition to degeneration triggered by oxidative stress in degenerative disorders. *Mol Psychiatry*. (2021) 26:736–46. doi: 10.1038/s41380-020-00943-9
35. Vatner SF, Zhang J, Oydanich M, Berkman T, Naftalovich R, Vatner DE. Healthful aging mediated by inhibition of oxidative stress. *Ageing Res Rev*. (2020) 64:101194. doi: 10.1016/j.arr.2020.101194
36. Martín-Vertedor D, Garrido M, Pariente JA, Espino J, Delgado-Adámez J. Bioavailability of bioactive molecules from olive leaf extracts and its functional value. *Phytother Res*. (2016) 30:1172–9. doi: 10.1002/ptr.5625
37. Medina E, Romero C, García P, Brenes M. Characterization of bioactive compounds in commercial olive leaf extracts, and olive leaves and their infusions. *Food Funct*. (2019) 10:4716–24. doi: 10.1039/c9fo00698b
38. Gorzynik-Debicka M, Przychodzen P, Cappello F, Kuban-Jankowska A, Marino Gammazza A, Knap N, et al. Potential health benefits of olive oil and plant polyphenols. *Int J Mol Sci*. (2018) 19:686. doi: 10.3390/ijms19030686
39. Martínez L, Castillo J, Ros G, Nieto G. Antioxidant and antimicrobial activity of rosemary, pomegranate and olive extracts in fish patties. *Antioxidants (Basel)*. (2019) 8:86. doi: 10.3390/antiox8040086

40. Schaffer S, Podstawa M, Visioli F, Bogani P, Müller WE, Eckert GP. Hydroxytyrosol-rich olive mill wastewater extract protects brain cells *in vitro* and *ex vivo*. *J Agric Food Chem*. (2007) 55:5043–9. doi: 10.1021/jf0703710
41. Sun L, Luo C, Liu J. Hydroxytyrosol induces apoptosis in human colon cancer cells through ROS generation. *Food Funct*. (2014) 5:1909–14. doi: 10.1039/c4fo00187g
42. Crupi R, Palma E, Siracusa R, Fusco R, Gugliandolo E, Cordaro M, et al. Protective effect of hydroxytyrosol against oxidative stress induced by the ochratoxin in kidney cells: *in vitro* and *in vivo* Study. *Front Vet Sci*. (2020) 7:136. doi: 10.3389/fvets.2020.00136
43. Loru D, Incani A, Deiana M, Corona G, Atzeri A, Melis MP, et al. Protective effect of hydroxytyrosol and tyrosol against oxidative stress in kidney cells. *Toxicol Ind Health*. (2009) 25:301–10. doi: 10.1177/0748233709103028
44. Martínez-Lara E, Peña A, Calahorra J, Cañuelo A, Siles E. Hydroxytyrosol decreases the oxidative and nitrosative stress levels and promotes angiogenesis through HIF-1 independent mechanisms in renal hypoxic cells. *Food Funct*. (2016) 7:540–8. doi: 10.1039/c5fo00928f
45. Lei XG, Zhu JH, Cheng WH, Bao Y, Ho YS, Redd2i AR, et al. Paradoxical roles of antioxidant enzymes: basic mechanisms and health implications. *Physiol Rev*. (2016) 96:307–64. doi: 10.1152/physrev.00010.2014
46. He L, He T, Farrar S, Ji L, Liu T, Ma X. Antioxidants maintain cellular redox homeostasis by elimination of reactive oxygen species. *Cell Physiol Biochem*. (2017) 44:532–53. doi: 10.1159/000485089
47. Chen M, Cai W, Zhao S, Shi L, Chen Y, Li X, et al. Oxidative stress-related biomarkers in saliva and gingival crevicular fluid associated with chronic periodontitis: a systematic review and meta-analysis. *J Clin Periodontol*. (2019) 46:608–22. doi: 10.1111/jcpe.13112
48. Ahlawat S, Asha, Sharma KK. Gut-organ axis: a microbial outreach and networking. *Lett Appl Microbiol*. (2020). doi: 10.1111/lam.13333. [Epub ahead of print].
49. Ringseis R, Gessner DK, Eder K. The gut-liver axis in the control of energy metabolism and food intake in animals. *Annu Rev Anim Biosci*. (2020) 8:295–319. doi: 10.1146/annurev-animal-021419-083852
50. Fraga CG, Croft KD, Kennedy DO, Tomás-Barberán FA. The effects of polyphenols and other bioactives on human health. *Food Funct*. (2019) 10:514–28. doi: 10.1039/c8fo01997e
51. Gessner DK, Ringseis R, Eder K. Potential of plant polyphenols to combat oxidative stress and inflammatory processes in farm animals. *J Anim Physiol Anim Nutr (Berl)*. (2017) 101:605–28. doi: 10.1111/jpn.12579
52. Zhang H, Davies KJA, Forman HJ. Oxidative stress response and Nrf2 signaling in aging. *Free Radic Biol Med*. (2015) 88:314–36. doi: 10.1016/j.freeradbiomed.2015.05.036
53. Marinić J, Broznić D, Milin C. Preexposure to olive oil polyphenols extract increases oxidative load and improves liver mass restoration after hepatectomy in mice *via* stress-sensitive genes. *Oxid Med Cell Longev*. (2016) 2016:9191407. doi: 10.1155/2016/9191407
54. Has AL, Alotaibi MF, Bin-Jumah M, Elgebaly H, Mahmoud AM. *Olea europaea* leaf extract up-regulates Nrf2/ARE/HO-1 signaling and attenuates cyclophosphamide-induced oxidative stress, inflammation and apoptosis in rat kidney. *Biomed Pharmacother*. (2019) 111:676–85. doi: 10.1016/j.biopha.2018.12.112
55. Omidian K, Rafiei H, Bandy B. Polyphenol inhibition of benzo[a]pyrene-induced oxidative stress and neoplastic transformation in an *in vitro* model of carcinogenesis. *Food Chem Toxicol*. (2017) 106:165–74. doi: 10.1016/j.fct.2017.05.037
56. Yahfoufi N, Alsadi N, Jambi M, Matar C. The immunomodulatory and anti-inflammatory role of polyphenols. *Nutrients*. (2018) 10:1618. doi: 10.3390/nu10111618
57. Wauquier F, Mevel E, Krisa S, Richard T, Valls J, Hornedo-Ortega R, et al. Chondroprotective properties of human-enriched serum following polyphenol extract absorption: results from an exploratory clinical trial. *Nutrients*. (2019) 11:9071. doi: 10.3390/nu11123071
58. Kountouri AM, Kaliora AC, Koumbi L, Andrikopoulos NK. *In-vitro* gastric cancer prevention by a polyphenol-rich extract from olives through induction of apoptosis. *Eur J Cancer Prev*. (2009) 18:33–9. doi: 10.1097/CEJ.0b013e3282fb75f7
59. Tuck KL, Freeman MP, Hayball PJ, Stretch GL, Stupans I. The *in vivo* fate of hydroxytyrosol and tyrosol, antioxidant phenolic constituents of olive oil, after intravenous and oral dosing of labeled compounds to rats. *J Nutr*. (2001) 131:1993–6. doi: 10.1093/jn/131.7.1993
60. Visioli F, Galli C, Bornet F, Mattei A, Patelli R, Galli G, et al. Olive oil phenolics are dose-dependently absorbed in humans. *FEBS Lett*. (2000) 468:159–60. doi: 10.1016/s0014-5793(00)01216-3
61. D'Angelo S, Manna C, Migliardi V, Mazzoni O, Morrica P, Capasso G, et al. Pharmacokinetics and metabolism of hydroxytyrosol, a natural antioxidant from olive oil. *Drug Metab Dispos*. (2001) 29:1492–8. doi: 10.1016/S1359-6446(01)01977-8
62. Gaupp R, Ledala N, Somerville GA. Staphylococcal response to oxidative stress. *Front Cell Infect Microbiol*. (2012) 2:33. doi: 10.3389/fcimb.2012.00033
63. Giuliani C, Marzorati M, Daghio M, Franzetti A, Innocenti M, Van de Wiele T, et al. Effects of olive and pomegranate by-products on human microbiota: a study using the SHIME(®) *in vitro* simulator. *Molecules*. (2019) 24:3791. doi: 10.3390/molecules24203791
64. Wang H, Hu C, Cheng C, Cui J, Ji Y, Hao X, et al. Unraveling the association of fecal microbiota and oxidative stress with stillbirth rate of sows. *Theriogenology*. (2019) 136:131–7. doi: 10.1016/j.theriogenology.2019.06.028
65. Qiao Y, Sun J, Ding Y, Le G, Shi Y. Alterations of the gut microbiota in high-fat diet mice is strongly linked to oxidative stress. *Appl Microbiol Biotechnol*. (2013) 97:1689–97. doi: 10.1007/s00253-012-4323-6
66. Li Y, Liu H, Zhang L, Yang Y, Lin Y, Zhuo Y, et al. Maternal dietary fiber composition during gestation induces changes in offspring antioxidative capacity, inflammatory response, and gut microbiota in a sow model. *Int J Mol Sci*. (2019) 21:31. doi: 10.3390/ijms21010031
67. Nie Y, Hu J, Hou Q, Zheng W, Zhang X, Yang T, et al. Lactobacillus frumenti improves antioxidant capacity *via* nitric oxide synthase 1 in intestinal epithelial cells. *Faseb J*. (2019) 33:10705–16. doi: 10.1096/fj.201900253RR
68. Louis P, Flint HJ. Formation of propionate and butyrate by the human colonic microbiota. *Environ Microbiol*. (2017) 19:29–41. doi: 10.1111/1462-2920.13589
69. Ortega-Hernández A, Martínez-Martínez E, Gómez-Gordo R, López-Andrés N, Fernández-Celis A, Gutiérrrez-Miranda B, et al. The interaction between mitochondrial oxidative stress and gut microbiota in the cardiometabolic consequences in diet-induced obese rats. *Antioxidants (Basel)*. (2020) 9:640. doi: 10.3390/antiox9070640
70. Mariat D, Firmesse O, Levenez F, Guimarăes V, Sokol H, Doré J, et al. The Firmicutes/Bacteroidetes ratio of the human microbiota changes with age. *BMC Microbiol*. (2009) 9:123. doi: 10.1186/1471-2180-9-123
71. Chae JP, Pajarillo EA, Oh JK, Kim H, Kang DK. Revealing the combined effects of lactulose and probiotic enterococci on the swine faecal microbiota using 454 pyrosequencing. *Microb Biotechnol*. (2016) 9:486–95. doi: 10.1111/1751-7915.12370
72. Molist F, Manzanilla EG, Pérez JF, Nyachoti CM. Coarse, but not finely ground, dietary fibre increases intestinal Firmicutes:Bacteroidetes ratio and reduces diarrhoea induced by experimental infection in piglets. *Br J Nutr*. (2012) 108:9–15. doi: 10.1017/s0007114511005216
73. Hu R, He Z, Liu M, Tan J, Zhang H, Hou DX, et al. Dietary protocatechuic acid ameliorates inflammation and up-regulates intestinal tight junction proteins by modulating gut microbiota in LPS-challenged piglets. *J Anim Sci Biotechnol*. (2020) 11:92. doi: 10.1186/s40104-020-00492-9
74. Yu Z, Zhao-Xi D, Mao-Long H, Xin ML, Jian-Xin L, Haifeng W. Olive extract ameliorates oxidative stress and inflammation, and protects intestinal villus and microbiota in piglets induced by Lipopolysaccharides. *Res Square*. (2021). doi: 10.21203/rs.3.rs-101171/v1. [Epub ahead of print].

Conflict of Interest: The authors declare that the research was conducted in the absence of any commercial or financial relationships that could be construed as a potential conflict of interest.

ORIGINAL RESEARCH
published: 13 April 2021
doi: 10.3389/fnut.2021.675445

Gut Microbiota Influence Lipid Metabolism of Skeletal Muscle in Pigs

Choufei Wu [1], Wentao Lyu [2], Qihua Hong [3], Xiaojun Zhang [4], Hua Yang [2]* and Yingping Xiao [2]*

[1] Key Laboratory of Vector Biology and Pathogen Control of Zhejiang Province, School of Life Sciences, Huzhou University, Huzhou, China, [2] State Key Laboratory for Managing Biotic and Chemical Threats to the Quality and Safety of Agro-Products, Institute of Agro-Product Safety and Nutrition, Zhejiang Academy of Agricultural Sciences, Hangzhou, China, [3] College of Animal Sciences, Zhejiang University, Hangzhou, China, [4] Institute of Animal Husbandry and Veterinary Medicine, Jinhua Academy of Agricultural Sciences, Jinhua, China

Gut microbiota is recognized as a strong determinant of host physiology including fat metabolism and can transfer obesity-associated phenotypes from donors to recipients. However, the relationship between gut microbiota and intramuscular fat (IMF) is still largely unknown. Obese Jinhua pigs (JP) have better meat quality that is associated with higher IMF content than lean Landrace pigs (LP). The present study was conducted to test the contribution of gut microbiota to IMF properties by transplanting fecal microbiota of adult JP and LP to antibiotics-treated mice. Similar to JP donors, the mice receiving JP's microbiota (JM) had elevated lipid and triglyceride levels and the lipoprotein lipase activity, as well as reduced mRNA level of angiopoietin-like 4 (ANGPTL4) in the gastrocnemius muscles, compared to those in mice receiving LP's microbiota (LM). High-throughput 16S rRNA sequencing confirmed that transplantation of JP and LP feces differently reconstructed the gut microbiota in both jejunum and colon of mouse recipients. In colonic samples, we observed an elevated ratio of Firmicutes to Bacteroidetes and increased abundance of genus *Romboutsia* in JM, which were positively correlated with obesity. Furthermore, the abundance of *Akkermansia* decreased in JM, which is positively correlated with lean. Colonic concentrations of acetate ($P = 0.047$) and butyrate ($P = 0.014$) were significantly lower in JM than in LM, and consistently, the terminal genes for butyrate synthesis, butyryl CoA: acetate CoA transferase were less abundant in colonic microbiota of JM. Taken together, these gut microbiota of obese JP intrinsically promotes IMF accumulation and can transfer the properties to mouse recipients. Manipulation of intestinal microbiota will, therefore, have the potential to improve the meat quality and flavor of pigs and even to ameliorate the metabolic syndrome in human.

Keywords: gut microbiota, fecal microbiota transplantation, lipid metabolism, intramuscular fat, pig

Edited by:
*Jie Yin,
Hunan Agricultural University, China*

Reviewed by:
*E. Xu,
Guizhou University, China
Jiangchao Zhao,
University of Arkansas, United States*

***Correspondence:**
*Hua Yang
yanghua@zaas.ac.cn
Yingping Xiao
ypxiaozj@hotmail.com*

Specialty section:
This article was submitted to Nutrition and Microbes, a section of the journal Frontiers in Nutrition

Received: *03 March 2021*
Accepted: *19 March 2021*
Published: *13 April 2021*

Citation:
Wu C, Lyu W, Hong Q, Zhang X, Yang H and Xiao Y (2021) Gut Microbiota Influence Lipid Metabolism of Skeletal Muscle in Pigs. Front. Nutr. 8:675445. doi: 10.3389/fnut.2021.675445

INTRODUCTION

China has the largest pork industry in the world. Growth rate, meat quality, and meat flavor are economically important in pig production that influence consumer acceptance (1, 2). In the past few decades, increasing lean meat content and reducing backfat thickness were the main targets of pig breeding (3). However, improvement of the sensory properties and nutritional value of pork has become a priority in recent years (4, 5), which is closely related to fatness traits such as intramuscular fat (IMF) content (6). Many studies have suggested that IMF have positive correlations with pork tenderness, juiciness, shearing force, and taste (7–9). Chinese local breeds such as Jinhua pig (JP) have distinctively higher IMF content and better meat quality than the introduced pig breeds, such as the Landrace (LP), which is a lean-type breed characterized by a fast growth rate and high lean meat content (10, 11). As muscles with sufficient IMF content are particularly suitable for conversion to dry products, JP is the excellent raw material of Jinhua-Ham, one of the most famous brands in China (10).

The genetic basis of IMF contents across multiple pig breeds has been investigated in several researches (10, 12, 13). However, the fact that the average heritability of IMF in the literature is only about 0.5 (ranging from 0.21 to 0.86) (14) suggests that alternative mechanisms for this trait in pigs may exist. As a forgotten organ in mammals that contains more genes than mammalian genome and that add a broad range of biological functions that the host could not otherwise perform, the gut microbiota has been proved to be a major contributor of obesity-associated phenotypes, as the propensity for adipogenesis can be transferred from donors to recipients through fecal microbiota transplantation (FMT) (15–19). There are also a few lines of evidence showing that the depletion of gut microbiota leads to increased muscle fatty acid catabolism (20) and ingestion of probiotics/prebiotic influences the skeletal muscle development and metabolic profile (21, 22). Moreover, the skeletal muscle properties are transmissible via FMT (23). These findings suggest a link between the gut microbiota composition and fat deposition in skeletal muscle.

One postulated mechanism underlying the interactions between gut microbiota and host fat metabolism relates to the regulation of lipoprotein lipase (LPL), a key enzyme in lipid metabolism by modulating intestinal epithelial expression of angiopoietin-like protein 4 (ANGPTL4/fasting-induced adipose factor, FIAF), a circulating LPL inhibitor susceptible to gut microbiota (24–26). Another mechanism involves the production of short-chain fatty acids (SCFAs), the major fermentation products of undigestible carbohydrates that are available to the gut microbiota. They are rapidly absorbed and utilized by the host and elicit effects on lipid metabolism and adipose tissue at several levels (27). LPL and SCFAs have also been associated with the IMF contents (28–31), while their functions in gut microbiota-mediated intramuscular fat metabolism remain unclear.

We have recently revealed significantly different gut microbiota structures between Jinhua pigs (a slow-growing breed with a high propensity for adipogenesis) and Landrace pigs (a lean, fast-growing breed with the high carcass yield), and found that gut microbiota plays an important role in contributing to adiposity in pigs (11, 19, 32). In the present study, we further compared the propensity for IMF accumulation between the two pig breeds and identified the contribution of gut microbiota by transplanting their respective fecal microbiota to antibiotic-treated mice, and the gut microbial community structure and IMF contents were monitored in mouse recipients. Our study uncovered a critical role of the gut microbiota in regulating the fat metabolism of skeletal muscle and provided a better understanding of the molecular mechanism.

METHODS

Animals

Pigs: Ten Jinhua and 10 Landrace pigs, with 5 males and 5 females of similar weights in each breed, were housed in the same environmentally controlled room in a swine breeding farm and fed a regular commercial corn-soybean diet. At 240 days of age, spontaneously excreted feces were collected freshly from each animal, mixed in equal amounts within the same breed to generate a "representative" fecal material for each breed.

Mice: A total of 24 28-day-old C57BL/6J mice (12 male and female each) were maintained in gnotobiotic isolators in SPF Animal Technology Co. (Beijing, China) under a strict 12-h light/dark cycle, and fed an autoclaved chow diet *ad libitum*.

Fecal Microbiota Transplantation

The stool suspension was then prepared as previously described (19). In brief, the fecal samples were diluted 5-fold (v/w) and homogenized in sterile pre-reduced phosphate buffer (PBS, 0.1 mol/L, pH7.2). After being thoroughly mixed and standing for 1 min, the supernatant was withdrawn and stored at −80°C in aliquots until used as the fecal inoculum.

Prior to fecal microbiota transplantation, the intestinal commensal bacteria was first depleted by the administration of an antibiotic cocktail (0.5 g/L vancomycin, 1 g/L neomycin sulfate, 1 g/L metronidazole, 1 g/L ampicillin) in drinking water ad lib according to our previous procedures (19). After 28 days of continuous treatment, the mice were randomly divided into 2 groups (12 in each group, half male and half female) and infused by intragastric gavage with fecal suspension of Jinhua or Landrace pigs respectively. The dosage was 0.2 mL per mouse once daily for 7 days. The mice were maintained for another 28-day after inoculation.

Sample Collection of Donors and Recipients

The gastrocnemius muscles (GM) from the pigs ($n = 10$ per breed) and mice ($n = 12$ per group) were sampled at euthanasia for RNA extraction and biochemical measurements. The jejunum and colon contents were obtained for 16S rRNA gene sequencing, qPCR, and SCFA analysis.

Quantitative PCR (qPCR)

Total RNA from the GM was isolated with RNeasy Plus Mini kit (Qiagen) and reverse-transcribed to synthesize cDNA using SuperScript II Reverse Transcriptase (Invitrogen) according to the manufactures' instructions. The cDNA library of each sample was then subjected to qPCR reactions in triplicate on an ABI Prism 7700 Detection system (Applied Biosystems, Foster City, CA, USA) using an annealing temperature of 63°C. The primers for LPL, ANGPTL4 and the internal standard of GAPDH were listed in **Table 1**. Data were normalized to GAPDH or 18S rRNA and calculated by the $2\text{-}\Delta\Delta CT$ method (33).

TABLE 1 | Primers of the target genes for pig and mouse used in RT-qPCR.

Species	Gene	Genbank Accession	Primer sequences(5′ to 3′)	Size (bp)
Pig	LPL	NM_214286.1	CCCTATACAAGAGGGAACCGGAT	138
			CCGCCATCCAGTCGATAAACGT	
	ANGPTL4	NM_001038644.1	CGACCTCCGAGGAGACAAGAA	108
			CGAGGGATGGAATGGAAGTACTG	
	GAPDH	AF017079	GGCAAATTCCACGGCACAGTCA	82
			CTCGCTCCTGGAAGATGGTGAT	
	18S	NR_046261	GCCCTATCAACTTTCGATGGTAGTC	113
			CCTTGGATGTGGTAGCCGTTTCTCA	
Mouse	LPL	NM_008509.2	CCAAGCTGGTGGGAAATGATGTG	95
			GCTGTACCCTAAGAGGTGGACGTT	
	ANGPTL4	NM_020581.2	CCTACAAGGATGGCTTCGGAGAT	86
			GCTTCCTCGGTTCCCTGTGAT	
	GAPDH	GU214026.1	CAGTATGACTCCACTCACGGCAA	100
			CTCGCTCCTGGAAGATGGTGAT	
	18S	NR_003278	CGGACACGGACAGGATTGACA	94
			CCAGACAAATCGCTCCACCAACTA	

TABLE 2 | Primers of key bacteria and genes in butyrate production used in qPCR analysis.

Item	Primers (5′ → 3′)
Clostridial cluster I	F:TACCHRAGGAGGAAGCCAC
	R:GTTCTTCCTAATCTCTACGCAT
Clostridial cluster IV	F:ATGCAAGTCGAGCGA(G/T)G
	R:TATGCGGTATTAATCT(C/T)CCTTT
Clostridial cluster XIVa	F:CGGTACCTGACTAAGAAG
	R:AGTTT(C/T)ATTCTTGCGAAC
Butyryl-CoA acetate-CoA transferase	F: AAGGATCTCGGIRTICAYWSIGARATG
	R:GAGGTCGTCICKRAAITYIGGRTGNGC
Butyrate kinase	F:TGCTGTWGTTGGWAGAGGYGGA
	R:GCAACIGCYTTTTGATTTAATGCATGG

Measurement of IMF Content

The IMF contents were measured using the Soxhlet method according to our previous study (32).

Biochemical and Enzymatic Measurements

GM samples (∼100 mg) were homogenized in 1 ml of ice-cold PBS. After centrifugation at 2500 rpm for 10 min at 4°C, the supernatant was decanted for measuring LPL activity and the triglyceride content with a LPL assay kit and a triglyceride assay kit (Jiancheng Bioengineering Ltd, Nanjing, China) according to the manufacturer's instructions, respectively. The LPL activity was expressed as U/mg protein of muscle tissue, and the triglyceride content was expressed as mmol/g protein of muscle tissue.

DNA Extraction and Microbiota Analysis

The genomic DNA was extracted from the jejunal and colonic contents of mice using QIAamp DNA Stool Mini Kit (QIAGEN, Valencia, CA, USA). The 16S rRNA gene sequencing and data analysis were performed as described previously (34). Briefly, the V3 and V4 region of bacterial 16S rRNA gene was amplified from each genomic DNA sample by using the barcode-fusion primers 341F and 806R. The DNA libraries were then constructed using TruSeq DNA PCR-Free Library Preparation Kit (Illumina) and sequenced on an Illumina MiSeq platform. To obtain clean sequencing data, the chimeric reads were identified and removed by using USEARCH. Operational taxonomic units (OTUs) were assembled at 97% sequence similarity. A representative sequence was picked for each OTU and annotated with taxonomic information using the RDP classifier (35). Pie charts showing taxa distribution at the phylum and genus levels were constructed. Principal coordinate analysis (PCoA) was conducted to illustrate the β-diversity based on weighted UniFrac distances.

Analysis of Short-Chain Fatty Acids

The concentrations of SCFAs were measured by gas chromatography (GC) using the method as described in our previous report (36). Briefly, 0.1 g of the colonic contents were vortex-mixed vigorously with 10 mL deionized water. After the mixture were centrifuged (12,000 rpm for 10 min), 500 µL aliquots of the supernatant were added to 100 µL of 25% (w/v) metaphosphoric acid and crotonic acid (internal standard). The mixed solution was filtered with a 0.22 µm mesh and was then employed to measure the concentrations of SCFAs by GC (GC-2010 plus, Shimadzu, Kyoto, Japan).

qPCR Analysis of Key Bacteria and Genes in Butyrate Production

The abundances of the major butyrate-producing bacteria, clostridial cluster I, IV, and XIVa and the terminal genes for butyrate synthesis, butyrate kinase (BK) and butyryl CoA: acetate CoA transferase (BCoAT) in mice colon contents were assessed by qPCR on an ABI Prism 7700 detection system (Applied

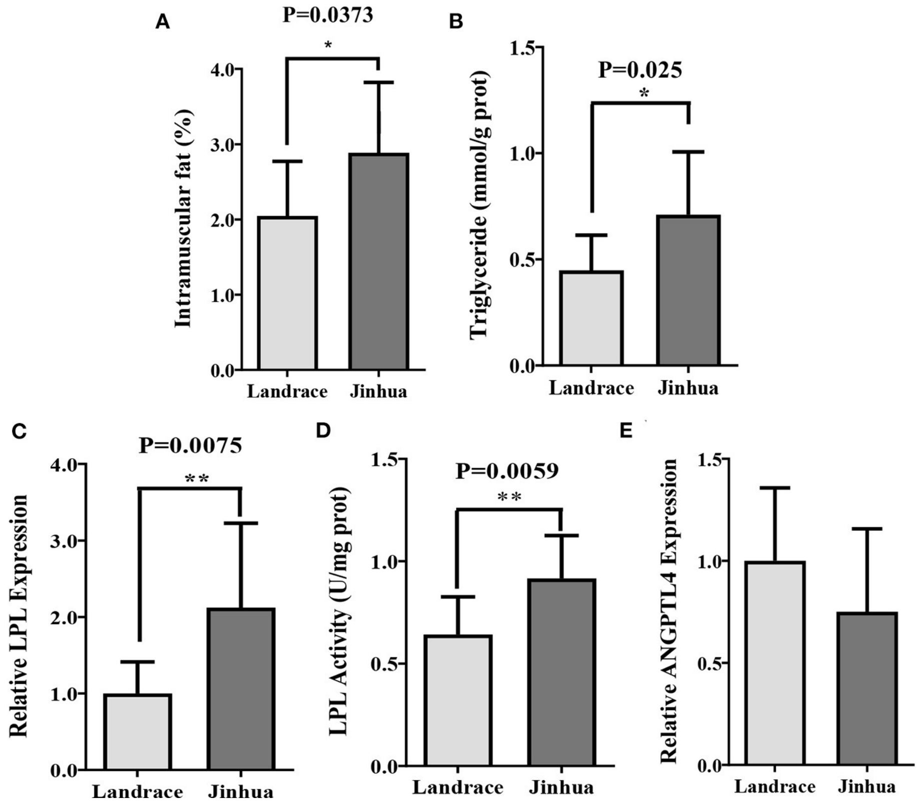

FIGURE 1 | Intramuscular fat deposition in Landrace and Jinhua pigs. Intramuscular fat **(A)**, triglyceride **(B)**, relative lipoprotein lipase (LPL) expression **(C)** and activity **(D)**, and relative ANGPTL4 expression **(E)** in gastrocnemius muscle of Landrace and Jinhua pigs. The results were shown as means ± SEM of 10 pigs. $^{*}P < 0.05$; $^{**}P < 0.01$.

Biosystems, Foster City, CA, USA) using the extracted DNA as templates and SYBR Green PCR Master Mix (Takara, Japan), as previously described (34, 37). DNA was amplified under the following conditions: 95°C for 2 min, and 35 cycles of 15 s at 95°C, 45 s at 58°C, and 1 min at 72°C. Each sample was analyzed in triplicate. The primer sets used were listed in **Table 2**. All qPCR results were expressed as gene copies per g of colon contents.

Statistical Analysis

Data are expressed as means ± SEM. All statistical analyses were performed using SPSS (SPSS, Chicago, IL, United States). Unpaired two-tailed Student's *t*-test was used to evaluate the differences between two groups. A *P*-value < 0.05 was considered a significant difference.

RESULTS

Jinhua Pigs Were More Efficient in IMF Deposition Than Landrace Pigs

To observe the differences in intramuscular fat (IMF) metabolism between the Jinhua and Landrace pigs, the two breeds were sacrificed at 240 days of age and the gastrocnemius muscles (GM) were sampled. As shown in **Figures 1A,B**, the Jinhua pigs had significantly higher level of intramuscular fat ($P = 0.0373$) and triglycerides ($P = 0.025$) than the Landrace pigs. Consistently, both the expression level ($P = 0.0075$) and activity ($P = 0.0059$) of lipoprotein lipase (LPL, **Figures 1C,D**) were elevated in GM samples of Jinhua pigs (**Figure 1E**). These findings were in accordance with the fact that Jinhua pigs are more efficient in IMF deposition than Landrace pigs.

Mouse Recipients Resembled Their Respective Pig Donors in IMF Deposition

To elucidate whether the IMF metabolic profiles were also affected by gut microbiota, FMT was carried out and triglyceride content, LPL expression and activity, as well as ANGPTL4 mRNA level in GM of mouse recipients were examined. Remarkably higher intramuscular levels of triglyceride content and LPL expression and activity in mouse recipients of Jinhua's feces (JM) than those in mouse recipients of Landrce pigs' feces (LM) were observed (**Figures 2A–C**). Furthermore, the ANGPTL4 mRNA expression level in JM was shown to be correspondingly was decreased compared to LM (**Figure 2D**). Collectively, the mouse recipients exhibited similar characteristics in IMF metabolism as their respective pig donors, suggesting that gut microbiota is capable of influencing and transferring the IMF trait across species.

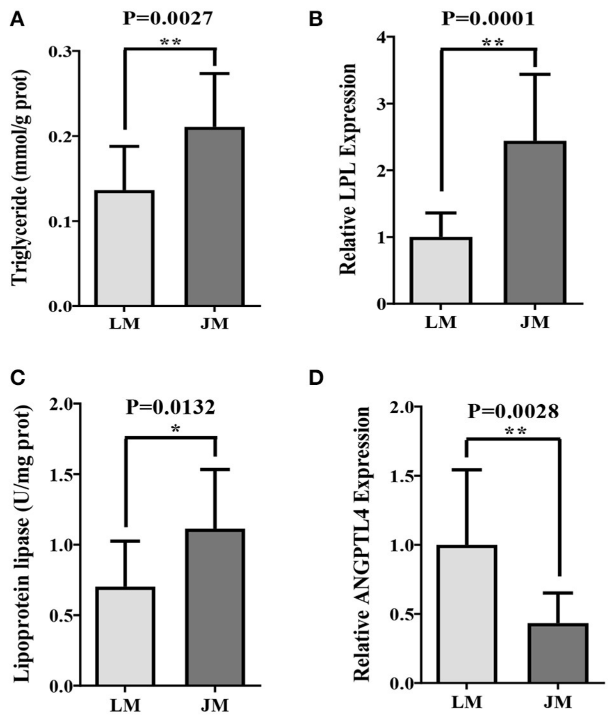

FIGURE 2 | Intramuscular fat deposition in mice receiving fecal microbiota of Landrace and Jinhua pigs. Intramuscular triglyceride **(A)**, relative lipoprotein lipase (LPL) expression **(B)** and activity **(C)**, and relative ANGPTL4 expression **(D)** in gastrocnemius muscle of mouse recipients. JM, mice receiving fecal microbiota from Jinhua pigs; LM, mice receiving fecal microbiota from Landrace pigs. $^{*}P < 0.05$; $^{**}P < 0.01$.

Gut Microbiota of Mouse Recipients Were Differently Reconstructed by FMT From Jinhua and Landrace Pigs

To identify the gut microbiota throughout the small and large intestine in the two groups of mouse recipients, the jejunal and colonic contents were obtained from individual mice and subjected to 16S rRNA gene sequencing. A total of 2,243,174 clean reads with an average length of 418 bps were generated from all samples, which were further grouped into 682 OTUs at the 97% identity level, with an average OTU number of 173 per sample (range = 103 ∼ 355, SEM = 60.70). Taxonomic analysis showed that Firmicutes, Bacterioidetes, Verrucomicrobia, and Proteobacteria were the most abundant phyla in both jejunum and colon, accounting for more than 90% of the total sequences in most samples (**Figures 3**, **4**). The ratio of Firmicutes to Bacteroidetes that was associated with the obesity phenotype was remarkably lower in jejunal samples of JM group than in those of LM group (**Figure 3A**), while it was elevated in colonic samples of JM group as compared to those of LM group (**Figure 4A**). Verrucomicrobia was greatly less abundant in both jejunum and colon of JM group as compared to LM group, while Proteobacteria was more prevalent in the jejunum of JM group than in LM group.

At the genus level, Lactobacillus, Akkermansia, Streptophyta, Bacteroides, and Clostridium XIVa were among the most abundant genera in the jejunum (**Figure 3**). Lactobacillus and Akkermansia made up larger proportions in the jejunum of LM group than in JM group, while Streptophyta and Bacteroides were more enriched in JM group. Notably, Clostridium XIVa, a main genus of butyrate-producing bacteria was remarkably reduced in the jejunum of JM (**Figures 3A,B**). In colon samples, Bacteroides, Lactobacillus, Akkermansia, Parabacterioides, and Rombontsia constituted the top five genera in both groups of mice. Among them, Bacteroides and Akkermansia decreased while Lactobacillus, and Rombontsia increased in the colon of JM group compared to LM (**Figure 4B**).

To evaluate the degree of discrepancy between the bacterial community structures of mouse recipients, a principal coordinate analysis (PCoA) was performed. As delineated in **Figure 5**, the microbiota in the jejunum and colon were significantly different by both PCoA1 and PCoA2. They were further separated according to their respective donors by PCoA1 (for jejunal samples) or both coordinates (for colonic samples), suggesting that transplantation of Landrace and Jinhua feces differently reconstructed the gut microbiota in both small and large intestines of mouse recipients.

Colonic Concentrations of Acetate and Butyrate Were Lower in JM

To investigate the difference of SCFA in the mouse recipients, the colonic concentrations of acetate, propionate, butyrate, iso-butyrate, valerate, and iso-valerate were assessed. The concentrations of acetate ($P = 0.047$) and butyrate ($P = 0.014$), as well as total SCFA ($P = 0.042$) were significantly lower in the colon of JM than in LM, while no differences were observed in propionate, butyrate, iso-butyrate, valerate, and iso-valerate between the two groups (**Table 3**).

Key Genes in Butyrate Biosynthesis Were Less Abundant in Colonic Microbiome of JM

Based on the observation that butyrate was remarkably decreased in the colon of LM, we further examined the abundances of the major butyrate-producing bacteria, clostridial cluster I, IV, and XIVa and the terminal genes for butyrate synthesis, butyrate kinase (BK) and butyryl CoA: acetate CoA transferase (BCoAT) in colonic contents of the two groups of mouse recipients by qPCR. As shown in **Table 4**, although the abundance of clostridial clusters of butyrate-producing bacteria was comparable in between JM and LM, the copies of BK and BCoAT genes were significantly fewer in the colonic samples of JM, consistent with the diminished production of butyrate in JM.

DISCUSSION

Over the last decade, extensive research has revealed a critical role of gut microbiota in the physiology of both fat deposition and obesity by affecting host energy harvest and fat metabolism (16–19, 38). There is substantial evidence indicating that skeletal

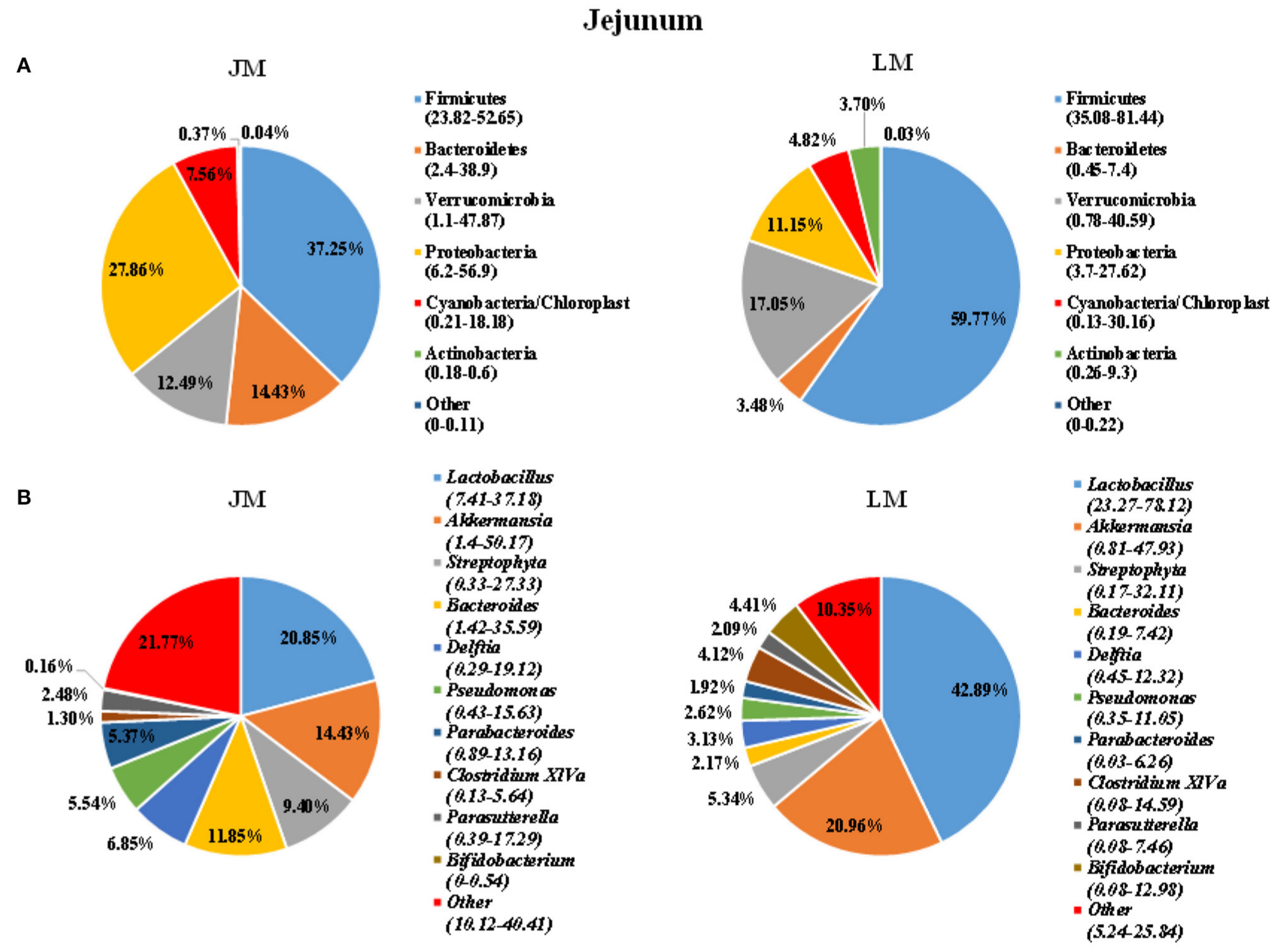

FIGURE 3 | Pie charts showing taxa distribution of bacterial community in jejunum of mouse recipients at the phylum **(A)** and genus **(B)** levels. Top 6 phyla and top 10 genera are shown.

muscle properties including lipid metabolic profile and fiber characteristics are closely linked to the presence of obesity (23, 39). Some researchers suggest that a gut microbiota-muscle axis might exist in the body (40). However, less attention has been paid to the association between the gut microbiota and IMF accumulation.

Jinhua and Landrace pigs display notable differences in the body fat content and propensity for adipogenesis, which make them good models to study human overweight and obesity (32, 41, 42). Our previous study has proved that gut microbiota of obese Jinhua pigs is capable of enhancing adipogenesis and fat deposition than that of lean Landrace pigs, and that the obesity-associated phenotypes is transferrable across species (23). Here, we further demonstrated that Jinhua pig-derived microbiota also enhances IMF content in their mouse recipients (JM) of FMT. Both Jinhua pig and JM exhibited higher triglyceride concentrations and LPL expression and activity in skeletal muscle as compared to LP and LM, respectively. LPL provides fatty acid for tissue utilization and storage and can be inhibited by ANGPTL4 that is susceptible to regulation by gut microbiota and its metabolites, SCFA (24–26). In line with the increased expression and activity of LPL, the expression level of ANGPTL4 in GM was found to be correspondingly decreased in both Jinhua pigs and JM. These findings support an implication of gut microbiota in intramuscular adipogenesis.

The feces and large intestinal contents are often analyzed to indicate the alterations in gut microbiota of FMT recipients. However, the impact of FMT on the microbiota in small intestine is barely known. To clarify that, jejunum microbiota of mouse recipients was analyzed in our present study. Significant differences were found between the two groups of mice. The phyla of Bacterioidetes and Proteobacteria, and the genera of Streptophyta and Bacteroides were more enriched in jejunum samples of JM group, while the phylum of Firmicutes and Verrucomicrobia and the genera of Lactobacillus, Akkermansia and Clostridium XIVa were more abundant in jejunum samples of LM. This data suggested that microbiota in small intestines of mouse recipients were also reconstructed following FMT.

In colonic samples, we observed an elevated ratio of Firmicutes to Bacteroidetes in JM, which may led to the

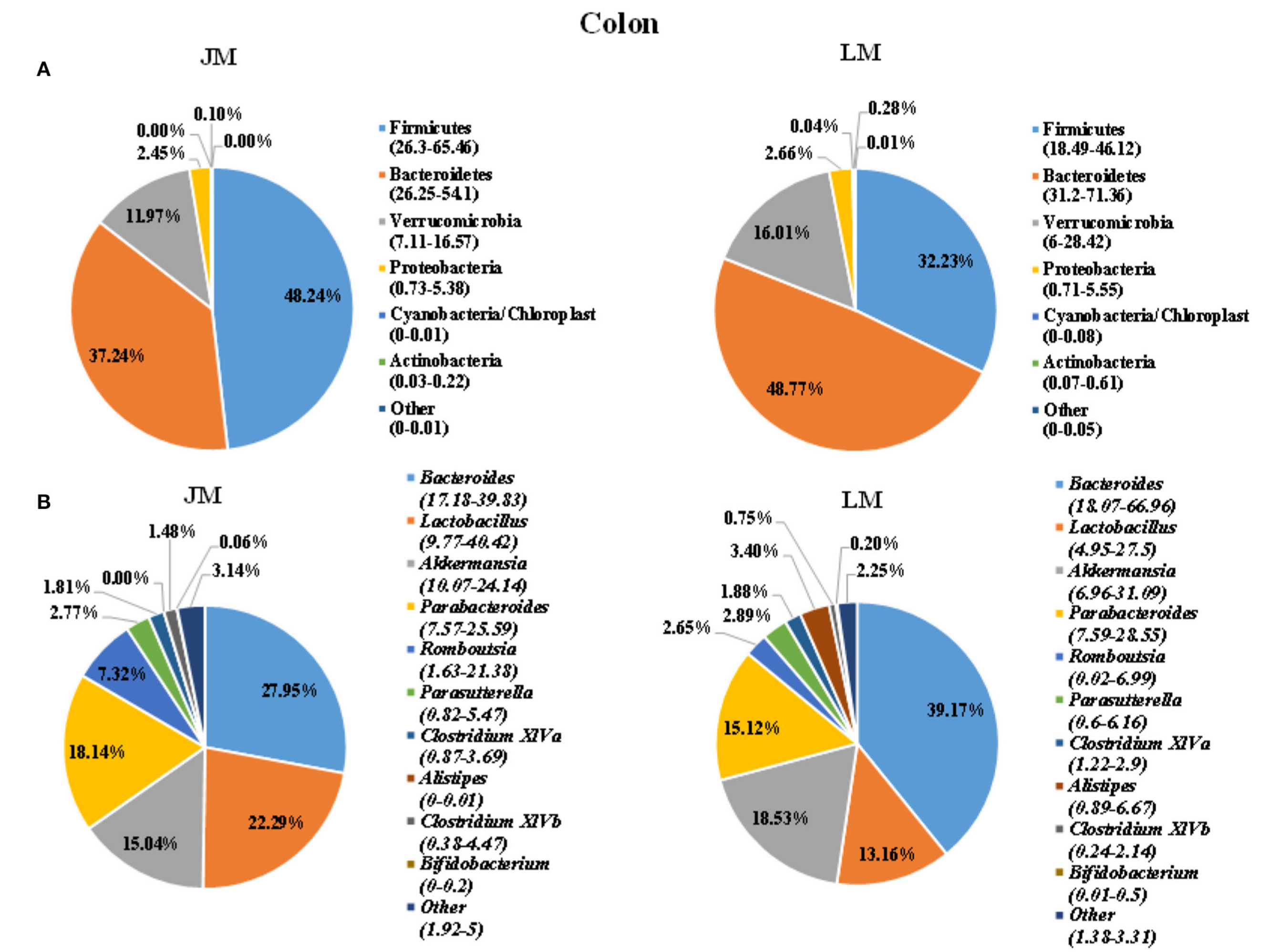

FIGURE 4 | Pie charts showing taxa distribution of bacterial community in colon of mouse recipients at the phylum **(A)** and genus **(B)** levels. Top 6 phyla and top 10 genera are shown.

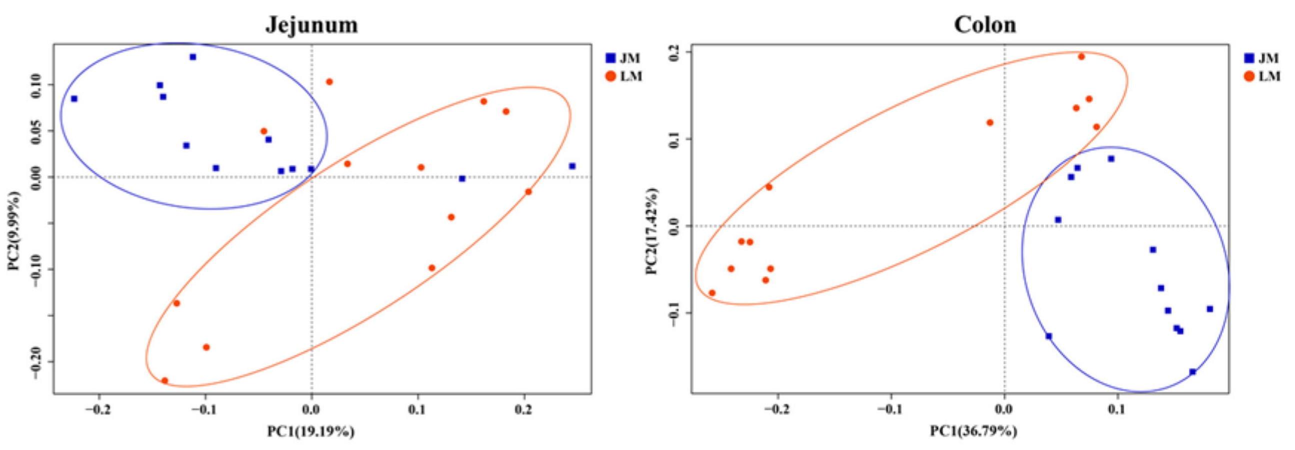

FIGURE 5 | Principal coordinates analysis (PCoA) of the jejunum and colon bacterial community composition of mouse recipients based on unweighted unifrac distance.

TABLE 3 | The concentration of short-chain fatty acids in the colon of mice receiving fecal microbiota of Jinhua and Landrace pigs.

Items	JM	LM	SEM	*P*-value
Acetate	1.84	2.37	0.21	0.047
Propionate	0.44	0.41	0.11	0.721
Butyrate	0.30	0.52	0.08	0.014
Iso-butyrate	0.22	0.25	0.07	0.589
Valerate	0.18	0.10	0.09	0.314
Iso-valerate	0.16	0.19	0.1	0.263
Total SCFAs	3.14	3.84	0.32	0.042

The concentrations of SCFAs were expressed as mg/g of fresh colonic contents.

TABLE 4 | The abundances of butyrate-producing bacteria and terminal genes for butyrate synthesis in the colon of mice receiving fecal microbiota of Jinhua and Landrace pigs.

Item	JM	LM	SEM	*P*-value
Clostridial cluster I	6.56	7.21	0.93	0.109
Clostridial cluster IV	5.85	6.08	0.52	0.210
Clostridial cluster XIVa	8.15	8.43	1.09	0.662
Butyryl-CoA acetate-CoA transferase	6.21	7.19	0.58	0.041
Butyrate kinase	5.97	6.63	0.71	0.076

The abundance of bacterial groups was expressed as log10 16S rRNA gene copies/g of fresh colonic contents and of genes related to butyrate synthesis was expressed as log10 gene copies of total DNA/g of fresh colonic contents.

development of obesity in human and rodents (24). Genus Romboutsia that is positively correlated with obesity (43) was also increased in the colon of JM. On the other hand, a significant diminishment of genus Bacteroides, an important SCFA producer, was observed, which was consistent with the reduced level of colonic SCFAs in JM. SCFAs act as substrates or signal molecules, which are transported into blood from the intestinal lumen and subsequently taken up by body organs in the host (44, 45). The SCFA can induce the transcription and secretion of ANGPTL4 in intestinal cells and adipocyte, and the elevations of ANGPTL4 have been reported to be associated with the inhibition of fat deposition (46). Taken together, the modulation of colonic microbiota and the decreased SCFAs generation esp. acetate and butyrate in JM might positively contribute to the intramuscular adipogenesis in mouse recipients.

Some researchers have reported that dietary supplementation of butyrate can prevent diet-induced insulin resistance and obesity by promoting energy expenditure and induce mitochondria function (46, 47) and can decrease IMF content in mice and Broilers (30, 48). Here we found a remarkable decrease of colonically derived butyrate in JM compared with that in LM, which might contribute to the higher IMF content in JM. However, the abundances of the major butyrate-producing bacteria, clostridial cluster I, IV, and XIVa were comparable in the colon between JM and LM as determined by qPCR, perhaps because these clostridial clusters still harbor a diverse collection of non-butyrate producers. Therefore, assessing terminal genes of butyrate synthesis pathways, namely, the butyrate kinase (BK) pathway and the butyryl CoA: acetate CoA transferase (BCoAT) pathway, could be valuable to indicate the activity of the butyrate producer (37, 49). Fewer copies of BK and BCoAT genes were detected in the colon of JM samples by qPCR, suggesting a decreased abundance or activity of butyrate-producing bacterial community and explaining the diminished production of butyrate in JM.

CONCLUSION

Our results demonstrated that Jinhua pig has a higher IMF content than Landrace pig and the phenotype could be recapitulated by gut microbiota in respective mouse recipients. The mechanism might be related to the regulation of ANGPTL4 and consequently LPL expression and activity, as well as to the modulation of colonically derived SCFAs. This study has opened possibilities for manipulating the meat quality and the sensory properties of lean commercial pig breeds through modulating the gut microbiota. Moreover, it might provide a model to investigate the link of gut microbiota with the distribution of adipose tissue and deposition of ectopic fat in human.

DATA AVAILABILITY STATEMENT

The datasets presented in this study can be found in online repositories. The names of the repository/repositories and accession number(s) can be found here: NCBI Sequence Read Archive (SRA) with accession number PRJNA707602.

ETHICS STATEMENT

The animal study was reviewed and approved by the Animal Care and Use Committee of Zhejiang Academy of Agricultural Sciences.

AUTHOR CONTRIBUTIONS

CW, YX, and HY designed the experiment. CW, WL, QH, XZ, and YX conducted the animal experiments. CW, HY, and YX wrote and revised the manuscript. CW, QH, HY, and YX did experimental analysis, collected, and analyzed the data. All authors reviewed the manuscript.

FUNDING

This research was funded by the National Natural Science Foundation of China (31972999) and State Key Laboratory for Managing Biotic and Chemical Threats to the Quality and Safety of Agro-products (2010DS700124-ZZ1905).

REFERENCES

1. Sato S, Uemoto Y, Kikuchi T, Egawa S, Kohira K, Saito T, et al. Genome-wide association studies reveal additional related loci for fatty acid composition in a Duroc pig multigenerational population. *Anim Sci J.* (2017) 88:1482–90. doi: 10.1111/asj.12793
2. Won S, Jung J, Park E, Kim H. Identification of genes related to intramuscular fat content of pigs using genome-wide association study. *Asian-Australas J Anim Sci.* (2018) 31:157–62. doi: 10.5713/ajas.17.0218
3. Dong Q, Liu H, Li X, Wei W, Zhao S, Cao J. A genome-wide association study of five meat quality traits in Yorkshire pigs. *Front Agric Sci Eng.* (2014) 1:137–43. doi: 10.15302/J-FASE-2014014
4. Fan B, Lkhagvadorj S, Cai W, Young J, Smith RM, Dekkers JCM, et al. Identification of genetic markers associated with residual feed intake and meat quality traits in the pig. *Meat Sci.* (2010) 84:645–50. doi: 10.1016/j.meatsci.2009.10.025
5. Franco D, Vazquez JA, Lorenzo JM. Growth performance, carcass and meat quality of the Celta pig crossbred with Duroc and Landrance genotypes. *Meat Sci.* (2014) 96:195–202. doi: 10.1016/j.meatsci.2013.06.024
6. Hausman GJ, Dodson MV, Ajuwon K, Azain M, Barnes KM, Guan LL, et al. BOARD-INVITED REVIEW: The biology and regulation of preadipocytes and adipocytes in meat animals. *J Anim Sci.* (2009) 87:1218–46. doi: 10.2527/jas.2008-1427
7. Hocquette J, Gondret F, Baéza E, Médale F, Jurie C, Pethick D. Intramuscular fat content in meat-producing animals: development, genetic and nutritional control, and identification of putative markers. *Animal.* (2010) 4:303–19. doi: 10.1017/S1751731109991091
8. Cho I, Yoo C, Lee J, Jung E, Han S, Lee S, et al. Genome-wide QTL analysis of meat quality-related traits in a large F 2 intercross between Landrace and Korean native pigs. *Genet Sel Evol.* (2015) 47:7. doi: 10.1186/s12711-014-0080-6
9. Gong H, Xiao S, Li W, Huang T, Huang X, Yan G, et al. Unravelling the genetic loci for growth and carcass traits in Chinese Bamaxiang pigs based on a 1.4 million SNP array. *J Anim Breed Genet.* (2018) 136:3–14. doi: 10.1111/jbg.12365
10. Wu T, Zhang Z, Yuan Z, Lo L, Chen J, Wang Y, et al. Distinctive genes determine different intramuscular fat and muscle fiber ratios of the longissimus dorsi muscles in Jinhua and landrace pigs. *PLoS ONE.* (2013) 8:e53181. doi: 10.1371/journal.pone.0053181
11. Gong Y, Zou X, Xia W, Wen X, Yang H. Comparative metabolomic analysis of caecal digesta between Jinhua pig and Landrace pig. *Czech J Anim Sci.* (2019) 64:332–42. doi: 10.17221/43/2018-CJAS
12. Wang Z, Li Q, Chamba Y, Zhang B, Shang P, Zhang H, et al. Identification of genes related to growth and lipid deposition from transcriptome profiles of pig muscle tissue. *PLoS One.* (2015) 10:e0141138. doi: 10.1371/journal.pone.0141138
13. Ding R, Yang M, Quan J, Li S, Zhuang Z, Zhou S, et al. Single-locus and multi-locus genome-wide association studies for intramuscular fat in Duroc pigs. *Front Genet.* (2019) 10:619. doi: 10.3389/fgene.2019.00619
14. Davoli R, Luise D, Mingazzini V, Zambonelli P, Braglia S, Serra A, et al. Genome-wide study on intramuscular fat in Italian Large White pig breed using the PorcineSNP60 BeadChip. *J Anim Breed Genet.* (2016) 133:277–82. doi: 10.1111/jbg.12189
15. Ley RE, Lozupone CA, Hamady M, Knight R, Gordon JI. Worlds within worlds: evolution of the vertebrate gut microbiota. *Nat Rev Microbiol.* (2008) 6:776–88. doi: 10.1038/nrmicro1978
16. Turnbaugh PJ, Hamady M, Yatsunenko T, Cantarel BL, Duncan A, Ley RE, et al. A core gut microbiome in obese and lean twins. *Nature.* (2009) 457:480–4. doi: 10.1038/nature07540
17. Turnbaugh PJ, Bäckhed F, Fulton L, Gordon JI. Diet-induced obesity is linked to marked but reversible alterations in the mouse distal gut microbiome. *Cell Host Microbe.* (2008) 3:213–23. doi: 10.1016/j.chom.2008.02.015
18. Turnbaugh PJ, Ley R, Mahowald M, Magrini V, Mardis ER, Gordon JI. An obesity-associated gut microbiome with increased capacity for energy harvest. *Nature.* (2006) 444:1027–31. doi: 10.1038/nature05414
19. Yang H, Xiang Y, Robinson K, Wang J, Zhang G, Zhao J, et al. Gut microbiota is a major contributor to adiposity in pigs. *Front Microbiol.* (2018) 9:3045. doi: 10.3389/fmicb.2018.03045
20. Bäckhed F, Manchester JK, Semenkovich CF, Gordon JI. Mechanisms underlying the resistance to diet-induced obesity in germ-free mice. *Proc Natl Acad Sci USA.* (2007) 104:979–84. doi: 10.1073/pnas.0605374104
21. Murakami Y, Ojima-Kato T, Saburi W, Mori H, Matsui H, Tanabe S, et al. Supplemental epilactose prevents metabolic disorders through uncoupling protein-1 induction in the skeletal muscle of mice fed high-fat diets. *Brit J Nutr.* (2015) 114:1774–83. doi: 10.1017/S0007114515003505
22. Liu Y, Li Y, Feng X, Wang Z, Xia Z. Dietary supplementation with Clostridium butyricum modulates serum lipid metabolism, meat quality, and the amino acid and fatty acid composition of Peking ducks. *Poult Sci.* (2018) 97:3218–29. doi: 10.3382/ps/pey162
23. Yan H, Diao H, Xiao Y, Li W, Yu B, He J, et al. Gut microbiota can transfer fiber characteristics and lipid metabolic profiles of skeletal muscle from pigs to germ-free mice. *Sci Rep.* (2016) 6:31786. doi: 10.1038/srep31786
24. Bäckhed F, Ding H, Wang T, Hooper LV, Koh GY, Nagy A, et al. The gut microbiota as an environmental factor that regulates fat storage. *Proc Natl Acad Sci USA.* (2004) 101:15718–23. doi: 10.1073/pnas.0407076101
25. Dijk W, Kersten S. Regulation of lipid metabolism by angiopoietin-like proteins. *Curr Opin Lipidol.* (2016) 27:249–56. doi: 10.1097/MOL.0000000000000290
26. Olshan DS, Rader DJ. Angiopoietin-like protein 4: A therapeutic target for triglycerides and coronary disease? *J Clin Lipidol.* (2018) 12:583–7. doi: 10.1016/j.jacl.2018.01.012
27. Morrison DJ, Preston T. Formation of short chain fatty acids by the gut microbiota and their impact on human metabolism. *Gut Microbes.* (2016) 7:189–200. doi: 10.1080/19490976.2015.1134082
28. Huang Y, Wang J, Chen B, Jiang Q, Guo Y, Lan G, et al. Gene expression and enzyme activity of lipoprotein lipase correlate with intramuscular fat content in Guangxi san-huang and Arbor Acres chickens. *Genet Mol Res.* (2016) 15:414. doi: 10.4238/gmr.15027414
29. Zappaterra M, Deserti M, Mazza R, Braglia S, Zambonelli P, Davoli R. A gene and protein expression study on four porcine genes related to intramuscular fat deposition. *Meat Sci.* (2016) 121:27–32. doi: 10.1016/j.meatsci.2016.05.007
30. Walsh ME, Bhattacharya A, Sataranatarajan K, Qaisar R, Sloane L, Rahman MM, et al. The histone deacetylase inhibitor butyrate improves metabolism and reduces muscle atrophy during aging. *Aging Cell.* (2015) 14:957–70. doi: 10.1111/acel.12387
31. Nayananjalie WA, Wiles TR, Gerrard DE, McCann MA, Hanigan MD. Acetate and glucose incorporation into subcutaneous, intramuscular, and visceral fat of finishing steers. *J Anim Sci.* (2015) 93:2451–9. doi: 10.2527/jas.2014-8374
32. Xiao Y, Kong F, Xiang Y, Zhou W, Wang J, Yang H, et al. Comparative biogeography of the gut microbiome between Jinhua and Landrace pigs. *Sci Rep.* (2018) 8:5985. doi: 10.1038/s41598-018-24289-z
33. Xiao Y, Wu C, Li K, Gui G, Zhang G, Yang H. Association of growth rate with hormone levels and myogenic gene expression profile in broilers. *J Anim Sci Biotechnol.* (2017) 8:43. doi: 10.1186/s40104-017-0170-8
34. Du X, Xiang Y, Lou F, Tu P, Zhang X, Hu X, et al. Microbial community and short-chain fatty acid mapping in the intestinal tract of quail. *Animals.* (2020) 10:1006. doi: 10.3390/ani10061006
35. Wang Q, Garrity GM, Tiedje JM, Cole JR. Naive Bayesian classifier for rapid assignment of rRNA sequences into the new bacterial taxonomy. *Appl Environ Microbiol.* (2007) 73:5261–7. doi: 10.1128/AEM.00062-07
36. Xiao Y, Li K, Xiang Y, Zhou W, Gui G, Yang H. The fecal microbiota composition of boar Duroc, Yorkshire, Landrace and Hampshire pigs. *Asian-Australas J Anim Sci.* (2017) 30:1456–63. doi: 10.5713/ajas.16.0746
37. Xu J, Verbrugghe A, Lourenço M, Cools A, Liu DJX, Van de Wiele T, et al. The response of canine faecal microbiota to increased dietary protein is influenced by body condition. *BMC Vet Res.* (2017) 13:374. doi: 10.1186/s12917-017-1276-0
38. Gerard P. Gut microbiota and obesity. *Cell Mol Life Sci.* (2016) 73:147–62. doi: 10.1007/s00018-015-2061-5
39. Houmard JA, Pories WJ, Dohm GL. Severe obesity: evidence for a deranged metabolic program in skeletal muscle? *Exerc Sport Sci Rev.* (2012) 40:204. doi: 10.1097/JES.0b013e31825d53fc
40. Bindels LB, Delzenne NM. Muscle wasting: the gut microbiota as a new therapeutic target? *Int J Biochem Cell B.* (2013) 45:2186–90. doi: 10.1016/j.biocel.2013.06.021

41. Miao Z, Wang L, Xu Z, Huang J, Wang Y. Developmental changes of carcass composition, meat quality and organs in the Jinhua pig and Landrace. *Animal.* (2009) 3:468–73. doi: 10.1017/S1751731108003613
42. Guo J, Shan T, Wu T, Zhu L, Ren Y, An S, et al. Comparisons of different muscle metabolic enzymes and muscle fiber types in Jinhua and Landrace pigs. *J Anim Sci.* (2011) 89:185–91. doi: 10.2527/jas.2010-2983
43. Hu S, Xu Y, Gao X, Li S, Jiang W, Liu Y, et al. Long-chain bases from sea cucumber alleviate obesity by modulating gut microbiota. *Marine Drugs.* (2019) 17:55. doi: 10.3390/md17080455
44. Neis EP, van Eijk HM, Lenaerts K, Olde Damink SW, Blaak EE, Dejong CH, et al. Distal versus proximal intestinal short-chain fatty acid release in man. *Gut.* (2019) 68:764–5. doi: 10.1136/gutjnl-2018-316161
45. Zhang L, Liu C, Jiang Q, Yin Y. Butyrate in energy metabolism: There is still more to learn. *Trends Endocrin Met.* (2021) 32:159–69. doi: 10.1016/j.tem.2020.12.003
46. Alex S, Lange K, Amolo T, Grinstead JS, Haakonsson AK, Szalowska E, et al. Short-chain fatty acids stimulate angiopoietin-like 4 synthesis in human colon adenocarcinoma cells by activating peroxisome proliferator-activated receptor γ. *Mol Cell Biol.* (2013) 33:1303–16. doi: 10.1128/MCB.00858-12
47. Gao Z, Yin J, Zhang J, Ward RE, Martin RJ, Lefevre M, et al. Butyrate improves insulin sensitivity and increases energy expenditure in mice. *Diabetes.* (2009) 58:1509–17. doi: 10.2337/db08-1637
48. Xiong J, Qiu H, Bi Y, Zhou H, Guo S, Ding B. Effects of dietary supplementation with tributyrin and coated sodium butyrate on intestinal morphology, disaccharidase activity and intramuscular fat of lipopolysaccharide-challenged broilers. *Braz J Poultry Sci.* (2018) 20:707–16. doi: 10.1590/1806-9061-2018-0787
49. Louis P, Duncan SH, McCrae SI, Millar J, Jackson MS, Flint HJ. Restricted distribution of the butyrate kinase pathway among butyrate-producing bacteria from the human colon. *J Bacteriol.* (2004) 186:2099–106. doi: 10.1128/JB.186.7.2099-2106.2004

Conflict of Interest: The authors declare that the research was conducted in the absence of any commercial or financial relationships that could be construed as a potential conflict of interest.

frontiers in Nutrition

ORIGINAL RESEARCH
published: 16 April 2021
doi: 10.3389/fnut.2021.660598

Check for updates

Bovine Lactoferrin Protects Dextran Sulfate Sodium Salt Mice Against Inflammation and Impairment of Colonic Epithelial Barrier by Regulating Gut Microbial Structure and Metabolites

*Shalong Wang[1], Jingyu Zhou[1], Da Xiao[2], Guoshun Shu[1] and Li Gu[3]**

[1] Department of General Surgery, The Second Xiangya Hospital of Central South University, Changsha, China, [2] Department of General Surgery, Shekou People's Hospital of Central South University, Shenzhen, China, [3] Department of Gastroenterology, The Second Xiangya Hospital of Central South University, Changsha, China

OPEN ACCESS

Edited by:
Hui Han,
Chinese Academy of Sciences (CAS), China

Reviewed by:
Ming Qi,
Chinese Academy of Sciences, China
Jing Wang,
University of California, Los Angeles, United States

Correspondence:
Li Gu
Ligu0423@csu.edu.cn

Specialty section:
This article was submitted to Nutrition and Microbes, a section of the journal Frontiers in Nutrition

Received: *29 January 2021*
Accepted: *08 March 2021*
Published: *16 April 2021*

Citation:
Wang S, Zhou J, Xiao D, Shu G and Gu L (2021) Bovine Lactoferrin Protects Dextran Sulfate Sodium Salt Mice Against Inflammation and Impairment of Colonic Epithelial Barrier by Regulating Gut Microbial Structure and Metabolites. Front. Nutr. 8:660598. doi: 10.3389/fnut.2021.660598

Background: Ulcerative colitis is characterized by relapsing and remitting mucosal inflammation. Bovine lactoferrin (BL) is a multifunctional protein that could regulate the intestinal flora and has anti-inflammatory effects. The aim of this study was to investigate the therapeutic effect of BL on colitis.

Methods: Dextran sulfate sodium salt (DSS) was utilized to establish a mouse model of colitis. BL was administered to treat DSS mice. The weight, the activity, and fecal status of the mice were recorded every day. Disease activity index was calculated. After the mice were euthanized, the colon length was measured. Hematoxylin and eosin staining was used to observe the pathological changes of the colon, and histological activity index was calculated. The myeloperoxidase (MPO) activity of colon tissue was measured. Western blot and immunohistochemistry were used to detect the expressions of Claudin-1, Occludin, and ZO-1. The expressions of IL-1β, IL-6, IL-10, TNF-α, and TGF-β in colon tissue were detected by ELISA. The protein expressions of MUC2, Reg3γ, β-defensin (HBD-2), and cAMP were detected by immunofluorescence (IF). 16S rDNA sequencing determined the type and structure of intestinal flora. Liquid chromatography–tandem mass spectrometry (LC-MS/MS) measured the metabolites of the intestinal flora.

Results: Compared with the DSS group, the mice's weight in the BL group was higher and the length of the colon was longer. At the 14th day, MPO activity was higher in the BL group. The expressions of Claudin-1, Occludin, and ZO-1 in the colon were up-regulated in the BL group compared with the DSS group. The expressions of IL-1β, IL-6, and TNF-α were lower. The expressions of IL-10 and TGF-β were higher. IF showed that the expressions of MUC2 and β-defensin (HBD-2) were down-regulated, and the expressions of Reg3γ and cAMP were up-regulated. The 16S rDNA sequencing results showed that the alpha diversity and beta diversity were notably changed in the DSS mice treated with BL. Metabolomics results showed that BL changed purine metabolism in the DSS mice.

Conclusion: BL alleviated colitis in mice by improving the inflammatory response and the structure of the colon barrier in the colon. BL changed the composition and metabolites of the intestinal flora. Thus, BL might be an effective nutritional supplement for colitis treatment.

Keywords: colitis, gut microbiota, intestinal epithelial barrier, gut microbial, bovine lactoferrin

BACKGROUNDS

The multifactorial pathophysiology of UC includes genetic predisposition, epithelial barrier defects, dysregulated immune responses, microbial dysbiosis, and environmental factors. Colitis could cause frequent abdominal pain, diarrhea, and even colon cancer (1, 2). But most of the drugs used in colitis, such as 5-aminosalicylic acid (5-ASA) or corticosteroids, would interfere with the patient's metabolism and would cause side effects. Therefore, we need to seek a safer and better drug for colitis patients.

Colitis is caused by inflammation of the intestinal tissue and destroys the intestinal barrier. The dextran sulfate sodium salt (DSS) colitis model is the most widely used inflammatory enteritis model (3). In DSS colitis models, the intestinal mucosa and epithelial cells were destroyed and inflammatory cells were activated (4). In addition, the lack of adaptive immunity in the intestines made bacteria and monocytes enter the intestinal mucosa, leading to an intestinal barrier imbalance (5). Therefore, it is crucial to maintain a stable microenvironment in the intestines. Many proteins regulate intestinal homeostasis, such as Claudin-1, Occludin, and ZO-1. Claudin-1 is involved in the regulation of intestinal epithelial barrier homeostasis by regulating Notch signal (6). In the area of damaged intestinal, the expression of Claudin-1 is up-regulated (7). Occludin is a transmembrane junction protein, and its C-terminus could directly interact with tight junction protein ZO-1 (8). By regulating CASP3 transcription and Caspase-3 expression, ZO-1 could regulate epithelial cell apoptosis and survival (9).

Intestinal inflammation is related to the imbalance of intestinal flora (10). The metabolites of intestinal flora affected the host's immune homeostasis, normal metabolism, and the integrity of the mucosa (11). Most studies have proved that fecal microbiota transplantation (FMT) could help colitis patients in recovering better (12). Intestinal microorganisms might produce abundant metabolites, among which butyrate could provide energy to colon cells, maintain the integrity of colon mucosa, and have anti-inflammatory and anticancer effects (13).

Bovine lactoferrin (BL) is a non-heme iron-binding glycoprotein (14), which promotes the proliferation and differentiation of intestinal epithelial cells (15). Besides, BL also has antibacterial and antiviral properties (16, 17). Studies have shown that in the early stage of antiviral treatment, BL may prevent the virus from entering colon host cells (18). Thus, BL is a natural immune molecule. Moreover, BL regulated the synthesis of ferroportin through down-regulation of IL-6 and up-regulated anemia in pregnant women (19). These results indicate that BL could play a therapeutic role by improving inflammation. However, there are few studies on the treatment of colitis with BL

Therefore, our study aims to prove the effect of BL on the inflammation and intestinal barrier of the DSS mice. We also intend to explore the effect of BL on the structure of intestinal flora and its metabolites in colitis and provide a new idea for the treatment of colitis.

METHODS

Dextran Sulfate Sodium Salt Model

Thirty-six mice were purchased from Animal Experiment Center of Xiangya Medical College, Central South University. All mice were fed for 7 days to adapt to the environment before the experiment. Colitis mouse model was induced using DSS. All mice were randomly divided into three groups, with 12 mice in each group. The control group drank water normally during the experiment. In the model group (DSS) group, the mice drank 4% DSS solution (20) freely for 7 days and then were fed with normal saline for 14 days. In the DSS+BL group, 4% DSS solution was drunk freely for 7 days, and then BL (100 mg/kg) (21) was gavaged for 14 days. Seven days after intragastric administration of DSS, the mice's weight was recorded every day, and the disease activity index (DAI) was calculated according to the weight and defecation of the mice for 14 consecutive days. After 14 days, the mice were sacrificed, and the length of their colon was measured. All experimental protocols were approved by Animal Ethics of the Second Xiangya Hospital, Central South University (2020844). The care and handling of animals comply with the guidelines of the National Institutes of Health.

Determination of Disease Activity Index

By measuring the DAI, the health of the rats was evaluated. We calculate the total weight loss, diarrhea, and blood in the stool from the first day as the clinical disease score. Grading rules are as follows: 0 points, mice weight changes within 1%, stool shape normal, and no rectal bleeding; 1 point, mice lost 1–5% weight, and stool became softer with weak hemoccult; 2 points, mice lost 5–10% weight, accompanied with moderate diarrhea and blood in the stool; 3 points, mice lost 10–15% weight, accompanied with diarrhea and fresh rectal bleeding; and 4 points, mice lost more than 15% of body weight, accompanied with severe bloody stools.

H&E Staining

The mice were sacrificed 14 days later, and colon tissue was taken. Leica microtome sliced the embedded tissue at 15 μm, following the steps in the H&E kit (Wellbio, China) instructions for staining. According to the results of H&E staining, goblet cells, inflammatory cells, and crypts in colon tissue were calculated to determine histological activity index (HAI). The histological activity scoring rules are as follows: (1) intestinal epithelial injury [no injury (0 points), massive loss of goblet cells (1 point), small number of crypts + massive loss of goblet cells (3 points), and large numbers of crypts absent (4 points)]; and (2) inflammatory cell infiltration [no inflammatory cell infiltrated (0 points), inflammatory cell infiltrated around the crypt (1 point), inflammatory cell infiltrated into the muscularis mucosa (2 points), inflammatory cell infiltrated to the muscularis mucosa with edema (3 points), and inflammatory cells infiltrated the submucosa (4 points)]. The scores of the above two items are added to get the HAI score (0–8 points).

Immunohistochemistry

The slices were dewaxed in water and then placed in xylene for 20 min, which were performed three times. After that, the sections were placed in 100, 95, 85, and 75% ethanol for 5 min. Slices were soaked in distilled water for 5 min. The slices were immersed in 0.01 M of citrate buffer (pH 6.0) and boiled for 20 min. After being cooled to room temperature, the slices were washed with 0.01 M of PBS (pH 7.2∼7.6) for 3 min, which were performed three times. Then 1% periodic acid was added, and the slices were placed at room temperature for 10 min. Slices were washed with PBS for 3 min, which were performed three times. Diluted primary antibodies Claudin-1 (1:100, rabbit, 13050-1-AP, PTG), Occludin (1:100, rabbit, 13050-1-AP, PTG), and ZO-1 (1:100, rabbit, 13050-1-AP, PTG) were added to the slices and put at 4°C overnight. Pan secondary antibody was added, and slices were incubated at 37°C for 30 min. DAB (Nakasugi Golden Bridge) was added to dye slices for 5–10 min. Hematoxylin (Wellbio, China) was used to dye cell nuclei for 5–10 min, and then they were washed with distilled water. They were dehydrated in all levels of alcohol (60–100%) and transparent in xylene. The slides were mounted with neutral gum (Sigma) and then observed.

Immunofluorescence

We deparaffinized the sections to water and placed in xylene for 20 min, which were performed three times. Slices were put in 100, 95, 85, and 75% ethanol in sequence for 5 min at each level. Slices were washed with distilled water for 5 min. The slices were immersed in citrate buffer (pH 6.0) and boiled in an electric furnace or microwave oven. After being cooled, slices were washed with 0.01 M of PBS (pH 7.2 ∼ 7.6) for 3 min, which were performed three times. Slices were place in sodium borohydride solution at room temperature for 30 min. The sections were placed in Sudan black dye solution at room temperature for 5 min. Slices were blocked with 10% normal serum/5% bovine serum albumin (BSA) for 60 min. Slices were placed in appropriate first antibody, cAMP (1:50, rabbit, ab76238, Abcam, UK), MUC2 (1:50, rabbit, ab76774, Abcam, UK), Reg3γ (1:50, rabbit, ab233480, Abcam, UK), β-defensin (HBD-2) (1:50, rabbit, bs-1296r, Bioss, China), Claudin-1 (1:50, rabbit, 13050-1-AP, PTG), and ZO-1 (1:50, rabbit, 21773-1-AP, PTG), overnight at 4°C. Slices were incubated with CoraLite488-conjugated Affinipure Goat Anti-Rabbit IgG(H+L) (SA00013-2, Proteintech, USA) and incubated at 37°C for 90 min. Slices were stained in the nucleus with DAPI (Wellbio, China) working solution at 37°C for 10 min. Slices were stored in the dark or observed under a fluorescence microscope.

Western Blot

After the colon tissue was taken out, 200 μl of radioimmunoprecipitation assay (RIPA), protease inhibitor mixture was added, and the tissue sample was broken by ultrasonic for 1.5 min and lysis on ice for 10 min. The supernatant was collected after centrifugation at 4°C and 12,000 rpm for 15 min. Bicinchoninic acid (BCA) protein quantification kit was used to quantitatively analyze the protein. In the protein supernatant, 5× loading buffer was added, mixed well, boiled for 7 min, and places in an ice box for quick cooling. Twenty micrograms of protein sample was added into 10% separating gel and 4.8% concentrated gel, and electrophoresis was performed. Protein was transferred to polyvinylidene difluoride (PVDF) membrane. After being blocked with 5% milk at room temperature for 2 h, the protein band was incubated with the primary antibody overnight at 4°C. The primary antibodies were Claudin-1 (1:2,000, rabbit, ab211737, Abcam, UK), Occludin (1:2,000, rabbit, ab45171, Abcam, UK), ZO-1 (1:2,000, rabbit, 21773-1-AP, Proteintech, USA), MUC2 (1:500, rabbit, ab76774, Abcam, UK), Reg3γ (1:500, rabbit, ab233480, Abcam, UK), HBD-2 (1:500, rabbit, bs-1296r, Bioss, China), cAMP (1:500, rabbit, ab76238, Abcam, UK), and β-actin (1:5,000, rabbit, 60008-1-Ig, Proteintech, USA). The antigen species of the primary antibody was incubated with a suitable secondary antibody at room temperature for 2 h and then developed with enhanced chemiluminescence (ECL) solution kit. The band pictures were analyzed with ImageJ to obtain protein expression data.

Enzyme-Linked Immunosorbent Assay

The tissues were added with 200 μl of RIPA and protease inhibitor and sonicated for 1.5 min. The supernatant was obtained from centrifuging the tissue homogenate at 4°C and 12,000 rpm for 20 min. According to the instructions of the ELISA kit, by measuring the optical density (OD) value with the microplate reader, the concentration of IL-1β (CSB-E08054m, Wuhan Huamei Biological Engineering Co., Ltd., China), IL-6 (CSB-E04639m, Wuhan Huamei Biological Engineering Co., Ltd., China), IL-10 (CSB-E04594m, Wuhan Huamei Biological Engineering Co., Ltd., China), TNF-α (CSB-E04741m, Wuhan Huamei Biological Engineering Co., Ltd., China), and TGF-β1 (CSB-E04726m, Wuhan Huamei Biological Engineering Co., Ltd., China) factors was calculated.

Myeloperoxidase Activity Measurement

According to the instructions, the peroxidase activity in rat colon tissue was determined by the guaiacol colorimetric method. Myeloperoxidase (MPO) activity could be calculated by comparing tissue OD value with A value. The unit of enzyme

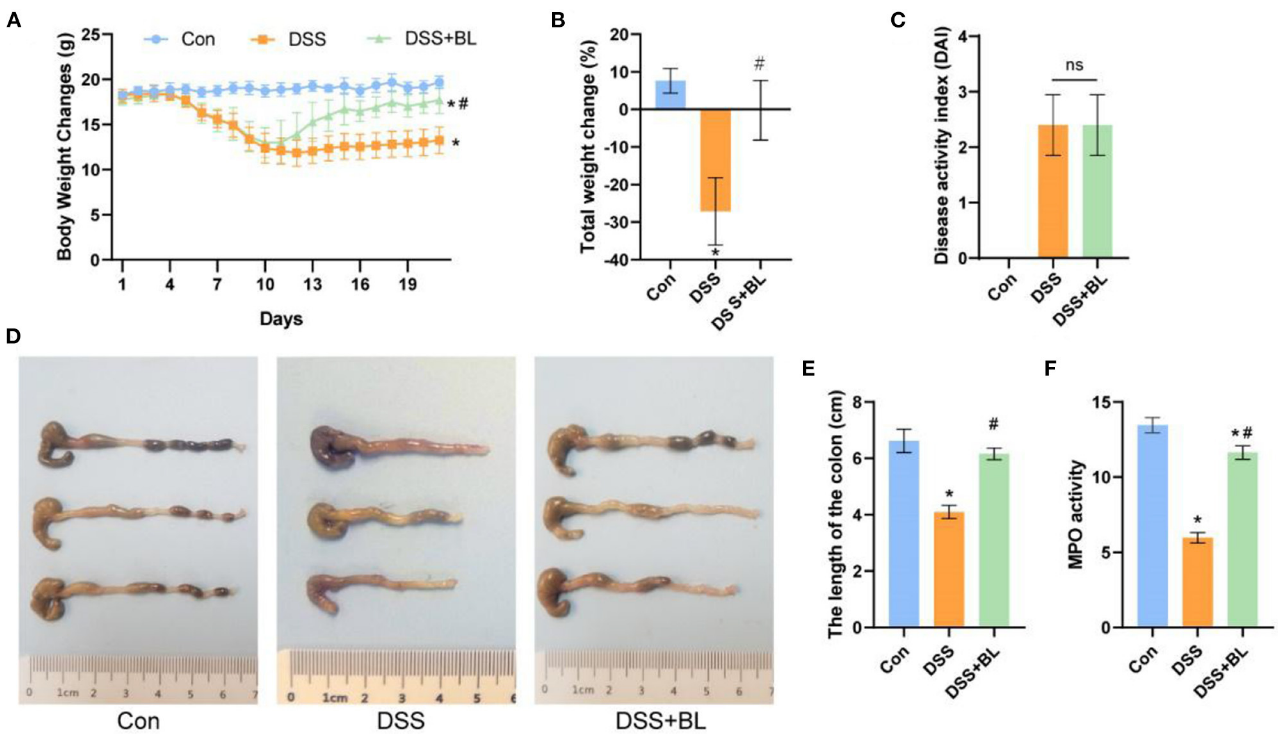

FIGURE 1 | Effects of bovine lactoferrin (BL) on changes in body weight, colon morphology, and myeloperoxidase (MPO) activity in dextran sulfate sodium salt (DSS) mice. **(A)** Changes of body weight of mice in each group within 19 days since start of modeling. **(B)** Changes of the rate of total weight of mice in each group within 19 days. **(C)** Changes of disease activity index (DAI) index on the seventh day after modeling. **(D)** Pictures of colons in each group. **(E)** Changes of colon length of mice in each group. **(F)** Changes of MPO activity in colon of mice in each group. One-way ANOVA was used to compare the three groups. $^{*}P < 0.05$ vs. control; $^{\#}P < 0.05$ vs. DSS. $n = 6$.

activity is the number of micromoles of xylophenol oxidized by the enzyme contained in a 1-g sample within 1 min.

Intestinal Flora Metabolomics

The intestinal excrement of mice was placed into 1.5-ml centrifuge tubes. There were eight sample replicates in each group. Liquid nitrogen was added to the centrifuge tube and weighed. According to the weight, nine times of the volume of the internal standard substance containing ^{13}C stable isotope was added with the pre-cooled extract liquid and mixed. Then, samples were left on ice for 5–10 min. Samples were in high-speed low-temperature centrifugation for 10 min at 4°C in 16,000 rpm. The supernatant was taken, and liquid chromatography–tandem mass spectrometry (LC-MS/MS) analysis was utilized. After obtaining the original data, we analyzed and sorted the data.

16S rDNA Sequencing

DNA was extracted from a single mouse stool sample by repeated beading and column purification methods. DNA quality was checked by agarose gel and quantified by Quant-iT dsDNA analysis kit (Cat.12640ES76, Shanghai Yisheng Biological Technology Co., Ltd.). The DNA was subjected to MiSeq sequencing (Illumina) according to the 2 × 300 pair termination protocol. The V4–V5 hypervariable region (primer sets 515F and 806R) of the 16S rDNA gene was amplified and sequenced using the method/manual of the manufacturer. After the raw data were processed, each species' operational taxonomic units (OTUs) were obtained, and species annotations were made for each OTU. According to the obtained species information and based on the species' abundance distribution, the final results were plotted.

Data Analysis

The data were analyzed using GraphPad Prism 7.0 (GraphPad Software Inc., San Diego, CA). All data were expressed as mean ± standard deviation. We used one-way ANOVA for data analysis between multiple groups. $P < 0.05$ was statistically significant. We utilized Kruskal–Wallis test (between multiple groups) and Wilcoxon test (between two groups) to analyze the relative abundance of species. Principal component analysis (PCA) and principal coordinate analysis (PCoA) were performed using the Anosim analysis, Adonis analysis, and analysis of differences in bacterial species abundance based on the Wald test method. The Spearman analysis was used to analyze the correlation between different microorganisms and different metabolites.

RESULTS

Bovine Lactoferrin Alleviated Dextran Sulfate Sodium Salt-Induced Colitis in Mice

In order to explore the therapeutic effect of BL on the DSS mice, we tested the changes in the overall health of the mice

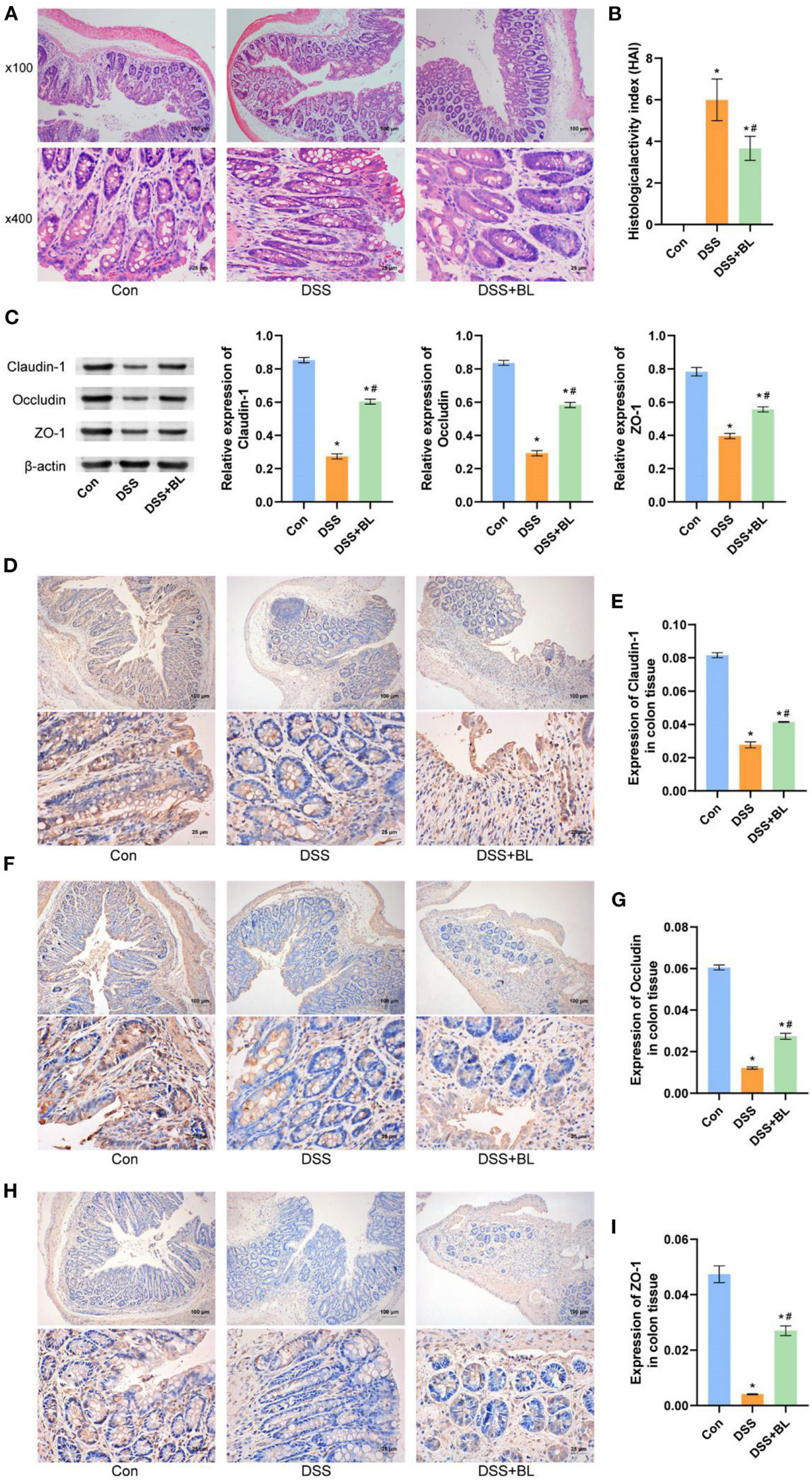

FIGURE 2 | Effects of bovine lactoferrin (BL) on colon tissue morphology and expression of colonic barrier-related connexin proteins in dextran sulfate sodium salt (DSS) mice. **(A)** H&E staining of colon tissue in mice. **(B)** Changes of histological activity index of colon tissue in mice. **(C)** Western blot results and analysis of Claudin-1, Occludin, and ZO-1. **(D,E)** Immunohistochemistry results and analysis of Claudin-1. **(F,G)** Immunohistochemistry results and analysis of Occludin. **(H,I)** Immunohistochemistry results and analysis of ZO-1. One-way ANOVA was used to compare the three groups. $^{*}P < 0.05$ vs. control; $^{\#}P < 0.05$ vs. DSS. $n = 6$.

during the administration period after modeling. We found that on the seventh day after modeling, the weight of the DSS mice decreased significantly, and the DAI score of two DSS groups was higher than that of the control group ($P < 0.05$), indicating that the colitis models were successfully created. After the 10th day, compared with that of the DSS group, the weight of the DSS+BL group increased gradually (**Figure 1A**). Compared with the first day, the weight of the control group increased by 8%, the weight of the DSS group decreased by 26% ($P < 0.01$), and the weight of the DSS+BL group changed little (**Figure 1B**). On the 14th day, we calculated the DAI based on the overall weight change and defecation of the mice. The DAI scores of the control group were the lowest. The scores of the DSS group and DSS+BL group increased, compared with the control group (**Figure 1C**). But the DAI between the two DSS groups had no significant difference. Meanwhile, we found that the length of the colon in the DSS group had been shortened to 4 cm, while the colon length of the control group and the DSS+BL group remained around 6 cm (**Figures 1D,E**; $P < 0.05$). The MPO activity was measured, and we found that the peroxidase activity in the DSS+BL group was up-regulated, compared with the DSS group (**Figure 1F**; $P < 0.05$). Therefore, these results suggested that BL reduced the related symptoms of the DSS mice.

Effects of Bovine Lactoferrin on Intestinal Epithelial Barrier in Dextran Sulfate Sodium Salt Mice

In order to explore the effect of BL on the intestinal epithelial barrier of the DSS mice, we utilized H&E staining to detect the pathological changes of colon tissue (**Figure 2A**). In the DSS groups, lymphocytes infiltration was increased and gathered into the crypts, epithelial cells were damaged, and goblet cells were markedly decreased, as compared with those in the DSS+BL groups ($P < 0.01$). We counted the goblet cells, inflammatory cells, and crypts in colon tissue and calculated the HAI. The HAI results showed that the HAI index of the DSS+BL groups was significantly lower than that of the DSS groups (**Figure 2B**; $P < 0.05$). Then, we performed Western blot (WB) and immunohistochemistry (IHC) to detect the level of the colonic barrier-related connexin proteins Claudin-1, Occludin, and ZO-1. WB (**Figure 2C**) and IHC (**Figures 2D–I**) results showed that the level of three proteins was the lowest in the DSS group. In the DSS+BL group, the expression of the three proteins enhanced than the DSS group and tended to the normal level ($P < 0.05$). These results indicated that BL could help damage colonic epithelial barrier recovery in the DSS mice.

Effects of Bovine Lactoferrin on Intestinal Inflammation and Colonic Mucosa in Dextran Sulfate Sodium Salt Mice

In order to test the effect of BL on colon inflammation in the DSS mice, we used ELISA to examine the expression of related inflammatory factors or anti-inflammatory factors in the colon. The ELISA results showed that, compared with those of the DSS group, the levels of inflammatory factors IL-1β, IL-6, and TNF-α (**Figures 3A,B,D**) were down-regulated in the DSS+BL groups, and the expression levels of anti-inflammatory factor IL-10 and TGF-β (**Figures 3C,E**) were up-regulated ($P < 0.05$). We used immunofluorescence (IF) to assess the expressions of colonic mucosa-related defense proteins, MUC2, Reg3γ, β-defensin (HBD-2), and cAMP. Compared with those in the DSS group, the expressions of MUC2 (**Figure 3F**) and cAMP (**Figure 3I**) significantly ascended in the DSS+BL groups ($P < 0.05$), while the expressions of Reg3γ (**Figure 3G**) and β-defensin (HBD-2) (**Figure 3H**) were inhibited. These results shown that BL might decrease the inflammation and promote the repair of colonic mucosa in the colon of the DSS mice.

Effects of Bovine Lactoferrin on Gut Microbial Metabolites in Dextran Sulfate Sodium Salt Mice

In order to detect the effect of BL on the metabolic function of the intestinal flora in the DSS mice, we collected the metabolites of the flora in the feces of mice for metabonomic analysis. We utilized PCA and partial least squares discriminant analysis (PLS-DA) to analyze the data of metabolomics, although PCA results showed that the difference between the control group and the DSS+BL group was unapparent (**Figure 4A**). PLS-DA displayed that the metabolite composition was significantly different among the three groups ($P < 0.05$; **Figure 4B**). We analyzed the relative abundance of the top 25 metabolites (**Figure 4C**). Compared with control groups, in the DSS group, 22 metabolites were significantly increased ($P < 0.05$). The relative abundance of PIPECOLATE was the highest in the control group. In the DSS+BL groups, the relative abundance of OPHTHALMATE and 1,1-dimethylbiguanide was the highest. The other 22 metabolites, such as L-malic acid and MALATE, were highly expressed in the intestines of the DSS mice ($P < 0.05$). Next, we analyzed the top 10 metabolites of each groups (**Figure 4D**). We found that, in the control group and DSS+BL group, NICOTINAMIDE HYPOXANTHINE DINUCLEOTIDE had the highest proportion. In the DSS group, deoxyadenosine monophosphate had the largest proportion. We analyzed the relative abundance of the top eight metabolites in the three groups (**Figures 4E–L**). Except for PIPECOLATE, the expressions of the rest of the metabolites were up-regulated in the DSS group and decreased in the DSS+BL group. These results showed that BL participated in regulating the secretion of intestinal microbial metabolites flora in the DSS mice.

Effects of Bovine Lactoferrin on Gut Microbial Structure in Dextran Sulfate Sodium Salt Mice

In order to detect the influence of BL on the structure and composition of the intestinal flora in the DSS mice, we collected the feces of three groups of mice and performed the sequence analysis of the microbes in the intestines for 16S rDNA sequencing to obtain the structure of the gut flora. In our results, three groups shared seven core bacterial groups in the Venn diagram (**Figure 5A**). The heat map showed that in the DSS+BL group, the expressions of *Akkermansia* were higher than those

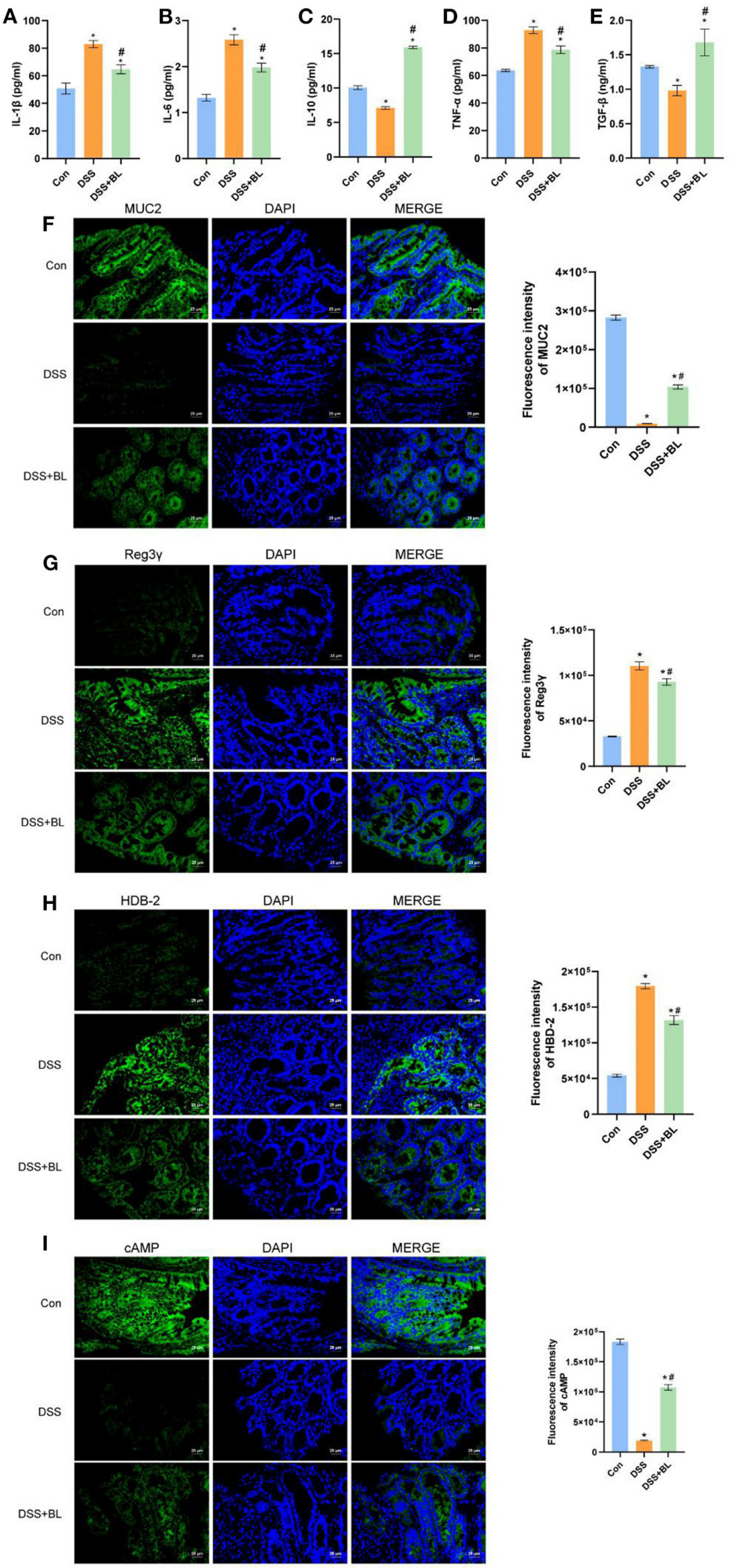

FIGURE 3 | Effects of bovine lactoferrin (BL) on inflammatory factors and expression of colonic mucosa-related defense proteins in dextran sulfate sodium salt (DSS) mice. **(A–E)** ELISA of inflammatory factors, IL-1β, IL-6, IL-10, TGF-α, and TNF-β of colon tissue in mice. **(F)** Immunofluorescence results and analysis of MUC2. **(G)** Immunofluorescence results and analysis of Reg3γ. **(H)** Immunofluorescence results and analysis of HBD-2. **(I)** Immunofluorescence results and analysis of cAMP. One-way ANOVA was used to compare the three groups. $^{*}P < 0.05$ vs. control; $^{\#}P < 0.05$ vs. DSS.

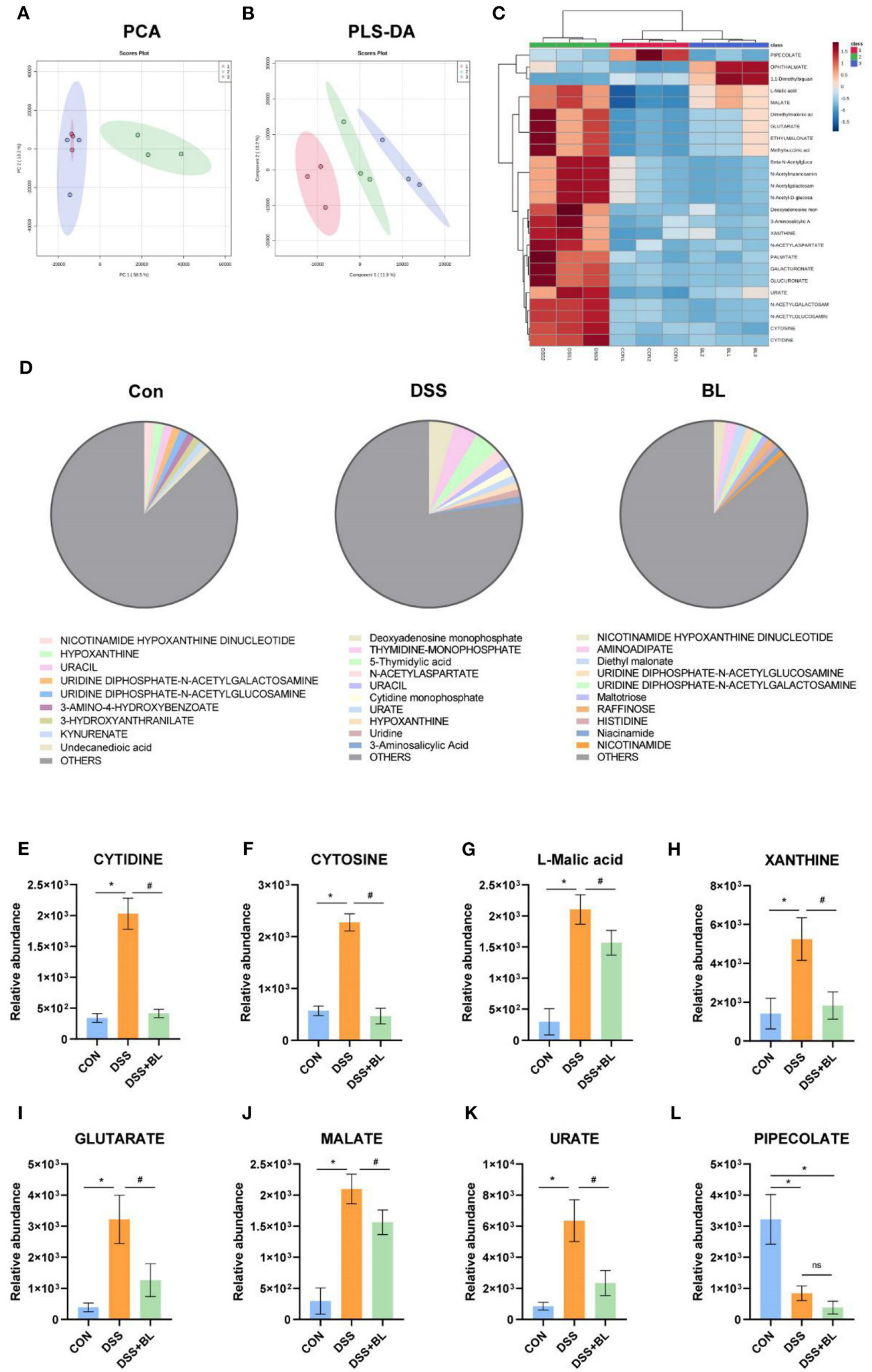

FIGURE 4 | Effects of bovine lactoferrin (BL) on gut microbial metabolites in dextran sulfate sodium salt (DSS) mice. **(A)** Principal component analysis (PCA) of intestinal flora metabolites. **(B)** Partial least squares discriminant analysis (PLS-DA) of intestinal flora metabolites. **(C)** Top 25 common metabolites. **(D)** Proportion of top 10 metabolites in each group. **(E–L)** Relative abundance of top eight metabolites. One-way ANOVA was used to compare the three groups. $^{*}P < 0.05$ vs. control; $^{\#}P < 0.05$ vs. DSS.

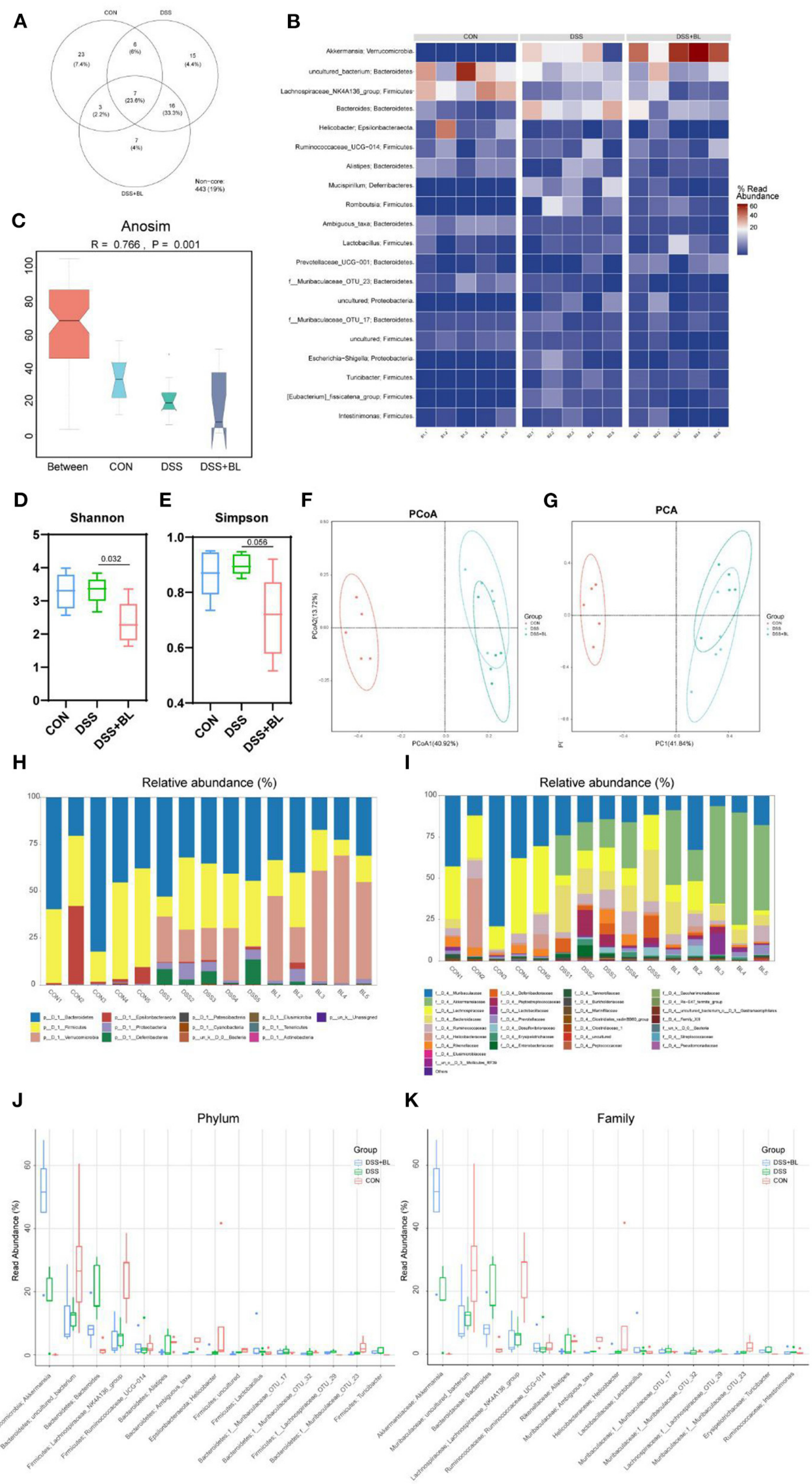

FIGURE 5 | Effects of bovine lactoferrin (BL) on gut microbial structure in dextran sulfate sodium salt (DSS) mice. **(A)** Venn diagram of colony structure. **(B)** Top 20 intestinal flora in each group. **(C)** Anosim analysis. **(D)** Shannon analysis of intestinal flora. **(E)** Simpson analysis of intestinal flora. **(F)** Principal coordinate analysis (PCoA) of intestinal flora. **(G)** Principal component analysis (PCA) of intestinal flora. **(H,J)** The expression of phylum relative abundance. **(I,K)** The expression of family relative abundance. One-way ANOVA was used to compare the three groups. *P < 0.05 vs. control; #P < 0.05 vs. DSS.

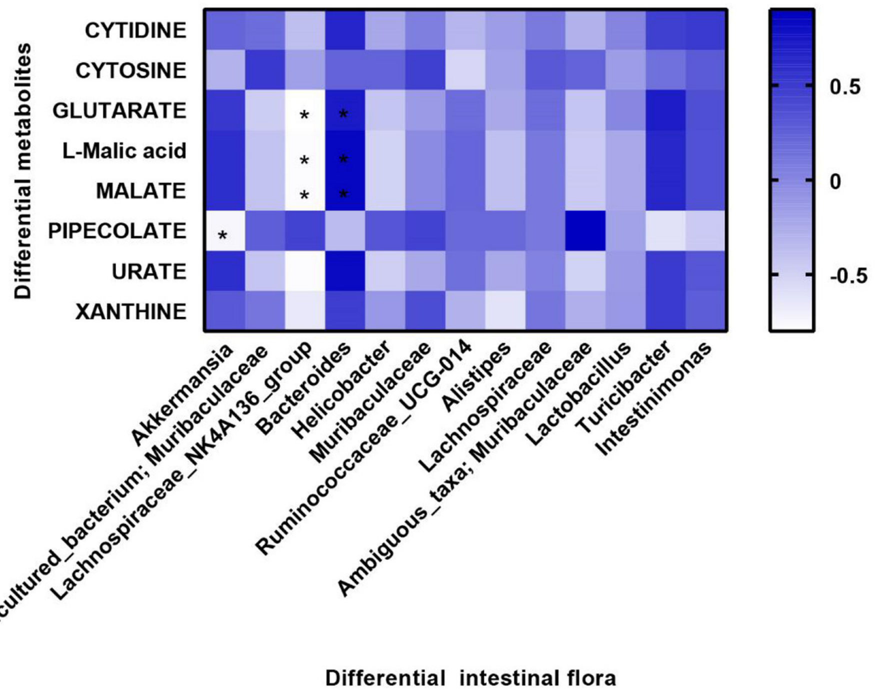

FIGURE 6 | Correlation between microbial diversity and metabolites. Differential metabolites are displayed on the y-axis, and differential flora are displayed on the x-axis. Blue color represents positive correlation, and white color represents negative correlation. Spearman analysis was used to compare all groups. *$P < 0.05$ differential metabolites vs. differential intestinal flora.

of the other groups ($P < 0.05$). The *uncultured_bacterium* and *Lachnospiraceae_NK4A136_group* were the lowest in the DSS groups compared with others (**Figure 5B**). The Anosim analysis showed that the difference between the groups of our results was greater than the difference within group ($P = 0.001$), and there was a significant difference (**Figure 5C**). The Shannon analysis showed that compared with that in the DSS group, the α-diversity of the gut flora in the DSS+BL group was significantly down-regulated (**Figure 5D**). However, in the Simpson analysis, there was no significant difference between the DSS group and DSS+BL group (**Figure 5E**). PCoA and PCA (β-diversity) showed that the genus difference between the DSS mice and normal mice was remarkable (**Figures 5F,G**). But the distance between the DSS group and the BL group is small and coincident. We analyzed the expressions of phylum (**Figures 5H,J**) and family (**Figures 5I,K**) relative abundance. In the phylum level, in the two colitis groups, Bacteroidetes and Firmicutes decreased, and Verrucomicrobia increased, compared with those in control group ($P < 0.05$). The proportion of Verrucomicrobia in the DSS+BL groups was higher than that in the DSS groups. In the family level, in colitis mice, Muribaculaceae and Lachnospiraceae decreased, and Akkermansiaceae increased, compared with that in the control group ($P < 0.05$). The proportion of Akkermansiaceae in the DSS+BL groups was higher than in the DSS groups. These results indicated that BL could change the structure and composition of the gut flora in the DSS mice, but the potential regulatory mechanism of BL on colitis requires our further exploration.

Relationship Between Gut Microbial Diversity and Gut Microbial Metabolites

Furthermore, we investigated the potential association between intestinal differential metabolites and intestinal microflora. We selected the top eight different intestinal metabolites and the top 15 different intestinal microflora at the family level of the three groups of mice for correlation analysis. The results showed that *Akkermansia* was negatively correlated with PIPECOLATE expression. *Lachnospiraceae_NK4A136* was negatively correlated with GLUTARATE, L-malic acid, and MALATE. However, *Bacteroides* was positively correlated with GLUTARATE, L-malic acid, and MALATE (**Figure 6**).

DISCUSSION

Colitis is a chronic inflammatory with hard recovery. BL is a kind of nutritional supplement that could repair the intestinal barrier function and intestinal microbiota to reduce enterohemorrhagic intestinal disease (22). Studies have shown that when BL was performed to treat colitis, the inflammatory response in the intestines was weakened and the barrier structure of the colon was protected (23). In our research, BL improved the damaged intestinal barrier in colitis and reduced inflammation in the colon. In addition, BL changed the intestinal microbes' structural diversity and metabolic function.

In our results, it was noted that BL alleviated the pathological symptoms of colitis and reduced body weight loss in colitis mice.

We found that BL regulated the expression of colonic barrier defense-related proteins and tight junction proteins in colitis. A previous study found that the defense protein MUC2$^{-/-}$ mice were suffering from malnutrition at 4 weeks old, and the abundance of the microbial community was more complicated than that of normal mice (24). Additionally, chitosan, another kind of nutritional supplement, attenuated the changes in colon tissue morphology and excessive inflammation caused by DSS, which was associated with increased ZO-1 expression (25). In this study, it was found that BL increased the expression of Claudin-1, Occludin, and ZO-1 in the intestines of colitis mice. In colitis, the epithelial barrier in the intestines was destroyed. The host's immune cells have increased contact with microorganisms in the intestinal tract, leading to frequent inflammatory reactions (26). Our results found that BL down-regulated the expressions of IL-1β, IL-6, and TNF-α inflammatory factors in the colon tissue of colitis mice and increased the expression levels of anti-inflammatory factors IL-10 and TGF-β. Therefore, we inferred that BL could be used as an auxiliary treatment to repair the colitis colonic barrier and reduce the inflammation in the colon.

It is well-known that intestinal microbes play a vital role in intestinal diseases. Gogokhia et al. showed that increasing bacteriophage levels could exacerbate colitis through TLR9 and IFN-γ (27). In our results, BL decreased the α-diversity of the flora, comparing with that in the DSS group. This means that BL inhibited the growth and reproduction of some intestinal flora in mice with colitis. The β-diversity showed that the distance between the DSS group and the BL group was coincident. This result showed that the types of flora in the BL group and the DSS group were similar. In our results, Muribaculaceae/Lachnospiraceae intestinal type in colitis mice with BL intervention turned into Akkermansiaceae/Bacteroidaceae intestinal type. Muribaculaceae acts a pivotal part in regulating the community composition and metabolites of microbial flora. Studies have shown that Muribaculaceae is a kind of bacteria beneficial to longevity in the intestinal flora (28, 29). Muribaculaceae participates in the degradation of polysaccharides, which will produce succinate, acetate, and propionate (30). These metabolites were beneficial to the intestinal barrier. Selective prebiotic-like effects on Akkermansiaceae also participated in the composition and metabolism of the flora and made the damaged intestines develop toward a healthy direction (31). However, the role of Lachnospiraceae and Bacteroidaceae for the host was still controversial (32). These results manifested that BL may change the structure of the excessively diverse intestinal flora in the DSS mice and made the composition of the flora move toward the direction of treating colitis. Meanwhile, BL reduced the expression of most of the metabolites of the intestinal flora, such as URATE. Excessive URATE could cause ventilation and kidney stones, which also made excessive inflammation in the intestines (33). Most of the metabolites that improved in the BL groups belong to purines. Therefore, we speculated that DSS colitis may cause a disorder of purine metabolism in the intestines. BL improved the structure of the intestinal flora, thereby restoring purine metabolism in the intestines. Tyson's research shows that *Saccharomyces cerevisiae* could treat colitis by improving purine metabolism (34). This experimental result shows that the intestinal flora of *Akkermansia* could decrease PIPECOLATE metabolite. *Lachnospiraceae_NK4A136* could decrease GLUTARATE, L-malic acid, and MALATE metabolites, while the effect of *Bacteroides* on the above three metabolites was opposite to that of *Lachnospiraceae_NK4A136*. In the future, we will do further experiments to specifically explore the effects of these intestinal flora and intestinal metabolites.

In the current study, we only found out that BL could regulate the gut flora in colitis mice, but the specific regulation mechanism of BL on intestinal flora and metabolism of mice with colitis still needs further research. In our next work, we will further explore this issue in order to clarify the mechanism of BL regulation of colitis.

CONCLUSION

In conclusion, BL could relieve colitis mice through reducing the inflammatory reaction in colitis, protecting the intestinal barrier, and regulating the structural composition and metabolic function of intestinal microorganism. Hence, as an adjuvant therapy, BL may be clinically valuable.

DATA AVAILABILITY STATEMENT

The datasets presented in this study can be found in online repositories. The name of the repository is SRA and accession number is PRJNA699346.

ETHICS STATEMENT

The animal study was reviewed and approved by Animal Ethics of the Second Xiangya Hospital, Central South University (2020844).

AUTHOR CONTRIBUTIONS

SW: conceptualization, validation, and formal analysis. JZ: methodology, formal analysis, and writing. DX: software, validation, and investigation. GS: formal analysis, investigation, and writing. LG: investigation, formal analysis, and writing. All authors: contributed to the article and approved the submitted version.

ACKNOWLEDGMENTS

The authors thank the laboratory of the Second Xiangya Hospital of Central South University for the support.

SUPPLEMENTARY MATERIAL

The Supplementary Material for this article can be found online at: https://www.frontiersin.org/articles/10.3389/fnut.2021.660598/full#supplementary-material

REFERENCES

1. Marion-Letellier R, Savoye G, Ghosh S. IBD: in food we trust. *J Crohns Colitis.* (2016) 10:1351–61. doi: 10.1093/ecco-jcc/jjw106
2. Gearry RB. IBD and environment: are there differences between East and West. *Dig Dis.* (2016) 34:84–9. doi: 10.1159/000442933
3. Chassaing B, Aitken JD, Malleshappa M, Vijay-Kumar M. Dextran sulfate sodium (DSS)-induced colitis in mice. *Curr Protoc Immunol.* (2014) 104:15.25.1–14. doi: 10.1002/0471142735.im1525s104
4. Drolia R, Tenguria S, Durkes AC, Turner JR, Bhunia AK. Listeria adhesion protein induces intestinal epithelial barrier dysfunction for bacterial translocation. *Cell Host Microbe.* (2018) 23:470–84.e7. doi: 10.1016/j.chom.2018.03.004
5. Monif GRG. Is ulcerative colitis a disease of a dysfunctional microbiota? *Med Hypotheses.* (2019) 131:109300. doi: 10.1016/j.mehy.2019.109300
6. Pope JL, Bhat AA, Sharma A, Ahmad R, Krishnan M, Washington MK, et al. Claudin-1 regulates intestinal epithelial homeostasis through the modulation of notch-signalling. *Gut.* (2014) 63:622–34. doi: 10.1136/gutjnl-2012-304241
7. Weber CR, Nalle SC, Tretiakova M, Rubin DT, Turner JR. Claudin-1 and claudin-2 expression is elevated in inflammatory bowel disease and may contribute to early neoplastic transformation. *Lab Invest.* (2008) 88:1110–20. doi: 10.1038/labinvest.2008.78
8. Fanning AS, Jameson BJ, Jesaitis LA, Anderson JM. The tight junction protein ZO-1 establishes a link between the transmembrane protein occludin and the actin cytoskeleton. *J Biol Chem.* (1998) 273:29745–53. doi: 10.1074/jbc.273.45.29745
9. Kuo WT, Shen L, Zuo L, Shashikanth N, Ong M, Wu L, et al. Inflammation-induced occludin downregulation limits epithelial apoptosis by suppressing caspase-3 expression. *Gastroenterology.* (2019) 157:1323–37. doi: 10.1053/j.gastro.2019.07.058
10. Togawa J, Nagase H, Tanaka K, Inamori M, Nakajima A, Ueno N, et al. Oral administration of lactoferrin reduces colitis in rats via modulation of the immune system and correction of cytokine imbalance. *J Gastroenterol Hepatol.* (2002) 17:1291–8. doi: 10.1046/j.1440-1746.2002.02868.x
11. Gao Y, Bi W, Wu X, Zhu X, Luo Y. [Bacterial resistance influences intestinal flora and host immune regulation]. *Sheng Wu Gong Cheng Xue Bao.* (2018) 34:1259–69. doi: 10.13345/j.cjb.180123
12. Shen ZH, Zhu CX, Quan YS, Yang ZY, Wu S, Luo WW, et al. Relationship between intestinal microbiota and ulcerative colitis: Mechanisms and clinical application of probiotics and fecal microbiota transplantation. *World J Gastroenterol.* (2018) 24:5–14. doi: 10.3748/wjg.v24.i1.5
13. O'Keefe SJ. Diet, microorganisms and their metabolites, and colon cancer. *Nat Rev Gastroenterol Hepatol.* (2016) 13:691–706. doi: 10.1038/nrgastro.2016.165
14. Wang B, Timilsena YP, Blanch E, Adhikari B. Lactoferrin: structure, function, denaturation and digestion. *Crit Rev Food Sci Nutr.* (2019) 59:580–96. doi: 10.1080/10408398.2017.1381583
15. Buccigrossi V, de Marco G, Bruzzese E, Ombrato L, Bracale I, Polito G, et al. Lactoferrin induces concentration-dependent functional modulation of intestinal proliferation and differentiation. *Pediatr Res.* (2007) 61:410–4. doi: 10.1203/pdr.0b013e3180332c8d
16. Bullen JJ, Rogers HJ, Leigh L. Iron-binding proteins in milk and resistance to *Escherichia coli* infection in infants. *Br Med J.* (1972) 1:69–75. doi: 10.1136/bmj.1.5792.69
17. Hasegawa K, Motsuchi W, Tanaka S, Dosako S. Inhibition with lactoferrin of *in vitro* infection with human herpes virus. *Jpn J Med Sci Biol.* (1994) 47:73–85. doi: 10.7883/yoken1952.47.73
18. Valenti P, Antonini G. Lactoferrin: an important host defence against microbial and viral attack. *Cell Mol Life Sci.* (2005) 62:2576–87. doi: 10.1007/s00018-005-5372-0
19. Lepanto MS, Rosa L, Cutone A, Conte MP, Paesano R, Valenti P. Efficacy of lactoferrin oral administration in the treatment of anemia and anemia of inflammation in pregnant and non-pregnant women: an interventional study. *Front Immunol.* (2018) 9:2123. doi: 10.3389/fimmu.2018.02123
20. Güvenç M, Cellat M, Özkan H, Tekeli I O, Uyar A, Gökçek I, et al. Protective effects of tyrosol against DSS-induced ulcerative colitis in rats. *Inflammation.* (2019) 42:1680–91. doi: 10.1007/s10753-019-01028-8
21. Zhu W, Kong F, Chen X. Therapeutic experiment of bovine lactoferrin on Helicobacter pylori infection in rats. *China Mod Appl Pharm.* (2008) 85–7. doi: 10.1016/S1872-2075(08)60042-4
22. Haiwen Z, Rui H, Bingxi Z, Qingfeng G, Jifeng Z, Xuemei W, et al. Oral administration of bovine lactoferrin-derived lactoferricin (Lfcin) B could attenuate enterohemorrhagic *Escherichia coli* O157:H7 induced intestinal disease through improving intestinal barrier function and microbiota. *J Agric Food Chem.* (2019) 67:3932–45. doi: 10.1021/acs.jafc.9b00861
23. Tanaka H, Gunasekaran S, Saleh DM, Alexander WT, Alexander DB, Ohara H, et al. Effects of oral bovine lactoferrin on a mouse model of inflammation associated colon cancer. *Biochem Cell Biol.* (2020) 99:159–65. doi: 10.1139/bcb-2020-0087
24. Wu M, Wu Y, Li J, Bao Y, Guo Y, Yang W. The dynamic changes of gut microbiota in Muc2 deficient mice. *Int J Mol Sci.* (2018) 19:2809. doi: 10.3390/ijms19092809
25. Wang J, Zhang C, Guo C, Li X. Chitosan ameliorates DSS-induced ulcerative colitis mice by enhancing intestinal barrier function and improving microflora. *Int J Mol Sci.* (2019) 20:5751. doi: 10.3390/ijms20225751
26. Ordás I, Eckmann L, Talamini M, Baumgart DC, Sandborn WJ. Ulcerative colitis. *Lancet.* (2012) 380:1606–19. doi: 10.1016/S0140-6736(12)60150-0
27. Gogokhia L, Buhrke K, Bell R, Hoffman B, Brown DG, Hanke-Gogokhia C, et al. Expansion of bacteriophages is linked to aggravated intestinal inflammation and colitis. *Cell Host Microbe.* (2019) 25:285–99.e8. doi: 10.1016/j.chom.2019.01.008
28. Smith BJ, Miller RA, Ericsson AC, Harrison DC, Strong R, Schmidt TM. Changes in the gut microbiome and fermentation products concurrent with enhanced longevity in acarbose-treated mice. *BMC Microbiol.* (2019) 19:130. doi: 10.1186/s12866-019-1494-7
29. Sibai M, Altuntaş E, Yildirim B, Öztürk G, Yildirim S, Demircan T. Microbiome and longevity: high abundance of longevity-linked muribaculaceae in the gut of the long-living rodent spalax leucodon. *Omics.* (2020) 24:592–601. doi: 10.1089/omi.2020.0116
30. Ormerod KL, Wood DL, Lachner N, Gellatly SL, Daly JN, Parsons JD, et al. Genomic characterization of the uncultured bacteroidales family S24-7 inhabiting the guts of homeothermic animals. *Microbiome.* (2016) 4:36. doi: 10.1186/s40168-016-0181-2
31. Rodríguez-Daza MC, Roquim M, Dudonné S, Pilon G, Levy E, Marette A, et al. Berry polyphenols and fibers modulate distinct microbial metabolic functions and gut microbiota enterotype-like clustering in obese mice. *Front Microbiol.* (2020) 11:2032. doi: 10.3389/fmicb.2020.02032
32. Vacca M, Celano G. The controversial role of human gut lachnospiraceae. *Microorganisms.* (2020) 8:573. doi: 10.3390/microorganisms8040573
33. Andrade-Oliveira V, Foresto-Neto O, Watanabe IKM, Zatz R, Câmara NOS. Inflammation in renal diseases: new and old players. *Front. Pharmacol.* (2019) 10:1192. doi: 10.3389/fphar.2019.01192
34. Chiaro TR, Soto R, Zac Stephens W. A member of the gut mycobiota modulates host purine metabolism exacerbating colitis in mice. (2017). 9:eaaf9044. doi: 10.1126/scitranslmed.aaf9044

Conflict of Interest: The authors declare that the research was conducted in the absence of any commercial or financial relationships that could be construed as a potential conflict of interest.

frontiers in Nutrition

ORIGINAL RESEARCH
published: 11 May 2021
doi: 10.3389/fnut.2021.667695

Lactobacillus acidophilus ATCC 4356 Alleviates Renal Ischemia–Reperfusion Injury Through Antioxidant Stress and Anti-inflammatory Responses and Improves Intestinal Microbial Distribution

Peng Zhang[†‡], *Xiuwu Han*[*†‡], *Xin Zhang*[‡] *and Xuhui Zhu*[‡]

Department of Urology, Beijing Chao-Yang Hospital, Capital Medical University, Beijing, China

OPEN ACCESS

Edited by:
Jie Yin,
Hunan Agricultural University, China

Reviewed by:
Tao Qiu,
Renmin Hospital of Wuhan University, China
Longlin Zhang,
Hunan Agricultural University, China

***Correspondence:**
Xiuwu Han
xiuwuhan@163.com

[†]*These authors share first authorship*

[‡]*These authors have contributed equally to this work*

Specialty section:
This article was submitted to Nutrition and Microbes, a section of the journal Frontiers in Nutrition

Received: *14 February 2021*
Accepted: *15 March 2021*
Published: *11 May 2021*

Citation:
Zhang P, Han X, Zhang X and Zhu X (2021) Lactobacillus acidophilus ATCC 4356 Alleviates Renal Ischemia–Reperfusion Injury Through Antioxidant Stress and Anti-inflammatory Responses and Improves Intestinal Microbial Distribution. Front. Nutr. 8:667695. doi: 10.3389/fnut.2021.667695

Background: Ischemia–reperfusion injury (IRI) is one of the main causes of acute kidney injury. Our previous results have shown that anti-oxidative stress decreased in the renal IRI model. This study aimed to investigate the effect of *Lactobacillus acidophilus* ATCC 4356 on oxidative stress, inflammation, and intestinal flora in renal IRI.

Methods: The model of renal IRI was established by cross-clamping the renal pedicle with non-traumatic vascular forceps. H&E staining was applied to observe the damage of kidney tissue in each group. The concentrations of serum blood urea nitrogen (BUN), creatinine (Cre), superoxide dismutase (SOD), glutathione (GSH), and malondialdehyde (MDA) were detected by biochemical kit. ELISA measured the concentrations of interleukin (IL)-1β, IL-8, IL-4, and IL-10. qRT-PCR was performed to detect molecular expressions of ATCC 4356, oxidative stress-related factors [nuclear factor-related factor 2 (Nrf2), heme oxygenase 1 (HO-1)], inflammatory factors [tumor necrosis factor (TNF)-α, IL-1β, IL-8, interferon (IFN)-γ, IL-4, IL-10], and apoptosis-related factors [caspase 3, Bax, Bcl2, high-mobility group box protein 1 (HMGB1)]. Except for ATCC 4356, the protein expression of the above indicators was detected by Western blot. The apoptosis level of renal tissue cells was detected by TdT-mediated dUTP nick end labeling (TUNEL). 16S rDNA gene sequencing was used to detect the changes of microbial species in the contents of the duodenum and screen out the differentially expressed flora.

Results: Both the glomeruli and renal tubules of ischemia/reperfusion (I/R) mice were severely damaged. H&E result displayed that *L. acidophilus* ATCC 4356 attenuated the infiltration of inflammatory cells caused by I/R. ATCC 4356 reduced the high expression of BUN and Cre in I/R mice with a dose effect. It also reduced the high expression of MDA, TNF-α, IL-1β, IL-8, IFN-γ, caspase 3, Bax, and HMGB1 in I/R mice, while it increased the low expression of SOD, GSH, Nrf2, HO-1, IL-4, IL-10, and Bcl2 in I/R mice. ATCC 4356 inhibited the high level of apoptosis in the kidney tissue of I/R mice. In IRI mice, the top 3 different gut microbiota were *Helicobacter*, *cultivated_bacterium*, and *k__Bacteria_ASV_3* compared with sham mice. Oral *L. acidophilus* ATCC 4356 reversed this change.

Conclusion: *L. acidophilus* ATCC 4356 attenuated renal IRI through anti-oxidative stress and anti-inflammatory response and improved the intestinal microbial distribution.

Keywords: *Lactobacillus acidophilus* (ATCC 4356), renal ischemia-reperfusion injury, intestinal microbial, antioxidant stress, anti-inflammatory

INTRODUCTION

Ischemia–reperfusion injury (IRI) is one of the main causes of acute kidney injury (AKI), which usually occurs during renal surgery (1). Renal IRI is a major clinical challenge faced by clinicians during the operation period of renal transplantation (2). Renal IRI is associated with high morbidity and mortality, and the pathophysiological process is complicated, while there is no good treatment method (3).

Oxidative stress, inflammation, and apoptosis are not only important causes of renal IRI but also key factors that cause renal insufficiency (4). For example, oxidative stress, inflammation, and apoptosis in diabetic rat models are intensified, thereby exacerbating rat renal IRI (5). Studies have found that resveratrol (RSV) decreased oxidative stress and inhibited inflammatory responses, which played a role in kidney protection (6). In addition, fibroblast growth factor 10 (FGF10) prevented renal IRI by regulating autophagy and inflammatory signal transduction (7). Similarly, nobiletin inhibited inflammatory cytokines and regulated inducible nitric oxide synthase (iNOS)–endothelial nitric oxide synthase (eNOS) expression, thereby protecting rats from renal IRI (8). Gastrin attenuated renal IRI by anti-apoptosis (9). Congruously, our previous results have indicated that anti-oxidative stress could alleviate renal IRI. Therefore, it may be a feasible way to prevent or reduce renal IRI by inhibiting oxidative stress, inflammation, and apoptosis.

Importantly, oral *Lactobacillus acidophilus* has the effect of anti-inflammation, anti-oxidative stress, and regulating intestinal microflora homeostasis, thus contributing to health benefits (10). In terms of antioxidant stress, oral *L. acidophilus* ATCC 4356 relieved the process of atherosclerosis by anti-oxidative stress (11). Oral *L. acidophilus* ATCC 4356 alleviated diabetic complications by antioxidant stress (12). In terms of anti-inflammation, oral *L. acidophilus* attenuated traumatic brain injury by anti-inflammatory response (13). We suspected that *L. acidophilus* ATCC 4356 was likely to exert an effect on renal IRI by regulating oxidative stress and inflammation.

A growing body of evidence has shown that the intestinal flora plays an important role in health and disease by regulating local and systemic immunity. Effective interventions of probiotic supplements on the composition of the intestinal flora can improve health and prevent the onset of certain diseases. For example, oral *L. acidophilus* reduced bacterial translocation and liver cell damage by regulating intestinal flora (14). We speculated that *L. acidophilus* ATCC 4356 alleviated renal IRI by regulating intestinal flora. In mechanism, the intestinal flora reached two sites [kidney and bone marrow (BM)] at the same time due to circulation. On the one hand, it reduced the maturation state of macrophages/monocytes. On the other hand, it inhibited the release of chemokines [monocyte chemoattractant protein (MCP)-1 and macrophage inflammatory protein (MIP)-2α] and the main functions (migration capacity). This reduced the influx of granulocytes to protect the kidney from damage (15).

In summary, this study will explore the effect of *L. acidophilus* ATCC 4356 on oxidative stress, inflammation, and intestinal flora in the renal IRI model. Our findings may provide a new prevention and treatment strategy for renal IRI diseases.

MATERIALS AND METHODS

Renal Ischemia/Reperfusion Model Construction

Eight-week-old specific pathogen-free (SPF)-grade C57/BL6 male mice were housed in standard laboratory cages and allowed free access to food and water. All experimental protocols were approved by the Animal Ethics Committee of Capital Medical University. The mice were anesthetized by intraperitoneal injection of sodium pentobarbital (50 mg/kg body weight). It was then placed on a heating pad to maintain the body temperature at 37°C. Laparotomy was performed on the animal. The renal hilum was exposed bilaterally. The bilateral renal pedicle was cross-clamped with non-traumatic vascular forceps for 28 min to complete renal ischemia. Before the end of the ischemic period, the cross-clamped with non-traumatic vascular forceps were removed. Renal ischemia during clamping and subsequent renal reperfusion after release of clamping were visually monitored by renal discoloration and recoloration, respectively. The bilateral kidney was observed for 5 min to ensure reperfusion for 48 h. The animals in the Sham group underwent the same operation without clamping the kidney pedicle. The abdomen was sutured with 5.0 Monocryl sutures (Ethicon, USA).

Preparation of *Lactobacillus acidophilus* ATCC 4356

L. acidophilus ATCC 4356 was obtained from ATCC (Manassas, Virginia, USA). The original culture was stored in 40% (volume/volume) glycerin at −80°C prior to use. The 1% inoculum was grown in sterile De Man, Rogosa, and Sharpe broth (DIFCO, Detroit, Michigan, USA). The organisms were subcultured three times and then grown at 37°C for 16 h. The inoculum was stored at 4°C between transfers.

Lactobacillus Acidophilus ATCC 4356 Intervention

Sixty 8-week-old SPF C57/BL6 male mice were randomly divided into five groups (n = 10). The 40 mice were established with renal IRI model. Model mice were given vehicle, 1 * 10^8 CFU/ml, 5 * 10^8 CFU/ml, 1 * 10^9 CFU/ml *L. acidophilus* ATCC 4356 by intragastric gavage, 0.2 ml/head/day for 4 weeks, respectively. The remaining 10 mice were in the Sham group, which were given an equal-volume vehicle. The experiment was divided into Sham group, ischemia/reperfusion (I/R) group, La.L group, La.M group, and La.H group. At the fourth weekend of the intervention, all animals were sacrificed. Samples needed for testing were collected.

Hematoxylin–Eosin Staining

The mouse kidney tissue was fixed in 4% paraformaldehyde for more than 24 h. The tissue was flushed with running water. The tissue was dehydrated by gradient ethanol and was transparent by xylene. Subsequently, the tissue was embedded in paraffin. A paraffin microtome (YD-315, Yidi, China) was used to prepare 4-µm-thick sections. The slices were baked in a 62°C oven for more than 8 h. The tissue was deparaffinized and rehydrated with xylene and gradient ethanol. The cytoplasm was stained with eosin to varying degrees of pink or red, in sharp contrast to the blue nucleus stained with hematoxylin. The sections were observed under an optical microscope (BA210T; Motic, Singapore).

Biochemical Testing

Experimental procedures were strictly performed according to the biochemical kit (C013-1, C011-2-1, A001-3, A006-2-1, A003-1-2; Nanjing Jiancheng Bioengineering Institute, China). The absorbance values of each group at 640-, 546-, 450-, 405-, and 532-nm wavelengths were detected using a microplate reader (MB-530, Huisong, China). The contents of blood urea nitrogen (BUN), creatinine (Cre), superoxide dismutase (SOD), glutathione (GSH), and malondialdehyde (MDA) in serum were calculated through the formula.

ELISA

The blood was centrifuged at 1,000g for 20 min at 2–8°C. The supernatant was collected. ELISA kits (CSB-E08054m, CSB-E04634m, CSB-E04594m; Wuhan Huamei, China) and (ml063162; Shanghai Meilian, China) were used to detect the concentrations of interleukin (IL)-1β, IL-4, IL-10, and IL-8. The experimental instructions were strictly implemented. The absorbance values of each group at 450-nm wavelength were detected through the microplate reader.

Quantitative Real-Time Polymerase Chain Reaction

Total RNA was isolated from kidney tissues in each group using TRIzol® reagent (Thermo Fisher, 15596026, USA). The cDNAs were synthesized using mRNA reverse transcription kit (CW2569, Kangwei reagent, China). UltraSYBR Mixture (CW2601, Kangwei Reagent, China) was used for PCR reaction. The fluorescent quantitative PCR system was ThermoFisher (PikoReal 96). Glyceraldehyde 3-phosphate dehydrogenase (GAPDH) was used as an internal reference. The relative expression level was calculated using the $2^{-\Delta\Delta Ct}$ method. The sequences of mRNA primers are in **Table 1**.

TABLE 1 | Primer sequences.

Name	Sequences
Nrf2	Forward GCTCCTATGCGTGAATCCCAA Reverse TTTGCCCTAAGCTCATCTCGT
HO-1	Forward TCCATGTTGACTGACCACGACT Reverse CCCACCCCTCAAAAGATAGCC
TNF-α	Forward AGCACAGAAAGCATGATCCG Reverse CACCCCGAAGTTCAGTAGACA
IL-1β	Forward TGAAATGCCACCTTTTGACAGT Reverse TTCTCCACAGCCACAATGAGT
IL-8	Forward AGACAGAGATACCGCCACGTTC Reverse AGAGAAAGCCTACACACAGTCCT
IFN-γ	Forward GCCACGGCACAGTCATTGA Reverse TGCTGATGGCCTGATTGTCTT
IL-4	Forward ATGTACCAGGAGCCATATCCACGG Reverse TCCCTTCTCCTGTGACCTCGTT
IL-10	Forward GTTCCCCTACTGTCATCCCC Reverse AGGCAGACAAACAATACACCA
Caspase 3	Forward TCTGACTGGAAAGCCGAAACTCT Reverse AGCCATCTCCTCATCAGTCCCA
Bax	Forward TGAAGACAGGGGCCTTTTTG Reverse AATTCGCCGGAGACACTCG
Bcl2	Forward TTGAAAACCGAACCAGGAATTGC Reverse GTCCTGTGCCACTTGCTCT
HMGB1	Forward ATCGTTCTCTTAAAGTGCCAGT Reverse ACGCAAATGTAAAGAACCCAAG
GAPDH	Forward GCGACTTCAACAGCAACTCCC Reverse CACCCTGTTGCTGTAGCCGTA

GAPDH, glyceraldehyde 3-phosphate dehydrogenase; HMGB1, high-mobility group box protein 1; HO-1, heme oxygenase 1; IFN-γ, interferon-γ; IL-4, interferon; Nrf2, nuclear factor-related factor 2; TNF-α, tumor necrosis factor-α.

Bacterial Quantitative Real-Time Polymerase Chain Reaction

According to the manufacturer's instructions, the QIAamp DNA Fecal Mini Kit (Qiagen, Hilden, Germany) was used to extract bacterial DNA from the digestion of the colon of C57/BL6 mice. UltraSYBR Mixture (CW2601, Kangwei Reagent, China) was used for PCR reaction. The fluorescent quantitative PCR system was ThermoFisher (PikoReal 96). The primers to quantify *L. acidophilus* ATCC 4356 are listed in **Table 2**. The initial DNA denaturation step was at 95°C for 10 min. Thirty amplification cycles (95°C for 15 s, 55°C for 25 s, and 72°C for 20 s) were performed. The Cp-value was drawn by using the DNA ASSAY kit (Qiagen, Hilden, Germany). The standard curve was drawn. Real-time monitoring

TABLE 2 | Sequence of primers used for detection of bacteria.

Target	Sequence
Sequences of primers used for detection of bacteria	Forward CTTCGGTGATGACGTTGGGA Reverse CTTCGGTGATGACGTTGGGA

was achieved by measuring fluorescence at the end of the extension phase.

Western Blot

The kidney tissues of each group were taken out at −80°C. Appropriate amount of radioimmunoprecipitation assay (RIPA) lysis buffer (P0013B; Shanghai Biyuntian, China) was added to lyse the samples. The cell supernatant was collected through centrifugation. The instructions of the bicinchoninic acid (BCA) protein quantitative kit were strictly implemented to determine the protein concentration. Next, we took the same mass of protein and loaded it on the Bolt Bis-Tris gel. After electrophoresis, the protein was transferred to the membrane. The membrane was immersed in 5% skimmed milk powder and sealed at room temperature for 1 h. The sample was incubated with an appropriate amount of primary antibody at room temperature for 90 min, including Nrf2 (16396-1-AP, 1:1,000; Proteintech, USA), heme oxygenase 1 (HO-1; 10701-1-AP, 1:3,000; Proteintech, USA), tumor necrosis factor (TNF)-α (ab6671, 1:2,000; Abcam, UK), IL-1β (16806-1-AP, 1:2,000; Proteintech, USA), IL-8 (ab10727, 1:1,000; Abcam, UK), interferon (IFN)-γ (15365-1-AP, 1:2,000; Proteintech, USA), IL-4 (ab239508, 1:5,000; Abcam, UK), IL-10 (ab133575, 1:1,000; Abcam, UK), caspase 3 (19677-1-AP, 1:2,000; Proteintech, USA), Bax (50599-2-lg, 1:6,000; Proteintech, USA), Bcl2 (12789-1-AP, 1:6,000; Proteintech, USA), high-mobility group box protein 1 (HMGB1; 10829-1-AP, 1:1,500; Proteintech, USA), and internal reference β-actin (60008-1-Ig, 1:5,000; Proteintech, USA). The samples were incubated with secondary antibody horseradish peroxidase (HRP)-goat anti-rabbit IgG (SA00001-2, 1:6,000; Proteintech, USA) or HRP goat anti-mouse IgG (SA00001-1, 1:5,000; Proteintech, USA) at room temperature for 90 min. The sample was exposed to enhanced chemiluminescence (ECL) development.

TdT-Mediated dUTP Nick End Labeling

Mouse kidney tissue was fixed in 4% paraformaldehyde for more than 24 h. The tissue was dehydrated by gradient ethanol and was transparent by xylene. Subsequently, the tissue was embedded in paraffin. A paraffin microtome (YD-315, Yidi, China) was used to prepare 4-μm-thick sections. The slices were baked in a 62°C oven for more than 8 h. The tissue was deparaffinized and rehydrated with xylene and gradient ethanol. The instructions of TdT-mediated dUTP nick end labeling (TUNEL) kit (40306ES50, Yeasen, China) were strictly carried out. The apoptosis of kidney tissues in each group was observed under a fluorescence microscope (BA410T; Motic, Singapore). Here, 3–5 400× visual fields for each group were randomly selected. Apoptosis rate (number of positive nuclei under the field of view/total number of nuclei under the field of view) was evaluated in each group.

16s rDNA

Based on the manufacturer's recommendations, microbial genomic DNA was extracted from the duodenal contents using the QIAamp® Fast DNA Stool Mini Kit (QIAGEN). The quality of the extracted DNA was detected using the Agilent 4200 Tapestation (Agilent Technologies) Kit. The NextEra XT DNA Sample Prep Kit (Illumina) was used to generate the sequencing library. The Agilent 4200 Tapestation confirmed the quality of the library. The whole genome of the samples was sequenced on HiSeq 2500 platform (Illumina) to obtain the original data for quality control.

Data Analysis

All data are expressed as mean ± standard deviation. All experiments were repeated three times independently. GraphPad Prism 8.0 statistical software was used to compare the data between two or three groups using Student's T-test or one-way analysis of variance. $P < 0.05$ was considered statistically significant.

RESULTS

Lactobacillus acidophilus ATCC 4356 Relieved Renal Injury in Mice With Ischemia/Reperfusion

H&E results showed that the I/R model caused serious damage to the glomerulus and renal tubules, and a large number of inflammatory cell infiltrates was seen in the renal tissue. *L. acidophilus* ATCC 4356 attenuated the damage and the inflammatory cell infiltration caused by I/R (**Figure 1A**). ELISA was applied to detect the changes of serum urea nitrogen (BUN) and Cre in each group. Renal IRI caused a significant increase in the expression of BUN and Cre in serum, while ATCC 4356 decreased the expression of BUN and Cre (**Figures 1B,C**). qRT-PCR was used to detect the colonization of ATCC 4356 in the colon. The results showed that there were a certain number of copies of ATCC 4356 in I/R mice (**Figure 1D**). The effect of ATCC 4356 showed a dose effect. Therefore, ATCC 4356 (1×10^9 CFU/ml) was selected for the follow-up study. In summary, *L. acidophilus* ATCC 4356 alleviated renal injury in mice with I/R.

Lactobacillus acidophilus ATCC 4356 Attenuated the Level of Oxidative Stress in Mice With Renal Ischemia–Reperfusion Injury

The Nrf2/antioxidant responsive element (ARE) signaling pathway is a key pathway in the anti-oxidative damage. Our previous experimental results proved that the expression of Nrf2 and HO-1 decreased in the renal IRI model, which indicated that the level of oxidative stress elevated. To determine the effect of ATCC 4356 on oxidative stress levels in mice with renal IRI, we used ELISA to detect the expression of SOD, GSH, and MDA in serum. Compared with the Sham group, the levels of SOD and

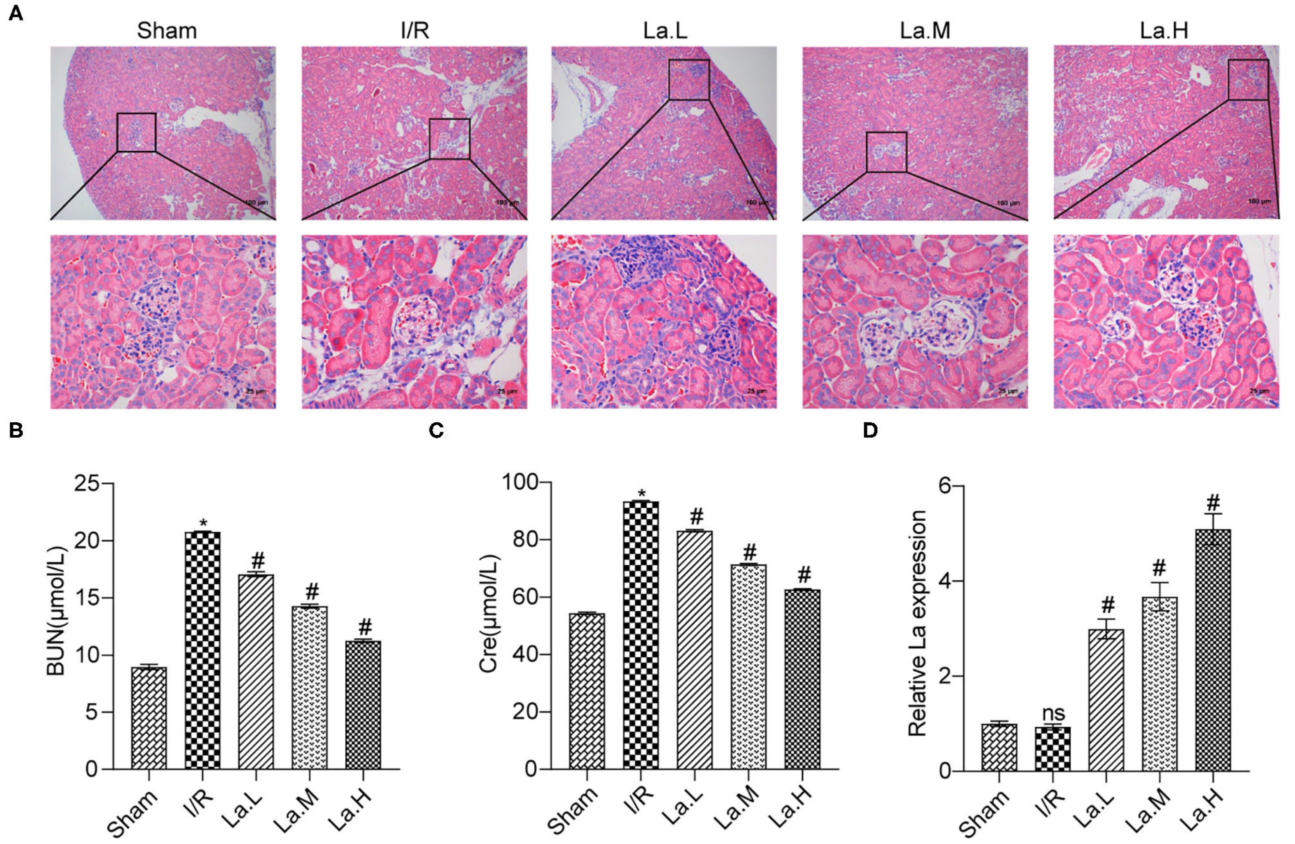

FIGURE 1 | *Lactobacillus acidophilus* ATCC 4356 relieved renal injury in mice with ischemia/reperfusion (I/R). **(A)** The kidney tissue damage was observed by H&E staining in each group. **(B)** *L. acidophilus* ATCC 4356 reduced serum blood urea nitrogen (BUN) expression in I/R mice. **(C)** *L. acidophilus* ATCC 4356 decreased serum creatinine (CRE) expression in I/R mice. **(D)** *L. acidophilus* ATCC 4356 was colonized in the intestine of I/R mice. All data are expressed as mean ± standard deviation. All experiments were repeated three times independently. Statistical significance was calculated using one-way analysis of variance. $^*p < 0.05$ vs. Sham, $^\#p < 0.05$ vs. I/R.

GSH in the I/R group decreased, and the levels of MDA increased. ATCC 4356 elevated the expression of SOD (**Figure 2A**) and GSH (**Figure 2B**) in I/R mice, while it decreased the expression of MDA (**Figure 2C**) in I/R mice. The expression of Nrf2 and HO-1 molecules and protein in kidney tissue were detected by qRT-PCR and Western blot. ATCC 4356 increased the levels of Nrf2 and HO-1 molecules in the kidney tissue of I/R mice (**Figure 2D**). The protein level and molecular level of the above two indicators were consistent (**Figure 2E**). *L. acidophilus* ATCC 4356 reduced the level of oxidative stress in mice with renal IRI.

Lactobacillus acidophilus ATCC 4356 Inhibited the Expression of Inflammatory Factors in Mice With Renal Ischemia–Reperfusion Injury

We have previously confirmed that *L. acidophilus* ATCC 4356 could alleviate renal IRI. Renal IRI is often accompanied by inflammatory response. Based on this, we examined inflammatory factors in mice with renal IRI. The results of the ELISA experiment showed that ATCC 4356 reduced the expression of pro-inflammatory factors (IL-1β and IL-8) in the serum of I/R mice, while it elevated the expression of anti-inflammatory factors (IL-4 and IL-10) (**Figures 3A–D**). The above indicator expressions in the kidney tissue were also obtained by qRT-PCR and Western blot experimental methods, and the expression trend was consistent with that in ELISA. In addition, ATCC 4356 inhibited the high expression of TNF-α and IFN-γ in kidney tissue induced by I/R significantly (**Figures 3E,F**).

Lactobacillus acidophilus ATCC 4356 Inhibited Cell Apoptosis in Mice With Renal Ischemia–Reperfusion Injury

In order to further clarify the effect of *L. acidophilus* ATCC 4356 on cell apoptosis in mice with renal IRI, we first detected the expression of apoptosis-related proteins in kidney tissue. The results showed that ATCC 4356 decreased the expression of pro-apoptotic factors (caspase 3, Bax, and HMGB1) and promoted the expression of anti-apoptotic factor Bcl2 at both the transcription level (**Figure 4A**) and translation level (**Figure 4B**).

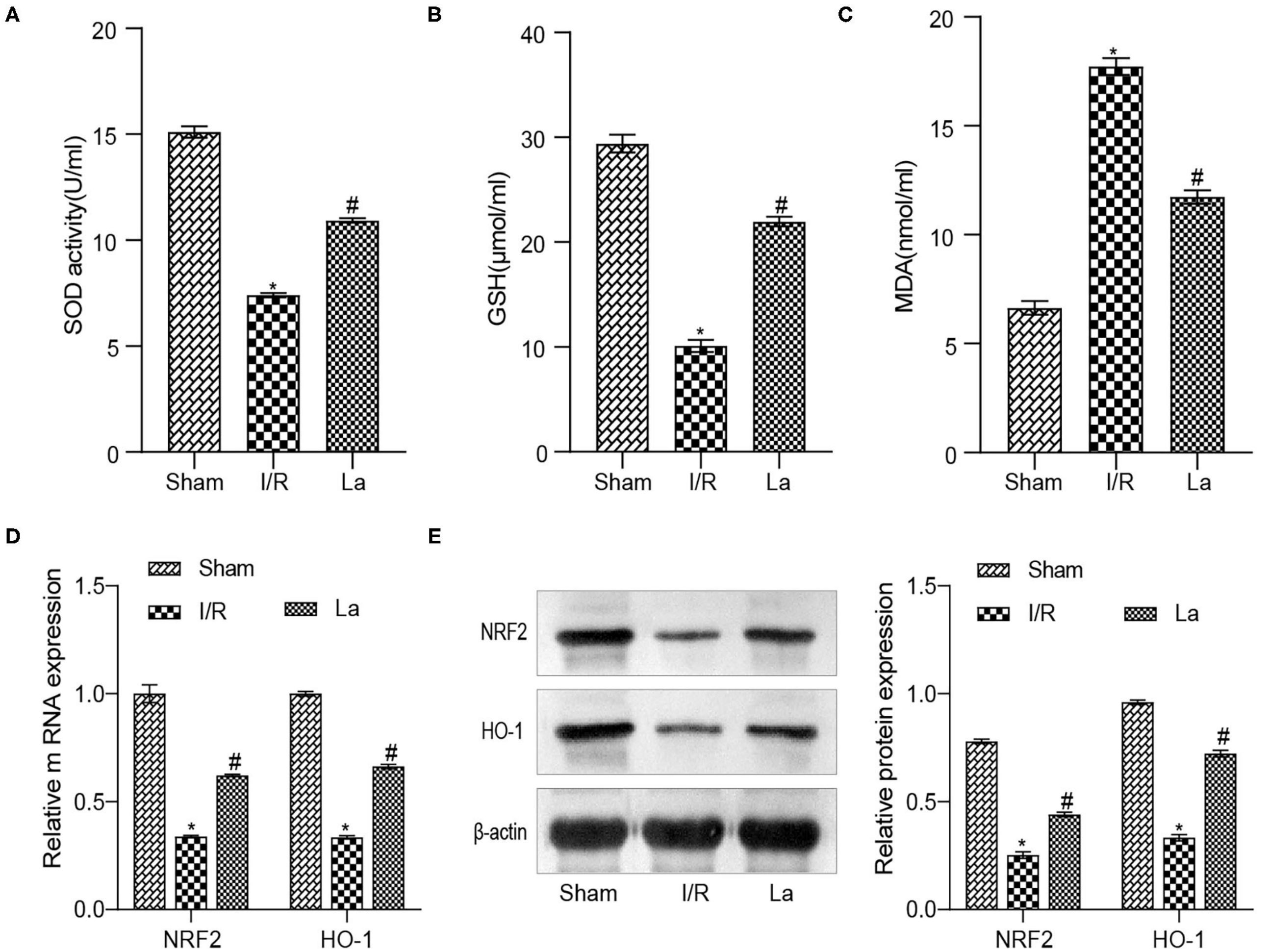

FIGURE 2 | *Lactobacillus acidophilus* ATCC 4356 reduced the level of oxidative stress in mice with renal ischemia–reperfusion injury (IRI). **(A)** ATCC 4356 elevated superoxide dismutase (SOD) concentration in ischemia/reperfusion (I/R) mice. **(B)** ATCC 4356 promoted glutathione (GSH) expression in I/R mice. **(C)** ATCC 4356 decreased malondialdehyde (MDA) levels in I/R mice. **(D)** ATCC 4356 promoted the expression of nuclear factor-related factor 2 (Nrf2) and heme oxygenase 1 (HO-1) mRNA in I/R mice. **(E)** ATCC 4356 increased Nrf2 and HO-1 protein expression in I/R mice. All data are expressed as mean ± standard deviation. All experiments were repeated three times independently. Statistical significance was calculated using one-way analysis of variance. $^{*}p < 0.05$ vs. Sham, $^{\#}p < 0.05$ vs. I/R.

Next, TUNEL fluorescence experiment was applied to evaluate the level of apoptosis in kidney tissue. It could be seen from **Figure 4C** that ATCC 4356 reduced the apoptosis rate of renal tissue in I/R mice. The above results indicated that *L. acidophilus* ATCC 4356 inhibits cell apoptosis in mice with renal IRI.

Effect of *Lactobacillus acidophilus* ATCC 4356 on the Gut Microbiota in Mice With Renal Ischemia–Reperfusion Injury

At the level of the intestinal flora, we randomly selected five mice from each group of Sham, I/R, and La group to detect the contents of the duodenum. It further showed the effect of oral *L. acidophilus* ATCC 4356 on the imbalance of intestinal flora in mice with renal IRI. The principal coordinates analysis (PCoA) was used to determined β diversity (**Figure 5A**). It could be seen that the gut microorganisms between the Sham group and the I/R group showed their own uniqueness, while the gut microorganisms in the La group showed a correlation with those in the Sham group. Analysis of similarities (anosim) was a statistical method that was mainly used to analyze the similarity between high-dimensional data groups (**Figure 5B**). Anosim analysis showed that there were significant differences among Sham, I/R, and La groups ($r = 0.18$, $P = 0.012$). The heatmap showed the top 20 differential microorganisms, and the top 3 were *Helicobacter*, *cultivated_bacterium*, and *k__Bacteria_ASV_3* (**Figure 5C**). The relative abundance of all samples at class and order levels was listed (**Figures 5D,E**). We further found that the relative abundance of *Helicobacter* in the Sham group was significantly higher than that in the I/R group at class and order levels. In the Sham group, the *uncultured_Bacteria* and *K__Bacteria_ASV_3* were significantly lower than those of the I/R group. At the same time, the relative abundance of these three flora

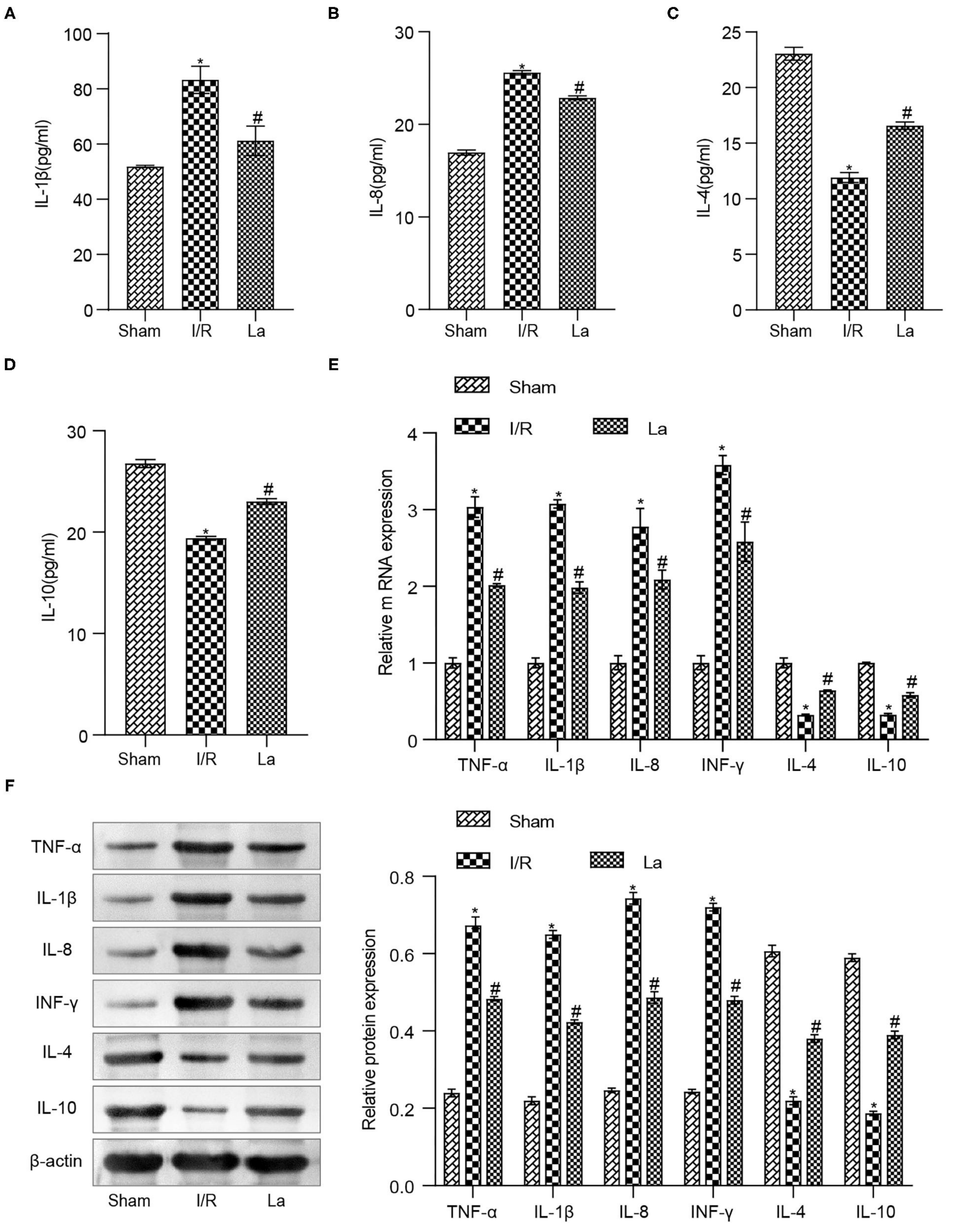

FIGURE 3 | *Lactobacillus acidophilus* ATCC 4356 inhibited the expression of inflammatory factors in mice with renal ischemia–reperfusion injury (IRI). **(A)** Interleukin (IL)-1β concentration in serum. **(B)** IL-8 concentration in serum. **(C)** IL-4 concentration in serum. **(D)** IL-10 concentration in serum. **(E)** Molecular levels of tumor necrosis factor (TNF)-α, IL-1β, IL-8, interferon (IFN)-γ, IL-4, and IL-10 in kidney tissue. **(F)** Protein levels of TNF-α, IL-1β, IL-8, IFN-γ, IL-4, and IL-10 in kidney tissue. All data are expressed as mean ± standard deviation. All experiments were repeated three times independently. Statistical significance was calculated using one-way analysis of variance. *$p < 0.05$ vs. Sham, #$p < 0.05$ vs. I/R.

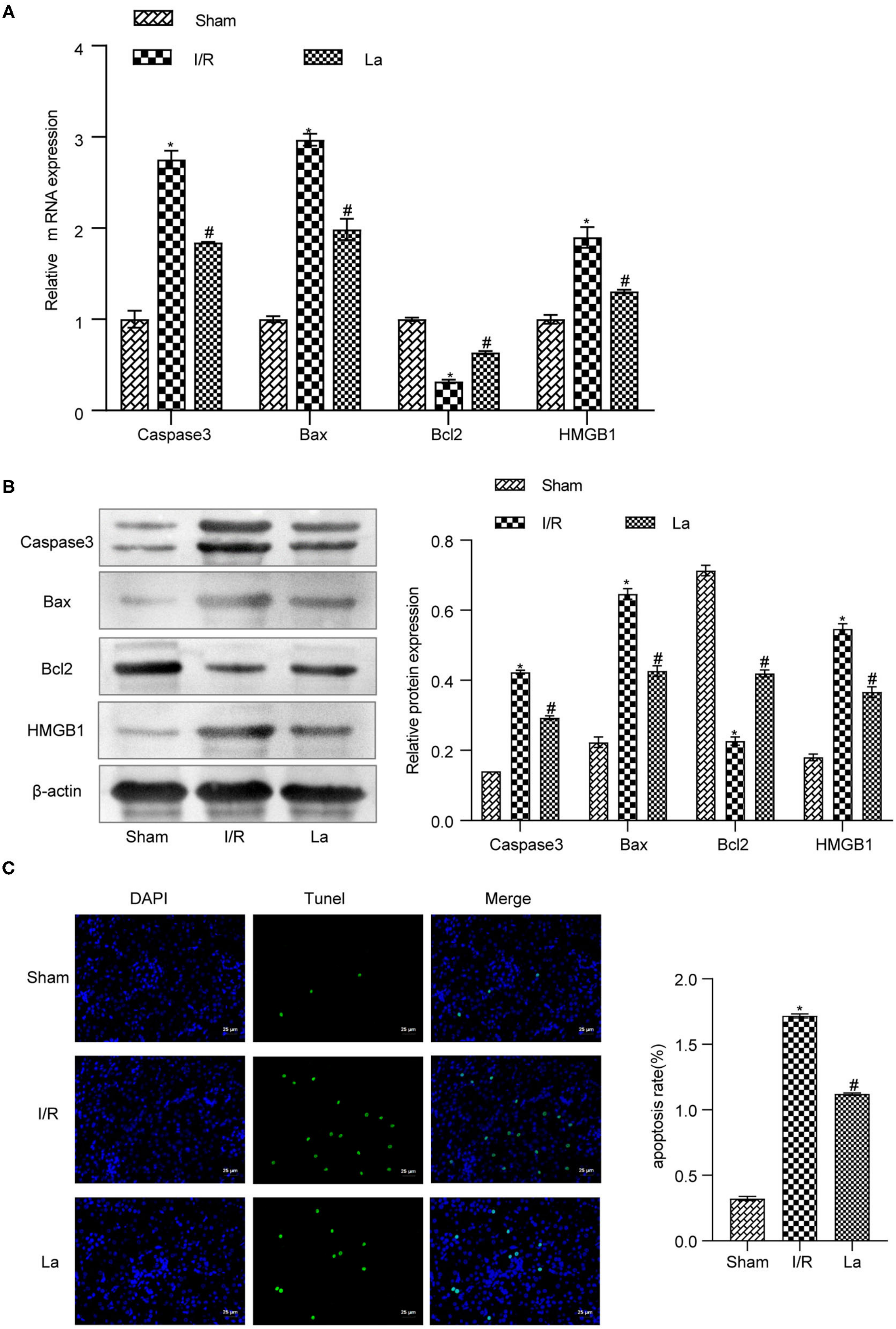

FIGURE 4 | *Lactobacillus acidophilus* ATCC 4356 inhibited cell apoptosis in mice with renal ischemia–reperfusion injury (IRI). **(A)** Relative mRNA levels of caspase 3, Bax, Bcl2, and high-mobility group box protein 1 (HMGB1) in renal tissues of each group. **(B)** The relative protein expression of caspase 3, Bax, Bcl2, and HMGB1 in kidney tissues of each group. **(C)** TdT-mediated dUTP nick end labeling (TUNEL; 400×, scale bar = 25 μm) to evaluate the apoptosis level of renal tissue in each group. All data are expressed as mean ± standard deviation. All experiments were repeated three times independently. Statistical significance was calculated using one-way analysis of variance. $^{*}p < 0.05$ vs. Sham, $^{\#}p < 0.05$ vs. I/R.

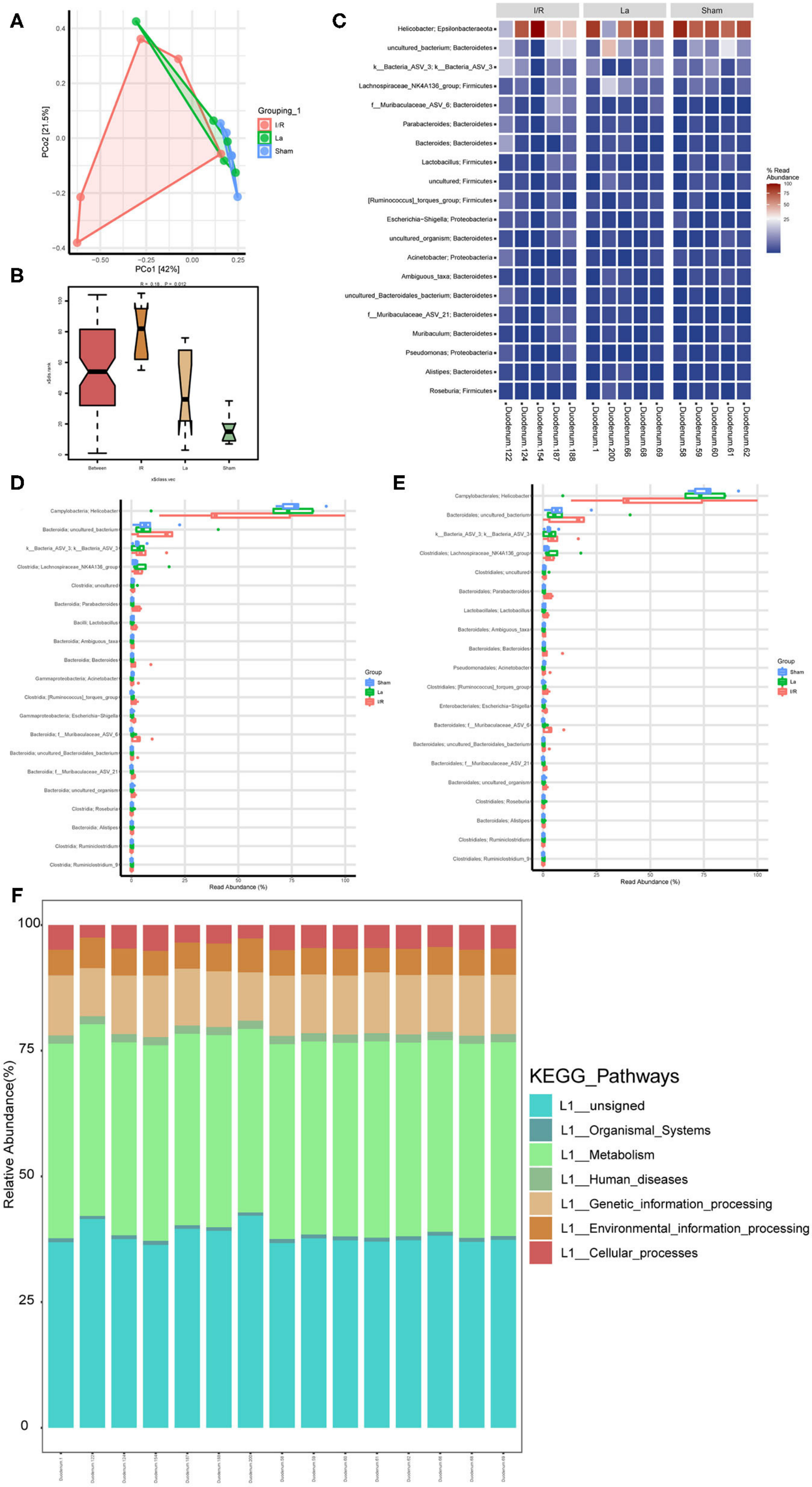

FIGURE 5 | Gut microbiota composition profiles in mice with renal ischemia–reperfusion injury (IRI). **(A)** Scatter plots of principal coordinates analysis (PCoA) for gut microbiota composition to show β-diversity in Sham, ischemia/reperfusion (I/R), and La group. **(B)** Anosim analysis to evaluate the overall similarity among Sham, I/R, and *(Continued)*

FIGURE 5 | and La group (R > 0 and $P < 0.05$). **(C)** Heatmap to show the different expressed metabolites between Sham, I/R, and La group. **(D)** Boxplot showed the top 20 microorganisms differentially expressed among the Sham, I/R, and La groups at the class level. **(E)** Boxplot showed the top 20 microorganisms differentially expressed among the Sham, I/R, and La groups at the order level. **(F)** Kyoto Encyclopedia of Genes and Genomes (KEGG) pathway showed the gene function enrichment of each sample.

in the La group was closer to that in the Sham group, which indicated that oral *L. acidophilus* ATCC 4356 effectively changed the abundance of flora. Kyoto Encyclopedia of Genes and Genomes (KEGG) annotation was performed on different groups of intestinal microorganisms (**Figure 5F**). The results showed that organismal systems, metabolism, human diseases, genetic information processing, environmental information processing, and cellular processes may have a certain effect on renal IRI. In conclusion, we could clearly understand that renal IRI can cause changes in intestinal microorganisms. At the same time, oral *L. acidophilus* ATCC 4356 could improve the intestinal flora imbalance caused by renal IRI.

DISCUSSION

Renal IRI research has always been a research hotspot of organ transplantation and general surgery (16). This study preliminarily explained the potential mechanism of ATCC 4356 to relieve renal IRI. In our study, we found that oral *L. acidophilus* ATCC 4356 alleviated the oxidative stress, inflammation, and cell apoptosis in the renal IRI mice. At the same time, ATCC 4356 regulated the homeostasis of intestinal flora in renal IRI mice. These suggested that ATCC 4356 might exert anti-oxidative stress, anti-inflammatory, and anti-apoptotic effects and improve the intestinal microbial distribution, thereby alleviating the process of renal IRI.

Decades of studies have shown that kidney tissue damage could be alleviated by reducing oxidative stress, inflammation, and cell death (17). Oral *L. acidophilus* could improve the cardiac function of mice with myocardial infarction (18). In this study, ATCC 4356 reduced the concentration of BUN and Cre in the serum of renal IRI mice. Meanwhile, H&E results showed that ATCC 4356 relieved the damage of kidney tissue in IRI mice. Oral *L. acidophilus* could protect against liver injury through its antioxidant effect, which included decreasing the expression of MDA and promoting the expression of SOD and Nrf2 (19). In renal IRI mice, we noted that ATCC 4356 increased the levels of SOD and GSH in the serum, while MDA level was reversed. This implied that ATCC 4356 played an anti-oxidative stress role in renal IRI. Nrf2/downstream antioxidant factor HO-1 (Nrf2/HO-1) axis acts an important role in anti-oxidative stress (20). On this basis, we further detected the expression of Nrf2 and HO-1 in kidney tissue at the mRNA and protein levels. The results showed that the expressions of both were upregulated with ATCC 4356 treatment in renal IRI mice. This suggested that ATCC 4356 may alleviate renal IRI through antioxidant stress.

Renal tissue damage can also be alleviated by an anti-inflammatory response. Previous studies have found that oral *L. acidophilus* could play an anti-inflammatory role in mouse colitis (21). ATCC 4356 inhibited the expression of IL-17, TNF-α, and IFN-γ, thereby mediating colon injury (22). These showed that ATCC 4356 had the potential of reducing inflammation. Our research supported this view. We found that ATCC 4356 upregulated the levels of anti-inflammatory factors (IL-4, IL-10) in renal IRI mice but downregulated the levels of pro-inflammatory factors (IL-1β, IL-8, TNF-α, and IFN-γ). In addition, ATCC 4356 exhibited an inhibitory effect on pro-apoptotic factors (caspase 3, Bax, and HMGB1) and a promotion on the anti-apoptotic factor (Bcl2). From TUNEL, it was noted that the apoptosis of kidney tissue in IRI mice was reduced *via* ATCC 4356 intervention. Therefore, we speculated that ATCC 4356 may relieve renal IRI through its influence on inflammatory signal pathway transduction. Our next work will focus on the potential signaling pathways and target cells of ATCC 4356 in renal IRI. As far as we know, changes in the structure and composition of the intestinal flora are associated with host function. Regulation of intestinal flora significantly reduced renal IRI (15). VSL#3 probiotics alleviate renal IRI by maintaining the required number of beneficial intestinal flora and inhibiting the proliferation of harmful bacteria (23). From a recent study, oral *L. acidophilus* modulated the intestinal flora structure and composition, thereby increasing the production of short-chain fatty acids (SCFAs) and reducing the number of Gram-negative bacteria to prevent chronic alcoholic liver injury in mice (24). Therefore, we suspected that ATCC 4356 alleviated renal IRI, which may be related to the intestinal flora. In this study, we further explored the effect of ATCC 4356 on the intestinal flora of renal IRI mice. The 16s DNA results showed that the relative abundance of *Helicobacter* in the Sham group was significantly higher than that in the I/R group at class and order levels. In the Sham group, the *uncultured_Bacteria* and *K__Bacteria_ASV_3* were significantly lower than those of the I/R group. And we found that the abundance of these intestinal microorganisms tended to be normal by oral *L. acidophilus* ATCC 4356, which indicated that ATCC 4356 could effectively improve the effect of IRI on the abundance of intestinal microorganisms in mice. Furthermore, it may be the reason that ATCC 4356 alleviates renal IRI, including organism system, metabolism, human diseases, genetic information processing, environmental information processing, and cellular processes.

We found that *L. acidophilus* ATCC 4356 could improve the results and composition of the intestinal flora of IRI mice, which may be a regulator of alleviating renal IRI. Intestinal flora imbalance affects the development of kidney and other diseases, which may be related to the destruction of intestinal epithelial barriers (biological barriers, physical barriers, and immune barriers) (25). Intestinal flora influences the biological barrier to participate in the process of kidney injury by secreting different metabolites, such as SCFA and trimethylamino-N-oxide (TMAO) (26). In addition, intestinal flora influences the immune barrier to participate in the process of kidney injury by targeting immune cells (27). We suspected that ATCC 4356 changes the structure of the intestinal flora, leading to changes in metabolites, and thus had a positive regulatory effect on IRI mice. This possibility and possible mechanism need further study.

Considering the limited space and budget, the mechanism study and cell model will be our next research content. Based on previous studies, bromodomain protein 4 (BRD4) inhibition alleviates renal IRI by blocking the phosphoinositide 3-kinase (PI3K)/Akt pathway to block apoptosis and oxidative stress in proximal renal tubular epithelial cells (1). *L. acidophilus* can play an anti-inflammatory role by regulating the PI3K/Akt signaling pathway (28). We will use hypoxia and reoxygenation of proximal renal tubular epithelial cells (TECs) to simulate the renal I/R model *in vivo*. Then, *L. acidophilus* ATCC 4356, PI3K agonist, or PI3K inhibitor will be used to intervene the cells. Meanwhile, qRT-PCR and Western blot will be used to detect the expression of PI3K/Akt signaling pathway, oxidative stress, inflammation, and apoptosis-related factors in cells and renal tissues. Through the above experiments, we will further investigate the mechanism of *L. acidophilus* ATCC 4356 in reducing renal IRI.

CONCLUSION

In summary, *L. acidophilus* ATCC 4356 relieved renal IRI through anti-oxidative stress and anti-inflammatory response and improved the intestinal microbial distribution on renal IRI mice. This study explored the relationship between ATCC 4356 and renal IRI for the first time, which provided evidence that ATCC 4356 alleviated renal IRI. The regulation of intestinal microbiome may be a new potential mechanism for renal IRI.

DATA AVAILABILITY STATEMENT

The datasets presented in this study can be found in online repositories. The names of the repository/repositories and accession number(s) can be found at: https://www.ncbi.nlm.nih.gov/Traces/study/?acc=PRJNA703751.

ETHICS STATEMENT

The animal study was reviewed and approved by the Animal Ethics Committee of Capital Medical University.

AUTHOR CONTRIBUTIONS

All authors listed have made a substantial, direct and intellectual contribution to the work, and approved it for publication.

FUNDING

This work was supported by the Special Fund for Clinical Research of the Wu Jieping Medical Foundation (320.6750.16218).

ACKNOWLEDGMENTS

We thank the Special Fund for Clinical Research of the Wu Jiping Medical Foundation and the Capital Medical University for all the support.

REFERENCES

1. Liu H, Wang L, Weng X, Chen H, Du Y, Diao C, et al. Inhibition of Brd4 alleviates renal ischemia/reperfusion injury-induced apoptosis and endoplasmic reticulum stress by blocking FoxO4-mediated oxidative stress. *Redox Biol.* (2019) 24:101195. doi: 10.1016/j.redox.2019.101195
2. Smith SF, Hosgood SA, Nicholson ML. Ischemia-reperfusion injury in renal transplantation: 3 key signaling pathways in tubular epithelial cells. *Kidney Int.* (2019) 95:50–6. doi: 10.1016/j.kint.2018.10.009
3. Hosszu A, Fekete A, Szabo AJ. Sex differences in renal ischemia-reperfusion injury. *Am J Physiol Renal Physiol.* (2020) 319:F149–54. doi: 10.1152/ajprenal.00099.2020
4. Gholampour H, Moezi L, Shafaroodi H. Aripiprazole prevents renal ischemia/reperfusion injury in rats, probably through nitric oxide involvement. *Eur J Pharmacol.* (2017) 813:17–23. doi: 10.1016/j.ejphar.2017.07.032
5. Gong DJ, Wang L, Yang YY, Zhang JJ, Liu XH. Diabetes aggravates renal ischemia and reperfusion injury in rats by exacerbating oxidative stress, inflammation, and apoptosis. *Ren Fail.* (2019) 41:750–61. doi: 10.1080/0886022X.2019.1643737
6. Li J, Li L, Wang S, Zhang C, Zheng L, Jia Y, et al. Resveratrol alleviates inflammatory responses and oxidative stress in rat kidney ischemia-reperfusion injury and H2O2-induced NRK-52E cells via the Nrf2/TLR4/NF-κB pathway. *Cell Physiol Biochem.* (2018) 45:1677–89. doi: 10.1159/000487735
7. Tan X, Zhu H, Tao Q, Guo L, Jiang T, Xu L, et al. FGF10 protects against renal ischemia/reperfusion injury by regulating autophagy and inflammatory signaling. *Front Genet.* (2018) 9:556. doi: 10.3389/fgene.2018.00556
8. Güvenç M, Cellat M, Uyar A, Özkan H, Gokcek I, Isler CT, et al. Nobiletin protects from renal ischemia-reperfusion injury in rats by suppressing inflammatory cytokines and regulating iNOS-eNOS expressions. *Inflammation.* (2020) 43:336–46. doi: 10.1007/s10753-019-01123-w
9. Liu C, Chen K, Wang H, Zhang Y, Duan X, Xue y, et al. Gastrin attenuates renal ischemia/reperfusion injury by a PI3K/Akt/Bad-mediated anti-apoptosis signaling. *Front Pharmacol.* (2020) 11:540479. doi: 10.3389/fphar.2020.540479
10. Cavalcanti Neto MP, Aquino JS, Romão da Silva LF, de Oliveira Silva R, Guimarães KSL, de Oliveira Y, et al. Gut microbiota and probiotics intervention: a potential therapeutic target for management of cardiometabolic disorders and chronic kidney disease? *Pharmacol Res.* (2018) 130:152–63. doi: 10.1016/j.phrs.2018.01.020
11. Chen L, Liu W, Li Y, Luo S, Liu Q, Zhong Y, et al. Lactobacillus acidophilus ATCC 4356 attenuates the atherosclerotic progression through modulation of oxidative stress and inflammatory process. *Int Immunopharmacol.* (2013) 17:108–15. doi: 10.1016/j.intimp.2013.05.018
12. Sheikh Hosseini S, Gol A, Khaleghi M. The effects of the Lactobacillus acidophilus ATCC 4356 on the oxidative stress of reproductive system in diabetic male rats. *Int J Reprod Biomed.* (2019) 17:493–502. doi: 10.18502/ijrm.v17i7.4861
13. Ma Y, Liu T, Fu J, Fu S, Hu C, Sun B, et al. Lactobacillus acidophilus exerts neuroprotective effects in mice with traumatic brain injury. *J Nutr.* (2019) 149:1543–52. doi: 10.1093/jn/nxz105

14. Adawi D, Ahrné S, Molin G. Effects of different probiotic strains of Lactobacillus and Bifidobacterium on bacterial translocation and liver injury in an acute liver injury model. *Int J Food Microbiol.* (2001) 70:213–20. doi: 10.1016/S0168-1605(01)00550-5
15. Emal D, Rampanelli E, Stroo I, Butter LM, Teske GJ, Claessen N, et al. Depletion of gut microbiota protects against renal ischemia-reperfusion injury. *J Am Soc Nephrol.* (2017) 28:1450–61. doi: 10.1681/ASN.2016030255
16. Jonker SJ, Menting TP, Warlé MC, Ritskes-Hoitinga M, Wever KE. Preclinical evidence for the efficacy of ischemic postconditioning against renal ischemia-reperfusion injury, a systematic review and meta-analysis. *PLoS ONE.* (2016) 11:e0150863. doi: 10.1371/journal.pone.0150863
17. Yang Y, Song M, Liu Y, Liu H, Sun L, Peng Y, et al. Renoprotective approaches and strategies in acute kidney injury. *Pharmacol Ther.* (2016) 163:58–73. doi: 10.1016/j.pharmthera.2016.03.015
18. Sadeghzadeh J, Vakili A, Sameni HR, Shadnoush M, Bandegi AR, Zahedi Khorasani M, et al. The Effect of Oral Consumption of Probiotics in Prevention of Heart Injury in a Rat Myocardial Infarction Model: a Histopathological, Hemodynamic and Biochemical Evaluation *Iran Biomed J.* (2017) 21:174–81. doi: 10.18869/acadpub.ibj.21.3.174
19. Malyar RM, Naseri E, Li H, Ali I, Farid RA, Liu D, et al. Hepatoprotective effects of selenium-enriched probiotics supplementation on heat-stressed wistar rat through anti-inflammatory and antioxidant effects. *Biol Trace Elem Res.* (2020). doi: 10.1007/s12011-020-02475-3
20. Diao C, Chen Z, Qiu T, Liu H, Yang Y, Liu X, et al. Inhibition of PRMT5 attenuates oxidative stress-induced pyroptosis via activation of the Nrf2/HO-1 signal pathway in a mouse model of renal ischemia-reperfusion injury. *Oxid Med Cell Longev.* (2019) 2019:2345658. doi: 10.1155/2019/2345658
21. Wang Y, Gu Y, Fang K, Mao K, Dou J, Fan H, et al. Lactobacillus acidophilus and Clostridium butyricum ameliorate colitis in murine by strengthening the gut barrier function and decreasing inflammatory factors. *Benef Microbes.* (2018) 9:775–87. doi: 10.3920/BM2017.0035
22. Jiang Y, Yang G, Meng F, Yang W, Hu J, Ye L, et al. Immunological mechanisms involved in probiotic-mediated protection against Citrobacter rodentium-induced colitis. *Benef Microbes.* (2016) 7:397–407. doi: 10.3920/BM2015.0119
23. Ding C, Han F, Xiang H, Wang Y, Li Y, Zheng J, et al. Probiotics ameliorate renal ischemia-reperfusion injury by modulating the phenotype of macrophages through the IL-10/GSK-3β/PTEN signaling pathway. *Pflugers Arch.* (2019) 471:573–81. doi: 10.1007/s00424-018-2213-1
24. Li H, Shi J, Zhao L, Guan J, Liu F, Huo G, et al. Lactobacillus plantarum KLDS1.0344 and *Lactobacillus acidophilus* KLDS1.0901 mixture prevents chronic alcoholic liver injury in mice by protecting the intestinal barrier and regulating gut microbiota and liver-related pathways. *J Agric Food Chem.* (2020) 69:183–97. doi: 10.1021/acs.jafc.0c06346
25. Gong J, Noel S, Pluznick JL, Hamad ARA, Rabb H. Gut microbiota-kidney cross-talk in acute kidney injury. *Semin Nephrol.* (2019) 39:107–16. doi: 10.1016/j.semnephrol.2018.10.009
26. Sun G, Yin Z, Liu N, Bian X, Yu R, Su X, et al. Gut microbial metabolite TMAO contributes to renal dysfunction in a mouse model of diet-induced obesity. *Biochem Biophys Res Commun.* (2017) 493:964–70. doi: 10.1016/j.bbrc.2017.09.108
27. Aa LX, Fei F, Qi Q, Sun RB, Gu SH, Di ZZ, et al. Rebalancing of the gut flora and microbial metabolism is responsible for the anti-arthritis effect of kaempferol. *Acta Pharmacol Sin.* (2020) 41:73–81. doi: 10.1038/s41401-019-0279-8
28. Wang H, Zhang L, Li Q, Xu S, Lu R. Surface-layer protein produced by *Lactobacillus crispatus* JCM 2009 ameliorates lipopolysaccharide-induced inflammation through autophagy cross-talk with the NF-κB signaling pathway. *Int J Biol Macromol.* (2021) 166:633–40. doi: 10.1016/j.ijbiomac.2020.10.221

Conflict of Interest: The authors declare that the research was conducted in the absence of any commercial or financial relationships that could be construed as a potential conflict of interest.

frontiers in Nutrition

ORIGINAL RESEARCH
published: 19 May 2021
doi: 10.3389/fnut.2021.690138

Allobaculum Involves in the Modulation of Intestinal ANGPTLT4 Expression in Mice Treated by High-Fat Diet

Zibin Zheng[1,2], *Wentao Lyu*[1], *Ying Ren*[2], *Xiaoqiong Li*[1], *Shenjun Zhao*[2], *Hua Yang*[1] and *Yingping Xiao*[1]*

[1] State Key Laboratory for Managing Biotic and Chemical Threats to the Quality and Safety of Agro-Products, Institute of Agro-Product Safety and Nutrition, Zhejiang Academy of Agricultural Sciences, Hangzhou, China, [2] Hubei Key Laboratory of Animal Nutrition and Feed Science, Wuhan Polytechnic University, Wuhan, China

OPEN ACCESS

Edited by:
Jie Yin,
Hunan Agricultural University, China

Reviewed by:
Shiyu Tao,
Huazhong Agricultural University, China
Daxi Ren,
Zhejiang University, China

***Correspondence:**
Yingping Xiao
ypxiaozj@hotmail.com

Specialty section:
This article was submitted to Nutrition and Microbes, a section of the journal Frontiers in Nutrition

Received: 02 April 2021
Accepted: 26 April 2021
Published: 19 May 2021

Citation:
Zheng Z, Lyu W, Ren Y, Li X, Zhao S, Yang H and Xiao Y (2021) Allobaculum Involves in the Modulation of Intestinal ANGPTLT4 Expression in Mice Treated by High-Fat Diet. Front. Nutr. 8:690138. doi: 10.3389/fnut.2021.690138

Increasing studies have shown that obesity is the primary cause of cardiovascular diseases, non-alcoholic fatty liver diseases, type 2 diabetes, and a variety of cancers. The dysfunction of gut microbiota was proved to result in obesity. Recent research indicated ANGPTL4 was a key regulator in lipid metabolism and a circulating medium for gut microbiota and fat deposition. The present study was conducted to investigate the alteration of gut microbiota and ANGPTL4 expression in the gastrointestinal tract of mice treated by the high-fat diet. Ten C57BL/6J mice were randomly allocated to two groups and fed with a high-fat diet (HFD) containing 60% fat or a normal-fat diet (Control) containing 10% fat. The segments of ileum and colon were collected for the determination of ANGPTL4 expression by RT-qPCR and immunohistochemical analysis while the ileal and colonic contents were collected for 16S rRNA gene sequencing. The results showed HFD significantly increased mice body weight, epididymal fat weight, perirenal fat weight, liver weight, and the lipid content in the liver ($P < 0.05$). The relative expression of ANGPTL4 and the ANGPTL4-positive cells in the ileum and colon of mice was significantly increased by HFD treatment. Furthermore, 16S rRNA gene sequencing of the ileal and colonic microbiota suggested that HFD treatment changed the composition of the gut microbiota. The ratio of Firmicutes to Bacteroidetes and the abundance of *Allobaculum* was significantly higher in the HFD group than in the Control group while the abundance of *Adlercreutzia, Bifidobacterium*, *Prevotellaceae UCG-001*, and *Ruminococcus* was significantly decreased. Interestingly, the abundance of *Allobaculum* was positively correlated with the expression of ANGPTL4. These findings provide a theoretical foundation for the development of strategies to control the obesity and related diseases by the regulation of ANGPTL4 and gut microbiota.

Keywords: gut microbiota, ANGPTL4, fat deposition, high-fat diet, mice

INTRODUCTION

The epidemic rise in obesity has chronically challenged human health, performance and quality of life with affecting more than 2 billion people in the world and being related to diabetes, cancers and cardiovascular diseases (1, 2). Gut microbiota is composed of numerous bacteria that contribute to nutrition absorption and energy homeostasis (3, 4). Increasing evidences indicate that gut microbiota directly participates in obesity and many other metabolic diseases (4, 5). A recent study have shown that obesity could be induced by the high-fat diet (HFD) (6). Meanwhile, the dysregulation in the composition and metabolic functions of gut microbiota would promote the development of obesity (7). The microbiota transplantation from girls with or without obesity to mice showed a close relationship between gut microbiota and obesity (8). Furthermore, the significant higher abundance ratio of Firmicutes to Bacteroidetes is generally regarded as a marker signal of obesity (9). Therefore, gut microbiota is closely related to host lipid metabolism, the disorder of which alters the composition of gut microbiota. The dysfunctional gut microbiota would further affects the host lipid metabolism in turn (10).

Angiogenin-like protein 4 (ANGPTL4), also known as a fasting induction factor (FIAF), plays an important role in lipid deposition by inhibiting lipoprotein lipase (LPL) to regulate lipid metabolism (11, 12). ANGPTL4 can be secreted in intestines, adipose tissue, liver, skeletal muscle, heart and other tissues, and is subsequently cleaved into N-terminal and C-terminal fragments. The N-terminal of ANGPTL4 acts as a LPL inhibitor (13, 14). LPL is transported by the GPIHBP1 protein to the lumen side of capillary endothelial cells and catalyzes the hydrolysis of triglycerides (TG) into fatty acids. This process allows lipids transported from the circulation into skeletal muscle, heart and adipose tissue after absorption (15, 16). In addition, ANGPTL4 is an endogenous inhibitor for intestinal fat digestive enzymes, especially pancreatic lipase, to prevent excessive fatty acids intake and lipid overload in intestinal cells (17, 18). Furthermore, ANGPTL4 has been considered as a circulating mediator between gut microbiota and fat storage (19). The germ-free (GF) mice with a normal microbiota harvested from the cecum of conventionally raised mice could improve the TG storage in fat cells with inhibition of ANGPTL4 expression in gut, suggesting gut microbiota might promote fat deposition by modulating ANGPTL4 expression (19). The expression of lipogenic genes in the abdominal fat of mice receiving the fecal microbiota of Jinhua pigs (obese) was higher than that in the mice receiving the fecal microbiota of Landrace pigs (lean) with reduction of ANGPTL4 expression in the gastrointestinal tract (20). Therefore, the ANGPTL4 expression might be one of the key regulators for obesity induced by the dysfunction of gut microbiota.

ANGPTL4 acts as a circulating medium for the gut microbiota and fat deposition in the body, so it is of great significance to explore how the gut microbiota affects the expression of ANGPTL4. However, the research on the regulation of ANGPTL4 expression by gut microbiota in obesity is limited. Accordingly, the objective of the present study is to explore the relationship among the gut microbiota structure, the ANGPTL4 expression and fat deposition.

MATERIALS AND METHODS

Animals and Sampling

Ten specific pathogen-free (SPF) C57BL/6J male mice weaned at the age of 28 days were purchased from GemPharmatech Co., Ltd (Nanjing, China). The mice were raised in cages at 25 ± 2°C for 12 h light/dark cycles with free access to water and mouse chow. After acclimatization for 1 week, the mice were weighed and randomly divided into Control group and high-fat diet (HFD) group. Mice in the Control and HFD groups were fed with a commercial standard diet with 10% fat content and the standard diet supplemented with 60% fat, respectively for 12 weeks (21, 22). At the end of 12-week study, all mice were weighed individually and sacrificed by decapitation following a CO_2 stun. The epididymal fat and perirenal fat of each mice were isolated and weighed. The ileal and colonic contents were collected and stored at −20°C until DNA isolation and 16S rRNA gene sequencing. Segments of liver, ileum and colon were collected and fixed in 4% paraformaldehyde for further analysis. Ileum and colon segments were isolated, rinsed with 0.9% NaCl, immediately frozen in liquid nitrogen, and stored at −80°C until RNA extraction.

DNA Extraction, Sequencing, and Data Analysis

Microbial genomic DNA was extracted from ileal and colonic contents using QIAamp DNA Stool Mini Kit (QIAGEN, Valencia, CA, US). The V4∼V5 region of bacterial 16S rRNA gene was amplified from each genomic DNA sample by using the barcode-fusion primers 515F and 907R. Sequencing libraries were then constructed using TruSeq DNA PCR-Free Library Preparation Kit (Illumina) and sequenced on an Illumina HiSeq platform at Mingke Biotechnology (Hangzhou) Co., Ltd. The sequencing data were analyzed using QIIME software package (23). The non-repeating sequences were analyzed by operational classification unit (OTU) with 97% similarity. Species matching was performed for all representative sequences of OTU using RPD databases (24). Pie charts were generated to show taxa distribution at the phylum and genus levels. Principal coordinate analysis (PCoA) was performed to analyze the beta diversity. For further identify the specific genera related to fat deposition, this study also analyzed the raw data of gut microbiota combining with other two similar studies on mice fed with high-fat diets (DDBJ Accession Number: PRJDB7523) (25) (NCBI Accession Number: SRP113647) (26).

RNA Extraction and Real-Time Quantitative PCR

Total RNA was isolated using TRIzol®Plus RNA Purification Kit (Invitrogen) and RNase-Free DNase Set (Qiagen) followed by reverse transcription using the SuperScript™ III First-Strand Synthesis SuperMix (Invitrogen) strictly according to the manufacturer's instructions. Real-time qPCR was performed in triplicate on an ABI Prism 7700 Sequence Detector system

TABLE 1 | Primers used in the RT-qPCR analysis.

Gene	Genbank accession	Primer sequences (5′-3′)	Size (bp)
Pig GAPDH	NM_001206359.1	CCAGGGCTGCTTTTAACTCTG GTGGGTGGAATCATACTGGAACAT	104
Pig ANGPTL4	NM_001038644.1	GACTGCCAAGAGCTGTTTGAAGA CTGAATTACAGTCCAGCCTCCAT	126

(Applied Biosystems, Foster City, CA, USA) using an annealing temperature of 63°C and gene-specific primers listed in **Table 1**. The data were normalized to GAPDH or 18S rRNA and calculated by $2^{-\Delta\Delta CT}$ method (27).

Histological Staining and Immunohistochemistry

The liver egments were fixed in 4% paraformaldehyde for 1 h at room temperature, cryoprotected in 20% sucrose at 4°C overnight, and embedded in OCT. The prepared series of 12-µm cryosections were stained with Oil Red O (Sigma-Aldrich, St. Louis, MO, United States).

The ileal and colonic sections were deparaffinized and microwaved in sodium citrate buffer for antigen retrieval. After being rinsed with phosphate buffered saline (PBS), slides were incubated with PBS containing normal goat serum. After blocking, sections were incubated with primary antibody (proteintech ANGPTL4 18374-1-AP) at 4°C overnight. After wash with PBS and incubation with secondary antibody for 50 min at room temperature, slides were rinsed with PBS for three times and added with a few drops of chromogenic substrate DAB with incubation for 15 min. Finally, slides were rinsed in water and counterstained using hematoxylin solution for picture caption.

Statistical Analysis

All statistical analyses were performed by SPSS 23.0 (IBM, New York, NY, United States) using unpaired two-tailed Student's *t*-test (20). Data are presented as the mean ± SEM. Results were considered significant when $P < 0.05$.

RESULT

Obesity Induced by HFD

To confirm whether obesity was induced by the HFD, we weighed each mouse, liver, epididymal fat, and perirenal fat individually in both of Control and HFD groups. The body weight, liver weight, epididymal fat, and perirenal fat in the HFD-treated mice were significantly higher than those of the Control group by 82.31% ($P < 0.0001$), 106.58% ($P = 0.0234$), 194.08% ($P = 0.0011$), and 627.91% ($P = 0.0046$), respectively (**Figures 1A–D**). To observe the fat content in the liver, we stained liver segments of mice in the Control and HFD groups. The number of lipid droplets in the liver of HFD group (**Figure 1F**) was obviously more and larger than that in Control group (**Figure 1E**), suggesting obesity had been induced by HFD.

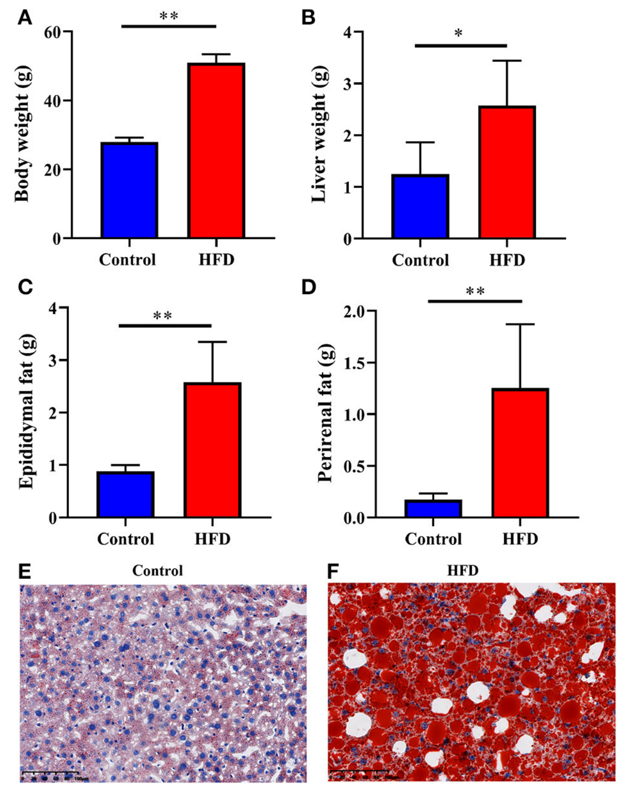

FIGURE 1 | Characterization of the obesity induced by HFD. The Control and HFD groups mice were analyzed for body weight **(A)**, liver weight **(B)**, epididymal fat weight **(C)**, perirenal fat weight **(D)**. Oil-red O stains of paraformaldehyde-fixed liver sections prepared from the Control **(E)** and HFD **(F)** group mice. Data were expressed as mean ± SEM and statistically analyzed by using unpaired two-tailed Students' *t*-test ($n = 5$). Asterisks (* and **) represent significant differences with $P < 0.05$ and $P < 0.01$, respectively.

HFD Increased the Expression of ANGPTL4 in the Gastrointestinal Tract

To examine whether the ANGPTL4 expression is involved in fat deposition, we determined the ANGPTL4 expression in the gastrointestinal tract by RT-qPCR analysis following RNA isolation and reverse transcription. Compared with the Control group, the relative expression of ANGPTL4 in the ileum ($P = 0.0452$) and colon ($P = 0.0409$) of mice in HFD group was increased significantly (**Figures 2A,B**). Furthermore, immunohistochemistry revealed the ANGPTL4-positive cells seemed to be more abundant in the HFD group (**Figures 2D,F**) than the Control group (**Figures 2C,E**), which was consistent with the trend of the relative expression of ANGPTL4 in the ileum and colon of mice in two groups.

HFD Altered the Gut Microbiota

To investigate the structure of gut microbiota in mice of the Control and HFD groups, we collected the ileal and colonic contents from mice of the Control and HFD groups and analyzed the alpha -diversity of gut microbiota. The alpha-diversity

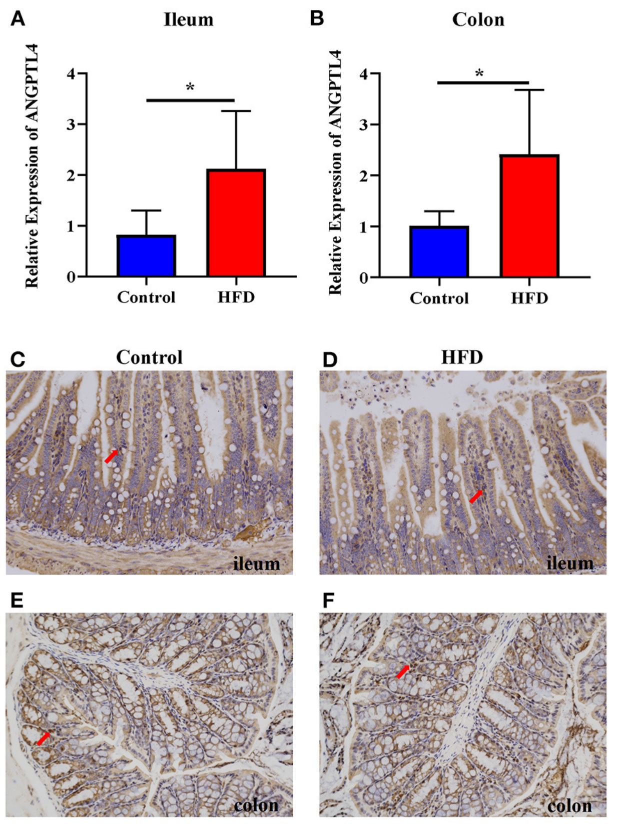

FIGURE 2 | The expression of ANGPTL4 in the ileum and colon of the Control and HFD groups. The mRNA expression level of ANGPTL4 was measured in the ileum **(A)** and colon **(B)** of mice in the Control and HFD groups using RT-qPCR analysis followed by RNA isolation. Sections of the ileum **(C,D)** and colon **(E,F)** in Control group **(C,E)** and HFD group **(D,F)** were stained with rabbit polyclonal antibodies to mouse ANGPTL4. The arrowhead points in the direction where ANGPTL4-positive cells are present. Data were expressed as mean ± SEM and statistically analyzed by using unpaired two-tailed Students' *t*-test ($n = 5$). Asterisks (*) represent significant differences with $P < 0.05$.

indicated that the number of OTU, Shannon index, and Chao1 index in the Control group were significantly higher than that in the HFD group ($P < 0.05$) while the Simpson index was significantly lower of Control group compared to HFD group (**Table 2**).

Next, we analyzed the composition of gut microbiota in the ileum and colon of mice in the Control and HFD groups. Taxonomic analysis showed that the dominant bacteria phyla were Firmicutes, Bacteroidetes, Actinobacteria, Proteobacteria, Deferribacteres, and Cyanobacteria in both of ileum and colon, accounting for more than 99.12% of the total sequences in most samples (**Figures 3A**, **4A**). The ratio of Firmicutes to Bacteroidetes, that was associated with the obesity phenotype, was remarkably higher in the ileum and colon of mice in the HFD group than those of the Control group (**Figures 3**, **4**). Compared to the Control group, the relative abundance of Firmicutes in the HFD group was increased by 38.81 and 15.00% in ileum and colon ($P < 0.05$), respectively. However, the relative abundance

TABLE 2 | Indices of alpha-diversity.

Gut	Item	Control	HFD	SEM	*P*-value
Ileum	OTU number	333^{a}	218^{b}	22.04	0.001
	Shannon index	3.26^{a}	2.50^{b}	0.18	0.022
	Simpson index	0.098^{b}	0.196^{a}	0.025	0.044
	Chao1 index	382^{a}	248^{b}	26.02	0.001
Colon	OTU number	379^{a}	204^{b}	29.86	<0.001
	Shannon index	4.38^{a}	3.52^{b}	0.16	0.001
	Simpson index	0.255^{b}	0.643^{a}	0.008	0.009
	Chao1 index	402^{a}	225^{b}	30.34	<0.001

The different superscript letters in the same row represent a significant difference ($p < 0.05$).

of Bacteroidetes in the HFD group was decreased by 48.45 and 20.02% in ileal and colonic samples relative to the Control group ($P < 0.05$), respectively (**Figures 3A**, **4A**). Cyanobacteria was less abundant in both of the ileum and colon of HFD group compared to Control group.

At the genus level, *Bacteroidales S24-7 group_norank*, *Faecalibaculum*, *Erysipelotrichaceae _uncultured*, *Alistipes*, *Lactobacillus*, *Coriobacteriaceae UCG-002*, *Lachnospiraceae_uncultured*, *Odoribacter*, *Lachnospiraceae NK4A136dium*, and *Peptoclostri* were the most abundant genera in both of the ileum and colon (**Figures 3B**, **4B**). Compared to the Control group, the relative abundance of *Bacteroidales S24-7 group_norank* in the HFD group was decreased by 51.58% and 56.76% in ileum and colon ($P < 0.05$), respectively, while the relative abundance of *Faecalibaculum* was increased by 37.27 and 68.18% in the ileal and colonic samples ($P < 0.05$), respectively (**Figures 3B**, **4B**). The relative abundance of *Lactobacillus* and *Odoribacter* was decreased while Alistipes and Peptoclostridium were increased in the ileum and colon (**Figures 3B**, **4B**) of the HFD group as compared to the Control group.

Hierarchical clustering together with a heat-map was performed to reveal the distinct characteristics of the significantly different bacterial genera (including the 21 from 248 total ileal bacterial genera, and 46 from 248 total colonic bacterial genera) based on the abundance of the identified bacterial genera in the Control group and HFD group (**Figure 5**). For example, the relative abundance of *Allobaculum* in ileum and colon of mice in the HFD group was significantly higher than that in the Control group ($P < 0.05$) (**Figure 5**). The relative abundance of *Adlercreutzia*, *Bifidobacterium*, *Prevotellaceae UCG-001* and *Ruminococcus* in the ileum and colon in HFD group was significantly lower than those in Control group ($P < 0.05$; **Figure 5**).

To evaluate the degree of discrepancy between the bacterial community structures of the Control group and HFD group mice, a principal coordinate analysis (PCoA) was performed. The ileal and colonic microbiota in the HFD group and the Control group were clearly separated from each other (**Figure 6A**). There was also a differently clustering of the bacterial community structure between the Control and HFD groups in ileum and colon (**Figures 6B,C**), indicating that the structure of the ileum

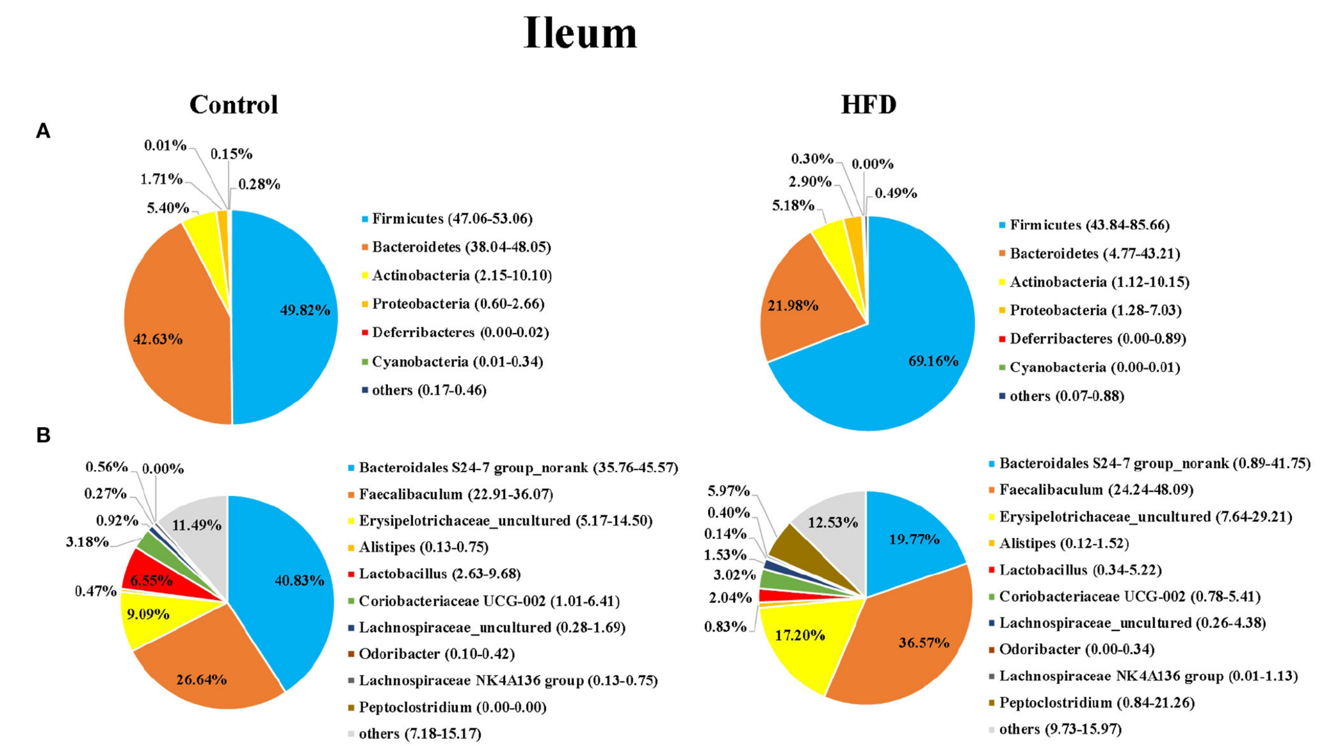

FIGURE 3 | The bacterial community in ileum of the Control group and HFD group mice at the phylum **(A)** and genus **(B)** levels. The top 6 phyla and top 10 genera are shown.

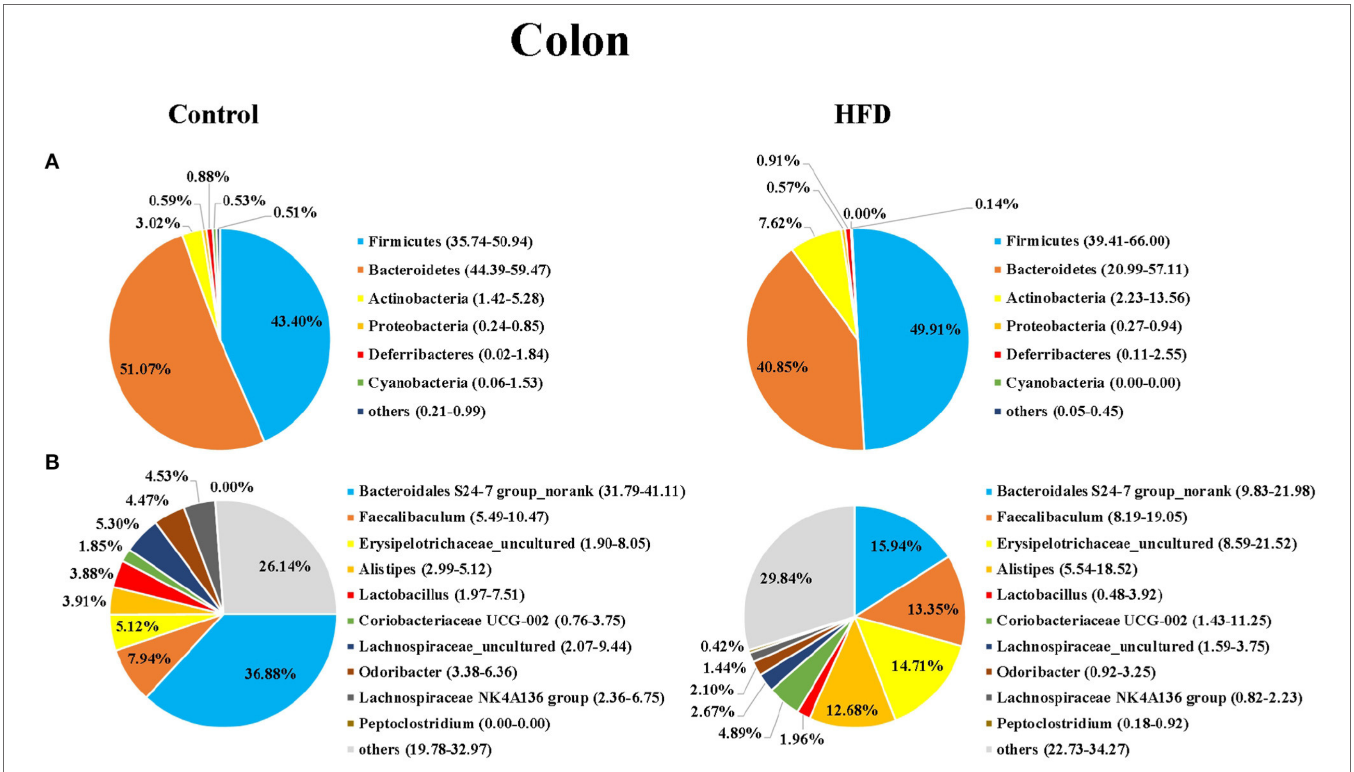

FIGURE 4 | The bacterial community in colon of mice in the Control group and HFD group at the phylum **(A)** and genus **(B)** levels. The top 6 phyla and top 10 genera are shown.

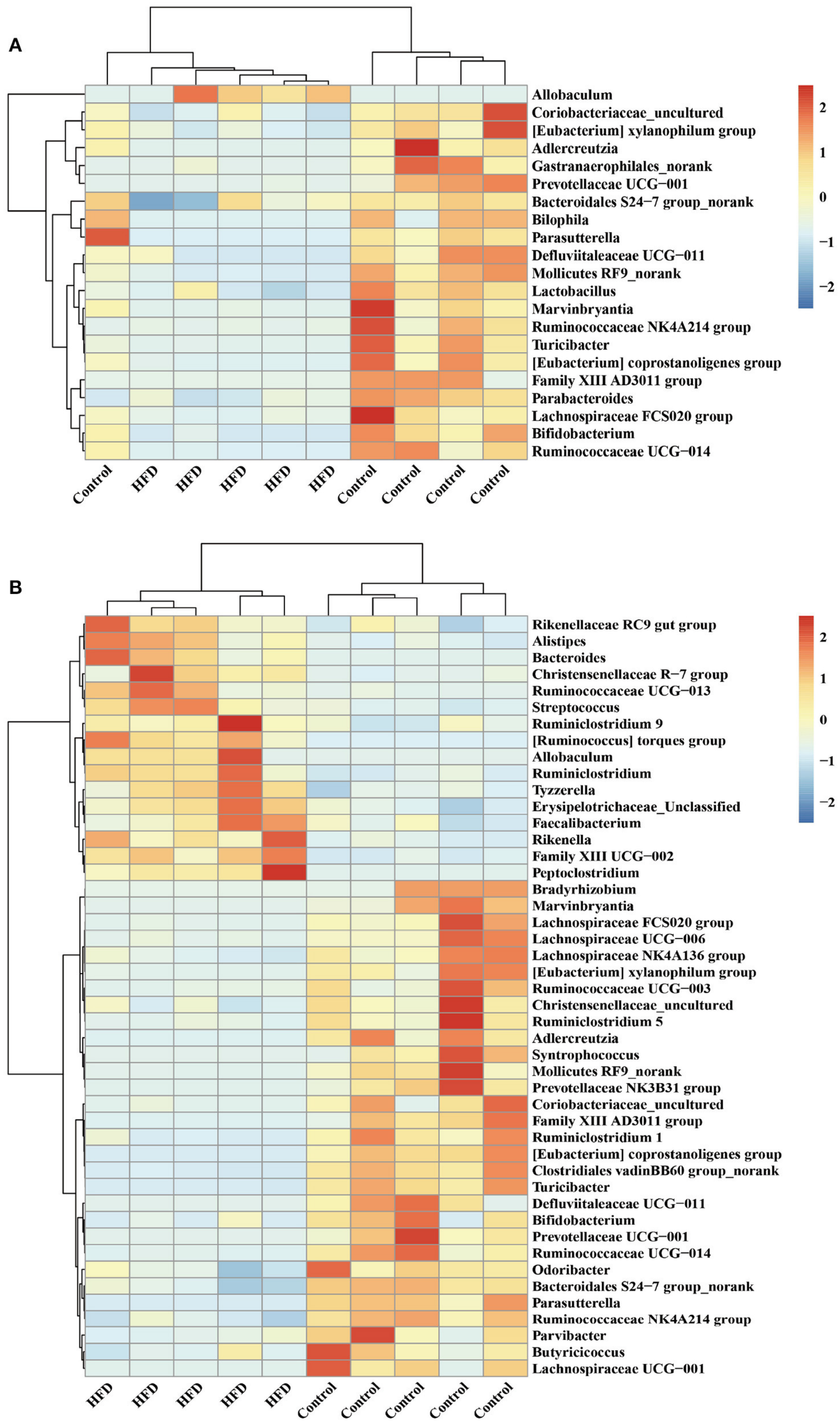

FIGURE 5 | Hierarchically clustered heat map for the significantly different bacterial genera in ileum **(A)** and colon **(B)** of mice.

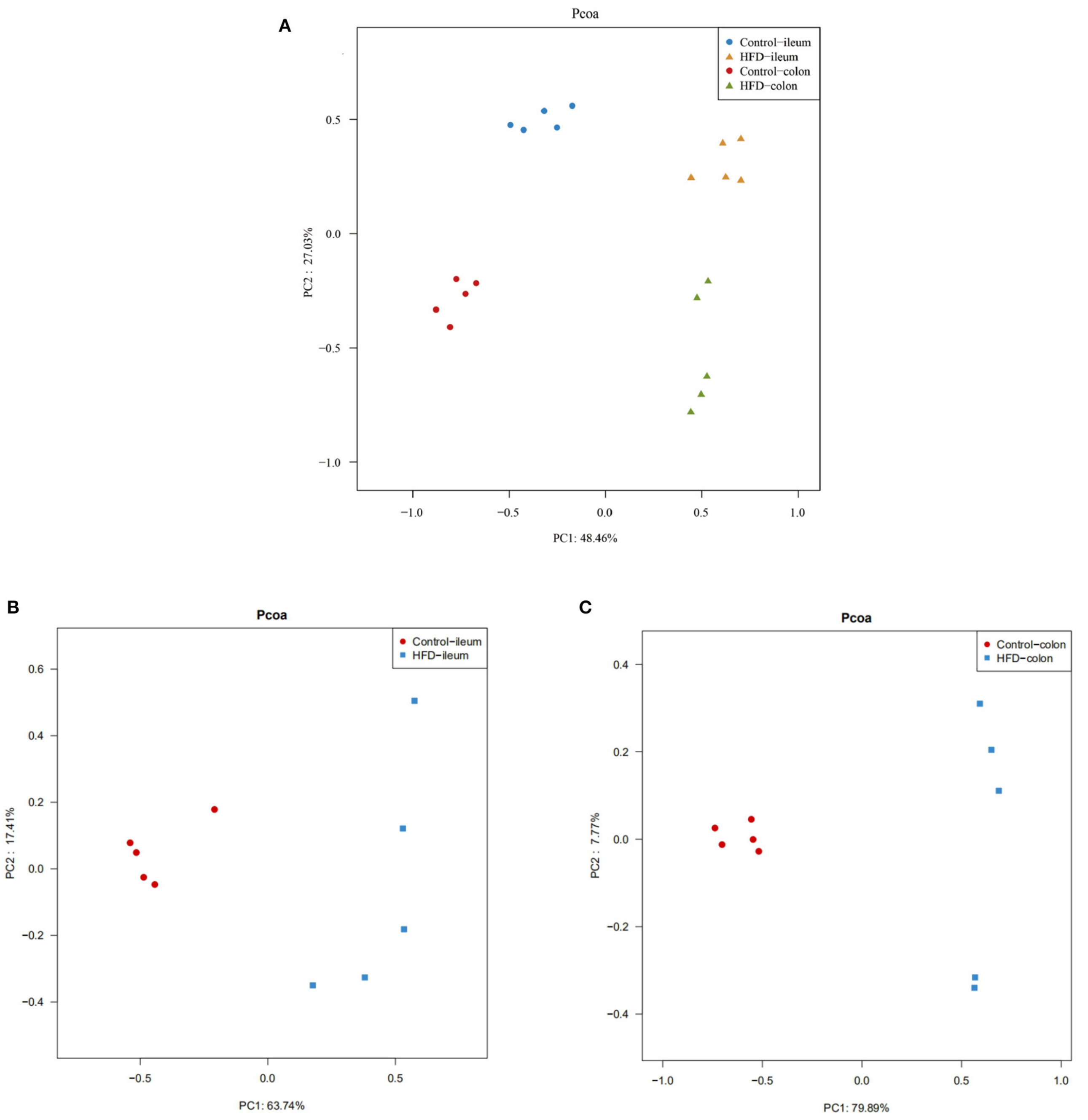

FIGURE 6 | PCoA of the ileum and colon microbial community composition of the Control and HFD mice based on weighted unifrac distance. **(A)** The overall characteristics of all 20 samples were analyzed by a principal coordinate analysis. The differences in ileum **(B)** and colon **(C)** microbial community structure between the Control group and HFD group.

and colon microbiota of the mice had a great difference between the Control and HFD groups.

Correlation Between the Gut Microbiota and ANGPTL4 Expression

To investigate the effect of gut microbiota on the expression of ANGPTL4, the correlation analysis was conducted. The microorganism positively correlated with ANGPTL4 expression was *Allobaculum*, and others were negatively correlated with ANGPTL4 expression including *Adlercreutzia*, *Bacteroidales S24–7 group_norank*, *Bifidobacterium*, *Coriobacteriaceae_uncultured*, *Defluviitaleaceae UCG−011*, *Family XIII AD3011 group*, *Lachnospiraceae FCS020 group*, *Marvinbryantia*, *Mollicutes RF9_norank*, *Parasutterella*, *Prevotellaceae UCG−001, Ruminococcaceae NK4A214 group, Ruminococcaceae UCG−014, Turicibacter, (Eubacterium) coprostanoligenes group, (Eubacterium) xylanophilum group* (**Figure 7**). Combining with the raw data from other similar studies, it was found that the relative abundance of *Allobaculum* in feces, ileum, cecum, and colon was increased significantly in HFD group compared to Control group (**Figure 8A**). Correlation analysis confirmed the positive association between the abundance of *Allobaculum* and the expression of ANGPTL4 in the ileum and colon, wherein, the *Allobaculum* was much more relevant to the ANGPL4 expression in colon ($R = 0.8928$, $P = 0.0005$) (**Figure 8B**).

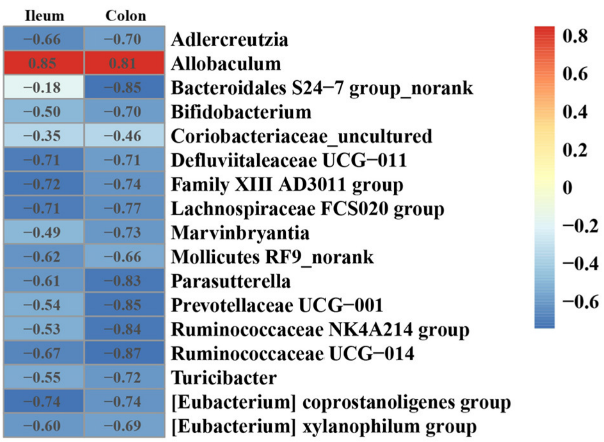

FIGURE 7 | Heatmap of Spearman correlation between the relative expression of ANGPTL4 and microbial genus in ileum and colon of mice.

DISCUSSION

Obesity is one of the most important health topics worldwide. The incidence rate of obesity keeps increasing for many years due to the improvement of living standards, excessive calorie intake and lack of physical exercise (28). High-fat diet is the direct cause of obesity (6). Extensive researches showed ANGPTL4 was an important regulator of TG metabolism by inhibiting LPL and pancreatic lipase (29, 30). This study found that the body weight of the mice was increased by 82.31% ($P < 0.05$) with the HFD treatment. Compared to the Control group, the expression of ANGPTL4 in the ileum and colon of the HFD

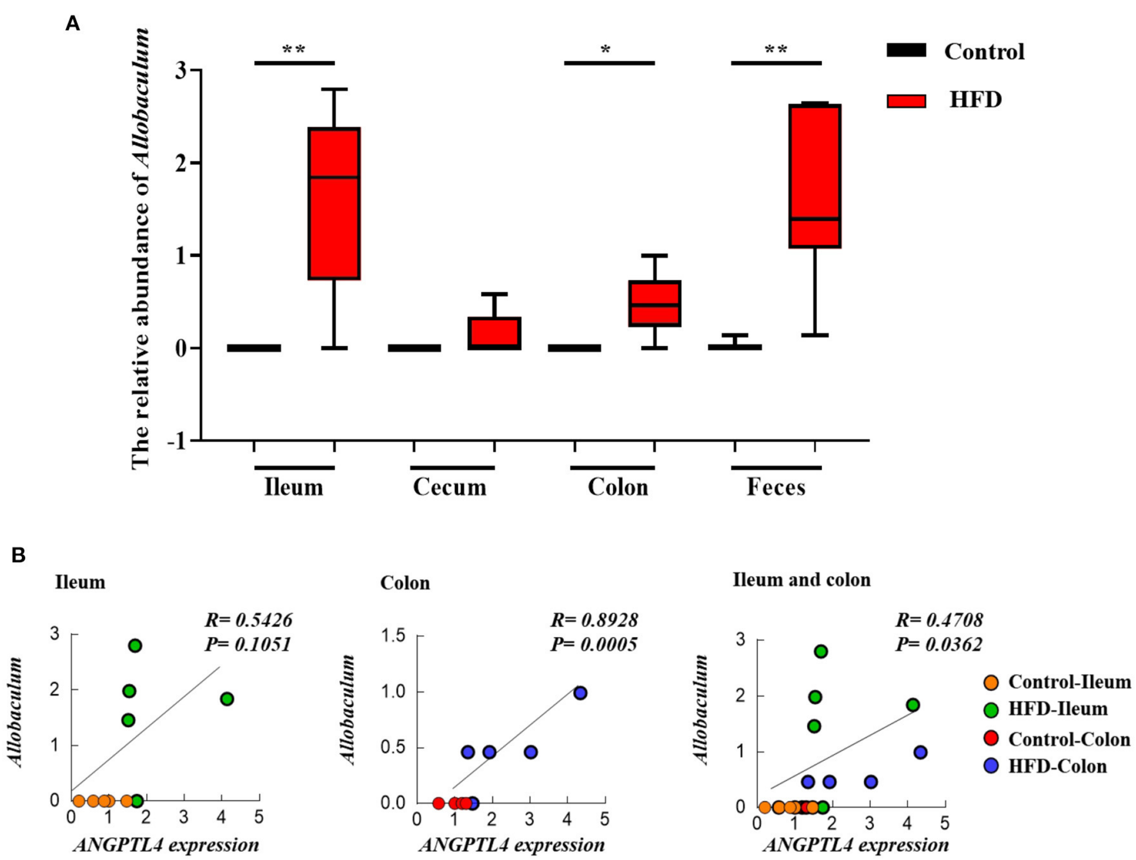

FIGURE 8 | The relative abundance of *Allobaculum* in ileum, cecum, colon, and feces of Control group and HFD group mice **(A)**, and the correlation between the *Allobaculum* and ANGPTL4 expression **(B)** in ileum and colon. The data of cecum and feces were obtained from the NCBI database (DDBJ Accession Number: PRJDB7523 and NCBI Accession Number: SRP113647) **(A)**. Asterisks (* and **) represent significant differences with $P < 0.05$ and $P < 0.01$, respectively.

group was increased significantly. Similar studies showed that the expression of ANGPTL4 mRNA in small intestine (17) and liver (31) of mice was significantly increased with the HFD intervention. With the treatment of HFD, the absence of any regulation on TG digestion may lead to excess fatty acid uptake into enterocytes. The excess fatty acids would beyond the ability of re-esterification and chyle granule secretion, resulting in the lipid overload of intestinal cells. Therefore, the HFD regulated the expression of ANGPTL4 through a negative feedback mechanism to inhibit the excessive intake of TG. This feedback mechanism aimed to match the lipid uptake amounts of intestinal cells with the capacity for TG secretion. Similarly, the protection of ANGPTL4 against lipid overload in cardiomyocytes (32) and macrophages (18) had also been found. Additionally, Wostmann first discovered that the growth rate of GF mice was slower than normal mice. Gut microbiota also contributes to fat deposition (33). Bäckhed et al. (19) proved that gut microbiota could inhibit the expression of LPL cycle inhibitor, ANGPTL4, in the intestine. The ANGPTL4 expression level of GF mice were higher resulting in slower body weight gain of mice. The ANGPTL4 knock-out GF mice were more obese than the wild-type mice (34). These findings indicate that ANGPTL4 was a circulating medium between gut microbiota and fat deposition. However, the specific mechanism in the microbial regulation by ANGPTL4 expression is still unclear. Meantime, research on the modulation mechanism of ANGPTL4 expression have never stopped. Alex et al. (35) found that short chain fatty acids (SCFAs), as the main metabolites of gut microbiota, could effectively induce the expression of ANGPTL4 in human colon cancer cells T84 and HT29. Aronsson's research showed that by being fed with the high-fat diet supplemented with Lactobacillus paraliquefaciens (F19), the body fat of mice was decreased significantly with the significant increase in the expression of ANGPTL4 (36). All of these prove that ANGPTL4 is involved in the regulation of gut microbiota on obesity.

Extensive studies have shown that the gut microbiota affects the body's immune response (37), neural signal (38), and bone density (39), regulates intestinal endocrine function (40), provides energy (41), synthesizes vitamins (42) and many other compounds (43). Therefore, the changes of gut microbiota structure will induce gastrointestinal diseases even a series of diseases in other tissues or systems such as liver, heart, nervous system, respiratory system, and so on (44). In recent years, studies have found that gut microbiota are widely involved in host lipid metabolism and obesity (7, 45). By comparing the response of GF and normal mice to the HFD treatment, researchers found that GF mice had a resistance to HFD, but microbial remodeling led to obesity for GF mice (46, 47). Therefore, gut microbiota is an important factor regulating fat deposition. In this study, the relative abundance ratio of Firmicutes to Bacteroidetes was increased significantly in the ileum and colon of mice in the HFD group. Similar studies found that the relative abundance ratio of Firmicutes to Bacteroidetes in the gut microbiota of mice showed a downward trend through exercise (48). In the obese humans and mice, the relative abundance of Firmicutes and Bacteroidetes was improved and reduced, respectively (49, 50). These findings were consistent with the results of this experiment.

In order to further explore the effect of gut microbiota on the expression of ANGPTL4, we preformed a correlation analysis between the microbial community composition and ANGTPL4 mRNA level. The results showed that the expression of ANGPTL4 was positively correlated with the relative abundance of *Allobaculum*, but negatively correlated with *Adlercreutzia, Bifidobacterium*, *Prevotellaceae UCG-001*, *and Ruminococcus*. *Allobaculum* cells are rod-shaped, stain Gram-positive and are arranged in pairs or chains (51). Related research showed that *Allobaculum* could produce butyric acid, and positively correlated with ANGPTL4 expression (52, 53). Butyric acid could transactivate PPARγ and regulated ANGPTL4, the target gene of PPARγ, in colon cells (54). Early studies have shown that SCFAs play an important role in the human gastrointestinal system, especially in regulating the host fat storage (55, 56). Janssen found that ANGPTL4$^{-/-}$ mice had significantly lower butyric acid levels than the wild-type mice. The butyrate-producing *Allobaculum* was less abundant in than the wild-type mice but *Adlercreutzia* abundance was significantly increased in ANGPTL4$^{-/-}$ mice (52). Similar alteration in *Allobaculum* abundance was found in other studies (25, 26). The relative abundances of *Adlercreutzia* (26), *Bifidobacterium* (57), *Prevotellaceae UCG-001* and *Ruminococcus* (58) were significantly decreased in obese mice induced by HFD. These findings were consistent with the results of this study. On the other hand, studies revealed that the abundance of *Allobaculum* might be negatively correlated with inflammation, insulin resistance and obesity with the intervention of ginger (59), berberine and metformin (60), or prebiotics (61) in mice. Consistent with these studies, our results found the significant increase in the relative abundance of *Allobaculum* and the expression level of ANGPTL4 by the HFD treatment in mice. The increase in ANGPTL4 expression also had an inhibitory effect on the lipid absorption. These results indicate that *Allobaculum* could be a promising target for the strategy to control obesity.

CONCLUSION

This study demonstrated that the HFD treatment significantly increased the expression of ANGPTL4 in the ileum and colon of mice with the enhancement of body weight, liver weight, epididymal fat weight, perirenal fat weight, and the lipid contents in the liver. This might be associated with the change in the composition of gut microbiota in mice including the significantly increased abundance of *Allobaculum* and the significantly decreased abundance of *Adlercreutzia, Bifidobacterium*, *Prevotellaceae UCG-001*, *and Ruminococcus* in the HFD mice. This work identified the positive correlation between the ANGPTL4 expression and the *Allobaculum* abundance and highlighted their important role in the regulation of lipid metabolism. This is meaningful to explore the regulation of ANGPTL4 by gut microbiota in the treatment of obesity.

DATA AVAILABILITY STATEMENT

The datasets presented in this study can be found in online repositories. The names of the repository/repositories and accession number(s) can be found below: https://www.ncbi.nlm.nih.gov/, PRJNA715938.

ETHICS STATEMENT

The animal study was reviewed and approved by Institutional Animal Care and Use Committee of Zhejiang Academy of Agricultural Sciences.

AUTHOR CONTRIBUTIONS

ZZ and YX designed the experiment. ZZ, WL, SZ, XL, and YX conducted the animal experiments. ZZ, WL, HY, and YX wrote and revised the manuscript. ZZ, WL, YR, HY, and YX did experimental analysis, collected, and analyzed the data. All authors reviewed the manuscript.

FUNDING

This study was funded by the National Natural Science Foundation of China (31972999), the Open Project of Hubei Key Laboratory of Animal Nutrition and Feed Science (201806), and State Key Laboratory for Managing Biotic and Chemical Threats to the Quality and Safety of Agro-products (2010DS700124-ZZ1905).

REFERENCES

1. Aron-Wisnewsky J, Warmbrunn MV, Nieuwdorp M, Clément K. Metabolism and metabolic disorders and the microbiome: the intestinal microbiota associated with obesity, lipid metabolism, and metabolic health-pathophysiology and therapeutic strategies. *Gastroenterology*. (2021) 160:573–99. doi: 10.1053/j.gastro.2020.10.057
2. Caballero B. Humans against obesity: who will win? *Adv Nutr*. (2019) 10:S4–9. doi: 10.1093/advances/nmy055
3. Chang CJ, Lin CS, Lu CC, Martel J, Ko YF, Ojcius DM, et al. Ganoderma lucidum reduces obesity in mice by modulating the composition of the gut microbiota. *Nat Commun*. (2015) 6:7489. doi: 10.1038/ncomms8489
4. Sekirov I, Russell SL, Antunes LC, Finlay BB. Gut microbiota in health and disease. *Physiol Rev*. (2010) 90:859–904. doi: 10.1152/physrev.00045.2009
5. He X, Zheng N, He J, Liu C, Feng J, Jia W, et al. Gut microbiota modulation attenuated the hypolipidemic effect of simvastatin in high-fat/cholesterol-diet fed mice. *J Proteome Res*. (2017) 16:1900–10. doi: 10.1021/acs.jproteome.6b00984
6. Kaya SD, Sinen O, Bülbül M. Gastric motor dysfunction coincides with the onset of obesity in rats fed with high-fat diet. *Clin Exp Pharmacol Physiol*. (2021) 48:553–62. doi: 10.1111/1440-1681.13448
7. Abenavoli L, Scarpellini E, Colica C, Boccuto L, Salehi B, Sharifi-Rad J, et al. Gut microbiota and obesity: a role for probiotics. *Nutrients*. (2019) 11:2690. doi: 10.3390/nu11112690
8. Ridaura VK, Faith JJ, Rey FE, Cheng J, Duncan AE, Kau AL, et al. Gut microbiota from twins discordant for obesity modulate metabolism in mice. *Science*. (2013) 341:1241214. doi: 10.1126/science.1241214
9. Yin J, Li Y, Han H, Ma J, Liu G, Wu X, et al. Administration of exogenous melatonin improves the diurnal rhythms of the gut microbiota in mice fed a high-fat diet. *mSystems*. (2020) 5:e00002–20. doi: 10.1128/mSystems.00002-20
10. Gérard P. Gut microbiota and obesity. *Cell Mol Life Sci*. (2016) 73:147–62. doi: 10.1007/s00018-015-2061-5
11. Li J, Li L, Guo D, Li S, Zeng Y, Liu C, et al. Triglyceride metabolism and angiopoietin-like proteins in lipoprotein lipase regulation. *Clin Chim Acta*. (2020) 503:19–34. doi: 10.1016/j.cca.2019.12.029
12. Fernández-Hernando C, Suárez Y. ANGPTL4: a multifunctional protein involved in metabolism and vascular homeostasis. *Curr Opin Hematol*. (2020) 27:206–13. doi: 10.1097/MOH.0000000000000580
13. Lichtenstein L, Kersten S. Modulation of plasma TG lipolysis by angiopoietin-like proteins and GPIHBP1. *Biochim Biophys Acta*. (2010) 1801:415–20. doi: 10.1016/j.bbalip.2009.12.015
14. Chen YQ, Pottanat TG, Siegel RW, Ehsani M, Qian YW, Roell WC, et al. Angiopoietin-like protein 4(E40K) and ANGPTL4/8 complex have reduced, temperature-dependent LPL-inhibitory activity compared to ANGPTL4. *Biochem Biophys Res Commun*. (2021) 534:498–503. doi: 10.1016/j.bbrc.2020.11.053
15. Dijk W, Kersten S. Regulation of lipid metabolism by angiopoietin-like proteins. *Curr Opin Lipidol*. (2016) 27:249–56. doi: 10.1097/MOL.0000000000000290
16. Kersten, Sander. Physiological regulation of lipoprotein lipase. *Biochim Biophys Acta*. (2014) 1841:919–33. doi: 10.1016/j.bbalip.2014.03.013
17. Mattijssen F, Alex S, Swarts HJ, Groen AK, Van Schothorst EM, Kersten S. Angptl4 serves as an endogenous inhibitor of intestinal lipid digestion. *Mol Metab*. (2013) 3:135–44. doi: 10.1016/j.molmet.2013.11.004
18. Lichtenstein L, Mattijssen F, Wit NJD, Georgiadi A, Hooiveld GJ, Meer RVD, et al. Angptl4 protects against severe proinflammatory effects of saturated fat by inhibiting fatty acid uptake into mesenteric lymph node macrophages. *Cell Metab*. (2010) 12:580–92. doi: 10.1016/j.cmet.2010.11.002
19. Bäckhed F, Ding H, Wang T, Hooper LV, Koh GY, Nagy A, et al. The gut microbiota as an environmental factor that regulates fat storage. *Proc Natl Acad Sci USA*. (2004) 101:15718–23. doi: 10.1073/pnas.0407076101
20. Yang H, Xiang Y, Robinson K, Wang J, Zhang G, Zhao J, et al. Gut microbiota is a major contributor to adiposity in pigs. *Front Microbiol*. (2018) 9:3045. doi: 10.3389/fmicb.2018.03045
21. Shi X, Zhou X, Chu X, Wang J, Xie B, Ge J, et al. Allicin improves metabolism in high-fat diet-induced obese mice by modulating the gut microbiota. *Nutrients*. (2019) 11:2909. doi: 10.3390/nu11122909
22. An Y, Li Y, Wang X, Chen Z, Xu H, Wu L, et al. Cordycepin reduces weight through regulating gut microbiota in high-fat diet-induced obese rats. *Lipids Health Dis*. (2018) 17:276. doi: 10.1186/s12944-018-0910-6
23. Lawley B, Tannock GW. Analysis of 16S rRNA gene amplicon sequences using the QIIME software package. *Methods Mol Biol*. (2017) 1537:153–63. doi: 10.1007/978-1-4939-6685-1_9
24. Wang Q, Garrity GM, Tiedje JM, Cole JR. Naive Bayesian classifier for rapid assignment of rRNA sequences into the new bacterial taxonomy. *Appl Environ Microbiol*. (2007) 73:5261–7. doi: 10.1128/AEM.00062-07
25. Ushiroda C, Naito Y, Takagi T, Uchiyama K, Mizushima K, Higashimura Y, et al. Green tea polyphenol (epigallocatechin-3-gallate) improves gut dysbiosis and serum bile acids dysregulation in high-fat diet-fed mice. *J Clin Biochem Nutr*. (2019) 65:34–46. doi: 10.3164/jcbn.18-116
26. Jiao X, Wang Y, Lin Y, Lang Y, Li E, Zhang X, et al. Blueberry polyphenols extract as a potential prebiotic with anti-obesity effects on C57BL/6 J mice by modulating the gut microbiota. *J Nutr Biochem*. (2019) 64:88–100. doi: 10.1016/j.jnutbio.2018.07.008
27. Xiao Y, Wu C, Li K, Gui G, Zhang G, Yang H. Association of growth rate with hormone levels and myogenic gene expression profile in broilers. *J Anim Sci Biotechnol*. (2017) 8:43. doi: 10.1186/s40104-017-0170-8
28. NCD-RisC. Trends in adult body-mass index in 200 countries from 1975 to 2014: a pooled analysis of 1698 population-based measurement studies with 19·2 million participants. *Lancet*. (2016) 387:1377–96. doi: 10.1016/S0140-6736(16)30054-X
29. Aryal B, Price NL, Suarez Y, Fernández-Hernando C. ANGPTL4 in metabolic and cardiovascular disease. *Trends Mol Med*. (2019) 25:723–34. doi: 10.1016/j.molmed.2019.05.010
30. Alex S, Lichtenstein L, Dijk W, Mensink RP, Tan NS, Kersten S. ANGPTL4 is produced by entero-endocrine cells in the human intestinal tract. *Histochem Cell Biol*. (2014) 141:383–91. doi: 10.1007/s00418-013-1157-y

31. Gao J, Ding G, Li Q, Gong L, Huang J, Sang Y. Tibet kefir milk decreases fat deposition by regulating the gut microbiota and gene expression of Lpl and Angptl4 in high fat diet-fed rats. *Food Res Int*. (2019) 121:278–87. doi: 10.1016/j.foodres.2019.03.029
32. Georgiadi A, Lichtenstein L, Degenhardt T, Boekschoten MV, van Bilsen M, Desvergne B, et al. Induction of cardiac Angptl4 by dietary fatty acids is mediated by peroxisome proliferator-activated receptor beta/delta and protects against fatty acid-induced oxidative stress. *Circ Res*. (2010) 106:1712–21. doi: 10.1161/CIRCRESAHA.110.217380
33. Wostmann BS, Larkin C, Moriarty A, Bruckner-Kardoss E. Dietary intake, energy metabolism, and excretory losses of adult male germfree Wistar rats. *Lab Anim Sci*. (1983) 33:46–50. doi: 10.2307/3808211
34. Bäckhed F, Manchester JK, Semenkovich CF, Gordon JI. Mechanisms underlying the resistance to diet-induced obesity in germ-free mice. *Proc Natl Acad Sci USA*. (2007) 104:979–84. doi: 10.1073/pnas.0605374104
35. Alex S, Lange K, Amolo T, Grinstead JS, Haakonsson AK, Szalowska E, et al. Short-chain fatty acids stimulate angiopoietin-like 4 synthesis in human colon adenocarcinoma cells by activating peroxisome proliferator-activated receptor γ. *Mol Cell Biol*. (2013) 33:1303–16. doi: 10.1128/MCB.00858-12
36. Aronsson L, Huang Y, Parini P, Korach-André M, Håkansson J, Gustafsson J, et al. Decreased fat storage by *Lactobacillus paracasei* is associated with increased levels of angiopoietin-like 4 protein (ANGPTL4). *PLoS ONE*. (2010) 5:e13087. doi: 10.1371/journal.pone
37. Fulde M, Hornef MW. Maturation of the enteric mucosal innate immune system during the postnatal period. *Immunol Rev*. (2014) 260:21–34. doi: 10.1111/imr.12190
38. Yano JM, Yu K, Donaldson GP, Shastri GG, Ann P, Ma L, et al. Indigenous bacteria from the gut microbiota regulate host serotonin biosynthesis. *Cell*. (2015) 161:264–76. doi: 10.1016/j.cell.2015.02.047
39. Cho I, Yamanishi S, Cox L, Methé BA, Zavadil J, Li K, et al. Antibiotics in early life alter the murine colonic microbiome and adiposity. *Nature*. (2012) 488:621–6. doi: 10.1038/nature11400
40. Neuman H, Debelius JW, Knight R, Koren O. Microbial endocrinology: the interplay between the microbiota and the endocrine system. *FEMS Microbiol Rev*. (2015) 39:509–21. doi: 10.1093/femsre/fuu010
41. Canfora EE, Jocken JW, Blaak EE: Short-chain fatty acids in control of body weight and insulin sensitivity. *Nat Rev Endocrinol*. (2015) 11:577–91. doi: 10.1038/nrendo.2015.128
42. Yatsunenko T, Rey FE, Manary MJ, Trehan I, Dominguez-Bello MG, Contreras M, et al. Human gut microbiome viewed across age and geography. *Nature*. (2012) 486:222–7. doi: 10.1038/nature11053
43. Devlin AS, Fischbach MA. A biosynthetic pathway for a prominent class of microbiota-derived bile acids. *Nat Chem Biol*. (2015) 11:685–90. doi: 10.1038/nchembio.1864
44. Lynch SV, Pedersen O. The human intestinal microbiome in health and disease. *N Engl J Med*. (2016) 375:2369–79. doi: 10.1056/NEJMra1600266
45. Schoeler M, Caesar R. Dietary lipids, gut microbiota and lipid metabolism. *Rev Endocr Metab Disord*. (2019) 20:461–72. doi: 10.1007/s11154-019-09512-0
46. Turnbaugh PJ, Bäckhed F, Fulton L, Gordon JI. Diet-induced obesity is linked to marked but reversible alterations in the mouse distal gut microbiome. *Cell Host Microbe*. (2008) 3:213–23. doi: 10.1016/j.chom.2008.02.015
47. Velagapudi VR, Hezaveh R, Reigstad CS, Gopalacharyulu P, Yetukuri L, Islam S, et al. The gut microbiota modulates host energy and lipid metabolism in mice. *J Lipid Res*. (2010) 51:1101–12. doi: 10.1194/jlr.M002774
48. Evans CC, LePard KJ, Kwak JW, Stancukas MC, Laskowski S, Dougherty J, et al. Exercise prevents weight gain and alters the gut microbiota in a mouse model of high fat diet-induced obesity. *PLoS ONE*. (2014) 9:e92193. doi: 10.1371/journal.pone.0092193
49. Turnbaugh PJ, Ley RE, Mahowald MA, Magrini V, Mardis ER, Gordon JI. An obesity-associated gut microbiome with increased capacity for energy harvest. *Nature*. (2006) 444:1027–31. doi: 10.1038/nature05414
50. Parnell JA, Reimer RA. Prebiotic fiber modulation of the gut microbiota improves risk factors for obesity and the metabolic syndrome. *Gut Microbes*. (2012) 3:29–34. doi: 10.4161/gmic.19246
51. Greetham HL, Gibson GR, Giffard C, Hippe H, Merkhoffer B, Steiner U, et al. Allobaculum stercoricanis gen. nov., sp. nov., isolated from canine feces. *Anaerobe*. (2004) 10:301–7. doi: 10.1016/j.anaerobe
52. Janssen AWF, Katiraei S, Bartosinska B, Eberhard D, Willems van Dijk K, Kersten S. Loss of angiopoietin-like 4 (ANGPTL4) in mice with diet-induced obesity uncouples visceral obesity from glucose intolerance partly *via* the gut microbiota. *Diabetologia*. (2018) 61:1447–58. doi: 10.1007/s00125-018-4583-5
53. Li S, Qi Y, Ren D, Qu D, Sun Y. The structure features and improving effects of polysaccharide from astragalus membranaceus on antibiotic-associated diarrhea. *Antibiotics (Basel)*. (2019) 9:8. doi: 10.3390/antibiotics9010008
54. Kumar J, Rani K, Datt C. Molecular link between dietary fibre, gut microbiota and health. *Mol Biol Rep*. (2020) 47:6229–37. doi: 10.1007/s11033-020-05611-3
55. Galvez J, Rodríguez-Cabezas ME, Zarzuelo A. Effects of dietary fiber on inflammatory bowel disease. *Mol Nutr Food Res*. (2005) 49:601–8. doi: 10.1002/mnfr.200500013
56. Murphy EF, Cotter PD, Healy S, Marques TM, O'Sullivan O, Fouhy F, et al. Composition and energy harvesting capacity of the gut microbiota: relationship to diet, obesity and time in mouse models. *Gut*. (2010) 59:1635–42. doi: 10.1136/gut.2010.215665
57. Cani PD, Neyrinck AM, Fava F, Knauf C, Burcelin RG, Tuohy KM, et al. Selective increases of bifidobacteria in gut microflora improve high-fat-diet-induced diabetes in mice through a mechanism associated with endotoxaemia. *Diabetologia*. (2007) 50:2374–83. doi: 10.1007/s00125-007-0791-0
58. Kong C, Gao R, Yan X, Huang L, Qin H. Probiotics improve gut microbiota dysbiosis in obese mice fed a high-fat or high-sucrose diet. *Nutrition*. (2019) 60:175–84. doi: 10.1016/j.nut.2018.10.002
59. Wang J, Wang P, Li D, Hu X, Chen F. Beneficial effects of ginger on prevention of obesity through modulation of gut microbiota in mice. *Eur J Nutr*. (2020) 59:699–718. doi: 10.1007/s00394-019-01938-1
60. Zhang X, Zhao Y, Xu J, Xue Z, Zhang M, Pang X, et al. Modulation of gut microbiota by berberine and metformin during the treatment of high-fat diet-induced obesity in rats. *Sci Rep*. (2015) 5:14405. doi: 10.1038/srep14405
61. Everard A, Lazarevic V, Gaïa N, Johansson M, Ståhlman M, Backhed F, et al. Microbiome of prebiotic-treated mice reveals novel targets involved in host response during obesity. *ISME J*. (2014) 8:2116–30. doi: 10.1038/ismej.2014.45

Conflict of Interest: The authors declare that the research was conducted in the absence of any commercial or financial relationships that could be construed as a potential conflict of interest.

frontiers in Nutrition

ORIGINAL RESEARCH
published: 07 June 2021
doi: 10.3389/fnut.2021.675640

Methyl-Donor Micronutrient for Gestating Sows: Effects on Gut Microbiota and Metabolome in Offspring Piglets

Qin He[1,2], Tiande Zou[1,2], Jun Chen[1,2], Jia He[1,2], Li Jian[1,2], Fei Xie[1,2], Jinming You[1,2]* and Zirui Wang[1,2]*

[1] Key Laboratory of Animal Nutrition in Jiangxi Province, Jiangxi Agricultural University, Nanchang, China, [2] Key Innovation Center for Industry-Education Integration of High-Quality and Safety Livestock Production in Jiangxi Province, Jiangxi Agricultural University, Nanchang, China

OPEN ACCESS

Edited by:
Jie Yin,
Hunan Agricultural University, China

Reviewed by:
Hongkui Wei,
Huazhong Agricultural University, China
Yulan Liu,
Polytechnic University, China

***Correspondence:**
Jinming You
youjinm@163.com
Zirui Wang
wangzirui@jxau.edu.cn

Specialty section:
This article was submitted to Nutrition and Microbes, a section of the journal Frontiers in Nutrition

Received: 03 March 2021
Accepted: 22 April 2021
Published: 07 June 2021

Citation:
He Q, Zou T, Chen J, He J, Jian L, Xie F, You J and Wang Z (2021) Methyl-Donor Micronutrient for Gestating Sows: Effects on Gut Microbiota and Metabolome in Offspring Piglets. Front. Nutr. 8:675640. doi: 10.3389/fnut.2021.675640

This study aimed to investigate the effects of maternal methyl-donor micronutrient supplementation during gestation on gut microbiota and the fecal metabolic profile in offspring piglets. Forty-three Duroc × Erhualian gilts were assigned to two dietary groups during gestation: control diet (CON) and CON diet supplemented with MET (folic acid, methionine, choline, vitamin B6, and vitamin B12). The body weights of offspring piglets were recorded at birth and weaning. Besides this, fresh fecal samples of offspring piglets were collected at 7, 14, and 21 days. The gut microbiota composition, metabolic profile, and short-chain fatty acid (SCFA) profiles in the fecal samples were determined using 16S rDNA sequencing, liquid chromatography-mass spectrometry metabolomics, and gas chromatography methods, respectively. The results showed that maternal methyl-donor micronutrient supplementation increased the microbiota diversity and uniformity in feces of offspring piglets as indicated by increased Shannon and Simpson indices at 7 days, and greater Simpson, ACE, Chao1 and observed species indices at 21 days. Specifically, at the phylum level, the relative abundance of Firmicutes and the Firmicutes to Bacteroidetes ratio were elevated by maternal treatment. At the genus level, the relative abundance of SCFA-producing *Dialister*, *Megasphaera*, and *Turicibacter*, and lactate-producing *Sharpea* as well as *Akkermansia*, *Weissella*, and *Pediococcus* were increased in the MET group. The metabolic analyses show that maternal methyl-donor micronutrient addition increased the concentrations of individual and total SCFAs of 21-day piglets and increased metabolism mainly involving amino acids, pyrimidine, and purine biosynthesis. Collectively, maternal methyl-donor micronutrient addition altered gut microbiota and the fecal metabolic profile, resulting in an improved weaning weight of offspring piglets.

Keywords: gilts, metabolic profiles, methyl-donor micronutrient, microbial community, offspring piglets

INTRODUCTION

The gut microbiota and fecal metabolic profile of neonates are closely related to immunity, disease, growth, and development. The colonization of microbial communities in the intestines is a key process in infant development (1); the intestinal microbial establishment is mainly determined and easily affected by diet, mother-to-child transmission, and the environment (2). The indigestible nutrients that are metabolized by bacteria in the neonatal intestines improve energy harvesting for growth but expose developing mammals to a variety of chemicals (3). The stability of gut microbiota systems can adapt to such environmental fluctuations. Therefore, a dysbiosis in the gut microbial community not only results in higher disease risk, but also causes short- and long-lasting adverse effects on neonates' health. Diet is an important determinant of maternal offspring's microbial communities and health outcomes. Maternal nutritional status has a great influence on fetal development, pregnancy outcome, and offspring disease development (4–6). Therefore, a specific diet plan for pregnant women may be a cost-effective intervention to promote intestinal microbiota colonization of offspring.

Methyl-donor micronutrients (MET), including folate, choline, betaine, methionine, cobalamin, pyridoxine, and so forth, are demonstrated to participate in the synthesis of nucleotides, proteins, and lipids via epigenetic mechanisms (7); meanwhile, the epigenetic mechanisms also modify the metabolome (8). However, the intergenerational effect of MET on the physiological metabolism of offspring in the early stage is hardly documented. Maternal diet during pregnancy may have a significant impact on the establishment of the neonatal microbiota, and may play a role in infant development (9). Additionally, there is increasing evidence that microbiota-derived metabolites are key factors regulating animal metabolism, growth, and development (10). Maternal-MET supplementation induces a specific intestinal microenvironment, limiting pathobiont colonization [such as adherent-invasive Escherichia coli (AIEC)] of the offspring gut (11). Conversely, other studies report that maternal-MET supplementation or deficiency leads to an increase in the sensitivity to colitis in the offspring (12, 13), suggesting the central role of MET in the intestinal microenvironment. Therefore, differences in the metabolome of control and MET offspring in the early stages after birth need to be further studied.

In our previous study, we found no differences in the reproduction performance of sows between CON and MET (number of total born, born alive, and weaned piglets per litter, etc.). However, maternal MET supplementation during pregnancy promotes skeletal muscle differentiation and maturity in newborn and weaning pigs and improves the growth performance of the offspring (14). This means that some changes in the suckling piglets may be important for growth and development. Therefore, this study was conducted to test the hypothesis that maternal methyl-donor micronutrient supplementation during gestation could beneficially regulate the gut microbiota and fecal metabolic profile and enhance the growth performance of offspring piglets.

MATERIALS AND METHODS

Ethics Statement

This study was conducted under the Chinese guidelines for animal welfare. All animal experiments were approved by the Animal Care and Use Committee of Jiangxi Agricultural University (Ethic Approval Code: JXAUA01).

Animals and Experimental Design

A total of 43 crossbred gilts (Duroc × Erhualian, body weight: 102.8 ± 6.3 kg) were artificially inseminated and then allotted by body weight to two dietary treatments. The two experimental diets were supplemented with or without methyl-donor micronutrients in the basal diet. There were 21 and 22 gilts in the control group (CON group) and Methyl-donor micronutrients group (MET group), respectively. The MET-supplemented diet contained 4,700 mg kg^{-1} methionine (CJ BIO, Malaysia, purity ≥99%), 16.3 mg kg^{-1} folic acid (Sigma-Aldrich, St. Louis, MO, USA, purity ≥97%), 2,230 mg kg^{-1} choline (NB GROUP, Shangdong, China, purity = 60%), 0.15 mg kg^{-1} vitamin B12 (Sigma-Aldrich, St. Louis, MO, USA, purity ≥98%), and 1,180 mg kg^{-1} vitamin B6 (Jiangxi Tianxin Pharmaceutical, Jiangxi, China, purity ≥98%). The dosage of methyl-donor micronutrients was added according to previous studies (15–18). Dietary treatment started at the last insemination and lasted until parturition. Ingredients and composition of pregnant gilt diets are show in **Supplementary Table 1**. During gestation, sows were fed 2.28 kg/day during days 1–80, 2.40 kg/day during days 80–90, and 3.00 kg/day of diet from day 91 until farrowing. Sows were fed discretely twice daily at 0800 and 1,400 h with 50% of the daily ration during each feeding. On day 110 of gestation, sows were transferred to farrowing pens. After parturition, all sows received a standard lactation diet (**Supplementary Table 2**) three times per day (i.e., 0800, 1,200, and 1,500 h). Piglets were weaned at 24 days. All animals were free to drink water. The experiment began with 54 gilts, 27 gilts per treatment. Pregnancy was confirmed by ultrasonic examination 30 days post-mating; 11 gilts were eliminated due to failure of pregnancy.

Data and Sample Collection

Sample Collection

After parturition, body weights (BW) were measured at birth and weaning (24 days). Six litters per group were selected, and one median-birth-weight piglet from each litter were sampled for feces collection at days 7, 14, and 21 and then snap-frozen in liquid nitrogen and stored at −80°C for gut microbiota, short-chain fatty acid (SCFA), and metabolomics analyses. Fecal 16S rDNA sequencing and liquid chromatography-mass spectrometry (LC-MS) metabolomics were performed according to the manufacturer's instructions (Shanghai Applied Protein Technology, Shanghai, China).

Serum S-Adenosylmethionine and Homocysteine

Serum from newborn and weaning offspring was analyzed for S-adenosylmethionine (SAM) and homocysteine (Hcy) using the enzyme-linked immunosorbent assay (ELISA) kits purchased from MLBIO (Shanghai, China).

Fecal DNA Extraction and 16S rDNA Gene Amplicon Sequencing Analysis

The total genomic DNA was extracted from fecal samples with the Cetyltrimethylammonium Bromide (CTAB) method. DNA concentration and purity were monitored on an agarose gel. The DNA was then diluted accordingly using sterile water. The bacterial 16S rDNA gene of various regions (3–4) was amplified by polymerase chain reaction (PCR) using a specific primer (Uni340F: 5′-CCTAYGGGRBGCASCAG-3′, Uni806R: 5′-GGACTACNNGGGTATCTAAT-3′). The PCR product was detected with 2% agarose gel and purified with the Qiagen Gel Extraction Kit (Qiagen, Germany) following the manufacturer's instructions. The library was generated by TruSeq® DNA PCR-Free Sample Preparation Kit (Illumina, USA) and quantified using a Qubit @ 2.0 Fluorometer (Thermo Scientific). Finally, 250 base pair paired-end sequencing was performed using the Illumina HiSeq 2500 platform.

Sequencing data were analyzed using the quantitative insights into microbial ecology (QIIME) (V1.9.1, http://qiime.org/scripts/split_libraries_fastq.html). Paired-end reads were merged using Fast Length Adjustment of Short reads (FLASH, V1.2.7, http://ccb.jhu.edu/software/FLASH/). The clean data were obtained by specific splice and filtering of the raw sequence data. Sequences with ≥97% similarity were assigned to the same operational taxonomic units (OTUs) and the OTU was screened for further annotation; analysis was performed using Uparse software (Uparse v7.0.1001, http://drive5.com/uparse/). The abundance information of OTUs was normalized using the serial number standard corresponding to the sample with the least sequence and both alpha (observed species, Chao1, Shannon, Simpson, ACE) and beta diversity (principal coordinate analysis (PCoA) and unweighted pair-group method with arithmetic means) were performed based on the normalized data of OTU abundance information. The alpha and beta diversity were calculated with QIIME and displayed with R software (Version 2.15.3). PCoA was based on unweighted UniFrac distances using the *WGCNA*, *stat*, and *ggplot2* packages in R. To determine the significance test of community structure differences between groups, permutational multivariate analysis of variance (PERMANOVA, Adonis procedure with 999 permutations) was performed in R to calculate *P*-values. Additionally, to further explore the differences in the community structure (phylum and genus) between the two groups of samples, the linear discriminant analysis (LDA) effect size (LEfSe) method was used to compare the differences in the taxonomic levels; the LDA score was set at 2.0 for a biomarker. In LEfSe analysis, the non-parametric factorial Kruskal–Wallis (KW) sum-rank test was used to detect all species with significant differential abundance, and the Wilcoxon rank-sum test was used to investigate biological consistency among subclasses.

Concentration of SCFA in the Fecal

Approximately 1 g of fecal samples were weighed, diluted with 2 mL of ultra-pure water and centrifuged at 12,000 g (4°C) for 15 min to obtain a supernatant. Then 25% of metaphosphoric acid solution was added in a ratio of 9:1 before centrifugation at 3,000 g for 10 min. The supernatant was aspirated with a syringe and filtered through a 0.45 mm filter membrane. Acetic acid, propionic acid, isobutyric acid, butyric acid, isovaleric acid, valeric acid, and total SCFA were determined using capillary column gas chromatography (Shimadzu Gas Chromatography 2014, Japan; capillary column length was 30 m, inner diameter was 0.25 mm, and film thickness was 0.25 μm), column temperature = 120°C, injector temperature = 220°C, detector temperature = 250°C, and each injection volume was 1 μL.

The standard substances of SCFAs are as follows: acetic acid (A116165, Shanghai Aladdin Bio-Chem Technology Co., LTD, Shanghai, China), propionic acid (P110443, Aladdin), isobutyric acid (I103521, Aladdin), butyric acid (B110439, Aladdin), isovaleric acid (I108280, Aladdin), and valeric acid (V108269, Aladdin).

Fecal Untargeted Metabolomic Analysis

Aliquots of 100 mg of fecal samples were homogenized with 200 μL of ultra-pure water and mixed with 800 L methanol/acetonitrile (1:1, v/v) to remove the protein. After centrifugation (14,000 g, 20 min, 4°C), the supernatant was collected for analysis.

LC-MS Analysis and Data Processing

Analyses were performed using liquid chromatography (1,290 infinity liquid, Agilent) coupled with quadrupole time-of-flight (Triple TOF 6600, AB Sciex). For hydrophilic interaction liquid chromatography (HILIC) separation, samples were analyzed using a 2.1 × 100 mm ACQUIY UPLC BEH Amide 1.7 μm column (Waters, Ireland). Chromatographic conditions and Q-TOF mass spectrometry conditions were as outlined by Liu et al. (19), electrospray ionization (ESI) positive mode was used for detection.

The raw MS data were converted to MzXML format using ProteoWizard MSConvert and processed using the XCMS online package (version 1.20.1) for further processing. Metabolites were identified by accuracy mass (<25 ppm) and secondary spectral matching to retrieve a self-built database from the laboratory (Shanghai Applied Protein Technology). After data preprocessing by Pareto-scaling, multidimensional statistical analysis [orthogonal partial least squares discriminant analysis (OPLS-DA)] and Student's *t*-test analysis were performed. Significantly different metabolites were identified based on the combination of a statistically significant threshold of variable influence on projection (VIP) values obtained from the OPLS-DA model and two-tailed Student's *t*-test (*p*-value) from the raw data. VIP > 1.00 and $P < 0.05$ were considered as significantly different metabolites. VIP > 1.00 and $0.05 < P < 0.10$ were regarded as differential metabolites.

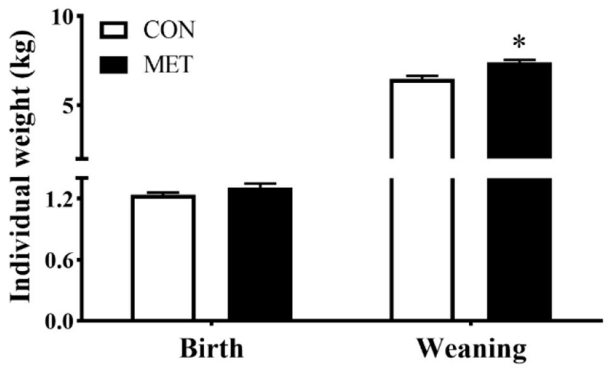

FIGURE 1 | Effect of maternal methyl-donor micronutrient supplementation during gestation on birth weight and weaning weight of offspring piglets ($n = 21$). No difference was observed for litter size of lactating sows between treatments [data not shown, see reference (14)]. The litter of each sow was considered as the experimental unit to calculate the individual weight of piglets at birth and weanling. CON, the control group; MET, the methyl-donor micronutrients group. *$P < 0.05$. Values are expressed as means ± standard error of mean (SEM).

TABLE 1 | Effect of maternal MET supplementation during gestation on the concentration of S-adenosylmethionine (SAM) and homocysteine (Hcy) in the serum of newborn and weaning piglets ($n = 6$).

Items	CON	MET	*P*-value
Birth			
SAM, μmol/mL	22.31 ± 0.86	24.55 ± 0.57	0.061
Hcy, nmol/mL	13.21 ± 0.24	11.90 ± 0.65	0.089
Weaning			
SAM, μmol/mL	19.40 ± 1.25	30.81 ± 2.81	0.002
Hcy, nmol/mL	13.15 ± 0.68	10.44 ± 0.98	0.037

CON, the control group; MET, the methyl-donor micronutrients group. Data are reported as means ± standard error of mean (SEM).

Statistical Analysis

Data were tested for normality using the Shapiro–Wilk test before statistical analysis. The growth performance, SCFA, and serum methyl metabolite profile between CON and MET piglets was assessed by independent-samples *t*-test. The individual sow was considered as the experimental unit for growth performance, one piglet per pen was used as the experimental unit for SCFA and methyl metabolite profile and microbial and metabolite analysis. Statistical analysis was performed on SPSS 24.0 software (SPSS Inc.). Correlations between altered metabolites screened from fecal metabonomic and perturbed gut microbe genera screened from 16S rDNA gene sequencing analysis were assessed by Spearman's correlation analysis. GraphPad Prism 8.0 (San Diego, CA, USA) was used to plot the images. Data are shown as means ± SEM. A value of $P < 0.05$ was considered statistical significance.

RESULTS

Growth Performance and Serum SAM and Hcy Concentrations of Offspring Piglets

There was no statistical difference in offspring birth weight between dietary treatments ($P > 0.05$). However, the body weight at weaning was greater for piglets from sows fed the MET vs. CON diet ($P < 0.05$) (**Figure 1**).

Maternal MET supplementation during gestation decreased serum Hcy concentration in the offspring at birth ($P = 0.089$, **Table 1**). Likewise, there was a significantly lower concentration of serum Hcy in the weaning offspring of the MET group compared with the CON group ($P < 0.05$). Moreover, the serum SAM concentration in piglets at birth and weaning was increased in the MET group ($P = 0.061$, $P < 0.05$, respectively).

Fecal Microbiota Diversity

The alpha diversity indices of fecal microbiota in suckling piglets are shown in **Table 2**. The Shannon and Simpson indices of the fecal bacterial community were higher in 7-day piglets from sows fed the MET vs. CON diet ($P < 0.05$). The ACE, Chao1, observed species, and Simpson indices were higher in 21-day piglets from sows fed the MET vs. CON diet ($P < 0.05$).

Figure 2 presents the PCoA analysis of the fecal microbial community in suckling piglets from sows fed the MET vs. CON diet. PERMANOVA (Adonis procedure with 999 permutations) revealed distinct clustering patterns of feces microbiota in offspring piglets between two treatments at 7 days ($R^2 = 0.17$, $P < 0.05$) and 21 days ($R^2 = 0.14$, $P < 0.05$).

Fecal Microbial Composition at Phylum and Genus Level

In both treatment groups, the Bacteroidetes, Firmicutes, Fusobacteria, and Proteobacteria were the dominant microbial phyla in the feces of offspring piglets, followed by Spirochaetes, Euryarchaeota, Actinobacteria, unidentified_Bacteria, Acidobacteria, and Tenericutes (**Figure 3A**). The relative abundance of Firmicutes and the Firmicutes/Bacteroidetes ratio were increased, and the relative abundance of Bacteroidetes were decreased in the feces of 21-day piglets from the MET group compared with the CON group ($P < 0.05$) (**Figures 3B–D**).

The 10 most abundant genera in the feces of offspring piglets are *unidentified_Prevotellaceae*, *Lactobacillus*, *Bacteroides*, *unidentified_Muribaculaceae*, *unidentified_Ruminococcaceae*, *Fusobacterium*, *Streptococcus*, *Phascolarctobacterium*, *Alloprevotella*, *unidentified_Spirochaetaceae* (**Figure 4A**). The relative abundances of *Megasphaera* and *Dialister* were increased in the feces of 7-day piglets, and relative abundances of *Sharpea*, *Weissella*, and *Pediococcus* were increased in the feces of 21-day piglets when their mothers were fed the MET vs. CON diet ($P < 0.05$) (**Figures 4B–F**).

Differential Fecal Microbial Communities

Differences in the relative abundances of the microbial community components of CON and MET offspring were

TABLE 2 | Effect of maternal methyl-donor micronutrient supplementation during gestation on the alpha diversity indices of fecal microbiota in suckling piglets ($n = 6$)[1].

Items	7 days old		14 days old		21 days old	
	CON	MET	CON	MET	CON	MET
Shannon	5.23 ± 0.12^b	5.69 ± 0.14^a	5.64 ± 0.23	6.02 ± 0.21	5.71 ± 0.21	6.04 ± 0.21
Simpson	0.91 ± 0.01^b	0.94 ± 0.01^a	0.93 ± 0.02	0.95 ± 0.01	0.94 ± 0.01^b	0.96 ± 0.01^a
ACE	800.36 ± 21.96	879.75 ± 34.39	940.12 ± 35.24	913.13 ± 65.47	815.08 ± 23.23^b	889.63 ± 18.09^a
Chao1	797.97 ± 25.79	886.62 ± 40.21	936.55 ± 25.46	904.09 ± 65.59	806.62 ± 24.45^b	882.62 ± 15.08^a
Observed species	618.50 ± 12.41	679.17 ± 25.41	718.17 ± 22.17	733.00 ± 50.68	651.83 ± 11.12^b	705.00 ± 12.88^a

CON, the control group; MET, the methyl-donor micronutrients group. At each time point, different letters indicate statistical difference in the same row ($P < 0.05$). Values are expressed as means ± standard error of mean (SEM). [1]n = 6: Six litters per group were selected, and one median-birth-weight piglet from each litter was sampled for feces collection at 7, 14, and 21 days.

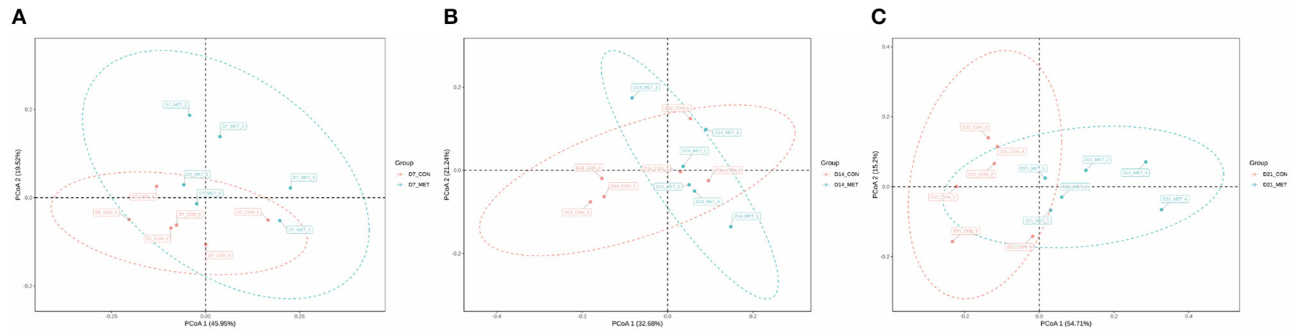

FIGURE 2 | The PCoA analysis of the fecal microbial community in suckling piglets from sows fed the MET vs. CON diet. The PCoA plot was generated by the weighted UniFrac distances. Each dot represents an individual sample of piglet ($n = 6$). $n = 6$: Six litters per group were selected, and one median-birth-weight piglet from each litter was sampled for feces collection at 7 **(A)**, 14 **(B)**, and 21 days **(C)**. CON, the control group; MET, the methyl-donor micronutrients group.

further analyzed by LEfSe. Compared with the CON group, including unknown bacteria, 14 microbial phlotypes were higher and 14 were lower in the 7-day suckling piglets from MET-fed sows (**Figure 5A**). At the age of 14 days, compared with the CON group, only one microbial phlotype was higher and two were lower in the MET offspring (**Figure 5B**). There were 42 higher and 16 lower microbial phlotypes in 21-day piglets from sows fed the MET vs. CON diet (**Figure 5C**).

Specific differentiated phylotypes were identified in 7-day suckling piglets from sows fed the MET vs. CON diet: increased genera *Dialister*, *Ralstonia*, *Megasphaera*, *Intestinimonas*, *Terrisporobacter*, *Anaerotrumcus* and families *Peptostretococcaceae*, *Chitinophagales* and order *Chitinophagaceae* ($P < 0.05$), decreased genera *Faecalibacterium*, *Rothia*, *Sedimentibacter*, *Aerosharea*, *unidentified-Prevotellaceae*, *Chlamydia* and families *Chlamydiaceae*, *Prevotellaceae*, *unidentified-Solibacterales* and order *Solibacterales*, *Chlamydiales* and class *unidentified-Chlamydiae*, phylum Chlamydiae ($P < 0.05$). At the age of 14 days, the suckling piglets from sows fed MET had significantly higher family *Christensenellaceae* ($P < 0.05$); at the age of 21 days, the suckling piglets from sows fed MET had increased genera *Streptococcus*, *Romboutsia*, *Agathobacter*, *Akkermansia*, *Sharpea*, *Rothia*, *Rubrobacter*, *Paraeggerthella*, *Pediococcus*, *Kurthia*, *Mogibacterium*, *Turicibacter*, *Foumirerlla* and families *Streptococcaceae*, *Akkermansiaceae*, *Micromonosporaceae*, *unidentified-Rubrobacterales*, *Micrococcaceae*, *Pseudomonadaceae*, *Flavobacteriaceae* and orders *Lactobacillales*, *Clostridiales*, *Verrucomicrobiales*, *Micromonosporaceae*, *Oceanospirillales*, *Rubrobacterales*, *Gaiellales*, *Micrococcales*, *Pseudomonadales* and classes *Bacilli*, *Clostridia*, *Rubrobacteria*, *Verrucomicrobia*, *unidentified-Actinobacteria*, *Thermoleophilia* and phyla Firmicutes, Verrucomicrobia ($P < 0.05$), decreased genera *Odoribater*, *Parabacteroides*, *unidentified-Cyanobacteria*, *Ochrobactrum* and families *Tanerellaceae*, *unidentified-Cyanobacteria*, *Rikenellaceae* and order *unidentified-Cyanobacteria*, *Bacteroidales* and classes *unidentified-Cyanobacteria*, *Bacteroidia* and phyla Cyanobacteria, Bacterioidetes ($P < 0.05$).

Fecal SCFA Concentration

As displayed in **Table 3**, no statistical differences were observed in the fecal SCFA concentration of 7-day piglets between maternal dietary treatments ($P > 0.05$). However, the concentration of acetate, butyrate, and total SCFA were increased in the feces of 14-day piglets from sows fed the MET vs. CON diet ($P < 0.05$). Besides this, maternal MET supplementation increased the concentration of acetate, propionate, isobutyrate, butyrate, isovalerate, valerate, valerate, and total SCFA in the feces of 21-day piglets ($P < 0.05$).

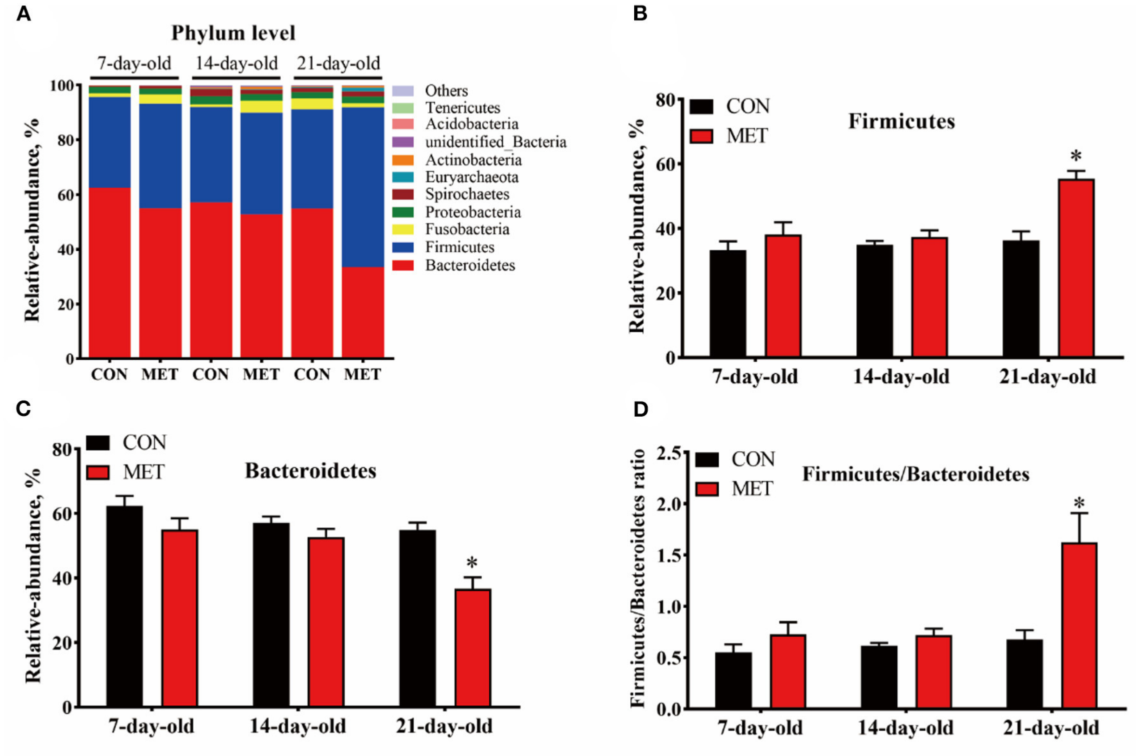

FIGURE 3 | The composition of fecal microbiota in suckling piglets from sows fed the MET vs. CON diet at the phylum level. The relative abundance of the top 10 phyla **(A)** and the bacterial phyla differed **(B–D)** between suckling piglets from CON- and MET-fed sow. Each dot represents an individual piglet ($n = 6$), and * indicates $P < 0.05$. $n = 6$: Six litters per group were selected, and one median-birth-weight piglet from each litter was sampled for feces collection at 7, 14, and 21 days. CON, the control group; MET, the methyl-donor micronutrients group.

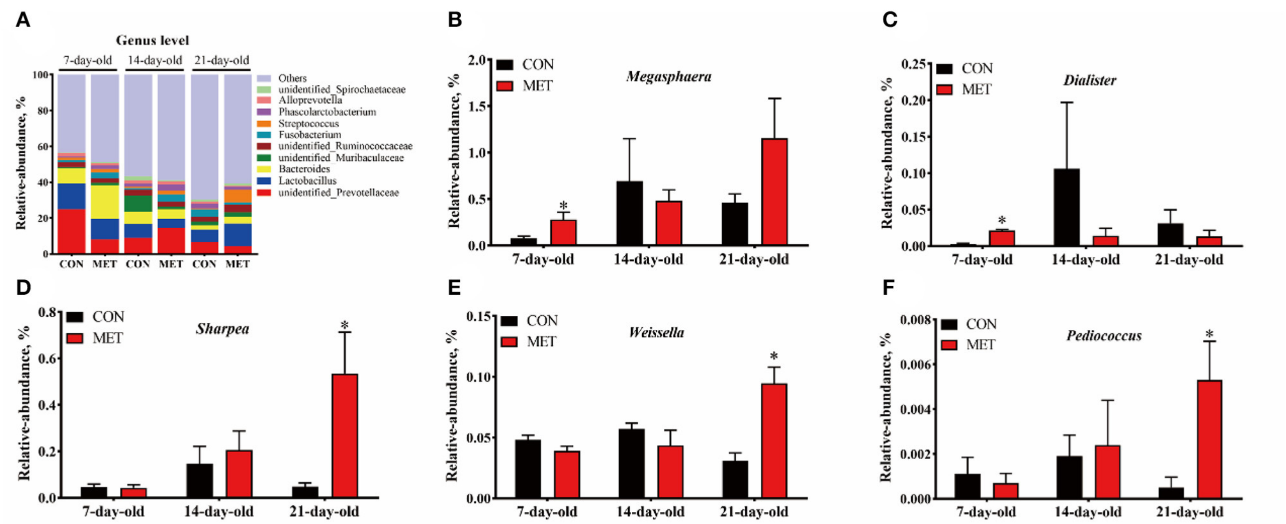

FIGURE 4 | The composition of fecal microbiota in suckling piglets from sows fed the MET vs. CON diet at the genus level. The relative abundance of the top 10 genera **(A)** and the bacterial genera differed **(B–F)** between suckling piglets from CON- and MET-fed sow. Each dot represents an individual piglet ($n = 6$), and * indicates $P < 0.05$. $n = 6$: Six litters per group were selected, and one median-birth-weight piglet from each litter was sampled for feces collection at 7, 14, and 21 days. CON, the control group; MET, the methyl-donor micronutrients group.

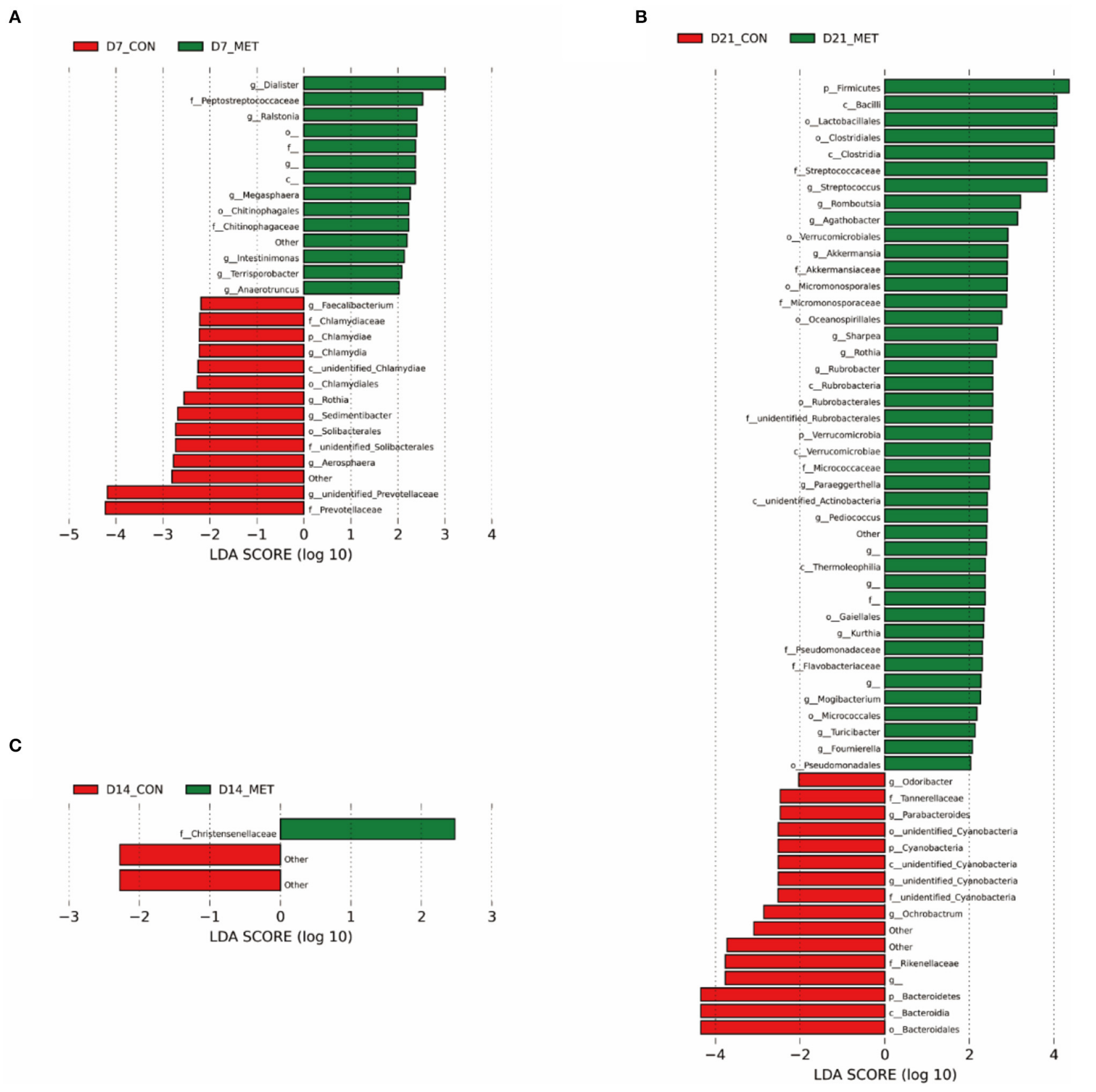

FIGURE 5 | The LEfSe analysis of the fecal bacterial community in 7 **(A)**, 14 **(B)**, and 21- day **(C)** suckling piglets from sows fed the MET vs. CON diet ($n = 6$). The default parameter of the LDA score is 4. The bacteria that are not named in the figure are those that have not yet been named. $n = 6$: Six litters per group were selected, and one median-birth-weight piglet from each litter was sampled for feces collection at 7, 14, and 21 days. CON, the control group; MET, the methyl-donor micronutrients group; LDA, linear discriminant analysis; p_, phylum; c_, class; o_, order; f_, family; g_, genus.

Fecal Metabolic Profiling

As graphed in **Figure 6**, the separation in positive ionization mode between the two groups by the OPLS-DA method was evaluated. OPLS-DA plots of the fecal metabolomics data show a clear separation with no overlap for each group, the parameters for the explanatory and predictive values of the intercepts (R2, Q2), which were stable and good to fitness and prediction (**Supplementary Figure 1**).

Differential Metabolites and Bioinformatics Analysis

Based on the VIP of the OPLS-DA model and the *p*-value of the Student's *t*-test, the biologically important difference metabolites were mined. Including significantly differential and differential metabolites, a total of 24 differentiated metabolites were identified from two data sets in 7-day suckling piglets (**Figure 7A**), 42 differentiated metabolites were identified from

TABLE 3 | Effect of maternal methyl-donor micronutrient supplementation during gestation on the concentration of short-chain fatty acids (SCFA) in feces of suckling piglets (mg/g) ($n = 6$)[1].

Items	7 days old		14 days old		21 days old	
	CON	MET	CON	MET	CON	MET
Acetate	1.74 ± 0.14	2.19 ± 0.19	1.95 ± 0.14[b]	2.67 ± 0.12[a]	2.17 ± 0.14[b]	2.9 ± 0.28[a]
Propionate	0.83 ± 0.11	1.07 ± 0.10	0.99 ± 0.08	1.24 ± 0.13	1.15 ± 0.12[b]	1.56 ± 0.10[a]
Isobutyrate	0.16 ± 0.03	0.18 ± 0.03	0.17 ± 0.02	0.24 ± 0.03	0.16 ± 0.02[b]	0.40 ± 0.07[a]
Butyrate	0.52 ± 0.03	0.55 ± 0.06	0.59 ± 0.08[b]	0.96 ± 0.11[a]	0.60 ± 0.05[b]	1.86 ± 0.28[a]
Isovalerate	0.39 ± 0.07	0.40 ± 0.07	0.38 ± 0.05	0.50 ± 0.06	0.41 ± 0.04[b]	1.11 ± 0.16[a]
Valerate	0.24 ± 0.03	0.36 ± 0.08	0.27 ± 0.05	0.43 ± 0.09	0.25 ± 0.03[b]	0.51 ± 0.05[a]
The ratio of acetate to propionate	2.29 ± 0.31	2.11 ± 0.09	2.01 ± 0.11	2.33 ± 0.34	1.94 ± 0.13	1.88 ± 0.19
Total SCFA	3.87 ± 0.36	4.79 ± 0.47	4.34 ± 0.40[b]	6.03 ± 0.24[a]	4.75 ± 0.37[b]	8.33 ± 0.86[a]

SCFA, short-chain fatty acid; CON, the control group; MET, the methyl-donor micronutrients group. At each time point, different letters indicate statistical difference in the same row ($P < 0.05$). Values are expressed as means ± standard error of mean (SEM). [1]n = 6: Six litters per group were selected, and one median-birth-weight piglet from each litter was sampled for feces collection at 7, 14, and 21 days.

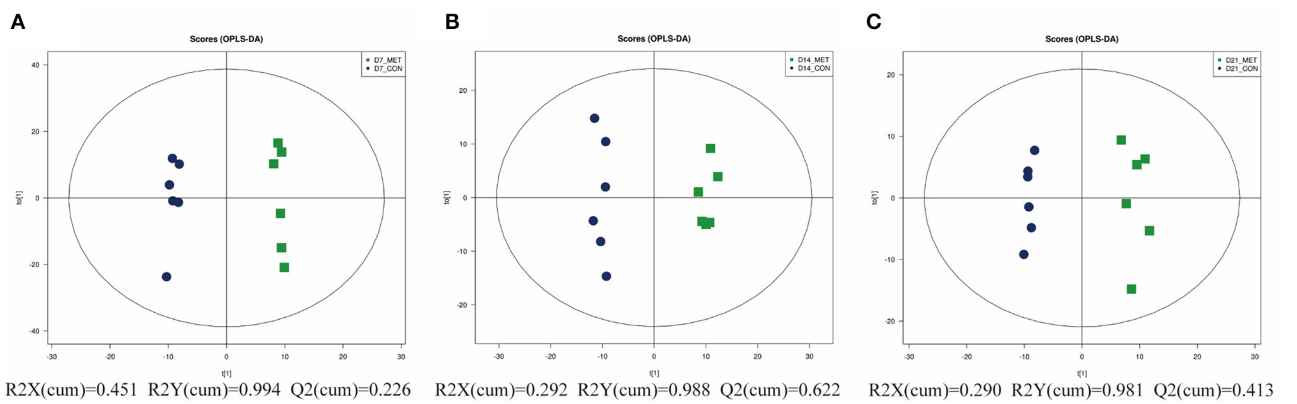

FIGURE 6 | The OPLS-DA analysis (orthogonal partial least squares discriminant analysis) of fecal microbial metabolites in 7 **(A)**, 14 **(B)**, and 21- day **(C)** suckling piglets from sows fed the MET vs. CON diet ($n = 6$). $n = 6$: Six litters per group were selected, and one median-birth-weight piglet from each litter was sampled for feces collection at 7, 14, and 21 days. CON, the control group; MET, the methyl-donor micronutrients group.

two data sets in 14-day suckling piglets (**Figure 7B**), and 29 differentiated metabolites were identified from two data sets in 21-day suckling piglets (**Figure 7C**). We subsequently analyzed the significantly metabolite differences in the Kyoto Encyclopedia of Genes and Genomes (KEGG) pathway database (http://www.genome.jp/kegg/) to pathways in offspring that may have been influenced by maternal MET during gestation. These findings revealed that the potential biomarkers contribute to various processes, including biosynthesis of amino acids, amino acid metabolism, pyrimidine metabolism, purine metabolism, amino sugar and nucleotide sugar metabolism, bile secretion, thiamine metabolism, vitamin B6 metabolism, riboflavin metabolism, nicotinate and nicotinamide metabolism, sulfur metabolism, and glutathione metabolism (**Tables 4–6**).

Specific differentiated metabolites were identified in 7-day suckling piglets of CON-fed and MET-fed sows: Deoxycytidine closely related to pyrimidine metabolism was increased 5.187-fold in MET piglets compared with CON piglets ($P < 0.05$). Pyridoxal closely related to vitamin B6 metabolism was increased 1.770- fold in MET compared with the CON group ($P < 0.05$). Indoleacetic acid closely related to tryptophan metabolism was decreased 0.191-fold in MET piglets compared with CON piglets ($P < 0.05$). Riboflavin metabolism (flavin adenine dinucleotide and flavin mononucleotide) were decreased 0.59- and 0.42-fold in MET piglets compared with CON piglets ($P < 0.05$). In the 14-day suckling piglets, critical metabolites (1-aminocyclopropanecarboxylic acid, anthranilic acid) closely related to biosynthesis of amino acids were increased by 4.95- and 2.16-fold in the MET group compared with the CON group, respectively ($P < 0.05$). Thymine, 2'-deoxyuridine, uracil, urea, and deoxycytidine, which are involved in pyrimidine metabolism, were increased in the MET compared with the CON group by 2.36-, 3.22-, 2.68-, 1.45-, and 7.63-fold, respectively ($P < 0.05$), and concentrations of adenosine, adenine, and deoxyinosine, which are involved in purine metabolism, were increased in the MET compared with the CON group by 1.39-, 3.81-, and 1.18-fold, respectively ($P < 0.05$). Critical metabolites (dopamine, bilirubin, and cholic acid) closely related to bile secretion were decreased in the MET group. In addition, critical metabolites closely related to amino acid and vitamin B6 metabolism were increased in the MET group compared with the CON group ($P < 0.05$). In the 21-day suckling piglets,: critical

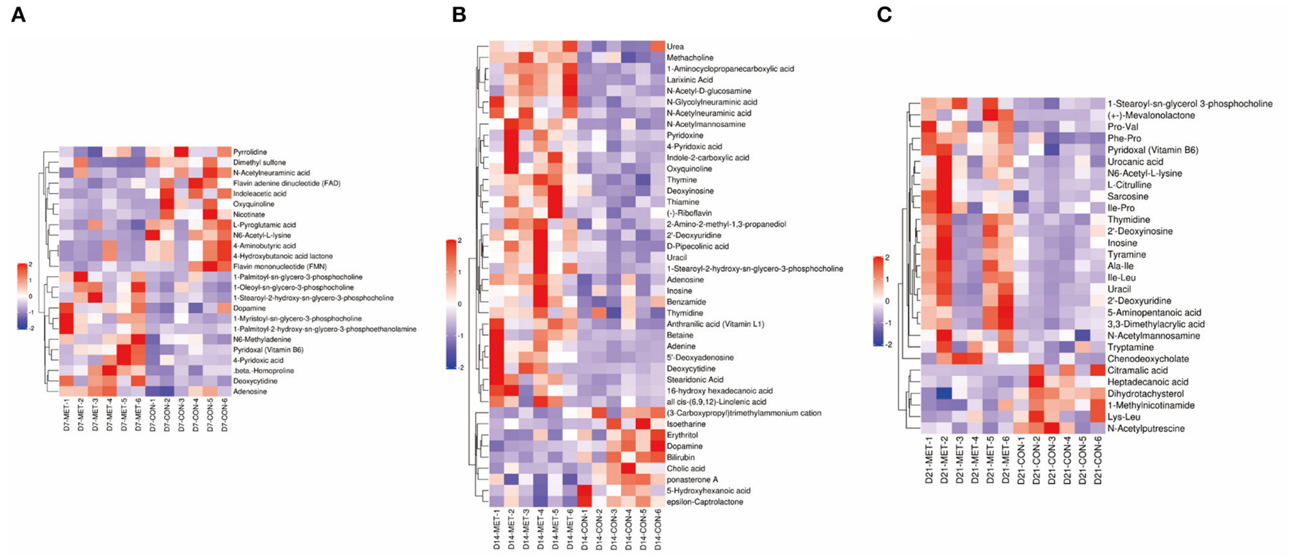

FIGURE 7 | The hierarchical clustering of fecal metabolic profile in 7 **(A)**, 14 **(B)**, and 21- day **(C)** suckling piglets from sows fed the MET vs. CON diet ($n = 6$). The color scale ranges from saturated purple (−2) to blank (0) to saturated red (2). Red and purple color represent increased and decreased metabolites, respectively. X axis: sample code, Y axis: metabolite name. $n = 6$: Six litters per group were selected, and one median-birth-weight piglet from each litter was sampled for feces collection at 7, 14, and 21 days. CON, the control group; MET, the methyl-donor micronutrients group.

TABLE 4 | The significantly changed fecal metabolites in 7-day suckling piglets from sows fed the MET vs. CON diet ($n = 6$)[1].

Metabolites	Fold change (MET vs. CON)	*P*-value	VIP	*m/z*	Pathway
Deoxycytidine	5.187	0.007	1.397	455.188	Pyrimidine metabolism
Indoleacetic acid	0.191	0.008	2.425	176.069	Tryptophan metabolism
Pyridoxal (Vitamin B6)	1.770	0.022	1.053	168.064	Vitamin B6 metabolism
Flavin adenine dinucleotide (FAD)	0.589	0.040	1.247	786.165	Riboflavin metabolism
Flavin mononucleotide (FMN)	0.418	0.049	1.125	457.110	Riboflavin metabolism
Nicotinate	0.191	0.038	1.364	124.041	Nicotinate and nicotinamide metabolism
N6-acetyl-l-lysine	0.403	0.009	2.201	189.122	Lysine degradation
Dimethyl sulfone	0.433	0.035	1.197	226.986	Sulfur metabolism
L-pyroglutamic acid	0.619	0.045	1.593	190.070	Glutathione metabolism
Beta-homoproline	3.459	0.008	1.007	130.085	Other
1-Myristoyl-sn-glycero-3-phosphocholine	3.068	0.017	1.150	468.307	Other
1-Oleoyl-sn-glycero-3-phosphocholine	1.912	0.028	2.715	522.355	Other
1-Stearoyl-2-hydroxy-sn-glycero-3-phosphocholine	4.347	0.036	1.757	506.358	Other

CON, the control group; MET, the methyl-donor micronutrients group. VIP variable importance for the projection, m/z mass to charge ratio. [1]n = 6: Six litters per group were selected, and one median-birth-weight piglet from each litter was sampled for feces collection at 7 days.

metabolites related to biosynthesis of amino acids, amino acid metabolism, and vitamin B6 metabolism, were increased in the MET group compared with CON group although bile secretion was decreased in MET piglets ($P < 0.05$).

Correlation Analysis for Differential Metabolites and Microbes

A Spearman's correlation matrix was generated to explore the correlation between the bacterial genera and candidate compounds that were affected by maternal nutrition. As shown in **Figure 8**, significant associations could be identified between the gut microbial and the altered metabolite profiles from 7- and 21-day suckling piglets. In the 21-day suckling piglets (**Figure 8A**), the correlation analysis revealed that deoxycytidine was positively correlated with the genera *Dialister* and *Anaerotrumcus* and negatively associated with the genera *Rothia*, *Sedimentibacter*, *and unidentified-Prevotellaceae* ($P < 0.05$). Indoleacetic acid was negatively associated with the genera *Dialister* and *Terrisporobacter* and positively correlated with the genera *Sedimentibacter*, *unidentified-Prevotellaceae*, and *Chlamydia* ($P < 0.05$). The genera *Dialister*, *Megasphaera*, and *Terrisporobacter*

TABLE 5 | The significantly changed fecal metabolites in 14-day suckling piglets from sows fed the MET vs. CON diet ($n = 6$)[1].

Metabolites	Fold change (MET vs. CON)	P-value	VIP	m/z	Pathway
1-Aminocyclopropanecarboxylic acid	4.947	0.000	1.449	84.043	Biosynthesis of amino acids
Anthranilic acid (Vitamin L1)	2.160	0.005	2.151	138.054	Biosynthesis of amino acids
Thymine	2.357	0.001	4.485	127.049	Pyrimidine metabolism
2'-Deoxyuridine	3.223	0.002	1.044	229.08	Pyrimidine metabolism
Uracil	2.675	0.024	1.155	113.033	Pyrimidine metabolism
Urea	1.450	0.043	1.137	61.039	Pyrimidine metabolism
Deoxycytidine	7.633	0.048	1.482	455.188	Pyrimidine metabolism
Adenosine	2.25	0.007	1.385	268.103	Purine metabolism
Adenine	3.111	0.011	3.814	136.061	Purine metabolism
Deoxyinosine	2.731	0.016	1.182	253.092	Purine metabolism
N-Acetylmannosamine	3.443	0.002	1.750	204.086	Amino sugar and nucleotide sugar metabolism
N-Acetylneuraminic acid	5.873	0.005	2.319	310.112	Amino sugar and nucleotide sugar metabolism
N-Acetyl-D-glucosamine	4.727	0.006	1.521	443.186	Amino sugar and nucleotide sugar metabolism
N-Glycolylneuraminic acid	2.558	0.007	1.172	326.107	Amino sugar and nucleotide sugar metabolism
Dopamine	0.508	0.005	1.937	136.074	Bile secretion
Bilirubin	0.228	0.007	5.162	585.269	Bile secretion
Cholic acid	0.310	0.047	1.652	426.319	Bile secretion
Thiamine	2.299	0.014	4.665	265.112	Thiamine metabolism
4-Pyridoxic acid	2.672	0.043	2.394	184.059	Vitamin B6 metabolism
Betaine	6.706	0.028	7.651	118.086	Glycine, serine and threonine metabolism
Erythritol	0.367	0.044	2.214	164.090	ABC transporters
Methacholine	2.472	0.001	1.141	160.132	Other
Larixinic acid	4.992	0.002	3.898	144.064	Other
Oxyquinoline	3.131	0.002	1.555	146.059	Other
D-Pipecolinic acid	5.572	0.003	7.555	130.086	Other
Epsilon-captrolactone	0.496	0.004	2.425	156.101	Other
5'-Deoxyadenosine	4.760	0.004	7.327	252.109	Other
(3-Carboxypropyl) Trimethylammonium cation	0.285	0.013	3.409	146.116	Other
2-Amino-2-methyl-1,3-propanediol	2.512	0.014	1.886	70.064	Other
Ponasterone A	0.439	0.015	1.376	482.345	Other
Indole-2-carboxylic acid	5.840	0.021	3.140	162.054	Other
Stearidonic acid	2.479	0.024	2.942	277.215	Other
1-Stearoyl-2-hydroxy-sn-glycero-3-phosphocholine	3.972	0.028	1.829	506.356	Other

CON, the control group; MET, the methyl-donor micronutrients group. VIP variable importance for the projection, m/z mass to charge ratio. [1]n=6: Six litters per group were selected, and one median-birth-weight piglet from each litter was sampled for feces collection at 14 days.

were positively correlated with vitamin B6 ($P < 0.05$). In addition, the genus *Sedimentibacter* was positively correlated with flavin adenine dinucleotide and flavin mononucleotide ($P < 0.05$). In the 21-day suckling piglets (**Figure 8B**), sarcosine was negatively associated with the genera *Parabacteroides* and *unidentified-Cyanobacterir* and positively correlated with the genera *Rothia*, *Rubrobacter*, *Pediococcus*, and *Mogibacterium* ($P < 0.05$). 1-Methylnicotinamide was negatively associated with the genera *Agathobacter*, *Paraeggerthella*, and *Pediococcus* and positively correlated with the genera *Odoribater* and *Ochrobactrum* ($P < 0.05$). Nine genera, including *Streptococcus*, *Akkermansia*, *Rothia*, *Rubrobacter*, *Pediococcus*, *Mogibacterium*, *Turicibacter*, and *Foumirerlla* were positively correlated with vitamin B6 ($P < 0.05$).

DISCUSSION

In a previous study, we found no differences in reproductive performance of sows between CON and MET; however, we observed that the offspring of sows fed with the MET diet grew faster than control offspring, and maternal MET exposure can promote skeletal muscle differentiation and maturity and improve the skeletal muscle mass of weaning piglets (14). Previous research reports the intestinal tract of the monogastric animal plays a crucial role in nutrient digestion and absorption and maintains the barrier function against malignant pathogens and antigens (20). In addition, gut microbiota contributes to muscle mass and muscle fiber types through the gut–muscle axis (21). Thus, in the present

TABLE 6 | The significantly changed fecal metabolites in 21-day suckling piglets from sows fed the MET vs. CON diet ($n = 6$)[1].

Metabolites	Fold change (MET vs. CON)	*P*-value	VIP	*m/z*	Pathway
Sarcosine	2.169	0.035	1.415	150.075	Biosynthesis of amino acids
1-Methylnicotinamide	0.457	0.017	2.128	137.070	Bile secretion
Pyridoxal (Vitamin B6)	2.056	0.012	1.844	168.064	Vitamin B6 metabolism
N6-Acetyl-L-lysine	3.092	0.048	1.020	189.122	Lysine degradation
Dihydrotachysterol	0.578	0.000	1.346	465.320	Other
Phe-Pro	2.199	0.001	2.128	263.138	Other
1-Stearoyl-sn-glycerol 3-phosphocholine	3.303	0.006	2.147	568.339	Other
Pro-Val	2.994	0.020	2.184	215.138	Other
Ile-Leu	2.964	0.033	1.547	245.186	Other
3,3-Dimethylacrylic acid	2.520	0.034	2.222	101.059	Other
Ala-Ile	3.760	0.044	2.163	203.138	Other
Ile-Pro	2.184	0.045	3.157	229.154	Other
(+-)-Mevalonolactone	3.800	0.045	1.183	148.095	Other

CON, the control group; MET, the methyl-donor micronutrients group. VIP, variable importance for the projection, m/z mass to charge ratio. [1]*n = 6: Six litters per group were selected, and one median-birth-weight piglet from each litter was sampled for feces collection at 21 days.*

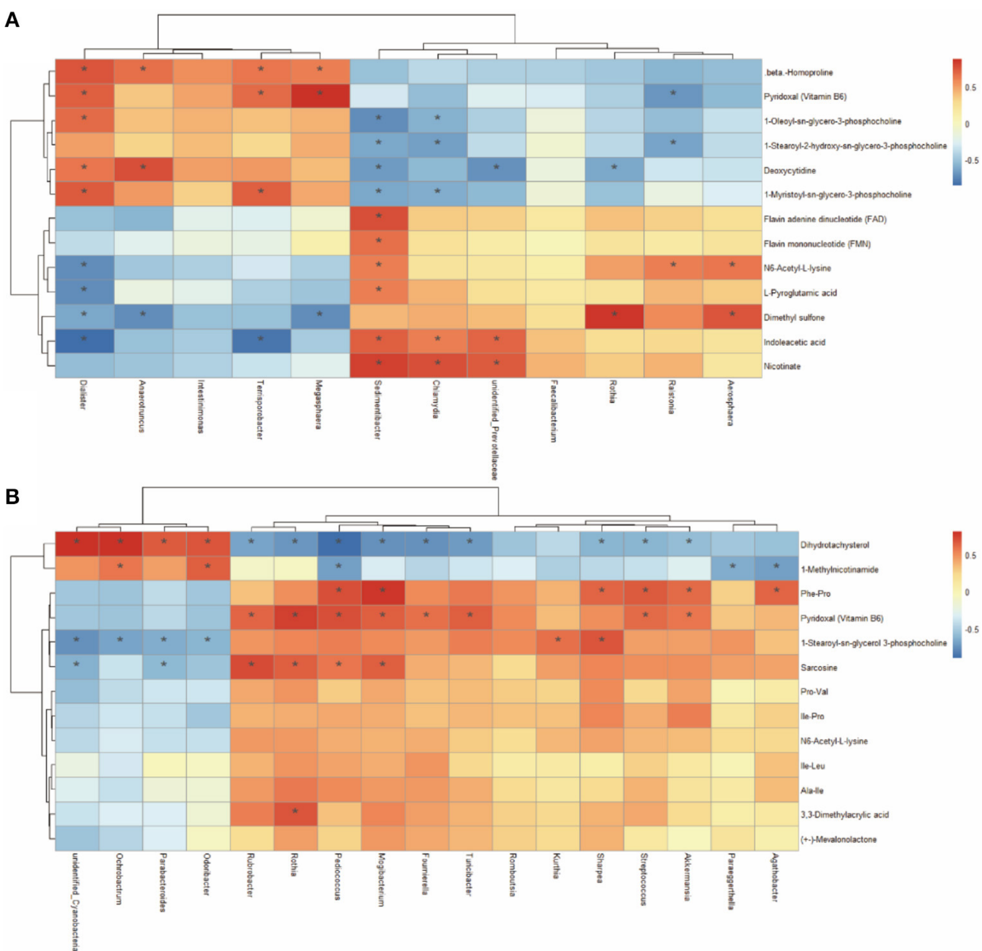

FIGURE 8 | Spearman correlation analysis between genera and metabolite concentrations in 7 **(A)** and 21- day **(B)** suckling piglets from sows fed the MET vs. CON diet ($n = 6$). *Asterisks indicate significant correlations between genera and metabolite concentrations. Cells are colored based on the Spearman correlation coefficient between the significantly altered genera and metabolites; red represents a significantly positive correlation, blue represents a significantly negative correlation ($P < 0.05$), and white represents no significant correlation ($P > 0.05$). $n = 6$: Six litters per group were selected, and one median-birth-weight piglet from each litter was sampled for feces collection at 7, 14, and 21 days.

study, we collected fresh fecal samples from piglets at 7, 14, and 21 days and further analyzed the effects of MET on intestine microbiota colonization and metabolism in offspring. Our findings show that the establishment of the suckling piglets' gut microbiota was strongly affected by maternal MET, and the MET offspring have a higher growth performance, which is concomitant with alterations in the intestinal microbiota alpha diversity, microbiota composition, SCFA, and the biosynthesis of amino acids. Furthermore, we found associations between the differentially abundant genera and metabolites in the CON and MET groups.

Establishment of the Gut Microbial Community in Suckling Piglets

The gut microbiota diversity is highly related to host health and metabolic capacity (22). The low diversity of intestinal microbiota is considered a mark of intestinal dysbiosis, which may lead to autoimmune diseases, inflammatory bowel diseases, diarrhea, and metabolic diseases (23, 24). Increased bacterial richness and diversity is a marker of the establishment of intestinal microbiota (10). Our findings show that bacterial richness and diversity were increased in 7-day piglets from the MET sows compared with those from the CON sows. In addition, bacterial richness and uniformity were significantly higher in MET offspring at 21 days of age, suggesting that MET offspring had a more diversified intestinal microbiota. However, there was no difference in the microbiota diversity of 14-day piglets, this is probably because the gut microbial community is unstable and in a stage of rapid change. The bacterial communities were dominated by Firmicutes and Bacteroidetes in agreement with a previous study (25, 26). The increase in Firmicutes phylum is considered a marker of the establishment of intestinal microbiota (1, 27, 28). Previous studies found that the F/B is proportional to body weight because the increase in Firmicutes is closely related to energy intake (29, 30), and the relative abundance of Bacteroidetes is associated with degradation of proteins and carbohydrates (31). In our study, the microbiota of MET piglets showed an increase in F/B over time, characterized by increases in Firmicutes abundance. This suggesting that the intestinal microbiota of MET offspring may be more efficient than CON offspring at extracting energy from their diet, and consequently, they gain more weight.

Differences in the Gut Microbiota Between CON and MET Offspring During Suckling Period

As is previously reported, an increase in methionine intake from the diet would lead to an increased amount of methionine in the lumen and provide an excellent fuel source for the rapid proliferation of bacteria (32). However, a lack of methyl donors can affect the differentiation and barrier functions of the small intestine and increase the concentration of Hcy, which subsequently promotes oxidative stress and activates interrelated pro-inflammatory mechanisms, ultimately aggravating inflammatory bowel disease in rats (13, 33). MET supplementation through the diet limits pathobiont colonization of the gut via inducing a specific intestinal micro-environment (11). When the harmful bacteria decrease, the beneficial bacteria may increase relatively. In our study, maternal MET supplementation during gestation decreased serum Hcy concentration in the offspring. Moreover, we identified that MET offspring at 7 days had a significantly higher abundance of *Dialister* and *Megasphaera* in the feces than CON offspring, and MET offspring at 21 days had a significantly higher abundance of *Romboutsia*, *Akkermansia*, *Sharpea*, *Turicibacter weissella*, and *pediococcus* in the feces than CON offspring. *Dialister* populations utilize succinate and produce propionate, *Megasphaera* can convert lactic acid to propionate via the acrylate pathway (34), and the *Sharpea* is beneficial to lactate production (35). Previous studies indicate that *Akkermansia* is linked with improved metabolic parameters; hosts with low *Akkermansia* content are susceptible to obesity, inflammation, and type 2 diabetes (36). As putatively beneficial gut microbiota, *Akkermansia* reinforces the gut barrier function and eventually reduces plasma lipopolysaccharide (37, 38). Previous studies also show that high relative abundances of *Romboutsia* are associated with decreased risk for infection in kidney transplant recipients (39), the *Turicibacter* might play a role in inflammatory bowel diseases and was proportional in concentration to that of butyric acid (40, 41). *Weissella* and *pediococcus* are recognized probiotic genera, which play a role in improving the health of the host (42, 43). Our data show that the relative abundance of beneficial bacteria is increased in MET piglets, which could play an inhibitory role in the growth of intestinal pathogenic bacteria and relieve metabolic diseases and intestinal inflammation (44, 45).

Changes in Feces SCFA Between CON and MET Offspring During Suckling Period

Our results indicate that maternal MET supplementation during gestation increased the concentrations of individual and total SCFAs of offspring at 21 days of age. As for the reason for the increased SCFAs in the feces of suckling piglets, a previous study reports that acetate, propionate, and butyrate were formed from cysteine, whereas the main products of methionine metabolism were propionate and butyrate (46). Supplementing DL-MHA (a methionine substitute) in the diet increased the concentration of acetic acid, valeric acid, and total SCFAs in the cecum of piglets (47). Due to the sparing effect between methionine and cysteine, the supplementation of MET may lead to quantities of residual Cys in the gut to produce the SCFAs. In addition, the relative abundance of SCFA-producing *Dialister*, *Megasphaera*, *Turicibacter*, and *Sharpea* were increased in the MET group, which may also explain the increased production of SCFAs in the intestine. As the main source of energy for epithelial cells, SCFA can increase the proliferation of intestinal tissues (48, 49), butyrate can decrease intestinal inflammation, and as it enhances the intestinal barrier function (50), propionate can be used by hepatocyte cells of the liver for gluconeogenesis (51). That beneficial bacteria were increased in the MET offspring may be associated with the increase of SCFAs, which destroy microbial pathogens (52). However, no alteration in the concentrations of individual or total SCFAs was observed when the offspring piglets were 7 days old. Although the butyric- and lactic-producing bacteria were increased, the total intestinal microbiota of 7-day piglets was relatively low, and the amount of SCFA produced was also low, so the difference is not significant.

Changes in Feces Metabolism Between CON and MET Offspring During Suckling Period

Maternal nutrition is clearly an important determinant of offspring gut microbiota, which has in turn linked with host metabolism and health (53, 54). The increase in BW at weaning might result from the increased metabolism of biosynthesis of amino acids, pyrimidine, and purine, which are positively correlated with growth. Previously, it was reported that amino acids not only serve as substances for synthesis of tissue proteins, but also as substrates for the synthesis of many low-molecular-weight substances (55). In our study, we found that maternal exposure to MET increased the concentrations of amino acid metabolism (including anthranilic acid, 1-aminocyclopropanecarboxylic acid, and sarcosine) in the offspring at 14 or 21 days. Meanwhile, the concentrations of metabolites involved in purine and pyrimidine metabolism increased, which indicated an enhanced function in nucleic acid metabolism via one-carbon metabolism (56) mainly because folate metabolism provides building blocks (10-formyl-tetrahydrofolate, methylene-tetrahydrofolate, respectively) for purine and pyrimidine synthesis. Furthermore, the amino and nucleotide sugars were increased in 14-day offspring of MET-supplemented sows. Notably, bile acid metabolites (cholic acid, dopamine, bilirubin, and 1-methylnicotinamide) were increased in 14- or 21-day offspring of sows in the CON group. The increase in bile acid metabolites could be caused by reduced reabsorption in the intestine (57). Bile acids (BAs) play an important role in the intestines, facilitating fat digestion and the absorption of lipids and liposoluble vitamins. Approximately 90% of bile acids return from the intestinal cavity to the liver via the portal vein (58). High concentrations of bile acid are toxic to mammalian cells (59). Cholic acid, as one of the BAs produced by the liver, is involved in the primary BA biosynthesis pathway (60). The elevation of cholic acid is a potential biomarker of liver injury, and extra cholic acid may partly lead to an increased risk of inflammation (61, 62). Total bilirubin is another indirect marker of liver function. Therefore, the decreased levels of cholic acid and bilirubin suggest that maternal exposure to MET during pregnancy may improve liver function of offspring.

The maternal metabolic status during gestation exerts a significant influence on the infant microbiota at the beginning of life (63). Maternal MET exposure can alter serum one-carbon metabolism of sows (14) and offspring. One-carbon metabolism participates in the synthesis of nucleotides, proteins, and lipids by integrating glucose, amino acid status, and vitamins in suckling piglets (8). In addition, there is increasing evidence that microbiota-derived metabolites act as key factors regulating animal metabolism, growth, and development (10). In this study, Spearman's correlation revealed an association between the abundance of specific bacterial genera and metabolites that were significantly influenced by maternal exposure to MET. Particularly, the VB6 and sarcosine were positively correlated with the genera *Rothia*, *Rubrobacter*, *Pediococcus*, and *Mogibacterium*. Altogether, the establishment of a gut microbial community and metabolic homeostasis could be a major underlying factor that induces improved growth and development of MET suckling piglets.

CONCLUSION

Collectively, maternal methyl-donor micronutrient addition altered gut microbiota and the fecal metabolic profile, resulting in an improved weaning weight of offspring piglets.

DATA AVAILABILITY STATEMENT

The raw sequences used in this study were stored on the Sequence Read Archive (SRA) of NCBI, and the SRA accession number is PRJNA694233.

ETHICS STATEMENT

The animal study was reviewed and approved by the Animal Care and Use Committee of Jiangxi Agricultural University (Ethic Approval Code: JXAUA01).

AUTHOR CONTRIBUTIONS

JY and TZ designed the study. QH, LJ, and JH performed the animal feeding experiment and sample analysis. FX assisted with SCFAs analysis. QH collected the data and wrote the manuscript. ZW and JC finalized the manuscript. All authors agree to be accountable for the content of the work.

FUNDING

The work was supported by the National Key Research and Development Program of China (2018YFD0500401).

SUPPLEMENTARY MATERIAL

The Supplementary Material for this article can be found online at: https://www.frontiersin.org/articles/10.3389/fnut.2021.675640/full#supplementary-material

REFERENCES

1. Muinck EJ, Trosvik P. Individuality and convergence of the infant gut microbiota during the first year of life. *Nat Commun*. (2018) 9:2233. doi: 10.1038/s41467-018-04641-7
2. Sonnenburg JL, Bäckhed F. Diet–microbiota interactions as moderators of human metabolism. *Nature*. (2016) 535:56–64. doi: 10.1038/nature18846
3. Ganal-Vonarburg SC, Hornef MW, Macpherson AJ. Microbial-host molecular exchange and its functional consequences in early mammalian life. *Science*. (2020) 368:604–7. doi: 10.1126/science.aba0478
4. Steegers-Theunissen RPM, Twigt J, Pestinger V, Sinclair KD. The periconceptional period, reproduction and long-term health of offspring: the importance of one-carbon metabolism. *Hum Reprod Update*. (2013) 19:640–55. doi: 10.1093/humupd/dmt041
5. Gabbianelli R. Modulation of the epigenome by nutrition and xenobiotics during early life and across the life span: the key role of lifestyle. *Lifestyle Genomics*. (2018) 11:9–12. doi: 10.1159/000490751
6. Vickers M. Early life nutrition, epigenetics and programming of later life disease. *Nutrients*. (2014) 6:2165–78. doi: 10.3390/nu6062165
7. Yu W, Wang Z, Zhang K, Chi Z, Xu T, Jiang D, et al. One-Carbon metabolism supports s-adenosylmethionine and histone methylation to drive inflammatory macrophages. *Mol Cell*. (2019) 75:1147–60. doi: 10.1016/j.molcel.2019.06.039
8. Wu S, Zhang J, Li F, Du W, Zhou X, Wan M, et al. One-Carbon metabolism links nutrition intake to embryonic development via epigenetic mechanisms. *Stem Cells Int*. (2019) 2019:1–8. doi: 10.1155/2019/3894101
9. Garcia-Mantrana I, Selma-Royo M, Gonzalez S, Parra-Llorca A, Martinez-Costa C, Collado MC. Distinct maternal microbiota clusters are associated with diet during pregnancy: impact on neonatal microbiota and infant growth during the first 18 months of life. *Gut Microbes*. (2020) 11:962–78. doi: 10.1080/19490976.2020.1730294
10. Li N, Huang S, Jiang L, Wang W, Li T, Zuo B, et al. Differences in the gut microbiota establishment and metabolome characteristics between low- and normal-birth-weight piglets during early-life. *Front Microbiol*. (2018) 9:1798. doi: 10.3389/fmicb.2018.01798
11. Gimier E, Chervy M, Agus A, Sivignon A, Billard E, Privat M, et al. Methyl-donor supplementation prevents intestinal colonization by Adherent-Invasive *E. coli* in a mouse model of Crohn's disease. *Sci Rep*. (2020) 10:12922. doi: 10.1038/s41598-020-69472-3
12. Mir SA, Nagy-Szakal D, Dowd SE, Szigeti RG, Smith CW, Kellermayer R. Prenatal methyl-donor supplementation augments colitis in young adult mice. *PLoS ONE*. (2013) 8:e73162. doi: 10.1371/journal.pone.0073162
13. Bressenot A, Pooya S, Bossenmeyer-Pourie C, Gauchotte G, Germain A, Chevaux J, et al. Methyl donor deficiency affects small-intestinal differentiation and barrier function in rats. *Brit J Nutr*. (2013) 109:667–77. doi: 10.1017/S0007114512001869
14. He Q, Zou T, Chen J, Jian L, He J, Xia Y, et al. Maternal methyl-donor micronutrients supplementation during pregnancy promotes skeletal muscle differentiation and maturity in newborn and weaning pigs. *Front Nutr*. (2020) 30:609022. doi: 10.3389/fnut.2020.609022
15. Oster M, Nuchchanart W, Trakooljul N, Murani E, Zeyner A, Wirthgen E, et al. Methylating micronutrient supplementation during pregnancy influences foetal hepatic gene expression and IGF signalling and increases foetal weight. *Eur J Nutr*. (2016) 55:1717–27. doi: 10.1007/s00394-015-0990-2
16. Matte JJ, Guay F, Girard CL. Folic acid and vitamin B 12 in reproducing sows: new concepts. *Can J Anim Sci*. (2006) 86:197–205. doi: 10.4141/A05-059
17. Zhao Y, Jin C, Xuan Y, Zhou P, Fang Z, Che L, et al. Effect of maternal or post-weaning methyl donor supplementation on growth performance, carcass traits, and meat quality of pig offspring. *J Sci Food Agr*. (2019) 99:2096–107. doi: 10.1002/jsfa.9402
18. Guay F, Matte JJ, Girard CL, Palin MF, Giguere A, Laforest JP. Effect of folic acid and glycine supplementation on embryo development and folate metabolism during early pregnancy in pigs. *J Anim Sci*. (2002) 80:2134–43. doi: 10.1093/ansci/80.8.2134
19. Liu Y, Wu X, Jiang H. Combined maternal and post-weaning high fat diet inhibits male offspring's prostate cancer tumorigenesis in transgenic adenocarcinoma of mouse prostate model. *Prostate*. (2018) 79:544–53. doi: 10.1002/pros.23760
20. Azad M, Gao J, Ma J, Li T, Tan B, Huang X, et al. Opportunities of prebiotics for the intestinal health of monogastric animals. *Anim Nutr*. (2020) 6:379–88. doi: 10.1016/j.aninu.2020.08.001
21. Yan H, Diao H, Xiao Y, Li W, Yu B, He J, et al. Gut microbiota can transfer fiber characteristics and lipid metabolic profiles of skeletal muscle from pigs to germ-free mice. *Sci Rep*. (2016) 6:31786. doi: 10.1038/srep31786
22. Clarke SF, Murphy EF, O'Sullivan O, Lucey AJ, Humphreys M, Hogan A, et al. Exercise and associated dietary extremes impact on gut microbial diversity. *Gut*. (2014) 63:1913–20. doi: 10.1136/gutjnl-2013-306541
23. Ott SJ. Reduction in diversity of the colonic mucosa associated bacterial microflora in patients with active inflammatory bowel disease. *Gut*. (2004) 53:685–93. doi: 10.1136/gut.2003.025403
24. Duca FA, Sakar Y, Lepage P, Devime F, Langelier B, Dore J, et al. Replication of obesity and associated signaling pathways through transfer of microbiota from obese-prone rats. *Diabetes*. (2014) 63:1624. doi: 10.2337/db13-1526
25. Xiao L, Estellé J, Kiilerich P, Ramayo-Caldas Y, Xia Z, Feng Q, et al. A reference gene catalogue of the pig gut microbiome. *Nat Microbiol*. (2016) 1:16161. doi: 10.1038/nmicrobiol.2016.161
26. Liu H, Hou C, Li N, Zhang X, Zhang G, Yang F, et al. Microbial and metabolic alterations in gut microbiota of sows during pregnancy and lactation. *FASEB J*. (2018) 33:4490–501. doi: 10.1096/fj.201801221RR
27. Olivares M, Walker AW, Capilla A, Benitez-Paez A, Palau F, Parkhill J, et al. Gut microbiota trajectory in early life may predict development of celiac disease. *Microbiome*. (2018) 6:36. doi: 10.1186/s40168-018-0415-6
28. Stewart CJ, Ajami NJ, O'Brien JL, Hutchinson DS, Smith DP, Wong MC, et al. Temporal development of the gut microbiome in early childhood from the TEDDY study. *Nature*. (2018) 562:583–88. doi: 10.1038/s41586-018-0617-x
29. Zhang W, Ma C, Xie P, Zhu Q, Wang X, Yin Y, et al. Gut microbiota of newborn piglets with intrauterine growth restriction have lower diversity and different taxonomic abundances. *J Appl Microbiol*. (2019) 127:354–69. doi: 10.1111/jam.14304
30. Singh P, Karimi A, Devendra K, Waldroup PW, Cho KK, Kwon YM. Influence of penicillin on microbial diversity of the cecal microbiota in broiler chickens. *Poultry Sci*. (2013) 92:272–6. doi: 10.3382/ps.2012-02603
31. Thomas F, Hehemann JH, Rebuffet E, Czjzek M, Michel G. Environmental and gut bacteroidetes: the food connection. *Front Microbiol*. (2011) 2:93. doi: 10.3389/fmicb.2011.00093
32. Miousse IR, Pathak R, Garg S, Skinner CM, Melnyk S, Pavliv O, et al. Short-term dietary methionine supplementation affects one-carbon metabolism and DNA methylation in the mouse gut and leads to altered microbiome profiles, barrier function, gene expression and histomorphology. *Genes Nutr*. (2017) 12:22. doi: 10.1186/s12263-017-0576-0
33. Chen M, Peyrin-Biroulet L, George A, Coste F, Bressenot A, Bossenmeyer-Pourie C, et al. Methyl deficient diet aggravates experimental colitis in rats. *J Cell Mol Med*. (2011) 15, 2486–97. doi: 10.1111/j.1582-4934.2010.01252.x
34. Canfora EE, Meex RCR, Venema K, Blaak EE. Gut microbial metabolites in obesity, NAFLD and T2DM. *Nat Rev Endocrinol*. (2019) 15:261–73. doi: 10.1038/s41574-019-0156-z
35. Kamke J, Kittelmann S, Soni P, Li Y, Tavendale M, Ganesh S, et al. Rumen metagenome and metatranscriptome analyses of low methane yield sheep reveals a Sharpea-enriched microbiome characterised by lactic acid formation and utilisation. *Microbiome*. (2016) 4:56. doi: 10.1186/s40168-016-0201-2
36. Plovier H, Everard A, Druart C, Depommier C, Van Hul M, Geurts L, et al. A purified membrane protein from *Akkermansia muciniphila* or the pasteurized bacterium improves metabolism in obese and diabetic mice. *Nat Med*. (2017) 23:107–13. doi: 10.1038/nm.4236
37. Depommier C, Everard A, Druart C, Plovier H, Van Hul M, Vieira-Silva S, et al. Supplementation with *Akkermansia muciniphila* in overweight and obese human volunteers: a proof-of-concept exploratory study. *Nat Med*. (2019) 25:1096–103. doi: 10.1038/s41591-019-0495-2
38. Liu J, Yue S, Yang Z, Feng W, Meng X, Wang A, et al. Oral hydroxysafflor yellow A reduces obesity in mice by modulating the gut microbiota and serum metabolism. *Pharmacol Res*. (2018) 134:40–50. doi: 10.1016/j.phrs.2018.05.012
39. Magruder M, Edusei E, Zhang L, Albakry S, Satlin MJ, Westblade LF, et al. Gut commensal microbiota and decreased risk for *Enterobacteriaceae bacteriuria* and urinary tract infection. *Gut microbes*. (2020) 12:1805281. doi: 10.1080/19490976.2020.1805281

40. Zhong Y, Nyman M, Fåk F. Modulation of gut microbiota in rats fed high-fat diets by processing whole-grain barley to barley malt. *Mol Nutr Food Res*. (2015) 59:2066–76. doi: 10.1002/mnfr.201500187
41. Zheng B, Wang T, Wang H, Chen L, Zhou Z. Studies on nutritional intervention of rice starch- oleic acid complex (resistant starch type V) in rats fed by high-fat diet. *Carbohydr Polym*. (2020) 246:116637. doi: 10.1016/j.carbpol.2020.116637
42. Singh S, Bhatia R, Singh A, Singh P, Kaur R, Khare P, et al. Probiotic attributes and prevention of LPS-induced pro-inflammatory stress in RAW264.7 macrophages and human intestinal epithelial cell line (Caco-2) by newly isolated *Weissella cibaria* strains. *Food Funct*. (2018) 9:1254–64. doi: 10.1039/C7FO00469A
43. Chen P, Xu H, Tang H, Zhao F, Yang C, Kwok LY, et al. Modulation of gut mucosal microbiota as a mechanism of probiotics-based adjunctive therapy for ulcerative colitis. *Microb Biotechnol*. (2020) 13:2032–43. doi: 10.1111/1751-7915.13661
44. Cheng S, Ma X, Geng S, Jiang X, Li Y, Hu L, et al. Fecal microbiota transplantation beneficially regulates intestinal mucosal autophagy and alleviates gut barrier injury. *Msystems*. (2018) 3:e00137–18. doi: 10.1128/mSystems.00137-18
45. Turroni F, Milani C, Duranti S, Mahony J, van Sinderen D, Ventura M. Glycan utilization and cross-feeding activities by bifidobacteria. *Trends Microbiol*. (2018) 26:339–50. doi: 10.1016/j.tim.2017.10.001
46. Smith EA, Macfarlane GT. Dissimilatory amino acid metabolism in human colonic bacteria. *Anaerobe*. (1997) 3:327–37. doi: 10.1006/anae.1997.0121
47. Kaewtapee C, Krutthai N, Bunchasak C. Effects of supplemental liquid DL-methionine hydroxy analog free acid in diet on growth performance and gastrointestinal functions of piglets. *Asian-Australas J Anim Sci*. (2016) 29:1166–72. doi: 10.5713/ajas.15.0579
48. Hooda S, Boler BMV, Serao MCR, Brulc JM, Staeger MA, Boileau TW, et al. 454 pyrosequencing reveals a shift in fecal microbiota of healthy adult men consuming polydextrose or soluble corn fiber. *J Nutr*. (2012) 142:1259–65. doi: 10.3945/jn.112.158766
49. Poll BG, Cheema MU, Pluznick JL. Gut microbial metabolites and blood pressure regulation: Focus on SCFAs and TMAO. *Physiology*. (2020) 35:275–84. doi: 10.1152/physiol.00004.2020
50. Kelly CJ, Zheng L, Campbell EL, Saeedi B, Scholz CC, Bayless AJ, et al. Crosstalk between microbiota-derived short-chain fatty acids and intestinal epithelial HIF augments tissue barrier function. *Cell Host Microbe*. (2015) 17:662–71. doi: 10.1016/j.chom.2015.03.005
51. He J, Guo H, Zheng W, Xue Y, Zhao R, Yao W. Heat stress affects fecal microbial and metabolic alterations of primiparous sows during late gestation. *J Anim Sci Biotechno*. (2019) 10:84. doi: 10.1186/s40104-019-0391-0
52. Vinolo MAR, Rodrigues HG, Nachbar RT, Curi R. Regulation of inflammation by short chain fatty acids. *Nutrients*. (2011) 3:858–76. doi: 10.3390/nu3100858
53. Yin J, Li Y, Han H, Ma J, Liu G, Wu X, et al. Administration of exogenous melatonin improves the diurnal rhythms of the gut microbiota in mice fed a high-fat diet. *Msystems*. (2020) 5:e00002-20. doi: 10.1128/mSystems.00002-20
54. Li Y, Ma J, Yao K, Su W, Tan B, Wu X, et al. Circadian rhythms and obesity: Timekeeping governs lipid metabolism. *J Pineal Res*. (2020) 69:e12682. doi: 10.1111/jpi.12682
55. Wu G, Bazer FW, Dai Z, Li D, Wang J, Wu Z. Amino acid nutrition in animals: protein synthesis and beyond. *Annu Rev Anim Biosci*. (2014) 2:387–417. doi: 10.1146/annurev-animal-022513-114113
56. Brosnan ME, Brosnan JT. Formate: The neglected member of one-carbon metabolism. *Annu Rev Nutr*. (2016) 36:369–88. doi: 10.1146/annurev-nutr-071715-050738
57. Gu Z, Li L, Tang S, Liu C, Fu X, Shi Z, et al. Metabolomics reveals that crossbred dairy buffaloes are more thermotolerant than holstein cows under chronic heat stress. *J Agr Food Chem*. (2018) 66:12889–97. doi: 10.1021/acs.jafc.8b02862
58. Hagenbuch B, Dawson P. The sodium bile salt cotransport family SLC10. *Pflugers Archiv*. (2004) 447:566–70. doi: 10.1007/s00424-003-1130-z
59. Amaral JD, Viana RJS, Ramalho RM, Steer CJ, Rodrigues CMP. Bile acids: regulation of apoptosis by ursodeoxycholic acid. *J Lipid Res*. (2009) 50:1721–34. doi: 10.1194/jlr.R900011-JLR200
60. Suzuki Y, Kaneko R, Nomura M, Naito H. Simple and rapid quantitation of 21 bile acids in rat serum and liver by UPLC-MS-MS: Effect of high fat diet on glycine conjugates of rat bile acids. *Nagoya J Med Sci*. (2013) 75:57–72. doi: 10.1002/lary.23585
61. Shimada T, Nakanishi T, Toyama A, Yamauchi S, Kanzaki A, Fujiwake H, et al. Potential implications for monitoring serum bile acid profiles in circulation with serum proteome for carbon tetrachloride-induced liver injury/regeneration model in mice. *J Proteome Res*. (2010) 9:4490–500. doi: 10.1021/pr1002388
62. Zhang J, Gao Y, Guo H, Ding Y, Ren W. Comparative metabolome analysis of serum changes in sheep under overgrazing or light grazing conditions. *BMC Vet Res*. (2019) 15:469. doi: 10.1186/s12917-019-2218-9
63. Calatayud M, Koren O, Collado MC. Maternal microbiome and metabolic health program microbiome development and health of the offspring. *Trends Endocrinol Metab*. (2019) 30:735–44. doi: 10.1016/j.tem.2019.07.021

Conflict of Interest: The authors declare that the research was conducted in the absence of any commercial or financial relationships that could be construed as a potential conflict of interest.

frontiers in Nutrition

ORIGINAL RESEARCH
published: 10 June 2021
doi: 10.3389/fnut.2021.667130

β-Sitosterol Ameliorates Endometrium Receptivity in PCOS-Like Mice: The Mediation of Gut Microbiota

Yanyan Yu[1], Ying Cao[2], Wenling Huang[1], Yanxia Liu[1], Ying Lu[1] and Jiajing Zhao[1]*

[1] *Department of Gynecology, Dongfang Hospital, Beijing University of Chinese Medicine, Beijing, China,* [2] *College of Traditional Chinese Medicine, North China University of Science and Technology, Tangshan, China*

Background: Polycystic ovary syndrome (PCOS), one of the most common endocrine diseases in women of childbearing age, has been found to be accompanied by changes in the gut microbiota. The Bu Shen Yang Xue formula (BSYXF) is a traditional Chinese medicine widely used for the treatment of PCOS. This study aimed to investigate whether the protective effects of β-sitosterol, the main active ingredient of BSYXF, on PCOS was mediated by regulating gut microbiota.

Methods: The presence of β-sitosterol in BSYXF was detected by liquid chromatography-mass spectrometry. The PCOS-like mouse model was induced by dehydroepiandrosterone. The fecal supernatant of β-sitosterol-treated mice was prepared for fecal microbiota transplantation (FMT). Body weight and wet weight of the uterus and ovary of the mice were recorded for organ index calculation. Hematoxylin and eosin stain was used to assess the endometrial morphology and microenvironment changes. Expression of endometrial receptivity markers cyclooxygenase-2 (COX-2), Integrin αvβ3, leukemia inhibitory factor (LIF), and homeobox A10 (HOXA10) in the endometrium were determined by immunohistochemistry and western blot analysis. Enzyme-linked immunosorbent assay was employed to detect the expression of follicle stimulating hormone (FSH), luteinizing hormone (LH), progesterone (P), and testosterone (T) in the serum. The diversity of gut microbiota was examined by 16S rDNA gene sequencing.

Results: With the treatment of β-sitosterol and β-sitosterol-FMT, the uterine index of PCOS-like mice increased, the ovarian index decreased, levels of COX-2, LH and T decreased, and levels of Integrin αvβ3, LIF, HOXA10, FSH, and P increased. Under β-sitosterol treatment, the structure of the gut microbiota in PCOS-like mice was also changed.

Conclusion: β-sitosterol regulates the endometrial receptivity of PCOS and harmonizes the sex hormone balance, which may be related to the changes in the structure and composition of gut microbiota, thus affecting the pathological process of PCOS.

Keywords: PCOS, gut microbiota, β-sitosterol, endometrium receptivity, Bu Shen Yang Xue formula

OPEN ACCESS

Edited by:
Jie Yin,
Hunan Agricultural University, China

Reviewed by:
Mei Yang,
Hunan Agricultural University, China
Alicia Motta,
University of Buenos Aires, Argentina

****Correspondence:***
Yanyan Yu
bjyyy2020@126.com

Specialty section:
This article was submitted to Nutrition and Microbes, a section of the journal Frontiers in Nutrition

Received: *12 February 2021*
Accepted: *19 May 2021*
Published: *10 June 2021*

Citation:
Yu Y, Cao Y, Huang W, Liu Y, Lu Y and Zhao J (2021) β-Sitosterol Ameliorates Endometrium Receptivity in PCOS-Like Mice: The Mediation of Gut Microbiota. Front. Nutr. 8:667130. doi: 10.3389/fnut.2021.667130

INTRODUCTION

Polycystic ovary syndrome (PCOS), one of the most common metabolic and endocrine disorders, affects 6–20% of women of childbearing age worldwide (1, 2). PCOS is characterized by excessive androgen secretion, low ovulation rate, and polycystic ovary (3), and is often accompanied by obesity and insulin resistance (4). Nowadays, research on women with infertility and PCOS mainly focuses on the aspects of ovulation dysfunction, sex hormones, and insulin resistance (5–7). However, insulin resistance could lead to insufficient glucose supply of endometrial cells, interfering with their growth and activity, thereby affecting endometrium receptivity (8), indicating that PCOS was closely related to endometrium receptivity.

Clinical trials have shown that PCOS is associated with decreased endometrium receptivity (9). Moreover, endocrine and metabolic abnormalities of PCOS have been found to affect the endometrium, causing endometrium disorders and leading to infertility (10). The decreased endometrium receptivity in PCOS might be caused by the noticeable imbalance of key proteins (or molecules) and signal cascades in the endometrial tissue (11). Among them, the expression of Integrin αvβ3, HOXA10, COX-2, and LIF in endometrium was different (9, 12, 13). Improving endometrium receptivity was reported to improve infertility in women with PCOS (14). We hypothesized that the improvement of endometrial receptivity may be a key factor in the treatment of PCOS. The level of testosterone increased in PCOS-like mice induced by DHEA (15), and testosterone was the regulator of HOXA10 (16). In addition, DHEA induces impaired decidua and endometrial receptivity in mice (17), so it is often used to simulate PCOS *in vivo*.

Intestinal microorganism disorders could cause intestinal mucosal damage and destroy the integrity of the intestinal barrier, leading to a series of diseases including PCOS (18). Clinical studies have found that changes in the gut microbiota are significantly related to the PCOS phenotype of women (19). Torres et al. (20) have conducted co-living studies with PCOS mouse model, indicating that dysbiosis of gut microbiota may be one of the causes of PCOS. A study demonstrated that *lactobacillus* and fecal microbiota transplantation (FMT) in healthy rats could treat rats with PCOS (21). In endometriosis rats treated with broad-spectrum antibiotics, metronidazole sensitive gut microbiota may promote the growth of endometrial lesions, and the feces of endometriosis rats can promote endometriosis progression (22). This suggests that intestinal microorganism plays a certain regulatory role in the development of PCOS. Gut microbiota dysregulation could lead to insulin resistance by inducing inflammation, which is closely related to endometrium receptivity (8, 23). These results suggested that the gut microbiota might influence the endometrium receptivity of PCOS through a potential mechanism.

Traditional Chinese medicine is widely used in the clinical treatment of PCOS. Studies have shown that Chinese herbal medicine has significant efficacy in promoting hormone normalization, estrus cycle recovery, insulin resistance and lipid metabolism improvement in patients with PCOS (24). The Bu Shen Yang Xue formula (BSYXF) is a traditional Chinese medicine compound, which is composed of 15 g of *Rehmannia glutinosa* (Gaertn.) DC., 15 g of *Dioscorea opposita* Thunb., 12 g of *Cervi Cornu* Colla, 15 g of *Angelica sinensis* (Oliv.) Diels, 15 g of *Dipsacus asper* Wall., 15 g of *Ligustrum lucidum* Ait., and 15 g of *Astragalus membranaceus* Moench. It has been reported that Bu Shen Huo Xue Decoction (BSHXF) has a positive effect on assisted reproduction, which was achieved by improving the morphology of rat endometrium (25). Both *Angelica sinensis* (Oliv.) Diels and *Ligustrum lucidum* Ait. in BSYXF contain β-sitosterol. β-sitosterol is one of the effective monomers in Moutan Cortex and provides an antioxidative stress effect (26). It is reasonable to assume that β-sitosterol is one of the main active ingredients in BSYXF for the treatment of PCOS. Therefore, in this study, β-sitosterol was extracted from BSYXF to investigate its influence on PCOS.

Researchers have shown that traditional Chinese medicine can improve metabolic disorders by regulating the composition and functional structure of the gut microbiota (27). For example, Guizhi Fuling Wan as a Chinese herbal medicine could control inflammation by regulating the gut microbiota, and had a certain therapeutic effect on PCOS (28). This study aimed to explore whether the effect of β-sitosterol in BSYXF on PCOS-like mice is achieved by gut microbiota, so as to provide new therapeutic targets for the treatment of PCOS.

MATERIALS AND METHODS

Liquid Chromatography-Tandem Mass Spectrometry

The amount of β-sitosterol in BSYXF was determined by LC-MS (LC-MS-MS-8050, Shimazu, Tokyo, Japan). LC-MS analysis was performed on Waters ACQUITY UPLC T3 C18 column (100 mm × 2.1 mm, 1.7 μm). β-sitosterol (RFS-G00202004022, Chengdu Herbpurify CO., Chengdu, China) was dissolved by water to prepare the standard substance solutions. The calibration samples consisted of five nonzero concentrations of β-sitosterol, namely, 10, 20, 50, 100, and 200 ng/mL, and were used to generate the calibration curve. Approximately 1 g of BSYXF (Beijing Tcmages Pharmaceutical Co., Beijing, China) was weighed, and dissolved in 50 mL of methanol, eddied for 1 min, and centrifuged for 10 min at 10,000 rpm/min. The supernatant was diluted 100 times. The injection volume was 1 μL. The amount of β-sitosterol in each group was calculated using the standard curve of β-sitosterol.

Animal Model of PCOS Induced by DHEA

For this study, 40 female pre-puberty C57BL/6 mice (21 days old, 17.80 ± 0.50 g) were purchased from Hunan Slack Jingda Experimental Animal Co., Ltd. (Changsha, China). All mice were randomly divided into four groups: Sham group, PCOS group, PCOS+β-sitosterol group and PCOS+β-sitosterol-FMT group, with 10 mice in each group. The PCOS group, PCOS+β-sitosterol group (β-sitosterol group), and PCOS+β-sitosterol-FMT group (β-sitosterol-FMT group) received subcutaneous injection of DHEA (20200707, OKA Biotechnology Co., Beijing, China) (6 mg/100 g body weight), 0.09 mL of sesame oil and 0.01 mL of 95% ethanol, once a day for 21 days. The Sham group was subcutaneously injected with 0.09 mL of sesame oil and 0.01 mL of 95% ethanol once a day for 21 days. The estrus cycle (proestrus, estrus, metestrus, and diestrus) was observed by a vaginal smear. When the estrus cycle of mice in the treatment group was disordered, the PCOS model was successfully established.

β-Sitosterol Treatment and FMT

After the successful establishment of the PCOS mouse model, the β-sitosterol group was given intragastric β-sitosterol-treatment (25 mg/kg/d) for 14 consecutive days. In the β-sitosterol group, 10 g of fresh fecal samples were collected every morning after intragastric administration. The feces were stirred and mixed with 20 mL of sterile physiological saline at 37°C for 1 min, centrifuged at 1,000 g for 5 min, and the supernatant was collected. The OD value was tested at 620 nm (adjusting fecal bacterial concentration to 2×10^9 CFU/mL). The supernatant was prepared for the FMT. The β-sitosterol-FMT group was given 0.2 mL of fecal supernatant from the β-sitosterol group mice by gavage for 14 consecutive days. Meanwhile, the Sham group and PCOS group were given the same amount of normal saline intragastric gavage for 14 consecutive days.

Specimen Collection

On the last day of intragastric administration, the Sham group mice were in the metestrus stage, the PCOS group mice were constantly in the metestrus phase or diestrus phase, the β-sitosterol group and β-sitosterol-FMT group mice were in the proestrus or diestrus. All mice were weighed and then anesthetized with 2% pentobarbital sodium (30 mg/kg) for laparotomy. Abdominal aorta blood, ovaries and uterine tissues were collected. All ovaries and uterine tissues were weighed. The uterine index and ovarian index were calculated using the following formula.

$$\text{Uterine index} = \text{wet weight of uterus/body weight}$$
$$\text{Ovarian index} = \text{wet weight of ovary/body weight}$$

Hematoxylin and Eosin Staining

After fixation with 4% paraformaldehyde for 4 h, the ovaries and uterine tissues of mice were dehydrated, embedded, sectioned, stained with H&E, and photographed under a microscope (BA210T, Motic, Xiamen, China) to observe the pathological structure of the ovaries and uterine tissues.

Immunohistochemistry

The paraffin-embedded tissues were divided into four groups. The sections were dewaxed to water, antigens were heat-repaired, and endogenous enzymes were inactivated and incubated with the following primary antibodies: cyclooxygenase-2 (COX-2; ab15191, 1:1,000, Abcam, Cambridge, UK), homeobox A10 (HOXA10; ab191470, 1:5,000, Abcam, Cambridge, UK), leukemia inhibitory factor (LIF; ab138002, 1:5,000, Abcam, Cambridge, UK), and Integrin αvβ3 (ab179475, 1:5,000, Abcam, Cambridge, UK) at 4°C overnight. After washing with phosphate-buffered saline (PBS), the secondary antibody was incubated for 30 min, and developed with DBA, then the hematoxylin was restained, and the slices were sealed. The figures were observed and photographed under microscope (BA410T, Motic, Xiamen, China) and analyzed by image processing software (Image-Pro-Plus 6.0, Media Cybernetics, Silver Spring, USA).

Western Blot

Total proteins were extracted from mice endometrial tissues. WB was used to detect the expression of proteins COX-2, Integrin αvβ3, LIF, and HOXA10. The protein was adsorbed on the PVDF membrane by gel electrophoresis and sealed with 5% skim milk solution for 2 h at room temperature. The primary antibody was incubated with COX-2 (ab15191, 1:1,000, Abcam, Cambridge, UK), HOXA10 (ab191470, 1:5,000, Abcam, Cambridge, UK), LIF (ab138002, 1:5,000, Abcam, Cambridge, UK), Integrin αvβ3 (ab179475, 1:5,000, Abcam, Cambridge, UK) and β-actin (66009-1-Ig, 1:5,000, Proteintech, USA) overnight at 4°C, washed three times with PBS with Tween (PBST), and secondary antibodies anti-rabbit IgG (#SA00001-2, dilution 1:6,000, Proteintech, Chicago, USA) and anti-mouse IgG (#SA00001-1, dilution 1:5,000, Proteintech, Chicago, USA) were incubated for 1.5 h at room temperature. The PBST was washed three times, and the membrane was incubated with SuperECL Plus (#K-12045-D50, Advansta, Menlo Park, USA) for 1 min. The chemiluminescence imaging system (ChemiScope 6100, Clinx, Shanghai, China) was used for scanning and imaging. β-actin was used as an internal reference for detecting relative expression levels.

Enzyme-Linked Immunosorbent Assay

All blood samples were centrifuged at 1,000 g for 10 min and the serum was collected. Concentrations of follicle stimulating hormone (FSH), progesterone (P), luteinizing hormone (LH), and testosterone (T) in serum samples were determined by ELISA kit (CSB-E06871m, CSB-E05104m, CSB-E12770m, CSB-E05101m, CusaBio, Wuhan, China) according to the manufacturer's instructions, and all samples were repeated three times.

16S rDNA Sequencing

The fresh feces of all groups were collected on the last day of intragastric administration. Microbial genomic DNA was extracted from each fecal sample at 200 mg using the Fecal Genomic DNA Kit (DP328, Tiangen, Beijing, China). Moreover, 4200 TapeStation Instrument (Version 4200, Agilent Technologies, Santa Clara, USA) was used to test the quality of the extracted DNA. The whole genome of the sample was sequenced on Illumina NovaSeq platform (NovaSeq 6000, Illumina, San Diego, USA). After obtaining the original data for quality control, species composition in the samples was analyzed by comparing with the Silva-132-99 database. Data analysis was conducted using R software (Version 4.0.2, R Foundation, Vienna, Austria). First, the R software was used to generate samples or groups that had operational taxonomic unit (OTU) list, and these specific OTUs were then visualized with the help of jvenn (http://www.bioinformatics.com.cn/static/others/jvenn/example.html). Nonmetric dimensional scaling (NMDS) and analysis of similarity (ANOSIM) analysis were performed by the vegan package. The QIIME2 pipeline (2020.2) (29) was used to calculate the alpha-diversity metrics (Observe, Chao1, ACE, Shannon, and Simpon). Differential abundance at the phylum and species level was determined using the Wald test method. All plots were visualized by the package ggplot2 in R software (Version 4.0.2, R Foundation, Vienna, Austria).

Statistical Analysis

Data are expressed as mean ± standard error of mean (SEM). GraphPad Prism 8 software (GraphPad Software, Inc., San Diego, USA) was used for statistical analysis. Comparisons among multiple groups were evaluated by one-way analysis of variance, followed by Tukey's *post-hoc* test. $P < 0.05$ was considered significant. All experiments were repeated three times. The measurement data conforms to normal distribution. The nonlinear model was used for the statistical analysis.

RESULTS

Determination of β-Sitosterol in BSYXF by LC-MS

LC-MS was used to analyze the total content of β-sitosterol in Bu Shen Yang Xue formula, which was 368.636 mg/kg (**Supplementary Figure 1**).

Effects of β-Sitosterol on Ovaries and Uterus in PCOS-Like Mice

To investigate the curative effect of β-sitosterol on PCOS-like mice, we first evaluated the physiological state of mice in different groups. The ovarian index of the PCOS group was significantly higher than that of the Sham group, while the uterine index of the PCOS group was lower than that of the Sham group. Both indices were notably reversed after β-sitosterol treatment (**Figures 1A,B**). After β-sitosterol treatment, results of H&E staining showed that excessive ovarian vesicles were reduced and absent granulosa cell layers were evidently increased in PCOS-like mice (**Figure 1C**). From uterine H&E staining, the average thickness of the endometrium of mice in the PCOS+β-sitosterol group was thicker than that in the PCOS group (**Figure 1D**). These results implied that β-sitosterol is capable of improving the uterine and ovary status of PCOS-like mice.

Effects of β-Sitosterol on the Expression of Endometrium Receptivity Markers and Related Hormones in PCOS-Like Mice

To further verify the effect of β-sitosterol on the endometrium receptivity of PCOS-like mice, the expressions of COX-2, Integrin αvβ3, LIF and HOXA10 in the endometrium of each group was detected by IHC and then WB. IHC results showed that the expression of COX-2 was markedly downregulated after β-sitosterol treatment in PCOS-like mice (**Figure 2A**). Meanwhile, β-sitosterol effectively inhibited the excessive decrease in expressions of integrins αvβ3, LIF, and HOXA10 in the endometrium of PCOS-like mice (**Figures 2B–D**). Results of WB were consistent (**Figure 3A**). Then, ELISA was used to detect the serum sex hormone levels of mice in each group. β-sitosterol treatment was observed to increase FSH and P levels in PCOS-like mice. By contrast, serum LH and T levels were significantly reduced in PCOS-like mice treated with β-sitosterol (**Figure 3B**). These results indicated that β-sitosterol has a positive effect on endometrial receptivity and on the sex hormone balance of PCOS-like mice.

Effects of β-Sitosterol on the Composition of Gut Microbiota in PCOS-Like Mice

Studies have shown that abnormal changes in gut microbiota was implicated in PCOS (21). Therefore, we hypothesized that regulating gut microbiota may play a role in the improvement effect of β-sitosterol on PCOS. Thereafter, the 16S rDNA gene sequencing was used to analyze the gut microbiota diversity. Based on the species annotation analysis of OTU, the Venn plot showed that the unique OTUs in the Sham group, PCOS group, and β-sitosterol group were 77, 57, and 81, respectively (**Figure 4A**). Moreover, alpha diversity was statistically analyzed. Unexpectedly, an undifferentiated distinction in microbial diversity as displayed by the observed index, Chao1 index, Ace index, Shannon index, and Simpon index, was observed in the three groups (**Figure 4B**). ANOSIM is a nonparametric test to check whether the differences between groups are significantly greater than the differences within groups, and therefore whether the grouping is meaningful. ANOSIM showed that this observation ($R = 0.738$, $P = 0.001$) was significant in the study groups (**Figure 4C**). Uniformly, NMDS analysis results showed that all groups of samples were separated clearly (**Figure 4D**). Therefore, it is reasonable to infer that β-sitosterol treatment may exert a protective effect by altering the species and structure of specific gut microbiota.

Effects of β-Sitosterol on the Abundance of Specific Microbiota in PCOS-Like Mice

To further explore the differences in the relative abundance of bacterial taxa, the relative abundance of the top 20 bacterial taxa in the three groups was assessed by the cluster heat map (**Figure 5A**). Moreover, differences in the relative abundance of the gut microbiota in each group at the phylum level were statistically analyzed. The top five different categories of bacteria in the phylum level were analyzed emphatically. Abundances of *Firmicutes-Lactobacillus*, *Bacteroidetes-f_Muribaculaceae_ASV_4*, and *Bacteroidetes-Alistipes* showed an upward trend in PCOS group, while in β-sitosterol group the change in these taxa was reversed. Inversely, after treatment with β-sitosterol, the decrease in *Firmicutes-Lactobacillus*, *Bacteroidetes-alloprevotella*, *Bacteroidetes-parabacteroides*, and *Bacteroidetes-f_Muribaculaceae_ASV_4* in PCOS-like mice was improved (**Figure 5B**). Furthermore, the abundance of the top 10 bacteria at the species level was analyzed. Although the abundances of *Ambiguous_taxa-Rikenella*, *Lactobacillus_johnsonii-Lactobacillus*, *f_Muriba culaceae_ASV_16*, *f_Muribaculaceae_ASV_4*, *uncultured_ bacterium-Alistipes*, *uncultured_bacterium-Dubosiella*, and *uncultured_bacterium-Lachnospiraceae_NK4A136_group* de monstrated an upward trend in the PCOS group compared

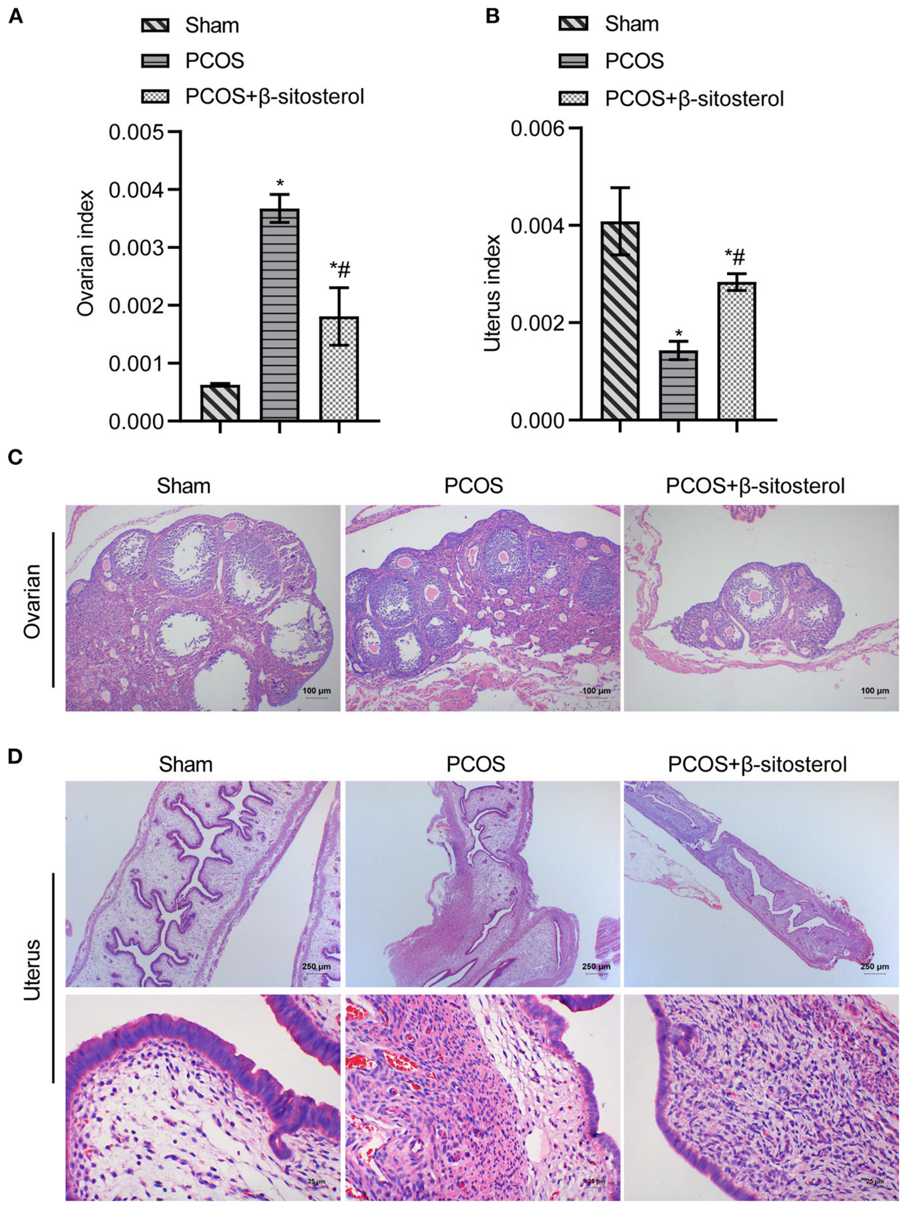

FIGURE 1 | Effect of β-sitosterol on ovaries and uterus in PCOS-like mice. **(A)** Ovarian index. **(B)** Uterine index. **(C)** Hematoxylin and eosin (H&E) staining was performed to observe pathological changes of ovarian tissue in each group (magnification, 100×; scale bar = 100 μm). **(D)** H&E staining showed pathological changes of uterine tissue in each group. Upper images are magnified 40-fold (scale bar = 250 μm), and local magnification (underneath) is magnified 400-fold (Scale bar = 25 μm). Data are presented as mean ± SEM. *$P < 0.05$ vs. Sham. #$P < 0.05$ vs. PCOS. PCOS, polycystic ovary syndrome.

with that in the Sham group, all these taxa abundances were reduced to some extent by β-sitosterol. In addition, the relative abundance of *Ambiguous_taxa-Alloprevotella*, *uncultured_Bacteroidales_bacterium-Parabacteroides*, and *uncultured_bacterium-Muribaculum* in the β-sitosterol group was counter to that in PCOS-like mice, which showed a partial increasing trend (**Figure 5C**). Although certain microbial strains such as *Firmicutes-Lactobacillus and Ambiguous_taxa-Alloprevotella* showed no significant difference among all groups, the variation tendency was still observed. These results indicated that β-sitosterol has the potential to change the intestinal microflora structure of PCOS-like mice and restore it to near normal levels.

Effects of β-Sitosterol-FMT on Ovaries and Uterus in PCOS-Like Mice

Furthermore, feces of mice from the β-sitosterol treatment group were transplanted into PCOS-like mice to confirm that β-sitosterol plays a positive role in PCOS through the intestinal flora. Compared with the PCOS group, the uterine index of

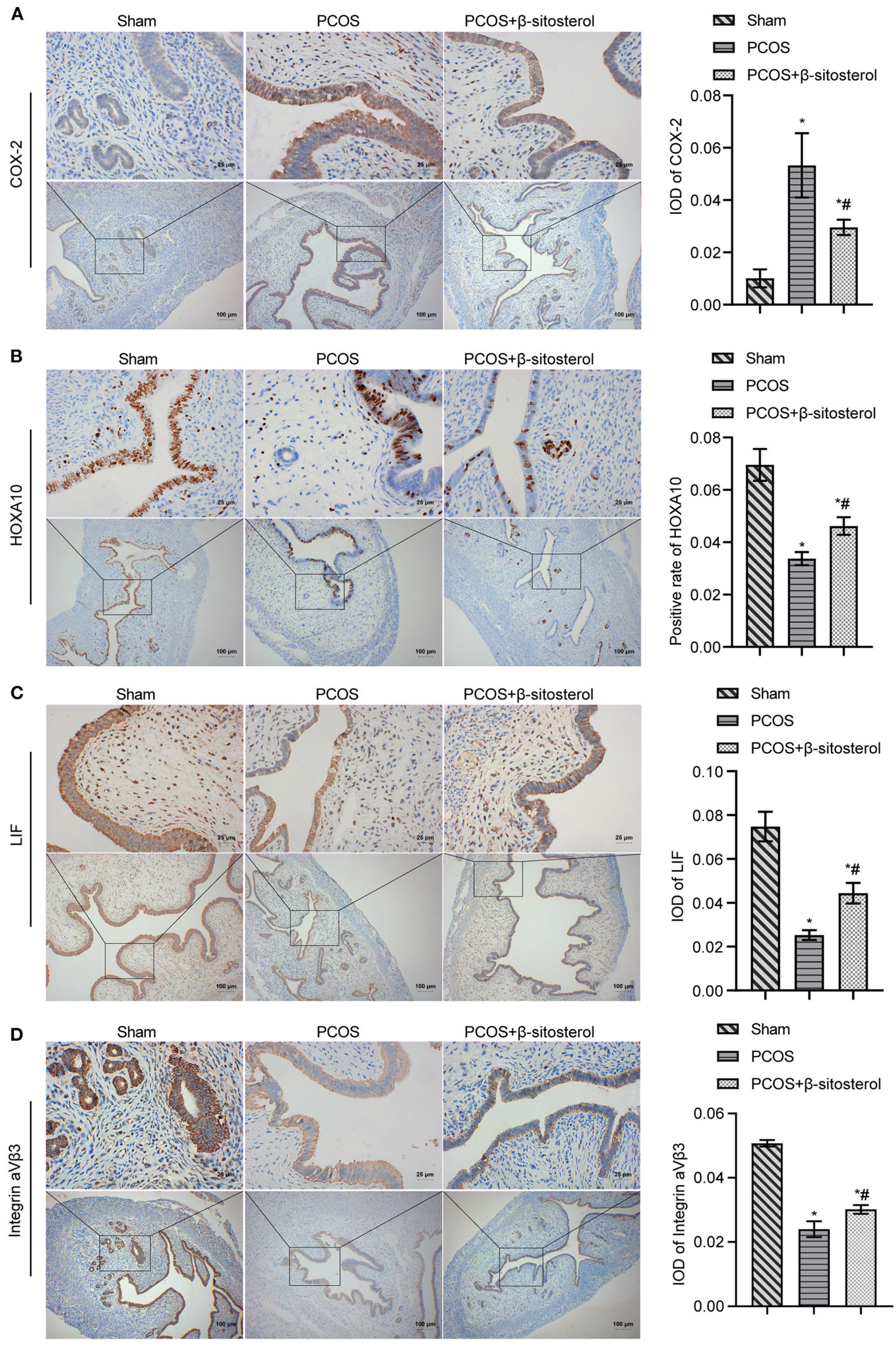

FIGURE 2 | Effect of β-sitosterol on the expression of endometrium receptivity markers and related hormones in PCOS-like mice. **(A–D)** Expressions of COX-2, HOXA10, LIF, and Integrin αvβ3 in the endometrium of mice in each group detected by IHC. Upper images are magnified 400-fold (scale bar = 25 μm) and lower images are magnified 100-fold (scale bar = 100 μm). Data are presented as mean ± SEM. $^{*}P < 0.05$ vs. Sham. $^{\#}P < 0.05$ vs. PCOS. PCOS, polycystic ovary syndrome; COX-2, cyclooxygenase-2; HOXA10, homeobox A10; LIF, leukemia inhibitory factor; ELISA, enzyme-linked immunosorbent assay.

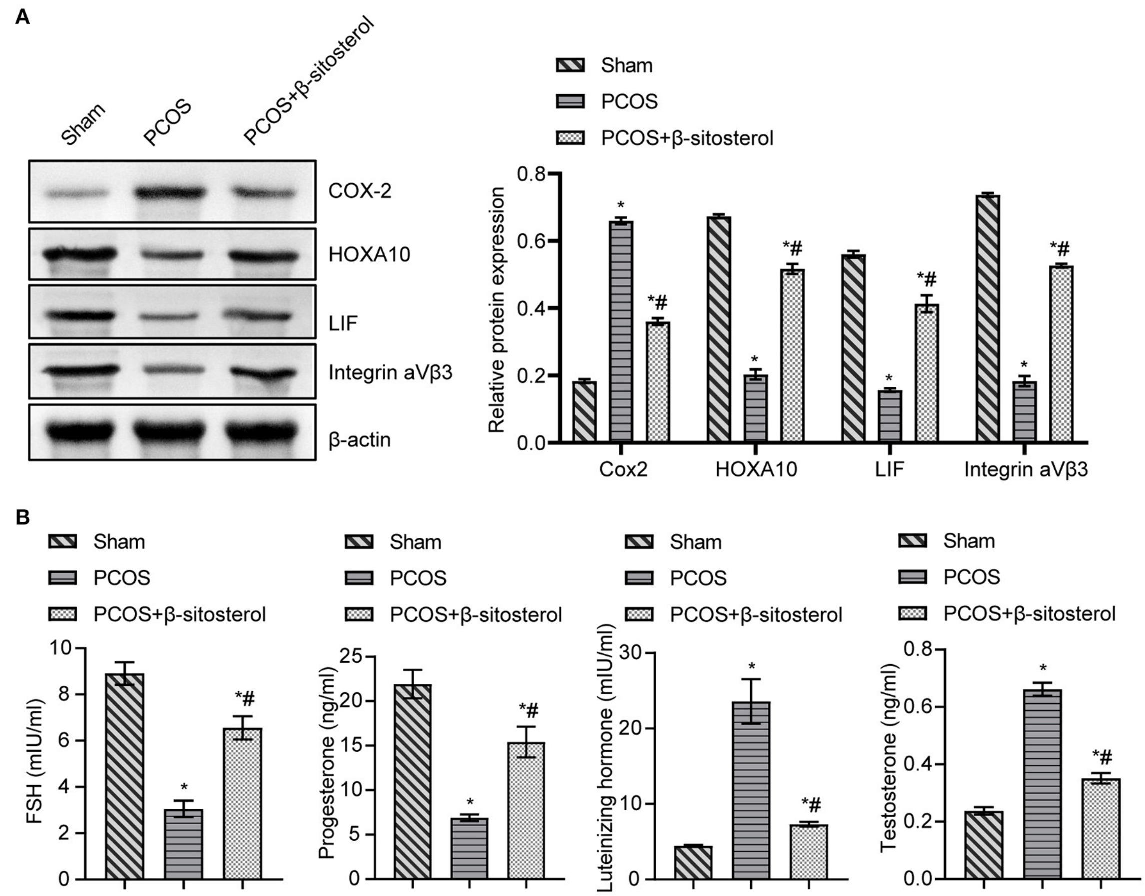

FIGURE 3 | Effect of β-sitosterol on the expression of endometrium receptivity markers and related hormones in PCOS-like mice. **(A)** Expressions of COX-2, HOXA10, LIF, and Integrin αvβ3 in the endometrium of mice in each group were detected by western blot. **(B)** Levels of FSH, P, LH, and T in the serum of mice in each group were detected by ELISA. Data are presented as mean ± SEM. $^{*}P < 0.05$ vs. Sham. $^{\#}P < 0.05$ vs. PCOS. FSH, follicle-stimulating hormone; P, progesterone; LH, luteinizing hormone; T, testosterone; PCOS, polycystic ovary syndrome.

mice in the β-sitosterol-FMT group showed a marked increase, compared with that of the ovarian index (**Figures 6A,B**). H&E staining results showed that, after β-sitosterol-FMT treatment, cystic follicles decreased and granulosa cell layer increased in PCOS-like mice (**Figure 6C**). H&E staining of the endometrium showed that the average thickness of the endometrium of mice in the β-sitosterol-FMT group increased compared with the mice in the PCOS group (**Figure 6D**). Therefore, the gut microbiota may be a potential pathway for β-sitosterol to ameliorate PCOS.

Effect of β-Sitosterol-FMT on the Expression of Endometrium Receptivity Markers and Related Hormones in PCOS-Like Mice

To further investigate the effect of β-sitosterol-FMT on the endometrium receptivity of PCOS-like mice, the expressions of endometrial receptivity marker proteins in each group was detected by IHC and WB. As a result, the expression of COX-2 was significantly decreased (**Figure 7A**) and the expressions of Integrin αvβ3, LIF, and HOXA10 were significantly increased in the β-sitosterol-FMT group compared with that in the PCOS group (**Figures 7B–D**). As shown in **Figure 8A**, WB detection results were consistent with IHC results, which demonstrated that β-sitosterol-FMT improves the endometrium receptivity of PCOS-like mice. According to ELISA results (**Figure 8B**), the levels of FSH and P in the β-sitosterol-FMT group mice were significantly increased compared with those in the PCOS group. By contrast, when PCOS-like mice were treated with β-sitosterol-FMT, the levels of LH and T were significantly lower than those in the PCOS group. The above results manifested that β-sitosterol-FMT treatment also have a positive effects on the sex hormone balance of PCOS-like mice.

DISCUSSION

In our study, we established a mouse model of PCOS induced by DHEA, and found that β-sitosterol improved endometrial receptivity and balanced sex hormone levels in mice with PCOS. In addition, β-sitosterol can improve the composition of gut

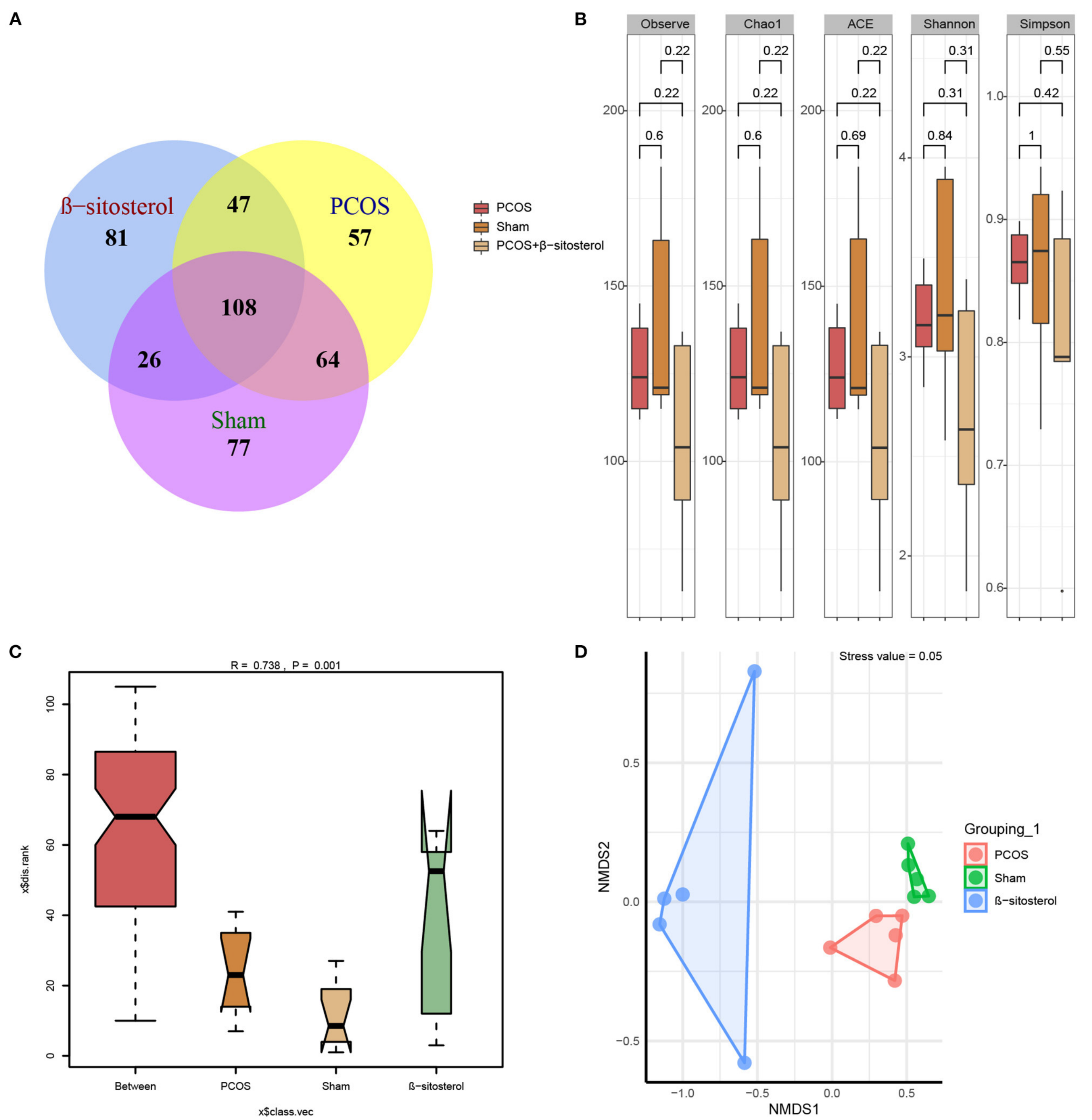

FIGURE 4 | Effects of β-sitosterol on the composition of gut microbiota in PCOS-like mice. **(A)** Venn diagrams demonstrated the results of operational taxonomic units in groups. **(B)** Changes in Observe, Chao1, ACE, Shannon, and Simpon indices. **(C)** Analysis of similarities showed differences in groups. **(D)** Nonmetric multidimensional scaling analysis showed differences in groups. PCOS, polycystic ovary syndrome; FSH, follicle-stimulating hormone; P, progesterone; LH, luteinizing hormone; T, testosterone.

microbiota in PCOS-like mice. The gut microbiota composition of PCOS-like mice was improved after β-sitosterol treatment. The feces of β-sitosterol-treated mice were transplanted into PCOS, demonstrating that β-sitosterol may have a positive effect on PCOS-like mice by regulating gut microbiota. Our study suggested that β-sitosterol is capable of altering the gut microbiota imbalance in the pathogenesis of PCOS and of improving the development process of PCOS.

Many literature have reported that DHEA induced rodent models with remarkable characteristics of polycystic ovary syndrome (30–33). The reversal of FSH/LH ratio is an important clinical feature of PCOS (34). In addition, it has been reported

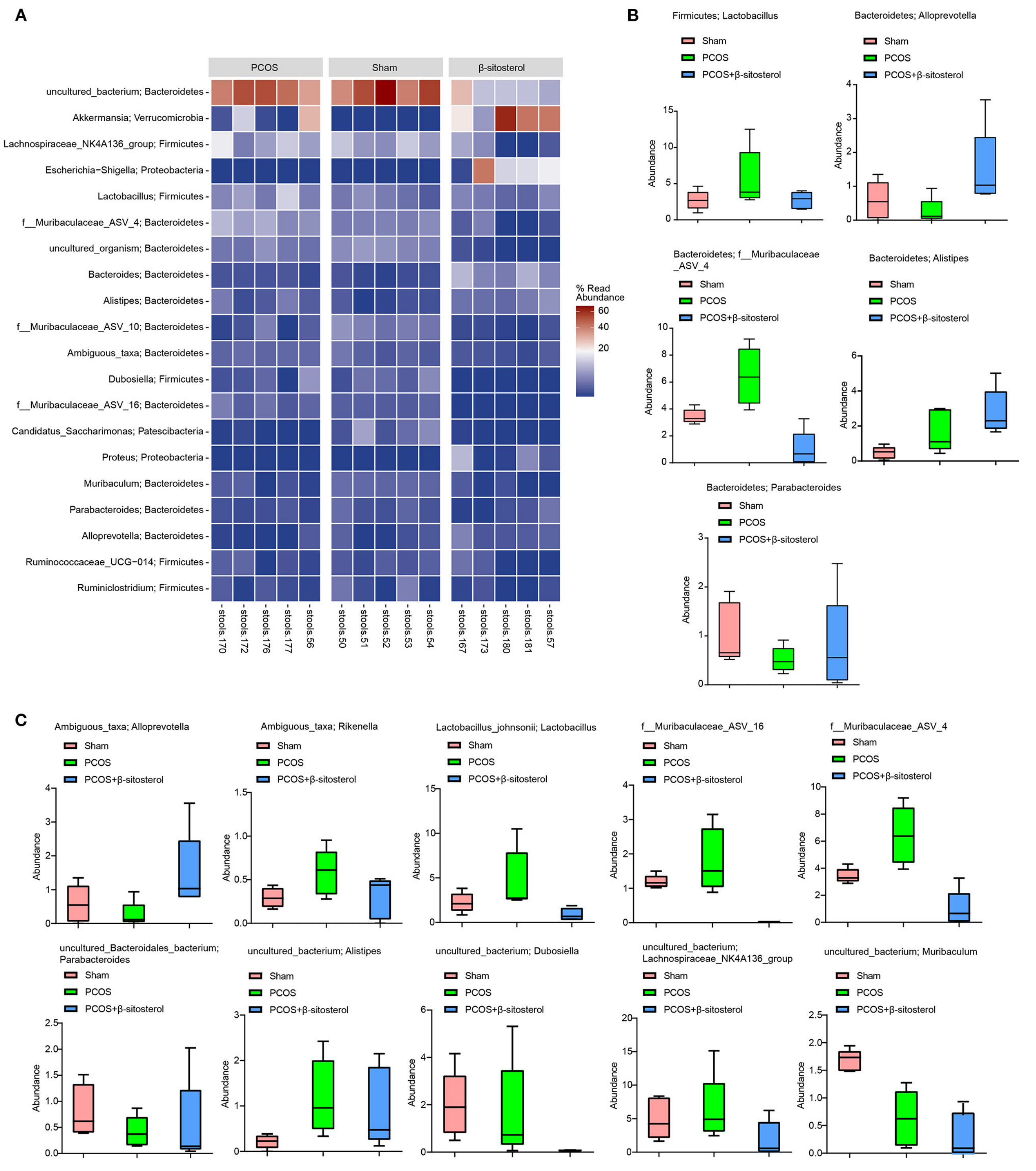

FIGURE 5 | Effects of β-sitosterol on the abundance of specific microbiota in PCOS-like mice. **(A)** Heat map showed that the abundances of the first 20 species were differentially expressed in groups. **(B)** Relative abundance of the five bacterial categories at the phylum level. Top five bacteria: *Firmicutes-Lactobacillus*, *Bacteroidetes-Alloprevotella*, *Bacteroidetes-Parabacteroides*, *Bacteroidetes-f_Muribaculaceae_ASV_4*, and *Bacteroidetes-Alistipes.* **(C)** Relative abundance of the top 10 bacterial categories at the species level. Top 10 bacteria: *Ambiguous_taxa-Alloprevotella*, *Ambiguous_taxa-Rikenella*, *Lactobacillus_johnsonii-Lactobacillus*, *f_Muribaculaceae_ASV_16*, *f_Muribaculaceae_ASV_4*, *uncultured_Bacteroidales_bacterium-Parabacteroides*, *uncultured_bacterium-Alistipes*, *uncultured_bacterium-Dubosiella*, *uncultured_bacterium-Lachnospiraceae_NK4A-136_group*, and *uncultured_bacterium-Muribaculum*. PCOS, polycystic ovary syndrome.

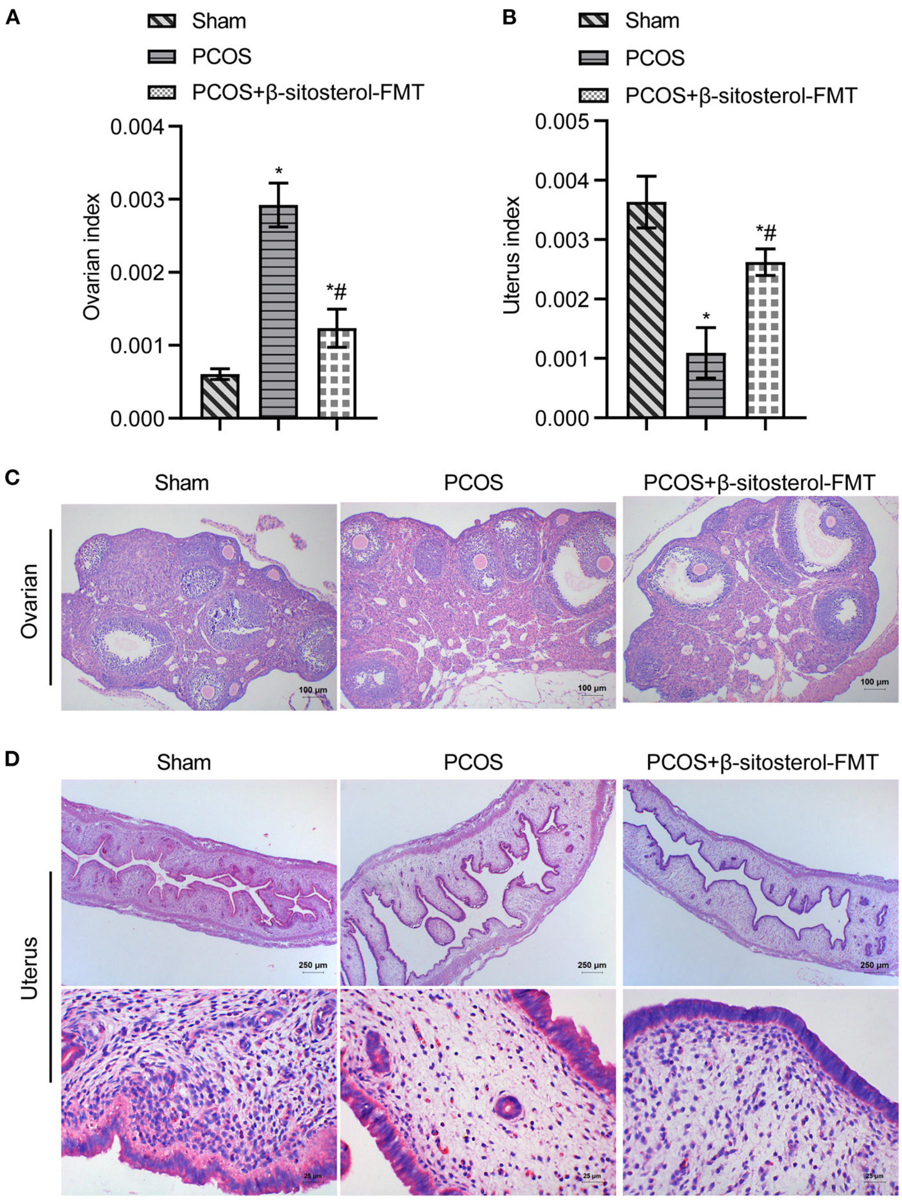

FIGURE 6 | Effects of β-sitosterol-FMT on ovaries and uterus in mice with PCOS. **(A)** Ovarian index. **(B)** Uterine index. **(C)** Hematoxylin and eosin (H&E) staining showed pathological changes of ovarian tissue in each group. Images are magnified 100-fold (scale bar = 100 μm). **(D)** HE staining showed pathological changes of uterine tissue in each group. Upper images are magnified 40-fold (scale bar = 250 μm), and underneath images are magnified 400-fold (scale bar = 25 μm). Data are presented as mean ± SEM. $^{*}P < 0.05$ vs. Sham. $^{\#}P < 0.05$ vs. PCOS. PCOS, polycystic ovary syndrome.

that LH level increased (15) and FSH expression level decreased (35) in PCOS model induced by DHEA. Therefore, the DHEA induced PCOS model is a feasible method. However, it has been reported that there may be no difference in LH and/or FSH levels between DHEA-induced PCOS model and control group, which may be the result of the difference in model establishment. In addition, DHEA treatment can significantly increase the number of cystic follicles and the thickness of membrane cell layer in mice, and significantly reduce the number of corpus luteum and dominant follicles, indicating that DHEA can induce the formation of PCOS in mice (36). This is consistent with our research.

PCOS was an important cause of female infertility, which might cause various serious complications (37, 38). Thus, studying effective treatment of PCOS is an urgent issue to improve the physical condition of patients with PCOS. Previous studies have confirmed that β-sitosterol was very effective in treating anti-inflammatory (39), antioxidative stress (40) and antitumor (41). In this study, β-sitosterol treatment significantly improved the uterine and ovary structure in PCOS group, we

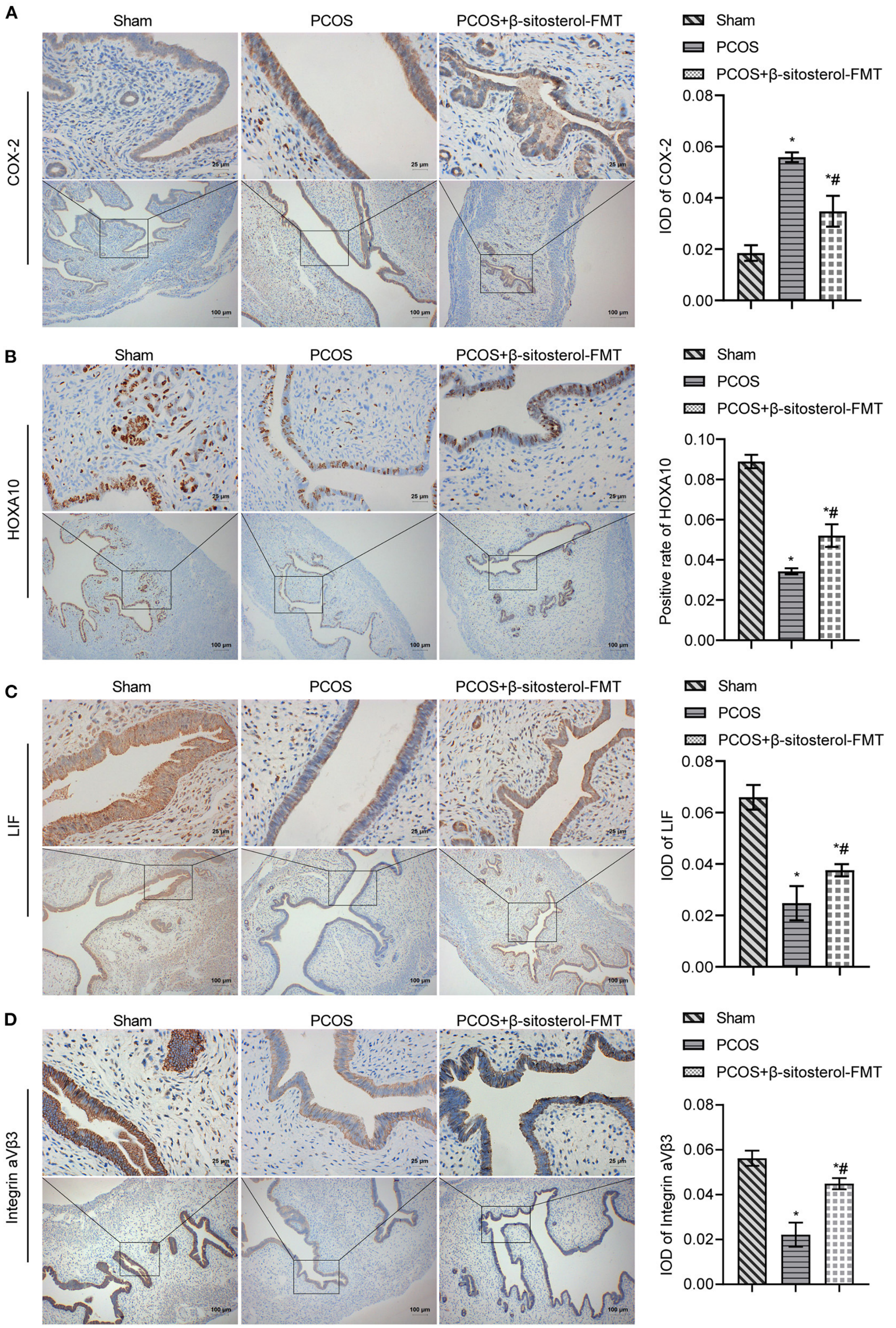

FIGURE 7 | Effect of β-sitosterol-FMT on the expressions of endometrium receptivity markers and related hormones in mice with PCOS. **(A–D)** Expressions of COX-2, HOXA10, LIF, and Integrin αvβ3 in the endometrium of mice in each group were detected by IHC. Upper images are magnified 400-fold (scale bar = 25 µm), and underneath images are magnified 100-fold (scale bar = 100 µm). Data are presented as mean ± SEM. *$P < 0.05$ vs. Sham. #$P < 0.05$ vs. PCOS. PCOS, polycystic ovary syndrome; COX-2, cyclooxygenase-2; HOXA10, homeobox A10; LIF, leukemia inhibitory factor; ELISA, enzyme-linked immunosorbent assay.

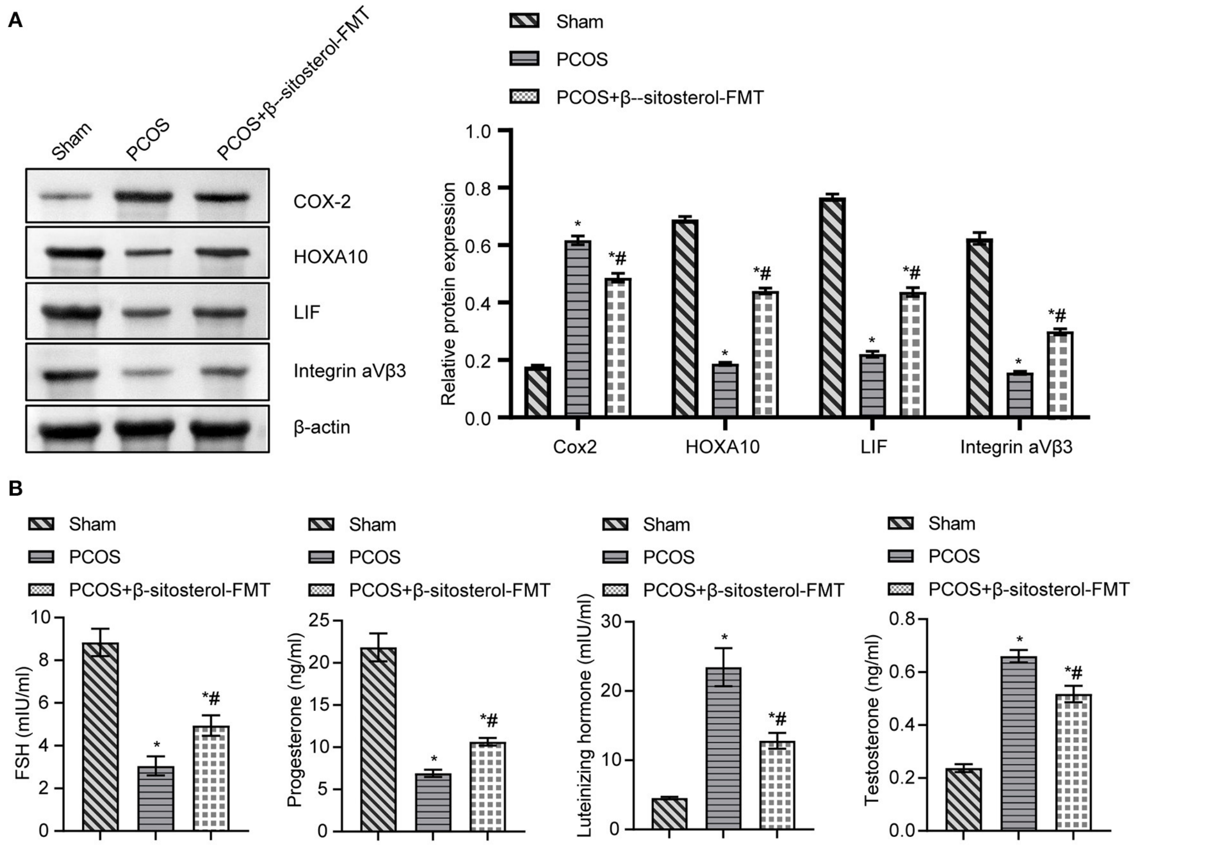

FIGURE 8 | Effect of β-sitosterol-FMT on the expressions of endometrium receptivity markers and related hormones in mice with PCOS. **(A)** Expressions of COX-2, HOXA10, LIF, and Integrin αvβ3 in the endometrium of mice in each group were detected by western blot. **(B)** Levels of FSH, P, LH, and T in the serum of mice in each group were detected by ELISA. Data are presented as mean ± SEM. **P* < 0.05 vs. Sham. #*P* < 0.05 vs. PCOS. PCOS, polycystic ovary syndrome; COX-2, cyclooxygenase-2; HOXA10, homeobox A10; LIF, leukemia inhibitory factor; ELISA, enzyme-linked immunosorbent assay.

therefore hypothesize from these observations that β-sitosterol treatment may have some effect on the improvement of PCOS. Studies have shown that decreased endometrium receptivity is an important indicator of infertility in patients with PCOS (42). Endometrial receptivity was reduced when PCOS occurs, and relevant biomarkers are abnormally expressed (9). We first investigated the therapeutic effect of β-sitosterol on the endometrial receptivity of PCOS-like mice. The observation of β-sitosterol evidently reversed a low expression of Integrin αvβ3, LIF, and HOXA10 and a high expression of COX-2 in the PCOS group, suggests β-sitosterol in PCOS group altered these abnormal expressions of markers in the endometrium. A disorder of sex hormone secretion was another cause of PCOS (43). In our study, β-sitosterol distinctly reduced the production of serum FSH and P in PCOS-like mice and promoted the production of LH and T. It is tempting to speculate from these observations that β-sitosterol could not only modulate endometrial receptivity, but also coordinate sex hormone balance in PCOS-like mice.

During the past decades, the regulatory roles of gut microbiota on various diseases, including PCOS, have gained increasing attention (44, 45). β-sitosterol could improve rumen fermentation in sheep by reducing microbial community and metabolic disorders induced by high grain feed (46). Therefore, we have reason to suspect that the protective effect of β-sitosterol on PCOS may be related to gut microbiota. In this study, 16S rDNA sequencing of gut microbiota showed that β-sitosterol had a regulatory effect on gut microbiota of mice in the PCOS group. Nevertheless, β- sitosterol showed no significant effect on the alpha diversity of PCOS-like mice. In a study that explored the composition of the gut flora in women with PCOS, no change was found in the alpha-diversity of the gut flora between patients with PCOS and people with good health status (47). We speculate that this may be due to the small sample size of the intestinal microbiome. To our delight, we found significant differences in beta diversity among various treatments. Moreover, the relative abundance of some bacterial communities changed significantly with the addition of β-sitosterol. A study found that *bacteroidetes* in PCOS has a lower relative abundance (48). Our results are consistent with such finding. In addition, we found that *Ambiguous_taxa-Alloprevotella* and *Parabacteroides* decreased in the intestinal tract of PCOS-like mice. After treatment with β-sitosterol, the structure of the gut microbiota in the PCOS group was significantly changed. Zhu et al. (28) found that the relative abundance of *Alloprevotella* was decreased significantly in PCOS. However, *Bacteroidete-Alloprevotella* and *Ambiguous_taxa-Alloprevotella* were upregulated by β-sitosterol administration, whereas *Firmicutes-Lactobacillus*, *Bacteroidetes-f_Muribaculaceae_ASV_4*, and *f_Muribaculaceae_ASV_16* were downregulated. Therefore, it is reasonable to speculate that β-sitosterol affects PCOS by changing the structure of the gut microbiota.

FMT was an innovative method for the treatment of PCOS. Gut microbiota disorders could be restored by FMT from healthy donors to recipients (49). FMT of healthy rats could improve the estrus cycle and ovarian disorder of PCOS rats (21). In our study, FMT in β-sitosterol treated mice restored endometrium receptivity of PCOS-like mice. It also decreased the levels of FSH and P and increased the levels of LH and T. β-sitosterol-FMT assisted in the treatment of PCOS-like mice. It is tempting to speculate from these observations that β-sitosterol has the ability to harmonize gut microbiota homeostasis in PCOS-like mice.

Our results indicate that the therapeutic effect of β-sitosterol on PCOS-like mice is at least partially mediated by the improvement of intestinal microbiota composition, suggesting that β-sitosterol may be an effective treatment for PCOS. However, it is unclear how β-sitosterol in the gut microbiota improves endometrial receptivity of PCOS. Given the small sample sizes no significant difference was found in the relative abundance of some intestinal microorganisms among the experimental groups. The exact cellular and molecular mechanisms by which β-sitosterol change the composition of gut microbes these changes is also unclear. In our next experiment, we will collect more samples for more precise experiments. In addition, we will further explore the influence of intestinal flora on PCOS in combination with clinical and animal experiments, as well as the ways through which β-sitosterol influences intestinal flora, so as to exert its alleviating effect on PCOS.

CONCLUSION

We found that β-sitosterol can regulate endometrial receptivity and sex hormone balance in PCOS-like mice, which may be related to its regulation effect on gut microbiota. At the same time, β-sitosterol-treated mice feces transplanted into PCOS-like mice, also contributed to the improvement of PCOS. Results suggested that β-sitosterol has a good clinical application prospect in the treatment of PCOS.

DATA AVAILABILITY STATEMENT

The datasets presented in this study can be found in online repositories. The names of the repository/repositories and accession number(s) can be found below: https://www.ncbi.nlm.nih.gov (PRJNA703774).

ETHICS STATEMENT

The animal study was reviewed and approved by the Ethics Committee of the Beijing University of Chinese Medicine Animal Care and Use Committee.

AUTHOR CONTRIBUTIONS

YY and YC performed the experiment and analyzed the data. JZ, YiL, and YaL performed the experiment. WH, YC, and YY guided the experiment, reviewed, and edited the manuscript. All authors contributed to the article and approved the submitted version.

ACKNOWLEDGMENTS

The authors would like to thank the Dongfang Hospital, Beijing University of Chinese Medicine for their support.

SUPPLEMENTARY MATERIAL

The Supplementary Material for this article can be found online at: https://www.frontiersin.org/articles/10.3389/fnut.2021.667130/full#supplementary-material

Supplementary Figure 1 | Determination of β-sitosterol in Bu Shen Yang Xue formula by liquid chromatography-tandem mass spectrometry.

REFERENCES

1. Wang FF, Pan JX, Wu Y, Zhu YH, Hardiman PJ, Qu F. American, European, and Chinese practice guidelines or consensuses of polycystic ovary syndrome: a comparative analysis. *J Zhejiang Univ Sci B.* (2018) 19:354–63. doi: 10.1631/jzus.B1700074
2. Escobar-Morreale HF. Polycystic ovary syndrome: definition, aetiology, diagnosis and treatment. *Nat Rev Endocrinol.* (2018) 14:270–84. doi: 10.1038/nrendo.2018.24
3. Sanchez-Garrido MA, Tena-Sempere M. Metabolic dysfunction in polycystic ovary syndrome: pathogenic role of androgen excess and potential therapeutic strategies. *Mol Metab.* (2020) 35:100937. doi: 10.1016/j.molmet.2020.01.001
4. Zhang Z, Hong Y, Chen M, Tan N, Liu S, Nie X, et al. Serum metabolomics reveals metabolic profiling for women with hyperandrogenism and insulin resistance in polycystic ovary syndrome. *Metabolomics.* (2020) 16:20. doi: 10.1007/s11306-020-1642-y
5. Marshall CJ, Prescott M, Campbell RE. Investigating the NPY/AgRP/GABA to GnRH neuron circuit in prenatally androgenized PCOS-like mice. *J Endocr Soc.* (2020) 4:1. doi: 10.1210/jendso/bvaa129
6. Liu X, Sun C, Zou K, Li C, Chen X, Gu H, et al. Novel PGK1 determines SKP2-dependent AR stability and reprograms granular cell glucose metabolism facilitating ovulation dysfunction. *EBioMedicine.* (2020) 61:103058. doi: 10.1016/j.ebiom.2020.103058
7. Kelley AS, Smith YR, Padmanabhan V. A narrative review of placental contribution to adverse pregnancy outcomes in women with polycystic ovary syndrome. *J Clin Endocrinol Metab.* (2019) 104:5299–315. doi: 10.1210/jc.2019-00383
8. He FF Li YM, Role of gut microbiota in the development of insulin resistance and the mechanism underlying polycystic ovary syndrome: a review. *J Ovarian Res*. (2020) 13:73. doi: 10.1186/s13048-020-00670-3
9. Piltonen TT. Polycystic ovary syndrome: endometrial markers. *Best Pract Res Clin Obstet Gynaecol.* (2016) 37:66–79. doi: 10.1016/j.bpobgyn.2016.03.008
10. Giudice LC. Endometrium in PCOS: implantation and predisposition to endocrine CA. *Best Pract Res Clin Endocrinol Metab.* (2006) 20:235–44. doi: 10.1016/j.beem.2006.03.005
11. Alikhani M, Amjadi F, Mirzaei M, Wu Y, Shekari F, Ashrafi M, et al. Proteome analysis of endometrial tissue from patients with PCOS reveals

proteins predicted to impact the disease. *Mol Biol Rep*. (2020) 47:8763–74. doi: 10.1007/s11033-020-05924-3
12. Kara M, Ozcan SS, Aran T, Kara O, Yilmaz N. Evaluation of endometrial receptivity by measuring HOXA-10, HOXA-11, and leukemia inhibitory factor expression in patients with polycystic ovary syndrome. *Gynecol Minim Invasive Ther*. (2019) 8:118–22. doi: 10.4103/GMIT.GMIT_112_18
13. Cha J, Sun X, Dey SK. Mechanisms of implantation: strategies for successful pregnancy. *Nat Med*. (2012) 18:1754–67. doi: 10.1038/nm.3012
14. Shang K, Jia X, Qiao J, Kang J, Guan Y. Endometrial abnormality in women with polycystic ovary syndrome. *Reprod Sci*. (2012) 19:674–83. doi: 10.1177/1933719111430993
15. Furat Rencber S, Kurnaz Ozbek S, Eraldemir C, Sezer Z, Kum T, Ceylan S, et al. Effect of resveratrol and metformin on ovarian reserve and ultrastructure in PCOS: an experimental study. *J Ovarian Res*. (2018) 11:55. doi: 10.1186/s13048-018-0427-7
16. Cermik D, Selam B, Taylor HS. Regulation of HOXA-10 expression by testosterone *in vitro* and in the endometrium of patients with polycystic ovary syndrome. *J Clin Endocrinol Metab*. (2003) 88:238–43. doi: 10.1210/jc.2002-021072
17. Li SY, Song Z, Song MJ, Qin JW, Zhao ML, Yang ZM. Impaired receptivity and decidualization in DHEA-induced PCOS mice. *Sci Rep*. (2016) 6:38134. doi: 10.1038/srep38134
18. Natividad JM, Verdu EF, Modulation of intestinal barrier by intestinal microbiota: pathological and therapeutic implications. *Pharmacol Res*. (2013) 69:42–51. doi: 10.1016/j.phrs.2012.10.007
19. Liu R, Zhang C, Shi Y, Zhang F, Li L, Wang X, et al. Dysbiosis of gut microbiota associated with clinical parameters in polycystic ovary syndrome. *Front Microbiol*. (2017) 8:324. doi: 10.3389/fmicb.2017.00324
20. Torres PJ, Ho BS, Arroyo P, Sau L, Chen A, Kelley ST, et al. Exposure to a healthy gut microbiome protects against reproductive and metabolic dysregulation in a PCOS mouse model. *Endocrinology*. (2019) 160:1193–204. doi: 10.1210/en.2019-00050
21. Guo Y, Qi Y, Yang X, Zhao L, Wen S, Liu Y, et al. Association between polycystic ovary syndrome and gut microbiota. *PLoS One*. (2016) 11:e0153196. doi: 10.1371/journal.pone.0153196
22. Chadchan SB, Cheng M, Parnell LA, Yin Y, Schriefer A, Mysorekar IU, et al. Antibiotic therapy with metronidazole reduces endometriosis disease progression in mice: a potential role for gut microbiota. *Hum Reprod*. (2019) 34:1106–16. doi: 10.1093/humrep/dez041
23. Scheithauer TPM, Rampanelli E, Nieuwdorp M, Vallance BA, Verchere CB, van Raalte DH, et al. Gut microbiota as a trigger for metabolic inflammation in obesity and type 2 diabetes. *Front Immunol*. (2020) 11:571731. doi: 10.3389/fimmu.2020.571731
24. Kwon CY, Cho IH, Park KS. Therapeutic effects and mechanisms of herbal medicines for treating polycystic ovary syndrome: a review. *Front Pharmacol*. (2020) 11:1192. doi: 10.3389/fphar.2020.01192
25. Gong X, Yu Y, Tong Q, Ren Y, Jin Z. Effects of "Bu Shen Huo Xue Decoction" on the endometrial morphology and expression of leukaemia inhibitory factor in the rat uterus during the oestrous cycle. *Evid Based Complement Alternat Med*. (2013) 2013:496036. doi: 10.1155/2013/496036
26. Zhang B, Yu D, Luo N, Yang C, Zhu Y. Four active monomers from Moutan Cortex exert inhibitory effects against oxidative stress by activating Nrf2/Keap1 signaling pathway. *Korean J Physiol Pharmacol*. (2020) 24:373–84. doi: 10.4196/kjpp.2020.24.5.373
27. Zhang HY, Tian JX, Lian FM, Li M, Liu WK, Zhen Z, et al. Therapeutic mechanisms of traditional Chinese medicine to improve metabolic diseases via the gut microbiota. *Biomed Pharmacother*. (2020) 133:110857. doi: 10.1016/j.biopha.2020.110857
28. Zhu Y, Li Y, Liu M, Hu X, Zhu H. Guizhi Fuling Wan, Chinese Herbal Medicine, ameliorates insulin sensitivity in PCOS model rats with insulin resistance via remodeling intestinal homeostasis. *Front Endocrinol (Lausanne)*. (2020) 11:575. doi: 10.3389/fendo.2020.00575
29. Bolyen E, Rideout JR, Dillon MR, Bokulich NA, Abnet CC, Al-Ghalith GA, et al. Reproducible, interactive, scalable and extensible microbiome data science using QIIME 2. *Nat Biotechnol*. (2019) 37:852–7. doi: 10.1038/s41587-019-0209-9
30. Safaei Z, Bakhshalizadeh S, Nasr-Esfahani MH, Akbari Sene A, Najafzadeh V, Soleimani M, et al. Vitamin D3 affects mitochondrial biogenesis through mitogen-activated protein kinase in polycystic ovary syndrome mouse model. *J Cell Physiol*. (2020) 235:6113–26. doi: 10.1002/jcp.29540
31. Motta AB. Dehydroepiandrosterone to induce murine models for the study of polycystic ovary syndrome. *J Steroid Biochem Mol Biol*. (2010) 119:105–11. doi: 10.1016/j.jsbmb.2010.02.015
32. Fatemi Abhari SM, Khanbabaei R, Hayati Roodbari N, Parivar K, Yaghmaei P. Curcumin-loaded super-paramagnetic iron oxide nanoparticle affects on apoptotic factors expression and histological changes in a prepubertal mouse model of polycystic ovary syndrome-induced by dehydroepiandrosterone - a molecular and stereological study. *Life Sci*. (2020) 249:117515. doi: 10.1016/j.lfs.2020.117515
33. Kim EJ, Jang M, Choi JH, Park KS, Cho IH. An improved dehydroepiandrosterone-induced rat model of polycystic ovary syndrome (PCOS): post-pubertal improve PCOS's features. *Front Endocrinol (Lausanne)*. (2018) 9:735. doi: 10.3389/fendo.2018.00735
34. Paoli A, Mancin L, Giacona MC, Bianco A, Caprio M. Effects of a ketogenic diet in overweight women with polycystic ovary syndrome. *J Transl Med*. (2020) 18:104. doi: 10.1186/s12967-020-02277-0
35. Dou L, Zheng Y, Li L, Gui X, Chen Y, Yu M, et al. The effect of cinnamon on polycystic ovary syndrome in a mouse model. *Reprod Biol Endocrinol*. (2018) 16:99. doi: 10.1186/s12958-018-0418-y
36. Xie Q, Xiong X, Xiao N, He K, Chen M, Peng J, et al. Mesenchymal stem cells alleviate DHEA-induced polycystic ovary syndrome (PCOS) by inhibiting inflammation in mice. *Stem Cells Int*. (2019) 2019:9782373. doi: 10.1155/2019/9782373
37. Joham AE, Teede HJ, Ranasinha S, Zoungas S, Boyle J. Prevalence of infertility and use of fertility treatment in women with polycystic ovary syndrome: data from a large community-based cohort study. *J Womens Health (Larchmt)*. (2015) 24:299–307. doi: 10.1089/jwh.2014.5000
38. Yu HF, Chen HS, Rao DP, Gong J. Association between polycystic ovary syndrome and the risk of pregnancy complications: A PRISMA-compliant systematic review and meta-analysis. *Medicine (Baltimore)*. (2016) 95:e4863. doi: 10.1097/MD.0000000000004863
39. Zhang F, Liu Z, He X, Li Z, Shi B, Cai F. β-Sitosterol-loaded solid lipid nanoparticles ameliorate complete Freund's adjuvant-induced arthritis in rats: involvement of NF-κB and HO-1/Nrf-2 pathway. *Drug Deliv*. (2020) 27:1329–41. doi: 10.1080/10717544.2020.1818883
40. Zhao R, Zhang MM, Wang D, Peng W, Zhang Q, Liu J, et al. Network pharmacology and molecular docking approaches to investigating the mechanism of action of Zanthoxylum bungeanum in the treatment of oxidative stress-induced diseases. *Comb Chem High Throughput Screen*. (2020). doi: 10.2174/1386207323999201117112316
41. Baraya YS, Yankuzo HM, Wong KK, Yaacob NS. Strobilanthes crispus bioactive subfraction inhibits tumor progression and improves hematological and morphological parameters in mouse mammary carcinoma model. *J Ethnopharmacol*. (2020) 267:113522. doi: 10.1016/j.jep.2020.113522
42. Lin XH, Liu ME, Xu HY, Chen XJ, Wang H, Tian S, et al. Leptin down-regulates γ-ENaC expression: a novel mechanism involved in low endometrial receptivity. *Fertil Steril*. (2015) 103:228–35.e3. doi: 10.1016/j.fertnstert.2014.10.002
43. Zheng J, Huang S, Tong Y, Wei S, Chen G, Huang S, et al. *In-situ* layer-by-layer synthesized TpPa-1 COF solid-phase microextraction fiber for detecting sex hormones in serum. *Anal Chim Acta*. (2020) 1137:28–36. doi: 10.1016/j.aca.2020.08.047
44. Zhou L, Ni Z, Yu J, Cheng W, Cai Z, Yu C. Correlation between fecal metabolomics and gut microbiota in obesity and polycystic ovary syndrome. *Front Endocrinol (Lausanne)*. (2020) 11:628. doi: 10.3389/fendo.2020.00628
45. Chu W, Han Q, Xu J, Wang J, Sun Y, Li W, et al. Metagenomic analysis identified microbiome alterations and pathological association between intestinal microbiota and polycystic ovary syndrome. *Fertil Steril*. (2020) 113:1286–1298.e4. doi: 10.1016/j.fertnstert.2020.01.027
46. Xia G, Sun J, Fan Y, Zhao F, Ahmed G, Jin Y, et al. β-Sitosterol Attenuates High Grain Diet-Induced Inflammatory Stress and Modifies Rumen Fermentation and Microbiota in Sheep. *Animals (Basel)*. (2020) 10:171. doi: 10.3390/ani10010171

47. Insenser M, Murri M, Del Campo R, Martínez-García M, Fernández-Durán E, Escobar-Morreale HF. Gut microbiota and the polycystic ovary syndrome: influence of sex, sex hormones, and obesity. *J Clin Endocrinol Metab.* (2018) 103:2552–62. doi: 10.1210/jc.2017-02799
48. Jobira B, Frank DN, Pyle L, Silveira LJ, Kelsey MM, Garcia-Reyes Y, et al. Obese adolescents with PCOS have altered biodiversity and relative abundance in gastrointestinal microbiota. *J Clin Endocrinol Metab.* (2020) 105:e2134–44. doi: 10.1210/clinem/dgz263
49. Quaranta G, Sanguinetti M, Masucci L. Fecal microbiota transplantation: a potential tool for treatment of human female reproductive tract diseases. *Front Immunol.* (2019) 10:2653. doi: 10.3389/fimmu.2019.02653

Conflict of Interest: The authors declare that the research was conducted in the absence of any commercial or financial relationships that could be construed as a potential conflict of interest.

frontiers in Nutrition

ORIGINAL RESEARCH
published: 11 June 2021
doi: 10.3389/fnut.2021.689818

Exposure to High Aerial Ammonia Causes Hindgut Dysbiotic Microbiota and Alterations of Microbiota-Derived Metabolites in Growing Pigs

Shanlong Tang[1†], Ruqing Zhong[1†], Chang Yin[1], Dan Su[1,2], Jingjing Xie[1], Liang Chen[1], Lei Liu[1] and Hongfu Zhang[1*]

[1] State Key Laboratory of Animal Nutrition, Institute of Animal Science, Chinese Academy of Agricultural Sciences, Beijing, China, [2] College of Animal Science and Technology, Qingdao Agricultural University, Qingdao, China

OPEN ACCESS

Edited by:
Yong Su,
Nanjing Agricultural University, China

Reviewed by:
Tongxing Song,
Huazhong Agricultural University, China
Sylvie Françoise Rebuffat,
Muséum National d'Histoire Naturelle, France

***Correspondence:**
Hongfu Zhang
zhanghongfu@caas.cn

† These authors have contributed equally to this work

Specialty section:
This article was submitted to Nutrition and Microbes, a section of the journal Frontiers in Nutrition

Received: 01 April 2021
Accepted: 13 May 2021
Published: 11 June 2021

Citation:
Tang S, Zhong R, Yin C, Su D, Xie J, Chen L, Liu L and Zhang H (2021) Exposure to High Aerial Ammonia Causes Hindgut Dysbiotic Microbiota and Alterations of Microbiota-Derived Metabolites in Growing Pigs. Front. Nutr. 8:689818. doi: 10.3389/fnut.2021.689818

Ammonia, an atmospheric pollutant in the air, jeopardizes immune function, and perturbs metabolism, especially lipid metabolism, in human and animals. The roles of intestinal microbiota and its metabolites in maintaining or regulating immune function and metabolism are irreplaceable. Therefore, this study aimed to investigate how aerial ammonia exposure influences hindgut microbiota and its metabolites in a pig model. Twelve growing pigs were treated with or without aerial ammonia (35 mg/m^3) for 25 days, and then microbial diversity and microbiota-derived metabolites were measured. The results demonstrated a decreasing trend in leptin ($p = 0.0898$) and reduced high-density lipoprotein cholesterol (HDL-C, $p = 0.0006$) in serum after ammonia exposure. Besides, an upward trend in hyocholic acid (HCA), lithocholic acid (LCA), hyodeoxycholic acid (HDCA) ($p < 0.1$); a downward trend in tauro-deoxycholic acid (TDCA, $p < 0.1$); and a reduced tauro-HDCA (THDCA, $p < 0.05$) level were found in the serum bile acid (BA) profiles after ammonia exposure. Ammonia exposure notably raised microbial alpha-diversity with higher Sobs, Shannon, or ACE index in the cecum or colon and the Chao index in the cecum ($p < 0.05$) and clearly exhibited a distinct microbial cluster in hindgut indicated by principal coordinate analysis ($p < 0.01$), indicating that ammonia exposure induced alterations of microbial community structure and composition in the hindgut. Further analysis displayed that ammonia exposure increased the number of potentially harmful bacteria, such as *Negativibacillus*, *Alloprevotella,* or *Lachnospira*, and decreased the number of beneficial bacteria, such as *Akkermansia* or *Clostridium_sensu_stricto_1*, in the hindgut (FDR < 0.05). Analysis of microbiota-derived metabolites in the hindgut showed that ammonia exposure increased acetate and decreased isobutyrate or isovalerate in the cecum or colon, respectively ($p < 0.05$). Unlike the alteration of serum BA profiles, cecal BA data showed that high ammonia exposure had a downward trend in cholic acid (CA), HCA, and LCA ($p < 0.1$); a downward trend in deoxycholic acid (DCA) and HDCA ($p < 0.05$); and an upward trend in glycol-chenodeoxycholic acid (GCDCA, $p < 0.05$). Mantel test and correlation analysis revealed associations between microbiota-derived metabolites and ammonia exposure-responsive cecal bacteria. Collectively, the findings illustrated that high ammonia exposure induced the dysbiotic microbiota in the hindgut, thereby affecting the production of microbiota-derived short-chain fatty acids and BAs, which play a pivotal role in the modulation of host systematic metabolism.

Keywords: high ammonia, microbiota, bile acid, short-chain fatty acid, growing pigs

INTRODUCTION

Ammonia (NH_3), the sole alkaline gas in the atmosphere, is the predominant source of active nitrogen. The primary sources of aerial ammonia are agricultural production, such as emission from animal husbandry and release of ammonia-based fertilizer (1, 2), and industrial production (e.g., chemical pant), land or sea release. Human activities (e.g., automobiles and airplane emissions) also give off ammonia (3). There is increasing attention to ammonia release over the past few decades, because of it having adverse influences on animal and human health. Besides, pernicious effects of aerial ammonia on the formation of atmospheric particles and reduction of air visibility have been reported (4, 5). Numerous studies have demonstrated that atmospheric ammonia has hazardous effects on many organs of animals, causing cardiac autophagy or liver apoptosis *via* the mitochondrial pathway or the PETEN/AKT/mTOR pathway (6–8), leading to respiratory tract infection and inflammation response (9), bringing about intestinal microvilli deficiency (10) and microbial disturbance in the small intestine (11), giving rise to dysfunction of immune organs (12, 13).

Previous studies in our laboratory have proved metabolic disorders induced by aerial ammonia exposure in animals. Ammonia exposure modulated the distribution of body fat in broilers by regulating the transcripts of lipid metabolism-related enzymes in the liver or breast muscle (14, 15). The previous results exhibited that high ammonia exposure disordered lipid metabolism *via* activation of the mTOR pathway, consequently upregulating genes involved in lipogenesis and downregulating lipolysis genes in the muscle of growing pigs (16), and impaired the branched-chain amino acid (BCAA) catabolism by suppressing the expression of BCAA catabolism-related enzymes (unpublished data). Attractively, the type of skeletal myofiber, especially increased myosin heavy chain (MyHC) *IIx* or decreased MyHC *I*, was notably altered after aerial ammonia exposure, which indicated that the metabolic type of skeletal muscle changed from oxidative to glycolytic type (16, 17). However, the specific mechanism that aerial ammonia jeopardizes animal health, causing metabolic disorder, is still unclear.

Microbiota is a crucial "microbial organ" of mammals, and is closely related to many physiological functions, such as metabolism, immunity, and nutrition. Recent studies have displayed that microbiota plays a momentous role in the function and metabolism of skeletal muscles (18–20). The absence of gut microbiota induces muscle mass loss and causes metabolic disturbance containing BCAA dysbolism and alteration of muscular myofibers or glucose homeostasis (19, 20). These results caused by the absence of gut microbiota are similar to those induced by aerial ammonia exposure, indicating that the role of gut microbiota in muscular dysbolism caused by ammonia exposure is irreplaceable. Besides, there is a wide array of evidence that microbial metabolites, such as short-chain fatty acid (SCFA), bile acid (BA), microbial tryptophan catabolites, and succinate, are pivotal inducers that regulate host metabolism and inflammatory response (21). However, it is still unclear whether or how ammonia exposure affects the composition of gut microbiota and its metabolites. Therefore, this study aimed to investigate the impacts of aerial ammonia on the constitution of gut microbiota (in the cecum and colon) and its metabolites [SCFA, BA, and amino acid (AA)].

MATERIALS AND METHODS

Animal Experimental Ethics

All procedures performed in this study were reviewed and approved by the Experimental Animal Welfare and Ethical Committee of the Institute of Animal Science of the Chinese Academy of Agricultural Sciences (IAS2017-2). Minimum numbers of pigs were used in an effort to minimize stress during handling.

Animals and Exposure Conditions

A total of twelve 70-day-old pigs (Yorkshire × Landrace, 20.27 ± 0.36 kg) purchased from a commercial pig farm (Beijing Breeding Pig Co., Ltd., Beijing, China) were randomly distributed into two groups, the control and high ammonia groups. All the pigs were individually penned, and each group was maintained in a separate controlled environment chamber. The pigs in the

Abbreviations: AA, amino acid; ALT, alanine aminotransferase; AST, aspartate aminotransferase; BA, bile acid; BCAA, branched-chain amino acid; BW, body weight; BWG, body weight gain; CA, cholic acid; CDCA, chenodeoxycholic acid; DCA, deoxycholic acid; FXR, farnesoid X receptor; GCA, glycol-cholic acid; GCBA, glycine-conjugated bile acid; GCDCA, glycol-chenodeoxycholic acid; GHCA, glycol-hyocholic acid; GUDCA, glycol-ursodeoxycholic acid; HCA, hyocholic acid; HDCA, hyodeoxycholic acid; HDL-C, high-density lipoprotein cholesterol; Ile, isoleucine; LCA, lithocholic acid; LDL-C, low-density lipoprotein cholesterol; Leu, leucine; LPS, lipopolysaccharide; MyHC, myosin heavy chain; NH_3, ammonia; OTU, operational taxonomic unit; PBA, primary bile acid; PCoA, principal coordinate analysis; Phe, phenylalanine; RDA, redundancy analysis; SBA, secondary bile acid; SCFA, short-chain fatty acid; TBA, total bile acid; TC, total cholesterol; TCA, tauro-cholic acid; TCBA, taurine-conjugated bile acid; TCDCA, tauro-chenodeoxycholic acid; TDCA, tauro-deoxycholic acid; TG, total triglycerides; TGR5, takeda G protein-coupled receptor 5; THDCA, tauro-hyodeoxycholic acid; TLCA, tauro-lithocholic acid; TUDCA, tauro-ursodeoxycholic acid; Tyr, tyrosine; UDCA, ursodeoxycholic acid; Val, valine; VLDL, very low density lipoprotein.

ammonia chamber were exposed to 35 mg/m^3 ammonia for 25 days, while pigs in the control group were housed in another chamber without ammonia during the experimental period. ToxiRAE Pro Ammonia (NH_3) Detector (RAE systems, San Jose, CA, USA) was used to monitor ammonia concentration in the chamber, and ammonia was sent into the chamber *via* a ventilation system before being mixed with air. Over the 25-day experimental period, all pigs had free access to clean water and consumed commercial feed (**Supplementary Table 1**) that was equal to 4–5% of body weight (BW) per day. The BW of each pig was taken weekly, and all animals were allowed to adapt to the chamber for 7 days under control group conditions before the start of the experiment.

Collecting Samples

At the end of the experiment, blood samples were acquired from the jugular vein *via* a sterilized syringe before the pigs were sacrificed by electric stunning (Xingye Butchery Machinery Co. Ltd., Changde, China). Then, the blood was centrifuged at 3,000 rpm for 15 min to obtain serum after 3 h incubation at room temperature. The serum was aliquoted and stored at −80°C for BA quantification or other metabolite analysis. Sections of the cecum and proximate colon were *in situ* ligated before the whole intestine was removed from the abdominal cavity. Then, the digesta in the cecum and proximal colon was aseptically collected in 2-ml sterile tubes, immediately frozen in liquid nitrogen, and stored at −80°C for sequencing of microbial 16S genes and analysis for SCFA and BA quantification.

Serum Metabolites

Serum leptin and adiponectin were measured by ELISA for antigen detection using commercial assay kits (Cat # KAP2281 for leptin, Cat # KAPME09 for adiponectin) from Beijing North Institute of Biological Technology (Beijing, China). According to the instruction of the manufacturer, the concentrations of high-density lipoprotein cholesterol (HDL-C, Cat # A112-2-1), low-density lipoprotein cholesterol (LDL-C, Cat # A113-2-1), very low-density lipoprotein (VLDL, Cat # H249), alanine aminotransferase (ALT, Cat # C009-2-1), and aspartate aminotransferase (AST, Cat # C010-2-1) in the serum were detected *via* commercial assay kits purchased from Nanjing Jiancheng Bioengineering Institute (Nanjing, China).

Quantification of Bile Acids in Serum and Intestinal Digesta

The BA in the serum was extracted according to the methods described by Fang et al. (22). Briefly, 200 µl of the serum was added into an equal amount of pre-cold sodium acetate (50 mM, pH 5.6) and triple ethanol (chromatography grade), and then the mixture was vortexed for 2 min to mix evenly. After centrifugation at 20,000 g for 20 min, the supernatant was diluted five times with a sodium acetate buffer and applied to a Bond Elute C18 cartridge (500 mg/6 ml, Varian, Harbor City, CA, USA) pre-activated by 5 ml methanol. The cartridge was then washed with 25% ethanol, and the BA was eluted with 5 ml methanol. The residue was dissolved in 1 ml methanol after the solvent was evaporated with nitrogen gas and finally passed through a 0.45-µm Milled-LG filter (Millipore, Billerica, MA, USA) for BA analysis. The BA in the intestinal digesta was extracted according to the methods described by Fang et al. (22). Approximate 50–80 mg lyophilized digesta in cecum was suspended in a mixture of pre-cold sodium acetate buffer (50 mM, pH 5.6) and ethanol, and then the same method was used as described above.

The BA in the serum and intestinal digesta was profiled with a Waters Xevo TQ-S LC/MS mass spectrometer (Waters, Milford, MA, USA) equipped with an ESI source and the assay condition used in the previous report by Fang et al. (22). Briefly, a 10-µl filtrate was injected into a ZORBAX Eclipse plus C18 column (95 Å, 1.8 µm, 2.1 × 100 mm) from Agilent (Santa Clara, CA, United States) to separate the BA. The mobile phases consisted of 5% acetonitrile and 0.1% formic acid (mobile phase A) and 95% acetonitrile and 0.1% formic acid (mobile phases B). The gradient for BA elution was gradually changed at a total flow rate of 0.4 ml/min as follows: mobile phase A:B (9:1, v/v) from 0 to 1 min, mobile phase A:B (7:3, v/v) from 1 to 1.5 min, mobile phase A:B (2:3, v/v) from 1.5 to 5.5 min, and mobile phase A:B (9:1, v/v) from 5.5 to 7 min. The spray voltage and vaporizer temperature were set at 2.91 kV and 500°C, respectively. The gas flow was set at 550 L/h. A total of 18 BA standards were purchased from Sigma-Aldrich (Merck KGaA, Darmstadt, Germany). The quantification of each BA was based upon the series dilutions of available standards, and good linearity was confirmed.

Quantification of Short-Chain Fatty Acids in Intestinal Digesta

To extract SCFA, about 0.5 g wet digesta was thoroughly mixed with 5 ml ultrapure water, then shocked for 30 min to mix evenly, and finally incubated at 4°C for 24 h. After centrifugation at 12,000 rpm for 20 min, the supernatant was mixed with 25% metaphosphoric acid at a ratio of 9:1, vortexed, and incubated at room temperature for 4 h. Then, the mixture was passed through a 0.45-µm Milled-LG filter (Millipore, Billerica, MA, USA) and subjected to SCFA analysis.

The Agilent 7890N gas chromatograph (Agilent, Santa Clara, CA, USA) was utilized to detect the SCFA in the samples. Briefly, a 2-µl sample was injected (split ratio 1:50) into the gas chromatograph equipped with a DB-FFAP column (15 m × 0.32 mm × 0.25 µm). The initial oven temperature was set at 100°C and then raised to 120°C at 2°C/min held at 120°C for 10 min. Nitrogen served as the carrier gas at a constant flow rate of 0.8 ml/min, and the constant pressure was 21.8 kPa. The injector and detector temperatures were 250 and 280°C, respectively. Individual SCFAs were identified by comparing their retention times with those in the standard mix of SCFA standards purchased from Sigma-Aldrich (Merck KGaA, Darmstadt, Germany).

DNA Extraction, Amplification, and Sequencing

Total bacterial DNA was extracted from the intestinal digesta using the EZNATM Soil DNA kit (D5625-02, Omega Bio-Tek Inc., Norcross, GA, USA) according to the instructions of the manufacturer. The V3-V4 hypervariable regions of the bacterial 16S rDNA were amplified by a two-step PCR method using primers 338F (5′-ACTCCTRCGGGAGGCAGCAG-3′) and 806R (5′-GGACTACCVGGGTATCTAAT-3′) with unique 8-bp barcodes to facilitate multiplexing, and sequencing was carried out with an Illumina sequencing platform using Miseq PE300.

Data Analysis and Statistical Test

Student's t-test of the data on serum metabolites (ALT, AST, LDL-C, VLDL, HDL-C, leptin, adiponectin, and BAs), microbial metabolites (intestinal BAs and SCFAs), and bacterial alpha-diversity indices (Sobs, Shannon, ACE, and Chao) was performed using the JMP software (JMP® version 10.0.0, SAS Institute, Cary, NC, USA) for Windows. $P < 0.05$ was regarded as statistically significant, while $0.05 < p < 0.1$ was set as significant trend.

Raw data obtained from gut microbiota were processed using the free online platform of Majorbio I-Sanger Cloud Platform (www.i-sanger.com), and redundant sequences were filtered. UPARSE (version 7.1, http://drive5.com/uparse/) was used to cluster operational taxonomic units (OTUs) at 97% similarity cutoff, and each presentative OTU was mapped to the Silva 138 database by RDP classifier (http://rdp.cme.msu.edu/) at a confidence threshold of 0.7. The principal coordinate analysis, triplot of redundancy analysis (RDA), and network for correlation analysis were employed using Majorbio I-Sanger Cloud Platform, and the Spearman's or Mantel's correlation analysis was applied using the ggcor R package. The significant difference between the control group and the ammonia group at genus level was tested by the DESeq2 method (MicrobiomeAnalyst, https://www.microbiomeanalyst.ca/) with corrected p-value (FDR) < 0.05.

RESULTS

Serum Metabolites Related to Lipids and Amino Acids

Although no changes in serum adiponectin, ALT, AST, LDL-C, and VLDL were observed in pigs exposed to high ammonia ($p > 0.05$, **Figures 1A–C**, **Supplementary Table 2**), serum HDL-C was diminished ($p = 0.0006$, **Figure 1C**, **Supplementary Table 2**), and serum leptin had a reduced trend ($p = 0.0898$, **Figure 1A**, **Supplementary Table 2**) after high ammonia exposure.

The results of other serum metabolites and free AAs, as described by Tang et al. (16), demonstrated that high ammonia exposure increased the concentration of serum total triglycerides (TG, $p = 0.0294$, **Supplementary Table 2**) and ApoB ($p = 0.0061$, **Supplementary Table 2**).Compared with the control pigs, the serum BCAA [leucine (Leu), $p < 0.0001$; isoleucine (Ile), $p = 0.0016$; valine (Val), $p = 0.0047$] and aromatic AA [tyrosine (Tyr), $p < 0.0001$; phenylalanine (Phe), $p = 0.0002$] were also notably increased in pigs exposed to high atmospheric ammonia (**Supplementary Table 2**). A previous study found that no alterations in feed intake, BW, and body weight gain (BWG) were observed in high ammonia exposed pigs ($p > 0.05$, **Supplementary Figures 1A–C**) (16).

Serum Bile Acid Profiles

In the growing pig serum, ∼88% of the BA existed in free form (**Figure 2D**). The most abundant BA was hyodeoxycholic acid (HDCA, 54.62%) or chenodeoxycholic acid (CDCA, 24.74%) in the secondary BAs (SBAs) or primary BAs (PBAs), respectively, which consisted of ∼97% of total serum BAs with glyco-CDCA (GCDCA, 6.24%), hyocholic acid (HCA, 6.20%), tauro-CDCA (TCDCA, 2.4%), tauro-ursodeoxycholic acid (TUDCA, 1.74%), and lithocholic acid (LCA, 1.6%) (**Figures 2C,D**). Among them, serum HCA ($p = 0.0605$), LCA ($p = 0.0799$) and HDCA ($p = 0.0841$) had an upward trend in pigs exposed to high ambient ammonia, while serum tauro-deoxycholic acid (TDCA, $p = 0.0751$) had a downward trend. and tauro-HDCA (THDCA, $p = 0.0050$) notably decreased in pigs exposed to high ammonia (**Figure 2A**; **Supplementary Table 2**). Despite higher differences from a trend point of view, no significant difference was observed in serum total BA (TBA) and PBA ($p > 0.05$, **Figure 2B**; **Supplementary Table 2**), and high ammonia exposure tended to increase serum SBA ($p = 0.0865$, **Figure 2B**; **Supplementary Table 2**).

Global Assessments for Sequencing Data

After data trimming and quality control, a total of 809,102 sequences from the cecum digesta and 690,575 sequences from the colon digesta were acquired with the number of sequences ranging from 38,754 to 73,486 per sample. The filtered 539,136 or 343,896 sequences from the cecum or the colon digesta, based on the normalized depth of 44,928 or 28,658 reads per sample, were clustered into 634 or 807 OTUs for all the samples at a 97% sequence similarity value, and were further clustered into 190 or 197 genera, 87 or 82 families, 53 or 51 orders, 25 or 25 classes, and 15 or 16 phyla. Most of the microbial diversity and bacterial communities in the cecum or the colon digesta samples had been sufficiently captured, indicated by good coverage (>0.999) and rarefaction curves (**Supplementary Figure 2**).

Variation in Alpha and Beta Diversities of Gut Microbiota

Compared with the control group pigs, the ammonia-exposed pigs exhibited higher Sobs ($p = 0.009$, **Figure 3A**), ACE ($p = 0.0354$, **Figure 3C**), and Chao indexes ($p = 0.0268$, **Figure 3D**) and showed a higher trend in the Shannon index ($p = 0.0762$, **Figure 3B**) in the cecum digesta at the OTU level. In the colon digesta, although no difference in the Chao index was observed ($p > 0.05$, **Figure 3D**), the Sobs ($p = 0.0238$, **Figure 3A**) and Shannon indexes ($p = 0.0115$, **Figure 3B**) were markedly greater and the ACE index ($p = 0.0801$, **Figure 3C**) showed an upward trend in the ammonia-exposed pigs at the OTU level. The principal coordinates analysis (PCoA) based on Bray–Curtis distance and ANOSIM test revealed that beta-diversity shifted due to ambient ammonia exposure and notable differences were observed in the cecum and colon at the OTU level (cecum $R = 0.5315$, $p = 0.003$, **Figure 3E**; colon $R = 0.2667$, $p = 0.007$, **Figure 3F**).

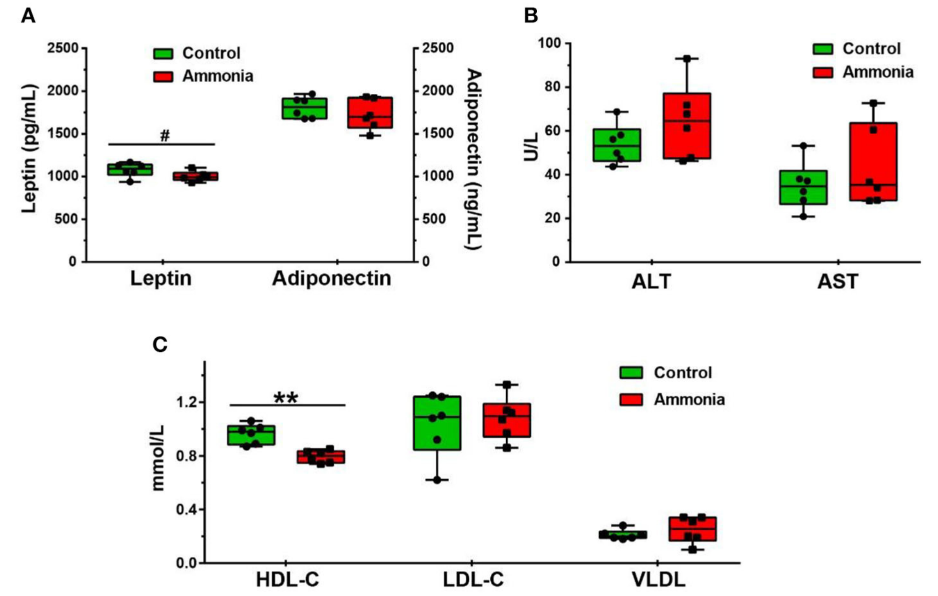

FIGURE 1 | The level of serum metabolites after atmospheric ammonia exposure. The contents of serum leptin and adiponectin after high ammonia exposure. **(A)** The level of ALT and AST in serum after high ammonia exposure. **(B)** The alteration of HDL-C, LDL-C, and VLDL in serum after ammonia exposure. **(C)** Data are expressed as min to max showing all points ($n = 6$), $^{\#}p < 0.1$ and $^{**}p < 0.01$.

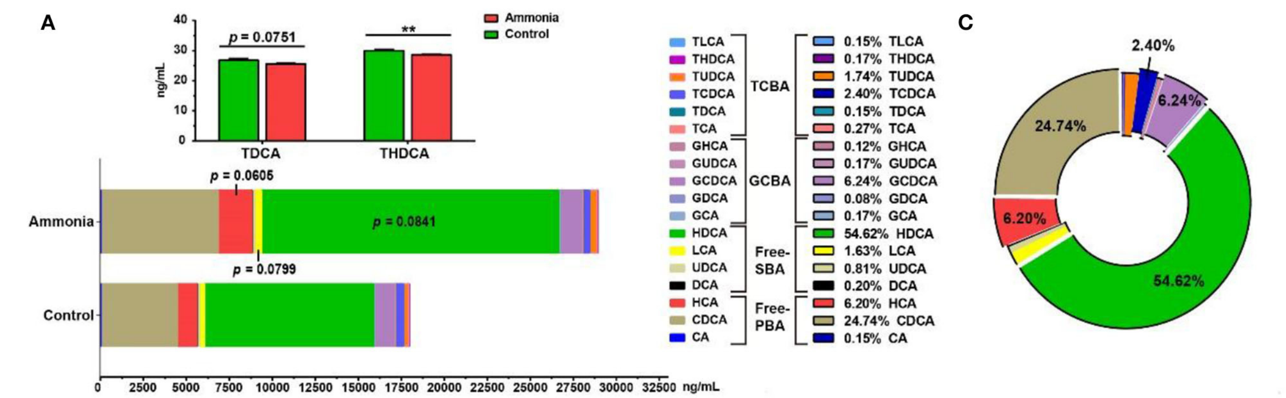

	Free-BA		TCBA		GCBA		total
PBA	HCA	6.20	THCA	—	GHCA	0.12	
	CA	0.15	TCA	0.27	GCA	0.17	
	CDCA	24.74	TCDCA	2.40	GCDCA	6.24	40.29
SBA	HDCA	54.62	THDCA	0.17	GHDCA	—	
	DCA	0.20	TDCA	0.15	GDCA	0.08	
	UDCA	0.81	TUDCA	1.74	GUDCA	0.17	
	LCA	1.63	TLCA	0.15	GLCA	—	59.72
total		88.35		4.88		6.78	

FIGURE 2 | The alteration in serum BA profiles caused by ammonia exposure. The changes in **(A)** each BA content and **(B)** each type of BA content in the serum of pigs exposed to high ammonia; **(C)** the compositions of each BA and **(D)** each type of BA in the serum of control pigs. Data are expressed as mean value or mean ± SE ($n = 6$), $^{**}p < 0.01$.

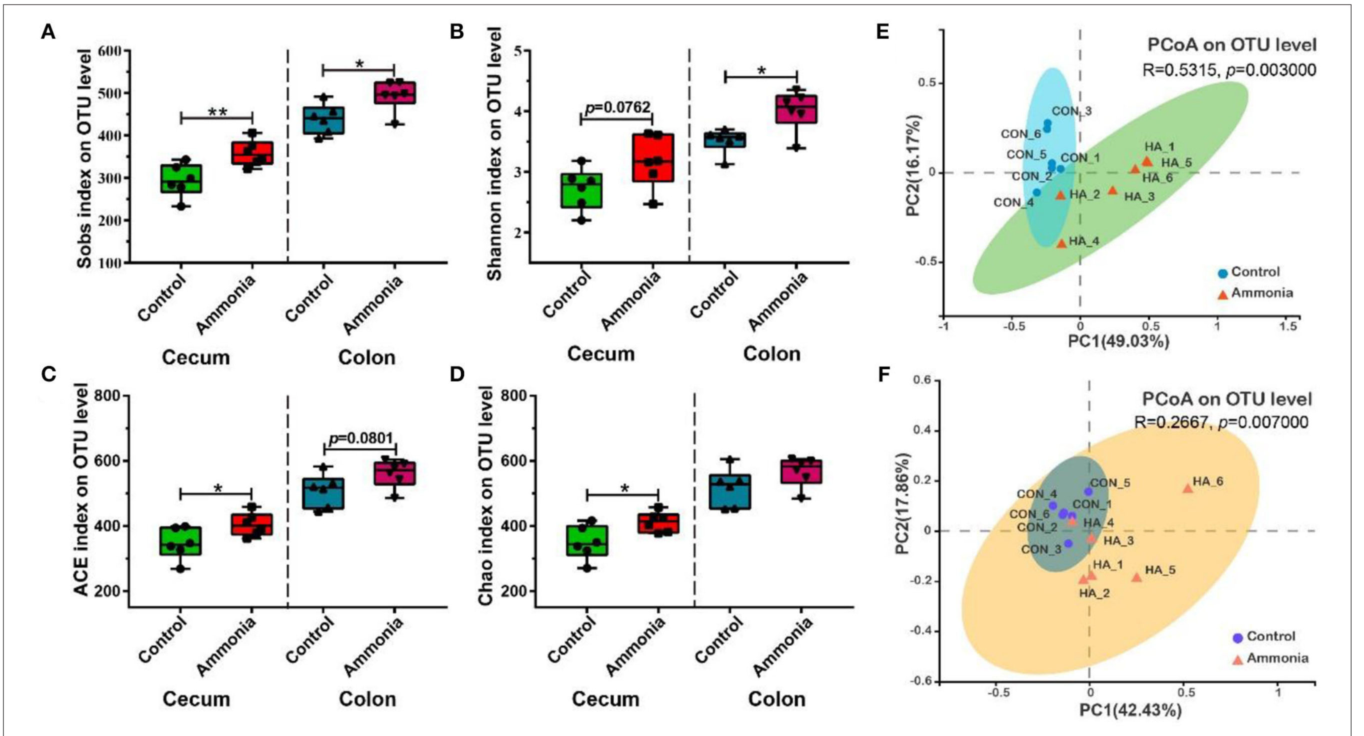

FIGURE 3 | Alpha and beta diversities of the microbial community in the cecum or colon digesta after ammonia exposure. **(A)** The Sobs, **(B)** Shannon, **(C)** ACE, and Chao indexes in the cecum or colon among two groups; PCoA (OTU level) of community membership based on the Bray–Curtis distance and ANOSIM test in **(E)** cecum and **(F)** colon. Data are expressed as min to max showing all points ($n = 6$), *$p < 0.05$, and **$p < 0.01$.

Alteration of Specific Gut Microbiota

A total of 17 microbiotas were identified at genus level in the cecum digesta of the pigs exposed to high ammonia, which included eight downregulated genera (*Ralstonia*, *Akkermansia*, *Gastranaerophilales*, *Terrisporobacter*, *unclassified_p__Firmicutes*, *Family_XIII_AD3011_group*, *Peptococcus*, and *Clostridium_sensu_stricto_1*) and nine upregulated genera (*norank_f__Muribaculaceae*, *Butyricicoccus*, *Lactobacillus*, *Anaerovibrio*, *Monoglobus*, *Lachnospira*, *Lachnospiraceae_UCG_010*, *norank_f__Butyricicoccaceae*, and *Alloprevotella*) (FDR < 0.05, **Figures 4A,B**). Besides, four microbiotas (increased *Bacteroidota* and *Spirochaetota*; decreased *Verrucomicrobiota* and *Cyanobacteria*) were notably altered at phylum level in the cecum digesta after ammonia exposure (FDR < 0.05, **Figure 4C**). In the colon digesta, high ammonia exposure increased genera *Lachnospira*, *Fournierella*, *Negativibacillus*, *Monoglobus*, *Butyricicoccaceae*, and decreased genus *Terrisporobacter* (FDR < 0.05, **Figures 4D,E**).

Gut Short-Chain Fatty Acid and Bile Acid Production

Based on microbiota alteration, further investigation of SCFA concentration in the cecum or colon was completed and shown in **Figure 5A** and **Supplementary Table 3**. In the cecum digesta, ammonia-exposed pigs exhibited lower concentration of isobutyrate ($p = 0.0002$) and isovalerate ($p < 0.0001$), while the higher concentration of acetate ($p = 0.0243$) and increased trend in total SCFA ($p = 0.0657$) were remarkably observed in the pigs exposed to ammonia. Compared with cecum SCFA, the colon SCFA profiles in either pigs exposed to ammonia or pigs not exposed to ammonia had similar alteration. In the colon digesta, high ammonia exposure decreased the content of isobutyrate ($p = 0.0115$) and isovalerate ($p = 0.0035$) and had a trend to increase acetate concentration ($p = 0.0624$). Besides, the contents of total SCFA, acetate, isobutyrate, butyrate, isovalerate, and valerate in the cecum were higher than those in colon.

Further investigation of BA concentration in the cecum was also finished. Among them, cecal cholic acid (CA, $p = 0.0586$), HCA ($p = 0.0703$), and LCA ($p = 0.0858$) had a downward trend, and deoxycholic acid (DCA $p = 0.0262$) and HDCA ($p = 0.0437$) dramatically decreased in the ammonia-exposed pigs, while cecal GCDCA ($p = 0.0128$) notably increased in the ammonia-exposed pigs (**Figure 5B**; **Supplementary Table 3**). Besides, there also was a downward trend in cecal TBA ($p = 0.0540$) and SBA ($p = 0.057$) after ammonia exposure, and high ammonia exposure significantly increased cecal glycine-conjugated BA (GCBA, $p = 0.0139$) (**Figure 5C**; **Supplementary Table 2**).

Microbiota-Metabolites Correlation

The triplot of RDA was shown in **Figure 6A** and revealed that the cecal samples from the control or the ammonia group were separated at the first constrained axis. *Clostridium_sensu_strictio_1*, *Terrisporobacter*, and *Turicibacter* were positively correlated with SBA, TBA, isovalerate, and

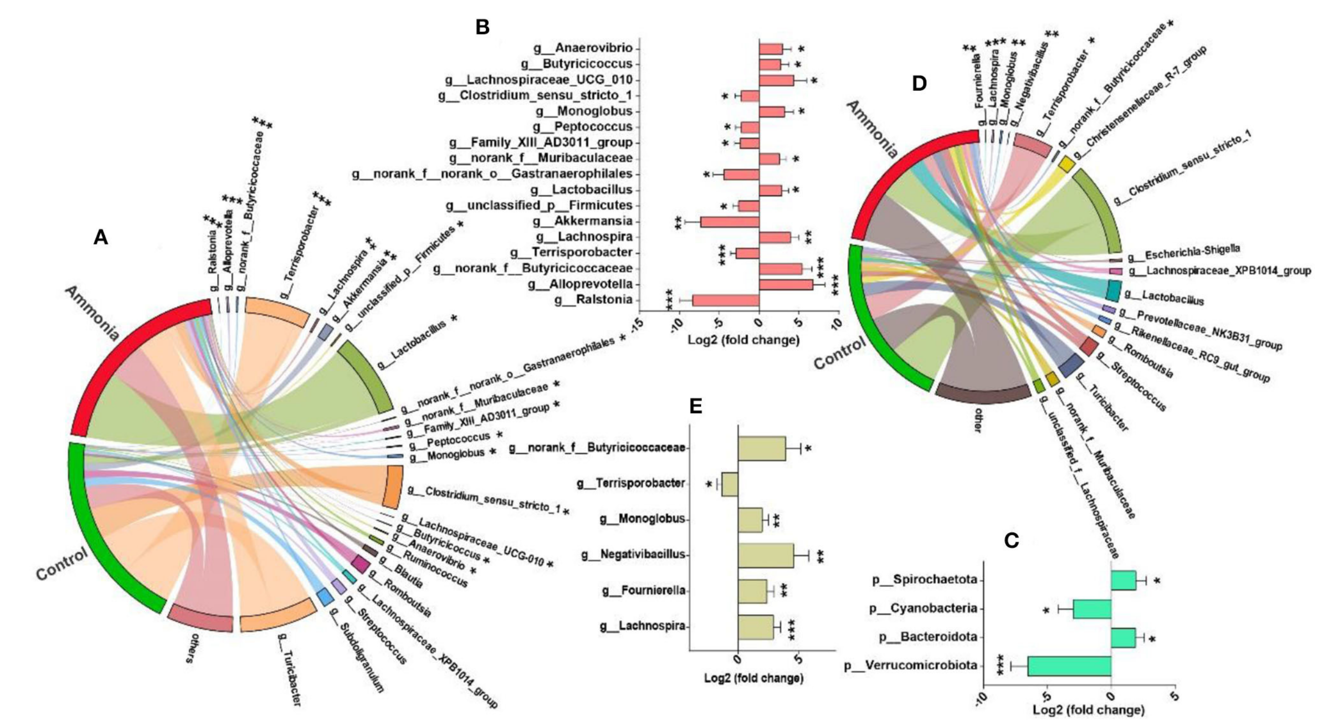

FIGURE 4 | Differentially abundant genera from the cecum or colon after ammonia exposure. The mainly enriched genera (including differentially abundant genera) from **(A)** the cecum or **(D)** colon in control group vs. ammonia group; the differentially abundant **(B)** genera or **(C)** phyla from the cecum and the differentially abundant **(E)** genera from the colon after high ammonia exposure. *FDR < 0.05, **FDR < 0.01, and ***FDR < 0.001, respectively.

isobutyrate in cecum chyme, while *Lactobacillus* was positively correlated with GCBA, taurine-conjugated BA (TCBA), acetate, butyrate, and propionate in cecum chyme. To further investigate the relationship between cecum bacteria and serum metabolites, the relevance network association analysis and Spearman or Mantel correlation analysis were established by the abundance of cecal genera, serum BCAA or aromatic AA, and lipid-related metabolites. The network analysis by Spearman correlation revealed that cecal *Akkermansia* and *Terrisporobacter* abundance were negatively associated with each BCAA in the serum, while *Alloprevotella*, *norank_f__Muribaculaceae*, *Lactobacillus*, *Monoglobus*, and *Lachnospira* abundance were positively associated with each serum BCAA (Spearman's r > 0.5, $p < 0.05$, **Figure 6B**). Because of the similarly altered trend between each BCAA and aromatic AA, the same genera and relationship were observed in each aromatic AA by network analysis (Spearman's r > 0.5, $p < 0.05$, **Figure 6B**). In addition, the Mantel correlation analysis demonstrated that a significant correlation was observed between five genera (*Ralstonia*, *Akkermansia*, *unclassified_p__Firmicutes*, *Terrisporobacter*, and *Family_XIII_AD3011_group*) and total BCAA (Mantel's r > 0.25, $p < 0.05$, **Figure 6C**). Apart from the same five genera, there were still two genera (*Lactobacillus* and *norank_f__Muribaculaceae*) which had a significant correlation with total aromatic AA by Mantel correlation analysis (Mantel's r > 0.25, $p < 0.05$, **Figure 6C**). For serum BAs, only serum SBA had a significant correlation with microorganisms (*Lactobacillus*, *norank_f__Muribaculaceae*, *Clostridium_sensu_stricto_1*, *Terrisporobacter*, *Alloprevotella*, *Akkermansia*, *Monoglobus*, and *Lachnospira*; r > 0.25, $p < 0.05$, **Figures 6B,C**). Spearman's correlation analysis showed that there was a strong correlation between BCAAs (Leu, Ile, Val), aromatic AAs (Tyr, Phe) or partial BAs (HCA, LCA, HDCA, TUDCA, THDCA), and lipid-related metabolites (TG, ApoB, HDL-C, VDL; $p < 0.05$, **Figure 6D**).

DISCUSSION

Increasing aerial ammonia, the most infamous atmospheric pollutant, has attracted much attention recently, owing to its adverse impacts on animal and human metabolic states. The serum lipid-related metabolites may reflect the overall metabolic state to a certain extent. Elevated serums, TG and ApoB, were observed in the previous study after high ammonia exposure (16). Evidence is given that a high level of ApoB is a superior indicator of vascular heart disease driving physiology than either total cholesterol (TC) or LDL-C (23). This study found no alteration in LDL-C, but there was a remarkable decline in HDL-C level after high ammonia exposure. HDL-C exhibited extraordinary anti-inflammation and antioxidant ability because of the existence of multiple antioxidant enzymes and the ability to neutralize bacterial lipopolysaccharide (LPS) (24). The low HDL-C level was usually associated with high triglyceride as the precursor of dysmetabolic events, such as insulin resistance.

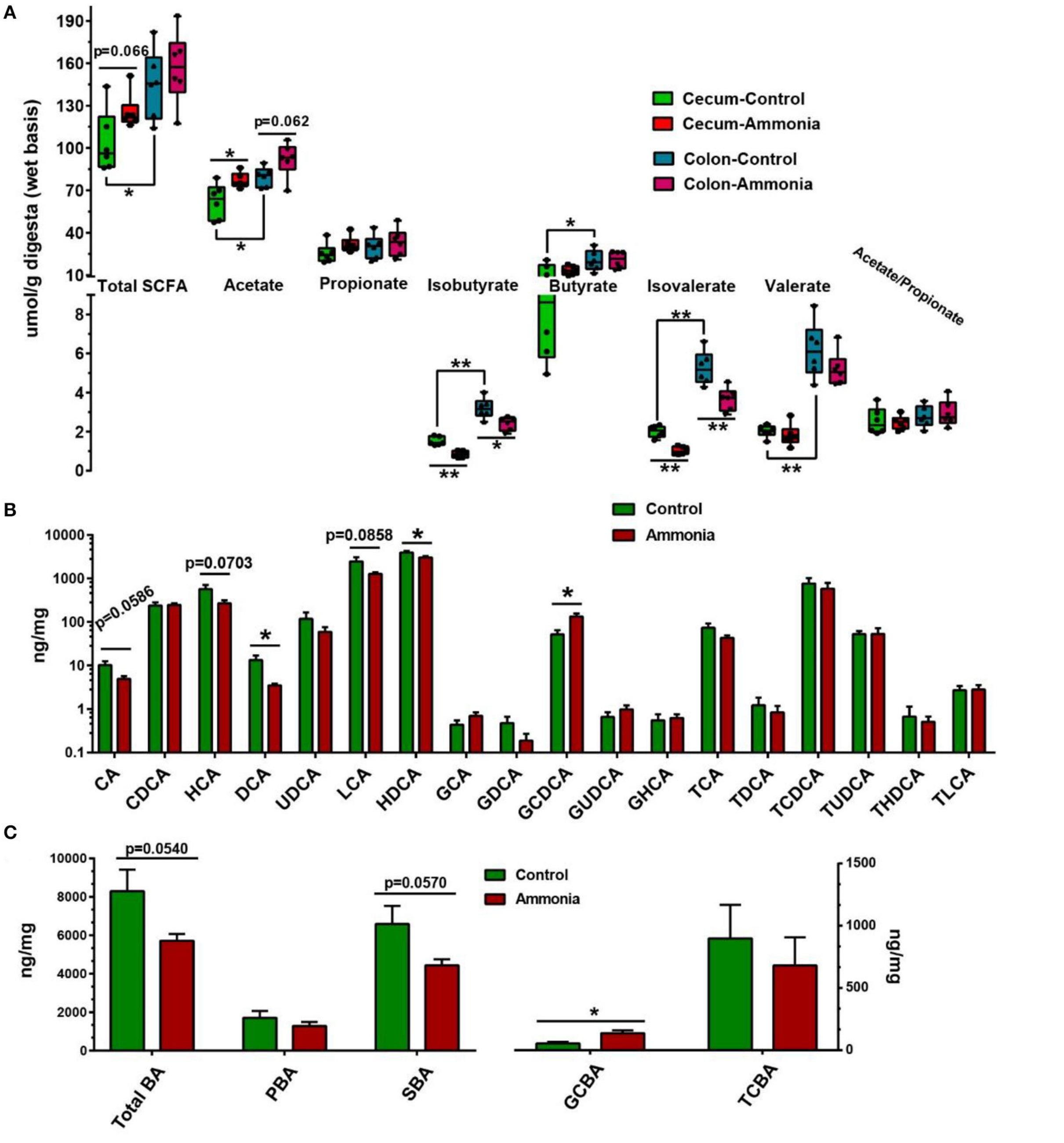

FIGURE 5 | SCFA and BA production from the cecum or colon digesta in pigs exposed to ammonia or not. **(A)** Changes in the SCFA profile of the cecum or colon after ammonia exposure; **(B)** changes in each BA content; and **(C)** each type of BA content in the cecum of pigs exposed to high ammonia. Data are expressed as min to max showing all points or mean ± SE ($n = 6$), *$p < 0.05$ and **$p < 0.01$.

The alterations in lipid-related metabolites, including TG, HDL-C, and ApoB, caused by ammonia exposure reflected the transformation of metabolic state, which was closely related to the serum microbiota-derived metabolites (such as BCAA, aromatic AA, HCA, LCA, HDCA, and THDCA) indicated by the Spearman's correlation analysis.

Lipid metabolism of skeletal muscle and metabolic state were altered in pigs after high aerial ammonia exposure in the previous or this study. Recent studies have shown that the action of gut microbiota in physiological muscle function and systemic metabolism was priceless (19, 20, 25). Therefore, gut microbiota diversity was assessed in the cecum and colon digesta by 16s rDNA sequencing of microorganisms. We observed that high ammonia exposure elevated the alpha diversity, indicated by the indexes of Sobs, Shannon, ACE, or Chao, and induced the transition of microbiota composition recommended by beta diversity in the cecum and colon. Among that, the explanation of microbial shift provided by the R value of PCoA suggested

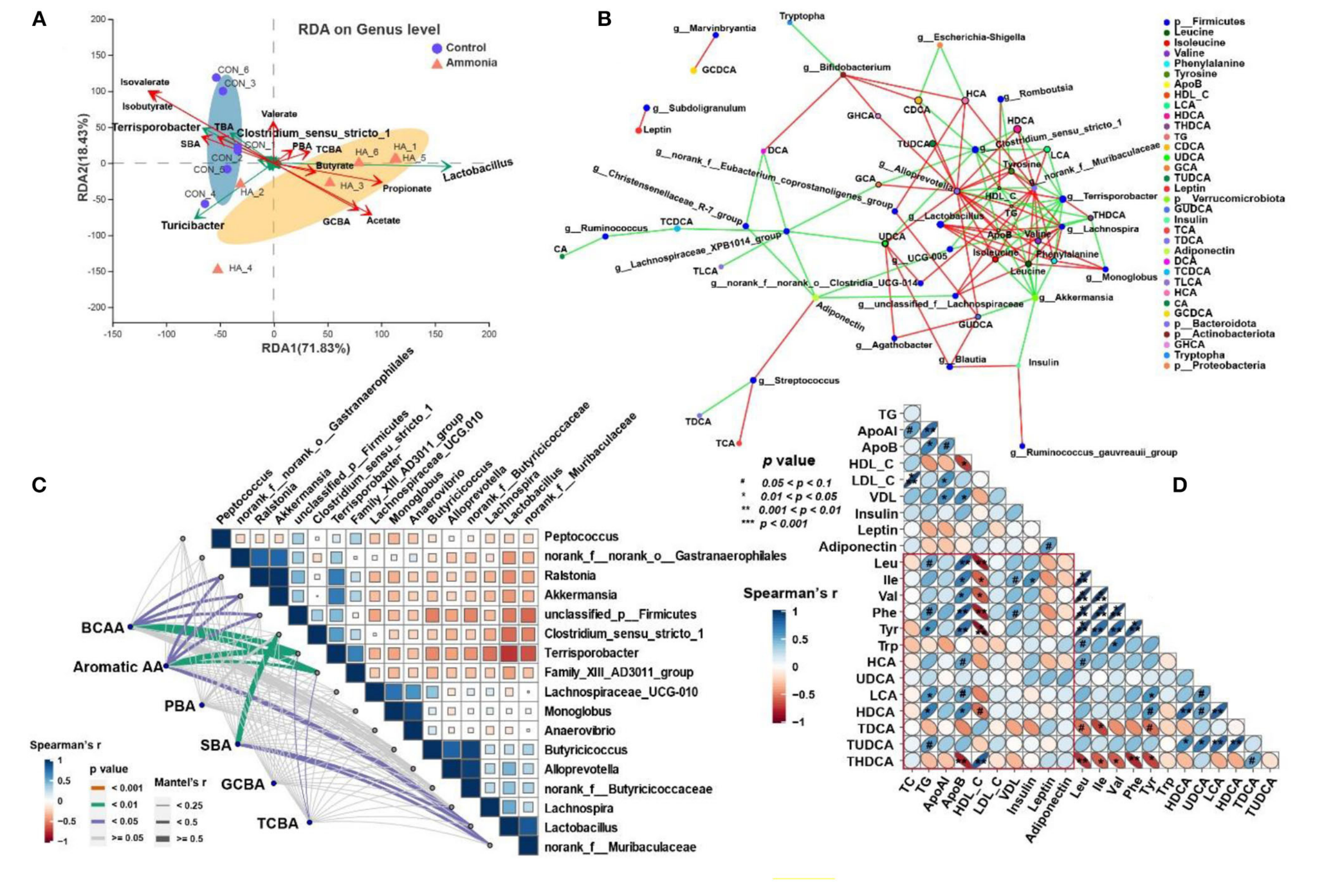

FIGURE 6 | Microbiota–metabolite correlation. **(A)** Triplot of RDA of the cecal microbial composition at genus level relative to cecal BAs and SCFAs. Microbiota from the control and ammonia groups is indicated by blue circles and orange triangles, respectively. Constrained explanatory variables (cecal TBA, PBA, SBA, GCBA, TCBA, and SCFA) are indicated by red arrows. Responding taxa are indicated by green arrows, and only those with higher fit in the ordination plot are labeled. The first (71.83% interpretation) and second coordinates (18.43% interpretation) are plotted. **(B)** A network for correlation analysis among the top 50 relative abundance of cecal bacterial genera, serum BA, and AA using relevant networking. Only correlations with Spearman's coefficient >0.5 and $p < 0.05$ are shown. The different color of nodes indicates various targets as demonstrated in legend. The line color represents correlation, and red and green represent positive and negative correlation, respectively. The more lines there are, the more connected the nodes are. **(C)** Pairwise comparisons of different cecal genera are demonstrated with a color gradient denoting Spearman's correlation coefficient. BCAA, aromatic AA, PBA, SBA, TCBA, and GCBA are related to each microbial genus by Mantel's correlation analysis. Edge width corresponds to the Mantel's r statistic for the corresponding distance correlation, and edge color denotes statistical significance. **(D)** Half Spearman's correlation matrix of serum BCAA (Leu, Ile, and Val), Aromatic AA (Phe, Tyr, and Trp), serum BA, and lipid parameters. The red and blue ellipses represent negative and positive correlations, respectively, and the width of ellipses represents strength of correlation (narrow ellipses mean stronger correlation).

that the cecal microbiota was more sensitive to aerial ammonia, which was consistent with the more remarkable alteration of microbiota in the cecum than that in the colon under the condition of ammonia exposure. Gut dysbiosis happens when the diversity, constitution, and functions of the gut microbiota are disturbed, negatively affecting an individual, for example, through interferece with intestinal homeostasis and disrupting immune response (26). The ratio of two main dominant phyla, Firmicutes and Bacteroidetes, displays a noticeable transition (decreased Firmicutes and increased Bacteroidetes) in patients with inflammatory bowel disease (27). In this study, greater abundance of Bacteroidetes and unchanged Firmicutes in the cecum were observed after ammonia exposure, which indicated that the lower ratio of Firmicutes/Bacteroidetes might contribute to inappropriate immune activation.

Specific bacteria (e.g., *Akkermansia*, *Alloprevotella*, *Lachnospira*, *Clostridium_sensu_stricto_1*, *Negativibacillus*, *Terrisporobacter*, and *Lactobacillus*) were identified to be enormously influenced by aerial ammonia exposure of the cecum or colon. For instance, *Akkermansia*, a commonly accepted beneficial inhabitant of the human microbiota, is crucial for fatty acid metabolism, which is conversely correlated with increased inflammation and reduction in patients with obesity or fatty liver disease (28). *Akkermansia* and its outer membrane protein AMUC_1100 could bind to a receptor on the membrane of intestinal epithelial cells and affect the downstream immune regulatory pathway, reducing inflammation response and LPS, regulating lipid and glucose metabolism (29, 30). Depletion of *Akkermansia* induced by ammonia exposure was observed, which might be a vital reason for metabolic disorder or inflammation after aerial ammonia exposure. Studies reported that the relatively great abundance of *Alloprevotella* and *Lachnospiraceae* was presented in the high-salt treatment, which could cause a metabolic disturbance, raising the risk of chronic disorders, tumors, and cardiovascular disease (31, 32). Although *Lachnospira* was well-described as a beneficial inhabitant for human and animal by fermenting fibers, thereby producing SCFA, it has been reported that aflatoxin B1 exposure induced a dramatic increment of *Lachnospira* (33), as *Lachnospira* was positively correlated with diarrhea in weaning pigs (34). All those reports indicated that *Alloprevotella* and *Lachnospira* might be potential pathogens under specific conditions. The data demonstrated that increased gut microbiota, *Alloprevotella* and *Lachnospira* might not be a beneficial signal for human and animal health under the condition of aerial ammonia exposure. Earlier research reported that the colonization of *Clostridium_sensu_stricto_1* could improve the aggregation of T cells regulated by CD41 in the colon of sterile mice (35) and strengthen the resistance of infant gut bacteria by hindering the colonization of pathogenic microbiota (36), which might explain the decrement of *Clostridium_sensu_stricto_1* induced by ammonia exposure in this study. Pathogenic bacteria *Negativibacillus* associated with gut dysbiosis or pediatric Crohn's disease (37, 38) was dramatically increased in this research after ammonia exposure. The results on specific different genera caused by ammonia exposure of the hindgut were quite different from those of the previous study on the small intestine (11), which is probably due to undigested or unabsorbed nutrients (induced by ammonia exposure in the small intestine) from the small intestine to enter the hindgut, interacting with ammonia exposure of the hindgut. Confusingly, *Lactobacillus,* identified as beneficial bacteria by numerous studies, was lifted in the intestine of ammonia-exposed pigs accompanied with metabolism disorder, especially lipid metabolism in skeletal muscle. Even so, a study still illustrated that a high-fat diet induced gut microbiota alteration (increased *Lactobacillus* and *Turicibacter*) in castrated mice and male androgen receptor knockout mice, causing metabolic disorder (39). Besides, Anhe et al. (40) found that camu camu (*Myrciaria dubia*) increased *Akkermansia* and decreased *Lactobacillus*, which increased heat production and made mice maintain metabolic homeostasis under the condition of high-fat and high-sugar intake. Therefore, the role of *Lactobacillus* raised by ammonia exposure needs to be further explored.

Microbial metabolites, closely related to the composition of intestinal microbiota, are incredibly crucial for the systemic metabolism and occurrence of metabolic diseases (21, 41, 42), and the BA profile, a kind of very vital microbial metabolites, was further analyzed in this research after ammonia exposure. The results demonstrated that the altered tendency of BA in the hindgut and serum was entirely dissimilar, which suggested that ammonia exposure enhanced the resorption of BAs, especially PBAs, in the ileum, causing a reduction in the PBA level entering the hindgut accompanied by decrement in SBAs produced by microbiota with PBA as substrate in the hindgut. The increment in BA resorption induced by ammonia exposure was consistent with the enhanced BA transport in the ileum after chronic heat exposure, and the serum THDCA level also declined in ammonia-exposed or heat-stressed pigs (43). However, heat stress had little effect on BA and BA-related bacteria in the hindgut, while ammonia exposure altered the hindgut BA profiles by disturbing the hindgut microbiota. The DCA and LCA, the most abundant metabolites in the gut microbiome, modify host energy and metabolism as well as gut barrier and inflammation (21, 42). For instance, the DCA and LCA, whose production is closely related to *Clostridium scindens*, are favorable for maintaining gut barrier integrity or accelerating intestinal crypt regeneration and wound repair *via* the farnesoid X receptor (FXR) and also detrimental for pathogen colonization (21, 44). We observed that the SBA content notably dropped with the relative abundance of *Clostridium_sensu_stricto_1* decreasing in the cecum after ammonia exposure, which might cause detrimental impacts on the intestinal barrier or inflammation and could lead to lipid or glucose metabolism disorder. Besides, the decreased SBA was affected by genera *Terrisporobacter*, *Clostridium_sensu_stricto_1*, *Turicibacter*, and *Lactobacillus* indicated by the RDA analysis. The increment in serum BA was essential in whole systemic metabolism after ammonia exposure in this research. Takeda G protein-coupled receptor 5 (TGR5), the plasma membrane-bound G protein-coupled receptor ubiquitously expressed with high expression in skeletal muscle, white adipose tissues, and gut (45, 46) is another crucial BA-responsive receptor that participated in host metabolism. The SBA (including LCA and DCA) is the primary ligand to activate TGR5 (47), and then the activation of TGR5 can regulate host metabolism through the mTOR pathway (48). The previous study showed that high ammonia exposure activated the mTOR-p70s6k pathway, leading to lipid metabolic disorder in skeletal muscle, which might be due to the increment in serums HCA, LCA, and HDCA induced by ammonia exposure in this study. Simultaneously, increased serum BA (including HCA, LCA, and HDCA) caused by ammonia exposure was affected by genera *Clostridium_sensu_stricto_1*, *Terrisporobacter*, *Alloprevotella*, *norank_f_Muribaculaceae*, and *Lactobacillus* indicated by the network analysis or Mantel's correlation in the research. The function of serum low abundance BA, such as TDCA or THDCA, being altered by ammonia exposure to host metabolism needs further *in vitro* trial investigation.

Short-chain fatty acid in the hindgut and specific serum AA (including BCAA and aromatic AA), two other kinds of crucial metabolites interacting with the gut microbiota to affect intestinal health, inflammation, and systemic metabolism (49, 50), was also measured in this study after ammonia exposure. Aerial ammonia exposure increased the content of hindgut acetate in this study. In addition, acetic-producing bacteria *Lactobacillus* increased, and the main reason for increased acetate in the hindgut was that ammonia exposure caused insufficient digestion and absorption of nutrients in pigs, resulting in starch and small molecular sugars entering the hindgut and fermenting to produce more acetate. Multitudinous studies have confirmed that ammonia exposure reduces animal growth performance (7, 51, 52). Despite lower values of BW on day 21 and day 25 in ammonia-exposed pigs, it did not reach the statistical

TABLE 1 | Summary of the altered metabolites from host serum or hindgut chyme after high ammonia exposure.

		Ammonia exposure
Serum AA (16)	BCAA	Ile ↑, Leu ↑, Val ↑
	Aromatic AA	Phe ↑, Tyr ↑
Serum BA	Free-PBA	HCA ↑
	Free-SBA	LCA ↑, HDCA ↑
	TCBA	TDCA ↓, THDCA ↓
		SBA ↑
Serum lipid-related metabolites		TG ↑ (16), ApoB ↑ (16), HDL-C ↓
Serum lipid-related hormones		Leptin ↓
Hindgut SCFA	Cecal SCFA	Total SCFA ↑, acetate ↑, isobutyrate ↓, isovalerate ↓
	Colonic SCFA	Acetate ↑, isobutyrate ↓, isovalerate ↓
Cecal BA	Free-PBA	CA ↓, HCA ↓
	Free-SBA	DCA ↓, LCA ↓, HDCA ↓
	GCBA	GCDCA ↑
		Total BA ↓, SBA↓, GCBA↑

↓ *Indicates decrease and* ↑ *indicates increase.*

level, suggesting that the adverse effect of impaired digestion and absorption of nutrients in the small intestine induced by ammonia exposure on growth performance of pigs could not be seen in the first 25 days. Simultaneously, undigested or unabsorbed nutrients entering the hindgut to provide substrates for hindgut microbiota might also be crucial for the increased microbial diversity in the hindgut. Studies confirmed that microbial-derived acetate takes part in the increment of fatty acid *de novo* synthesis and antibiotic-treated mice manifest decrement of fatty acid *de novo* synthesis (53), which might partly explain the results, namely disordered serum lipid-related metabolites and a decrease in fatty acid oxidation or an increase in fatty acid synthesis in skeletal muscle after ammonia exposure. Besides, the content of isobutyrate and isovalerate was declined with SCFA-related genera (*Terrisporobacter*, *Turicibacter*, and *Clostridium_sensu_stricto_1*) altered in this study after ammonia exposure. BCAAs are partly produced and metabolized by the gut microbiota, and increased BCAA ciculation with dysbiotic intestinal microbiota is closely associated with metabolic disorders, such as insulin resistance (54, 55). The research found that increased BCAA circulation induced by ammonia exposure was partly explained by altered genera *Ralstonia*, *Akkermansia*, *unclassified_p_Firmicutes*, *Terrisporbacter*, and *Fammilly_XIII_AD3011_group*, and another reason for increased BCAA circulation was the inhibition of BCAA catabolism in skeletal muscle and the liver (unpublished data). Although extremely crucial aromatic AA tryptophan was unaffected by ammonia exposure, serums Phe and Tyr were dramatically increased, which was closely related to altered genera *Ralstonia*, *Akkermansia*, *unclassified_p_Firmicutes*, *Terrisporbacter*, *Fammilly_XIII_AD3011_group*, *Lactobacillus*, and *norank_f_Muribaculaceae.*

CONCLUSION

In conclusion, high ammonia exposure damaged the bacterial composition and community structure of hindgut microbiota in growing pigs, increasing the presence of potentially pathogenic bacteria, such as *Negativibacillus*, *Alloprevotella*, or *Lachnospira*, and decreasing the presence of beneficial bacteria, such as *Akkermansia* or *Clostridium_sensu_stricto_1*. The dysbiotic microbiota caused the increment in hindgut acetate and decrement in cecal BAs (mainly including CA, HCA, DCA, LCA, and HDCA) and led to the increment in serum BAs (primarily involving HCA, LCA, and HDCA), BCAA, or aromatic AA, which might serve as signaling molecules to interact with host metabolism (**Table 1**). This study provides a novel sight to partly explain the metabolism disorder or tissue injury induced by atmospheric ammonia exposure.

DATA AVAILABILITY STATEMENT

The data used to support the findings of this study are available from the corresponding author upon request. The raw data on cecal or colonic digesta microbiota of pigs were deposited in NCBI's Sequence Read Archive (SRA) database and accessible through SRA accession number: PRJNA718995.

ETHICS STATEMENT

The animal study was reviewed and approved by the Experimental Animal Welfare and Ethical Committee of Institute of Animal Science of Chinese Academy of Agricultural Sciences.

AUTHOR CONTRIBUTIONS

ST, RZ, and HZ designed the research. ST, RZ, CY, and DS conducted the research. ST and LC analyzed the data. ST and HZ wrote the study and had primary responsibility for the final content. LL and JX provided the animals and expertise. All authors read and approved the final manuscript.

FUNDING

This research was supported by the National Key Research and Development Program of China (2016YFD0500501), Agricultural Research Outstanding Talents and Innovation Team (2016-nybrc-03), and the Fundamental Research Funds for the Central Institute, the Agricultural Science and Technology Innovation Program (ASTIP-IAS07).

ACKNOWLEDGMENTS

The authors would like to thank Ya Wang for helping with the animal feeding experiment.

SUPPLEMENTARY MATERIAL

The Supplementary Material for this article can be found online at: https://www.frontiersin.org/articles/10.3389/fnut.2021.689818/full#supplementary-material

REFERENCES

1. Zeng Y, Tian S, Pan Y. Revealing the sources of atmospheric ammonia: a review. *Curr Pollut Rep.* (2018) 4:189–97. doi: 10.1007/s40726-018-0096-6
2. Ti C, Xia L, Chang SX, Yan X. Potential for mitigating global agricultural ammonia emission: a meta-analysis. *Environ Pollut.* (2019) 245:141–8. doi: 10.1016/j.envpol.2018.10.124
3. Boyle E. Nitrogen pollution knows no bounds. *Science.* (2017) 356:700–1. doi: 10.1126/science.aan3242
4. Shen D, Wu S, Li Z, Tang Q, Dai P, Li Y, et al. Distribution and physicochemical properties of particulate matter in swine confinement barns. *Environ Pollut.* (2019) 250:746–53. doi: 10.1016/j.envpol.2019.04.086
5. Kim E, Kim BU, Kim HC, Kim S. Direct and cross impacts of upwind emission control on downwind $PM_{2.5}$ under various NH_3 conditions in Northeast Asia. *Environ Pollut.* (2020) 268:115794. doi: 10.1016/j.envpol.2020.115794
6. Xing H, Peng M, Li Z, Chen J, Zhang H, Teng X. Ammonia inhalation-mediated mir-202-5p leads to cardiac autophagy through PTEN/AKT/mTOR pathway. *Chemosphere.* (2019) 235:858–66. doi: 10.1016/j.chemosphere.2019.06.235
7. Xu Y, Li Z, Zhang S, Zhang H, Teng X. miR-187-5p/apaf-1 axis was involved in oxidative stress-mediated apoptosis caused by ammonia via mitochondrial pathway in chicken livers. *Toxicol Appl Pharmacol.* (2020) 388:114869. doi: 10.1016/j.taap.2019.114869
8. Zeng X, Liu R, Li Y, Li J, Zhao Q, Li X, et al. Excessive ammonia inhalation causes liver damage and dysfunction by altering gene networks associated with oxidative stress and immune function. *Ecotoxicol Environ Saf.* (2021) 217:112203. doi: 10.1016/j.ecoenv.2021.112203
9. Xiong Y, Tang X, Meng Q, Zhang H. Differential expression analysis of the broiler tracheal proteins responsible for the immune response and muscle contraction induced by high concentration of ammonia using iTRAQ-coupled 2D LC-MS/MS. *Sci China Life Sci.* (2016) 59:1166–76. doi: 10.1007/s11427-016-0202-8
10. Wang S, Li X, Wang W, Zhang H, Xu S. Application of transcriptome analysis: oxidative stress, inflammation and microtubule activity disorder caused by ammonia exposure may be the primary factors of intestinal microvilli deficiency in chicken. *Sci Total Environ.* (2019) 696:134035. doi: 10.1016/j.scitotenv.2019.134035
11. Li Y, Zhang R, Li X, Li J, Ji W, Zeng X, et al. Exposure to the environmental pollutant ammonia causes changes in gut microbiota and inflammatory markers in fattening pigs. *Ecotoxicol Environ Saf.* (2021) 208:111564. doi: 10.1016/j.ecoenv.2020.111564
12. Shah SWA, Chen D, Zhang J, Liu Y, Ishfaq M, Tang Y, et al. The effect of ammonia exposure on energy metabolism and mitochondrial dynamic proteins in chicken thymus: through oxidative stress, apoptosis, and autophagy. *Ecotoxicol Environ Saf.* (2020) 206:111413. doi: 10.1016/j.ecoenv.2020.111413
13. Zhao F, Qu J, Wang W, Li S, Xu S. The imbalance of Th1/Th2 triggers an inflammatory response in chicken spleens after ammonia exposure. *Poult Sci.* (2020) 99:3817–22. doi: 10.1016/j.psj.2020.04.029
14. Yi B, Chen L, Sa R, Zhong R, Xing H, Zhang H. High concentrations of atmospheric ammonia induce alterations of gene expression in the breast muscle of broilers (*Gallus gallus*) based on RNA-Seq. *BMC Genomics.* (2016) 17:598. doi: 10.1186/s12864-016-2961-2
15. Sa RN, Xing H, Luan SJ, Sun YB, Sun CY, Zhang HF. Atmospheric ammonia alters lipid metabolism-related genes in the livers of broilers (*Gallus gallus*). *J Anim Physiol Anim Nutr.* (2018) 102:e941–7. doi: 10.1111/jpn.12859
16. Tang S, Xie J, Wu W, Yi B, Liu L, Zhang H. High ammonia exposure regulates lipid metabolism in the pig skeletal muscle via mTOR pathway. *Sci Total Environ.* (2020) 740:139917. doi: 10.1016/j.scitotenv.2020.139917
17. Tang S, Xie J, Zhang S, Wu W, Yi B, Zhang H. Atmospheric ammonia affects myofiber development and lipid metabolism in growing pig muscle. *Animals.* (2019) 10:2. doi: 10.3390/ani10010002
18. Grosicki GJ, Fielding RA, Lustgarten MS. Gut microbiota contribute to age-Related changes in skeletal muscle size, composition, and function: biological basis for a gut-muscle axis. *Calcif Tissue Int.* (2018) 102:433–42. doi: 10.1007/s00223-017-0345-5
19. Lahiri S, Kim H, Garcia-Perez I, Reza MM, Martin KA, Kundu P, et al. The gut microbiota influences skeletal muscle mass and function in mice. *Sci Transl Med.* (2019) 11:eaan5662. doi: 10.1126/scitranslmed.aan5662
20. Nay K, Jollet M, Goustard B, Baati N, Vernus B, Pontones M, et al. Gut bacteria are critical for optimal muscle function: a potential link with glucose homeostasis. *Am J Physiol Endocrinol Metab.* (2019) 317:E158–71. doi: 10.1152/ajpendo.00521.2018
21. Zhang Z, Tang H, Chen P, Xie H, Tao Y. Demystifying the manipulation of host immunity, metabolism, and extraintestinal tumors by the gut microbiome. *Signal Transduct Target Ther.* (2019) 4:41. doi: 10.1038/s41392-019-0074-5
22. Fang W, Zhang L, Meng Q, Wu W, Lee YK, Xie J, et al. Effects of dietary pectin on the profile and transport of intestinal bile acids in young pigs. *J Anim Sci.* (2018) 96:4743–54. doi: 10.1093/jas/sky327
23. Pokharel Y, Mouhanna F, Nambi V, Virani SS, Hoogeveen R, Alonso A, et al. ApoB, small-dense LDL-C, Lp(a), LpPLA2 activity, cognitive change. *Neurology.* (2019) 92:e2580–93. doi: 10.1212/WNL.0000000000007574
24. Trieb M, Rainer F, Stadlbauer V, Douschan P, Horvath A, Binder L, et al. HDL-related biomarkers are robust predictors of survival in patients with chronic liver failure. *J Hepatol.* (2020) 73:113–20. doi: 10.1016/j.jhep.2020.01.026
25. Yan H, Diao H, Xiao Y, Li W, Yu B, He J, et al. Gut microbiota can transfer fiber characteristics and lipid metabolic profiles of skeletal muscle from pigs to germ-free mice. *Sci Rep.* (2016) 6:31786. doi: 10.1038/srep31786
26. Lee M, Chang EB. Inflammatory bowel diseases (IBD) and the microbiome-searching the crime scene for clues. *Gastroenterology.* (2021) 160:524–37. doi: 10.1053/j.gastro.2020.09.056
27. Nishino K, Nishida A, Inoue R, Kawada Y, Ohno M, Sakai S, et al. Analysis of endoscopic brush samples identified mucosa-associated dysbiosis in inflammatory bowel disease. *J Gastroenterol.* (2018) 53:95–106. doi: 10.1007/s00535-017-1384-4
28. Lang S, Fairfied B, Gao B, Duan Y, Zhang X, Fouts DE, et al. Changes in the fecal bacterial microbiota associated with disease severity in alcoholic hepatitis patients. *Gut Microbes.* (2020) 12:1785251. doi: 10.1080/19490976.2020.1785251
29. Zhai R, Xue X, Zhang L, Yang X, Zhao L, Zhang C. Strain-specific anti-inflammatory properties of two Akkermansia muciniphila strains on chronic colitis in mice. *Front Cell Infect Microbiol.* (2019) 9:239. doi: 10.3389/fcimb.2019.00239
30. Wang L, Tang L, Feng Y, Zhao S, Han M, Zhang C, et al. A purified membrane protein from Akkermansia muciniphila or the pasteurised bacterium blunts colitis associated tumourigenesis by modulation of CD8(+) T cells in mice. *Gut.* (2020) 69:1988–97. doi: 10.1136/gutjnl-2019-320105
31. Wang C, Huang Z, Yu K, Ding R, Ye K, Dai C, et al. High-salt diet has a certain impact on protein digestion and gut microbiota: a sequencing and proteome combined study. *Front Microbiol.* (2017) 8:1838. doi: 10.3389/fmicb.2017.01838
32. Dong Z, Liu Y, Pan H, Wang H, Wang X, Xu X, et al. The effects of high-salt gastric intake on the composition of the intestinal microbiota in wistar rats. *Med Sci Monit.* (2020) 26:e922160. doi: 10.12659/MSM.922160
33. Grosu IA, Pistol GC, Taranu I, Marin DE. The impact of dietary grape seed meal on healthy and aflatoxin B1 afflicted microbiota of pigs after weaning. *Toxins.* (2019) 11:25. doi: 10.3390/toxins11010025
34. Zhu JJ, Gao MX, Song XJ, Zhao L, Li YW, Hao ZH. Changes in bacterial diversity and composition in the faeces and colon of weaned piglets after feeding fermented soybean meal. *J Med Microbiol.* (2018) 67:1181–90. doi: 10.1099/jmm.0.000766
35. Liu B, Zhu X, Cui Y, Wang W, Liu H, Li Z, et al. Consumption of dietary fiber from different sources during pregnancy alters sow gut microbiota and improves performance and reduces inflammation in sows and piglets. *mSystems.* (2021) 6:e00591–20. doi: 10.1128/mSystems.00591-20
36. Louis P, Flint HJ. Diversity, metabolism and microbial ecology of butyrate-producing bacteria from the human large intestine. *FEMS Microbiol Lett.* (2009) 294:1–8. doi: 10.1111/j.1574-6968.2009.01514.x
37. Larzabal M, Da Silva WM, Multani A, Vagnoni LE, Moore DP, Marin MS, et al. Early immune innate hallmarks and microbiome changes across the gut during Escherichia coli O157: H7 infection in cattle. *Sci Rep.* (2020) 10:21535. doi: 10.1038/s41598-020-78752-x

38. Wang Y, Gao X, Zhang X, Xiao F, Hu H, Li X, et al. Microbial and metabolic features associated with outcome of infliximab therapy in pediatric Crohn's disease. *Gut Microbes.* (2021) 13:1–18. doi: 10.1080/19490976.2020.1865708
39. Harada N, Minami Y, Hanada K, Hanaoka R, Kobayashi Y, Izawa T, et al. Relationship between gut environment, feces-to-food ratio, and androgen deficiency-induced metabolic disorders. *Gut Microbes.* (2020) 12:1817719. doi: 10.1080/19490976.2020.1817719
40. Anhe FF, Nachbar RT, Varin TV, Trottier J, Dudonne S, Le Barz M, et al. Treatment with camu camu (*Myrciaria dubia*) prevents obesity by altering the gut microbiota and increasing energy expenditure in diet-induced obese mice. *Gut.* (2019) 68:453–64. doi: 10.1136/gutjnl-2017-315565
41. Wahlstrom A, Sayin SI, Marschall HU, Backhed F. Intestinal crosstalk between bile acids and microbiota and its impact on host metabolism. *Cell Metab.* (2016) 24:41–50. doi: 10.1016/j.cmet.2016.05.005
42. Wu J, Wang K, Wang X, Pang Y, Jiang C. The role of the gut microbiome and its metabolites in metabolic diseases. *Protein Cell.* (2020) 12:360–73. doi: 10.1007/s13238-020-00814-7
43. Fang W, Wen X, Meng Q, Wu W, Everaert N, Xie J, et al. Alteration in bile acids profile in Large White pigs during chronic heat exposure. *J Therm Biol.* (2019) 84:375–83. doi: 10.1016/j.jtherbio.2019.07.027
44. Jain U, Lai CW, Xiong S, Goodwin VM, Lu Q, Muegge BD, et al. Temporal regulation of the bacterial metabolite deoxycholate during colonic repair is critical for crypt regeneration. *Cell Host Microbe.* (2018) 24:353–63. doi: 10.1016/j.chom.2018.07.019
45. Maruyama T, Tanaka K, Suzuki J, Miyoshi H, Harada N, Nakamura T, et al. Targeted disruption of G protein-coupled bile acid receptor 1 (Gpbar1/M-Bar) in mice. *J Endocrinol.* (2006) 191:197–205. doi: 10.1677/joe.1.06546
46. Vassileva G, Golovko A, Markowitz L, Abbondanzo SJ, Zeng M, Yang S, et al. Targeted deletion of Gpbar1 protects mice from cholesterol gallstone formation. *Biochem J.* (2006) 398:423–30. doi: 10.1042/BJ20060537
47. Chen X, Lou G, Meng Z, Huang W. TGR5: a novel target for weight maintenance and glucose metabolism. *Exp Diabetes Res.* (2011) 2011:853501. doi: 10.1155/2011/853501
48. Zhai H, Li Z, Peng M, Huang Z, Qin T, Chen L, et al. Takeda G protein-coupled receptor 5-mechanistic target of rapamycin complex 1 signaling contributes to the increment of glucagon-like peptide-1 production after roux-en-Y gastric bypass. *EBioMedicine.* (2018) 32:201–14. doi: 10.1016/j.ebiom.2018.05.026
49. Yao Y, Yan L, Chen H, Wu N, Wang D. Cyclocarya paliurus polysaccharides alleviate type 2 diabetic symptoms by modulating gut microbiota and short-chain fatty acids. *Phytomedicine.* (2020) 77:153268. doi: 10.1016/j.phymed.2020.153268
50. Zhou C, Li L, Li T, Sun L, Yin J, Guan H, et al. SCFAs induce autophagy in intestinal epithelial cells and relieve colitis by stabilizing HIF-1alpha. *J Mol Med.* (2020) 98:1189–202. doi: 10.1007/s00109-020-01947-2
51. Drummond JG, Curtis SE, Simon J, Norton HW. Effects of aerial ammonia on growth and health of young pigs. *J Anim Sci.* (1980) 50:1085–91. doi: 10.2527/jas1980.5061085x
52. Wang T, He Q, Yao W, Shao Y, Li J, Huang F. The variation of nasal microbiota caused by low levels of gaseous ammonia exposure in growing pigs. *Front Microbiol.* (2019) 10:1083. doi: 10.3389/fmicb.2019.01083
53. Kindt A, Liebisch G, Clavel T, Haller D, Hormannsperger G, Yoon H, et al. The gut microbiota promotes hepatic fatty acid desaturation and elongation in mice. *Nat Commun.* (2018) 9:3760. doi: 10.1038/s41467-018-05767-4
54. Newgard CB, An J, Bain JR, Muehlbauer MJ, Stevens RD, Lien LF, et al. A branched-chain amino acid-related metabolic signature that differentiates obese and lean humans and contributes to insulin resistance. *Cell Metab.* (2009) 9:311–26. doi: 10.1016/j.cmet.2009.02.002
55. Lynch CJ, Adams SH. Branched-chain amino acids in metabolic signalling and insulin resistance. *Nat Rev Endocrinol.* (2014) 10:723–36. doi: 10.1038/nrendo.2014.171

Conflict of Interest: The authors declare that the research was conducted in the absence of any commercial or financial relationships that could be construed as a potential conflict of interest.

frontiers in Nutrition

ORIGINAL RESEARCH
published: 17 June 2021
doi: 10.3389/fnut.2021.676035

Effect of Dietary Tryptophan on Growth, Intestinal Microbiota, and Intestinal Gene Expression in an Improved Triploid Crucian Carp

Yawei Fu[1,2†], Xiaoxiao Liang[1,2†], Donghua Li[2†], Hu Gao[1], Yadong Wang[1,2], Wenting Li[2], Kang Xu[1,3*] and Fangzhou Hu[3*]

[1] CAS Key Laboratory of Agro-Ecological Processes in Subtropical Region, Hunan Provincial Key Laboratory of Animal Nutritional Physiology and Metabolic Process, National Engineering Laboratory for Pollution Control and Waste Utilization in Livestock and Poultry Production, Institute of Subtropical Agriculture, Chinese Academy of Sciences, Changsha, China, [2] College of Animal Science and Technology, Henan Agricultural University, Zhengzhou, China, [3] State Key Laboratory of Developmental Biology of Freshwater Fish, College of Life Sciences, Hunan Normal University, Changsha, China

OPEN ACCESS

Edited by:
Christophe Lacroix,
ETH Zürich, Switzerland

Reviewed by:
Jun Wang,
Shanghai Ocean University, China
Yongqing Hou,
Wuhan Polytechnic University, China

***Correspondence:**
Kang Xu
xukang2020@163.com
Fangzhou Hu
hufangzhou90@163.com

[†] These authors have contributed equally to this work

Specialty section:
This article was submitted to Nutrition and Microbes, a section of the journal Frontiers in Nutrition

Received: 04 March 2021
Accepted: 20 May 2021
Published: 17 June 2021

Citation:
Fu Y, Liang X, Li D, Gao H, Wang Y, Li W, Xu K and Hu F (2021) Effect of Dietary Tryptophan on Growth, Intestinal Microbiota, and Intestinal Gene Expression in an Improved Triploid Crucian Carp. Front. Nutr. 8:676035. doi: 10.3389/fnut.2021.676035

Tryptophan (Trp) has received increasing attention in the maintenance of intestinal function. In this study, improved triploid crucian carp (ITCC) fed diets containing 6.35 g kg^{-1} Trp had higher average daily gain (ADG) and improved villus height (VH) and crypt depth (CD) in the intestine compared to the control group. To elucidate the potential mechanisms, we used RNA sequencing (RNA-seq) to investigate changes in the intestinal transcriptome and 16S rRNA gene sequencing to measure the intestinal microbiota in response to 6.35 g kg^{-1} Trp feeding in ITCC. Dietary Trp altered intestinal gene expression involved in nutrient transport and metabolism. Differentially expressed transcripts (DETs) were highly enriched in key pathways containing protein digestion and absorption and the AMPK signaling pathway. 16S rRNA sequencing showed that 6.35 g kg^{-1} Trp significantly increased the abundance of the genus *Cetobacterium*, and the Firmicutes/Bacteroidetes ratio at the phylum level ($P < 0.05$). In addition, bacterial richness indices (Simpson index) significantly increased ($P < 0.05$) community evenness in response to 6.35 g kg^{-1} Trp. In conclusion, appropriate dietary Trp improves the growth performance, and influences the intestinal flora of ITCC. This study might be helpful to guide the supply of dietary exogenous Trp in ITCC breeding.

Keywords: tryptophan, improved triploid crucian carp, transcriptome, intestinal flora, 16S rRNA

INTRODUCTION

Improving the growth rate and feed conversion rate of fish is essential for the sustainable development of aquaculture (1, 2). Amino acids play important roles in the nutrient metabolism of cultured fishes. Dietary nutrients affect gut microbial diversity and composition (3). Numerous studies describe the link between Trp metabolism and fish health (4). Trp cannot be synthesized exogenously in fish, and must be obtained via food (5, 6). Appropriate feeding of Trp has positive effects on the growth performance and intestinal health status of fish by regulating intestinal immune tolerance, maintaining microbial homeostasis, and inhibiting inflammation (5, 6).

Besides, there is growing evidence that Trp deficiency could cause negative impacts on growth performance in fish (7–9). For example, fish growth performance and the structural integrity of the intestines were altered in a Trp deficient scenario, which translated into lower disease resistance (6, 10). Similarly, Trp deficiency causes depressed growth and efficiency of feed conversion and low protein retention, as reported for other fish species (11–14).

The microbial balance of the intestinal flora is associated with the gut health, which can be affected by dietary constituents and commensal bacteria (15, 16). The intestinal flora could affect food digestion and absorption, and nutrients can also affect the composition of intestinal microbes (17, 18). Previous studies have demonstrated that Trp could alter the intestinal microbial composition and diversity (19). The metabolism of Trp by the intestinal microbiome could also affect intestinal homeostasis (20, 21). Trp catabolites are essential signaling molecules in microbial communities, and important mediators for regulating a diverse array of physiological systems in fish (4). Gut microbes are primary participants in Trp metabolism; it is estimated that 90% of serotonin in the human body is produced by gut microbes (22).

In our previous studies, the ITCC was produced by crossing improved tetraploid males with improved diploid female red crucian carp, which has excellent traits of fast growth rate and sterility (23). With the expansion of improved triploid crucian carp farming, the breed of ITCC and research on the development of its feeding should be developed. However, information regarding the effects of amino acids on the growth performance and intestinal health status of ITCC is lacking. Moreover, little information has been done on the effect of Trp on the growth performance and intestinal health of ITCC. In this study, we aimed to explore the effects of Trp supplementation on growth, intestinal microbiota, and intestinal gene expression in ITCC. This study will provide guidance for developing effective nutritional strategies and feeding practices to improve ITCC health.

MATERIALS AND METHODS

Ethics Statement

All experimental animals used in this study were treated humanely, following the Animal Welfare Committee of the Institute of Subtropical Agriculture (201703-64C), Chinese Academy of Sciences, Changsha, China.

Experimental Animals and Tissue Samples

A total of 450 healthy ITCC and weight-matched ITCC (23) were randomly divided into five groups, with three biological replicates of each group, and 30 fishes per biological replicate. The Trp concentrations in the five experimental diets were determined to be 1.85 (control), 3.35, 4.85, 6.35, and 7.85 g kg^{-1} Trp diet (basal diets supplemented with 0, 1.5, 3.0, 4.5, and 6.0 g kg^{-1} Trp). The fishes were weighed at the beginning and end of the 4-week feeding trial.

Sample Collections

At the end of the feeding trial, all the experimental fish fasted for 12 h. Three fish from each replicate (a total of 45 fish) were randomly selected, anesthetized, sacrificed, and sampled according to the method described in a previous study (24). For other biochemical parameters and molecular analysis, the intestinal tract and distal intestinal contents were quickly removed, frozen in liquid nitrogen, and stored at −80°C until use. Meanwhile, we collected section samples from each group and fixed them in a 4% paraformaldehyde solution for histologic analysis (25).

RNA Extraction

Transcriptome sequencing was performed on a total of 6 samples from the 6.35 Trp group (6.35 g kg^{-1} Trp diet group) and the 1.85 Trp group (control group). Total RNA was isolated from the intestinal tract of fish using an RNAiso Plus kit (Takara, Kyoto, Japan). Total RNA was purified using a TruSeq RNA Sample Prep Kit 52 (New England Biolabs, Ipswich, MA, USA). RNA degradation and contamination were detected using 1% agarose gels. The purity of the total RNA was assessed with a NanoPhotometer® spectrophotometer (IMPLEN, CA, USA). The total RNA concentration was measured using a Qubit® RNA Assay Kit in Qubit® 2.0 Fluorometer (Life Technologies, CA, USA). The integrity of the total RNA was estimated using an RNA Nano 6000 Assay Kit of the Bioanalyzer 2100 system (Agilent Technologies, CA, USA).

Library Preparation for Transcriptome Sequencing

Three samples were pooled to make one biological replicate and experiment was done using three technical replicates. A total amount of 1.5 μg RNA per sample was used as input material for the RNA sample preparations. Sequencing libraries were generated using the NEBNext® Ultra™ RNA Library Prep Kit of Illumina® (NEB, USA) following the manufacturer's protocols, and index codes were added to attribute sequences to each sample. Briefly, mRNA was purified from total RNA using poly-T oligo-attached magnetic beads. Fragmentation was carried out using divalent cations under elevated temperature in NEBNext First Strand Synthesis Reaction Buffer (5X). First-strand cDNA was synthesized using random hexamer primers and M-MuL5 Reverse Transcriptase (RNase H). Second strand cDNA synthesis was subsequently performed using DNA Polymerase I and RNase H. The remaining overhangs were converted into blunt ends via exonuclease/polymerase activities. After adenylation of the 3′ ends of DNA fragments, NEBNext adaptor with a hairpin loop structure was ligated to prepare for hybridization. To preferentially select cDNA fragments 250–300 bp in length, the library fragments were purified with the AMPure XP system (Beckman Coulter, Beverly, USA). Then, 3 μl of USER Enzyme (NEB, USA) was used with size-selected, adaptor-ligated cDNA at 37°C for 15 min followed by 5 min at 95°C before PCR. Then PCR was performed with Phusion High-Fidelity DNA polymerase, universal PCR primers, and Index (X) Primer. Finally, PCR products were purified (AMPure XP system), and library quality was assessed on the Agilent Bioanalyzer 2100 system.

RNA-Seq Data Analysis

Clustering of the index-coded samples was performed on a cBot Cluster Generation System using TruSeq PE Cluster Kit 53-cBot-HS (Illumina) according to the manufacturer's instructions. Differential expression analysis of two groups (three biological replicates per group) was performed using the DESeq R package (1.10.1) (26). DESeq provides statistical routines for determining differential expression in digital gene expression data using a model based on the negative binomial distribution. The resulting *P*-values were adjusted using Benjamini and Hochberg's approach to control the false discovery rate. Genes with an adjusted $P < 0.05$ found by DESeq were assigned as differentially expressed. To obtain significantly different genes, we set the screening criteria as *P*-value (padj) $\leq$ 0.001 and difference multiple $|\text{FoldChange}| \geq 2$. Cluster analysis was used to cluster genes with the same or similar expression patterns, which might have similar functions or participate in the same biological process. Cluster analysis of a heat-map for DEGs was performed by the pheatmap R package (27).

Gene function was annotated based on the following databases: Nr (NCBI non-redundant protein sequence, ftp://ftp.ncbi.nih.gov/blast/db/); Nt (NCBI non-redundant nucleotide sequence); Pfam (Protein family http://pfam.xfam.org/); KOG/COG (Clusters of Orthologous Groups of proteins, http://www.ncbi.nlm.nih.gov/KOG/); Swiss-Prot (a manually annotated and reviewed sequence database http://www.uniprot.org/); KO (KEGG Ortholog database, http://ccb.jhu.edu/software/tophat/index.shtml); GO (Gene Ontology, and STRING database. The Protein–protein interaction networks (PPIs) information of these DEGs were predicted by STRING database. After mapping the DEGs into this database, and a combined score $\geq$0.4 were exported. Then, the PPIs of these SDEGs were visualized in Cytoscape, and the hub genes among the PPI network were identified and ranked using CytoHubba plugin and the maximal clique centrality (MCC) method of Cytoscape software (28).

Real-Time PCR Analysis

We randomly selected 8 genes (including four upregulated genes and four downregulated genes) for real-time PCR in 1.85Trp and 6.35Trp groups to confirm the reproducibility and accuracy of the RNA-seq gene expression data. Using an RNAiso Plus kit (Takara, Kyoto, Japan), total RNA was isolated from intestinal tract tissues of fishes. After checking the RNA quality, as described in the RNA extraction section, reverse transcription was performed using the PrimeScript™ RT Reagent Kit with gDNA Eraser (Takara, Kyoto, Japan) according to the manufacturer's protocol. Real-time PCR experiments were performed using a LightCycler® 96 Real-Time PCR system (Roche Applied Science) in a 25 μL reaction volume containing 12.5 μL of 2 ×SYBR® Premix Ex TaqTM II (Tli RNaseH Plus; Takara, Kyoto, Japan), 1.25 μL each of the forward and reverse primers (10 μM), 8 μL of deionized water, and 2 μL (∼100 ng) of cDNA. The β-actin gene was used as the reference gene, and the primers of eight genes were designed using Primer. The thermal cycling conditions were 3 min at 95°C, followed by 37 reaction cycles (95°C for 30 s, 60°C for 30 s, and 72°C for 30 s), and an extension for 10 min at 72°C. We calculated the relative gene expression levels with the comparative CT method (referred to as the $2^{-\Delta\Delta CT}$ method) (29), with three replicates for each reaction.

DNA Extraction, 16S rRNA Sequencing

DNA was extracted from the intestinal contents using a fecal DNA kit (Omega, USA) and then eluted in a 50 μL eluent buffer. The primers (F:5′-ACTCCTACGGGAGGCAGCAG-3′; R: 5′-GGACTACHVGGGTWT-CTAAT-3′) were used in the PCR amplification for the V3–V4 region of the bacterial 16S rRNA gene. PCR analysis was performed with 25 μL reactions containing 12.5 μL of PCR premix, 2.5 μL of each primer, 25 ng of template DNA, and PCR-grade water to equalize the final volumes. The PCR products were detected by 2% agarose gel electrophoresis and then purified using a gel recovery kit (Thermo Scientific, USA). The libraries were constructed using the Ion Plus Fragment Library Kit 48 reactions library building kit (Thermo Fisher, USA) and qualified by Qubit quantification and library assay, Single-ended sequencing was performed using Ion S5TMXL (Thermo Fisher, USA).

The clean reads of all samples were clustered using UPARSE software. The sequences were clustered into OTUs with 97% identity, and the sequences with the highest frequency of occurrence were selected as the representative sequences of OTUs. Species annotation analysis was performed using the Mothur method with the SSU rRNA database of SILVA132 for classification (threshold set between 0.8 and 1). Multiple sequence alignment was performed using MUSCLE software, and then the data were homogenized. Alpha diversity analysis and beta diversity analysis were based on the homogenized data. PCoA was plotted using R software (Version 2.15.3). The WGCNA, stats and ggplot2 were used for PCoA analysis. LEfSe was performed by LEfSe software.

Statistical Analysis

The qRT-PCR validation data were analyzed by using SPSS 18.0 (SPSS, USA). The significance of the difference between two groups was analyzed by Student's *t*-test. Differences were considered significant if the $P < 0.05$ and $P < 0.01$ were considered extremely significant. The results are presented as the mean and standard error of the mean (SEM).

RESULTS

Growth Performance and Gut Morphology

As shown in **Figure 1**, the average final weight and the ADG were significantly ($P < 0.05$) increased as affected by dietary 6.35 g kg^{-1} Trp levels compared with the control group. In this study, compared with the control group, dietary supplementation with different doses of Trp significantly altered the VH and CD ($p < 0.05$) in ITCC, and the effect was obvious when the fish were fed a diet containing 6.35 g kg^{-1}Trp, while there was no difference in the ratio of VH to CD (**Table 1**).

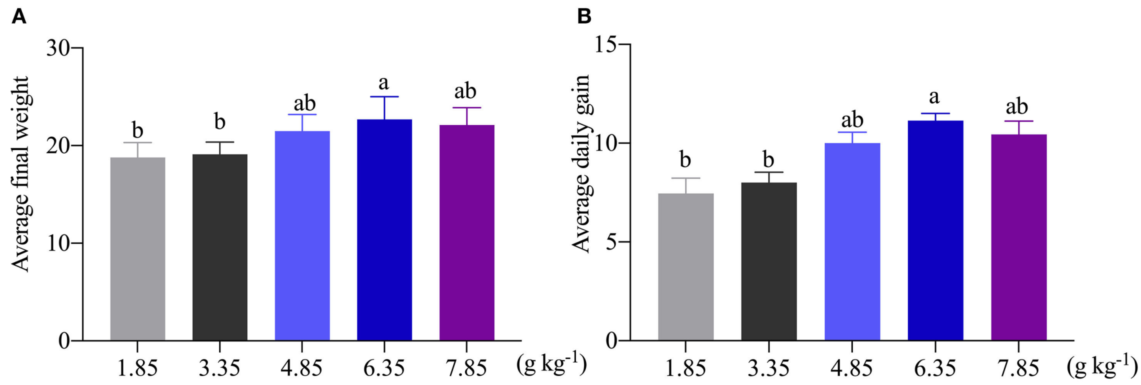

FIGURE 1 | Effects of dietary tryptophan on the growth performance of ITCC. **(A)** Average final weight of ITCC. **(B)** The average daily gain of ITCC. The Trp concentrations in the five experimental diets were determined to be 1.85 (control), 3.35, 4.85, 6.35, and 7.85 g kg^{-1} Trp diet (basal diets supplemented with 0, 1.5, 3.0, 4.5, and 6.0 g kg^{-1} Trp).

TABLE 1 | The effect of tryptophan on the morphology of the intestine in ITCC.

Item	1.85 Trp	6.35 Trp	*p*
Villous height, μm	331.68 ± 28.32^b	548.48 ± 82.46^a	0.003
Crypt depth, μm	94.12 ± 12.33^b	152.54 ± 33.28^a	0.001
VH:CD ratio	3.59 ± 0.62	4.03 ± 0.80	0.092

VH:CD ratio, villous height to crypt depth ratio.
^{a,b}Means without a common superscript in the same row differ ($P < 0.05$).
All the data were presented as mean ± SEM. They were subject to t-test.

RNA-Seq Analysis

To reveal the molecular regulatory mechanism, we used the pooled total RNA of the control and 6.35 g kg^{-1} Trp diet groups. The cDNA library of six intestinal tissues (1.85Trp_1, 1.85Trp _2, and 1.85Trp _3 from the control group; 6.35Trp _1, 6.35Trp _2, and 6.35Trp _3 from the group fed 6.35 g kg^{-1} Trp diets) were sequenced on an Illumina HiSeq platform, with 3.11 million reads in total being generated, of which 97.5% (3.04 million) passed the filter for clean reads. The GC contents of the clean reads were 45.61–47.29% (**Supplementary Table 1**). By comparing to the sequencing data of the two groups, 155,547 transcripts were identified, of which 140,907 and 143,462 transcripts were identified in the 6.35 Trp group and control group, respectively.

In total, we found 3,263 differentially expressed transcripts (1,443 upregulated and 1,820 downregulated transcripts) in the 6.35 Trp group compared with the control group (**Supplementary Table 2**). The heat map of cluster analysis of DETs showed that the gene expression patterns of DETs were clustered within groups, while the difference between the two groups was significant (**Figure 2**).

GO Enrichment Analysis of DETs

GO enrichment analysis was performed with 1,654 DETs. A total of 2,730 GO terms were enriched, including 1,559 biological process terms, 430 cellular component terms and 741 molecular function terms (**Supplementary Table 3**). The top 30 most significantly enriched GO terms are shown in **Figure 3**. The top GO terms of the 1,164 upregulated transcripts were molecular function including motor activity and ion binding. The top GO terms of the 490 downregulated transcripts were solute: sodium symporter activity, neurotransmitter transporter activity, and neurotransmitter: sodium symporter activity. The top 22 GO terms in the molecular functions are shown in **Figure 3**, including motor activity, ATP binding, adenyl ribonucleotide binding, and anion binding so on. As shown in **Figure 3**, the top 2 GO terms belong to the cellular component category, including the myosin complex and the actin cytoskeleton.

KEGG Pathway Analysis of DETs

The DETs were annotated into 273 KEGG pathways (**Supplementary Table 4**). The top 10 enriched pathways of the DETs are shown in **Table 2**. With regard to the KEGG pathway analysis of the upregulated genes, 11 pathways were enriched including "fatty acid biosynthesis," "AMPK signaling pathway," "protein digestion and absorption," "butanoate metabolism," and "Terpenoid backbone biosynthesis." With regard to KEGG pathway analysis of the downregulated genes, 19 pathways were enriched, including "bile secretion," "mineral absorption," "renin-angiotensin system," "cell cycle," "carbohydrate digestion and absorption," and "PPAR signaling pathway."

Protein-Protein Interaction (PPI) Network Analysis

After importing the PPI network of DETs, Cytoscape displayed modules in the default MCODE settings. Genes in these modules were then assembled for enrichment analysis using DAVID. Among them, the "metabolic pathways" was identified as the most significant pathway. Twenty-nine significant pathways were enriched in KEGG pathways. Based on the STRING database, the PPI network of 566 nodes and 2,154 protein pairs was obtained with a combined score >0.7 (**Supplementary Table 5**). In total, one module (module 1) with a score >13 was detected by MCODE. The hub gene ubiquitin A-52 residue

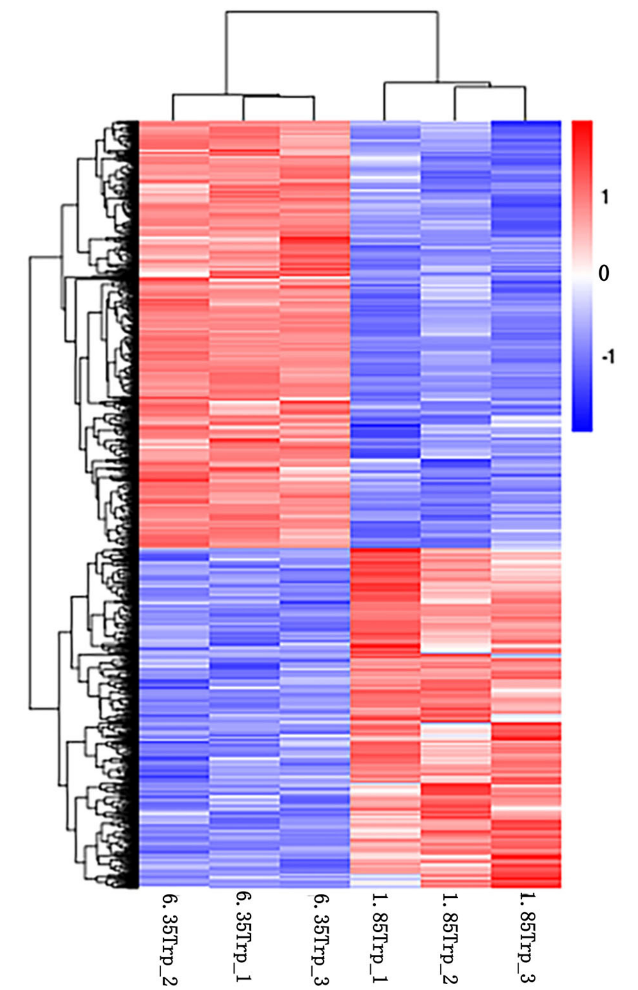

FIGURE 2 | Cluster analysis of DETs by the FPKM value. The X-axis indicates the samples in the different groups. The sample on the left is from the 6.35 Trp group, and the sample on the right is from the 1.85 Trp group. The Y-axis is the gene cluster across the 1.85 and 6.35 Trp groups. Color from red to blue, indicated that the log10 (FPKM+1) values were from large to small, red color indicates high expression level and blue color indicates low expression level.

ribosomal protein fusion product 1 (*UBA52*) (padj = 0.01911, $\log_2 FC = -2.4374$) was identified with Cytohubba and MCODE (**Supplementary Table 6**; **Figure 4**).

Real-Time PCR Validation

The real-time PCR results were consistent with the RNA-seq data (**Figure 5**). Eight transcripts were selected, and the RNA-seq data were further evaluated by real-time PCR experiments. The relative expression levels of carboxypeptidase A1 (*CPA1*), carboxypeptidase A5 (*CPA5*), chymotrypsin-like (*CTRL*), and endoplasmic reticulum resident protein 27-like (*Erp27*) were significantly increased in the 6.35 Trp group compared to those in the control group. In addition, the relative expression levels of period circadian protein homolog 1-like (*LOC109066737*), neuraminidase 3 (*NEU3*), period circadian regulator 2 (*Per2*), and single-stranded DNA binding protein 4 (*ssbp4*) were significantly decreased in the 6.35 Trp group compared to the control group.

Gut Microbial Composition

OTUs were defined as a read sharing 97% nucleotide-sequence identity (**Supplementary Table 7**). The number of observed species and indices of Shannon, Simpson, and Chao1 did not differ between the 6.35 Trp and control groups (**Figure 6**). Compared to the control group, the Simpson index ($P < 0.05$) in the 6.35 Trp group was decreased significantly, which indicated that the bacterial diversity was increased after 6.35 g kg^{-1} Trp diets treatment. PCoA is a comparative analysis of the microbial community composition of different samples (**Figure 7**). The unweighted UniFrac distance-based PcoA results showed that the microbiota compositions of the control group and the 6.35 Trp group were overt changes.

To identify the significantly different species of gut microbes between the control and 6.35 Trp groups, we analyzed the microbial community profiles using LEfSe software (**Figure 8**). There were seven significantly different biomarker, with enrichment of *p_Fusobacteria*, *o_Fusobacteriales*, *c_Fusobacteria*, *g_cetobacterium,* and *f_Fusobacteriaceae* in the 6.35 Trp group and *c_Bacteroidia*, and *c_Bacteroidetes,* in the control group. At the genus level, compared to the control group, Cetobacterium was significantly more abundant in the 6.35 Trp group ($P < 0.05$). At the phylum level, the abundance of *Fusobacteria* increased, but the abundance of *Proteobacteria* decreased in the 6.35 Trp group. The Firmicutes /B acteroidetes ratio was increased compared to that of the control group ($P < 0.05$).

DICUSSION

Growth Performance

Trp, an essential amino acid, is important for metabolic functions in fish (30–32). Some Trp metabolites are also important mediators to regulate partial physiological functions in fish (4). Previous studies have reported that different dietary levels of Trp affect growth performance in many fish, including juvenile silver catfish, and fingerling Indian catfish (11, 33). Trp improved hybrid catfish growth performance, digestive, and absorptive abilities (34). In this study, we found that the growth performance of ITCC increased as the dietary Trp levels increased (up to 6.35 g kg^{-1}). This result supports that optimal dietary Trp could improve the growth performance and feed efficiency as reported in juvenile Jian carp (*Cyprinus carpio* var. Jian) (13), silver catfish (33), red drum (14), Indian catfish (Ahmed et al., 2012), and Nile tilapia (35). Analogously, increases in the dietary Trp concentrations can promote the ADG, and a certain dose-dependent relationship has been found between dietary Trp and the growth performance of fishes (36–40). However, another study showed that dietary supplementation with Trp had no effects on the growth performance and body proximate of seabream (Sparus aurata) (41). A possible reason for

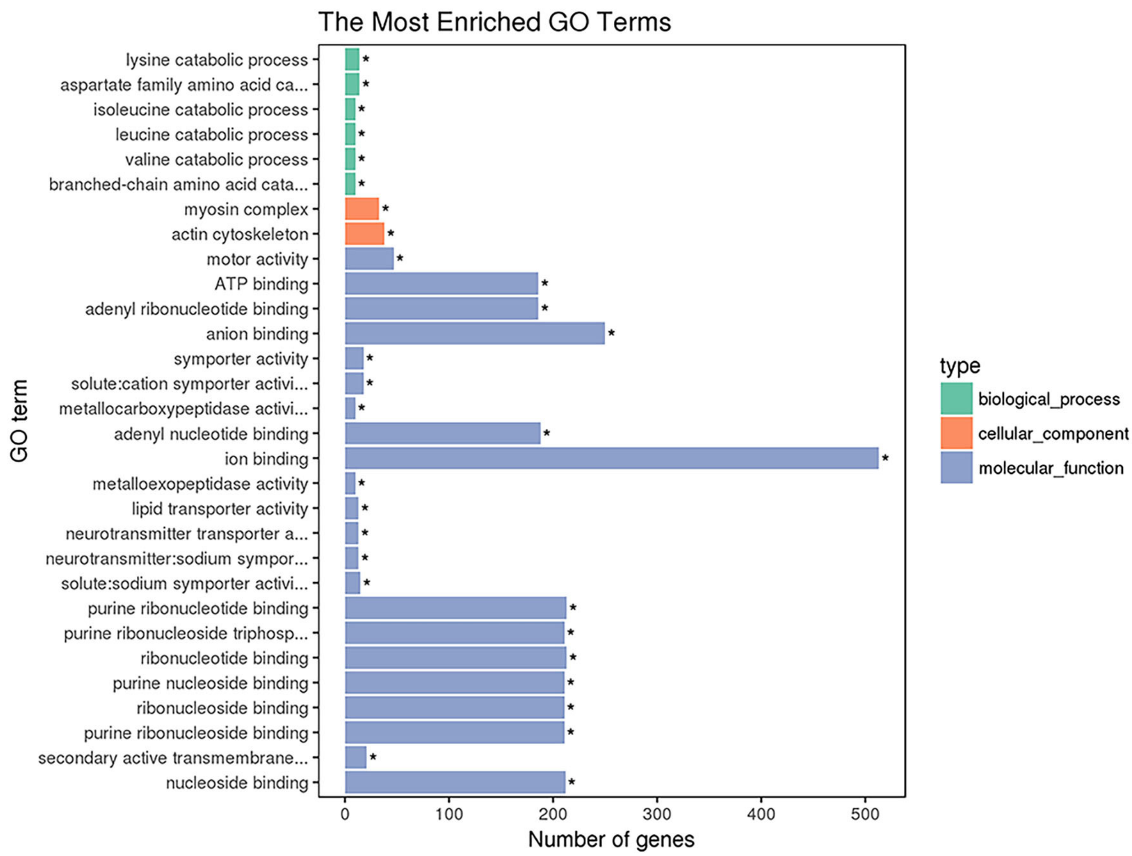

FIGURE 3 | The enriched GO terms of the DETs. The X-axis indicates the number of DETs for each GO term; the y-axis corresponds to the GO terms. *represent the significantly enriched terms ($p < 0.05$).

TABLE 2 | The top 10 significantly enriched KEGG pathway of DEGs.

ID	KEGG term	Corrected *P*-value
ko00061	Fatty acid biosynthesis	0.0000
ko04974	Protein digestion and absorption	0.0000
ko00650	Butanoate metabolism	0.0001
ko04152	AMPK signaling pathway	0.0001
ko00900	Terpenoid backbone biosynthesis	0.0001
ko04977	Vitamin digestion and absorption	0.0002
ko04973	Carbohydrate digestion and absorption	0.0011
ko00640	Propanoate metabolism	0.0013
ko04975	Fat digestion and absorption	0.0015
ko00140	Steroid hormone biosynthesis	0.0049

this discrepancy may be related to ethnic differences and different diets.

Trp Improved the Intestinal Morphology of ITCC

The integrity of the intestine is important for nutrient uptake and intestinal health (42–44). Generally, digestion and absorption depend on intestinal growth and development, as well as the activities of digestive enzymes in fish. The VH and CD are important indices of the functional capacity of enterocytes, and the VH: CD ratio affects the nutrient digestibility and absorption capacity of the intestinal mucosa (45, 46). The improvement of intestinal morphology was associated with increased nutrient absorption and growth performance of fish (47). Previous studies have demonstrated that fish have a special need for Trp in epithelial structures. Optimal Trp exerts beneficial effects on maintaining the intestinal structural integrity and intestinal development of fish (13, 48). In this study, feeding 6.35 g kg^{-1} Trp diets significantly increased villus height and crypt depth, which suggests that dietary Trp can influence the morphological structure of the intestine, which might be associated with nutrient digestion and absorption. Similar results showed that Trp improves the digestive and absorption capacity of fish (34, 49).

Trp Regulated the Expression of Genes in the Intestine of ITCC

Regarding the molecular mechanism by which Trp affects intestinal morphology, pathway enrichment of DEGs summarizes the complex networks of genes.

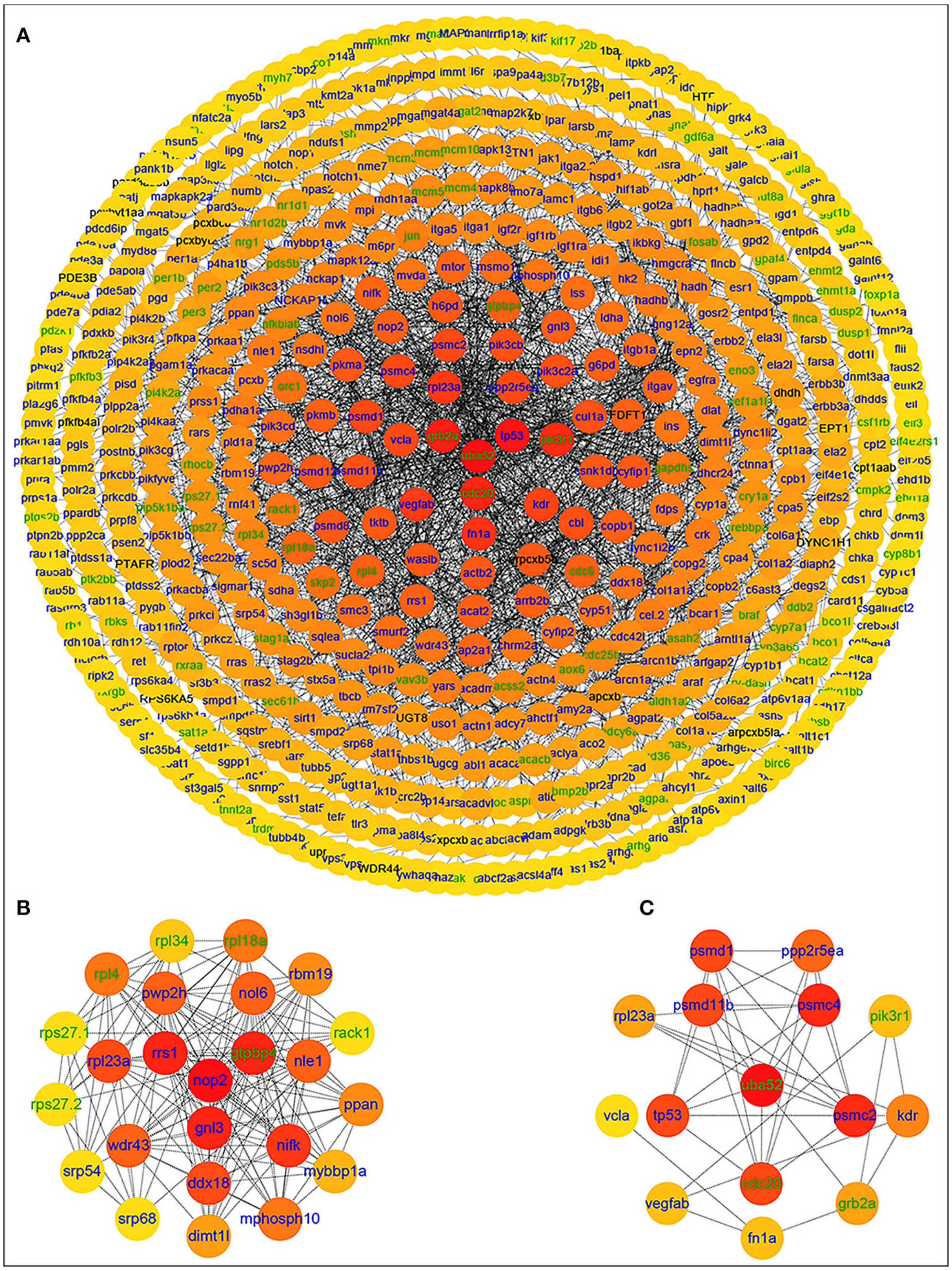

FIGURE 4 | PPI network of differentially expressed genes in the group fed 6.35 g kg^{-1} Trp diets compared with the control group and two significant modules identified among the PPI network using the molecular complex detection method with a score of >13. Blue nodes represent the upregulated genes; green nodes represent the downregulated genes; **(A)** PPI network of differentially expressed genes in the group fed 6.35 g kg^{-1} Trp diets compared with the control group; **(B)** module 1, MCODE score = 23; **(C)** protein-protein interaction network of 15 hub genes.

Fatty Acid Biosynthesis

Fatty acid biosynthesis capacity of fish varies among species, with trophic level hypothesized as a major factor (50). Fatty acid catabolism is a major source of energy in salmonid fish (51). In the present study, 6.35 g kg^{-1} Trp gut samples showed an upregulated expression of genes enriched significantly in Fatty acid biosynthesis signaling pathway (*ACSL*, *FADD*, *ACACA*, and *FASN*) compared with control group. This indicated that 6.35 g kg^{-1} Trp intake further promoted fatty acid biosynthesis in ITCC. Acetyl-CoA carboxylase (*ACACA*) and fatty acid synthase (*FASN*) are important rate-limiting enzymes that play a critical role in body weight differences in abdominal adipose tissue of growing animals (52). *FASN* plays a crucial role in the process from lipogenesis and is physiologically modulated by energy

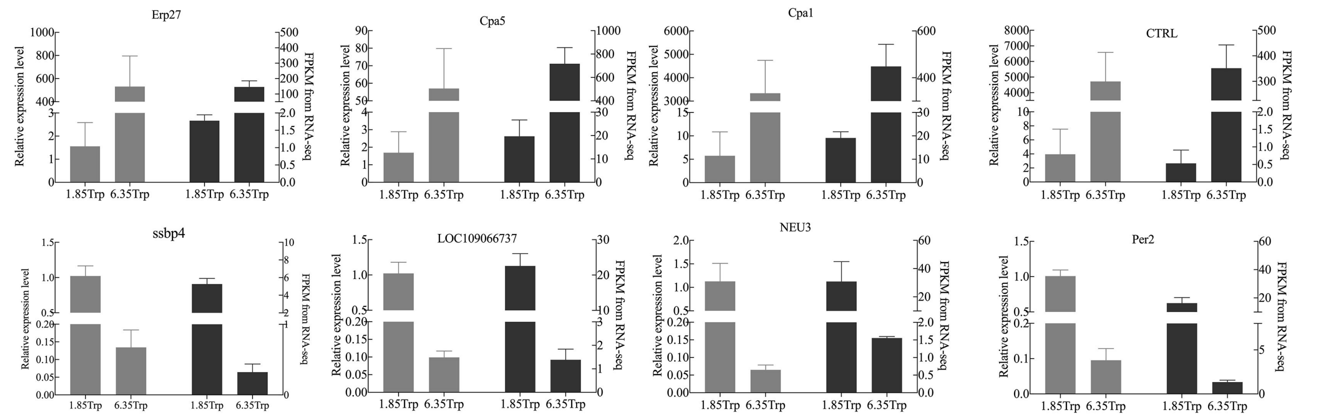

FIGURE 5 | Comparison of the gene expression levels of RNA-seq with real-time PCR. The right axis represents the expression levels determined by RNA-seq in FPKM units, and the left axis represents gene expression levels determined by real-time PCR. Bars represent the mean (±SE) of three samples. The black column indicates the FPKM value; the grey column indicates the real-time PCR using β-actin as a reference gene. Data represent relative mRNA expression of **(A)** *Erp27*, **(B)** *CPA5*, **(C)** *CPA1*, **(D)** *CTRL*, **(E)** *LOC109066737*, **(F)** *ssbp4*, **(G)** *NEU3*, and **(H)** *Per2* determined by quantitative real-time PCR.

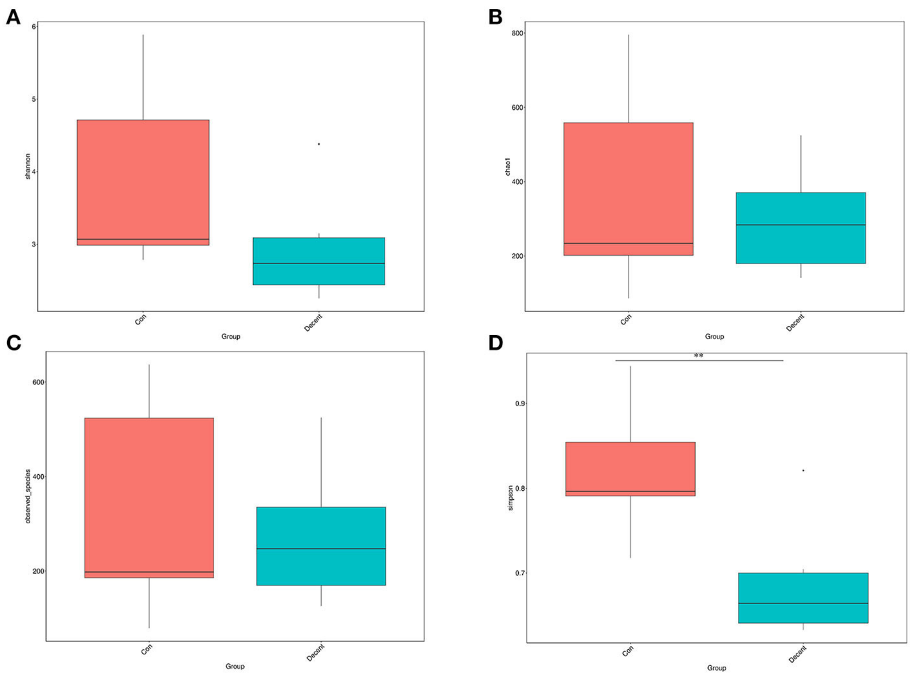

FIGURE 6 | Alpha diversity of the gut microbiota in control group and 6.35Trp group. **(A)** Shannon's diversity index. **(B)** Chao1. **(C)** Observed-species. **(D)** Simpson. **$p < 0.01$ vs. control group by Tukey's *post-hoc* test.

balance (53). So, the expression of *FASN* may be a good non-invasive indicator to study the role of Trp in growth and in studies on fatty acid biosynthesis in ITCC. Therefore, studying the regulation of *Fatty acid biosynthesis* has great significance for improving gut health.

Protein Digestion and Absorption

Fish growth is based on the digestion and absorption of nutrients (54). Fish are known to utilize proteins preferentially to lipids or carbohydrates as energy sources (55). Amino acids are important energy sources, satisfying 14–85% of the energy needs of teleost fish (54). A previous study showed that dietary Trp could improve the digestion and absorption ability of juvenile Jian carp (*Cyprinus carpio var*. Jian) (13). In this work, numerous genes related to "protein digestion and absorption" were upregulated in the intestine of fish fed 6.35 g kg^{-1} Trp diets, indicating that dietary Trp might influence associated with changed intestinal function in protein digestion and absorption of ITCC.

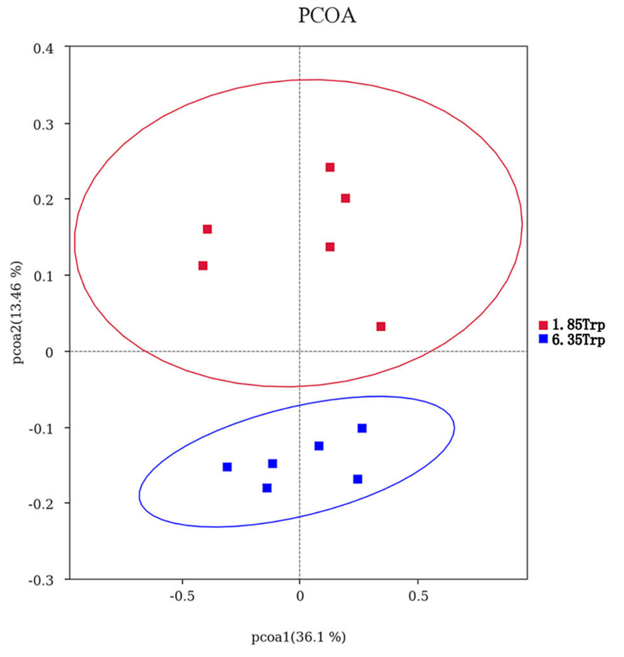

FIGURE 7 | Principal coordinate analysis (PCoA) of the microbial community composition of the control group and 6.35 Trp group. Horizontal coordinates indicate one principal component, vertical coordinates indicate another principal component, and percentages indicate the value of the principal component's contribution to sample differences; each point in the graph represents a sample, and samples from the same group are represented using the same color. Blue represents the 6.35 Trp group, and red represents the 1.85 Trp group.

AMPK Signaling Pathway

TOR can activate the AMPK signaling pathway and control the growth response of cells to nutrients, especially amino acids (56). *TOR* is a nutrient sensor that can affect cell growth by regulating of protein synthesis (57, 58). Previous studies have reported that dietary Trp supplementation increased the expression of *TOR* and *S6K1* mRNA levels and the phosphorylation level of *TOR* and *S6K1* in grass carp muscle (59, 60). In this work, dietary Trp levels (6.35 g kg^{-1} Trp diet) upregulated the relative expression of *TOR* mRNA in the intestinal tract, in agreement with the finding that dietary Trp increased the expression of *TOR* in hybrid catfish (34). Conversely, another study showed that dietary Trp improved young grass carp growth, which may be related to the downregulation of *TOR* in the intestine of young grass carp (36). These results suggest that Trp may activate the AMPK signaling pathway to coordinate nutrient uptake in fish through regulation of *TOR* gene expression. However, the mechanisms require further study.

Intestinal Microorganism and Tryptophan

Trp plays important roles in maintaining gut microflora and intestinal health. Deficiency in dietary Trp could alter the gut microbial community (61). In this study, we found that 6.35 g kg^{-1} Trp significantly increased the abundance of *Cetobacterium*, and the Firmicutes/Bacteroidetes ratio at the phylum level ($P < 0.05$). A study by Liang et al. reported that Trp can increase intestinal species richness (62). Studies have shown that the ratio of Firmicutes/Bacteroidetes is related to increased energy harvesting and growth performance (63–65). Similarly, it was found that the higher the ratio of the relative abundance of *Firmicutes* to *Bacteroidetes* in grass carp, the faster the growth of the fish (66). It is worth noting that Trp increased the richness and diversity of the intestinal microbiota, perhaps partly because Trp promoted the growth of the intestinal villi, thus increasing the nutrients available to the intestinal flora (34, 62, 67).

Moreover, *Cetobacterium* has been identified as an important component of gut microbiota in freshwater fishes, which is an indicator of healthy fish (68–71). A previous study found the effect of diet on the abundance of *Cetobacterium* in the intestine of zebrafish (72). Numerous studies have confirmed the effect of *Cetobacterium* on the digestion and absorption of food, and the general growth and development process of fishes (Yunlong Grouper, common carp, and tilapia) (73, 74). In the present study, the abundance of *Cetobacterium* was increased significantly by 6.35 g kg^{-1} Trp treatment in ITCC, suggesting that *Cetobacterium* might play a crucial role in digestive and nutritional processes.

In addition, it was also found that in the 6.35 Trp group, the abundance of *Fusobacteria* increased after dietary with 6.35 g kg^{-1} Trp. *Fusobacteria* is the most dominant phylum in the fish intestine and it may have a lasting positive impact on intestinal function (17, 75). *Fusobacteria* may be involved in the digestive process of fish by providing a variety of enzymes (76). Previous studies have shown that Trp catabolites are absorbed through the intestinal epithelium and enter the bloodstream, affecting host physiology and promoting intestinal and systemic homeostasis (31). Thus, the increase in the abundance of *Cetobacterium* and *Fusobacteria* might indicate the positive effect of Trp in balancing the gut microbiota, which may be most strongly linked to health performance.

Overall, our study suggests that dietary 6.35 g kg^{-1} Trp had a beneficial effect on gut microbes and regulated the abundance of gut microbes in ITCC. However, further work needs to be done determine the effects of Trp on certain beneficial intestinal bacteria.

CONCLUSIONS

In this study, dietary Trp was found to improve the growth performance and intestinal health of ITCC. We found that 6.35 g kg^{-1} Trp altered intestinal gene expression involved in protein digestion and absorption and the AMPK signaling pathway in the ITCC gut. In addition, 6.35 g kg^{-1} Trp significantly increased the abundance of *Cetobacterium* and the Firmicutes/Bacteroidetes ratio in the ITCC gut. However, more studies are needed to clarify the interaction between host gene expression and gut microbiota in ITCC fed a diet with 6.35 g kg^{-1} Trp.

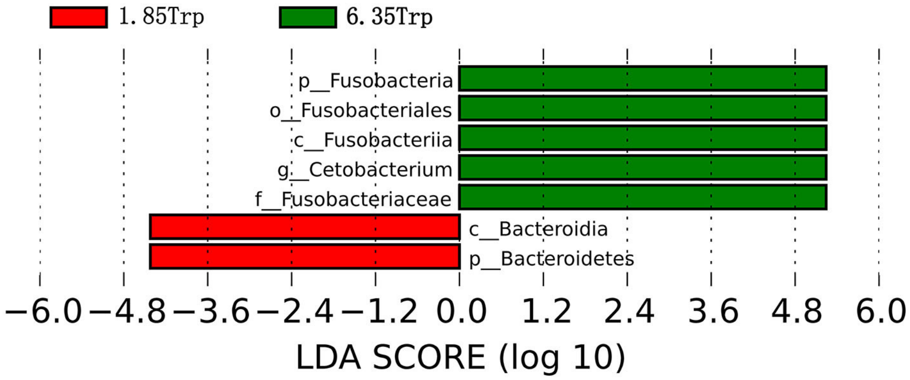

FIGURE 8 | Linear discriminant analysis coupled with effect size (LEfSe) of the control group and 6.35 Trp group. The LDA value distribution histogram shows species with an LDA score greater than the set value (set to 4 by default), and the biomarkers with statistically significant differences between groups. The prefixes "p," "c," "o," "f," "g," "s," and "t" represent the annotated level of phylum, class, order, family, genus, species, and strain. Green represents the 6.35 Trp group, and red represents the 1.85 Trp group.

DATA AVAILABILITY STATEMENT

The raw reads were deposited to Sequence Read Archive (SRA) database (PRJNA702642 for RNA-seq; BioProject: PRJNA704527 for 16S rRNA sequencing).

ETHICS STATEMENT

The animal study was reviewed and approved by the Animal Welfare Committee of the Institute of Subtropical Agriculture (201703-64C), Chinese Academy of Sciences, Changsha, China.

AUTHOR CONTRIBUTIONS

KX and FH conceptualized and designed this study. YF, XL, DL, HG, YW, and WL performed the main experiments and analyzed the data. FH participated in experimental animal management, tissue sampling, and data analysis. YF, XL, and DL drafted this manuscript. KX and FH reviewed this manuscript. KX acquired the funding and supervised this study. All authors read and approved the manuscript.

FUNDING

This work was supported by the Special Funds for the Construction of Innovative Provinces in Hunan (2020JJ5635, 2019RS1068, 2020WK2030, and 2019NK2193), Supported by State Key Laboratory of Developmental Biology of Freshwater Fish (Grant No. 2018KF008), the Natural Science Foundation of Guangxi Province (2020JJB130030), the National Natural Science Foundation of China (31601953), and the Open Fund of Key Laboratory of Agro-ecological Processes in Subtropical Region, Chinese Academy of Sciences (ISA2019304).

SUPPLEMENTARY MATERIAL

The Supplementary Material for this article can be found online at: https://www.frontiersin.org/articles/10.3389/fnut.2021.676035/full#supplementary-material

REFERENCES

1. Fry JP, Love DC, Macdonald GK, West PC, Engstrom PM, Nachman KE, et al. Environmental health impacts of feeding crops to farmed fish. *Environ Int.* (2016) 91:201–14. doi: 10.1016/j.envint.2016.02.022
2. Dourou M, Dritsas P, Baeshen MN, Elazzazy A, Al-Farga A, Aggelis G. High-added value products from microalgae and prospects of aquaculture wastewaters as microalgae growth media. *FEMS Microbiol. Lett.* (2020) 367:fnaa081. doi: 10.1093/femsle/fnaa081
3. Thorburn AN, Macia L, Mackay CR. Diet, metabolites, and "western-lifestyle" inflammatory diseases. *Immunity.* (2014) 40:833–42. doi: 10.1016/j.immuni.2014.05.014
4. David A, Lange A, Abdul-Sada A, Tyler CR, Hill EM. Disruption of the prostaglandin metabolome and characterization of the pharmaceutical exposome in fish exposed to wastewater treatment works effluent as revealed by nanoflow-nanospray mass spectrometry-based metabolomics. *Environ Sci Technol.* (2017) 51:616–24. doi: 10.1021/acs.est.6b04365
5. Farhat, Khan MA. Dietary L-tryptophan requirement of fingerling stinging catfish, *Heteropneustes fossilis* (Bloch). *Aquac Res.* (2014) 45:1224–35. doi: 10.1111/are.12066
6. Wen H, Feng L, Jiang W, Liu Y, Jiang J, Li S, et al. Dietary tryptophan modulates intestinal immune response, barrier function, antioxidant status and gene expression of TOR and Nrf2 in young grass carp (*Ctenopharyngodon idella*). *Fish Shellf Immunol.* (2014) 40:275–87. doi: 10.1016/j.fsi.2014.07.004
7. Walton MJ, Coloso RM, Cowey CB, Adron JW, Knox D. The effects of dietary tryptophan levels on growth and metabolism of rainbow trout (*Salmo gairdneri*). *Br J Nutr.* (1984) 51:279–87. doi: 10.1079/BJN19840032
8. Akiyama T, Murai T, Mori K. Role of tryptophan metabolites in inhibition of spinal deformity of chum salmon fry caused by tryptophan deficiency. *Nsugaf.* (1986) 52:1255–9. doi: 10.2331/suisan.52.1255
9. Hoseini SM, Perez-Jimenez A, Costas B, Azeredo R, Gesto M. Physiological roles of tryptophan in teleosts: current knowledge and perspectives for future studies. *Rev Aquac.* (2019) 11:3–24. doi: 10.1111/raq.12223

10. Machado M, Azeredo R, Domingues A, Fernandez-Boo S, Dias J, Conceicao LEC, et al. Dietary tryptophan deficiency and its supplementation compromises inflammatory mechanisms and disease resistance in a teleost fish. *Sci Rep.* (2019) 9:7689. doi: 10.1038/s41598-019-44205-3
11. Ahmed I. Dietary amino acidl-tryptophan requirement of fingerling Indian catfish, *Heteropneustes fossilis* (Bloch), estimated by growth and haemato-biochemical parameters. *Fish Physiol Biochem.* (2012) 38:1195–209. doi: 10.1007/s10695-012-9609-1
12. Ciji A, Sahu NP, Pal AK, Akhtar MSJR. Dietary L-tryptophan modulates growth and immuno-metabolic status of *Labeo rohita* juveniles exposed to nitrite. *Aquac Res.* (2013) 46:2013–24. doi: 10.1111/are.12355
13. Tang QQ, Feng L, Jiang WD, Liu Y, Jiang J, Li SH, et al. Effects of dietary copper on growth, digestive, and brush border enzyme activities and antioxidant defense of hepatopancreas and intestine for young grass carp (*Ctenopharyngodon idella*). *Biol Trace Elem Res.* (2013) 155:370–80. doi: 10.1007/s12011-013-9785-6
14. Pewitt E, Castillo S, Velásquez A, Gatlin DM III. The dietary tryptophan requirement of juvenile red drum, *Sciaenops* ocellatus. *Aquaculture*. (2017) 469:112–6. doi: 10.1016/j.aquaculture.2016.11.030
15. Koleva Z, Dedov I, Kizheva J, Lipovanska R, Moncheva P, Hristova P. Lactic acid microflora of the gut of snail. *Biotechnol Biotechnol Equip.* (2014) 28:627–34. doi: 10.1080/13102818.2014.947071
16. Azad MK, Gao J, Ma J, Li T, Tan B, Huang X, et al. Opportunities of prebiotics for the intestinal health of monogastric animals. *Anim Nutr.* (2020) 6:379–88. doi: 10.1016/j.aninu.2020.08.001
17. Knutie SA, Gabor CR, Kohl KD, Rohr JR. Do host-associated gut microbiota mediate the effect of an herbicide on disease risk in frogs? *J Anim Ecol.* (2018) 87:489–99. doi: 10.1111/1365-2656.12769
18. Zha Y, Eiler A, Johansson F, Svanbäck R. Effects of predation stress and food ration on perch gut microbiota. *Microbiome.* (2018) 6:28. doi: 10.1186/s40168-018-0400-0
19. Liang H, Dai Z, Liu N, Ji Y, Chen J, Zhang Y, et al. Dietary L-tryptophan modulates the structural and functional composition of the intestinal microbiome in weaned piglets. *Front Microbiol.* (2018) 9:1736. doi: 10.3389/fmicb.2018.01736
20. Dehhaghi M, Kazemi Shariat Panahi H, Guillemin GJ. Microorganisms, tryptophan metabolism, and kynurenine pathway: a complex interconnected loop influencing human health status. *Int J Tryptop Res.* (2019) 12:1178646919852996. doi: 10.1177/1178646919852996
21. Taleb S. Tryptophan dietary impacts gut barrier and metabolic diseases. *Front Immunol.* (2019) 10:2113. doi: 10.3389/fimmu.2019.02113
22. Lee-Sarwar KA, Lasky-Su J, Kelly RS, Litonjua AA, Weiss ST. Gut microbial-derived metabolomics of asthma. *Metabolites.* (2020) 10:97. doi: 10.3390/metabo10030097
23. Chen S, Wang J, Liu S, Qin Q, Xiao J, Duan W, et al. Biological characteristics of an improved triploid crucian carp. *Sci China Ser. C Life Sci.* (2009) 52:733–8. doi: 10.1007/s11427-009-0079-3
24. Xu K, Wen M, Duan W, Ren L, Hu F, Xiao J, et al. Comparative analysis of testis transcriptomes from triploid and fertile diploid cyprinid fish. *Biol Reprod.* (2015) 92:95. doi: 10.1095/biolreprod.114.125609
25. Liu X, Wu P, Jiang WD, Liu Y, Jiang J, Kuang SY, et al. Effects of dietary ochratoxin a on growth performance and intestinal apical junctional complex of juvenile grass carp (*Ctenopharyngodon idella*). *Toxins.* (2020) 13:11. doi: 10.3390/toxins13010011
26. Wang L, Feng Z, Wang X, Wang X, Zhang X. DEGseq: an R package for identifying differentially expressed genes from RNA-seq data. *Bioinformatics.* (2010) 26:136–8. doi: 10.1093/bioinformatics/btp612
27. Robinson MD, Mccarthy DJ, Smyth GKJB. edgeR: a Bioconductor package for differential expression analysis of digital gene expression data. *Bioinformatics.* (2010) 26:139–40. doi: 10.1093/bioinformatics/btp616
28. Shannon P, Markiel A, Ozier O, Baliga NS, Wang JT, Ramage D, et al. Cytoscape: a software environment for integrated models of biomolecular interaction networks. *Genome Res.* (2003) 13:2498–504. doi: 10.1101/gr.1239303
29. Schmittgen TD, Livak KJ. Analyzing real-time PCR data by the comparative C(T) method. *Nat Protoc.* (2008) 3:1101–8. doi: 10.1038/nprot.2008.73
30. Le Floc'h N, Otten W, Merlot E. Tryptophan metabolism, from nutrition to potential therapeutic applications. *Amino Acids.* (2011) 41:1195–205. doi: 10.1007/s00726-010-0752-7
31. Roager HM, Licht TR. Microbial tryptophan catabolites in health and disease. *Nat Commun.* (2018) 9:3294. doi: 10.1038/s41467-018-05470-4
32. Maslowski KM. Metabolism at the centre of the host-microbe relationship. *Clin Exp Immunol.* (2019) 197:193–204. doi: 10.1111/cei.13329
33. Pianesso D, Neto JR, Silva LPD, Goulart FR, Adorian TJ, Mombach PI, et al. Determination of tryptophan requirements for juvenile silver catfish (*Rhamdia quelen*) and its effects on growth performance, plasma and hepatic metabolites and digestive enzymes activity. *J Anim Feed Sci Technol.* (2015) 210:172–83. doi: 10.1016/j.anifeedsci.2015.09.025
34. Zhao Y, Wu XY, Xu SX, Xie JY, Xiang KW, Feng L, et al. Dietary tryptophan affects growth performance, digestive and absorptive enzyme activities, intestinal antioxidant capacity, and appetite and GH-IGF axis-related gene expression of hybrid catfish (*Pelteobagrus vachelli*♀ × *Leiocassis longirostris*♂). *Fish Physiol Biochem.* (2019) 45:1627–47. doi: 10.1007/s10695-019-00651-4
35. Zaminhan M, Boscolo WR, Neu DH, Feiden A, Barriviera Furuya VRB, Furuya WM. Dietary tryptophan requirements of juvenile Nile tilapia fed corn-soybean meal-based diets. *Anim Feed Sci Technol.* (2017) 227:62–7. doi: 10.1016/j.anifeedsci.2017.03.010
36. Tang L, Feng L, Sun CY, Chen GF, Jiang WD, Hu K, et al. Effect of tryptophan on growth, intestinal enzyme activities and TOR gene expression in juvenile Jian carp (*Cyprinus carpio* var. Jian): studies *in vivo* and *in vitro*. *Aquaculture.* (2013) 412–3:23–33. doi: 10.1016/j.aquaculture.2013.07.002
37. Tejpal CS, Pal AK, Sahu NP, Kumar JA, Muthappa NA, Vidya S, et al. Dietary supplementation of l-tryptophan mitigates crowding stress and augments the growth in *Cirrhinus mrigala* fingerlings. *Aquaculture*. (2009) 293:277. doi: 10.1016/j.aquaculture.2008.09.014
38. Ahmed I, Khan MA, Jafri AKJR. Dietary threonine requirement of fingerling Indian major carp, *Cirrhinus mrigala* (Hamilton). *Aquac Res.* (2004) 35:162–70. doi: 10.1111/j.1365-2109.2004.00997.x
39. Fatmaabidi S, Khan MJ. Dietary tryptophan requirement of fingerling rohu, *Labeo rohita* (Hamilton), based on growth and body composition. *J World Aquac Soc.* (2010) 41:700–9. doi: 10.1111/j.1749-7345.2010.00412.x
40. Cowan M, Petri WA, Jr. Microglia: immune regulators of neurodevelopment. *Front Immunol.* (2018) 9:2576. doi: 10.3389/fimmu.2018.02576
41. Cerqueira M, Schrama D, Silva TS, Colen R, Engrola SAD, Conceição LEC, et al. How tryptophan levels in plant-based aquafeeds affect fish physiology, metabolism and proteome. *J Proteom.* (2020) 221:103782. doi: 10.1016/j.jprot.2020.103782
42. Qian L, Tang M, Yang J, Wang Q, Cai C, Jiang S, et al. Targeted mutations in myostatin by zinc-finger nucleases result in double-muscled phenotype in Meishan pigs. *Sci Rep.* (2015) 5:14435. doi: 10.1038/srep14435
43. Qiu K, Qin CF, Luo M, Zhang X, Sun WJ, Jiao N, et al. Protein restriction with amino acid-balanced diets shrinks circulating pool size of amino acid by decreasing expression of specific transporters in the small intestine. *PLoS ONE.* (2016) 11:e0162475. doi: 10.1371/journal.pone.0162475
44. Yu Y, Lu J, Oliphant K, Gupta N, Claud K, Lu L. Maternal administration of probiotics promotes gut development in mouse offsprings. *PLoS ONE.* (2020) 15:e0237182. doi: 10.1371/journal.pone.0237182
45. Chang Y, Cai H, Liu G, Chang W, Zheng A, Zhang S, et al. Effects of dietary leucine supplementation on the gene expression of mammalian target of rapamycin signaling pathway and intestinal development of broilers. *Anim Nutr.* (2015) 1:313–9. doi: 10.1016/j.aninu.2015.11.005
46. Wu QJ, Zheng XC, Wang T, Zhang TY. Effect of dietary oridonin supplementation on growth performance, gut health, and immune response of broilers infected with. *Irish Vet J.* (2018) 71:16. doi: 10.1186/s13620-018-0128-y
47. Kumari R, Gupta S, Singh AR, Ferosekhan S, Kothari DC, Pal AK, et al. Chitosan nanoencapsulated exogenous trypsin biomimics zymogen-like enzyme in fish gastrointestinal tract. *PLoS ONE.* (2013) 8:e74743. doi: 10.1371/journal.pone.0074743
48. Poston HA, Rumsey GL. Factors affecting dietary requirement and deficiency signs of L-tryptophan in rainbow trout. *J Nutr.* (1983) 113:2568–77. doi: 10.1093/jn/113.12.2568

49. Blanco AM, Bertucci JI, Sánchez-Bretaño A, Delgado MJ, Valenciano AI, Unniappan S. Ghrelin modulates gene and protein expression of digestive enzymes in the intestine and hepatopancreas of goldfish (*Carassius auratus*) via the GHS-R1a: possible roles of PLC/PKC and AC/PKA intracellular signaling pathways. *Mol Cell Endocrinol.* (2017) 442:165–81. doi: 10.1016/j.mce.2016.12.027
50. Garrido D, Kabeya N, Betancor MB, Pérez JA, Acosta NG, Tocher DR, et al. Functional diversification of teleost Fads2 fatty acyl desaturases occurs independently of the trophic level. *Sci Rep.* (2019) 9:11199. doi: 10.1038/s41598-019-47709-0
51. Horn SS, Sonesson AK, Krasnov A, Moghadam H, Hillestad B, Meuwissen THE, et al. Individual differences in EPA and DHA content of Atlantic salmon are associated with gene expression of key metabolic processes. *Sci Rep.* (2019) 9:3889. doi: 10.1038/s41598-019-40391-2
52. Pitel F, Fillon V, Heimel C, Le Fur N, El Khadir-Mounier C, Douaire M, et al. Mapping of FASN and ACACA on two chicken microchromosomes disrupts the human 17q syntenic group well conserved in mammals. *Mammal Genome.* (1998) 9:297–300. doi: 10.1007/s003359900752
53. Kuhajda FP. Fatty acid synthase and cancer: new application of an old pathway. *Cancer Res.* (2006) 66:5977–80. doi: 10.1158/0008-5472.CAN-05-4673
54. Jiang J, Feng L, Tang L, Liu Y, Jiang W, Zhou X. Growth rate, body composition, digestive enzymes and transaminase activities, and plasma ammonia concentration of different weight Jian carp (var.). *Anim Nutr.* (2015) 1:373–7. doi: 10.1016/j.aninu.2015.12.006
55. Lee DH, Lim SR, Han JJ, Lee SW, Ra CS, Kim JD. Effects of dietary garlic powder on growth, feed utilization and whole body composition changes in fingerling sterlet sturgeon, *Acipenser ruthenus*. *Asian Austral J Anim Sci.* (2014) 27:1303–10. doi: 10.5713/ajas.2014.14087
56. González A, Hall MN. Nutrient sensing and TOR signaling in yeast and mammals. *EMBO J.* (2017) 36:397–408. doi: 10.15252/embj.201696010
57. Paoli PP, Wakeling LA, Wright GA, Ford D. The dietary proportion of essential amino acids and Sir2 influence lifespan in the honeybee. *Age.* (2014) 36:9649. doi: 10.1007/s11357-014-9649-9
58. Honda Y, Araki Y, Hata T, Ichihara K, Ito M, Tanaka M, et al. 10-Hydroxy-2-decenoic acid, the major lipid component of royal jelly, extends the lifespan of *Caenorhabditis elegans* through dietary restriction and target of rapamycin signaling. *J Aging Res.* (2015) 2015:425261. doi: 10.1155/2015/425261
59. Jiang WD, Wen HL, Liu Y, Jiang J, Kuang SY, Wu P, et al. The tight junction protein transcript abundance changes and oxidative damage by tryptophan deficiency or excess are related to the modulation of the signalling molecules, NF-κB p65, TOR, caspase-(3,8,9) and Nrf2 mRNA levels, in the gill of young grass carp (*Ctenopharyngodon idellus*). *Fish Shellfish Immunol.* (2015) 46:168–80. doi: 10.1016/j.fsi.2015.06.002
60. Jiang WD, Wen HL, Liu Y, Jiang J, Wu P, Zhao J, et al. Enhanced muscle nutrient content and flesh quality, resulting from tryptophan, is associated with anti-oxidative damage referred to the Nrf2 and TOR signalling factors in young grass carp (*Ctenopharyngodon idella*): avoid tryptophan deficiency or excess. *Food Chem.* (2016) 199:210–9. doi: 10.1016/j.foodchem.2015.12.003
61. Hashimoto T, Perlot T, Rehman A, Trichereau J, Ishiguro H, Paolino M, et al. (2012). ACE2 links amino acid malnutrition to microbial ecology and intestinal inflammation. *Nature.* 487, 477–81. doi: 10.1038/nature11228
62. Liang H, Dai Z, Kou J, Sun K, Chen J, Yang Y, et al. Dietary l-tryptophan supplementation enhances the intestinal mucosal barrier function in weaned piglets: implication of tryptophan-metabolizing microbiota. *Int J Mol Sci.* (2018) 20:20. doi: 10.3390/ijms20010020
63. Turnbaugh PJ, Ley RE, Mahowald MA, Magrini V, Mardis ER, Gordon JI. An obesity-associated gut microbiome with increased capacity for energy harvest. *Nature.* (2006) 444:1027–31. doi: 10.1038/nature05414
64. Moschen AR, Wieser V, Tilg H. Dietary factors: major regulators of the gut's microbiota. *Gut Liver.* (2012) 6:411–6. doi: 10.5009/gnl.2012.6.4.411
65. López-Cepero AA, Palacios C. Association of the intestinal microbiota and obesity. *Puerto Rico Health Sci J.* (2015) 34:60–4. doi: 10.1111/j.1472-765X.2007.02258.x
66. Li X, Yan Q, Xie S, Hu W, Yu Y, Hu Z. Gut microbiota contributes to the growth of fast-growing transgenic common carp (*Cyprinus carpio* L.). *PLoS ONE.* (2013) 8:e64577. doi: 10.1371/journal.pone.0064577
67. Gao J, Xu K, Liu H, Liu G, Bai M, Peng C, et al. Impact of the gut microbiota on intestinal immunity mediated by tryptophan metabolism. *Front Cell Infect Microbiol.* (2018) 8:13. doi: 10.3389/fcimb.2018.00013
68. Robins Wahlin TB, Wahlin A, Winblad B, Bäckman L. The influence of serum vitamin B12 and folate status on cognitive functioning in very old age. *Biol Psychol.* (2001) 56:247–65. doi: 10.1016/S0301-0511(01)00079-5
69. Tsuchiya C, Sakata T, Sugita H. Novel ecological niche of *Cetobacterium somerae*, an anaerobic bacterium in the intestinal tracts of freshwater fish. *Lett Appl Microbiol.* (2008) 46:43–8.
70. Van Kessel MA, Dutilh BE, Neveling K, Kwint MP, Veltman JA, Flik G, et al. Pyrosequencing of 16S rRNA gene amplicons to study the microbiota in the gastrointestinal tract of carp (*Cyprinus carpio* L.). *AMB Exp.* (2011) 1:41. doi: 10.1186/2191-0855-1-41
71. Ramírez C, Coronado J, Silva A, Romero J. *Cetobacterium* is a major component of the microbiome of giant amazonian fish (*Arapaima gigas*) in ecuador. *Animals.* (2018) doi: 10.3390/ani8110189
72. Zheng M, Lu J, Lin G, Su H, Sun J, Luan T. Dysbiosis of gut microbiota by dietary exposure of three graphene-family materials in zebrafish (*Danio rerio*). *Environ Pollut.* (2019) 254:112969. doi: 10.1016/j.envpol.2019.112969
73. Sugita H, Miyajima C, Deguchi Y. The vitamin-B12-producing Ability of the intestinal microflora of fresh-water fish. *Aquaculture.* (1991) 92:267–76. doi: 10.1016/0044-8486(91)90028-6
74. Ma C, Chen C, Jia L, He X, Zhang B. Comparison of the intestinal microbiota composition and function in healthy and diseased Yunlong Grouper. *AMB Exp.* (2019) 9:187. doi: 10.1186/s13568-019-0913-3
75. Clements KD, Angert ER, Montgomery WL, Choat JH. Intestinal microbiota in fishes: what's known and what's not. *Mol Ecol.* (2014) 23:1891–8. doi: 10.1111/mec.12699
76. Smriga S, Sandin SA, Azam F. Abundance, diversity, and activity of microbial assemblages associated with coral reef fish guts and feces. *FEMS Microbiol Ecol.* (2010) 73:31–42. doi: 10.1111/j.1574-6941.2010.00879.x

Conflict of Interest: The authors declare that the research was conducted in the absence of any commercial or financial relationships that could be construed as a potential conflict of interest.

frontiers in Nutrition

ORIGINAL RESEARCH
published: 28 June 2021
doi: 10.3389/fnut.2021.705763

Probiotic Effects of *Lactobacillus fermentum* ZJUIDS06 and *Lactobacillus plantarum* ZY08 on Hypercholesteremic Golden Hamsters

Dongting Yang [1†], Wentao Lyu [2†], Ziyi Hu [1†], Jiting Gao [1], Zhiyao Zheng [1], Weijun Wang [3], Jenni Firrman [4] and Daxi Ren [1*]

[1] College of Animal Sciences, Institute of Dairy Science, Zhejiang University, Hangzhou, China, [2] State Key Laboratory for Managing Biotic and Chemical Threats to the Quality and Safety of Agro-Products, Institute of Agro-Product Safety and Nutrition, Zhejiang Academy of Agricultural Sciences, Hangzhou, China, [3] Zhejiang Yiming Food Co. Ltd., Wenzhou, China, [4] Dairy and Functional Foods Research Unit, Eastern Regional Research Center, Agricultural Research Service, U.S. Department of Agriculture, Wyndmoor, PA, United States

OPEN ACCESS

Edited by:
*Jie Yin,
Hunan Agricultural University, China*

Reviewed by:
*Long Zhang,
China West Normal University, China
Wei Zhang,
Beijing Academy of Agricultural and Forestry Sciences, China*

***Correspondence:**
*Daxi Ren
dxren@zju.edu.cn*

[†] These authors have contributed equally to this work

Specialty section:
This article was submitted to Nutrition and Microbes, a section of the journal Frontiers in Nutrition

***Received:** 06 May 2021*
***Accepted:** 27 May 2021*
***Published:** 28 June 2021*

Citation:
Yang D, Lyu W, Hu Z, Gao J, Zheng Z, Wang W, Firrman J and Ren D (2021) Probiotic Effects of Lactobacillus fermentum ZJUIDS06 and Lactobacillus plantarum ZY08 on Hypercholesteremic Golden Hamsters. Front. Nutr. 8:705763. doi: 10.3389/fnut.2021.705763

Hypercholesteremia or high cholesterol is one of the important factors leading to atherosclerosis and other cardiovascular diseases. The application of probiotics with cholesterol-lowering characteristics has become increasingly popular over the past decade due to their contribution to human health. This study aimed to evaluate the probiotic effects of *Lactobacillus fermentum* ZJUIDS06 and *Lactobacillus plantarum* ZY08 on hyperlipidemic golden hamsters. A hyperlipidemic model was established through a high cholesterol diet in golden hamsters, after which lyophilized *Lactobacillus fermentum* ZJUIDS06 and *Lactobacillus plantarum* ZY08 were orally administered individually for 8 weeks. The physiological characteristics of golden hamsters and short chain fatty acid (SCFA) in the colon were assessed by automatic Biochemical Analyzer and gas choromatograph, respectively. A MiSeq sequencing-based analysis of the bacterial 16S rRNA gene (V3–V4 region) in the cecum content was performed to analyze the cecum microbiota. Correlations between sets of these variables were also investigated using the R package "corrplot." Results showed that neither *Lactobacillus fermentum* ZJUIDS06 nor *Lactobacillus plantarum* ZY08 inhibited body weight increase. However, supplementation with *Lactobacillus fermentum* ZJUIDS06 for 8 weeks increased colon SCFA levels ($P < 0.05$), decreased serum low-density lipoprotein, total cholesterol, and triglycerides levels, and also induced changes in the cecum microbiota of hyperlipidemic golden hamsters. Remarkably, oral administration of *Lactobacillus fermentum* ZJUIDS06 increased the relative abundance of *Parabacteroides* in the cecum, which served as a biomarker for colon SCFA production and improvement of serum cholesterol levels. In a word, *Lactobacillus fermentum* ZJUIDS06 improved hyperlipidemia in golden hamsters, which correlated with an increase in SCFA levels and relative abundance of *Parabacteroides,* indicating its potential importance in functional foods that can help lower cholesterol.

Keywords: *in vivo*, probiotic potential, *Lactobacillus fermentum*, *Lactobacillus plantarum*, cholesterol-lowering effects, intestinal microbiota

INTRODUCTION

Atherosclerosis is a type of cardiovascular disease that has become increasingly prevalent on a global scale and contributes to the etiology of multiple diseases, such as coronary heart disease, cerebral infarction, and peripheral vascular disease (1–3). The most commonly associated pathogenic factor for atherosclerosis is the increase in low-density lipoprotein cholesterol (LDL-C) levels in conjugation with a decrease in high-density lipoprotein cholesterol (HDL-C) levels (4, 5). The prescribed use of statin drugs reduces the risk of developing atherosclerotic cardiovascular disease (6, 7), cardiovascular-related death, and death in general, by lowering LDL-C levels (8–10). However, the use of statins on a regular basis has been associated with multiple adverse effects, including liver damage, liver necrosis, kidney damage, myopathy, and rhabodomyolysis (6, 11, 12), asks for the development of alternative agents or bioactives with cholesterol-lowering characteristics.

The administration of cholesterol-lowering probiotics has become increasingly popular over the past few decades due to their generally recognized as safe (GRAS) status and their contribution to the healthy microbiota of human mucosal surfaces. To date, a number of cholesterol-lowering strains have been isolated from feces of healthy people, fermented dairy products, and pickles, including *Lactobacillus plantarum*, *Lactobacillus fermentum*, *Lactobacillus acidophilus*, *Lactobacillus casei*, *Lactobacillus reuteri*, *Lactobacillus rhamnosus*, *Bifidobacterium*, and *Enterococcus faecium*. The LAB strains previously reported to exhibit the cholesterol-lowering effect *in vivo* mainly belong to *Lactobacillus* and *Enterococcus* (13, 14).

The cholesterol-lowering effects of *Lactobacillus fermentum* or *Lactobacillus plantarum* have been reported from both animal models and human clinical trials. *Lactobacillus fermentum* MJM60397 reduced the levels of serum triglycerides (TG) and LDL-C, and improved gene expression of LDL-R in livers of male ICR mice after a 7-week intervention period (15). Consumption of buffalo milk fermented by *Lactobacillus fermentum* improved serum lipids and biochemical indexes of livers in male Wistar rats (16). *Lactobacillus plantarum* EM fermented juice reduced the levels of serum TG, total cholesterol (TC), and LDL-C of Sprague-Dawley rats and improved the expression of 7 α-hydroxylase and LDL receptors in the rat liver (17). In addition, *Lactobacillus plantarum* colonizing the colon of rats reduced serum alanine aminotransferase (ALT), aspartate aminotransferase (AST), TC, TG, LDL, very low-density lipoprotein (VLDL), and the Atherogenic Index under hypercholesterolemic conditions (18). In human clinical trials, ingestion of *Lactobacillus fermentum* ME-3 for 4 weeks decreased serum TG and oxidized-LDL and increased serum HDL-C, and thus reducing the risk of developing cardiovascular disease and diabetes (19). Heat-inactivated *Lactobacillus plantarum* L-137 reduced the levels of serum TC, LDL-C, AST, and ALT in overweight people (20). In a human clinical trial, treatment with live *Lactobacillus plantarum* Q180 for 12 weeks decreased postprandial maximum concentrations of TG, LDL-C, Apo B-100, and Apo B-48 levels (21).

Several mechanisms for cholesterol reduction by lactic acid bacteria (LAB) have been proposed, such as deconjugation of bile salts by bile-salt hydrolase (BSH) (22–24), binding and incorporation of cholesterol to the LAB cellular surface (25–27), production of short-chain fatty acids (SCFAs) during the LAB growth (28, 29), and co-precipitation of cholesterol with deconjugated bile salts (30, 31). Nevertheless, the mechanism for cholesterol reduction by LAB needs to be studied on a case-to-case basis and the cholesterol-lowering effects of LAB still need to be elucidated.

In our previous study, two cholesterol-lowering probiotics, *Lactobacillus plantarum* ZY08 and *Lactobacillus fermentum* ZJUIDS06, were isolated from baby feces. Both strains demonstrated cholesterol-lowering effects *in vitro* (**Supplementary Figure 1**), were resistant to acid and bile salt, and had no antibiotic resistance. However, the *in vivo* cholesterol-lowering effects of these two strains were still unknown, and their effects on the intestine microbial community remained unclear. Therefore, the objectives of this study were to assess the effects of *Lactobacillus plantarum* ZY08 and *Lactobacillus fermentum* ZJUIDS06 on serum lipids, SCFA profiles, and gut microbiota in hyperlipidemic golden hamsters, and thus to provide deeper insights into the counter- hyperlipidemic effects of certain probiotics.

MATERIALS AND METHODS

Bacterial Strains, Culture Conditions, and Gavage Administration

Lactobacillus plantarum ZY08 and *Lactobacillus fermentum* ZJUIDS06 (**Supplementary Figure 2**) were isolated from breastfed baby (6 months old) feces in Hangzhou, Zhejiang Province, China. The two strains were grown in MRS broth (Beijing Land Bridge Technology Co. Ltd., Beijing, China) and incubated anaerobically at 37°C for 18 h. *In vitro* cholesterol-lowering characteristics for the two strains (**Supplementary Figure 1**) were determined following previously described methods (32). The two strains were lyophilized (WECARE-BIO Biotechnology Co. Ltd., Jiangsu, China) and stored at −20°C until use.

Golden Hamster Experimental

The *in vivo* experiment was conducted following a previous study with some modifications (33, 34). In this experiment, cholesterol (0.1%) and lard (10%) were added to the standard diet (**Supplementary Table 1**, Pluteng Biological Technology Co. Ltd., Shanghai, China) to produce the high cholesterol diet. Golden hamsters (*Mesocricetus auratus*, Vital River Laboratory Animal Technology Co. Ltd., Beijing, China) were fed the high cholesterol diet to develop the mixed hyperlipidemia model. Animal care and experimental procedures were approved prior to initiation (#17426), and the guidelines set by the Animal Care and Use Committee of Zhejiang University was followed.

Golden hamsters were selected as the animal model for this study because hamsters synthesize and excrete cholesterol and bile acids in a manner similar to that of humans,

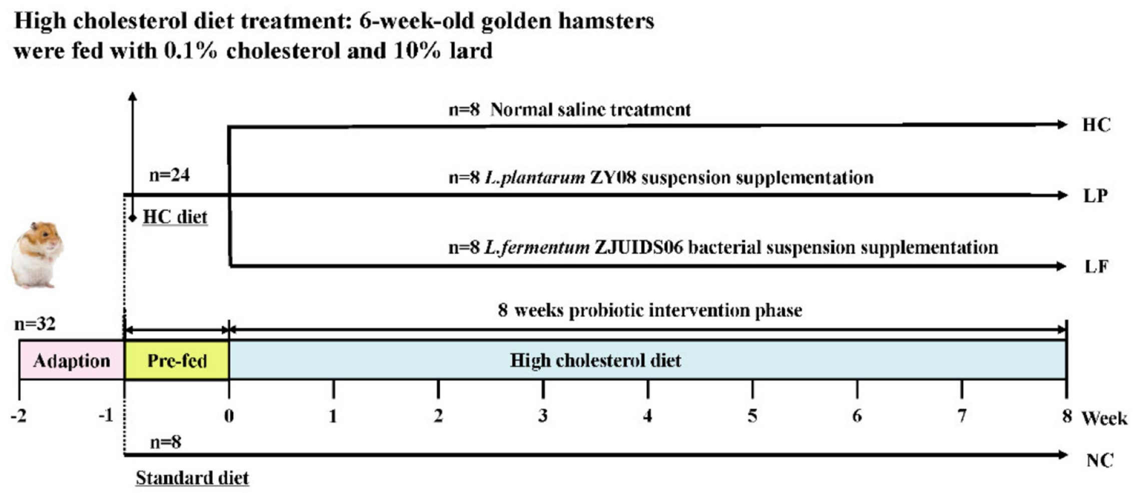

FIGURE 1 | Experimental design of animal study.

and they have become a standard model for evaluating the cholesterol-decreasing efficacy of probiotic strains (34–36). Male hamsters are considered a better model than females for developing hyperlipidemia and evaluating the cholesterol-decreasing efficacy because they are more susceptible to a high-fat diet induced weight gain (37). Accordingly, male hamsters were chosen as a model to assess the cholesterol-lowering effect of LAB *in vivo*. A flow chart summarizing the aims of our study can be found in **Figure 1**. A total of 32 male golden hamsters, 6 weeks old, were fed a standard diet for 1 week to allow them to adapt to their new environment. Subsequently, 24 hamsters were fed the high cholesterol diet for 8 weeks, and the other eight hamsters were maintained using a standard diet for 8 weeks and were considered as the negative control group (NC group). To initiate the experimental phase, the 24 hamsters fed the high cholesterol diet were randomly assigned to the following three groups according to their body weight: High cholesterol positive control group (HC group), *Lactobacillus plantarum* ZY08 intervention group (LP group), and *Lactobacillus fermentum* ZJUIDS06 intervention group (LF group). During the experimental period, golden hamsters in the NC group and HC group were given 1 mL normal saline per 100 g body weight per day. Hamsters in the LP group were given 1 mL of *Lactobacillus plantarum* ZY08 suspension (10^9 CFU/mL) per 100 g body weight per day, while hamsters in the LF group were given 1 mL *Lactobacillus fermentum* ZJUIDS06 suspension (10^9 CFU/mL) per 100 g body weight per day. The viable counts of lyophilized bacteria were enumerated on MRS agar by surface plating on a weekly basis. Lyophilized bacteria were suspended in saline and the viable cell counts in the suspension used for gavage administration were $\sim 10^9$ CFU/mL (35, 38, 39).

Body weight and food intake were measured every week and blood samples were collected every 2 weeks. After an 8-week intervention period, all golden hamsters were euthanized, and dissected before blood, liver, kidney, and intestine tract samples were collected and frozen −80°C until analyzed.

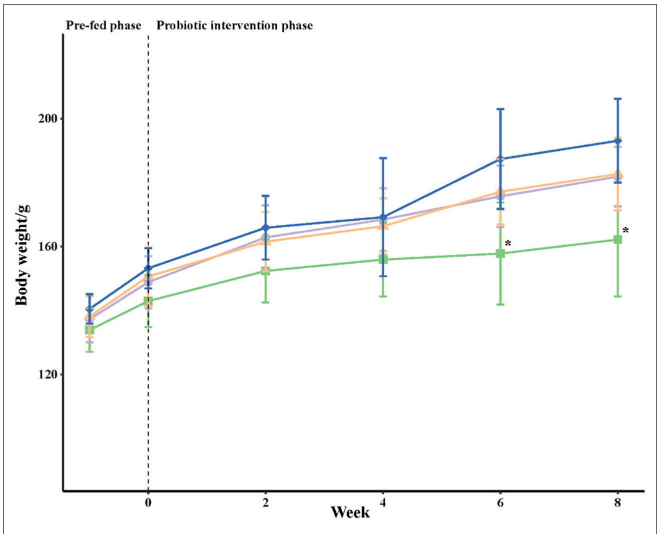

FIGURE 2 | Body weights (g) of golden hamsters over time. The body weight for each golden hamster was measured once a week; each point represents the mean per group ± SD ($n = 8$). Statistical analysis was performed using one-way ANOVA and a Tukey's test. At each time point, an asterisk (*) symbol indicates that the mean value was significantly lower than the mean value of the HC group. NC, negative control group; HC, positive control group; LP, *Lactobacillus plantarum* ZY08 supplemented group; LF, *Lactobacillus fermentum* ZJUIDS06 supplemented group. NC, HC, LP, and LF are colored in green (■), purple (•), orange (▲), and blue (♦), respectively.

Serum Lipids Determination

Blood samples were collected every 2 weeks from the intraorbital venous plexus of the golden hamsters using a flat-ending capillary (0.5 mm diameter) tube. The blood was stored at 4°C overnight and centrifuged at 3000× g for 10 min to harvest the serum for lipid profiling. The amounts of TC, LDL-C HDL-C, and TG in the serum were determined by automatic Biochemical

Analyzer (#3100, Hitachi, Ltd., Tokyo, Japan), according to the manufacturer's procedure.

Histological Examination of the Liver

The livers of the golden hamsters were frozen in liquid nitrogen immediately after dissection. The tissue was covered by an OCT embedding agent (Tissue-Tek O.C.T. Compound 4583, SAKURA Finetek USA, Torrance, USA), frozen, and then cut out using Cryotome E (Thermo Fisher Scientific, Waltham, USA). A coverslip (Servicebio Technology Co. Ltd., Wuhan, China) was applied to attach the tissue. Finally, the hematoxylin-eosin staining was performed, and the section was observed using an oil immersion lens (Eclipse E100, Nikon, Corp., Tokyo, Japan) and scanned by Pannoramic MIDI (3DHISTECH™ Ltd., Budapest, Hungary).

Determination of SCFA

SCFA in the colon content were determined following a previously described method with some modification (40). After dissection, the segmented colon sections were squeezed with sterile forceps, and the contents were removed and stored in cryopreservation tubes at −80°C. The colon contents were diluted five-fold with ultrapure water and vortexed for 3 min. Next, the suspension was rested for 5 min and then centrifuged at 4°C, 5000× g for 20 min. One milliliter of supernatant was mixed with 20 μL chromatogram grade phosphoric acid (Shanghai Aladdin Biochemical Technology Co. Ltd.), and the mixture was injected into a chromatographic vial (WondaVial, Shimadzu, Corp., Kyoto, Japan) through a 0.45 μm membrane filter for gas chromatography.

The gas chromatography machine (Shimadzu, Corp., Kyoto, Japan) consisted of an AOC-20S auto sampler and a GC-2010 equipped with a flame ionization detector. A SH-stabliwax (#227-36305-2, 30 × 0.25 × 0.25, Shimadzu, Corp., Kyoto, Japan) highly polar column was installed on the GC with nitrogen as the carrier gas at a flow rate of 3 mL/min. The sample injection volume was 0.2 μL with a split injection ratio of 50 and an injection temperature of 200°C. The ethyl acetate was injected as a blank solvent between every sample to remove any memory effects. The initial column temperature was set at 80°C and held for 1 min, then increased to 170°C at a rate of 8°C/min, then immediately increased to 220°C at a rate of 20°C/min and maintained for 4 min. The total time was 18.75 min. Finally, the content of SCFAs was calculated according to the SCFA standard curve, which was calibrated by the external standard method.

Tissue Weight

At the end of the experiment, the adipose tissue surrounding liver, kidney, and epididymis were collected, washed with PBS, and dried with clean filter paper. The tissues were then weighed by using an electronic balance (BSA124, Sartorius, Inc., Gottingen, Germany) and recorded.

DNA Extraction and Cecum Microbiota Analysis

The cecum content usually contains the highest absolute number and diversity of microorganisms in the gastrointestinal tract (41), and is thus particularly useful for the analysis of microbiota. After dissection, the segmented cecum was squeezed with sterile forceps to remove the content, which was stored in cryopreservation tubes at −80°C. DNA from the cecum content was extracted using the Fast DNA SPIN extraction kit (MP Biomedicals, Inc., Santa Ana, USA) following the manufacturer's protocol. Quantity and quality of the extracted DNA were measured using the NanoDrop DN-1000 spectrophotometer (Thermo Fisher Scientific, Inc., Waltham, USA) and agarose gel electrophoresis, respectively. PCR amplification of the bacterial 16S rRNA genes V3–V4 region was performed using the forward primer 338F (5′-ACTCCTACGGGAGGCAGCA-3′) and the reverse primer 806R (5′-GGACTACHVGGGTWTCTAAT-3′) (Personal Biotechnology Co. Ltd., Shanghai, China) (42–44). Sample-specific 7-bp barcodes were added to the primers for multiplex sequencing. The PCR components consisted of 5 μL of Q5 reaction buffer (5×), 5 μL of Q5 High-Fidelity GC buffer (5×), 0.25 μL of Q5 High-Fidelity DNA polymerase (5 U/μL), 2 μL (2.5 mmol/L) of dNTPs, 1 μL (10 μmol/L) of each forward and reverse primer, 2 μL of DNA template, and 8.75 μL of ddH_2O. Thermal cycling covered initial denaturation at 98°C for 2 min, followed by 25 cycles including denaturation at 98°C for 15 s, annealing at 50°C for 30 s, and extension at 72°C for 30 s, with a final extension of 5 min at 72°C. The Agencourt AMPure Beads (Beckman Coulter, Inc., Indianapolis, USA) were applied for PCR amplicon purification and a PicoGreen dsDNA Assay Kit (Invitrogen, Thermo Fisher Scientific, Waltham, USA) was used for quantification. Based on quantification, amplicons were gathered in equal amounts, and pair-end 2 × 300 bp sequencing was performed using the Illlumina MiSeq platform with the MiSeq Reagent Kit v3 at Shanghai Personal Biotechnology Co. Ltd. (Shanghai, China). The sequencing data were uploaded to the Sequence Read Archive (SRA) of NCBI and can be viewed with the following accession code: PRJNA727412.

Bioinformatics were applied to the sequencing data using QIIME2 (45) with slight modifications. Briefly, raw sequence data were demultiplexed using the demux plugin and then the primer removed with the cut adapt plugin (46). Sequences were quality filtered, de-noised, merged, and chimeras were removed using the DADA2 plugin (47). Mafft (48) was applied to align the non-singleton amplicon sequence variants (ASVs) and then the results were applied to construct a phylogeny with fasttree2 (49). The diversity plugin was applied to estimate the Alpha-diversity metrics Chao1 (50). The observed species, Shannon (51, 52), and Simpson (53), and the beta diversity metrics, weighted UniFrac (54), unweighted UniFrac (55), and Bray-Curtis dissimilarity were identified. All samples were rarefied to 56,522 sequences. The classify-sklearn naïve Bayes Taxonomy classifier in feature-classifier plugin (45) was applied to assign Taxonomy to ASVs set against the SILVA Release 132 Database (56).

Statistical Analysis

Experiments were performed in biological triplicates. All data are expressed as means ± SD. Differences between variables were tested for significance by one-way ANOVA with a Tukey's Test (General parameter data) or a Kruskal-Wallis test (Non-parametric data) using IBM SPSS version 24.0 (International

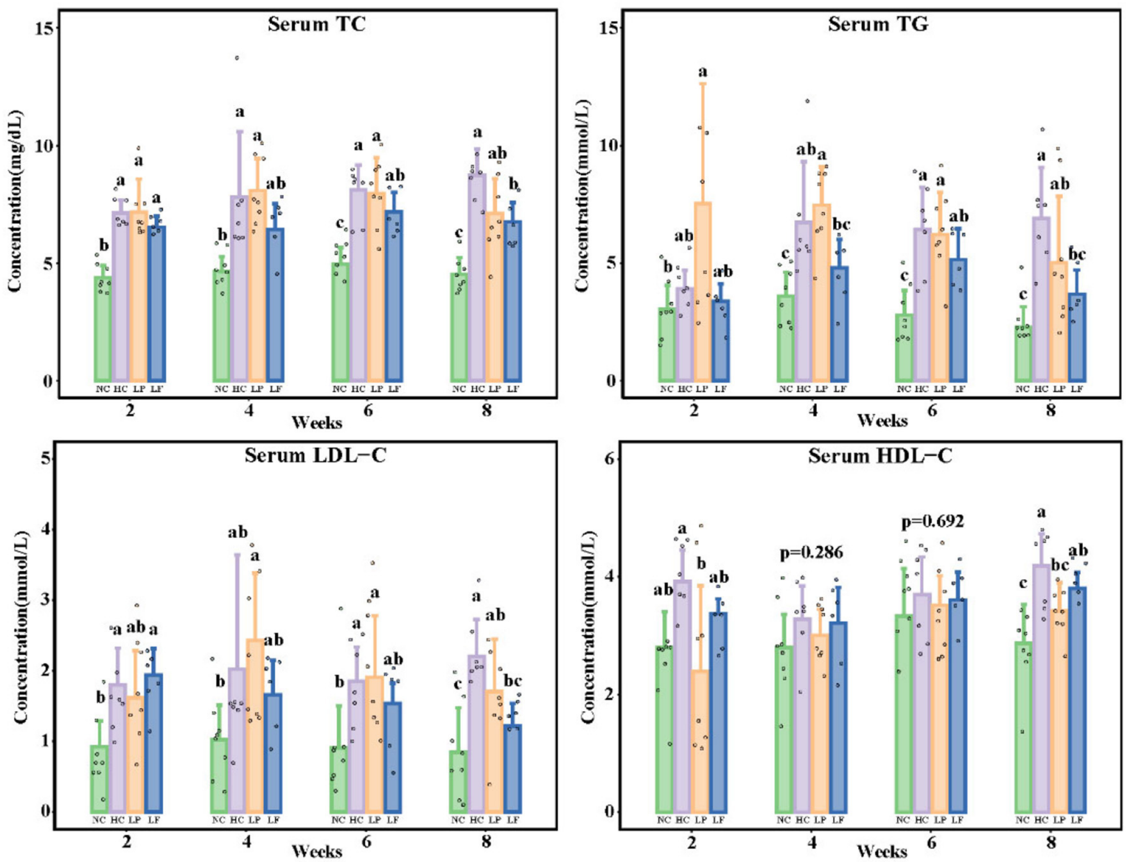

FIGURE 3 | Serum lipid levels of golden hamsters. Groups annotated with *a, b, c* are significantly different with $P < 0.05$ as determined by one-way ANOVA and a Tukey's test. TC, total cholesterol; TG, triglyceride; LDL-C, low-density lipoprotein cholesterol; HDL-C, high-density lipoprotein cholesterol; NC, negative control group; HC, positive control group; LP, *Lactobacillus plantarum* ZY08 supplemented group; LF, *Lactobacillus fermentum* ZJUIDS06 supplemented group. NC, HC, LP, and LF are colored in green, purple, orange, and blue, respectively.

Business Machines, Corp., Armonk, USA). Differences at $P < 0.05$ were considered significant. QIIME2 and R packages (v3.6.3) were used to analyze the sequencing data. The ASV table in QIIME2 was used to calculate the ASV-level alpha diversity indices, such as Chao1 richness estimator, Observed species, Shannon diversity index, Simpson index, Faith's PD, Pielou's evenness, Good's coverage, and to visualize box plots. The richness and evenness of ASVs between the samples were compared by the generated ASV-level ranked abundance curves. Bray-Curtis metrics (57), non-metric multidimensional scaling (NMDS), and unweighted pair-group method with arithmetic means (UPGMA) hierarchical clustering (58) were applied to investigate the structural variation of microbial communities across samples in Beta diversity analysis. PERMANOVA (Permutational multivariate analysis of variance) (59) and ANOSIM (Analysis of similarities) (60, 61) in QIIME2 were applied to assess the significance of differentiation for the microbiota structure among groups. LEfSe (Linear discriminant analysis effect size) was applied to detect differentially abundant taxa around the groups in the default parameters (62). The correlation between the genus level abundance of cecum microbiota and SCFA was analyzed by Spearman's correlation coefficient and plotted using the R package "corrplot."

RESULTS

Golden Hamster Body Weights and Daily Dietary Intake

The body weight for each golden hamster was recorded weekly and the means for each group were calculated (**Figure 2**). In the pre-fed and early intervention periods, the mean values of body weight were comparable among all groups. However, the mean body weights for golden hamsters in the positive control group (HC), *Lactobacillus plantarum* supplemented group (LP), and *Lactobacillus fermentum* supplemented group (LF) were higher than those in the negative control group (NC) after 6 and 8 weeks of the experiment. Similar results for body weights were observed in the three groups fed the high cholesterol diet (HC, LP, and LF). There was no significant difference in the daily nutritional intake between all groups.

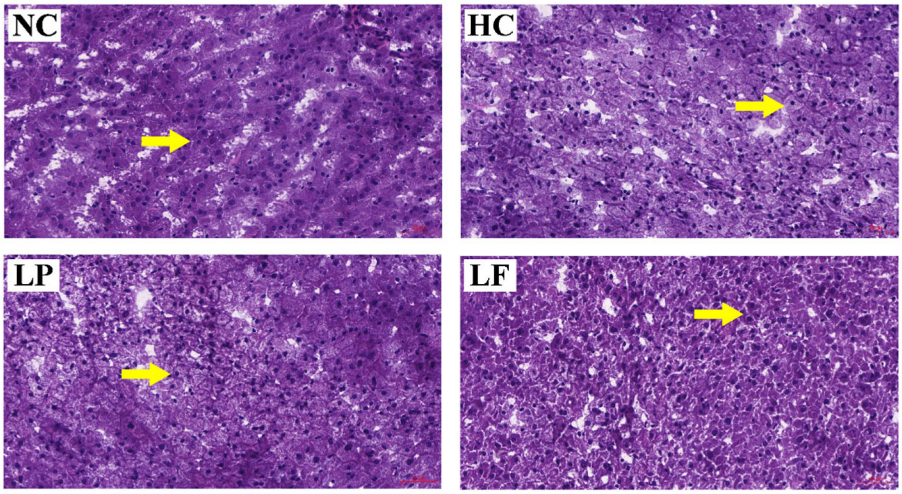

FIGURE 4 | Histological staining of liver tissues from hyperlipidemic golden hamsters after 8-weeks of treatment. Arrows indicate the situation of cytoplasm near the nucleus. Specimens were visualized and image captured using light microscopy (H & E stain, magnification: ×200, Scale bar, 50 μm). NC, negative control group; HC, positive control group; LP, *Lactobacillus plantarum* ZY08 supplemented group; LF, *Lactobacillus fermentum* ZJUIDS06 supplemented group.

Effect of LAB on Serum Lipids

Serum lipids, including TC, LDL-C, HDL-C, and TG were determined every 2 weeks. Exposing the golden hamsters to a high cholesterol diet for 2 weeks increased serum TC and LDL-C levels, indicating that the addition of 0.1% cholesterol and 10% lard to the feed was suitable for inducing hypercholesteremia. After 8 weeks, the serum TC, TG, HDL-C, and LDL-C levels were overall significantly different among all the groups (**Figure 3**). Ingestion of *Lactobacillus fermentum* ZJUIDS06 for 8 weeks reduced serum TC and TG levels in the golden hamsters fed the high cholesterol diet by 1.97 mg/dL and 3.21 mmol/L, respectively, and reduced serum LDL-C by 44.8%, while *Lactobacillus plantarum* ZY08 did not have such an effect. Ingestion of *Lactobacillus fermentation* ZJUIDS06 did not affect the serum HDL-C levels in golden hamsters fed the high cholesterol diet, while ingestion of *Lactobacillus plantarum* ZY08 reduced the HDL-C levels.

Liver Histology

Histopathological analysis was performed on the harvested livers using hematoxylin-eosin staining to assess the effects of LAB supplementation on hepatocyte steatosis (**Figure 4**). The cytoplasm near the nucleus was compact in the hepatocytes of golden hamsters in the NC group. In the HC and LP group, a large number of lipid droplets appeared in the cytoplasm near the nucleus of the hepatocytes. Remarkably, ingestion of *Lactobacillus fermentum* ZJUIDS06 reduced the number of lipid droplets that were present in the cytoplasm near the nucleus of the hepatocytes.

Effect of LAB on SCFA

The concentrations of acetic acid, butyric acid, and propionic acid in colon contents of golden hamsters are presented in **Figure 5**. The amount of total SCFAs in the NC group was lower than that of the HC group. Golden hamsters supplemented with *Lactobacillus fermentum* ZJUIDS06 had higher levels of total SCFAs compared to any other group. Ingestion of *Lactobacillus fermentum* ZJUIDS06 administration for 8 weeks increased acetic acid, propionic acid, and butyric acid by 1.06, 0.13, and 0.10 mmol/L, respectively, while ingestion of *Lactobacillus plantarum* ZY08 did not have similar effects.

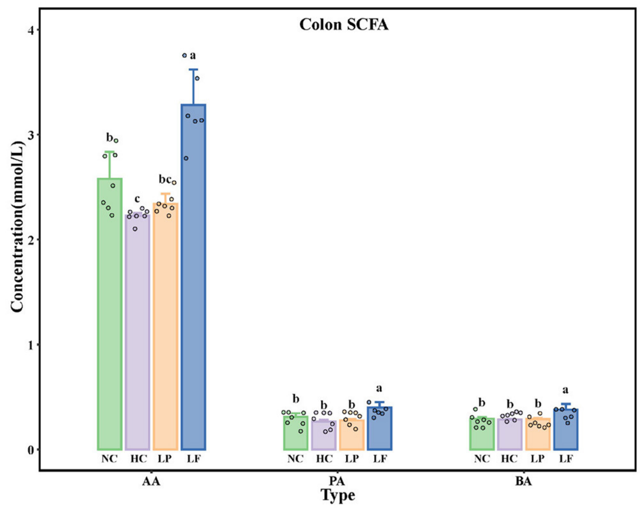

FIGURE 5 | Colon SCFA levels in golden hamsters after 8 weeks of treatment. Groups annotated with *a, b, c* differed significantly with $P < 0.05$ as determined by one-way ANOVA and a Tukey's test. AA, acetic acid; PA, propionic acid; BA, butyric acid; NC, negative control group; HC, positive control group; LP, *Lactobacillus plantarum* ZY08 supplemented group; LF, *Lactobacillus fermentum* ZJUIDS06 supplemented group. NC, HC, LP, and LF are colored in green, purple, orange, and blue, respectively.

Effect of LAB on Tissue Weight

Liver and the epididymal fat pad (EFP) are the two major adipose tissue depots in golden hamsters (63). Therefore, the liver and epididymal fat pad (EFP) weights were recorded to assess the effects of LAB on fat accumulation in the hamsters (**Supplementary Table 2**). The weights of these organs were comparable among the HC, LP, and LF groups. The liver and EFP weight of golden hamsters in the HC, LP, and LF groups were higher than those in the NC group.

Effect of LAB on Cecum Microbiota

To assess the effects of *Lactobacillus fermentum* ZJUIDS06 and *Lactobacillus plantarum* ZY08 intervention on the cecum microbiota of hyperlipidemic golden hamsters (**Supplementary Figure 3**), a MiSeq sequencing-based analysis of bacterial 16S rRNA (V3–V4 region) in cecum content was performed. After being spliced and optimized, 27 samples were delineated into 40,453 OTUs at a 95% similarity level with distance-based OTUs and richness, and rarefaction and Shannon index analysis indicating that the sequencing depth covered rare new phylotypes and most of the diversity (**Supplementary Figure 4**).

The caecal microbiota community was first assessed by analyzing species richness, or the number of species in a community, and species diversity, which is the number of species and abundance of each species that live in a particular location (64) (**Figure 6A**). The observed species and Chao indices of the LF group were significantly higher than the other groups, indicating that the *L. fermentum* ZJUIDS06 intervention increased cecal microbiota richness. However, the Simpson and Shannon indices showed no differences between any of the two groups, indicating that the LAB intervention did not influence the diversity of cecal microbiota.

Next, a Multidimensional Scaling (NMDS) analysis was applied to visualize the differences in community structure between the groups. NMDS is similar to a Principal coordinates analysis (PCoA) analysis, but MNDS analysis is decomposed by dimensionality reduction, and the data structure is simplified, so that the distribution characteristics of the samples can be described using a specific distance scale (65). Here, NMDS analysis revealed a distinct clustering of microbiota composition between the standard diet group (NC) and the high cholesterol diet groups (HC, LP, LF) (**Figure 6B**). The significant separation between groups was confirmed using an unweighted pair-group method with arithmetic means (UPGMA) hierarchical clustering (**Figure 6C**) which showed the similarity between samples in the form of a hierarchical tree and the clustering effect by branch length. An analysis of similarities (ANOSIM) revealed that the overall microbiota structure differed significantly between groups (**Supplementary Table 3**), indicating that the two LAB interventions induced different shifts in the structure of the caecal microbiota community.

Finally, discriminant taxonomic markers were identified with linear discriminant analysis effect size (LEfSe) using the non-parametric factorial Kruskal–Wallis H-test (**Figure 7**). The LEfSe analysis resulted in three parts: The abundance histogram showed the specific distribution of significantly enriched species in different groups of the samples (**Figure 7A**); The species classification cladogram showed the taxonomic hierarchical distribution of significantly enriched species from the phylum to the genus level for each group of the samples (**Figure 7B**); the distribution histogram displayed the LDA value (LDA >2) of significantly different species, which is used to identify the significantly enriched taxa for each group and the important species identified (**Figure 7C**). Based on the results of the LEfSe analysis, *Firmicutes* and *Bacteroidetes* were the dominant phyla in the cecum of all groups. The cecum microbiota of golden hamsters fed a high cholesterol diet was characterized by an increased *Firmicutes*-to-*Bacteroidetes* ratio (**Figure 7A**). Remarkably, at the genus level, *Lactobacillus fermentum* ZJUIDS06 administration increased the relative abundance of *Parabacteroides*, *Flavonifractor*, and *Lactobacillus plantarum* ZY08 increased that of *Faecalibaculum*, *Ruminococcus*, and *Desulfovibrio*.

Correlation Analysis

To demonstrate whether the identified biomarkers were correlated with serum lipid indexes or cecum SCFAs, we performed an association analysis using the R package "corrplot" (**Figure 8**). At the family level, six of 10 marker taxa in the NC group, *Muribaculaceae*, *Tannerellaceae*, *Atopobiaceae*, *Bacteroidaceae*, *Porphyromonadaceae*, and *Clostridiaceae,* showed negative correlations with serum lipid indexes (**Figure 8A**). Three of five marker taxa in the HC group, *Lachnospiraceae*, *Anaplasmataceae*, and *Ruminococcaceae,* showed positive correlations with serum lipid indexes. Only *Desulfomicrobiaceae* in the LP group showed a positive correlation with acetic acid with a Spearman's correlation coefficient of 0.504. The classes significantly correlated with serum lipid reduction and *Lactobacillaceae* and *Bifidobacteriaceae* are shown in **Figure 8B**.

At the genus level, three of the six identified biomarker taxa from the NC group, *Olsenella*, *Bacteroides*, and *Muribaculum,* showed negative correlations with serum lipid indexes. *Kineothrix*, *Dehalobacterium*, and *Wolbachia* from the HC group, *Flavonifractor* from the LF group, and *Desulfovibrio* from the LP group showed significantly positive correlations with serum lipid indexes. Interestingly, only *Parabacteroides* was enriched in the LF group presenting a negative correlation with LDL-C, as well as a positive correlation with SCFA levels, with a Spearman's correlation coefficient of 0.430 for acetic acid, 0.534 for pentanoic acid, and 0.416 for butyric acid, respectively (**Figure 8C**). In addition, *Lactobacillus fermentum* ZJUIDS06 administration increased both the relative abundance of *Parabacteroides* (**Figure 8D**) and the SCFA concentration in the colon content (**Figure 8A**).

DISCUSSION

Ingestion of LAB did not affect body weights of hyperlipidemic golden hamsters, while daily supplementation with *Lactobacillus fermentum* ZJUIDS06, at the dosages of 10^9 CFU per 100 g body weight for 8 weeks, significantly reduced LDL-C, TC, and TG levels in the hyperlipidemic golden hamsters. The lack of

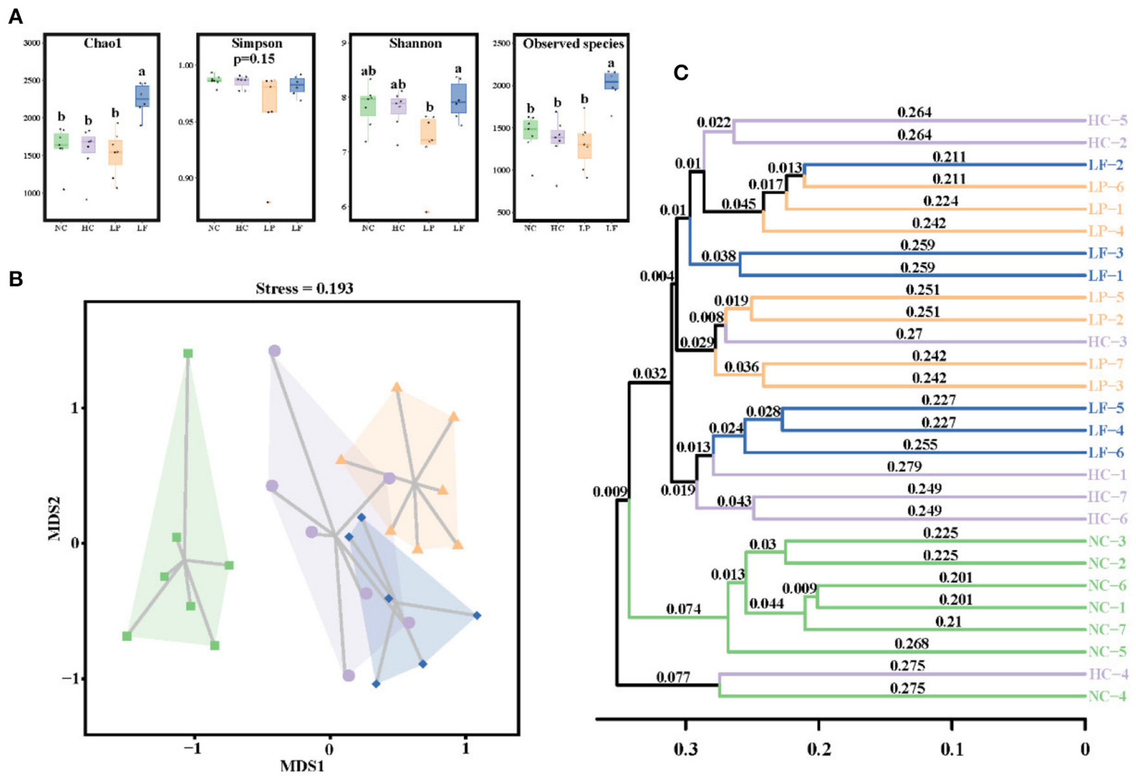

FIGURE 6 | (A) Box plot depicting alpha diversity in the experimental groups of golden hamsters. Groups annotated with *a, b* significantly differed with $P < 0.05$, respectively, as determined by a Kruskal-Wallis and Dunn's test. **(B)** NMDS based on Bray-Curtis distance. **(C)** Clustering tree depicting the samples clustering according to their similarity. NC, negative control group; HC, positive control group; LP, *Lactobacillus plantarum* ZY08 supplemented group; LF, *Lactobacillus fermentum* ZJUIDS06 supplemented group. NC, HC, LP, and LF are colored in green (■), purple (•), orange (▲), and blue (♦), respectively.

a decreasing body weight effect following LAB administration in golden hamsters may be related to the feeding methods used. In previous studies where golden hamsters were exposed to unpredictable chronic mild stress or LAB administration, ingestion of probiotics significantly decreased the body weight gain (66–68). However, in the studies where feeding was unrestricted but monitored, probiotic intervention had no effect on body weight gain (38, 39, 66, 69), which was consistent with our findings here. Remarkably, *Lactobacillus fermentum* ZJUIDS06 exhibited cholesterol-lowering effect while *Lactobacillus plantarum* ZY08 did not have such effect. The variation in cholesterol-lowering effect between these two strains may relate to their different interactions with the host, and still needs to be further elucidated (70). The observation that the reduction of LDL-C, TC, and TG levels by *Lactobacillus fermentum* ZJUIDS06 in hyperlipidemic golden hamsters positively correlated with the levels of colon SCFAs, indicated that oral administration of *Lactobacillus fermentum* ZJUIDS06 may reduce serum lipids by inducing increased colon SCFAs. The effects of SCFAs on cholesterol metabolism in cellular models, hyperlipidemic animal models, and in human clinical trials have been well-documented (citation). Previously, butyrate was found to increase the activity of the liver X receptor ABCG5 and G8 expression and to decrease NPC1L1 expression in Caco-2 cells (71). Concentration changes of SCFA indirectly activated ApoA-I expression with PPARα transactivation, increased transcription of PPARα and CPT1 and decreased transcription of KEAP1 in HepG2 cells (29). The dietary supply with SCFAs decreased serum lipids and promoted fecal excretion of bile acids in hyperlipidemic hamsters through up-regulation of SREBP2, LDLR, and CYP7A1 expression in the liver (28) and reduced the serum lipids in freshly weaned pigs by up-regulating the expression of hepatic FAS, CPT-1α, and SREBP-1 (72). Accordingly, the increase in colon SCFAs observed in this study may relate to the decrease in the serum lipids in hyperlipidemic golden hamsters. However, the role of SCFAs in mediating serum lipids still needs to be elucidated.

In previous reports, the cholesterol-lowering intervention strategies used in hyperlipidemic rodents increased the relative abundance of *Lactobacillus* or *Bifidobacteria* and decreased the ratio of *Firmicutes* to *Bacteroides* (39, 73–75). However, interventions used in this study did not have such effects (**Figure 8B**). The discrepancy between our research and other reports may relate to variations in the intestinal segments or animal models (41). Remarkably, in this research, *Parabacteroides* was the key symbiotic genus negatively correlated with LDL-C and positively correlated with colon SCFAs. Species of *Parabacteroides* have been reported as symbiotic bacteria that

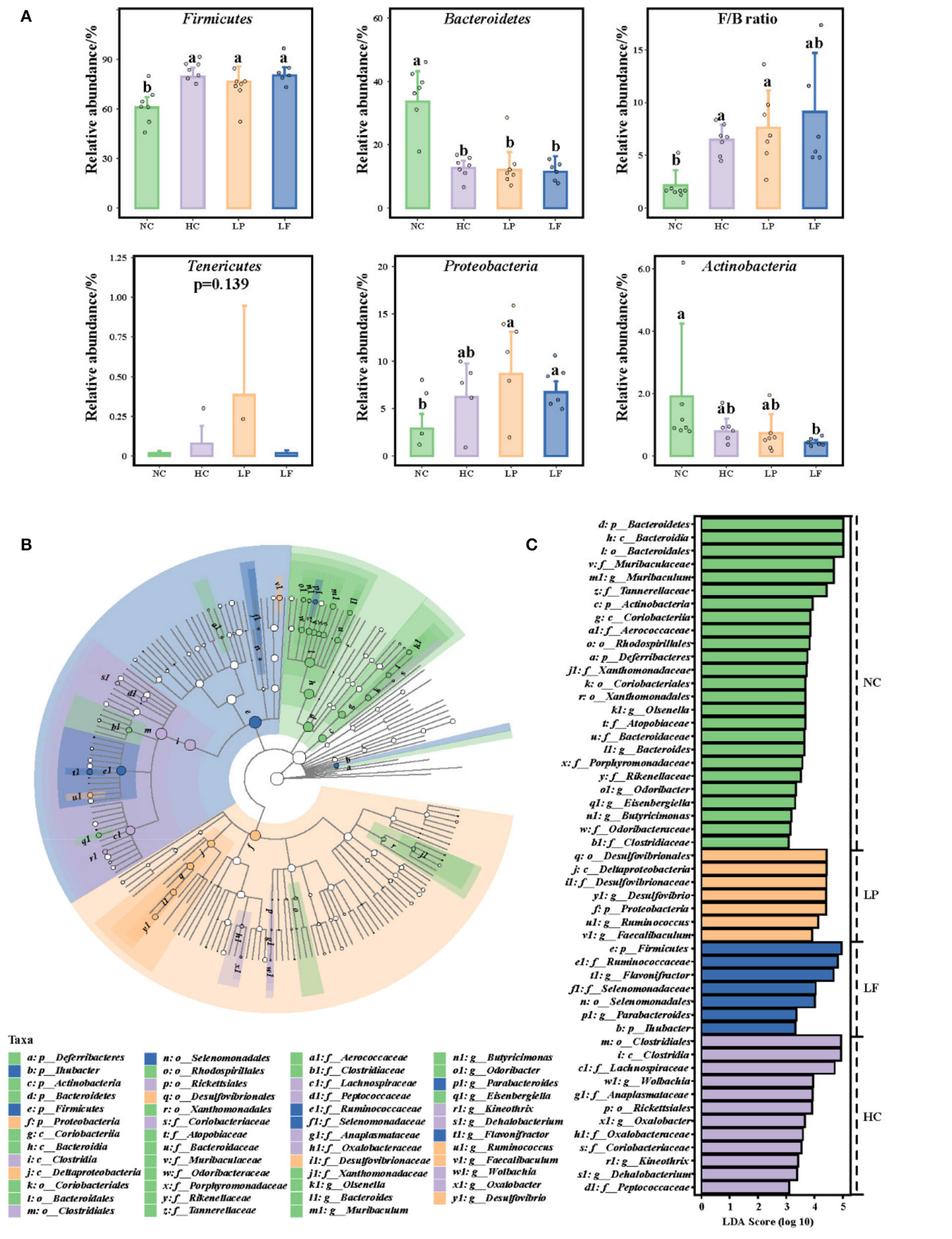

FIGURE 7 | (A) Caecum microbial composition of golden hamsters at the phylum level. **(B)** Taxa Lefse cladogram. **(C)** LDA Score (LDA >2). Groups annotated with letters *a, b* were significantly different with $p < 0.05$ as determined by a Kruskal-Wallis test and FDR correction. NC, negative control group; HC, positive control group; LP, *Lactobacillus plantarum* ZY08 supplemented group; LF, *Lactobacillus fermentum* ZJUIDS06 supplemented group. NC, HC, LP, and LF are colored in green, purple, orange, and blue, respectively.

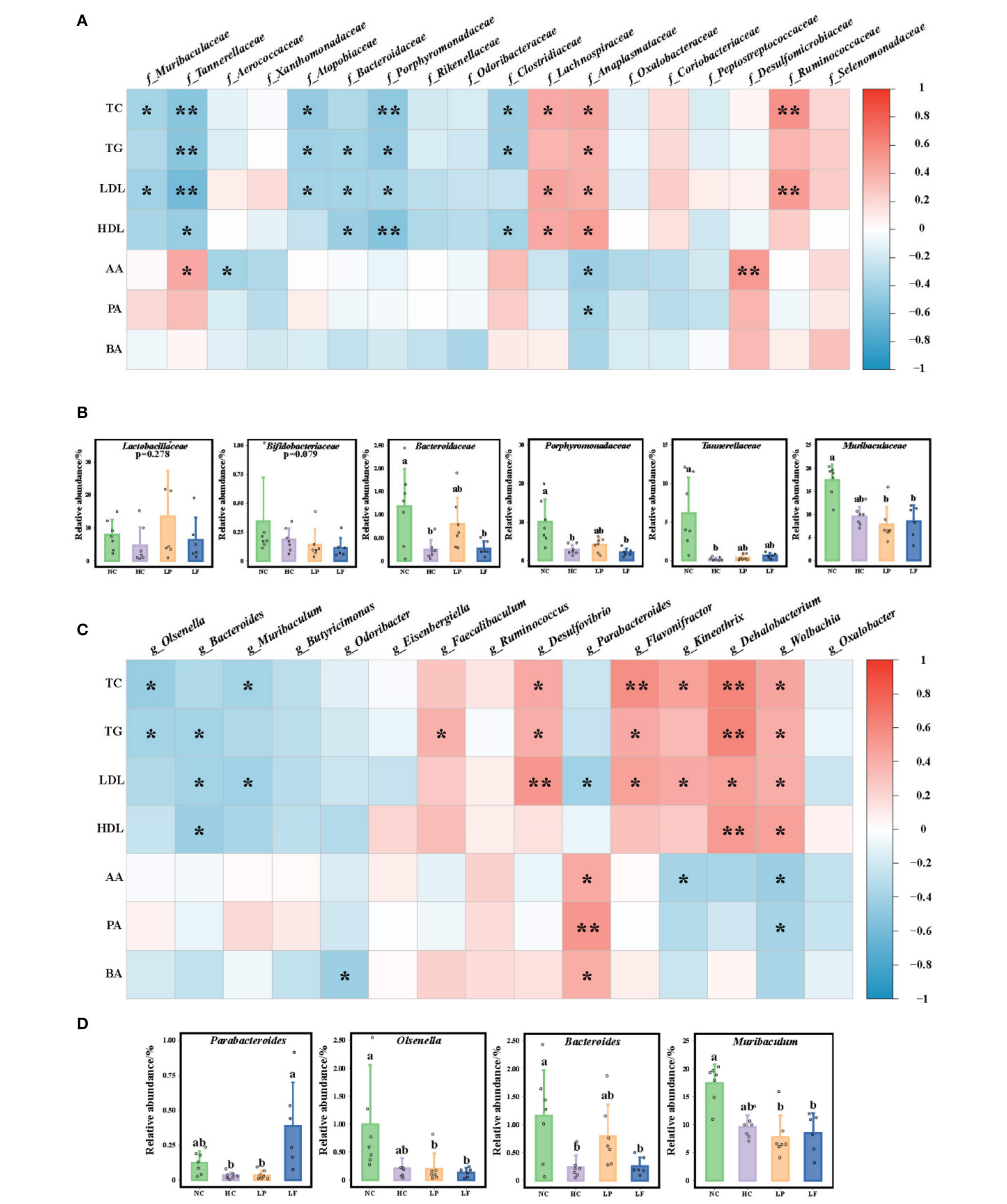

FIGURE 8 | (A) Heat map of Spearman's correlation coefficients between serum lipid indexes, colon SCFA, and marker taxa at the family level (f_bacteria). **(B)** The relative abundance of taxa at the family level that had a significantly negative correlation with the serum lipid indexes including *Lactobacillaceae* and *Bifidobacteriaceae*. *(Continued)*

FIGURE 8 | (C) Heat map of Spearman's correlation coefficient between serum lipid indexes, colon SCFA, and marker taxa at the genus level (g_bacteria). **(D)** The relative abundance of taxa at the genus level that had a significantly negative correlation with serum lipid indexes. Symbols * and ** represent $P < 0.05$ and <0.01, respectively. NC, negative control group; HC, positive control group; LP, *Lactobacillus plantarum* ZY08 supplemented group; LF, *Lactobacillus fermentum* ZJUIDS06 supplemented group; NC, HC, LP, and LF are colored in green, purple, orange, and blue, respectively. TC, serum total cholesterol; TG, serum triglyceride; LDL, serum LDL-C; HDL, serum HDL-C; AA, acetic acid in colon content; PA, propionic acid in colon content; BA, butyrate acid in colon content.

can alleviate obesity and metabolic dysfunction in mice (76). *Parabacteroides goldsteinii* relates to the anti-obesity effects of polysaccharides isolated from *Hirsutella sinensis* and water extract of *Ganoderma lucidum mycelium* in high-fat-diet (HFD) fed mice (77, 78). Oral treatment of HFD fed mice with live *P. goldsteinii* reduced obesity and was associated with increased adipose tissue thermogenesis. *P. goldsteinii* is a novel probiotic bacterium that may be used to treat obesity and associated metabolic disorders (78). These findings provide evidence that ingestion of *Lactobacillus fermentum* ZJUIDS06 may reduce serum lipids by enriching the commensal bacteria *Parabacteroides*.

Our results show that the oral administration of *Lactobacillus fermentum* ZJUIDS06 was not only positively correlated with *Parabacteroides*, but also with increased levels of SCFAs. The results of previous studies have found that some strains of *Parabacteroides* can produce SCFAs. For example, *Parabacteroides acidifaciens* sp. nov. ferments glucose into acetate acid, propionate, isobutyrate, and isopentanoate *in vitro* (79). However, the effects of *Parabacteroides* on *in vivo* SCFAs production remain inconclusive. Only one study found that oral administration of mice with alive *Parabacteroides distanonis* did not affect the level of acetate acid, propionate, isobutyrate, isopentanoate, and pentanoic acid in feces, but increased the level of jejunal succinic acid (76). Taken together, the correlation between *Parabacteroides* and *in vivo* SCFAs production still deserves further validation.

In conclusion, uptake of *Lactobacillus fermentum* ZJUIDS06 and *Lactobacillus plantarum* ZY08 did not prevent body weight gain in golden hamsters fed on a high cholesterol diet. However, oral administration of live *Lactobacillus fermentum* ZJUIDS06 in hyperlipidemic golden hamsters significantly increased colon SCFAs, and decreased the serum levels of LDL-C, TC, and TG, without affecting serum HDL-C, thus improving the colon SCFAs and serum lipid profiles. Both probiotics significantly altered the cecum microbiome, and the reduction of serum lipids following administration of *Lactobacillus fermentum* ZJUIDS06 was positively correlated with the relative abundance of *Parabacteroides*, which are commensal intestinal bacteria with probiotic characteristics. Our results give rise to a deeper understanding of the serum cholesterol-decreasing effects of certain probiotics.

DATA AVAILABILITY STATEMENT

The sequencing data was uploaded to the Sequence Read Archive (SRA) of NCBI and can be visited via accession number: PRJNA727412.

ETHICS STATEMENT

The animal study was reviewed and approved by the Animal Care and Use Committee of Zhejiang University.

AUTHOR CONTRIBUTIONS

DY, ZH, WL, and DR: research design. DY and JG performed *in-vivo* experiments. DY, JG, and ZZ collected the sample and data. DY and ZH analyzed the data. ZH, JF, WW, WL, and DR revised the paper. All authors participated in the conception, design of the study, read, and approved the final manuscript.

FUNDING

This research work was supported by the Zheng Jiang province for Key Research & Development Projects (Grant Number: 2019C02091).

SUPPLEMENTARY MATERIAL

The Supplementary Material for this article can be found online at: https://www.frontiersin.org/articles/10.3389/fnut.2021.705763/full#supplementary-material

REFERENCES

1. Stoekenbroek RM, Boekholdt SM, Fayyad R, Laskey R, Tikkanen MJ, Pedersen TR, et al. High-dose atorvastatin is superior to moderate-dose simvastatin in preventing peripheral arterial disease. *Heart.* (2015) 101:356–62. doi: 10.1136/heartjnl-2014-306906
2. Pothineni NVK, Subramany S, Kuriakose K, Shirazi LF, Romeo F, Shah PK, et al. Infections, atherosclerosis, and coronary heart disease. *Euro Heart J.* (2017) 38:3195–201. doi: 10.1093/eurheartj/ehx362
3. Ni T, Fu Y, Zhou W, Chen M, Shao J, Zhou W, et al. Carotid plaques and neurological impairment in patients with acute cerebral infarction. *PLoS ONE.* (2020) 15:e0226961. doi: 10.1371/journal.pone.0226961
4. Zhang Y, Wu N-Q, Li S, Zhu C-G, Guo Y-L, Qing P, et al. Non-HDL-C is a better predictor for the severity of coronary atherosclerosis compared with LDL-C. *Heart Lung Circul.* (2016) 25:975–81. doi: 10.1016/j.hlc.2016.04.025
5. März W, Kleber ME, Scharnagl H, Speer T, Zewinger S, Ritsch A, et al. HDL cholesterol: reappraisal of its clinical relevance. *Clin Res Cardiol.* (2017) 106:663–75. doi: 10.1007/s00392-017-1106-1
6. Bellosta S, Corsini A. Statin drug interactions and related adverse reactions: an update. *Expert Opinion Drug Safety.* (2018) 17:25–37. doi: 10.1080/14740338.2018.1394455
7. Wong ND, Toth PP, Amsterdam EA. American Society for Preventive Cardiology. Most important advances in preventive cardiology during this

past decade: viewpoint from the American Society for Preventive Cardiology. *Trends Cardiovasc Med.* (2021) 31:49–56. doi: 10.1016/j.tcm.2019.11.013

8. Kunwar S, Parekh JD, Chilukuri RS, Andukuri VA. Necrotizing autoimmune myopathy: a case report on statin induced rhabdomyolysis requiring immunosuppressive therapy. *Drug Discov Ther.* (2018) 12:315–7. doi: 10.5582/ddt.2018.01049
9. Özdemir IH, Copkiran Ö, Tikiz H, Tikiz C. Peripheral polyneuropathy in patients receiving long-term statin therapy. *Turk Kardiyol Dern Ars.* (2019) 47:554–63. doi: 10.5543/tkda.2019.78379
10. Paseban M, Butler AE, Sahebkar A. Mechanisms of statin-induced new-onset diabetes. *J Cell Physiol.* (2019) 234:12551–61. doi: 10.1002/jcp.28123
11. Liu A, Wu Q, Guo J, Ares I, Rodríguez JL, Martínez-Larrañaga MR, et al. Statins: adverse reactions, oxidative stress and metabolic interactions. *Pharmacol Ther.* (2019) 195:54–84. doi: 10.1016/j.pharmthera.2018.10.004
12. Janssen L, Allard NaE, Saris CGJ, Keijer J, Hopman MTE, Timmers S. Muscle toxicity of drugs: when drugs turn physiology into pathophysiology. *Physiol Rev.* (2020) 100:633–72. doi: 10.1152/physrev.00002.2019
13. Hlivak P, Odraska J, Ferencik M, Ebringer L, Jahnova E, Mikes Z. One-year application of probiotic strain Enterococcus faecium M-74 decreases serum cholesterol levels. *Bratisl Lek Listy.* (2005) 106:67–72.
14. Nguyen TDT, Kang JH, Lee MS. Characterization of *Lactobacillus plantarum* PH04, a potential probiotic bacterium with cholesterol-lowering effects. *Int J Food Microbiol.* (2007) 113:358–61. doi: 10.1016/j.ijfoodmicro.2006.08.015
15. Palaniyandi SA, Damodharan K, Suh JW, Yang SH. Probiotic Characterization of cholesterol-lowering Lactobacillus fermentum MJM60397. *Probiotics Antimicrob Proteins.* (2020) 12:1161–72. doi: 10.1007/s12602-019-09585-y
16. Yadav R, Khan SH, Mada SB, Meena S, Kapila R, Kapila S. Consumption of probiotic *Lactobacillus fermentum* MTCC: 5898-fermented milk attenuates dyslipidemia, oxidative stress, and inflammation in male rats fed on cholesterol-enriched diet. *Probiotics Antimicrobial Proteins.* (2019) 11:509–18. doi: 10.1007/s12602-018-9429-4
17. Jeon YB, Lee J-J, Chang HC. Characterization of juice fermented with EM and its cholesterol-lowering effects on rats fed a high-fat and high-cholesterol diet. *Food Sci Nutr.* (2019) 7:3622–34. doi: 10.1002/fsn3.1217
18. Aminlari L, Shekarforoush SS, Hosseinzadeh S, Nazifi S, Sajedianfard J, Eskandari MH. Effect of probiotics Bacillus coagulans and *Lactobacillus plantarum* on lipid profile and feces bacteria of rats fed cholesterol-enriched diet. *Probiotics Antimicrobial Proteins.* (2019) 11:1163–71. doi: 10.1007/s12602-018-9480-1
19. Kullisaar T, Zilmer K, Salum T, Rehema A, Zilmer M. The use of probiotic L. fermentum ME-3 containing Reg'Activ Cholesterol supplement for 4 weeks has a positive influence on blood lipoprotein profiles and inflammatory cytokines: an open-label preliminary study. *Nutr J.* (2016) 15:93. doi: 10.1186/s12937-016-0213-6
20. Tanaka Y, Hirose Y, Yamamoto Y, Yoshikai Y, Murosaki S. Daily intake of heat-killed *Lactobacillus plantarum* L-137 improves inflammation and lipid metabolism in overweight healthy adults: a randomized-controlled trial. *Eur J Nutr.* (2020) 59:2641–9. doi: 10.1007/s00394-019-02112-3
21. Park YE, Kim MS, Shim KW, Kim Y-I, Chu J, Kim B-K, et al. Effects of Q180 on postprandial lipid levels and intestinal environment: a double-blind, randomized, placebo-controlled, parallel trial. *Nutrients.* (2020) 12:255. doi: 10.3390/nu12010255
22. Choi S-B, Lew L-C, Yeo S-K, Nair Parvathy S, Liong M-T. Probiotics and the BSH-related cholesterol lowering mechanism: a Jekyll and Hyde scenario. *Crit Rev Biotechnol.* (2015) 35:392–401. doi: 10.3109/07388551.2014.889077
23. Bustos AY, Font De Valdez G, Fadda S, Taranto MP. New insights into bacterial bile resistance mechanisms: the role of bile salt hydrolase and its impact on human health. *Food Res Int.* (2018) 112:250–62. doi: 10.1016/j.foodres.2018.06.035
24. Jia E-T, Liu Z-Y, Pan M, Lu J-F, Ge Q-Y. Regulation of bile acid metabolism-related signaling pathways by gut microbiota in diseases. *J Zhejiang Univ Sci B.* (2019) 20:781–92. doi: 10.1631/jzus.B1900073
25. Bosch M, Fuentes MC, Audivert S, Bonachera MA, Peiró S, Cuñé J. *Lactobacillus plantarum* CECT 7527, 7528 and 7529: probiotic candidates to reduce cholesterol levels. *J Sci Food Agric.* (2014) 94:803–9. doi: 10.1002/jsfa.6467
26. Lim FT, Lim SM, Ramasamy K. Pediococcus acidilactici LAB4 and *Lactobacillus plantarum* LAB12 assimilate cholesterol and modulate ABCA1, CD36, NPC1L1 and SCARB1 *in vitro*. *Beneficial Microbes.* (2017) 8:97–109. doi: 10.3920/BM2016.0048
27. Mishra AK, Kumar SS, Ghosh AR. Probiotic *Enterococcus faecalis* AG5 effectively assimilates cholesterol and produces fatty acids including propionate. *FEMS Microbiol Lett.* (2019) 366:fnz039. doi: 10.1093/femsle/fnz039
28. Zhao Y, Liu J, Hao W, Zhu H, Liang N, He Z, et al. Structure-specific effects of short-chain fatty acids on plasma cholesterol concentration in male syrian hamsters. *J Agric Food Chem.* (2017) 65:10984–92. doi: 10.1021/acs.jafc.7b04666
29. Tayyeb JZ, Popeijus HE, Mensink RP, Konings MCJM, Mulders KHR, Plat J. The effects of short-chain fatty acids on the transcription and secretion of apolipoprotein A-I in human hepatocytes *in vitro*. *J Cell Biochem.* (2019) 120:17219–27. doi: 10.1002/jcb.28982
30. Zheng Y, Lu Y, Wang J, Yang L, Pan C, Huang Y. Probiotic properties of Lactobacillus strains isolated from Tibetan kefir grains. *PLoS ONE.* (2013) 8:e69868. doi: 10.1371/journal.pone.0069868
31. Bhat B, Bajaj BK. Multifarious cholesterol lowering potential of lactic acid bacteria equipped with desired probiotic functional *attributes*. *3 Biotech.* (2020) 10:200. doi: 10.1007/s13205-020-02183-8
32. Psomas EI, Fletouris DJ, Litopoulou-Tzanetaki E, Tzanetakis N. Assimilation of cholesterol by yeast strains isolated from infant feces and Feta cheese. *J Dairy Sci.* (2003) 86:3416–22. doi: 10.3168/jds.S0022-0302(03)73945-9
33. Sullivan MP, Cerda JJ, Robbins FL, Burgin CW, Beatty RJ. The gerbil, hamster, and guinea pig as rodent models for hyperlipidemia. *Lab Anim Sci.* (1993) 43:575–8.
34. Zhang Z, Wang H, Jiao R, Peng C, Wong YM, Yeung VSY, et al. Choosing hamsters but not rats as a model for studying plasma cholesterol-lowering activity of functional foods. *Mol Nutr Food Res.* (2009) 53:921–30. doi: 10.1002/mnfr.200800517
35. Guo CF, Yuan YH, Yue TL, Li JY. Hamsters are a better model system than rats for evaluating the hypocholesterolemic efficacy of potential probiotic strains. *Mol Nutr Food Res.* (2018) 62:e1800170. doi: 10.1002/mnfr.201800170
36. Dong B, Singh AB, Azhar S, Seidah NG, Liu J. High-fructose feeding promotes accelerated degradation of hepatic LDL receptor and hypercholesterolemia in hamsters via elevated circulating PCSK9 levels. *Atherosclerosis.* (2015) 239:364–74. doi: 10.1016/j.atherosclerosis.2015.01.013
37. Robins SJ, Fasulo JM, Patton GM, Schaefer EJ, Smith DE, Ordovas JM. Gender differences in the development of hyperlipemia and atherosclerosis in hybrid hamsters. *Metabolism.* (1995) 44:1326–31. doi: 10.1016/0026-0495(95)90038-1
38. Huang W-C, Chen Y-M, Kan N-W, Ho C-S, Wei L, Chan C-H, et al. Hypolipidemic effects and safety of *Lactobacillus reuteri* 263 in a hamster model of hyperlipidemia. *Nutrients.* (2015) 7:3767–82. doi: 10.3390/nu7053767
39. Sudun, L.iu S, Xiao C, Peng C, Liang L, He X, et al. Probiotic strains improve high-fat diet-induced hypercholesterolemia through modulating gut microbiota in ways different from atorvastatin. *Food Funct.* (2019) 10:6098–109. doi: 10.1039/C9FO00444K
40. Fei Y, Wang Y, Pang Y, Wang W, Zhu D, Xie M, et al. Xylooligosaccharide modulates gut microbiota and alleviates colonic inflammation caused by high fat diet induced obesity. *Front Physiol.* (2019) 10:1601. doi: 10.3389/fphys.2019.01601
41. Zmora N, Zilberman-Schapira G, Suez J, Mor U, Dori-Bachash M, Bashiardes S, et al. Personalized gut mucosal colonization resistance to empiric probiotics is associated with unique host and microbiome features. *Cell.* (2018) 174:1388–405. doi: 10.1016/j.cell.2018.08.041
42. Liu JH, Zhang ML, Zhang RY, Zhu WY, Mao SY. Comparative studies of the composition of bacterial microbiota associated with the ruminal content, ruminal epithelium and in the faeces of lactating dairy cows. *Microb Biotechnol.* (2016) 9:257–68. doi: 10.1111/1751-7915.12345
43. Yu HJ, Jing C, Xiao N, Zang XM, Zhang CY, Zhang X, et al. Structural difference analysis of adult's intestinal flora basing on the 16S rDNA gene sequencing technology. *Eur Rev Med Pharmacol Sci.* (2020) 24:12983–92. doi: 10.26355/eurrev_202012_24203
44. Zeng Q, An S. Identifying the biogeographic patterns of rare and abundant bacterial communities using different primer sets on the loess plateau. *Microorganisms.* (2021) 9:139. doi: 10.3390/microorganisms9010139

45. Bokulich NA, Kaehler BD, Rideout JR, Dillon M, Bolyen E, Knight R, et al. Optimizing taxonomic classification of marker-gene amplicon sequences with QIIME 2's q2-feature-classifier plugin. *Microbiome.* (2018) 6:90. doi: 10.1186/s40168-018-0470-z
46. Martin M. Cutadapt removes adapter sequences from high-throughput sequencing reads. *EMBnet J.* (2011) 17:13. doi: 10.14806/ej.17.1.200
47. Callahan BJ, Mcmurdie PJ, Rosen MJ, Han AW, Johnson AJA, Holmes SP. DADA2: High-resolution sample inference from Illumina amplicon data. *Nat Methods.* (2016) 13:581–3. doi: 10.1038/nmeth.3869
48. Katoh K, Misawa K, Kuma, K-I, Miyata T. MAFFT: a novel method for rapid multiple sequence alignment based on fast Fourier transform. *Nucl Acids Res.* (2002) 30:3059–66. doi: 10.1093/nar/gkf436
49. Price MN, Dehal PS, Arkin AP. FastTree: computing large minimum evolution trees with profiles instead of a distance matrix. *Mol Biol Evolut.* (2009) 26:1641–50. doi: 10.1093/molbev/msp077
50. Chao A. Nonparametric estimation of the number of classes in a population. *Scand J Stat.* (1984) 11:265–70.
51. Shannon CE. A mathematical theory of communication. *Bell Syst Tech J.* (1948) 27:379–423. doi: 10.1002/j.1538-7305.1948.tb01338.x
52. Shannon CE. A mathematical theory of communication. *Bell Syst Tech J.* (1948) 27:623–56. doi: 10.1002/j.1538-7305.1948.tb00917.x
53. Simpson EH. Measurement of diversity. *Nature.* (1949) 163:688. doi: 10.1038/163688a0
54. Lozupone CA, Hamady M, Kelley ST, Knight R. Quantitative and qualitative β diversity measures lead to different insights into factors that structure microbial communities. *Appl Environ Microbiol.* (2007) 73:1576–85. doi: 10.1128/AEM.01996-06
55. Lozupone C, Knight R. UniFrac: a new phylogenetic method for comparing microbial communities. *Appl Environ Microbiol.* (2005) 71:8228–35. doi: 10.1128/AEM.71.12.8228-8235.2005
56. Kõljalg U, Nilsson RH, Abarenkov K, Tedersoo L, Taylor AFS, Bahram M, et al. Towards a unified paradigm for sequence-based identification of fungi. *Mol Ecol.* (2013) 22:5271–7. doi: 10.1111/mec.12481
57. Bray JR, Curtis JT. An ordination of the upland forest communities of southern wisconsin. *Ecol Monogr.* (1957) 27:326–49. doi: 10.2307/1942268
58. Ramette A. Multivariate analyses in microbial ecology. *FEMS Microbiol Ecol.* (2007) 62:142–60. doi: 10.1111/j.1574-6941.2007.00375.x
59. Mcardle BH, Anderson MJ. Fitting multivariate models to community data: a comment on distance-based redundancy analysis. *Ecology.* (2001) 82:290–7. doi: 10.1890/0012-9658(2001)082[0290:FMMTCD]2.0.CO;2
60. Clarke KR. Non-parametric multivariate analyses of changes in community structure. *Austral Ecol.* (1993) 18:117–43. doi: 10.1111/j.1442-9993.1993.tb00438.x
61. Warton DI, Wright ST, Wang Y. Distance-based multivariate analyses confound location and dispersion effects. *Methods Ecol Evolut.* (2012) 3:89–101. doi: 10.1111/j.2041-210X.2011.00127.x
62. Segata N, Izard J, Waldron L, Gevers D, Miropolsky L, Garrett WS, et al. Metagenomic biomarker discovery and explanation. GenomeBiology.com. (2011) 12:R60. doi: 10.1186/gb-2011-12-6-r60
63. Harris RBS. Denervation as a tool for testing sympathetic control of white adipose tissue. *Physiol Behav.* (2018) 190:3–10. doi: 10.1016/j.physbeh.2017.07.008
64. Pyron M. Characterizing communities. *Nat Educ Knowl.* (2010) 3:39.
65. Legendre P, Legendre L. *Numerical Ecology: Second English Edition*. Amsterdam: Elsevier Science BV (1998). p. 870.
66. Ting W-J, Kuo W-W, Hsieh DJ-Y, Yeh Y-L, Day C-H, Chen Y-H, et al. Heat killed *Lactobacillus reuteri* GMNL-263 reduces fibrosis effects on the liver and heart in high fat diet-hamsters via TGF-β suppression. *Int J Mol Sci.* (2015) 16:25881–96. doi: 10.3390/ijms161025881
67. Hsieh F-C, Lan C-CE, Huang T-Y, Chen K-W, Chai C-Y, Chen W-T, et al. Heat-killed and live *Lactobacillus reuteri* GMNL-263 exhibit similar effects on improving metabolic functions in high-fat diet-induced obese rats. *Food Funct.* (2016) 7:2374–88. doi: 10.1039/C5FO01396H
68. Avolio E, Fazzari G, Zizza M, De Lorenzo A, Di Renzo L, Alò R, et al. Probiotics modify body weight together with anxiety states via pro-inflammatory factors in HFD-treated Syrian golden hamster. *Behav Brain Res.* (2019) 356:390–9. doi: 10.1016/j.bbr.2018.09.010
69. Bhathena J, Martoni C, Kulamarva A, Urbanska AM, Malhotra M, Prakash S. Orally delivered microencapsulated live probiotic formulation lowers serum lipids in hypercholesterolemic hamsters. *J Med Food.* (2009) 12:310–9. doi: 10.1089/jmf.2008.0166
70. Campana R, van Hemert S, Baffone W. Strain-specific probiotic properties of lactic acid bacteria and their interference with human intestinal pathogens invasion. *Gut Pathog.* (2017) 9:1–12. doi: 10.1186/s13099-017-0162-4
71. Chen Y, Xu C, Huang R, Song J, Li D, Xia M. Butyrate from pectin fermentation inhibits intestinal cholesterol absorption and attenuates atherosclerosis in apolipoprotein E-deficient mice. *J Nutr Biochem.* (2018) 56:175–82. doi: 10.1016/j.jnutbio.2018.02.011
72. Jiao AR, Diao H, Yu B, He J, Yu J, Zheng P, et al. Oral administration of short chain fatty acids could attenuate fat deposition of pigs. *PLoS ONE.* (2018) 13:e0196867. doi: 10.1371/journal.pone.0196867
73. Huang Y, Wang J, Cheng Y, Zheng Y. The hypocholesterolaemic effects of *Lactobacillus acidophilus* American type culture collection 4356 in rats are mediated by the down-regulation of Niemann-Pick C1-like 1. *Br J Nutr.* (2010) 104:807–12. doi: 10.1017/S0007114510001285
74. Xie N, Cui Y, Yin Y-N, Zhao X, Yang J-W, Wang Z-G, et al. Effects of two Lactobacillus strains on lipid metabolism and intestinal microflora in rats fed a high-cholesterol diet. *BMC Complement Alternative Med.* (2011) 11:53. doi: 10.1186/1472-6882-11-53
75. Liang T-T, Tong L-T, Geng D-H, Wang L-L, Zhou X-R, Pu H-Y, et al. Wheat Gluten regulates cholesterol metabolism by modulating gut microbiota in hamsters with hyperlipidemia. *J Oleo Sci.* (2019) 68:909–22. doi: 10.5650/jos.ess18257
76. Wang K, Liao M, Zhou N, Bao L, Ma K, Zheng Z, et al. Parabacteroides distasonis alleviates obesity and metabolic dysfunctions via production of succinate and secondary bile acids. *Cell Rep.* (2019) 26:222–35. doi: 10.1016/j.celrep.2018.12.028
77. Chang C-J, Lin C-S, Lu C-C, Martel J, Ko Y-F, Ojcius DM, et al. Ganoderma lucidum reduces obesity in mice by modulating the composition of the gut microbiota. *Nat Commun.* (2015) 6:7489. doi: 10.1038/ncomms8489
78. Wu T-R, Lin C-S, Chang C-J, Lin T-L, Martel J, Ko Y-F, et al. Gut commensal plays a predominant role in the anti-obesity effects of polysaccharides isolated from. *Gut.* (2019) 68:248–62. doi: 10.1136/gutjnl-2017-315458
79. Wang Y-J, Xu X-J, Zhou N, Sun Y, Liu C, Liu S-J, et al. *Parabacteroides acidifaciens* sp. nov., isolated from human faeces. *Int J Syst Evolut Microbiol.* (2019) 69:761–6. doi: 10.1099/ijsem.0.003230

Conflict of Interest: WW was employed by Zhejiang YIMING food CO. LTD.

The remaining authors declare that the research was conducted in the absence of any commercial or financial relationships that could have led to a potential conflict of interest.

frontiers in Nutrition

ORIGINAL RESEARCH
published: 13 July 2021
doi: 10.3389/fnut.2021.701760

NU9056, a KAT 5 Inhibitor, Treatment Alleviates Brain Dysfunction by Inhibiting NLRP3 Inflammasome Activation, Affecting Gut Microbiota, and Derived Metabolites in LPS-Treated Mice

Lu Chen[1], Wenxiang Qing[1], Zexiong Yi[2], Guoxin Lin[1], Qianyi Peng[3] and Fan Zhou[4]**

[1] Department of Anesthesiology, The Third Xiangya Hospital, Central South University, Changsha, China, [2] Medical College of Xiangya, Central South University, Changsha, China, [3] Department of Critical Care Medicine, Xiangya Hospital, Central South University, Changsha, China, [4] Department of Anesthesiology, The Second Xiangya Hospital, Central South University, Changsha, China

OPEN ACCESS

Edited by:
Jie Yin,
Hunan Agricultural University, China

Reviewed by:
Ilandarage Menu Neelaka Molagoda,
Jeju National University, South Korea
Suman Kapila,
National Dairy Research Institute (ICAR), India
Burak Ibrahim Arioz,
Dokuz Eylül University, Turkey

***Correspondence:**
Qianyi Peng
405905@csu.edu.cn
Fan Zhou
zhoufan_2005@csu.edu.cn

Specialty section:
This article was submitted to Nutrition and Microbes, a section of the journal Frontiers in Nutrition

Received: *28 April 2021*
Accepted: *11 June 2021*
Published: *13 July 2021*

Citation:
Chen L, Qing W, Yi Z, Lin G, Peng Q and Zhou F (2021) NU9056, a KAT 5 Inhibitor, Treatment Alleviates Brain Dysfunction by Inhibiting NLRP3 Inflammasome Activation, Affecting Gut Microbiota, and Derived Metabolites in LPS-Treated Mice. Front. Nutr. 8:701760. doi: 10.3389/fnut.2021.701760

Background: The pathogenesis of sepsis-associated encephalopathy (SAE) is complicated, while the efficacy of current treatment technologies is poor. Therefore, the discovery of related targets and the development of new drugs are essential.

Methods: A mouse model of SAE was constructed by intraperitoneal injection of lipopolysaccharide (LPS). LPS treatment of microglia was used to build an *in vitro* model of inflammation. Nine-day survival rates, behavioral testing, transmission electron microscopy (TEM), immunohistochemical (IHC), immunofluorescence (IF), and ELISA were performed. The expression levels of Occludin, Claudin 5, NLRP3, caspase-1, and ASC genes and proteins were detected by RT-qPCR or Western blot. Caspase-1 P10 (Casp-1 P10) protein expression was detected. 16S rDNA sequencing and gas chromatography-mass spectrometer (GC-MS) were used to analyze the gut microbiota and metabolism. Flow cytometric experiment and Cell Counting Kit-8 (CCK8) assay were performed.

Results: NU9056 improved the survival rate of mice and alleviated LPS-induced cognitive impairment, anxiety, and depression *in vivo*. The tight junctions were thickened via NU9056 treatment. Further, the mRNAs and proteins expression levels of Occludin and Claudin 5 were up-regulated by NU9056. NU9056 increased the expression level of DCX. The expression levels of Iba-1, NLRP3, IL-1β, ASC, and Casp-1 P10 were down-regulated by NU9056. The composition of the gut microbiota changed. Kyoto Encyclopedia of Genes and Genomes data predicted that the effects of NU9056 might be related to apoptosis and tight junction pathways. NU9056 up-regulated the concentration of acetate, propionate, and butyrate. NU9056 significantly reduced LPS-induced apoptosis of microglia, the average fluorescence intensity of ROS, and the release of IL-1β and IL-18, while improving cell viability *in vitro*.

Conclusions: NU9056 might effectively alleviate LPS-induced cognitive impairment and emotional disorder in experimental mice by inhibiting the NLRP3 inflammasome. The therapeutic effects may be related to gut microbiota and derived metabolites. NU9056 might be a potential drug of SAE prevention.

Keywords: NU9056, gut microbiota, NLRP3 inflammasome, derivative metabolites, sepsis-associated encephalopathy

INTRODUCTION

Sepsis is one of the leading causes of death in intensive care units (ICU) worldwide and often causes neurological disorders, such as sepsis-associated encephalopathy (SAE). SAE is characterized by pro-inflammatory and anti-inflammatory imbalance, multiple organ dysfunction, severe nervous system disorder, and cognitive and mental dysfunction (1). Although progress has been made in drug therapy and surgical treatment, and age-standardized morbidity and mortality rates have been declining, patients with SAE are still severely. They have a high mortality rate (2). Knowledge of the pathogenesis of sepsis is incomplete, and the discovery of SAE-related targets and the development of corresponding drugs remain crucial goals.

Blood-brain barrier (BBB) damage is closely associated with neuronal damage in SAE (3). Destruction of the BBB is also accompanied by the activation of the NLR family pyrin domain containing 3 (NLRP3, previously known as NACHT, LRR, and PYD domain-containing protein 3) inflammasome (4). The NLRP3 inflammasome is mainly composed of an intracellular sensor, NLRP3, an adaptor ASC and an effector caspase-1 (5). The NLRP3 inflammasome plays a vital role in neuro-inflammatory diseases, like Alzheimer's and Parkinson's disease (6). Related inhibitors, such as the NLRP3 inhibitor MCC950 and the caspase-1 inhibitor VX765, can significantly reduce the neuro-inflammatory damage caused by SAE (7, 8).

Intestinal flora and metabolic disorders are also major factors in the deterioration of SAE. Maintaining metabolic homeostasis contributes to the effective treatment of SAE (9, 10). Probiotics, such as *Clostridium butyricum,* may improve the cognitive impairment of SAE mice by regulating the gut microbiota (11). Related reports have indicated that the gut microbiota of NLRP3-deficient mice can improve depression by regulating astrocytes (12). The NLRP3 inflammasome is also a sensor of metabolic stress (13). Thus, inhibition of the NLRP3 inflammasome may have the potential for SAE treatment by regulating gut microbiota and metabolism.

The KAT5 (also known as Tip60), H4K16 histone acetyltransferase, is present in hypoxia-reoxygenation macrophages. The overexpression of KAT5 and myocardin-related transcription factor A (MRTF-A) synergistically activate the pro-inflammatory factor-induced nitric oxide synthase (iNOS) (14). NLRP3 self-aggregation and complete inflammasome activation require acetylation (15).

NU9056 is a specific inhibitor of KAT5 (16) related to the inhibition of NLRP3 inflammasome (15). However, relatively little is known regarding the underlying mechanism. In the present study, we investigated whether NU9056 has a significant therapeutic effect on SAE *in vivo* and *in vitro* and the main possible reasons for these effects.

MATERIALS AND METHODS

Animal Model

Ninety-five, 12-week-old C57BL/6J mice weighing 25–30 g were randomly divided into a control group, a lipopolysaccharide (LPS) group, and an NU9056 (LPS+NU9056, L. Nu) group. This study was approved by the Institutional Animal Care and Use Committee of the Third Xiangya Hospital, Central South University (No: LLSC (LA) 2018-035). The mice were purchased from Hunan Slack Jingda Experimental Animal Co., Ltd. Laboratory. The animals were adaptively fed for 7 days from the date of purchase. They were reared at room temperature (25 $\pm$ 2°C). The relative humidity was ~55%. Alternating 12 h cycles of light and dark were used. Mice had free access to food and water. LPS-treated mice received an intraperitoneal injection of LPS (10 mg/kg, cat# L2880, Sigma). Control mice were injected with the same amount of normal saline. NU9056 (5 mg/kg, cat#4903, TOCRIS) was intraperitoneally injected twice, 30 min before and 24 h after LPS injection. Sixteen hours after intraperitoneal injection of LPS, blood was collected transcardially. The supernatant was separated and collected. The experiment was performed immediately. Finally, the remaining samples were stored at −80°C. According to the process shown in **Supplementary Figure 1**, the brains and feces from the end of the colon were collected. A portion of the samples were fixed and tested, and the remainder were stored at −80°C. Another 43 mice were randomly divided into three groups with the same grouping and treatment methods as well as before. The animal survival rate and behavioral experiments were carried out. The mice were euthanized by intraperitoneal injection of sodium pentobarbital 150 mg/kg.

Cell Culture and Treatment

BV2 cells (cat# ZQ0397, Shanghai Zhong Qiao Xin Zhou Biotechnology Co., Ltd.) were cultured in DMEM (cat# C11995500BT, Gibco), supplemented with 10% fetal bovine serum (cat# 10099141, Gibco), 100 IU/mL penicillin, and 100 μg/mL streptomycin sulfate (cat# C0222, Beyotime Biotechnology). The cells were placed in a cell culture incubator in an atmosphere of 5% CO_2 at 37°C. Cells were divided into the control group, LPS, and L. Nu groups. The cells in the control group were treated with the same volume of solvent as LPS in the culture medium. The cells in the LPS group were pre-treated with a volume of solvent equivalent to the NU9056 volume for 30 min and followed by the addition of 1 μg/mL LPS and culture of the cells for 24 h. The cells of the L. Nu group were pre-treated with NU9056 (10 μM) for 30 min prior to the same treatment with LPS.

Survival of Animals and Behavioral Testing

The mice were observed daily for their survival. Animal behavior experiments included an open field test (OFT), novel object recognition (NOR), elevated plus maze (EPM), and mouse tail suspension test (TST). The tests were performed as described previously (7) and are briefly described below.

OFT

The open-field box was 40 × 40 × 40 cm. The total distance traveled in five min was analyzed using Smart Junior software (version 3.0; Panlab, Spain).

NOR

Each mouse was placed in a square space of 40 × 40 × 40 cm and underwent familiarization and discrimination. Each mouse could explore 10 min in the field in the familiarization phase with two identical objects (A1 and A2) located opposite and equidistant positions. Twenty-four hours later, each mouse was returned to the open field where one of the familiar objects (A2) was replaced by a novel object (A3). In the discrimination phase, each mouse could explore objects for 10 min, and the time of exploring each object was recorded. Preference indexes of training and test were analyzed.

EPM

The plus-maze height of 50 cm included a central square, two open arms, and two closed arms. The two closed arms were 30 cm in length and 5 cm in width and enclosed by walls with a height of 15 cm. Open arms had no walls. Mice were placed in the central square facing one of the open arms and allowed to explore individually for 5 min. The total time spent in open arms was calculated using the Smart Junior software (version 3.0; Panlab, Spain).

TST

The mice were fixed with the tip of their tail on a horizontal scaffold at the height of 50 cm with the head down. Next, the duration of immobility was recorded for 6 min by the Smart Junior software (version 3.0; Panlab, Spain).

Transmission Electron Microscopy (TEM)

As previously mentioned (17, 18), the samples were fixed in 2.5% glutaraldehyde for 2 h. The samples were washed three times with phosphate-buffered saline (pH 7.2–7.4). The samples were exposed to 1% osmium tetroxide for 1.5 h and then dehydrated. The samples were infiltrated using Poly/Bed 812 resin. TEM was performed using a model H-7700 transmission electron microscope (Hitachi).

TABLE 1 | All primer sequences were used in the study.

Gene	Sequences (5′-3′)
Occludin	F:GTTAAGGCACGGGTAGCACT
	R:TACTTCTGTGACACCGGCAC
Claudin	F: GTTAAGGCACGGGTAGCACT
	R: TACTTCTGTGACACCGGCAC
NLRP3	F: CCTCTTTGGCCTTGTAAACCAG
	R: TGGCTTTCACTTCAATCCACT
ASC	F: CAGAGTACAGCCAGAACAGGACACT
	R: AAGCATCCAGCACTCCGTCCAC
Caspase-1	F: ACAAGGCACGGGACCTATG
	R: TCCCAGTCAGTCCTGGAAATG
β-actin	F: ACATCCGTAAAGACCTCTATGCC
	R: TACTCCTGCTTGCTGATCCAC

Quantitative Reverse Transcription-Polymerase Chain Reaction (RT-qPCR)

RNA was extracted from tissues and cells using TRIzol (Invitrogen) according to the manufacturer's instructions. Next, the extracted RNA was reverse-transcribed into cDNA. The sequences of the target genes were searched using NCBI, and the primers were designed using Primer 5 software (Premier). The primer sequences for each gene were shown in **Table 1**. The relative expression of each target gene was calculated using the $2^{-\Delta\Delta Ct}$ method with β-actin as the internal reference.

Western Blot

Total proteins in each group of tissues were extracted and denatured. After sodium dodecyl sulfate-polyacrylamide gel electrophoresis, the proteins were transferred to nitrocellulose membranes. The membranes were incubated overnight at 4°C with primary antibodies to Occludin (1:2,000, cat# 27260-1-AP, Proteintech), Claudin5 (1:2,000, cat# ab131259, Abcam), NLRP3 (1:1,000, cat# ab263899, Abcam), ASC (1:1,000, cat# AG-25B-0006-C100, Adipogen), Casp-1(1:1,000, cat#24232, Cell Signaling Technology), and β-actin (1:5,000, cat# 60008-1-Ig, Proteintech). The membranes were then exposed to secondary antibody horseradish peroxidase (HRP)-conjugated goat anti-mouse IgG (1:5,000, cat# SA00001-1, Proteintech) or HRP goat anti-rabbit IgG (1:6,000, cat# SA00001-2, Proteintech) was incubated for 90 min at room temperature. β-Actin was used as an internal control. After ECL color exposure, the protein bands were analyzed using an Odyssey infrared imaging system (Li cor Biosciences).

Immunohistochemistry (IHC)

Tissue sections were first deparaffinized and heat-repaired for antigen retrieval and for other routine treatments. The sections were incubated in 3% H_2O_2 for 25 min to remove endogenous peroxidase activity and blocked in 3% BSA for 30 min at room temperature. The primary antibody doublecortin (DCX, cat# 4604S, Cell Signaling Technology) diluted 1:500 was added and incubated overnight at 4°C. The sections were rinsed in phosphate-buffered saline and incubated with goat anti-rabbit secondary antibody (100 μL; cat# PV-9000, ZSGB-BIO) at room temperature for 50 min. Subsequently, the avidin-biotin-peroxidase complex (ABC Elite Kit, Vector Laboratories) was added at room temperature. Positive expression was visualized using enhanced 3,3′ diaminobenzidine.

Immunofluorescence (IF)

Tissue sections were first deparaffinized and heat-repaired for antigen retrieval and for other routine treatments. The cell slides were fixed and permeabilized by routine processing. The primary antibodies Iba1 (1:100; cat# 10904-1-AP, Proteintech) and NLRP3 (2 μg/ml; cat# PA5-79740, ThermoFisher) were incubated overnight at 4°C. The next day, goat anti-rabbit IgG (1:200; cat# SA00013-2, Proteintech) was incubated at 37°C for 90 min. In addition, a 4′,6-diamidino-2-phenylindole (DAPI) working solution was used to stain the nucleus for 10 min. Finally, buffered glycerol was used to mount the slides, and the samples were stored in the dark and observed under a fluorescence microscope.

ELISA

Serum and cellular supernatants were collected. ELISA detection kit for interleukin (IL)-18 (cat# CSB-E04609m) was purchased from Cusabio Biotech Co., Ltd. ELISA detection kits, including IL-1β (cat#88-7013-77) and IL-6 (cat# 88-7064-77), were purchased from eBioscience. The concentrations of IL-1β, IL-6, and IL-18 were determined according to the manufacturer's instructions. A microplate reader (MB-530, Shenzhen Huisong Technology Development Co., Ltd.) was used to measure the optical density (OD) value of each well at 450 nm within 5 min after the termination of the reaction. The sample concentration was determined using a regression equation of the standard curve.

16S rDNA Sequencing Analysis

DNA was extracted following the stool genomic DNA kit instructions (cat# DP328-02, TIANGEN). The concentration of DNA using the dsDNA HS Assay Kit (cat# 12640ES76, Shanghai Yisheng Biotechnology Co., Ltd.) was measured. 16S rDNA sequencing was performed using a NovaSeq PE250 device (Illumina). Raw data were obtained and subjected to unlinking, filtering, deduplication, base correction, and removing the chimera sequence to obtain a valid sequence (clean data) for subsequent analysis. Sequence data were assessed using Qiime 2 (Qiime2-2020.2) and R software (4.0.2). Based on the Kyoto Encyclopedia of Genes and Genomes (KEGG) gene function spectrum data, the conversion calculation of the total metabolic function of the flora was performed and analyzed via KEGG differentiation pathway analysis.

Fecal Short-Chain Fatty Acid (SCFA) Detection

The concentration of SCFA consisting of acetate, propionic, isobutyric, butyric, isovalerate, and valerate were measured via gas chromatography-mass spectrometry (GC-MS) using a model 5977 B apparatus (Agilent). An appropriate amount of feces was added to 300 μL of normal saline containing 37.3 μg/mL d7 isobutyric acid and magnetic beads and homogenized at 60 Hz for 60 s. After centrifugation, acidification, extraction, and other treatments, the samples were analyzed using GC-MS with a DB-WAX capillary column (30 m × 0.250 mm × 0.25 μm) and 99.999% helium as the chromatographic carrier gas at a flow rate of 1 mL/min. The temperature of the injection port and auxiliary heater was 250 and 260°C, respectively. The oven temperature was programmed to start at 50°C and was increased at different rates. Finally, the temperature was increased to 240°C at a rate of 15°C/min and maintained for 5 min. The scanning range was 33–300 Da. The concentration of SCFA was quantified based on the peak area of the total ion current.

Flow Cytometric Experiment

The cells were collected after the abovementioned treatment. An Annexin V-FITC apoptosis detection kit (cat# KGA108, Nanjing KGI) was used to treat the cells according to the manufacturer's instructions. Apoptosis rates were analyzed using a flow cytometer (A00-1-1102, Beckman). The cells were treated with 10 μM of 2′,7′-dichlorofluorescein diacetate (DCFH-DA; cat# S0033S, Beyotime Biotechnology) and incubated at 37°C for 20 min. The fluorescence intensity of reactive oxygen species (ROS) was measured using flow cytometry.

Cell Counting Kit-8 (CCK8) Assay

Cells in the logarithmic growth phase were digested and counted. They were seeded in a 96-well plate at a density of 5×10^3 cells/well using 100 μL per well, with five replicate wells in each group. After 24 h, the cells were processed according to the above groups. The assay was performed according to the manufacturer's protocol. OD_{450nm} was measured on a microplate reader (Bio-Tek). The average value was calculated, and the survival rate curve was plotted.

Statistical Analyzes

Statistical analyzes were performed using GraphPad Prism 8 software (GraphPad Software). Unpaired *t*-tests were used to determine the statistical significance between the two groups. Three or more groups were determined using a one-way analysis of variance. Data are expressed as mean ± standard deviation (SD). Significance was indicated by a $P < 0.05$.

RESULTS

NU9056 Improved Survival Rate and Relieved Cognitive Dysfunction and Emotional Disorder in LPS-Induced Mice

In order to identify the effects of NU9056 on LPS-induced mice, a survival analysis was conducted. The results found that the survival percent in all of the animals in the control group was 100% during the 9 days in the study, suggesting they were normal. In contrast, the animals in the LPS group began to die the next day and continued to die on days 2–6, with an eventual survival rate of 60%. In the L. Nu group, the survival curve was relatively flat compared to the LPS group, and the eventual survival rate was 87% (**Figure 1**), suggesting that NU9056 has noticeable therapeutic effects in the LPS-induced mice. To verify the impact of NU9056 on cognitive and emotional dysfunction, OFT, NOR, EPM, and TST behavioral experiments were performed according to the experimental shown in **Supplementary Figure 1**. The OFT experiment results showed that there was no significant difference in the total distance moved by the mice in each group 5 days after LPS injection (**Figure 1B**). The results of the NOR experiment indicated that the preference index of training in the mice among the groups was not different for the left and right objects. In the testing phase, NU9056 increased the exploration index of the novel object induced by LPS in mice (**Figures 1C,D**). In the EPM experiment, the time in the open arms of the mice in the LPS group was significantly reduced compared with that in the control group, while the time for the mice in the L. Nu group increased significantly compared with that in the LPS group (**Figure 1E**). The TST results showed that the immobility duration of the L. Nu group markedly lower than that of the LPS group (**Figure 1F**). The collective results indicated that NU9056 reversed cognitive dysfunction and emotional disorder of mice in the LPS group.

NU9056 Might Inhibit Microglia Activation and Protect From BBB Damage by Downregulating the NLRP3 Inflammatory Pathway in the Mice Treated With LPS

TEM revealed that the tight junctions of the LPS group showed local thinning, indicating that the tight junctions and BBB were damaged. Compared with the mice in the LPS group, the tight junctions of the mice in the NU9056 group became thicker, and the structure tended to be normal, indicating that the BBB function was protected (**Figure 2A**). RT-qPCR and Western blot were used to explore the BBB function and molecular pathways related to NU9056. The expression levels of genes and proteins, including Occludin and Claudin 5 in the L. Nu group, were significantly higher than those in the LPS group (**Figures 2B,C**). To further verify the effects of NU9056 in LPS-induced mice on newborn brain neurons, IHC was performed. The results indicated that the L. Nu group reversed the LPS-induced decrease in the expression level of DCX, suggesting that NU9056 has a potential therapeutic effect in mice with SAE (**Figure 2D**). Altogether, NU9056 protected BBB and newborn neurons' function from damage *in vivo*.

To validate whether NU9056 activated hippocampal microglia, *in vivo* IF was performed. Compared with the control group, NU9056 reversed the abnormal activation of Iba-1 and NLRP3 in the hippocampus of mice stimulated with LPS (**Figures 3A,B**). In contrast to the LPS group, the expression level of the serum inflammatory factor IL-1β in the L. Nu group was significantly reduced, while there was no significant difference in IL-6 levels (**Figure 3C**). Moreover, in the hippocampus of mice, related inflammation and pyrolysis pathway indicators, the expression levels of NLRP3 and ASC genes and proteins were abnormally activated, and that of Casp-1 splicing body P10 protein was significantly increased. However, NU9056 reversed the above process (**Figures 3D,E**). In addition, the results suggested that NU9056 might inhibit the abnormal activation of microglia and inflammation induced by LPS by down-regulating the NLRP3 inflammatory pathway.

NU9056 Affected Fecal Microbiota in LPS-Induced Mice

To further identify whether the effects of NU9056 in alleviating SAE were related to the gut microbiota, 16S rDNA sequencing was performed. The rank-abundance graph showed that as the sequencing depth increased, the read abundance gradually increased and finally tended to be flat, indicating that each group of samples' species richness and uniformity were eligible (**Figure 4A**). The operational taxonomic unit (OTU) species annotation Venn diagram indicated that in terms of overall species diversity, the species abundance of the L. Nu group decreased (**Figure 4B**). The results of an OTU core species annotation Venn diagram suggested that compared with the control group, the endemic species clusters of the LPS group were up-regulated, while that of the L. Nu group tended to be similar to the normal group (**Figure 4C**). We then analyzed the alpha diversity of the samples among the groups. Compared with the LPS group, the Shannon, Simpson's, and J indices of the L. NU group decreased significantly, indicating that biodiversity was reduced (**Figure 4D**). The beta diversity results of the samples demonstrated that the degree of dispersion between LPS groups was greater, whereas it was significantly reduced after NU9056 treatment (**Figure 4E**). Subsequently, we analyzed the changes in fecal microbial abundance at the phylum and genus levels. At the phylum level, compared with the LPS group, the relative abundance of the *Verrucomicrobia* phylum in the L. Nu group showed an upward trend (**Figure 4F**). At the genus level, the abundance of the *Akkermansia* genus in the phylum *Verrucomicrobia* in the L. Nu group was notably higher than that in the LPS group (**Figure 4G**). The above results suggested that the mitigation effects of NU9056 might be related to the diversity and structural changes in the gut microbiota.

To further distinguish the function of changes caused by changes in species abundance, KEGG pathways were used for functional predictions. The results of data analysis at the level of the Class predicted a changing trend of cellular processing pathway enrichment in the L. Nu group (**Figure 4H**). Compared to the control group, the apoptosis signaling pathway in the LPS group was significantly enriched. In addition, the tight junction and signaling pathways regulating the pluripotency of stem cells in the L. Nu group displayed a trend of enrichment. The L. Nu group was less enriched in the apoptosis pathway than the LPS group (**Figure 4I**). These findings indicated that the therapeutic effects of NU9056 might be involved in inhibiting apoptosis, promoting tight junctions, and signaling pathways regulating the pluripotency of stem cells.

NU9056 in LPS-Induced Mice Might Be Associated With SCFA

Changes in the gut microbiota are often closely associated with metabolism. Therefore, we further studied the effects of

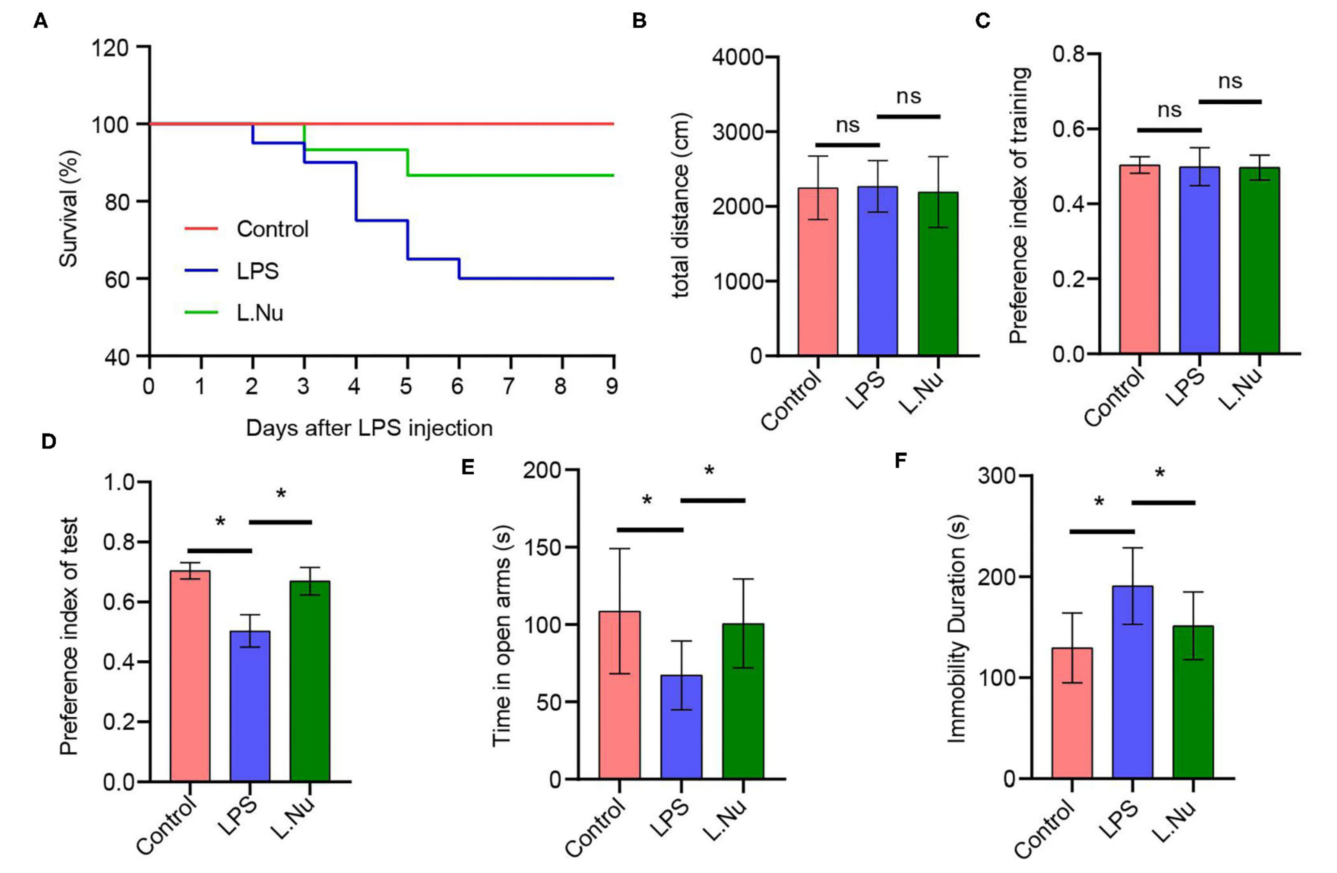

FIGURE 1 | NU9056 improved survival rate and relieved cognitive and emotional dysfunction in LPS-induced mice. **(A)** The 9-day survival rate of mice was determined. Twelve of twenty mice of the LPS group survived, 13 of 15 mice of the L. Nu group survived. **(B)** The total distance moved by each group of mice was detected in the OFT experiment. **(C,D)** The preference index of training and test were recorded in the NOR experiment. **(E)** The time in open arms was detected in the EPM assay. **(F)** The duration of immobility of the mice was analyzed using the TST experiment. *$P < 0.05$; ns, not significant; $n = 8$–20 mice/group.

NU9056 on SCFAs. GC-MS revealed that in contrast with the LPS group, the concentrations of acetate, propionate, and butyric markedly increased, while the overall concentrations of isobutyrate, isovalerate, and valerate were reduced and showed no evident change trend in the L. Nu group (**Figure 5**). These results suggested that the alleviating effects of NU9056 in LPS-induced mice might be associated with SCFA.

Gut Microbiota Was Related to SCFA and Inflammatory Factors in LPS-Induced Mice

The above results indicated that the effects of NU9056 may be related to the gut microbiota, SCFA, and inflammatory factors. To analyze the correlation among them, the Spearman correlation coefficient algorithm was used (**Figure 6**). The heatmap revealed that the concentration of acetate was negatively correlated with *Alloprevotella* ($r = -0.51$, $P = 0.036$), *Parabacteroides* ($r = -0.55$, $P = 0.021$), and *Bacteroides* ($r = -0.60$, $P = 0.029$), and positively correlated with *Lachnoclostridium* ($r = 0.54$, $P = 0.041$). Propionate was negatively correlated with *Bacteroides* ($r = -0.55$, $P = 0.036$) and *Escherichia-Shigella* ($r = -0.52$, $P = 0.048$). Butyrate was positively correlated with *Akkermansia* ($r = 0.54$, $P = 0.042$), but negatively correlated with *Alloprevotella* ($r = -0.57$, $P = 0.029$) and *Roseburia* ($r = -0.53$, $P = 0.047$). The inflammatory factor IL-1β was significantly positively correlated in *Alloprevotella* ($r = 0.55$, $P = 0.035$), *Bacteroides* ($r = 0.79$, $P = 0.001$), and *Escherichia-Shigella* ($r = 0.76$, $P = 0.002$). The inflammatory factor IL-6 was significantly positively correlated with *Bacteroides* ($r = 0.70$, $P = 0.005$) and *Escherichia-Shigella* ($r = 0.59$, $P = 0.023$). The inflammatory factor IL-6 was significantly negatively associated with *Roseburia* ($r = -0.66$, $P = 0.009$), *Lachnoclostridium* ($r = -0.54$, $P = 0.041$), and *Lachnospiraceae_NK4A136_group* ($r = -0.67$, $P = 0.008$).

NU9056 Inhibited Apoptosis and Inflammation of Microglia *in vitro*

The above results showed that NU9056 had therapeutic effects on LPS-induced mice. Subsequently, we wanted to verify its protective effects *in vitro* further. We detected the apoptosis rate and ROS levels in each group of cells. Compared to that in the LPS group. The apoptosis rate and average fluorescence intensity of BV2 cells in the L. Nu group were markedly lower

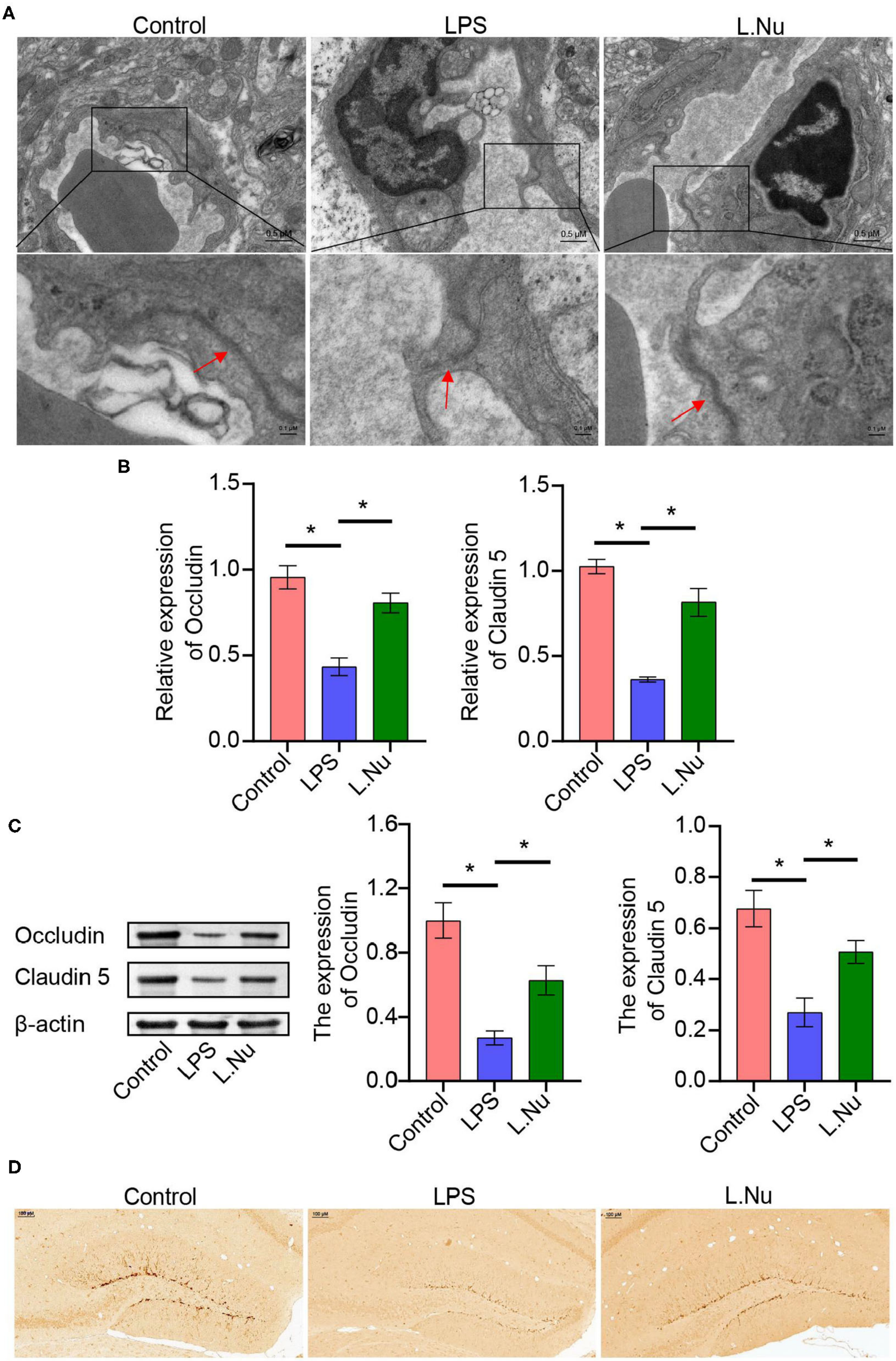

FIGURE 2 | NU9056 protected BBB, and newborn neurons function from damage *in vivo*. **(A)** The morphological changes of the tight junctions of the hippocampus in the mice were observed using TEM. The arrow points to a tight junctions structure. **(B,C)** The expression levels of Occludin and Claudin 5 genes and proteins in the mouse hippocampus were detected using RT-qPCR and Western blot. **(D)** The DCX expression level of newborn neurons in the brain tissue of mice was observed using IHC. *$P < 0.05$.

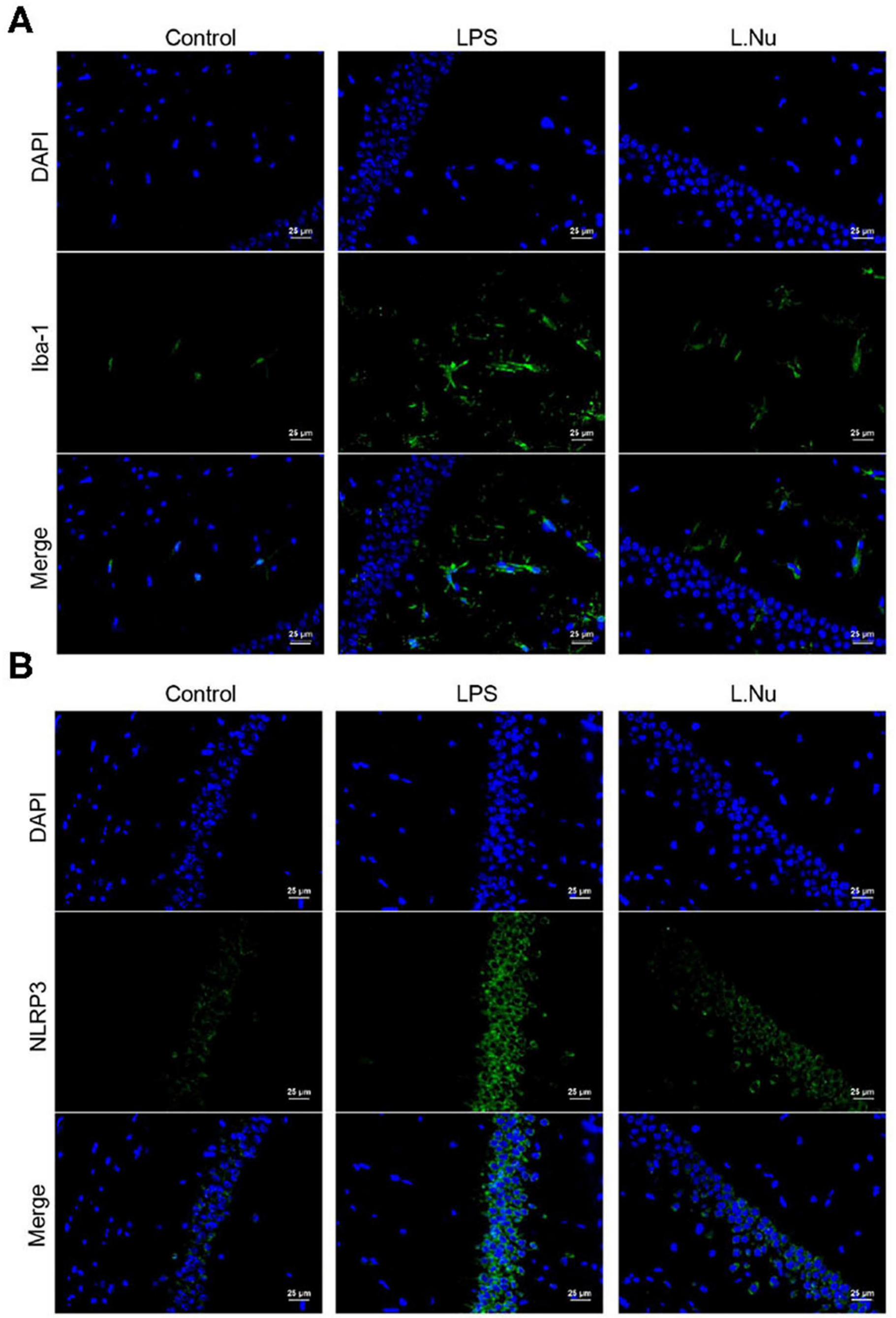

FIGURE 3 | Continued

(**Figures 7A,B**). The CCK8 results revealed that the cell viability of the L. Nu group was remarkably higher than that of the LPS group (**Figure 7C**). We further tested the inflammatory factors. ELISA results revealed that NU9056 suppressed the LPS-induced expression of IL-1β and Il-18 (**Figure 7D**). The collective results suggested that NU9056 also inhibited apoptosis and inflammation in microglia *in vitro*.

DISCUSSION

SAE occurs in 70% of patients admitted to the ICU, which might be related to abnormal activation of microglia, brain inflammation, neurotransmitter dysfunction, and other causes (19). In this study, the mitigation effects of NU9056 on LPS-stimulated mouse models of behavioral disorders, brain

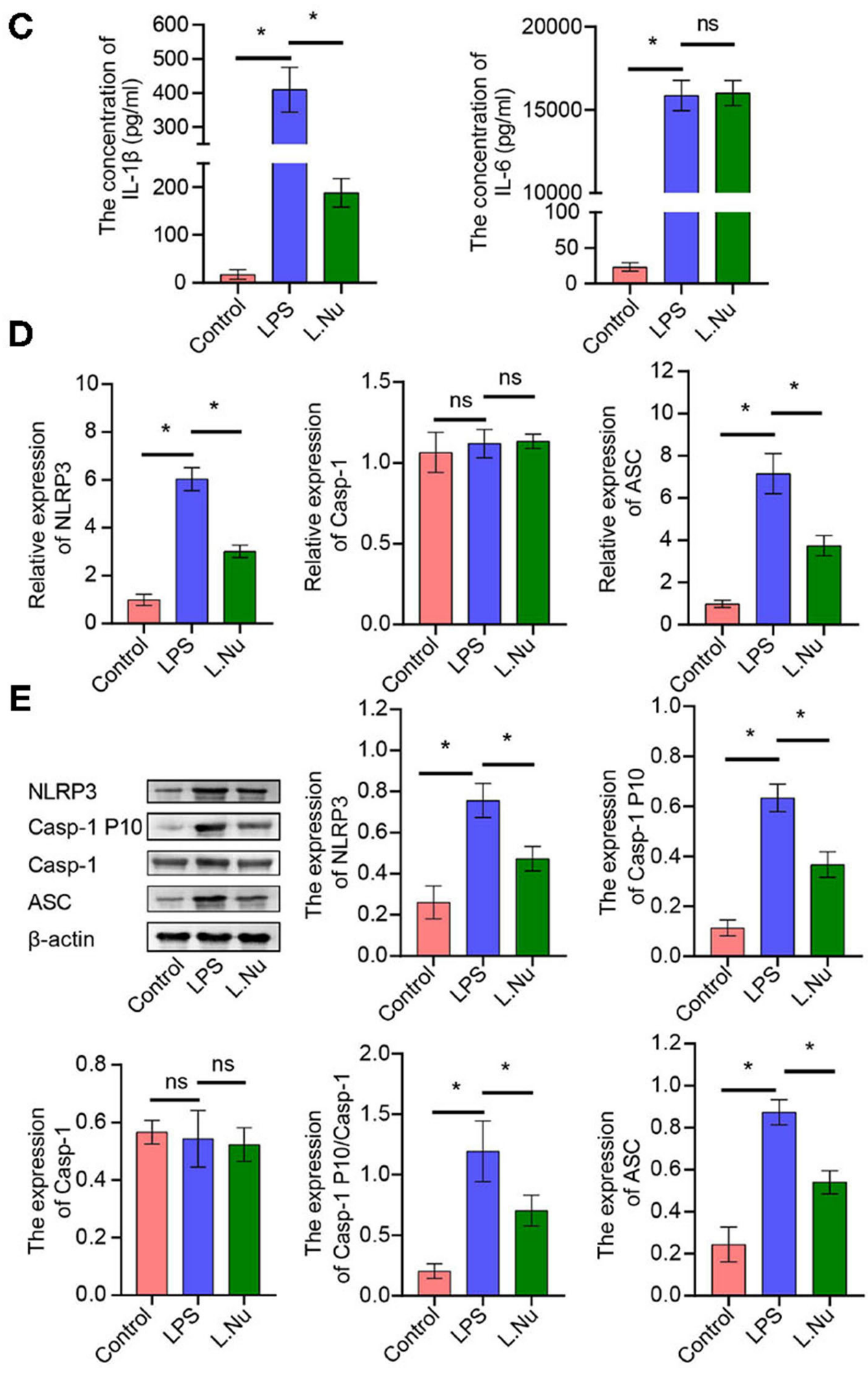

FIGURE 3 | NU9056 might inhibit microglia activation and inflammation by inhibiting the NLRP3 inflammatory pathway *in vivo*. **(A,B)** The expression level of Iba-1 and NLRP3 in hippocampal microglia of mice were detected using IF; **(C)** the concentrations of IL-1β and IL-6 in the serum of mice were tested using ELISA; **(D,E)** genes or proteins expression levels of NLRP3, ASC, Casp-1, and Casp-1 P10 in the hippocampus of mice were analyzed by RT-qPCR or Western blot. *$P < 0.05$; ns, not significant.

damage, abnormal activation of microglia, brain inflammation, and BBB function were investigated. NU9056 remarkably improved the survival rate of LPS-stimulated mice, relieved cognitive dysfunction, anxiety, and depression, reduced DCX expression, hindered abnormal activation of microglia, reduced neuroinflammation, protected BBB function, and affected the

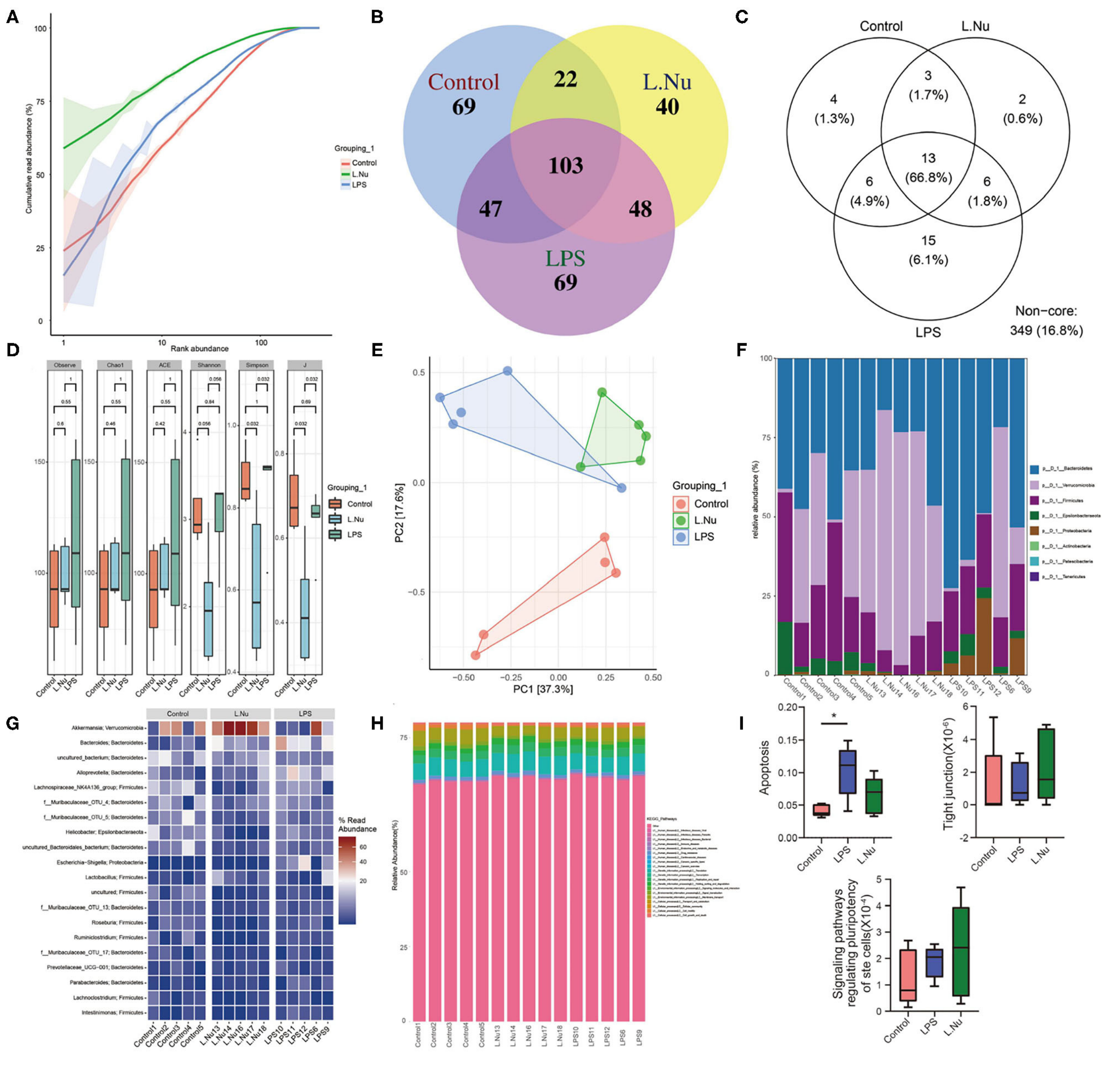

FIGURE 4 | NU9056 affected the fecal microbiota in LPS-induced mice. **(A)** Rank-abundance graph. **(B)** Venn diagram of the number of common and unique OTUs in each group. **(C)** Venn diagram of the number of common and unique core species OTUs in each group. **(D)** The alpha diversity of gut microbiota in each group was analyzed using 16S rDNA sequencing, consisting of (1) Observed OTUs, (2) Chao1 index, (3) ACE index, (4) Shannon index, (5) Simpson's index, and (6) J index. **(E)** Principal component analysis of the similarity of samples among groups. **(F)** Variation in the relative abundance of samples in each group at the phylum level. **(G)** Variation in the relative abundance of samples in each group at the genus level. **(H)** KEGG pathways predictions of functions of gut microbiota at the class level. **(I)** KEGG pathways predictions of enrichment of each group in apoptosis, tight junction, and signaling pathways regulating the pluripotency of stem cells. *$P < 0.05$.

composition of the gut microbiota. In addition, we validated the results of the LPS-induced inflammation model *in vitro*. The collective findings indicate that NU9056 treatment might have effectively alleviated damage in the LPS model mice by inhibiting the NLRP3 inflammasome to some extent.

The NLRP3 inflammasome is activated in the central nervous system, which can cause many neuroinflammatory diseases (20). The widely accepted view is that NLRP3 binds to ASC after activation and then binds to Casp-1. The active Casp-1 rapidly cleaves pro-IL-1β and pro-IL-18 to mature IL-1β and IL-18, respectively. Subsequently, IL-1β is released outside the cell, causing inflammation (21). IL-6 is another common inflammatory factor. Typically LPS induces an increase in the concentration of IL-6 (22). As an NLRP3 inhibitor, the

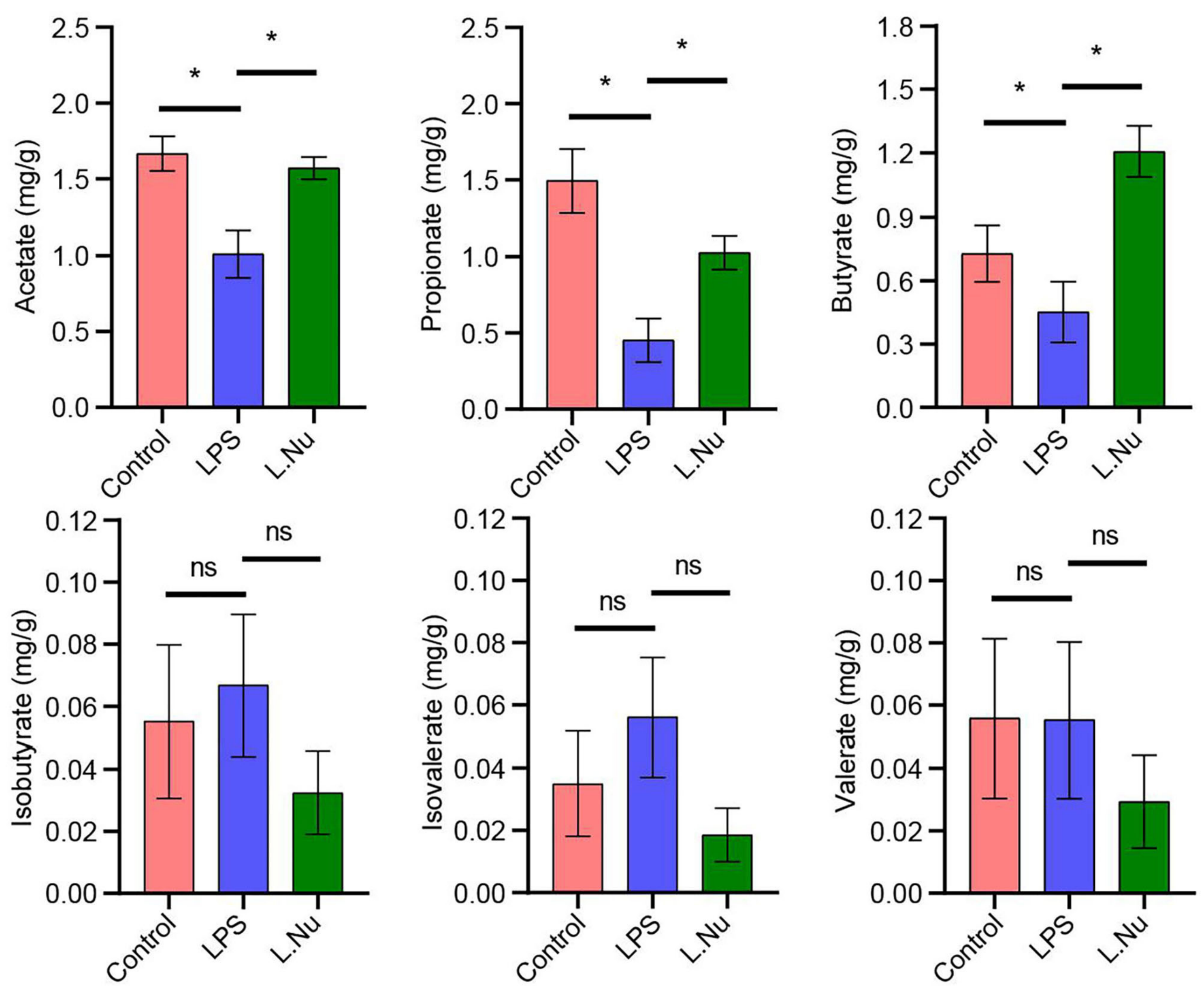

FIGURE 5 | NU9056 in LPS-induced mice might be associated with SCFA. GC-MS determination of the concentration of SCFA consisting of acetate, propionic, butyric, isobutyric, isovalerate, and valerate in the stools of mice. *$P < 0.05$; ns, not significant.

therapeutic effects of MCC950 on diabetic stroke rats were similar to those of NU9056 in the treatment of LPS-induced mice (23). In this study, we determined the concentrations of IL-1β and IL-6 in the blood of mice in each group *in vivo*. NU9056 could markedly downregulate the concentration of IL-1β without significantly affecting the IL-6 level in the blood. This was consistent with the research of Zhao et al. (15). NU9056 attenuated the release of IL-1β and IL-18 *in vitro*. This might be explained by the fact that NU9056 is a specific inhibitor of KAT5. It may have an anti-inflammatory effect by inhibiting the activation of NLRP3 inflammasomes. However, the downstream pathway of NLRP3 inflammasome may be mainly IL-1β and IL-18 (21). Therefore, NU9056 has no significant effect on IL-6 inflammatory cytokines.

Microglia, BV2 cells, are permanent immune cells in the brain and play an essential role in regulating inflammation in the brain (24). NOD-like receptor protein 3 (NLRP3) was also widely expressed in the cells (25). BV2 cells are often used to study the BBB function, inflammation, NLRP3 pathway, etc. (25, 26). Therefore, BV2 cells have been studied *in vitro*. Due to funding limitations, NU9056 has not been studied on other cells, such as astrocytes and neural cells. We will further explore NU9056 in microglia, astrocytes, neural cells, and other cellular mechanisms related to neuroinflammation in future studies. In addition, abnormal activation of microglia increases ROS levels abnormally and causes apoptosis in brain tissue (20). The present study results also showed that NU9056 could reverse LPS-induced activation of microglia to a certain extent. Activation of TLR4-NF-kB in LPS-induced BV2 cells has been reported in many papers (27, 28). If NU9056 could block the TLR4-NF-kB pathway simultaneously, it would be an essential basis for the possible action of NU9056 on other inflammatory

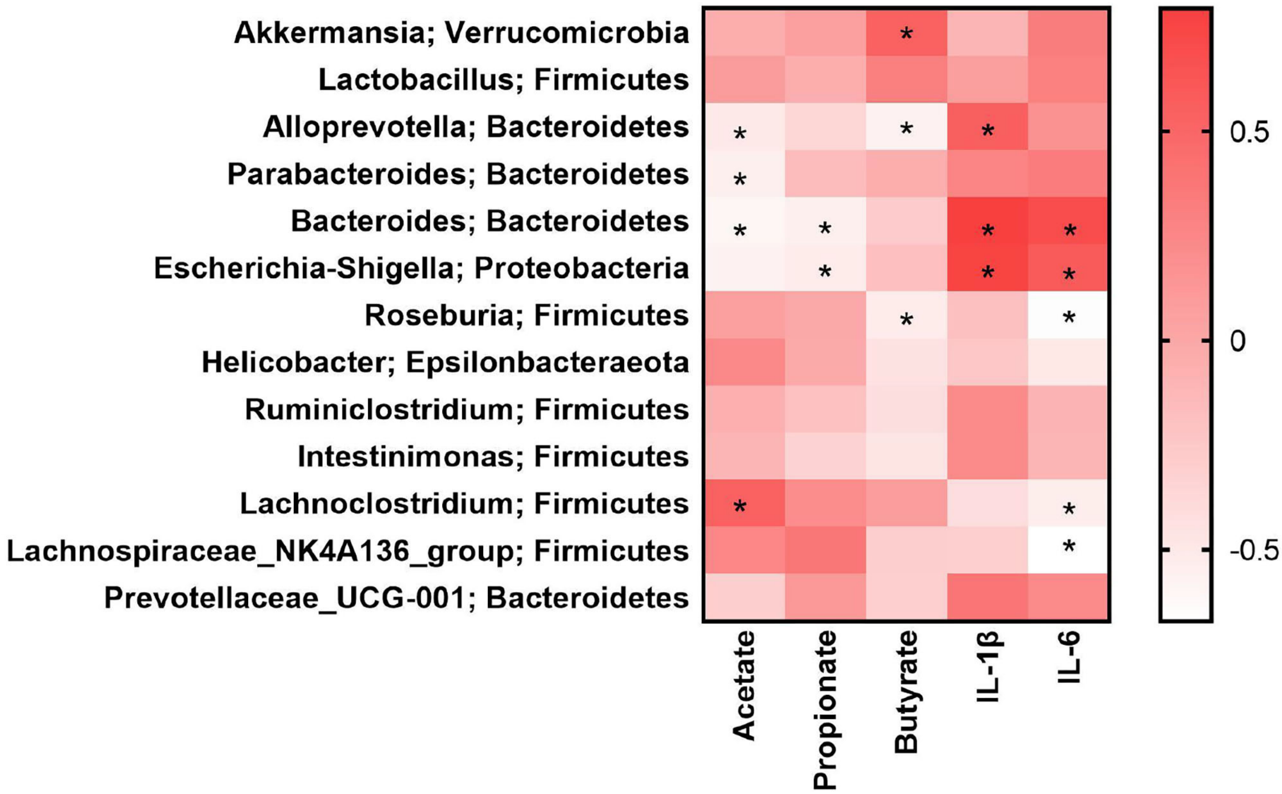

FIGURE 6 | Gut microbiota was related to SCFA and inflammatory factors in LPS-induced mice. *$P < 0.05$.

diseases. But due to the funding and time, we did not do that. Future studies will further investigate whether NU9056 can inhibit different inflammatory pathways other than NLRP3, such as TLR4-NF-kB.

BBB damage was involved in the occurrence and development of many neuroinflammatory diseases, including SAE. Therefore, many therapeutic drugs related to neurological diseases have the effect of protecting BBB (29). Our research revealed that NU9056 could alleviate the BBB damage of LPS-induced mice. The result of TEM found that the tight junctions become thicker; additionally, the BBB-related proteins Occludin and Claudin 5 also have an upward trend, suggesting that NU9056 has a relieving effect on BBB. It further illustrated the great potential of NU9056 as a treatment for SAE.

SAEs have been well-established to cause severe cognitive impairment (30). DCX is a classic marker of newborn neurons (31). Furthermore, in depression-like model mice, treatment with ghrelin increased the expression level of DCX (32). Consistent with these findings, we observed that the decrease in the expression level of DCX in the LPS model was reversed by NU9056, suggesting that NU9056 has the potential to protect newborn neurons and further alleviate cognitive impairment.

The cognitive ability of mice has been assessed through OFT, NOR, and other behavioral experiments (33). Liao et al. reported that S100A9 could contribute to the learning and memory impairment of experimental sepsis mice (34). In our study, different behavioral experiments were performed in mice treated with LPS and NU9056. The same animals were used for different behavioral experiments. The reality is that a behavioral experiment such as NOR often takes several hours. After a long period of the behavioral experiment, mice showed unstable mood and abnormal performance. The circadian rhythm also affected the mice's behavior. In addition, there may be some influence between different behavioral experiments. With these factors in mind, in our experiment, the mice were tested by OFT, NOR, EPM, and TST behavioral experiments on days 5, 6, 7, 8, and 9 after LPS modeling. OFT detected the recovery of activity ability of mice in each group. The total movement distance of the three groups of mice within a certain period of time was the same, which meant that their activity ability had returned to a consistent level. This could avoid the deviation of subsequent behavioral tests due to differences in activity ability (35, 36). Then, according to the size of the behavioral stimuli, NOR, EMP, and TST were performed to detect the memory, anxiety, and depression of the mice, respectively. In NOR, EMP, and TST experiments, NU9056 showed the effects of improving memory ability and alleviating anxiety and depression in sepsis mice.

Increasing evidence has shown that inflammation, BBB function, and cognitive dysfunction in SAE mice provide a key link to gut microbiota and metabolism (9). The NLRP3 inflammasome plays a crucial role in coordinating host

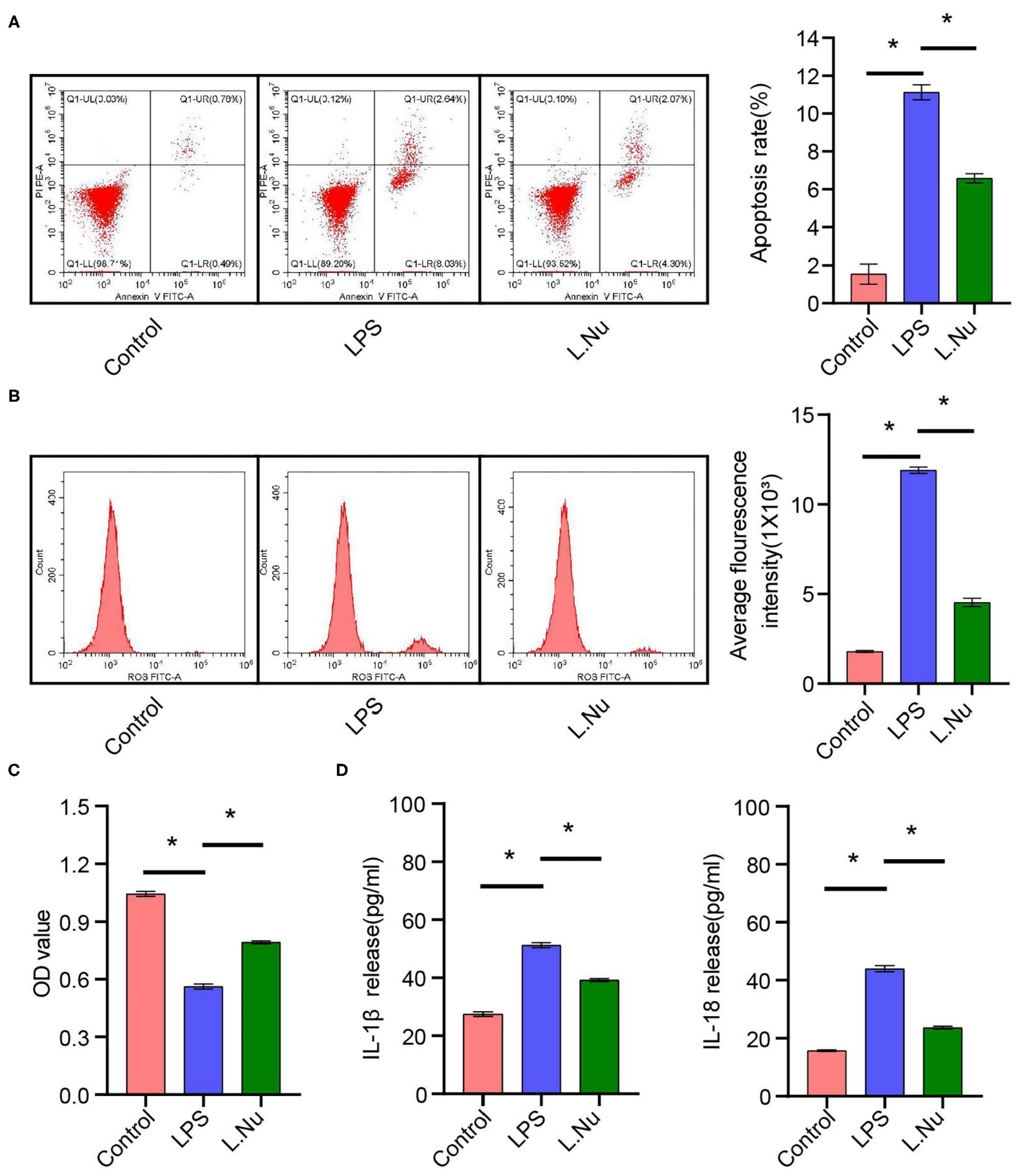

FIGURE 7 | NU9056 inhibited apoptosis and inflammation of microglia *in vitro*. **(A)** Apoptosis rate in each group was detected using flow cytometry. **(B)** The average fluorescence intensity of each group was measured using flow cytometry. **(C)** Cell viability was tested using CCK8 assay. **(D)** The IL-1β and IL-18 release were estimated using ELISA. $^*P < 0.05$.

physiology and shaping the peripheral and central immune and inflammatory responses of central nervous system diseases (37, 38). The "microbiota-gut-brain axis" view has been posited, discussed, and has become a hot research topic (39). Therefore, we speculate that the therapeutic effects of NU9056 may be related to the gut microbiota. *Akkermansia* has been studied recently as a probiotic with great potential. In cancer treatment, *Akkermansia* has great potential to combine with programmed death-1 immunotherapy to enhance its efficacy (40). *Akkermansia* has also been proven to be metabolically beneficial in obese and diabetic mice (41). In the present study, after NU9056 treatment, the abundance of *Akkermansia* in mice was significantly increased, suggesting that NU9056 might attenuate SAE by regulating the gut microbiota. The KEGG prediction results indicated that NU9056 could reduce the accumulation of the apoptosis pathway in the model mice and increase the enrichment of tight junctions and signaling pathways regulating pluripotency of stem cells. This also illustrated the possibility of using NU9056 to alleviate SAEs.

SCFAs have been the main fermentation metabolite of anaerobic bacteria in the gut. SCFAs are the main fermentation metabolites of anaerobic bacteria in the gut. Moreover, they have been considered as potential mediators of the influence of gut microbiota on intestinal immune function (42). The SCFA results revealed that acetate, butyrate, and propionate levels were reduced in patients with encephalitis (43). In the present study, NU9056 notably reversed the LPS-induced decrease in the concentrations of acetate, propionic acid, and butyrate. Due to economic and experimental limitations, its specific effects have not been deeply explored. In future studies, we will investigate the detailed mechanism of NU9056 as a potential SAE treatment. In view of previous studies, *in vivo* and *in vitro* experiments have shown that there is no significant difference between the NU9056 without LPS treatment group and the control group in function and NLRP3 pathway experiments (15, 44, 45). Therefore, in that design, NU9056 was not set without LPS treatment group. Considering the rigor of the experiment, we will set the NU9056 without LPS group in the future study to further study whether NU9056 has any effect on normal animals or cells.

SAE is an acute disease. Patients with SAE may have acute changes in consciousness, which is an important cause of death (19). LPS was used to establish a model that induced acute inflammation in mice, and the inflammatory indicators change significantly during 0–72 h (46). In the acute kidney injury study, inflammatory cytokines such as IL-1β, IL6, and TNF-α were measured in mice 16 h after intraperitoneal injection of LPS (47). Therefore, ELISA was performed at 16 h after modeling in the study. Many studies have shown that BBB markers were detected 24 h after modeling (24). Therefore, the indicators of BBB included Occludin and claudin-5, and the samples were collected 1 day after LPS modeling in the electron microscope experiment. The subsequently affected pathways often take a certain amount of time, so we chose 3 days to study pathways. Due to fund limitations, we did not conduct experiments on the changes of inflammatory indicators and pathway indicators over time. In future studies, we will collect blood and tissues at different time points for further research.

CONCLUSION

NU9056 might effectively alleviate the cognitive impairment, emotional disorder, inflammation, and BBB dysfunction of the experimental SAE by inhibiting the NLRP3 inflammasome. In addition, the therapeutic effects of NU9056 on experimental SAE may be related to the gut microbiota and derived metabolites.

DATA AVAILABILITY STATEMENT

The datasets presented in this study can be found in online repositories. The names of the repository/repositories and accession number(s) can be found at: https://www.ncbi.nlm.nih.gov accession number: PRJNA726029.

ETHICS STATEMENT

The animal study was reviewed and approved by Animal Care and Use Committee of the Third Xiangya Hospital, Central South University.

AUTHOR CONTRIBUTIONS

WQ, ZY, and GL had data collection and analysis, and manuscript preparation. LC, QP, and FZ supervised the whole study, data analysis, and manuscript preparation. All authors contributed to the article and approved the submitted version.

FUNDING

This work was supported by the Natural Science Foundation of Hunan Province (Project No: 2020JJ5918).

ACKNOWLEDGMENTS

We thank the Third Xiangya Hospital, Central South University, for all the support.

SUPPLEMENTARY MATERIAL

The Supplementary Material for this article can be found online at: https://www.frontiersin.org/articles/10.3389/fnut.2021.701760/full#supplementary-material

REFERENCES

1. Li Y, Yin L, Fan Z, Su B, Chen Y, Ma Y, et al. Microglia: a potential therapeutic target for sepsis-associated encephalopathy and sepsis-associated chronic pain. *Front Pharmacol.* (2020) 11:600421. doi: 10.3389/fphar.2020.600421
2. Rudd KE, Johnson SC, Agesa KM, Shackelford KA, Tsoi D, Kievlan DR, et al. Global, regional, and national sepsis incidence and mortality, 1990-2017: analysis for the Global Burden of Disease Study. *Lancet.* (2020) 395:200–11. doi: 10.1016/s0140-6736(19)32989-7
3. Haileselassie B, Joshi AU, Minhas PS, Mukherjee R, Andreasson KI, Mochly-Rosen D. Mitochondrial dysfunction mediated through dynamin-related protein 1 (Drp1) propagates impairment in blood brain barrier in septic encephalopathy. *J Neuroinflam.* (2020) 17:36. doi: 10.1186/s12974-019-1689-8
4. Chen S, Tang C, Ding H, Wang Z, Liu X, Chai Y, et al. Maf1 ameliorates sepsis-associated encephalopathy by suppressing the NF-kB/NLRP3 inflammasome signaling pathway. *Front Immunol.* (2020) 11:594071. doi: 10.3389/fimmu.2020.594071
5. Swanson KV, Deng M, Ting JP. The NLRP3 inflammasome: molecular activation and regulation to therapeutics. *Nat Rev Immunol.* (2019) 19:477–89. doi: 10.1038/s41577-019-0165-0
6. Wu AG, Zhou XG, Qiao G, Yu L, Tang Y, Yan L, et al. Targeting microglial autophagic degradation in NLRP3 inflammasome-mediated neurodegenerative diseases. *Ageing Res Rev.* (2021) 65:101202. doi: 10.1016/j.arr.2020.101202
7. Xu XE, Liu L, Wang YC, Wang CT, Zheng Q, Liu QX, et al. Caspase-1 inhibitor exerts brain-protective effects against sepsis-associated encephalopathy and cognitive impairments in a mouse model of sepsis. *Brain Behav Immun.* (2019) 80:859–70. doi: 10.1016/j.bbi.2019.05.038
8. Fu Q, Wu J, Zhou XY, Ji MH, Mao QH, Li Q, et al. NLRP3/caspase-1 pathway-induced pyroptosis mediated cognitive deficits in a mouse model of sepsis-associated encephalopathy. *Inflammation.* (2019) 42:306–18. doi: 10.1007/s10753-018-0894-4
9. Wang X, Buechler NL, Woodruff AG, Long DL, Zabalawi M, Yoza BK, et al. Sirtuins and immuno-metabolism of sepsis. *Int J Mol Sci.* (2018) 19:2738. doi: 10.3390/ijms19092738
10. Haak BW, Wiersinga WJ. The role of the gut microbiota in sepsis. *Lancet Gastroenterol Hepatol.* (2017) 2:135–43. doi: 10.1016/s2468-1253(16)30119-4
11. Liu J, Jin Y, Li H, Yu J, Gong T, Gao X, et al. Probiotics exert protective effect against sepsis-induced cognitive impairment by reversing gut microbiota abnormalities. *J Agric Food Chem.* (2020) 68:14874–83. doi: 10.1021/acs.jafc.0c06332
12. Zhang Y, Huang R, Cheng M, Wang L, Chao J, Li J, et al. Gut microbiota from NLRP3-deficient mice ameliorates depressive-like behaviors by regulating astrocyte dysfunction via circHIPK2. *Microbiome.* (2019) 7:116. doi: 10.1186/s40168-019-0733-3
13. Sokolova M, Ranheim T, Louwe MC, Halvorsen B, Yndestad A, Aukrust P. NLRP3 inflammasome: a novel player in metabolically induced inflammation-potential influence on the myocardium. *J Cardiovasc Pharmacol.* (2019) 74:276–84. doi: 10.1097/fjc.0000000000000704
14. Yang Y, Yang G, Yu L, Lin L, Liu L, Fang M, et al. An interplay between MRTF-A and the histone acetyltransferase TIP60 mediates hypoxia-reoxygenation induced iNOS transcription in macrophages. *Front Cell Dev Biol.* (2020) 8:484. doi: 10.3389/fcell.2020.00484
15. Zhao K, Zhang Y, Xu X, Liu L, Huang L, Luo R, et al. Acetylation is required for NLRP3 self-aggregation and full activation of the inflammasome. *BioRXiv.* (2019). doi: 10.1101/2019.12.31.891556
16. Brown JA, Bourke E, Eriksson LA, Kerin MJ. Targeting cancer using KAT inhibitors to mimic lethal knockouts. *Biochem Soc Trans.* (2016) 44:979–86. doi: 10.1042/bst20160081
17. Jiang X, Shen Z, Chen J, Wang C, Gao Z, Yu S, et al. Irisin protects against motor dysfunction of rats with spinal cord injury via adenosine 5'-monophosphate (AMP)-activated protein kinase-nuclear factor kappa-B pathway. *Front Pharmacol.* (2020) 11:582484. doi: 10.3389/fphar.2020.582484
18. Lu X, Qi X, Yi X, Jian Z, Gao T. Transcellular traversal of the blood-brain barrier by the pathogenic propionibacterium acnes. *J Cell Biochem.* (2018) 122:153–65. doi: 10.1002/jcb.28132
19. Mazeraud A, Righy C, Bouchereau E, Benghanem S, Bozza FA, Sharshar T. Septic-associated encephalopathy: a comprehensive review. *Neurotherapeutics.* (2020) 17:392–403. doi: 10.1007/s13311-020-00862-1
20. Zhong X, Xie L, Yang X, Liang F, Yang Y, Tong J, et al. Ethyl pyruvate protects against sepsis-associated encephalopathy through inhibiting the NLRP3 inflammasome. *Mol Med.* (2020) 26:55. doi: 10.1186/s10020-020-00181-3
21. Meyers AK, Zhu X. The NLRP3 inflammasome: metabolic regulation and contribution to inflammaging. *Cells.* (2020) 9:1808. doi: 10.3390/cells9081808
22. Huang ZS, Xie DQ, Xu LJ, Huang CS, Zheng M, Chen YJ, et al. Tetramethylpyrazine ameliorates lipopolysaccharide-induced sepsis in rats via protecting blood-brain barrier, impairing inflammation and nitrous oxide systems. *Front Pharmacol.* (2020) 11:562084. doi: 10.3389/fphar.2020.562084
23. Ward R, Li W, Abdul Y, Jackson L, Dong G, Jamil S, et al. NLRP3 inflammasome inhibition with MCC950 improves diabetes-mediated cognitive impairment and vasoneuronal remodeling after ischemia. *Pharmacol Res.* (2019) 142:237–50. doi: 10.1016/j.phrs.2019.01.035
24. Wang Y, Sha H, Zhou L, Chen Y, Zhou Q, Dong H, et al. The mast cell is an early activator of lipopolysaccharide-induced neuroinflammation and blood-brain barrier dysfunction in the hippocampus. *Mediat Inflamm.* (2020) 2020:8098439. doi: 10.1155/2020/8098439
25. Wang QS, Ding HG, Chen SL, Liu XQ, Deng YY, Jiang WQ, et al. Hypertonic saline mediates the NLRP3/IL-1β signaling axis in microglia to alleviate ischemic blood-brain barrier permeability by downregulating astrocyte-derived VEGF in rats. *CNS Neurosci Ther.* (2020) 26:1045–57. doi: 10.1111/cns.13427
26. Sui DM, Xie Q, Yi WJ, Gupta S, Yu XY, Li JB, et al. Resveratrol protects against sepsis-associated encephalopathy and inhibits the NLRP3/IL-1β axis in microglia. *Mediat Inflamm.* (2016) 2016:1045657. doi: 10.1155/2016/1045657
27. Zhang J, Zheng Y, Luo Y, Du Y, Zhang X, Fu J. Curcumin inhibits LPS-induced neuroinflammation by promoting microglial M2 polarization via TREM2/ TLR4/ NF-κB pathways in BV2 cells. *Mol Immunol.* (2019) 116:29–37. doi: 10.1016/j.molimm.2019.09.020
28. Kim SY, Jin CY, Kim CH, Yoo YH, Choi SH, Kim GY, et al. Isorhamnetin alleviates lipopolysaccharide-induced inflammatory responses in BV2 microglia by inactivating NF-κB, blocking the TLR4 pathway and reducing ROS generation. *Int J Mol Med.* (2019) 43:682–92. doi: 10.3892/ijmm.2018.3993
29. Catarina AV, Branchini G, Bettoni L, De Oliveira JR, Nunes FB. Sepsis-associated encephalopathy: from pathophysiology to progress in experimental studies. *Mol Neurobiol.* (2021) 58:2770–9. doi: 10.1007/s12035-021-02303-2
30. Shulyatnikova T, Verkhratsky A. Astroglia in sepsis associated encephalopathy. *Neurochem Res.* (2020) 45:83–99. doi: 10.1007/s11064-019-02743-2
31. Huang HJ, Chen XR, Han QQ, Wang J, Pilot A, Yu R, et al. The protective effects of Ghrelin/GHSR on hippocampal neurogenesis in CUMS mice. *Neuropharmacology.* (2019) 155:31–43. doi: 10.1016/j.neuropharm.2019.05.013
32. Ratto D, Corana F, Mannucci B, Priori EC, Cobelli F, Roda E, et al. Hericium erinaceus improves recognition memory and induces hippocampal and cerebellar neurogenesis in frail mice during aging. *Nutrients.* (2019) 11:715. doi: 10.3390/nu11040715
33. Savi FF, de Oliveira A, de Medeiros GF, Bozza FA, Michels M, Sharshar T, et al. What animal models can tell us about long-term cognitive dysfunction following sepsis: a systematic review. *Neurosci Biobehav Rev.* (2021) 124:386–404. doi: 10.1016/j.neubiorev.2020.12.005
34. Liao YL, Zhou XY, Ji MH, Qiu LC, Chen XH, Gong CS, et al. S100A9 upregulation contributes to learning and memory impairments by promoting microglia m1 polarization in sepsis survivor mice. *Inflammation.* (2021) 44:307–20. doi: 10.1007/s10753-020-01334-6
35. Zhang S, Wang X, Ai S, Ouyang W, Le Y, Tong J. Sepsis-induced selective loss of NMDA receptors modulates hippocampal neuropathology in surviving septic mice. *PLoS ONE.* (2017) 12:e0188273. doi: 10.1371/journal.pone.0188273
36. Qing W, Li F, Wang X, Quan C, Ouyang W, Liao Q. Inhibiting RIP1 improves chronic stress-induced cognitive impairments in d-galactose-induced aging mice. *Front Behav Neurosci.* (2018) 12:234. doi: 10.3389/fnbeh.2018.00234

37. Gordon R, Albornoz EA, Christie DC, Langley MR, Kumar V, Mantovani S, et al. Inflammasome inhibition prevents α-synuclein pathology and dopaminergic neurodegeneration in mice. *Sci Transl Med.* (2018) 10:eaah4066. doi: 10.1126/scitranslmed.aah4066
38. Kaufmann FN, Costa AP, Ghisleni G, Diaz AP, Rodrigues ALS, Peluffo H, et al. NLRP3 inflammasome-driven pathways in depression: clinical and preclinical findings. *Brain Behav Immun.* (2017) 64:367–83. doi: 10.1016/j.bbi.2017.03.002
39. Pellegrini C, Antonioli L, Calderone V, Colucci R, Fornai M, Blandizzi C. Microbiota-gut-brain axis in health and disease: Is NLRP3 inflammasome at the crossroads of microbiota-gut-brain communications? *Prog Neurobiol.* (2020) 191:101806. doi: 10.1016/j.pneurobio.2020.101806
40. Ansaldo E, Slayden LC, Ching KL, Koch MA, Wolf NK, Plichta DR, et al. *Akkermansia* muciniphila induces intestinal adaptive immune responses during homeostasis. *Science.* (2019) 364:1179–84. doi: 10.1126/science.aaw7479
41. Plovier H, Everard A, Druart C, Depommier C, Van Hul M, Geurts L, et al. A purified membrane protein from *Akkermansia* muciniphila or the pasteurized bacterium improves metabolism in obese and diabetic mice. *Nat Med.* (2017) 23:107–13. doi: 10.1038/nm.4236
42. Vinolo MA, Rodrigues HG, Nachbar RT, Curi R. Regulation of inflammation by short chain fatty acids. *Nutrients.* (2011) 3:858–76. doi: 10.3390/nu3100858
43. Xu R, Tan C, He Y, Wu Q, Wang H, Yin J. Dysbiosis of gut microbiota and short-chain fatty acids in encephalitis: a Chinese Pilot Study. *Front Immunol.* (2020) 11:1994. doi: 10.3389/fimmu.2020.01994
44. Tsai HD, Wu JS, Kao MH, Chen JJ, Sun GY, Ong WY, et al. Clinacanthus nutans protects cortical neurons against hypoxia-induced toxicity by downregulating HDAC1/6. *Neuromol Med.* (2016) 18:274–82. doi: 10.1007/s12017-016-8401-2
45. Castillo-Chabeco B, Figueroa G, Parira T, Napuri J, Agudelo M. Ethanol-induced modulation of GPR55 expression in human monocyte-derived dendritic cells is accompanied by H4K12 acetylation. *Alcohol.* (2018) 71:25–31. doi: 10.1016/j.alcohol.2018.05.008
46. Seemann S, Zohles F, Lupp A. Comprehensive comparison of three different animal models for systemic inflammation. *J Biomed Sci.* (2017) 24:60. doi: 10.1186/s12929-017-0370-8
47. Ren Q, Guo F, Tao S, Huang R, Ma L, Fu P. Flavonoid fisetin alleviates kidney inflammation and apoptosis via inhibiting Src-mediated NF-κB p65 and MAPK signaling pathways in septic AKI mice. *Biomed Pharmacother.* (2020) 122:109772. doi: 10.1016/j.biopha.2019.109772

Conflict of Interest: The authors declare that the research was conducted in the absence of any commercial or financial relationships that could be construed as a potential conflict of interest.

frontiers in Nutrition

ORIGINAL RESEARCH
published: 26 July 2021
doi: 10.3389/fnut.2021.702559

Effects of Different Treatment Methods of Dried Citrus Peel (*Chenpi*) on Intestinal Microflora and Short-Chain Fatty Acids in Healthy Mice

Yujiao Qian [1,2†], Zhipeng Gao [3†], Chen Wang [1], Jie Ma [3], Gaoyang Li [1,2], Fuhua Fu [1,2], Jiajing Guo [1,2] and Yang Shan [1,2*]*

[1] Longping Branch, Graduate School of Hunan University, Changsha, China, [2] International Joint Lab on Fruits & Vegetables Processing, Quality and Safety, Hunan Key Lab of Fruits & Vegetables Storage, Processing, Quality and Safety, Hunan Agriculture Product Processing Institute, Hunan Academy of Agricultural Sciences, Changsha, China, [3] College of Animal Science and Technology, Hunan Agricultural University, Changsha, China

OPEN ACCESS

Edited by:
Yong Su,
Nanjing Agricultural University, China

Reviewed by:
Senem Kamiloglu,
Uludağ University, Turkey
Sylvie Françoise Rebuffat,
Muséum National d'Histoire Naturelle, France

***Correspondence:**
Jiajing Guo
guojiajing1986@163.com
Yang Shan
sy6302@sohu.com

† These authors share first authorship

Specialty section:
This article was submitted to Nutrition and Microbes, a section of the journal Frontiers in Nutrition

Received: *29 April 2021*
Accepted: *21 June 2021*
Published: *26 July 2021*

Citation:
Qian Y, Gao Z, Wang C, Ma J, Li G, Fu F, Guo J and Shan Y (2021) Effects of Different Treatment Methods of Dried Citrus Peel (Chenpi) on Intestinal Microflora and Short-Chain Fatty Acids in Healthy Mice. Front. Nutr. 8:702559. doi: 10.3389/fnut.2021.702559

Chenpi is a kind of dried citrus peel from *Citrus reticulata*, and it is often used as traditional Chinese medicine to treat dyspepsia and respiratory tract inflammation. In this study, to determine which way of *chenpi* treatment plays a better effect on the prevention of obesity in healthy mice, we conducted 16S ribosomal RNA (rRNA) gene sequencing for intestinal microbiota and gas chromatography-mass spectrometry detector (GC/MSD) analysis for short-chain fatty acids (SCFAs) of female rats fed with either *chenpi* decoction or *chenpi* powder-based diet ($n = 10$ per group) for 3 weeks. *Chenpi* powder (CP) group significantly reduced abdominal adipose tissues, subcutaneous adipose tissue, and the serum level of total triacylglycerol (TG). At a deeper level, *chenpi* powder has a better tendency to increase the ratio of *Bacteroidetes* to *Firmicutes*. It alters the *Muribaculaceae* and *Muribaculum* in intestinal microbiota, though it is not significant. The concentrations of acetic acid, valeric acid, and butyric acid increased slightly but not significantly in the *CP* group. *Chenpi* decoction just reduced perirenal adipose tissues, but it shows better antioxidant activity. It has little effect on intestinal microbiota. No differences were found for SCFAs in the *chenpi* decoction (CD) group. The results indicated that *chenpi* powder has a better effect in preventing obesity in mice. It can provide a basis for the development of functional products related to *chenpi* powder.

Keywords: *chenpi* powder, *chenpi* decoction, intestinal microbiota, short chain fatty acids, different treatment methods

INTRODUCTION

Dried citrus peel (*chenpi*) is the mature dry pericarp of *Citrus reticulata*. As a traditional Chinese medicine, it has a good effect on treating dyspepsia and improving respiratory tract inflammation. *Chenpi* contains many active components, such as essential oil (1), flavonoid (2), pectin (3), insoluble fiber (4), and so on. Citrus peel essential oils may ameliorate hypercholesterolemia and hepatic steatosis by modulating lipid and cholesterol homeostasis, and most of them have good antimicrobial and antioxidant activities (5, 6). Polymethoxyflavones, a kind of flavonoid from citrus peel, have anti-obesity, anti-hyperglycemic, and antiviral activities; meanwhile, it may effectively prevent the progression of metabolic syndrome (7–10). Pectin polysaccharide has *in vitro* intestinal immunomodulatory activity (11). In addition to the abovementioned active substances, pure *chenpi* powder also contains a large amount of dietary fiber. The composition and activity of intestinal microbiota and the production of short-chain fatty acids (SCFAs) were affected by dietary fiber (12). Meanwhile, the production of SCFAs (in particular, acetate, propionate, and butyrate) is closely related to intestinal health and function (13).

Intestinal microbiota are microorganisms colonized in the human digestive tract, which is closely related to age, obesity, and inflammation (14–16). In recent years, the study on intestinal microbiota is a hot spot. Diet has different effects on intestinal microflora. More and more evidence shows that intestinal microflora is closely related to metabolism, host gene expression, and other factors (17–19). *Chenpi* has been proven to have a modulation effect on the composition of intestinal microbiota species, the abundance of microbiota, fecal SCFAs, intestinal barrier function, and gastrointestinal inflammation (20–22).

Obesity as a thorny issue worldwide is caused by many factors. Obesity can cause a series of complications, such as hypertension, hyperlipidemia, metabolic diseases, and increasing organ burden (23, 24). Several studies have observed the effects of extracts or natural products on intestinal microorganisms, SCFAs, glucose metabolism, and body weight of healthy mice model (25, 26). Looking for natural products that can alleviate and treat obesity is a healthy and safe method. Although there are some studies on the effect of reducing weight and lipid of *chenpi*, there is no study on which way of *chenpi* treatment can play a better effect. In this experiment, we observed the effect of the *chenpi* on healthy mice. Traditionally, *chenpi* was infused with boiling water to extract their effective components such as "decoction." In this study, we added *chenpi* to the normal diet of mice in two forms, both *chenpi* decoction and *chenpi* powder. This study aimed to investigate the modulation effect of two different types of *chenpi* on the accumulation of adipose, intestinal microbiota, antioxidant capacity, and SCFAs to unvail their potential application for obesity prevention, which may also provide a basis for the use of *chenpi* as a kind of anti-obesity food in the food industry.

MATERIALS AND METHODS

Mice and Housing

Forty four-week-old C57BL/six female mice (Tianqin Biotechnology Company, Changsha, China) were housed in a controlled room with a 12 h/day lighting cycle during the experimentation. Food and drinking water were freely available to mice. Following 1 week of acclimation, mice ($n = 10$) were randomly grouped to control (C), *chenpi* decoction (CD), control powder (P), *chenpi* powder (CP). They were all provided with a normal diet. The normal diet contained 54.9% corn, 5.6% casein, 18% soybean meal, 6.5% beer yeast, 0.7% lard, 0.8% bean oil, 0.5% salt, 1.4% fishmeal, and 1% premixture. The difference between granulated (C) and powder (P) groups is whether granulation is carried out. In the CD group and CP group, *chenpi* decoction and *chenpi* powder, respectively, were added to the normal diet. The body weight, food intake, and water intake were recorded once a week. After 3 weeks of administration, blood samples were collected by orbital bleeding. Liver, abdominal adipose tissues, subcutaneous adipose tissues, and perirenal adipose tissues were weighed and collected. Fecal samples were collected by 16S ribosomal RNA (rRNA) sequencing and analysis of SCFAs. The experimental protocol was approved by the Animal Care and Use Committee of Hunan Agricultural University.

Preparation of *Chenpi* Decoction and *Chenpi* Powder

Chenpi was purchased from Jiangmen Xinhui tangerine peel village market limited company, Guangdong Province. The variety of *chenpi* is red *Pericarpium Citri Reticulatae*, which is made by traditional sunlight drying. According to the traditional decocting method, 10 g *chenpi* was crushed into a coarse powder and 200 ml of water was added and boiled over 95°C for 30 min. The filtrate was filtered out and then added 20 times of water to decoct again in the same way. The filtrate was combined, evaporated, and concentrated to 10 ml and stored at 4°C. The concentration of *chenpi* decoction was 1 g/ml. CD group were administered 0.2 ml/day *chenpi* decoction by gavage. The mice in the C group were given distilled water at the same time. After grinding and sieving, the *chenpi* powder was sealed in vacuum and stored at 4°C. The CP group were given 0.2 g/day *chenpi* powder in the diet.

Histopathological Observation

Paraformaldehyde solution in 4% was used to fix adipose tissues. Then, they were dehydrated by ethanol solution, embedded, and prepared. The subcutaneous adipose tissue was stained with H&E. Images were obtained using a Nikon Eclipse E100 Upright optical microscope from Nikon Corporation, Japan (27).

Biochemical Analysis

The serum concentration of total cholesterol (TC), total triacylglycerol (TG), high-density lipoprotein cholesterol (HDL-C), and low-density lipoprotein cholesterol (LDL-C) were determined by using Kehua biological automatic biochemical analyzer. Biochemical kits were purchased from Shanghai Kehua Bio-Engineering Co., Ltd (Shanghai, China) (28).

Measurement of Hepatic Malondialdehyde (MDA) and Superoxide Dismutase (SOD) Levels

About 0.5 g of each liver tissue was homogenized in 4.5 ml frozen normal saline and then centrifuged and collected supernatant at 2,000 rpm for 10 min at 4°C for measurements. All these biochemical markers were measured using kits purchased from the Nanjing Jiancheng Bioengineering Institute (Nanjing, China). Coomassie Brilliant Blue was used to determine the concentration of protein (27). Each sample has a parallel sample.

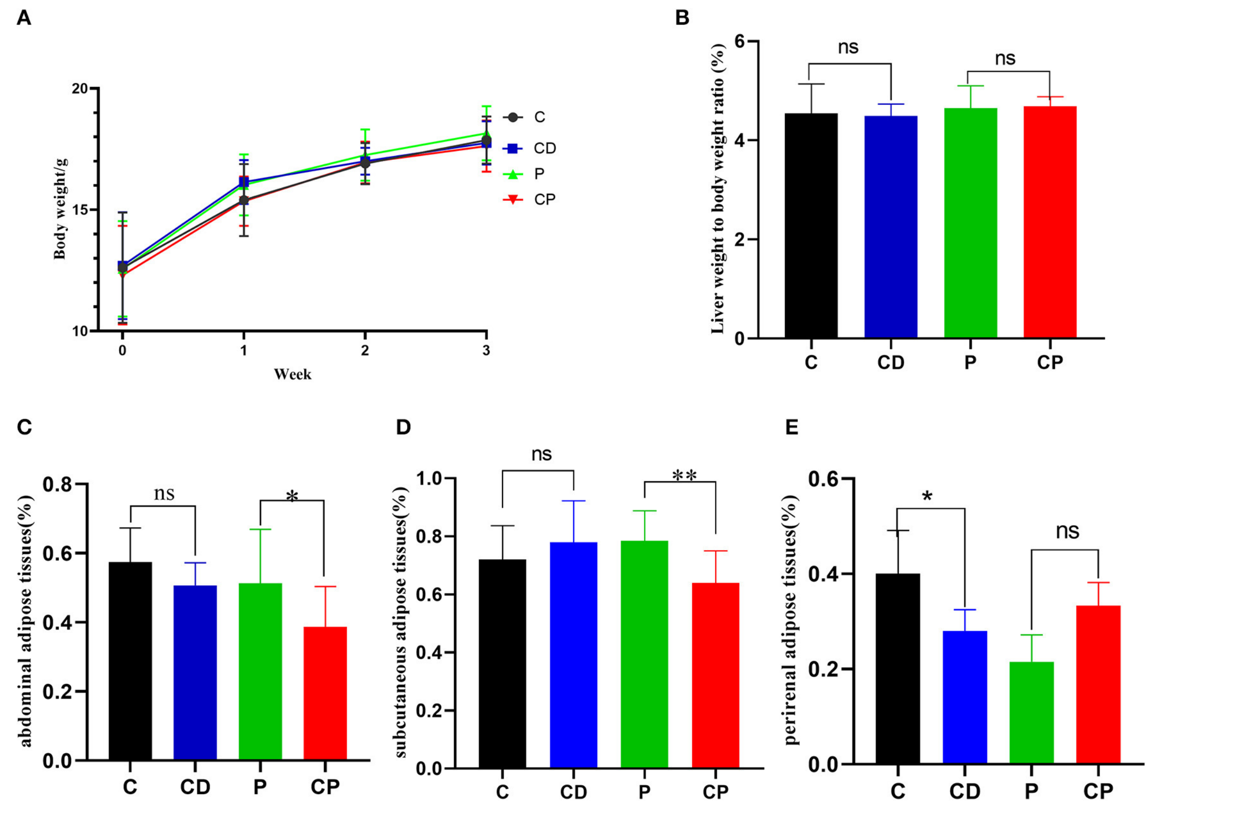

FIGURE 1 | Chenpi alleviated the accumulation of adipose in mice ($n = 9$–10). **(A)** The body weight in 3 weeks (g); **(B)** the relative weight of liver to body weight; **(C)** abdominal adipose tissues to body weight ratio (%); **(D)** subcutaneous adipose tissues to body weight ratio (%); and **(E)** perirenal adipose tissues to body weight ratio (%). * $P < 0.05$; ** $P < 0.01$; and ns $P > 0.05$.

16S Ribosomal RNA (rRNA) Gene Sequencing for Microbiota Profiling

Total genomic DNA was extracted from fecal samples and stored at −20°C using the DNA kit according to the instructions for 16S rRNA gene pyrosequencing. Paired-end sequencing was performed on the Illumina MiSeq platform (29). The V3-V4 regions were amplified using a specific primer with the barcode by thermocycler PCR system. In summary, α-diversity, β-diversity, and principal coordinate analysis (PCoA) were calculated and generated by Quantitative Insights Into Microbial Ecology (QIIME). The measurement was repeated three times for each sample. The online platform of Majorbio Cloud (http://www.majorbio.com/) was used to analyze data (30, 31).

Detection of SCFAs

A total of 100 mg feces were dissolved in 0.9 ml water, then mixed, and then centrifuged at 13,200 g force for 10 min at 4°C. A 1 μl supernatant of each sample was injected into the inlet for gas chromatography-mass spectrometry detector (GC/MSD) analysis. The levels of acetic, propionic, butyric, valeric, isobutyric, and isovaleric acids in SCFAs were measured using 8890B-5977B GC/MSD (Agilent Technologies Inc. CA, USA) (32, 33). The measurement was repeated three times for each sample.

Statistical Analysis

The statistical analyses were completed using IBM SPSS Statistics 26.0. The *t*-test was performed to determine the difference between groups. Values of $P < 0.05$ mean statistically significant.

RESULTS

Chenpi Alleviates Accumulation of Adipose in Mice

To determine the anti-obesity effect of *chenpi* on mice, body weight, liver, abdominal adipose tissues, subcutaneous adipose tissues, and perirenal adipose tissues were weighed. *Chenpi* treatment has a tendency to regulate body weight, but the difference was not significant ($P > 0.05$) (**Figure 1A**). Liver weight has basically no change in every group (**Figure 1B**). Weight of abdominal adipose tissues and subcutaneous adipose tissue was significantly reduced at 0.13 and 0.15% in the CP group compared with the P group ($P < 0.05$) (**Figures 1C,D**). Perirenal adipose tissues were significantly reduced in CD ($P < 0.05$) compared with the C group (**Figure 1E**). Serum concentrations of lipids were analyzed (**Figure 2**) to find out that *chenpi* powder can significantly reduce the serum level of TG by 24% compared to the P group ($P < 0.05$) (**Figure 2B**) but had no

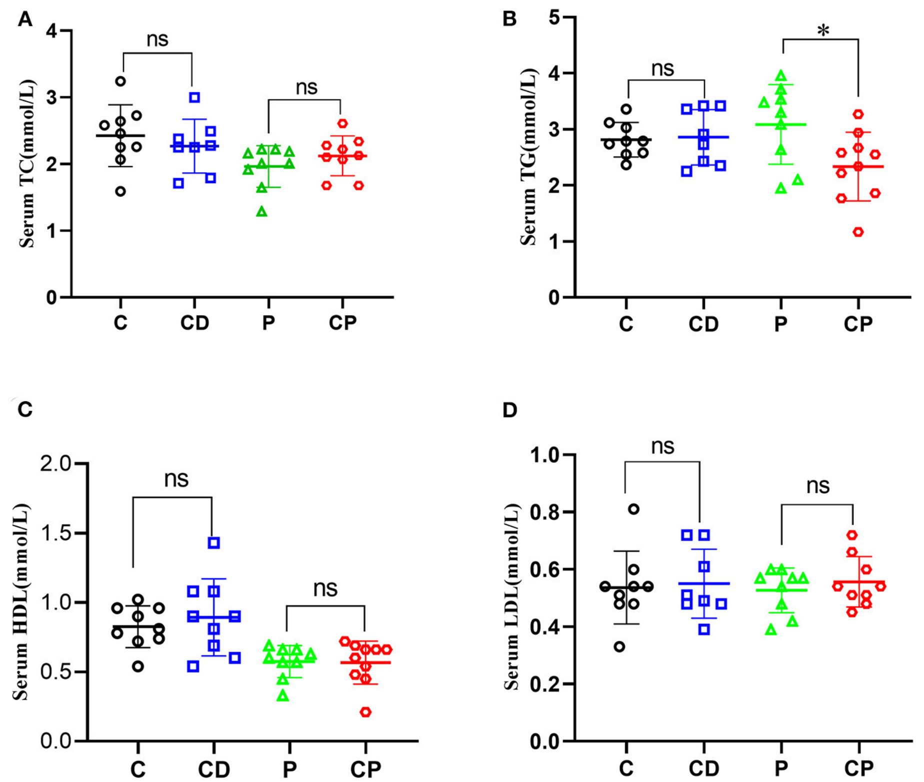

FIGURE 2 | Chenpi adjusted serum concentrations of lipids. Concentrations of total cholesterol (TC) **(A)**, total triacylglycerol (TG) **(B)**, high-density lipoprotein cholesterol (HDL-C) **(C)**, and low-density lipoprotein cholesterol (LDL-C) **(D)** in serum (*n* = 8–10). * $P < 0.05$; ns $P > 0.05$.

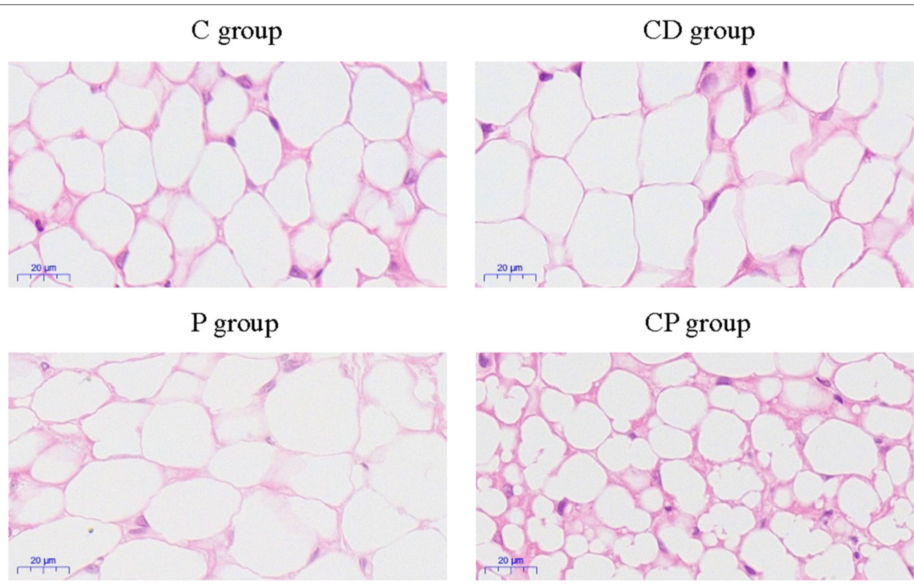

FIGURE 3 | The observation of subcutaneous adipose tissues by H&E staining of four treatment groups (×400).

remarkable effect on the serum levels of TC, LDL-C, and HDL-C. These items showed no significant changes in the CD group compared to the C group. The histopathological observation of adipose tissues showed that the CP group exhibited a strong inhibitory effect on the enlargement of adipocytes compared with the P group, while the difference was not significant in other groups (**Figure 3**). To sum up, compared with *chenpi* decoction, supplementation of *chenpi* powder in the diet significantly alleviated accumulation of lipid and serum TG metabolism, and it reduced the relative weight of abdominal adipose tissue and subcutaneous adipose tissue.

Chenpi Enhanced Antioxidant Capacity in the Liver

In order to test the antioxidant capacity of each group, the MDA index and SOD index of the liver were detected. The content of MDA was decreased in the CD group compared to the C group, while the content of MDA in the CP group was 1.35 nmol/mg higher than that of the P group ($P < 0.05$) (**Figure 4**). The activity of SOD was increased marginally in the CD group compared to the C group ($P > 0.05$).

Chenpi Modulated the Structural Composition of Intestinal Microbiota

Intestinal microbiota were known as a key factor in modulating obesity. Thus, to investigate whether *chenpi* influences the intestinal microbiota of mice, 16S rRNA sequencing was tested. We analyzed the composition and difference of intestinal microflora in different diet groups.

Microbial diversity and richness were evaluated by α-diversity and β-diversity. PCoA plot was applied to evaluate overall differences in β-diversity in unweighted UniFrac distance for the sample set (34, 35). As shown in **Figure 5**, different diets have strong effects on the gut microbial composition revealed by a clear separation among four groups. Shannon and Simpson's indexes evaluated the diversity of the microbiota. ACE and Chao indexes described the richness of the microbiota (36). As shown in **Figure 6**, the CD group exhibited a higher richness of microbiota evidenced by the increased ACE and Chao indexes compared to C ($P > 0.05$) (**Figures 6C,D**) but with no significant difference. Simpson's index in the CP group significantly increased, but other indexes reduced.

As shown in **Figure 7**, there were differences in microbial composition among the four groups at phylum, family, and genus levels. *Firmicutes* and *Bacteroidetes* are the two majorities at the phylum level. CD group had a 51% higher ratio of *Firmicutes* to *Bacteroidetes* compared with the C group ($P > 0.05$) (**Figures 7A**, **8A**). However, the CP group had a lower abundance of *Firmicutes* ($P = 0.07$) and a higher abundance of *Bacteroidetes* ($P = 0.06$) compared with the P group (**Figures 7A**, **8B**). The difference is not significant. The dominant genera are *Muribaculaceae*, *Lactobacillaceae,* and *Lachnobacterium* at the family level. The relative abundance of *Lactobacillaceae* in the CD group is higher than in the C group ($p > 0.05$) (**Figures 7B**, **8C**). The relative abundance of *Muribaculaceae* in two powder groups is higher than in two decoction groups (**Figure 7B**). The relative abundance of *Muribaculaceae* increased in the CP group compared with the P group ($P = 0.086$) (**Figures 7B**, **8D**). Similar alterations were observed for *norank_f_Muribaculaceae*, *Lactobacillus*, and *Lachnospiraceae _NK4A316_group* at the genus level (**Figures 7C**, **8E**). The relative abundance of *Muribaculaceae* ($p = 0.09$) and *Muribaculum* increased in the CP group compared with the P group ($P = 0.08$) (**Figure 8F**).

Chenpi Changed the Content of SCFAs in Feces

The content of SCFAs of feces is closely related to intestinal health. Here, the contents of acetic, propionic, butyric, valeric, isobutyric, and isovaleric acids were tested by GC/MSD. On the whole, the content of SCFAs in the two powder groups was higher than that in the decoction groups. There was no difference in the concentration of any SCFAs in feces in the CD group when compared with the control group. The group that consumed *chenpi* powder had higher concentrations of SCFAs than the P group, especially acetic, valeric, and butyric acids, but the difference was not significant (**Figure 9**).

DISCUSSION

We present the results of a study investigating the effects of different supplementation treatments with *chenpi* on various

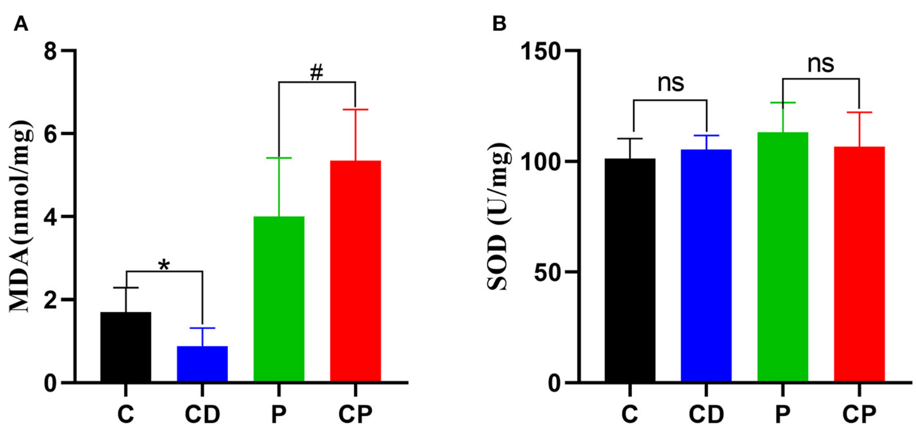

FIGURE 4 | The content of hepatic malonaldehyde (MDA) **(A)** and superoxide dismutase (SOD) **(B)** in liver ($n = 8$–10). * $P < 0.05$; #$P < 0.05$; and ns $P > 0.05$.

health parameters, microbial composition, and content of SCFAs. In healthy mice, *chenpi* supplement changed the accumulation of fat. In particular, *chenpi* powder can effectively reduce the weight of abdominal adipose tissues, subcutaneous adipose tissue, and the serum level of TG. Other studies also have shown that *chenpi* can reduce the gain of body weight, organ weight, and accumulation of lipid (37). Obesity is closely related to hyperlipidemia, and reducing the content of serum triglyceride can effectively alleviate hyperlipidemia (38). There was no significant change in body weight and liver weight in our study, perhaps because the feeding time was not long enough. The effect of *chenpi* on the antioxidant activity of the liver was analyzed. MDA is the most frequently measured biomarkers of lipid peroxidation and oxidative stress that is considered hazardous to health (39). Oxidative damage can lead to a decrease in the content of SOD (40, 41). Here, the decoction of *chenpi* shows stronger antioxidant activity, which might be explained as more antioxidants are released from *chenpi* after decoction treatment using a high temperature (42).

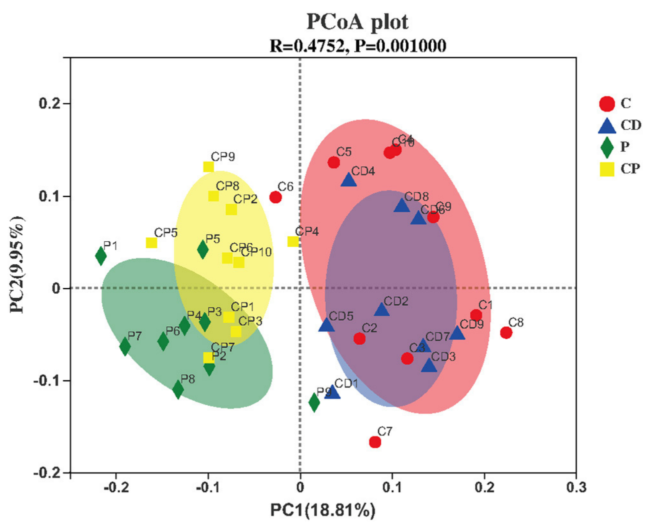

FIGURE 5 | Principal coordinate analysis (PCoA) and plot analysis of different treatment groups ($n = 10$).

Chenpi and its main active substances can affect the composition and richness of intestinal microorganisms. Hesperidin can increase the proportion of *Lactobacillus* in healthy mice. Citrus polymethoxyflavones can greatly enrich the bacterium *Bacteroides* in high-fat diet (HFD) mice (43–45). The abundance of *Proteobacteria* and the ratio of *Firmicutes* to *Bacteroidetes* were decreased by the *chenpi* extract in HFD mice. Although the addition of *chenpi* supplement did not significantly increase the abundance and diversity of intestinal microbiota in our study, it shows that *chenpi* powder has

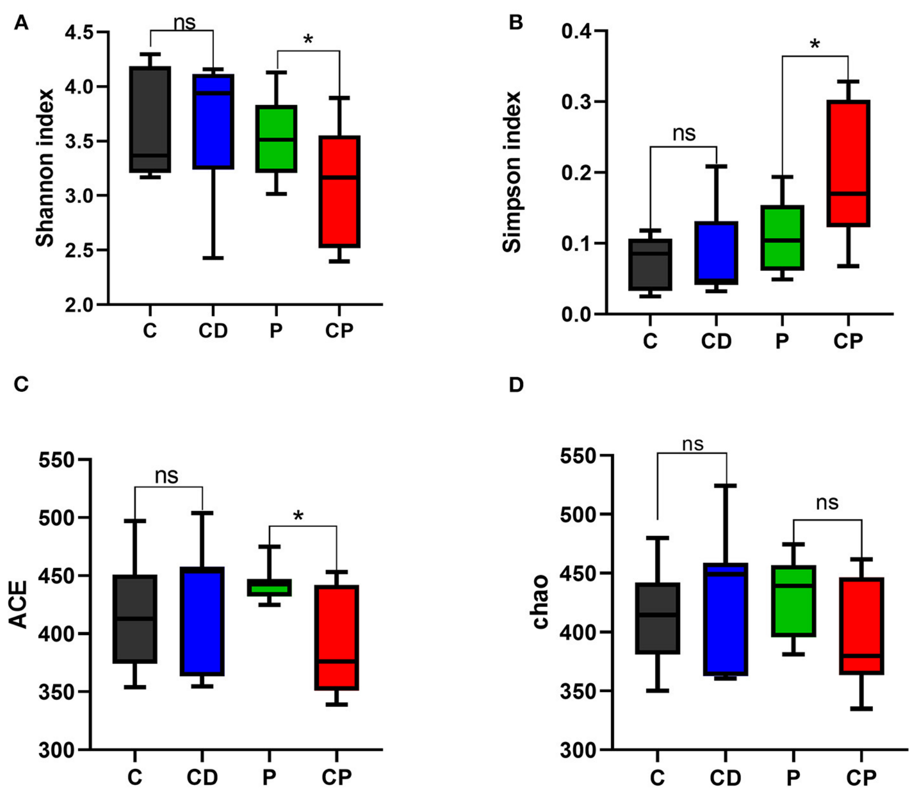

FIGURE 6 | Shannon **(A)**, Simpson's **(B)**, ACE **(C)**, and Chao **(D)** indexes in α-diversity analysis. * $P < 0.05$; ns $P > 0.05$ ($n = 10$).

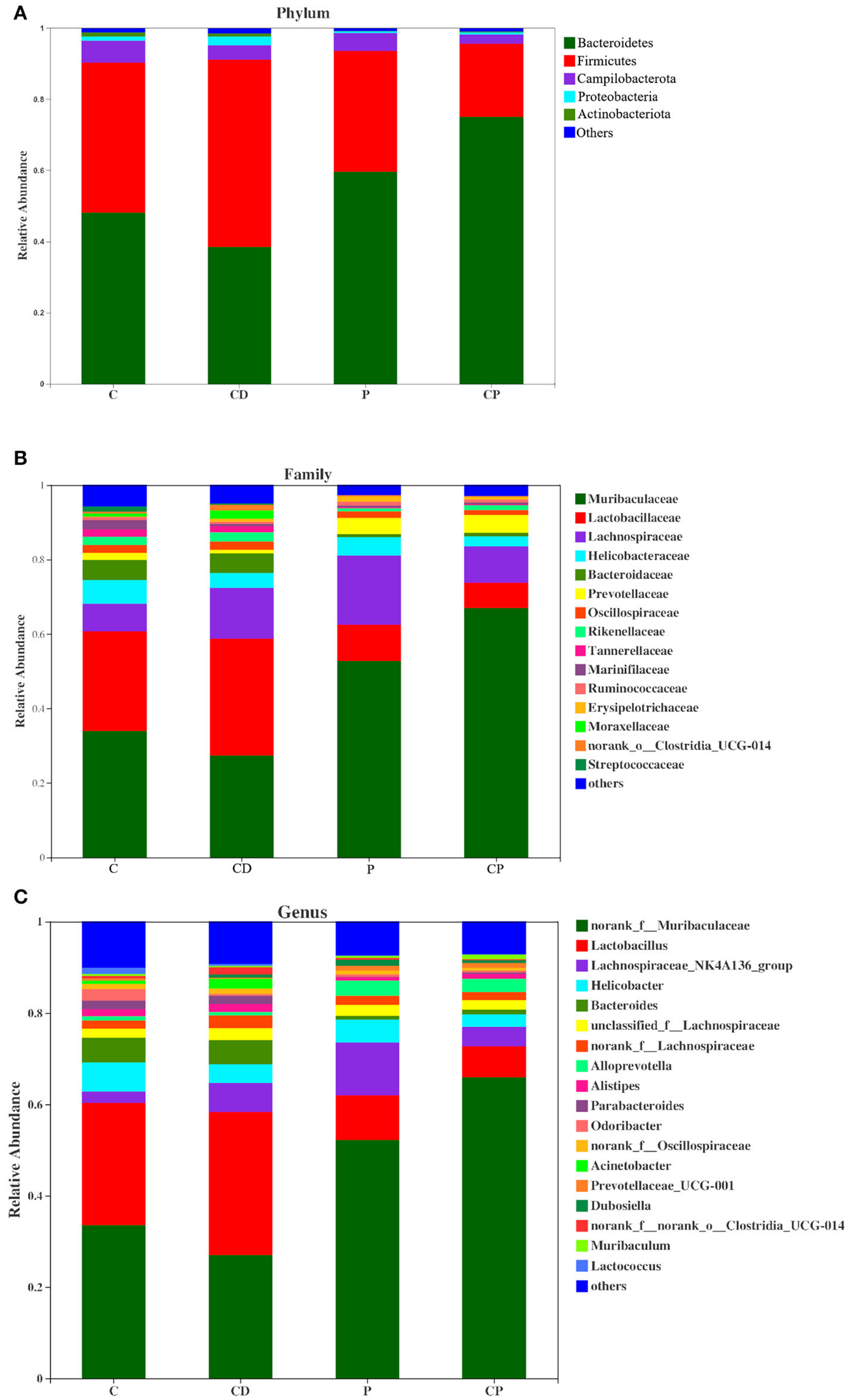

FIGURE 7 | Compositions of microbiota at the phylum **(A)**, family **(B)**, and genus levels **(C)** ($n = 10$).

a better tendency to increase the ratio of *Bacteroidetes* to *Firmicutes*. This may be because the decoction does not extract the active ingredients of *chenpi* very well and contains fewer ingredients than *chenpi* powder. Although active compounds such as hesperidin, naringenin, and nobiletin can be detected in the water decoction of *chenpi*, some components cannot

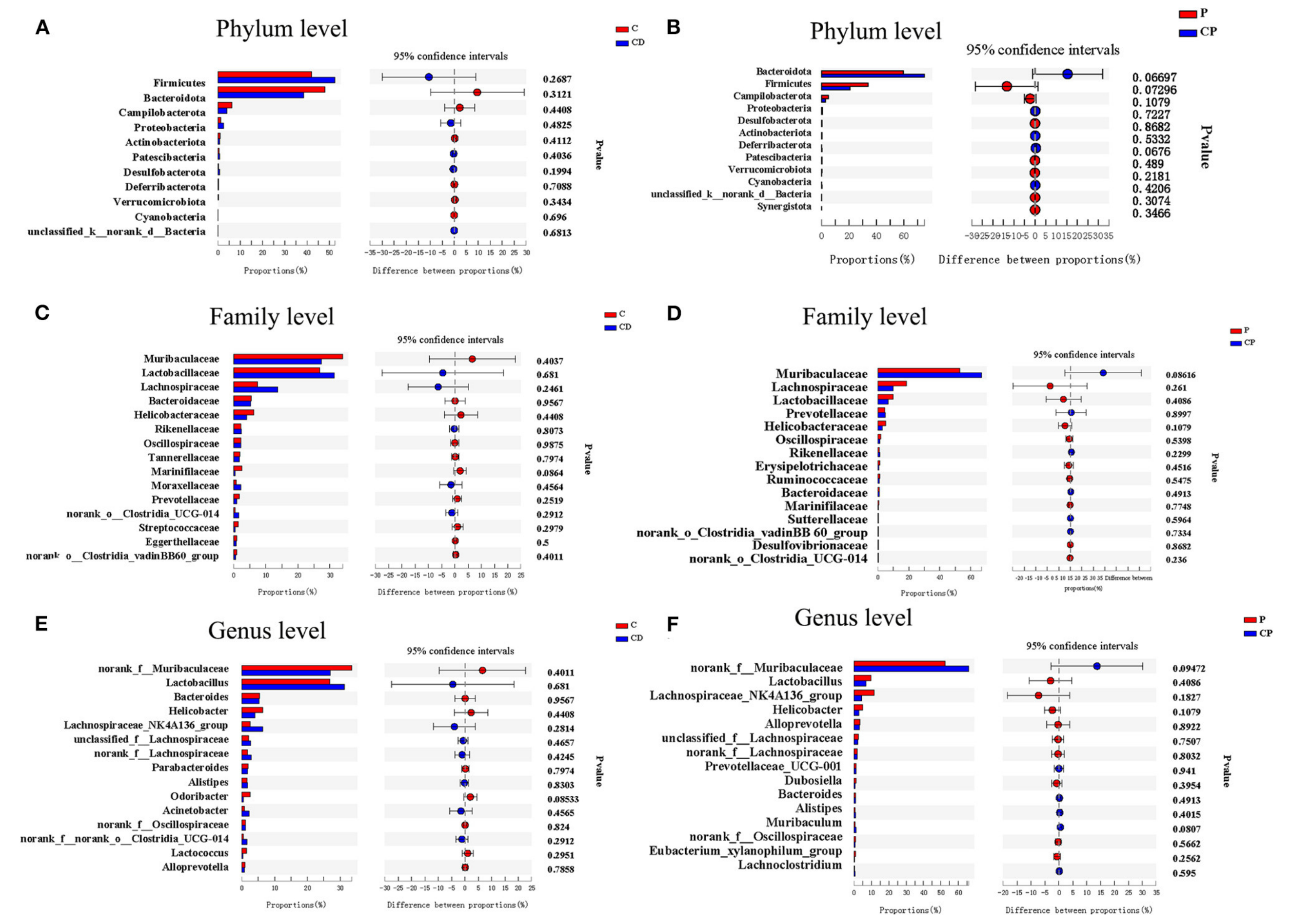

FIGURE 8 | Bar plots of Welch's *t*-test at the phylum, family, and genus levels (n = 9–10). **(A)** C group and CD group at the phylum level. **(B)** P group and CP group at the phylum level. **(C)** C group and CD group at the family level. **(D)** P group and CP group at the family level. **(E)** C group and CD group at the genus level. **(F)** P group and CP group at the genus level. $^{*}P < 0.05$.

be fully and effectively extracted because of their poor water solubility (46). A study showed that the water solubility of 5-demethylnobiletin and hesperidin in *chenpi* was low (47, 48). ACE and Chao indexes reduced in the CP group. This may be related to the reduction in harmful bacteria. Studies show that the abundance of *Bacteroidetes* was reduced by 50%, but *Firmicutes* was increased about 18% (49, 50), the abundance ratio of *Bacteroidetes* to *Firmicutes* will decrease in fat mice compared to lean mice (51, 52), and our results are consistent with them. In the control group, *Muribaculaceae*, *Lactobacillaceae,* and *Lachnospiraceae* are the dominant strain at the family level. *Chenpi* powder increased the abundance of *Muribaculaceae* significantly at family and genus levels. A high abundance of *Muribaculaceae* is associated with longevity in mice (53). *Chenpi* decoction can increase the abundance of *Lactobacillaceae* that are intestinal beneficial bacteria (54). It has correlation coefficients between bacterial abundances and serum lipid oxidative. The correlations between the abundance of *Lactobacillaceae,* serum TG, and MDA levels were negative (55). *Chenpi* increased intestinal beneficial bacteria and reduced microbial abundance associated with obesity. *Chenpi* powder is more outstanding in the regulation of intestinal microbiota.

The content of SCFAs is closely related to the diet structure. *Chenpi* contains not only many active ingredients but also a lot of dietary fiber. A fiber-rich diet can increase the content of SCFAs in mice. Dietary fiber can be fermented by colonic microbiota to produce SCFAs. Many studies have shown that a diet rich in dietary fiber can change the content of SCFAs. Passion fruit peel can increase the concentrations of butyrate and acetate in cecal content (56). Salami with citrus fiber increased the production of acetate, propionate, and butyrate (57). Dietary fibers from papayas promoted the production of SCFAs (58). Intestinal microorganisms are closely related to SCFAs. *Lachnospiraceae* plays an important role in the production of butyrate (59, 60). *Muribaculaceae* are helpful to the production of propionate (61). *Escherichia coli* could produce acetic acid (62). No significant changes in SCFAs were observed in our study, perhaps due to our shorter feeding cycle.

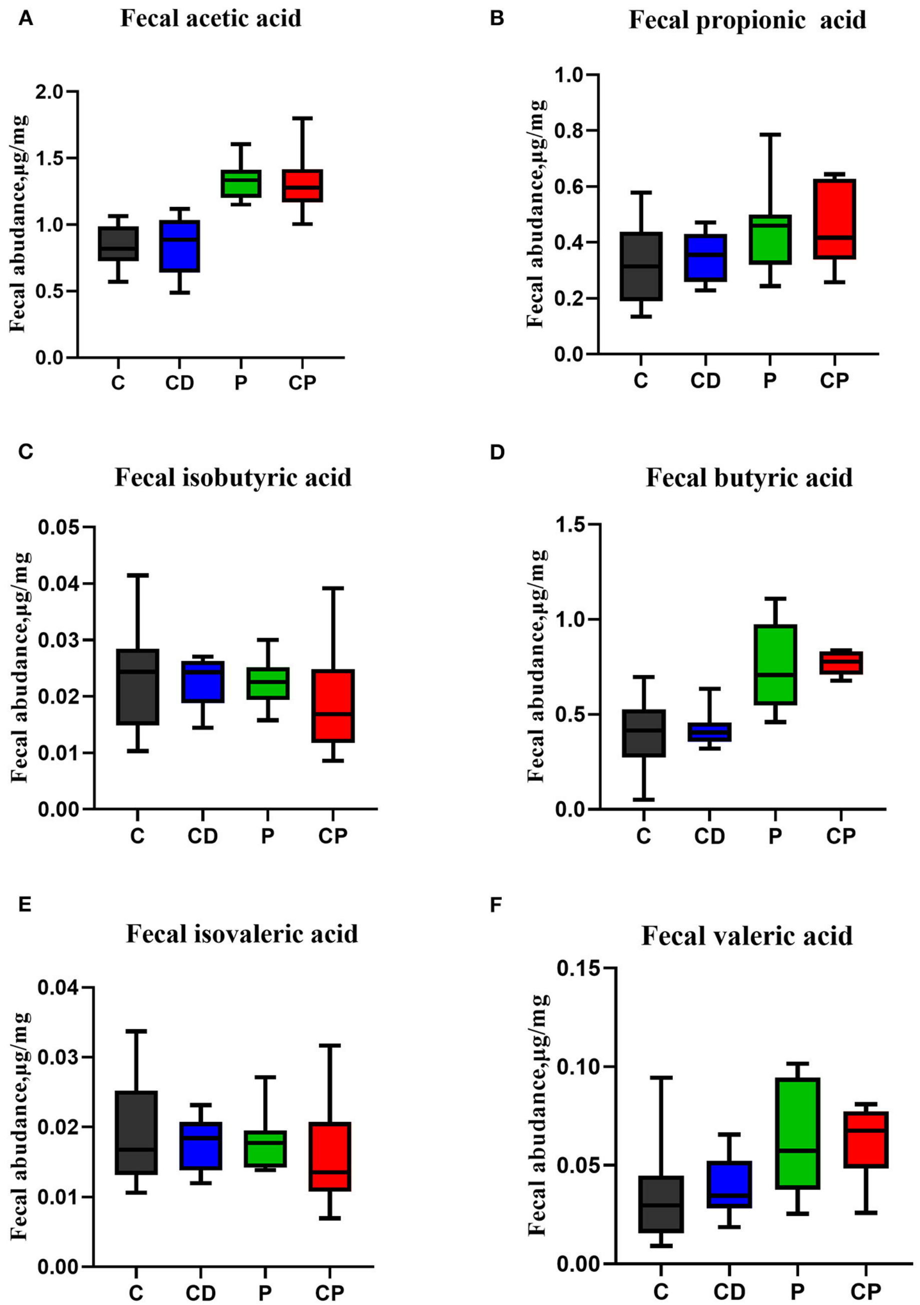

FIGURE 9 | The effect of chenpi on short-chain fatty acids (SCFAs) in the feces ($n = 9$–10). **(A)** Acetic acid, **(B)** propionic acid, **(C)** isobutyric acid, **(D)** butyric acid, **(E)** isovaleric acid, and **(F)** valeric acid.

In conclusion, daily consumption of *chenpi* has a certain effect on reducing weight and lipid. Compared with *chenpi* decoction, *chenpi* powder has a better effect in preventing obesity. *Chenpi* powder may be developed as supplementary functional food to prevent obesity in the future. In this study, we focused on the effect of different treatment methods of *chenpi* on healthy mice to predict the preventive effect on obesity. In the future, a high-fat model would be established to observe this effect in depth. It is our next direction to research study to develop a variety of popular *chenpi* functional foods.

DATA AVAILABILITY STATEMENT

The datasets presented in this study can be found in online repositories. The names of the repository/repositories and accession number(s) can be found below: PRJNA729616.

ETHICS STATEMENT

The animal study was reviewed and approved by Animal Care and Use Committee of Hunan Agriculture University.

AUTHOR CONTRIBUTIONS

JG: Conceptualization. YQ: methodology. YQ and JM: software. YQ, YS, and JG: writing-review and editing. YQ, CW, and ZG: visualization. GL, FF, and YS: supervision. YS: project administration and funding acquisition. All authors contributed to the article and approved the submitted version.

FUNDING

This research was supported by the National Key Research and Development Project of China (2017YFD0400701), the National Natural Science Foundation of China (32073020), the Changsha Municipal Natural Science Foundation (kq2014070), and the Hunan Innovative Province Construction Project (2019NK2041).

REFERENCES

1. Tranchida PQ, Bonaccorsi I, Dugo P, Mondello L, Dugo G. Analysis of citrus essential oils: state of the art and future perspectives. *A review Flavour and Fragr J.* (2012) 27:98–123. doi: 10.1002/ffj.2089
2. Huang R, Zhang Y, Shen S, Zhi Z, Cheng H, Chen S. Antioxidant and pancreatic lipase inhibitory effects of flavonoids from different citrus peel extracts: An in vitro study. *Food Chem.* (2020) 326:126785. doi: 10.1016/j.foodchem.2020.126785
3. Tian CH, Xu H, Li J, Han Z. Characteristics and intestinal immunomodulating activities of water-soluble pectic polysaccharides from *Chenpi* with different storage periods. *Sci Food Agri.* (2018) 98:3752–7. doi: 10.1002/jsfa.8888
4. Huang J, Liao J, Qi J, Jiang W, Yang X. Structural and physicochemical properties of pectin-rich dietary fiber prepared from citrus peel. *Food Hydrocoll.* (2020) 110:106140. doi: 10.1016/j.foodhyd.2020.106140
5. Feng K, Zhu X, Liu G, Kan Q, Chen T, Chen Y, et al. Dietary citrus peel essential oil ameliorates hypercholesterolemia and hepatic steatosis by modulating lipid and cholesterol homeostasis. *Food Funct.* (2020) 11:7217–30. doi: 10.1039/D0FO00810A
6. Raspo AM, Vignola BM, Andreatta AE, Juliani HR. Antioxidant and antimicrobial activity of citrus essential oils from Argentina and the United States. *Food Biosci.* (2020) 36:100651. doi: 10.1016/j.fbio.2020.100651
7. Gao Z, Wang ZY, Guo Y, Chu C, Zheng GD, Liu EH, et al. Enrichment of polymethoxyflavones from *Citrus reticulata* 'Chachi' peel and their hypoglycaemic effect. *J Chromatogr B.* (2019) 1124:226–32. doi: 10.1016/j.jchromb.2019.06.010
8. Guo J. TaoH, Cao Y, Ho CT, Jin S. Huang Q prevention of obesity and type 2 diabetes with aged citrus peel (Chenpi) extract. *J Agric Food Chem.* (2016) 64:2053–61. doi: 10.1021/acs.jafc.5b06157
9. Xu JJ, Wu X, Li MM, Li GQ, Yang YT, Luo HJ, et al. Antiviral activity of polymethoxylated flavones from "guang*Chenpi*", the edible and medicinal pericarps of citrus reticulata 'chachi'. *J. Agric. Food Chem.* (2014) 62:2182–2189. doi: 10.1021/jf404310y
10. Ling Y, Shi Z, Y X, Cai Z, Wang L, Wu X, et al. Hypolipidemic effect of pure total flavonoids from peel of Citrus (PTFC) on hamsters of hyperlipidemia and its potential mechanism. *Exp Gerontol.* (2020) 130:110786. doi: 10.1016/j.exger.2019.110786
11. Fu M, Zou B, An K, Yu Y, Tang D, Wu J, et al. Anti-asthmatic activity of alkaloid compounds from *Pericarpium Citri Reticulatae* (*Citrus reticulata* 'Chachi'). *Food Funct.* (2019) 10:903–11. doi: 10.1039/C8FO01753K
12. Gunaranjan P, Christine AB, Halina S, Thanuja DH, John AM. Short-term feeding of fermentable dietary fibres influences the gut microbiota composition and metabolic activity in rats. *Int J Food Sci Tech.* (2017) 52:2572–81. doi: 10.1111/ijfs.13543
13. Macfarlane GT, Macfarlane S. Fermentation in the human large intestine: its physiologic consequences and the potential contribution of prebiotics. *J Clin Gastroenterol.* (2011) 45:S120–7. doi: 10.1097/MCG.0b013e31822fecfe
14. Leigh SJ, Morris MJ. Diet, inflammation and the gut microbiome: mechanisms for obesity-associated cognitive impairment. *Biochim Biophys Acta Mol Basis Dis.* (2020) 1866:15767. doi: 10.1016/j.bbadis.2020.165767
15. Goyal D, Ali SA, Singh RK. Emerging role of gut microbiota in modulation of neuroinflammation and neurodegeneration with emphasis on Alzheimer's disease. *Prog Neuropsychopharmacol Biol Psychiatry.* (2020) 106:110112. doi: 10.1016/j.pnpbp.2020.110112
16. Ragonnaud E, Biragyn A. Gut microbiota as the key controllers of "healthy" aging of elderly people. *Immun Ageing.* (2021) 18:2. doi: 10.1186/s12979-020-00213-w
17. Xia Y, Tan D, Akbary R, Kong J, Seviour R, Kong Y. Aqueous raw and ripe Pu-erh tea extracts alleviate obesity and alter cecal microbiota composition and function in diet-induced obese rats. *Appl Microbiol Biotechnol.* (2019) 103:1823–35. doi: 10.1007/s00253-018-09581-2
18. Lee ES, Song EJ, Nam YD, Nam TG, Kim HJ, Lee BH, et al. Effects of enzymatically modified chestnut starch on the gut microbiome, microbial metabolome, and transcriptome of diet induced obese mice. *Int J Bio Macromolecules.* (2019) 145:245–243. doi: 10.1016/j.ijbiomac.2019.12.169
19. Liu M, Li X, Zhou S, Wang TTY, Zhou S, Yang K, et al. Dietary fiber isolated from sweet potato residues promote healthy gut microbiome profile. *Food Funct.* (2020) 11:689–99. doi: 10.1039/C9FO01009B
20. Zhang M, Zhu J, Zhang X, Zhao D, Ma Y, Li D, et al. Aged citrus peel (*Chenpi*) extract causes dynamic alteration of colonic microbiota in high-fat diet induced obese mice. *Food Funct.* (2020) 11:2667–78. doi: 10.1039/C9FO02907A
21. Tung YC, Chang WT, Li S, Wu JC, Bademeav V, Ho CT, et al. Citrus peel extracts attenuated obesity and modulated gut microbiota in a high-fat diet-induced obesity mice. *Food Funct.* (2018) 9:3363–73. doi: 10.1039/C7FO02066J
22. Yu M, Li Z, Chen W, Wang G, Cui Y, Ma X, et al. Dietary supplementation with citrus extract altered the intestinal microbiota and microbial metabolite profiles and enhanced the mucosal immune homeostasis in yellow-feathered broilers. *Front in microbiol.* (2019) 10:2662. doi: 10.3389/fmicb.2019.02662
23. Paavonsalo S, Hariharan S, Lackman MH, Karaman S. Capillary rarefaction in obesity and metabolic diseases-organ-specificity and possible mechanisms. *Cells.* (2020) 9:2683. doi: 10.3390/cells9122683
24. Gesta S, H Y, Tseng, Kahn CR. Developmental origin of fat: tracking obesity to its source. *Cell.* (2008) 135:366. doi: 10.1016/j.cell.2008.09.048
25. Shtriker MG, Hahn M, Taieb E, Nyska A, Moallem U, Tirosh O, et al. Fenugreek galactomannan and citrus pectin improve several parameters associated with glucose metabolism and modulate gut microbiota in mice. *Nutrition.* (2018) 134–42. doi: 10.1016/j.nut.2017.07.012
26. Liu X, Martin DA, Valdez JC, Sudakaran S, Rey F, Bolling BW. Aronia berry polyphenols have matrix-dependent effects on the gut microbiota. *Food Chem.* (2021) 359:129831. doi: 10.1016/j.foodchem.2021.129831
27. Hu Y, Hou Z, Yi R, Wang Z, Sun P, Li G, et al. Tartary buckwheat flavonoids ameliorate high fructose-induced insulin resistance and oxidative stress associated with the insulin signaling and Nrf2/HO-1 pathways in mice. *Food Funct.* (2017) 8:2803–16. doi: 10.1039/C7FO00359E
28. Yin J, Li Y, Han H, Chen S, Gao J, Liu G, et al. Melatonin reprogramming of gut microbiota improves lipid dysmetabolism in high-fat diet-fed mice. *J Pineal Res.* (2018) 65:e12524. doi: 10.1111/jpi.12524
29. Chen LC, Fan ZY, Wang HY, Wen DC, Zhang SY. Effect of polysaccharides from adlay seed on anti-diabetic and gut microbiota. *Food Funct.* (2019) 10:4372–80. doi: 10.1039/C9FO00406H
30. Fan L, Qi Y, Qu S, Chen X, Li A, Hendi M, et al. B. adolescentis ameliorates chronic colitis by regulating Treg/Th2 response and gut microbiota remodeling. *Gut Microbes.* (2021) 13:1–17. doi: 10.1080/19490976.2020.1826746
31. Ye M, Sun J, Chen Y, Ren Q, Li Z, Zhao Y, et al. Oatmeal induced gut microbiota alteration and its relationship with improved lipid profiles: a

secondary analysis of a randomized clinical trial. *Nutr Metab (Lond)*. (2020) 17:85. doi: 10.1186/s12986-020-00505-4
32. Xiao S, Liu C, Chen M, Zou J, Zhang Z, Cui X, et al. Scutellariae radix and coptidis rhizoma ameliorate glycolipid metabolism of type 2 diabetic rats by modulating gut microbiota and its metabolites. *Appl Microbiol Biotechnol.* (2020) 104:303–17. doi: 10.1007/s00253-019-10174-w
33. Tamura K, Sasaki H, Shiga K, Miyakawa H, Shibata S. The timing effects of soy protein intake on mice gut microbiota. *Nutrients.* (2019) 12:87. doi: 10.3390/nu12010087
34. Yin J, Han H, Li Y, Liu Z, Zeng X, Li T, et al. Lysine restriction affects feed intake and amino acid metabolism via gut microbiome in piglets. *Cell Physiol Biochem*. (2017) 44:1749–61. doi: 10.1159/000485782
35. Duan Y, Zhong Y, Xiao H, Zheng C, Song B, Wang W, et al. Gut microbiota mediates the protective effects of dietary beta-hydroxy-beta-methylbutyrate (HMB) against obesity induced by high-fat diets. *FASEB J.* (2019) 33:10019–33. doi: 10.1096/fj.201900665RR
36. Van den Brule S, Rappe M, Ambroise J, Bouzin C, Dessy C, Paquot A, et al. Diesel exhaust particles alter the profile and function of the gut microbiota upon subchronic oral administration in mice. *Part Fibre Toxicol.* (2021) 18:7. doi: 10.1186/s12989-021-00400-7
37. Guo J, Cao Y, Ho C-T, Jin S, Huang Q. Aged citrus peel (chenpi) extract reduces lipogenesis in differentiating 3T3-L1 adipocytes. *J Funct Foods.* (2017) 34:297–303. doi: 10.1016/j.jff.2017.04.042
38. Chen K, Ma Z, Yan X, Liu J, Xu W, Li Y, et al. Investigation of the lipid-lowering mechanisms and active ingredients of danhe granule on hyperlipidemia based on systems pharmacology. *Front Pharmacol.* (2020) 11:528. doi: 10.3389/fphar.2020.00528
39. Tsikas D. Assessment of lipid peroxidation by measuring malondialdehyde (MDA) and relatives in biological samples: Analytical and biological challenges. *Anal Biochem.* (2017) 524:13–30. doi: 10.1016/j.ab.2016.10.021
40. Zhang C, Zhao J, Famous E, Pan S, Peng X. Tian J. Antioxidant, hepatoprotective and antifungal activities of black pepper (Piper nigrum L) essential oil. *Food Chem.* (2021) 346:128845. doi: 10.1016/j.foodchem.2020.128845
41. Wu Q, Li W, Zhao J, Sun W, Yang Q, Chen C, et al. Apigenin ameliorates doxorubicin-induced renal injury via inhibition of oxidative stress and inflammation. *Biomed Pharmacother.* (2021) 137:111308. doi: 10.1016/j.biopha.2021.111308
42. Choi MY, Chai C, Park JH, Lim J, Lee J, Kwon SW. Effects of storage period and heat treatment on phenolic compound composition in dried Citrus peels (Chenpi) and discrimination of Chenpi with different storage periods through targeted metabolomic study using HPLC-DAD analysis. *J Pharm Biomed Anal.* (2011) 54:638–45. doi: 10.1016/j.jpba.2010.09.036
43. Stevens Y, Rymenant EV, Grootaert C, Camp JV, Possemiers S, Masclee A, et al. The intestinal fate of citrus flavanones and their effects on gastrointestinal health. *Nutrients.* (2019) 11:1464. doi: 10.3390/nu11071464
44. Estruel-Amades S, Massot-Cladera M, Perez-Cano FJ, Franch A, Castell M, Camps-Bossacoma M. Hesperidin effects on gut microbiota and gut-associated lymphoid tissue in healthy rats. *Nutrients.* (2019) 11:324. doi: 10.3390/nu11020324
45. Zeng SL, Li SZ, Xiao PT, Cia YY, Chu C, Chen BZ, et al. Citrus polymethoxyflavones attenuate metabolic syndrome by regulating gut microbiome and amino acid metabolism. *Sci Adv.* (2020) 6:eaax6208. doi: 10.1126/sciadv.aax6208
46. Cao R, Zhao Y, Zhou Z, Zhao X. Enhancement of the water solubility and antioxidant activity of hesperidin by chitooligosaccharide. *J Sci Food Agric.* (2018) 98:2422–7. doi: 10.1002/jsfa.8734
47. Ning F, Wang X, Zheng H, Zhang K, Bai C, Peng H. Improving the bioaccessibility and in vitro absorption of 5-demethylnobiletin from chenpi by se-enriched peanut protein nanoparticles-stabilized pickering emulsion. *J Funct Foods.* (2019) 55:76–85. doi: 10.1016/j.jff.2019.02.019
48. Zhang Y, Yu Y, Li H, Huang W, Wang P. Effects of Citri Reticulatae Pericarpium and grapefruit juice on the pharmacokinetics of omeprazole in rats. *J Food Bio.* (2021) 00:e13804. doi: 10.1111/jfbc.13804
49. Louis P, Flint HJ. Formation of propionate and butyrate by the human colonic microbiota. *Environ Microbiol.* (2017) 19:29–41. doi: 10.1111/1462-2920.13589
50. Ley RE, Backhed F, Turnbaugh P, Lozupone CA, Knight RD, Gordon JI. Obesity alters gut microbial ecology. *Proc Natl Acad Sci USA*. (2005) 102:11070–11075. doi: 10.1073/pnas.0504978102
51. Long JF, Yang JP, Henning SM, Woob SL, Hsu M. ChanB, et al. Xylooligosaccharide supplementation decreases visceral fat accumulation and modulates cecum microbiome in mice. *J Funct Foods.* (2019) 52:138–46. doi: 10.1016/j.jff.2018.10.035
52. Evans CC, LePard KJ, Kwak JW, Stancukas MC, Laskowski S, Dougherty J, et al. Exercise prevents weight gain and alters the gut microbiota in a mouse model of high fat diet-induced obesity. *PLoS ONE.* (2014) 9:e92193. doi: 10.1371/journal.pone.0092193
53. Sibai M, Altuntas E, Yildirim B, Ozturk G, Yildirim S, Demircan T. Microbiome and longevity: high abundance of longevity-linked muribaculaceae in the gut of the long-living rodent spalax leucodon. *Omics: a Journal of Integrative Biology.* (2020) 24:592–601. doi: 10.1089/omi.2020.0116
54. Liu H, Zhu H, Xia H, Yang X, Yang L, Wang S, et al. Different effects of high-fat diets rich in different oils on lipids metabolism, oxidative stress and gut microbiota. *Food Res Int.* (2020) 141:110078. doi: 10.1016/j.foodres.2020.110078
55. Ojo BA, O'Hara C, Wu L, El-Rassi D, Ritchey JW, Chowanadisai W, et al. Wheat germ supplementation increases lactobacillaceae and promotes an anti-inflammatory gut milieu in C57BL/6 mice fed a high-fat, high-sucrose diet. *J Nutr.* (2019) 149:1107–15. doi: 10.1093/jn/nxz061
56. Da Silva JK, Cazarin CBB, Bogusz Junior S, Augusto F, Maróstica Junior MR. Passion fruit (Passiflora edulis) peel increases colonic production of short-chain fatty acids in Wistar rats. *LWT - Food Sci Tech.* (2014) 59:1252–7. doi: 10.1016/j.lwt.2014.05.030
57. Pérez-Burillo S, Mehta T, Pastoriza S, Kramer DL, Paliy O, Rufian-Henares JA, et al. Potential probiotic salami with dietary fiber modulates antioxidant capacity, short chain fatty acid production and gut microbiota community structure. *Lebensm Wiss Technol.* (2019) 105:355–62. doi: 10.1016/j.lwt.2019.02.006
58. Do Prado SBR, Minguzzi BT, Hoffmann C, Fabi JP. Modulation of human gut microbiota by dietary fibers from unripe and ripe papayas: Distinct polysaccharide degradation using a colonic in vitro fermentation model. *Food Chem.* (2021) 348:129071. doi: 10.1016/j.foodchem.2021.129071
59. Rinninella E, Raoul P, Cintoni M, Franceschi F, Miggiano GAD, Gasbarrini A, et al. What is the healthy gut microbiota composition? a changing ecosystem across age, environment, diet, and diseases. *Microorganisms*. (2019) 7:14. doi: 10.3390/microorganisms7010014
60. Berger K, Burleigh S, Lindahl M, Bhattacharya A, Patil P, Stalbrand H, et al. Xylooligosaccharides increase bifidobacteria and lachnospiraceae in mice on a high-fat diet, with a concomitant increase in short-chain fatty acids, especially butyric acid. *J Agric Food Chem.* (2021) 69:3617–25. doi: 10.1021/acs.jafc.0c06279
61. Smith BJ, Miller RA, Ericsson AC, Harrison DC, Strong R, Schmidt TM. Changes in the gut microbiome and fermentation products concurrent with enhanced longevity in acarbose-treated mice. *BMC Microbiol.* (2019) 19:130. doi: 10.1186/s12866-019-1494-7
62. Nakkarach A, Foo HL, Song AA, Mutalib NEA, Nitisinprasert S, Withayagiat U. Anti-cancer and anti-inflammatory effects elicited by short chain fatty acids produced by Escherichia coli isolated from healthy human gut microbiota. *Microb Cell Fact.* (2021) 20:36. doi: 10.1186/s12934-020-0 1477-z

Conflict of Interest: The authors declare that the research was conducted in the absence of any commercial or financial relationships that could be construed as a potential conflict of interest.

frontiers in Nutrition

REVIEW
published: 04 August 2021
doi: 10.3389/fnut.2021.701511

Check for updates

Gut Microbiota and Their Role in Health and Metabolic Disease of Dairy Cow

Qingbiao Xu[1], *Qinqin Qiao*[2], *Ya Gao*[1], *Jinxiu Hou*[1], *Mingyang Hu*[1], *Yufeng Du*[1], *Ke Zhao*[3] *and Xiang Li*[1,4,5]*

[1] College of Animal Sciences and Technology, Huazhong Agricultural University, Wuhan, China, [2] College of Information Engineering, Fuyang Normal University, Fuyang, China, [3] Institute of Food Science, Zhejiang Academy of Agricultural Sciences, Hangzhou, China, [4] National Center for International Research on Animal Genetics, Breeding and Reproduction (NCIRAGBR), Huazhong Agricultural University, Wuhan, China, [5] Key Laboratory of Agricultural Animal Genetics, Breeding and Reproduction of Ministry of Education, College of Animal Sciences and Technology, Huazhong Agricultural University, Wuhan, China

OPEN ACCESS

Edited by:
Jie Yin,
Hunan Agricultural University, China

Reviewed by:
Hongbing Fan,
University of Alberta, Canada
Zuo Wang,
Hunan Agricultural University, China

***Correspondence:**
Xiang Li
xxianglli@mail.hzau.edu.cn

Specialty section:
This article was submitted to Nutrition and Microbes, a section of the journal Frontiers in Nutrition

Received: 28 April 2021
Accepted: 28 June 2021
Published: 04 August 2021

Citation:
Xu Q, Qiao Q, Gao Y, Hou J, Hu M, Du Y, Zhao K and Li X (2021) Gut Microbiota and Their Role in Health and Metabolic Disease of Dairy Cow. Front. Nutr. 8:701511. doi: 10.3389/fnut.2021.701511

Ruminants are mostly herbivorous animals that employ rumen fermentation for the digestion of feed materials, including dairy cows. Ruminants consume plant fibre as their regular diet, but lack the machinery for their digestion. For this reason, ruminants maintain a symbiotic relation with microorganisms that are capable of producing enzymes to degrade plant polymers. Various species of microflora including bacteria, protozoa, fungi, archaea, and bacteriophages are hosted at distinct concentrations for accomplishing complete digestion. The ingested feed is digested at a defined stratum. The polysaccharic plant fibrils are degraded by cellulolytic bacteria, and the substrate formed is acted upon by other bacteria. This sequential degradative mechanism forms the base of complete digestion as well as harvesting energy from the ingested feed. The composition of microbiota readily gets tuned to the changes in the feed habits of the dairy cow. The overall energy production as well as digestion is decided by the intactness of the resident communal flora. Disturbances in the homogeneity gastrointestinal microflora has severe effects on the digestive system and various other organs. This disharmony in communal relationship also causes various metabolic disorders. The dominance of methanogens sometimes lead to bloating, and high sugar feed culminates in ruminal acidosis. Likewise, disruptive microfloral constitution also ignites reticuloperitonitis, ulcers, diarrhoea, etc. The role of symbiotic microflora in the occurrence and progress of a few important metabolic diseases are discussed in this review. Future studies in multiomics provides platform to determine the physiological and phenotypical upgradation of dairy cow for milk production.

Keywords: gastrointestinal microflora, metabolic diseases, rumen, ruminants, dairy cow, omics

INTRODUCTION

Nearly 200 species of ruminants were identified till date, and among them, six were domesticated (1). Dairy cow was the most studied. Earlier studies provide insights into the knowledge of their digestive metabolism. Ruminants (mostly herbivores) employ foregut fermentation that allows them to digest cellulosic materials from plants. But during evolution, vertebrates lost the ability to produce enzymes that degrade cellulose and other complex polysaccharides (2). The ruminants rely upon a symbiotic relationship with microorganisms to digest such compounds. The microbiota produces enzymes to break the complex compounds into simpler molecules for easy absorption by the intestine. To carry out this, the host system has to provide an optimal environment and substrate for the survival of microflora. Thus, a commensal relationship is maintained where the host organism provides the substrates and maintains the environment required for the survival of the organism. In return, the microflora offers the nutrients required for the host organism (3).

The physiology and structure of the ruminant digestive system evolved billion years ago to ensure the effective digestion of cellulosic materials and various polysaccharides (4). The potency of the system lies in its design where the ingested feed material experiences a prolonged interaction with microflora (5). The ruminant stomach is a quadra compartmental digestive sac composed of the rumen, reticulum, omasum, and abomasum. Rumen internal environment is partitioned into different sacs by reticulo-ruminal fold in which the ingested food enters the rumen and then the reticulum (**Figure 1**). The rumen is lined with papillae, whereas the reticular epithelium forms a honeycomb structure. Feed consumed is directed toward the rumen through the reticulum (6). Reticulorumen (collective chamber of rumen and reticulum) stores the feed consumed for rumination and interaction with microflora. The feed is chewed to mix it with saliva and then swallowed. The ingested feed is then transferred to the anterior reticulorumen. Saliva is crucial for ingestion as well as rumination. It contains phosphate, potassium, and sodium bicarbonate in high concentrations to buffer the acids generated during fermentation. The reticulorumen appears to be a multifunctional fermentation sac with sizes varying from cattle (35–100 L) and sheep (3–5 L) (7). The physicochemical parameters of the rumen are described in **Table 1** (9–13). The host organism maintains the environment of rumen through various mechanisms. The atmosphere in the reticulorumen is mostly anaerobic with carbon dioxide (65%), methane (27%), nitrogen (7%), and hydrogen (0.2%) (14, 15). Along with these, traces of O_2, H_2S, and CO are also present. This gas composition is due to the rigorous fermentation in the rumen by resident microflora. The ingested feed is regurgitated to facilitate proper fermentation through interaction with microflora, a process called rumination.

Rumination helps in increasing the surface area and decreasing the size of the feed particles, thereby promoting proper fermentation (16–18). In continuation, after the degradation of feed particles into smaller compounds, the feed is passed into the following chamber omasum. Omasum plays the role of a filter through which lesser size (<2 mm) particles can freely pass through (19). Then the digested fodder moves to abomasum, the true stomach. The abomasum has a distinct enzyme component lysozyme that attacks the cell walls of bacteria (20, 21). In abomasum, the digestion of bacterial proteins as well as digesta is done in a similar fashion as the other non-ruminants (17). Host genetics also play a crucial role in deciding the fate and constitution of rumen microflora, which in turn has an effect on fermentation and the products (22). The maintenance of the rumen environment is crucial for the host to digest the feed and survive (23). This process in turn effects the ability of the dairy cattle to produce milk. The constitution of microflora is very important for all the above reasons. Deviation of the constitution of microflora or intrusion of infective organisms through feed, environmental, and other factors leads to disturbances in the metabolism of the host. This leads to diseases, and the regulation of such process is mandatory. Present review throws light on the roles of gut microbes in the health and metabolic diseases of ruminants.

WHAT IS THE NEED OF MICROFLORA?

Ruminants feed on plants that are the sources of complex polysaccharides, *viz.*, hemicellulose, cellulose, and lignin (24). However, due to the lack enzymatic system to degrade polysaccharides, they employ microflora that are capable of hydrolyzing these compounds in the gut for energy generation (25). These commensal microbes utilize the feed consumed by the host for survival, thereby establishing a healthy symbiotic relationship. The microbial population is habituated in the reticulorumen compartment. The reticulorumen environment is strictly anaerobic. It comprises dense and diverse microflora with eukarya (fungi and protozoa), archaea (methanogens), and bacteria at concentrations of 10^4, 10^6, and 10^{10}, respectively (26). These bacterial populations seem to be very sensitive and can be influenced by little changes in the rumen environment. Fermentation by the rumen microflora is a complex process in which microorganisms act in coordination to generate simpler compounds that are easily metabolized by the host (27). The polysaccharides are metabolized into two simpler forms. The former one is the proteins required for bacterial cell wall synthesis and the later form is the volatile fatty acid (VFA), which are end products of fermentation (28, 29). VFA plays a crucial role in ruminant metabolism and acts as a source of host energy. They participate in vital pathways such as fatty acid synthesis and gluconeogenesis. Recent findings indicate that VFA holds ∼70% of plant polysaccharides energy content (30, 31).

MEMBERS OF MICROBIAL CONSORTIUM

Primarily rumen is hosted by various microorganisms that assist the host organism in the digestion of complex polysaccharides of the dairy cow. The infants derive basal flora from the environment, feed consumed, partners, etc. The early gut microflora is developed from breast feeding (43%) and environment (28%), whereas non-breastfed lambs receive from

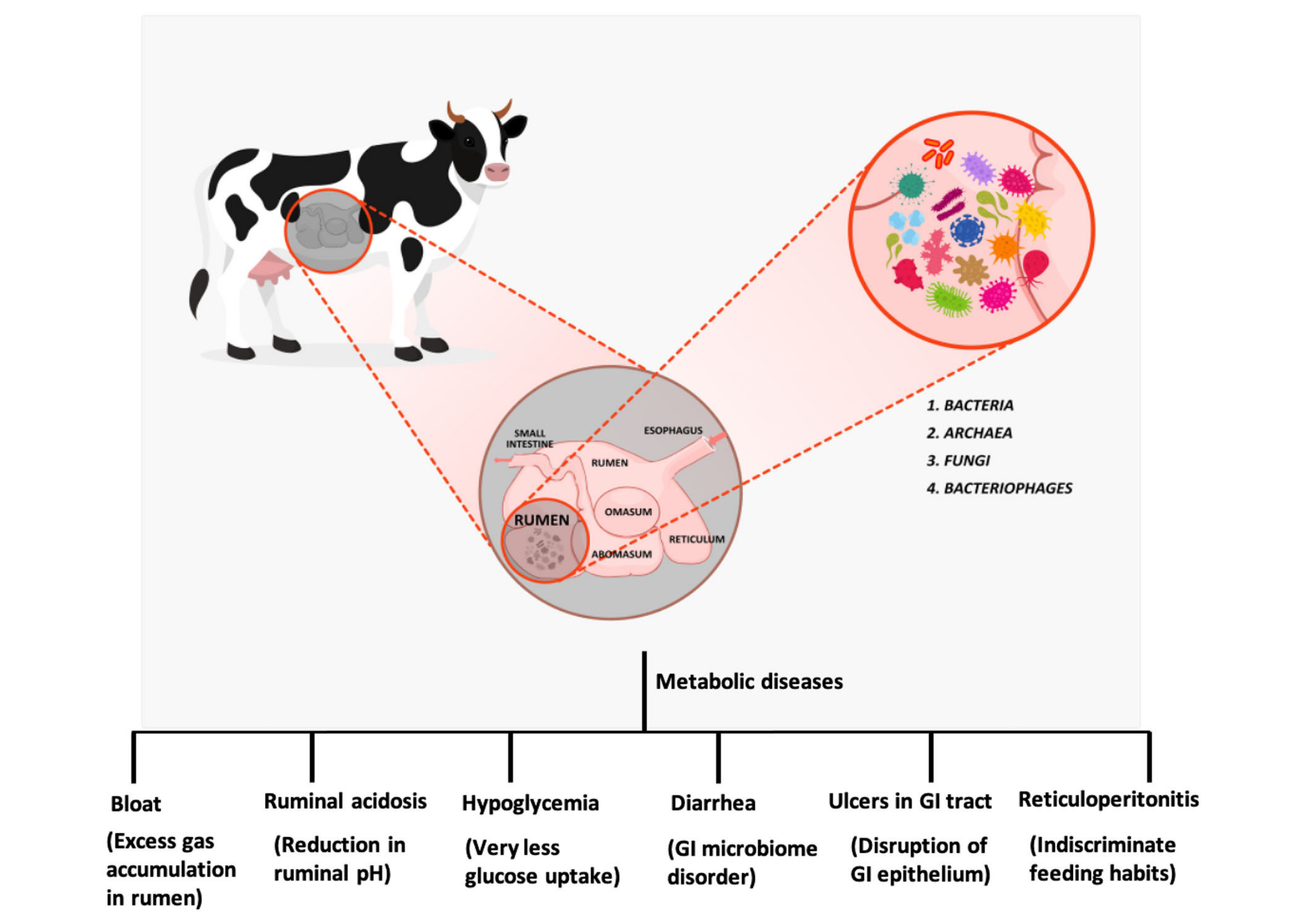

FIGURE 1 | Ruminant digestive system, microflora and metabolic diseases in ruminants.

vagina (46%) and air (31%) (32). The first floor of the rumen of neonates is colonized by enterococcus and streptococcus species which transform the gut environment to anaerobic (33). This helps in the recruitment of strict anaerobes in the gut to maintain the anaerobic ambience. Facultative anaerobes and aerobes are present in very less quantities, approximately 100-fold lesser in comparison with anaerobic organisms. The digestive capability of the dairy cow is directly proportional to the existing rumen microflora activity. Most of the organisms present in the rumen are non-culturable, whereas the culturable biota were studied in all aspects (34, 35).

The constitution of gut microbiota varies with the host, indicating a solid environmental-driven specificity of the host. The microbial composition of the feces in twins was more similar than in siblings (36). This implies the involvement of host genetics in deciding the individual gut microflora. Individuals also vary in fungal and archaeal compositions. The choice and development of gut microflora hence is a collaborative play of host genetics as well as environment. It is an ardent fact that the physiology of the individual has a strong relationship with gut microbial development. Apart from this, microflora differs from section to section in gut regions. Strict segregation of microflora between digestive and epithelium starts in the early stages of the life of a calf. The methanogenic composition also differs down the gastrointestinal tract. In neonatal calves the phylum *Bacteroides* is predominant, whereas in adult animals the phyla *Prevotella* and *Bacteroidetes* are abundant. Studies indicate that the microflora of 21-day-old calves has *Prevotella* (15.1%) and *Bacteroidetes* (15.8%), implying a starter-feed-driven rumen microbiome development during maturation. Methanogens and cellulolytic members were observed at 3–4 days of age, and this population is similar to that of matured mammals. Cellulolytic flora is present in 1-day individuals, indicating their importance in the ruminant system. Surprisingly, the rumen microflora of 14-day-old calves harbors more profuse yet ephemeral microorganisms in comparison with adult organisms. Metagenomic studies indicate that archaea (0.6–4%), eukarya (1.5%), and bacteria were present in ascending order of magnitude, with bacteria contributing 95% of the coding sequence.

Bacteria

Bacteria occupies the major portion of gut microflora, and their presence is crucial for the health of the dairy cow. They aid in the fermentation and degradation of plant polymers by the secretion of various enzymes (37, 38). Rumen contains about 1 × 10^3 bacteria/mL, and this consortium is complex in terms of functionality and taxon identification. The communal interaction of various bacteria enables the breakdown of the ingested fiber. The identification of these bacteria and their unique functionality has become the focal point of many studies. With the advancement of next generation sequencing technology, microbiological techniques, culture free approaches, and genetic engineering it has become easier to step forward in studying the role of commensal flora in host metabolism. Gene sequencing helped to identify and classify bacteria based on 16 s rRNA and physicochemical properties. The predominant microflora in the rumen are *Proteobacteria*, *Bacteroidetes,* and *Firmicutes*. In a study, *Prevotella* has also been identified with 42–60% of rRNA composition in two lactating cows. The coordinated metabolism of the microflora in which the metabolic product of one organism acts as a substrate for the other allows the sequential digestion of plant polymers (39, 40). The bacterial consortium is highly complex, and hence most of the bacteria are uncultured. The flora which are dominant and have a specific role in the metabolism are covered here so far.

The cell wall of a plant is comprised of a hemicellulose matrix with embedded cellulose fibers in it. The initial degradation of this matrix is carried out by a particular taxon of bacteria that secretes cellulolytic enzymes (24, 25). In general, bacteria contribute to most of the xylanase and endoglucanase activities in the rumen. These degrade the cellulose into smaller oligo/disaccharides which are then acted upon by other organisms. The first order cellulolytic bacteria includes *Ruminococcus flavefaciens*, *Ruminococcus albus*, and *Fibrobacter succinogenes*. Also, *Butyrivibrio fibrisolvens* is present in a lesser extent in comparison with the above said organisms. Apart from these, other uncultured bacteria can also act upon the substrate to degrade cellulose fibers. Some organisms like *Cellulosilyticum ruminicola H1*, from the rumen of Yak, also have the capability to produce lignocellulolytic enzymes. On the other hand, coculturing of some organisms implicated negative interaction and decreased enzyme efficiency (41). This inhibition is found to be an effect of the bacteriocins secreted as a part of the defense mechanism and competition for the substrate (42). For instance, *R. flavefaciens* and *R. albus* secrete bacteriocins in competition for cellulose (43, 44). Non-cellulolytic bacteria also secrete bacteriocins and are supposed to be tough competitors for different substrates in a rumen environment (45, 46).

The end products of cellulolytic bacterial interaction act as substrates for different microflora that start further degradation of such compounds. Other important polymers, such as starch, are hydrolyzed by *Selenomonas ruminantium, Succinomonas amylolytica, Butyrivibrio fibrisolvens, Streptococcus bovis*, *Ruminobacter amylophilus,* and *Prevotella* species, whereas pectin is degraded by *Lachnospira multiparus* and *Succinovibro dextrinosolvens.* Besides, the constitution of bacteria changes with the type of feed consumed by the host (5, 47, 48). Animal feeding differs in various places. High fiber feed is rich in cellulose whereas high grain feed is packed with starchy material. This influences the type of bacteria required to digest the material consumed and has a strong impact on microflora constitution in the gut environment (49, 50). Sugar and starch fermenters constitute most of the rumen bacteria. Maximum energy is extracted from the plant polysaccharides as the end products of bacterial fermentation serve as substrate to many other organisms. *Megasphaera elsdenii* acts upon lactate (end product of bacterial fermentation) and *Veillonella alcalescens* utilizes succinate, acetate, and hydrogen (51, 52).

TABLE 1 | Physicochemical properties of the rumen.

Parameter		References
Temperature	39°C (optimal), vary in between 38–41°C	(2, 8)
pH	∼6.5 (buffered in the range of 5.5–7.0)	
Dry content	Maintained constant around 10–20%	
Osmolality	250–400 mOsmol/Kg (increases with the feed intake)	
Redox potential	Lies within the range of −150 to −350 mv	
Gaseous composition	CO_2 (65%), CH_4 (27%) are the major gases produced by fermentation. N_2 (7%), O_2 (0.6%) H_2 (0.2%) are present in traces.	

Recent metagenomic studies on gut microflora of various mammalian species revealed that in ruminant and herbivore microflora the anabolic pathways for the synthesis of amino acids (AAs) are more prevalent in comparison to carnivores. This is because the diet of a carnivore would be rich in protein, and therefore the constitution of gut microbiota is chosen to be more proteolytic. In the point of herbivores, the diet is fiber rich, and carbohydrate is the core source of energy (53). Hence in the microbiota of rumen, the AA synthesis pathways are commonly seen. Indeed, a certain cellulolytic activity some organisms also exhibit potent proteolytic activity, such as *B. fibrisolvens, P. ruminicola, S. ruminantium,* and *R. amylophilus. P. ruminicola* exhibits deaminase and proteolytic activities and produces higher amounts of ammonia (NH_3) in the rumen. This activity is considered to be crucial as the rumen environment has lesser protein and ammonia that act as nitrogen sources for AA and protein synthesis (54). Other classes of bacteria include sulfate-reducing bacteria that assist in the reduction of sulfate to H_2S. In addition, it has to be noted that the rumen microbiota is fine-tuned depending upon the dietary changes to assist degradation and fermentation of various complex compounds. They also have communal relations with each other and with the host to ensure their survival as well as maximum energy production. They also play a role in supplying VFAs and proteins to the host organism. Disturbances in concentrations of microbiota sometimes have a heavy impact on the host system and may lead to diseases. Different types of bacteria are listed in **Table 2**.

Archaea

Anaerobic methanogens make up most of the archaea constituting ∼0.6–3.3% of the total rumen microbiota (65). Major archaea members of rumen microbiota are listed in **Table 3**. Metagenomic studies and 16 s rRNA sequencing analyses revealed the presence of archaea in the rumen environment. Studies revealed that about 3.6% of microbiota

TABLE 2 | Gut bacteria in ruminants (mostly rumen).

Bacteria type	Bacterial species	Gram staining	End products	References
Cellulolytic	*Fibrobacter succinogens*	Negative	Acetate, Formate, Ethanol, propionate	(55–60)
	Ruminococcus flavefaciens	Positive		
	Ruminococcus albus	Positive		
	Clostridium longisporum	Positive		
	Eubacterium cellulosolvens	Positive		
	Clostridium cellobioparum	Positive		
	Butyrivibrio fibrisolvens	Negative		
Hemi cellulolytic	*Eubacterium xylanophilum*	Positive	Acetate, Formate, Ethanol, propionate	(55–60)
	Eubacterium uniformis	Positive		
	Prevotella ruminicola	Negative		
Lipolytic	*Anaerovibrio lipolytica*	Negative	Acetate and propionate	(61)
Pectinolytic	*Treponema saccharophilum,*	Negative	Acetate and formate	(62)
	Lachnospira multiparus	Positive		
Proteolytic	*Prevotella sp.*	Negative	Amino acids, nitrogen	(63)
	Ruminobacter amylophilus,	Positive		
	Clostridium bifermentans	Positive		
Amylolytic	*Prevotella ruminicola*	Negative	Formate, propionateand Acetate	(64)
	Streptococcus Bovis,	Positive		
	Ruminobacter amylophilus	Positive		
Saccharolytic	*Succinivibrio sp.*	Negative	Lactate, Acetate, Fumarate, Succinate	(55–60)
	Lactobacillus sp.	Positive		
	Bifidobacterium ruminantium	Positive		
Tanninolytic	*Streptococcus Caprinus*	Positive	Lactate, Acetate, Fumarate, Succinate	(62)
	Eubacterium oxidoreducens	Positive		
Ureolytic	*Megasphaera elsdenii*	Negative	Ammonia and CO_2	(55–60)

in rumen exhibited autofluorescence, a distinctive property exhibited by methanogenic bacteria (71). Methanogens, as the name indicates, generate methane (CH_4) either by the reduction of CO_2 or by the hydrolysis of acetate to CH_4 and CO_2. Most of the ruminal methane is produced via the reduction of CO_2 rather than dissimilating acetate. The process of CO_2 reduction requires electrons which come from various sources, including methylamine, methanol, formate, and hydrogen produced as metabolic intermediates (72, 73). Archaea are clustered under Euryarchaeota and are classified as *Methanomicrobiales, Methanosarcinales, Methanococcales, Methanobacteriales,* and *Methanopyrales*. Most of the ruminant methanogens fall under one of the three categories identified. They are ordered as *Methnaomicrobiales* < *Methnaomicrobium* and *Methanobacteriales* (14.9%) < *Methanobrevibacter* (61.6%). Apart from this, another set of uncultured ruminal archaea were categorized under rumen cluster C (RCC). A study on the ruminal archaea community of red deer, cattle, and sheep disclosed the fact that their composition is maintained throughout different species. They are more conserved when compared to the bacterial members. The dominant archaea species stood same in all the rumens. Species belonging to *Methanobrevibacter* is found to be dominant in rumen. About 26.5% of the total archaea is occupied by members of RCC (55, 66).

Methane production by various archaea is mediated by cytochrome in few methanogens, whereas alternative complexes mediate this process in some methanogens. The genus *Methanosarcinales* comprises of methanogens and has the capability to grow on a wide range of substrates. Hydrogen concentration in the environment plays a crucial role in the production of methane. Cytochrome-based methanogens have higher growth yields when compared with non-cytochromic methanogens. Non-cytochromic methanogens need lesser hydrogen concentration to produce methane whereas cytochromic methanogens need about 10-fold higher concentrations of hydrogen for the optimal growth. This is the reason for the presence of non-cytochromic methanogens in higher concentrations in the rumen. Hydrogen utilization by methanogens is crucial as it decreases the pressure, allowing the conversion of endergonic metabolic reactions to exergonic reactions. This makes bacterial fermentation energetically favorable (74). Hydrogen consumption by methanogens stands as a good example of the symbiotic relationship between methanogenic and cellulolytic bacteria, wherein the hydrogen produced by the latter is consumed by the former for its survival. Coculturing of rumen methanogens and ruminal fungus has a heavy influence on cellulolytic and fermentation activities. Hydrogen transfer among methanogens and other microflora in rumen is best described by coculturing methanogens with

TABLE 3 | Various microflora in rumen.

Organism	Species	Mode of action	References
Archaea	*Methanobacterium formicicum, Methanobacterium bryantii, Methanobrevibacter ruminantium, Methanobrevibacter smithii, Methanomicrobium mobile, Methanosarcina barkeri, Methanoculleus olentangyi*	Strictly anaerobic and produce methane from CO_2 and H_2.	(65, 66)
Protozoa	*Entodinium bovis, Entodinium bubalum, Entodinium bursa, Entodinium caudatum, Entodinium chatterjeei, Entodinium parvum, Entodinium longinucleatum, Entodinium dubardi, Entodinium exiguum, Epidinium caudatum, Isotricha prostoma, Isotricha intestinalis, Dasytricha ruminantium, Diplodinium dendatum, Diplodinium indicum, Oligoisotricha bubali, Polyplastron multivesiculatum, Eremoplastron asiaticus, Eremoplastron bubalus*	Lignocellulosic digestion and degradation of complex compounds to reducing sugars	(67)
Bacteriophages	*Methanobacterium phage Ψ M1, Methanobacterium phage Ψ M10, Methanobacterium phage Ψ M100, Methanothermobacter phage Ψ M100, Methanobacterium phage ΨM2*	Strictly anaerobic and produce methane from CO_2 and H_2.	(3)
Fungus	*Piromyces communis, Piromyces mae, Piromyces minutus, Piromyces dumbonicus, Piromyces rhizinflatus, Piromyces spiralis, Piromyces citronii, Piromyces polycephalus, Anaeromyces mucronatus, Anaeromyces elegans, Caecomyces communis, Caecomyces equi, Caecomyces sympodialis, Cyllamyces aberensis, Cyllamyces icaris, Neocallimastix frontalis, Neocallimastix patriciarum, Neocallimastix hurleyensis, Neocallimastix variabilis, Orpinomyces joynii, Orpinomyces intercalaris*	Act upon lignin and cellulose fibers to and forms Formate, Succinate, Hydrogen, acetate and lactate.	(68–70)

protozoa. Even though archaea and bacteria fall prey to protozoa, methanogens get habituated inside and help in the generation of energy by consuming the hydrogen produced during the metabolism (74–76). Hydrogen consumption by methanogens forms the root of symbiosis with other microbiota in the rumen for maximal energy production (77–79). The commensal interactions of methanogens with protozoa and other rumen microbiota facilitate the complete degradation of complex plant polymers. The methane production is directly related to the amount of fodder and hemicellulose degradation (80–82). About 19% of the total energy of the feed is lost during the production of methane gas by methanogens. The commensal interaction of methanogens with other microbiota in the rumen enhances energy production to a maximum extent. But the gas production has a hinderance effect on the overall energy harvested from the ingested feed.

Protozoa

Protozoa are unicellular organisms bound by pellicle or cuticle in the rumen. They are the simplest forms of eukaryotes found in the universe (**Table 3**). Most of the protozoa are parasitic as they feed on microorganisms, organic matter, and cell debris. Ciliates are more prevalent in ruminant gut in comparison with several flagellate species. Ciliates are subcategorized into Vestibuliferida and Entodiniomorphida with 25 genera. Protozoa in the rumen have specialized functions tuned to survive in a rumen environment (83, 84). Most of the protozoa are anaerobic, but very few species are supposed to sequester oxygen. Oxygen sequestration from the environment is advantageous to the host as it maintains the anaerobic ambience of the reticulorumen. This also helps in the survival of strict anaerobes and promotes the digestive degradation. Various complex carbohydrates *viz*., lignocellulose, starch, and sugar are consumed by protozoa for energy production. Around 50% of the total biomass in the rumen is composed of protozoa. Degradation of fats, proteins, and carbohydrates is facilitated by direct engulfing (85). The lignocellulosic digestion capacity by protozoa is presumed to be the result of lateral gene transfer from the bacteria they engulf (86). Protozoa prey on selective species of bacteria, and the reason for feeding on particular bacteria is not clearly understood (87–89). Ciliates play a crucial role in fermentation and plant fiber degradation. The products obtained as a result of protozoan fermentation are found similar to that of bacteria. In contrast to bacteria, protozoa divide at a much slower rate (15–24 h). To overcome the washing out of protozoa before division, they tend to reside in the lower layers of the rumen. Many methanogens reside on the protozoan surface for H_2. Hydrogen gas is produced is used for the reduction of CO_2 to methane. Methanogens residing on protozoa account for around 9–25% of total rumen methane (77, 90). Protozoa are capable of engulfing and store more starch at once, which decreases acid production by lowering pH (91).

Protozoa (holotrich) produces pectin esterase, invertase, amylase, and polygalactouronase to degrade plant sugars and fibers. Protozoa also produce cellulolytic and hemicellulolytic bacteria in lower quantities compared with that of entodiniomorphids. Ciliates in the rumen secrete proteolytic enzymes, resulting in the production of AAs and ammonia. The type of engulfed microbiota decides the nitrogen metabolism of the protozoa. Generation of nitrogenous compounds in turn influences the recycling of nitrogen. Rumen ciliates also influence ammonia as well as VFA production. The symbiosis of protozoa and rumen bacteria were investigated and showed that the presence of rumen protozoa effected the bacterial composition in rumen. Absence of protozoa has a positive effect on the growth of cellulolytic and hemicellulolytic bacteria. Lambs with no protozoan population showed increased growth of wool as much as 10% when compared to lambs with rumen protozoa. No proper effect of protozoa on methane production is observed. Variations in the composition of digested material in both omasum and abomasum are observed in defaunated and faunated animals. It is an ardent fact that protozoa influence many processes in the metabolism of host (92–94).

Fungi

Rumen is a repository of anaerobic fungi with an explicit capacity of lignocellulose degradation. Fungi contribute to 20% of the overall microbiota in the rumen. They are deliberate members of plant fiber degradation. Fungi also exhibit proteolytic activity. In the fungal structure, polycentric or monocentric thallus is observed, and the zoospores are polyflagellate or uniflagellate. Asexual life cycle of anaerobic fungi is mostly observed (95). Most of the fungi are not present alone in the rumen of the animals but are vividly present along the digestive tract. Fungal species were also isolated from the feces and saliva of the dairy cow. Domestic animals host Chytridiomycetes for assisting their digestion. These organisms occupy about 8% of total ruminal microbiota in the animals fed on forage, which allows more retention in the rumen (45). But in the case of high grain diets, fungal population decreases. Enzymes secreted by fungal cultures degrade lignin, hemicellulose, starch, and cellulose (33). In addition, fungi are strict anaerobes, and hence carbohydrate fermentation is the sole source of energy production. Fungi are devoid of cytochromes and mitochondria that are coplayers of oxidative phosphorylation. Despite that, they contain Hygrogenosomes that facilitate the generation of energy. Hydrogenosomes are mitochondrial derivatives that occurred during evolution, and they are not only confined to fungal genera. Various anaerobic eukaryotes and trichomonads are also found to contain this organelle. Hydrogenosomes differ from conventional mitochondria by possessing pyruvate/ferredoxin reductase instead of dehydrogenase. They also provide room for ATP production and pyruvate conversion.

Commensal interplay of fungi and bacteria is a well-studied concept. *In vitro* studies were carried out to understand the degradative dynamics of fungi when cocultured with cellulolytic bacteria. Cellulose degradation capacity of the fungi increases manifold with *Megasphera elsdenii, Selenomonas ruminantium*, and *Viellonella alcalescens*. Xylan consumption is increased by coculturing *Neocallimastix frontalis* with cellulolytic bacteria like *Selenomonas ruminantium, Prevotella ruminicola,* and *Succinivibrio dextrinosolvens* (**Table 3**). On the other hand, coculturing with *Streptococcus brevis* or *Lachnospira sp.* has a negative effect on xylan degradation. *R. flavefaciens,* and *R. albus* coculturing with fungi have shown adverse effects on cellulolytic activity. These bacteria release a polypeptide into the broth that has detrimental effects on cellulolytic activity of the fungus. The fungal activity in the degradation of cellulosic materials is considered minimum than that of bacteria. This might be due to their larger doubling time, inhibition by bacteria, competition for substrates, and decreased retention. Nevertheless, they exhibit remarkable activity in the degradation of lignocellulosic material, as the rhizoids pervade the cell wall of plants and make it easily accessible by the rest of the rumen microbiota (96).

Bacteriophages

Bacteriophages are obligate parasites and play a crucial role in rumen microbiota. Bacteriophages infect bacteria and lyse them after their replication (**Table 3**). Through lysis, the overall bacterial population is maintained in the host digestive environment. Bacterial lysis releases bacterial proteins that act as precursors of AA synthesis (97). Bacteriophages are found to vary with the organism, i.e., they are specific for a particular organism. This may be used by the researchers to destroy a particular genus of microbes from the rumen environment. Very little information is known about the bacteriophages infecting protozoans, methanogens, and archaea. It was identified that siphophages are capable of infecting methanogenic bacteria. The knowledge about the enzymatic profile and genetic makeup of rumen phages is limited and yet to be explored to manipulate the rumen environment (98).

METABOLIC DISORDERS IN RUMINANTS

Disturbances in the homogeneity of gastrointestinal microflora have severe effects on the digestive system and various organs. This disharmony in the communal relationship also causes various metabolic disorders, including bloat, ruminal acidosis, hypoglycemia, diarrhea, ulcers in gastrointestinal (GI) tract, and retivuloperitonitis (**Figure 1**).

Bloat

The rumen tympany, also called as bloat, is associated with a condition in which excess gas is accumulated in the rumen. This is observed in animals fed with higher quantities of grains or forages (99), which can be categorized into free gas and frothy bloat. Free-gas bloat is associated with pathological/physical problems hindering gas release from the stomach of the dairy cow. Esophagus obstructions (external particles cloths and fruit material, etc.), cysts, blisters, tumors, thoracic or cervical enlargement, reticular dysfunction, and hypocalcemia are major conditions affecting gas belching (100–102). Frothy bloat is the result of feed ingestion, which continuously produces froth that cannot be easily expelled from the stomach. Testing with a stomach tube helps in figuring the type of bloat. If the causative agents are physical obstructions, they have to be removed manually to ensure the gas expulsion. Frothy bloat contains both hydrophobic and hydrophilic properties. The foam is the result of partial digestion of polymeric compounds including, lipopolysaccharides, fatty acids, glycans, and glycolipids. Presence of these partially digested compounds increases rumen viscosity and hinders gas removal. Gaseous distension exerts pressure on the nearby organs causing edema, pain, organ failure, and death. Several practices that are employed to treat free bloat and frothy bloat include using a stomach tube to remove gas and partially digested feed, anti-foaming agent administration, and the placement of fistula or cannula (103).

Apart from physical factors, the microbiota in the rumen also contribute to the development of gas. Gas is generated as a result of methanogenic bacterial action upon various substrates. This methane, hydrogen, and CO_2 gases produced in excess when left unattended by downstream flora results in the accumulation of gas in the stomach. The hydrogen gas produced as a part of methanogen metabolism also has to be addressed. It is a well-known fact that the rumen environment is highly anaerobic.

But excess CO_2 can cause subtle changes in the rumen. CO_2 can be reduced by methanogens to generate methane and/or as such CO_2 in excess can cause tympany. It is nevertheless necessary to attend to the excess production of these gases to maintain ruminal microbial harmony. Hence to maintain the environment, probiotics can be used to replenish the rumen flora. Treated and high fiber feed also helps in relieving the stress caused by methanogenic bacteria (104).

Ruminal Acidosis

Ruminal acidosis is caused by the consumption of more fermentable carbohydrate-rich feed material than grainy feeds (105, 106). Molasses, sugar beets, potatoes, and cereal grains result in acidosis. Fermentation of such compounds result in higher amounts of lactic acid production and hence pH of rumen is drastically reduced (107, 108). Due to this, many gram-negative bacteria are destroyed releasing endotoxin into the rumen. All these results in low pH, accumulation of fluid, disturbance of microbiota, and partial digestion. Low pH and acid production have destructive effects on the inner epithelium of the stomach causing ulcers as well as mucosal inflammation. Drastic fall in pH also inhibits the cellulolytic bacteria but enhances propionate-producing bacteria in the rumen. Rumen microbiota alteration leads to improper metabolism which can cause liver dysfunction, lung-related diseases, and can also lead to death (109–111).

Hypoglycemia

Hypoglycemia is a disorder observed when the rate of glucose uptake is very less in comparison to the rate of utilization (112, 113). Vitamin B_{12} plays a key role in the synthesis of glucose from propionate, and its deficiency is also related to the occurrence of hypoglycemia. In new-born calves and lambs in a cold environment, hypoglycemia leads to death. Gluconeogenesis does require NADH and ATP apart from substrates made available in the ruminant environment. For this reason, an organism depends primarily on dietary carbohydrates for glucose rather than synthesis. Deficiency in glucose supply caused hypoglycemia in all the animals. On the other hand, hypoglycemia is also seen in animals whose diet is rich in inhibitors of fatty acid beta oxidation in the kidney and liver. Required amounts of AAs, fatty acids, ambience, and vitamins have to be provided for treating hypoglycemia (114–116).

Most of the fed polysaccharides should be degraded to glucose for energy production. Disharmony in the activity of rumen microbiota contributes to impaired degradation of polysaccharides that in turn affects glucose turnover. Proper diet at regular intervals with the maintenance of a favorable environment and supplementing cellulolytic bacteria may also address this issue in less severe conditions (117, 118).

Ulcers in GI Tract

Ulcers in the dairy cow are more common in the duodenum and abomasum. They are often observed in cows and buffaloes than in sheep (119, 120). Ulcers are mostly associated with improper feed intake, over grazing stress, microbial infection, and malnutrition. These occur in concomitance with other diseases, *viz.*, salmonellosis and blue tongue (*Clostridium perfringens* abomasitis). Over usage of non-steroidal antiinflammatory drugs can also cause ulcers. Perforating ulcers are generally more infectious and have adverse effects on the epithelium of gastrointestinal tract than non-perforating ulcers (121).

The disruption of the outer epithelium of gastrointestinal tract is caused by acid production and can be alleviated by the administration of probiotics containing lactic acid bacteria. Antihistamine with iron injection can also reduce the pain and bleeding in adult ruminants (122).

Reticuloperitonitis

Reticuloperitonitis, also called as traumatic reticulitis or hardware disease, is mainly observed in cattle with unsystematic feeding (123, 124). Indiscriminate feeding habits of dairy cow leads to the disturbances in the harmony of rumen microbiota. Continuous feeding deters bacterial revival and causes improper digestion which may lead to bloat and ruminal acidosis. It is a noncontagious disease which if not properly observed causes devastating effects. Proper dietary consumption at regular intervals will enable bacterial resurgence and revival. Usage of probiotic syrups, administration of antibiotics, and digestive aids may help in the initial stages and rumenotomy is suggested during severity index (125).

Diarrhea

Diarrhea is a severe problem prevalent in young calf. It is associated with various symptoms including disturbance of electrolyte balance, dehydration, and weakness. The reason for the disease varies with geographical location, type of feed, type of infection, and host metabolic issues. In most of the time, the disease occurrence is multifactorial. Pathogens namely, bacteria, virus, parasites, and protozoa can trigger infection. Infection by bacterial diarrhea includes *Enterobacter sp. mycobacterium paratuberculosis, Clostridium perfringens, Salmonella sp.* as well as *Staphylococcus*. Rotavirus and adenoviruses contribute to viral infections. *Trichonema sp.* and *Strongylus sp.* are major parasites infecting the gastrointestinal tract of the dairy cow. Nonetheless, *Trichomonas sp., Entamoeba sp.,* and *Giardia sp.* contribute to protozoan infection. Infection of the ruminant flora by either of the above species causes disturbance in the homogeneity and functionality, culminating in disease. Malabsorption or hypersecretion of fluids into the gut usually results in the secretion of excessive fluid from the intestine. Severe outflux of fluids with salts leads to weakness. Things to be observed to treat diarrhea are suppressing the infection and adjusting physiological imbalance. This allows eradication of the causative agent helping in faster recovery. Usage of antibiotic drugs will also help in wiping out the existing infection and maintaining the functional role of microflora (126).

ROLE OF MULTIOMICS IN DAIRY COW

Gut microbiota plays a crucial role in ruminant digestion as well as energy production. Hence it is essential to study the genomic environment to predict the changes that cause genetic and metabolic disorders. But it is difficult to isolate and study the genome of a particular flora in the consortium. For this reason, the whole genome of the consortium is studied under the branch metagene "omics". The complete genome of the gut microflora, termed as gut microbiome, is obtained by sequencing methodologies and omics approaches (127). The identity of the microbiome is determined by general sequencing protocols, whereas "omics" determine the actual functionality of the microbiome present in rumen. Omics approaches embrace metabolomics, metaproteomics, metatranscriptomics, and metagenomics. The relationship between host and microbiota is well-studied by omics approaches. For instance, metagenomics approaches revealed that *Bacteroidetes* is energetically less favorable to the host in comparison to *Firmicutes*. The action of *Firmicutes* increases nutrient availability to the host, which culminated in obesity.

Role of omics in the physiology and functionality of livestock is an area which is yet to be explored. Many omics-related approaches succeeded in finding the relation between microbiome composition and livestock production (128). These studies also helped in revealing taxonomical differences in the ruminal microenvironment of the organisms based on the dietary changes and environmental variations (22, 129). Recent studies on profiling microbiome of the rumen in a large sample set (>700) revealed a diet-dependent relationship between the host and microflora. The type of feed ingest decides the flora in the rumen (130). In depth analysis of the rumen microbiome using omics approaches helps in identifying markers that decide the variability in feed efficiency in cattle. Omics-based studies also help in assessing colonization patterns in the dairy cow.

CONCLUSIONS AND FUTURE PERSPECTIVES

In the last few decades, the role of GI microbiota in health and disease has become the focal point of many studies. Involvement of gut microbiota in digestion and various diseases in humans is well-studied. However, in the case of dairy cows, the underlying mechanisms of host–microbial interactions are yet to be uncovered. The interaction of rumen or gut microflora is purely symbiotic in which one organism benefits the others. The higher organisms lost the capacity to degrade plant cell wall and other materials during evolution to use it as a source of energy. Hence, ruminants employed microorganisms to digest plant materials and in turn provided them nutrients required for survival. Several types of microorganisms reside in the rumen and gut of the dairy cow. These organisms are from all the main groups such as bacteria, protozoa, archaea fungi, and bacteriophages. Composition of rumen microbiota varies with the geographical location and type of regular feed. However, the dominant strains in the rumen environment are always conserved. Surprisingly, the microbiota adapts to the feed intake and changes its constitution to meet the requirement of the host. Bacteria occupy a major part of the ruminal microflora. Microorganisms are adopted in such a way that most of the energy is extracted from the provided substrate. Collaborative action of various species of organisms helps in proper digestion and energy production. The end product of one organism acts as a substrate for the secondary organism. In this manner, the degradation of the plant fiber is carried out to harvest maximum energy from the ingest.

To understand the metabolic disease of dairy cow, many factors have to be taken into consideration. This should start with the type of feed, interval of feed, grazing area, and response of the ruminant system to various drugs. Rumen microflora are the crucial role players in the digestion as well as energy generation for the dairy cow. Hence, it is nevertheless necessary for a dairy cow to maintain the ambience in the GI tract to ensure the proper symbiotic relationship with the resident bacteria. Infection by pathogens can lead to disharmony in the commensalism of the bacteria that culminates in various diseases. Prior identification of the infection, proper care, and treatment are required to rescue the organism. Preventive measures like proper ingest, probiotic supplementation, and vaccination protect the organisms from infections, thereby increasing the productivity. In depth analysis of microbiome using omics approaches helps in attaining knowledge about gut microbial mechanisms and functional activities at various conditions. Also, the variations in the gut microbiome have a strong impact on the phenotypic definition and physiology of the host. Gut microbiota has an influence on the health and productivity of dairy cow. Future studies in multiomics provide a platform to determine the physiological and phenotypical upgradation of the dairy cow for milk production.

AUTHOR CONTRIBUTIONS

QX and QQ wrote and prepared the original draft. YG, JH, MH, and YD edited the manuscript. QX, KZ, and XL critically reviewed the manuscript. All authors reviewed and approved the final manuscript.

FUNDING

This work was supported by grants from the Fundamental Research Funds for the Central Universities (2662019QD021), the Innovation Team of Development and Research on Food Technology of Fuyang Local Agricultural Products (FXKCT02), the State Key Laboratory of Animal Nutrition (2004DA125184F1906), the Open Project Program of Key Laboratory of Feed Biotechnology, Key Laboratory of Molecular Animal Nutrition of Zhejiang University, and the National Natural Science Foundation of China (C31802087).

REFERENCES

1. Russell JB. "Rumen," in *Encyclopedia of Microbiology*, ed. M. B. T.-E. of M. Third E. Schaechter Oxford: Elsevier p. 163–174. doi: 10.1016/B978-012373944-5.00061-4
2. Mackie RI. Mutualistic Fermentative Digestion in the Gastrointestinal Tract: Diversity and Evolution. *Integr Comp Biol.* (2002) 42:319–26. doi: 10.1093/icb/42.2.319
3. Choudhury P, Sirohi S, Puniya A, Chaudhary PP. "Harnessing the Diversity of Rumen Microbes using Molecular Approaches," in *Livestock Green House Gases: emission and options for mitigation.* Satish Serial Publishing House p. 65–82.
4. Oltjen JW, Beckett JL. Role of ruminant livestock in sustainable agricultural systems. *J Anim Sci.* (1996) 74:1406. doi: 10.2527/1996.7461406x
5. Krause DO, Denman SE, Mackie RI, Morrison M, Rae AL, Attwood GT, et al. Opportunities to improve fiber degradation in the rumen: microbiology, ecology, and genomics. *FEMS Microbiol Rev.* (2003) 27:663–93. doi: 10.1016/S0168-6445(03)00072-X
6. Castillo-González A, Burrola-Barraza M, Domínguez-Viveros J, Chávez-Martínez A. Rumen microorganisms and fermentation. *Arch Med Vet.* (2014) 46:349–61. doi: 10.4067/S0301-732X2014000300003
7. Sahu NP, Kamra DN. Microbial eco-system of the gastro-intestinal tract of wild herbivorous animals. *J Appl Anim Res.* (2002) 21:207–30. doi: 10.1080/09712119.2002.9706370
8. Castro-Montoya JM, Makkar HPS, Becker K. Chemical composition of rumen microbial fraction and fermentation parameters as affected by tannins and saponins using an in vitro rumen fermentation system. *Can J Anim Sci.* (2011) 91:433–48. doi: 10.4141/cjas2010-028
9. Hillman ET, Lu H, Yao T, Nakatsu CH. Microbial ecology along the gastrointestinal tract. *Microbes Environ.* (2017) 32:300–13. doi: 10.1264/jsme2.ME17017
10. Firkins JL Yu Z, Park T, Plank JE. Extending Burk Dehority's perspectives on the role of ciliate protozoa in the rumen. *Front Microbiol.* (2020) 11:123. doi: 10.3389/fmicb.2020.00123
11. Wahrmund JL, Ronchesel JR, Krehbiel CR, Goad CL, Trost SM, Richards CJ. Ruminal acidosis challenge impact on ruminal temperature in feedlot cattle1. *J Anim Sci.* (2012) 90:2794–801. doi: 10.2527/jas.2011-4407
12. Liu K, Zhang Y, Yu Z, Xu Q, Zheng N, Zhao S, et al. Ruminal microbiota–host interaction and its effect on nutrient metabolism. *Anim Nutr.* (2021) 7:49–55. doi: 10.1016/j.aninu.2020.12.001
13. Matthews C, Crispie F, Lewis E, Reid M, O'Toole PW, Cotter PD. The rumen microbiome: A crucial consideration when optimising milk and meat production and nitrogen utilisation efficiency. *Gut Microbes.* (2019) 10:115–32. doi: 10.1080/19490976.2018.1505176
14. Burns JC, ASAS. Centennial Paper: Utilization of pasture and forages by ruminants: A historical perspective1. *J Anim Sci.* (2008) 86:3647–63. doi: 10.2527/jas.2008-1240
15. Kingston-Smith AH, Marshall AH, Moorby JM. Breeding for genetic improvement of forage plants in relation to increasing animal production with reduced environmental footprint. *Animal.* (2013) 7:79–88. doi: 10.1017/S1751731112000961
16. McAllister TA, Bae HD, Jones GA, Cheng K-J. Microbial attachment and feed digestion in the rumen. *J Anim Sci.* (1994) 72:3004–18. doi: 10.2527/1994.72113004x
17. Merchen NR, Elizalde JC, Drackley JK. Current perspective on assessing site of digestion in ruminants. *J Anim Sci.* (1997) 75:2223–34. doi: 10.2527/1997.7582223x
18. Hoover WH, Miller TK. Rumen digestive physiology and microbial ecology. *Vet Clin North Am Food Anim Pract.* (1991) 7:311–25. doi: 10.1016/S0749-0720(15)30801-X
19. Weimer PJ. Why don't ruminal bacteria digest cellulose faster? *J Dairy Sci.* (1996) 79:1496–502. doi: 10.3168/jds.S0022-0302(96)76509-8
20. Jollès P, Schoentgen F, Jollès J, Dobson DE, Prager EM, Wilson AC. Stomach lysozymes of ruminants. II Amino acid sequence of cow lysozyme 2 and immunological comparisons with other lysozymes. *J Biol Chem.* (1984) 259:11617–25. doi: 10.1016/S0021-9258(18)90908-7
21. Jollès J, Jolles P, Bowman BH, Prager EM, Stewart C-B, Wilson AC. Episodic evolution in the stomach lysozymes of ruminants. *J Mol Evol.* (1989) 28:528–35. doi: 10.1007/BF02602933
22. Li F, Li C, Chen Y, Liu J, Zhang C, Irving B, et al. Host genetics influence the rumen microbiota and heritable rumen microbial features associate with feed efficiency in cattle. *Microbiome.* (2019) 7:92. doi: 10.1186/s40168-019-0699-1
23. Suttle N. "NUTRIENTS, DIGESTION AND ABSORPTION | Absorption of Minerals and Vitamins," In: *Encyclopedia of Dairy Sciences*, ed. H. B. T.-E. of D. S. Roginski. Oxford: Elsevier p. 2127–2132. doi: 10.1016/B0-12-227235-8/00363-1
24. Flint HJ, Bayer EA. Plant Cell Wall Breakdown by Anaerobic Microorganisms from the Mammalian Digestive Tract. *Ann N Y Acad Sci.* (2008) 1125:280–8. doi: 10.1196/annals.1419.022
25. Flint HJ, Bayer EA, Rincon MT, Lamed R, White BA. Polysaccharide utilization by gut bacteria: potential for new insights from genomic analysis. *Nat Rev Microbiol.* (2008) 6:121–31. doi: 10.1038/nrmicro1817
26. Ozutsumi Y, Tajima K, Takenaka A, Itabashi H. The effect of protozoa on the composition of rumen bacteria in cattle using 16S rRNA gene clone libraries. *Biosci Biotechnol Biochem.* (2005) 69:499–506. doi: 10.1271/bbb.69.499
27. Mcallister Ta Rode LM, Major DJ Cheng K-J, Buchanan-Smith JG. Effect of ruminal microbial colonization on cereal grain digestion. *Can J Anim Sci.* (1990) 70:571–9. doi: 10.4141/cjas90-069
28. Kay RNB. Digestion of protein in the intestines of adult ruminants. *Proc Nutr Soc.* (1969) 28:140–51. doi: 10.1079/PNS19690025
29. Strom E, Øskov ER. The nutritive value of rumen micro-organisms in ruminants. *Br J Nutr.* (1984) 52:613–20. doi: 10.1079/BJN19840128
30. Russell JB, Muck RE, Weimer PJ. Quantitative analysis of cellulose degradation and growth of cellulolytic bacteria in the rumen. *FEMS Microbiol Ecol.* (2009) 67:183–97. doi: 10.1111/j.1574-6941.2008.00633.x
31. Weimer PJ, Russell JB, Muck RE. Lessons from the cow: What the ruminant animal can teach us about consolidated bioprocessing of cellulosic biomass. *Bioresour Technol.* (2009) 100:5323–31. doi: 10.1016/j.biortech.2009.04.075
32. Bi Y, Cox MS, Zhang F, Suen G, Zhang N, Tu Y, et al. Feeding modes shape the acquisition and structure of the initial gut microbiota in newborn lambs. *Environ Microbiol.* (2019) 21:2333–46. doi: 10.1111/1462-2920.14614
33. Jami E, Israel A, Kotser A, Mizrahi I. Exploring the bovine rumen bacterial community from birth to adulthood. *ISME J.* (2013) 7:1069–79. doi: 10.1038/ismej.2013.2
34. Malmuthuge N, Li M, Goonewardene LA, Oba M, Guan LL. Effect of calf starter feeding on gut microbial diversity and expression of genes involved in host immune responses and tight junctions in dairy calves during weaning transition. *J Dairy Sci.* (2013) 96:3189–200. doi: 10.3168/jds.2012-6200
35. Fonty G, Gouet P, Jouany J-P, Senaud J. Establishment of the microflora and anaerobic fungi in the rumen of lambs. *Microbiology.* (1987) 133:1835–43. doi: 10.1099/00221287-133-7-1835
36. Dill-McFarland KA, Breaker JD, Suen G. Microbial succession in the gastrointestinal tract of dairy cows from 2 weeks to first lactation. *Sci Rep.* (2017) 7:40864. doi: 10.1038/srep40864
37. Li F, Wang Z, Dong C, Li F, Wang W, Yuan Z, et al. Rumen bacteria communities and performances of fattening lambs with a lower or greater subacute ruminal acidosis risk. *Front Microbiol.* (2017) 8:1–10. doi: 10.3389/fmicb.2017.02506
38. Zhou M, Chen Y, Guan LL. "Rumen Bacteria," in *Rumen Microbiology: From Evolution to Revolution* (New Delhi: Springer India), 79–95. doi: 10.1007/978-81-322-2401-3_6
39. Brulc JM, Antonopoulos DA, Berg Miller ME, Wilson MK, Yannarell AC, Dinsdale EA, et al. Gene-centric metagenomics of the fiber-adherent bovine rumen microbiome reveals forage specific glycoside hydrolases. *Proc Natl Acad Sci.* (2009) 106:1948–53. doi: 10.1073/pnas.0806191105
40. Mizrahi I, Jami E. Review: The compositional variation of the rumen microbiome and its effect on host performance and methane emission. *Animal.* (2018) 12:s220–32. doi: 10.1017/S1751731118001957
41. Cai S, Li J, Hu FZ, Zhang K, Luo Y, Janto B, et al. Cellulosilyticum ruminicola, a newly described rumen bacterium that possesses redundant

fibrolytic-protein-encoding genes and degrades lignocellulose with multiple carbohydrate- borne fibrolytic enzymes. *Appl Environ Microbiol.* (2010) 76:3818–24. doi: 10.1128/AEM.03124-09

42. Kalmokoff ML, Teather RM. Isolation and characterization of a bacteriocin (Butyrivibriocin AR10) from the ruminal anaerobe Butyrivibrio fibrisolvens AR10: evidence in support of the widespread occurrence of bacteriocin-like activity among ruminal isolates of B. *fibrisolvens Appl Environ Microbiol.* (1997) 63:394–402. doi: 10.1128/aem.63.2.394-402.1997
43. Saluzzi L, Smith A, Stewart CS. Analysis of bacterial phospholipid markers and plant monosaccharides during forage degradation by Ruminococcus flavefaciens and Fibrobacter succinogenes in co-culture. *J Gen Microbiol.* (1993) 139:2865–73. doi: 10.1099/00221287-139-11-2865
44. Odenyo AA, Mackie RI, Stahl DA, White BA. The use of 16S rRNA-targeted oligonucleotide probes to study competition between ruminal fibrolytic bacteria: development of probes for Ruminococcus species and evidence for bacteriocin production. *Appl Environ Microbiol.* (1994) 60:3688–96. doi: 10.1128/aem.60.10.3688-3696.1994
45. Rychlik JL, Russell JB. Bacteriocin-like activity of Butyrivibrio fibrisolvens JL5 and its effect on other ruminal bacteria and ammonia production. *Appl Environ Microbiol.* (2002) 68:1040–6. doi: 10.1128/AEM.68.3.1040-1046.2002
46. Chen J, Stevenson DM, Weimer PJ, Albusin B. A bacteriocin from the ruminal bacterium ruminococcus albus 7 that inhibits growth of ruminococcus flavefaciens. *Appl Environ Microbiol.* (2004) 70:3167–70. doi: 10.1128/AEM.70.5.3167-3170.2004
47. Erickson DL, Nsereko VL, Morgavi DP, Selinger LB, Rode LM, Beauchemin KA. Evidence of quorum sensing in the rumen ecosystem: detection of N-acyl homoserine lactone autoinducers in ruminal contents. *Can J Microbiol.* (2002) 48:374–8. doi: 10.1139/w02-022
48. Mitsumori M, Xu L, Kajikawa H, Kurihara M, Tajima K, Hai J, et al. Possible quorum sensing in the rumen microbial community: detection of quorum-sensing signal molecules from rumen bacteria. *FEMS Microbiol Lett.* (2003) 219:47–52. doi: 10.1016/S0378-1097(02)01192-8
49. Callaway TR, Dowd SE, Edrington TS, Anderson RC, Krueger N, Bauer N, et al. Evaluation of bacterial diversity in the rumen and feces of cattle fed different levels of dried distillers grains plus solubles using bacterial tag-encoded FLX amplicon pyrosequencing1. *J Anim Sci.* (2010) 88:3977–83. doi: 10.2527/jas.2010-2900
50. Fernando SC, Purvis HT, Najar FZ, Sukharnikov LO, Krehbiel CR, Nagaraja TG, et al. Rumen microbial population dynamics during adaptation to a high-grain diet. *Appl Environ Microbiol.* (2010) 76:7482–90. doi: 10.1128/AEM.00388-10
51. Johns A. Isolation of a bacterium, producing propionic acid, from the rumen of sheep. *J Gen Microbiol.* (1951) 5:317–25. doi: 10.1099/00221287-5-2-317
52. Elsden SR, Volcani BE, Gilchrist FMC, Lewis D. Properties of a fatty acid forming organism isolated from the rumen of sheep. *J Bacteriol.* (1956) 72:681–689. doi: 10.1128/jb.72.5.681-689.1956
53. Muegge BD, Kuczynski J, Knights D, Clemente JC, Gonzalez A, Fontana L, et al. Diet drives convergence in gut microbiome functions across mammalian phylogeny and within humans. *Science (80-).* (2011) 332:970–4. doi: 10.1126/science.1198719
54. Stevenson DM, Weimer PJ. Dominance of prevotella and low abundance of classical ruminal bacterial species in the bovine rumen revealed by relative quantification real-time PCR. *Appl Microbiol Biotechnol.* (2007) 75:165–74. doi: 10.1007/s00253-006-0802-y
55. Jeyanathan J, Kirs M, Ronimus RS, Hoskin SO, Janssen PH. Methanogen community structure in the rumens of farmed sheep, cattle and red deer fed different diets. *FEMS Microbiol Ecol.* (2011) 76:311–26. doi: 10.1111/j.1574-6941.2011.01056.x
56. Pfister P, Wasserfallen A, Stettler R, Leisinger T. Molecular analysis of Methanobacterium phage ΨM2. *Mol Microbiol.* (1998) 30:233–44. doi: 10.1046/j.1365-2958.1998.01073.x
57. Luo Y, Pfister P, Leisinger T, Wasserfallen A. The genome of archaeal prophage ΨM100 encodes the lytic enzyme responsible for autolysis ofmethanothermobacter wolfeii. *J Bacteriol.* (2001) 183:5788–92. doi: 10.1128/JB.183.19.5788-5792.2001
58. Kamra DN. Rumen microbial ecosystem. *Curr Sci.* (2005) 89:124–135. Available at: http://www.jstor.org/stable/24110438
59. Wright A-DG, Klieve A V. Does the complexity of the rumen microbial ecology preclude methane mitigation? *Anim Feed Sci Technol.* (2011) 166–167:248–253. doi: 10.1016/j.anifeedsci.2011.04.015
60. Kumar S, Choudhury PK, Carro MD, Griffith GW, Dagar SS, Puniya M, et al. New aspects and strategies for methane mitigation from ruminants. *Appl Microbiol Biotechnol.* (2014) 98:31–44. doi: 10.1007/s00253-013-5365-0
61. Fuentes MC, Calsamiglia S, Cardozo PW, Vlaeminck B. Effect of pH and level of concentrate in the diet on the production of biohydrogenation intermediates in a dual-flow continuous culture. *J Dairy Sci.* (2009) 92:4456–66. doi: 10.3168/jds.2008-1722
62. Duskova D, Marounek M. Fermentation of pectin and glucose, and activity of pectin-degrading enzymes in the rumen bacterium Lachnospira multiparus. *Lett Appl Microbiol.* (2001) 33:159–63. doi: 10.1046/j.1472-765x.2001.00970.x
63. Sales-Duval M, Lucas F, Blanchart G. Effects of exogenous ammonia or free amino acids on proteolytic activity and protein breakdown products in streptococcus bovis, prevotella albensis, and butyrivibrio fibrisolvens. *Curr Microbiol.* (2002) 44:435–43. doi: 10.1007/s00284-001-0013-9
64. Cotta MA, Hespell RB. Proteolytic activity of the ruminal bacterium Butyrivibrio fibrisolvens. *Appl Environ Microbiol.* (1986) 52:51–8. doi: 10.1128/aem.52.1.51-58.1986
65. Yanagita K, Kamagata Y, Kawaharasaki M, Suzuki T, Nakamura Y, Minato H. Phylogenetic Analysis of Methanogens in Sheep Rumen Ecosystem and Detection of Methanomicrobium mobile by Fluorescence In Situ Hybridization. *Biosci Biotechnol Biochem.* (2000) 64:1737–42. doi: 10.1271/bbb.64.1737
66. Hook SE, Wright A-DG, McBride BW. Methanogens: methane producers of the rumen and mitigation strategies. *Archaea.* (2010) 2010:1–11. doi: 10.1155/2010/945785
67. Coleman GS. The metabolism of free amino acids by washed suspensions of the rumen ciliate entodinium caudatum. *J Gen Microbiol.* (1967) 47:433–47. doi: 10.1099/00221287-47-3-433
68. Moniello G, Richardson AJ, Duncan SH, Stewart CS. Effects of coumarin and sparteine on attachment to cellulose and cellulolysis by Neocallimastix frontalis RE1. *Appl Environ Microbiol.* (1996) 62:4666–8. doi: 10.1128/aem.62.12.4666-4668.1996
69. Hodrová B, Kopečný J, Petr O. Interaction of the rumen fungus Orpinomyces joyonii with Megasphaera elsdenii and Eubacterium limosum. *Lett Appl Microbiol.* (1995) 21:34–7. doi: 10.1111/j.1472-765X.1995.tb01001.x
70. Dashtban M, Schraft H, Qin W. Fungal bioconversion of lignocellulosic residues; opportunities & perspectives. *Int J Biol Sci.* (2009) 5:578–95. doi: 10.7150/ijbs.5.578
71. Gorris LG, van der Drift C. Cofactor contents of methanogenic bacteria reviewed. *Biofactors.* (1994) 4:139–45. Available at: http://www.ncbi.nlm.nih.gov/pubmed/79\penalty-\@M16957
72. Thauer RK, Kaster A-K, Seedorf H, Buckel W, Hedderich R. Methanogenic archaea: ecologically relevant differences in energy conservation. *Nat Rev Microbiol.* (2008) 6:579–91. doi: 10.1038/nrmicro1931
73. Hungate RE, Smith W, Bauchop T, Yu I, Rabinowitz JC. Formate as an intermediate in the bovine rumen fermentation. *J Bacteriol.* (1970) 102:389–97. doi: 10.1128/jb.102.2.389-397.1970
74. Stams AJM, Plugge CM. Electron transfer in syntrophic communities of anaerobic bacteria and archaea. *Nat Rev Microbiol.* (2009) 7:568–77. doi: 10.1038/nrmicro2166
75. Latham MJ, Wolin MJ. Fermentation of cellulose by Ruminococcus flavefaciens in the presence and absence of Methanobacterium ruminantium. *Appl Environ Microbiol.* (1977) 34:297–301. doi: 10.1128/aem.34.3.297-301.1977
76. Pavlostathis SG, Miller TL, Wolin MJ. Kinetics of insoluble cellulose fermentation by continuous cultures of Ruminococcus albus. *Appl Environ Microbiol.* (1988) 54:2660–3. doi: 10.1128/aem.54.11.2660-2663.1988
77. Vogels GD, Hoppe WF, Stumm CK. Association of methanogenic bacteria with rumen ciliates. *Appl Environ Microbiol.* (1980) 40:608–12. doi: 10.1128/aem.40.3.608-612.1980

78. Krumholz LR, Forsberg CW, Veira DM. Association of methanogenic bacteria with rumen protozoa. *Can J Microbiol.* (1983) 29:676–80. doi: 10.1139/m83-110
79. Tóthová T, Piknová M, Kišidayová S, Javorský P, Pristaš P. Distinctive archaebacterial species associated with anaerobic rumen protozoan Entodinium caudatum. *Folia Microbiol (Praha).* (2008) 53:259–62. doi: 10.1007/s12223-008-0039-5
80. Joblin KN, Naylor GE, Williams AG. Effect of methanobrevibacter smithii on xylanolytic activity of anaerobic ruminal fungi. *Appl Environ Microbiol.* (1990) 56:2287–95. doi: 10.1128/aem.56.8.2287-2295.1990
81. Marvin-Sikkema FD, Richardson AJ, Stewart CS, Gottschal JC, Prins RA. Influence of hydrogen-consuming bacteria on cellulose degradation by anaerobic fungi. *Appl Environ Microbiol.* (1990) 56:3793–3797. doi: 10.1128/aem.56.12.3793-3797.1990
82. Teunissen MJ, Kets EPW, Op den. Camp HJM, Huis in't Veld JHJ, Vogels GD. Effect of coculture of anaerobic fungi isolated from ruminants and non-ruminants with methanogenic bacteria on cellulolytic and xylanolytic enzyme activities. *Arch Microbiol.* (1992) 157:176–82. doi: 10.1007/BF00245287
83. Keiji Ogimoto SI. Atlas of Rumen Microbiology. *Q Rev Biol.* (1983) 58:92–92. doi: 10.1086/413111
84. Dehority BA. Effects of microbial synergism on fibre digestion in the rumen. *Proc Nutr Soc.* (1991) 50:149–59. doi: 10.1079/PNS19910026
85. Stewart CS, Duncan SH, Richardson AJ, Backwell C, Begbie R. The inhibition of fungal cellulolysis by cell-free preparations from ruminococci. *FEMS Microbiol Lett.* (1992) 97:83–7. doi: 10.1111/j.1574-6968.1992.tb05444.x
86. Ricard G, McEwan NR, Dutilh BE, Jouany J-P, Macheboeuf D, Mitsumori M, et al. Horizontal gene transfer from Bacteria to rumen Ciliates indicates adaptation to their anaerobic, carbohydrates-rich environment. *BMC Genomics.* (2006) 7:22. doi: 10.1186/1471-2164-7-22
87. Gutierrez J. Observations on Bacterial Feeding by the Rumen Ciliate Isotricha prostoma. *J Protozool.* (1958) 5:122–6. doi: 10.1111/j.1550-7408.1958.tb02538.x
88. Gutierrez J, Davis RE. Bacterial ingestion by the rumen ciliates entodinium and diplodinium. *J Protozool.* (1959) 6:222–6. doi: 10.1111/j.1550-7408.1959.tb04361.x
89. Mah RA. Factors influencing the in vitro culture of the rumen ciliate ophryoscolex purkynei stein. *J Protozool.* (1964) 11:546–52. doi: 10.1111/j.1550-7408.1964.tb01796.x
90. Newbold CJ, Lassalas B, Jouany JP. The importance of methanogens associated with ciliate protozoa in ruminal methane production in vitro. *Lett Appl Microbiol.* (1995) 21:230–4. doi: 10.1111/j.1472-765X.1995.tb01048.x
91. Ranilla MJ, Jouany J-P, Morgavi DP. Methane production and substrate degradation by rumen microbial communities containing single protozoal species in vitro. *Lett Appl Microbiol.* (2007) 45:675–80. doi: 10.1111/j.1472-765X.2007.02251.x
92. Sirohi SK, Choudhury PK, Dagar SS, Puniya AK, Singh D. Isolation, characterization and fibre degradation potential of anaerobic rumen fungi from cattle. *Ann Microbiol.* (2013) 63:1187–94. doi: 10.1007/s13213-012-0577-6
93. Sirohi SK, Singh N, Dagar SS, Puniya AK. Molecular tools for deciphering the microbial community structure and diversity in rumen ecosystem. *Appl Microbiol Biotechnol.* (2012) 95:1135–54. doi: 10.1007/s00253-012-4262-2
94. Sirohi SK, Chaudhary PP, Singh N, Singh D, Puniya AK. The 16S rRNA and mcrA gene based comparative diversity of methanogens in cattle fed on high fibre based diet. *Gene.* (2013) 523:161–6. doi: 10.1016/j.gene.2013.04.002
95. Dehority BA, Tirabasso PA. Antibiosis between Ruminal Bacteria and Ruminal Fungi. *Appl Environ Microbiol.* (2000) 66:2921–7. doi: 10.1128/AEM.66.7.2921-2927.2000
96. Bernalier A, Fonty G, Bonnemoy F, Gouet P. Inhibition of the cellulolytic activity of Neocallimastix frontalis by Ruminococcus flavefaciens. *J Gen Microbiol.* (1993) 139:873–80. doi: 10.1099/00221287-139-4-873
97. Klieve A V, Heck GL, Prance MA, Shu Q. Genetic homogeneity and phage susceptibility of ruminal strains of Streptococcus bovis isolated in Australia. *Lett Appl Microbiol.* (1999) 29:108–12. doi: 10.1046/j.1365-2672.1999.00596.x
98. McAllister TA, Newbold CJ. Redirecting rumen fermentation to reduce methanogenesis. *Aust J Exp Agric.* (2008) 48:7. doi: 10.1071/EA07218
99. Shenkoru T, Faciola A, Schultz B. Perryman B. Frothy Bloat (Primary Ruminal Tympany) Potential and Nutrient Content of Forage Kochia (Bassia prostrata L). J Arid Land Studies. (2015) 180:177–80.
100. Kaba T, Abera B, Kassa T. Esophageal groove dysfunction: a cause of ruminal bloat in newborn calves. *BMC Vet Res.* (2018) 14:276. doi: 10.1186/s12917-018-1573-2
101. Clarke RTJ, Reid CSW. Foamy Bloat of Cattle. *A Review J Dairy Sci.* (1974) 57:753–85. doi: 10.3168/jds.S0022-0302(74)84964-7
102. Priyanka M, Dey S. Ruminal impaction due to plastic materials - An increasing threat to ruminants and its impact on human health in developing countries. *Vet World.* (2018) 11:1307–15. doi: 10.14202/vetworld.2018.1307-1315
103. Rahman MM, Bhuiyan MMU, Islam MT, Shamsuddin M. Efficacy of simethicone for treatment of bloat in ruminants. *Asian J Med Biol Res.* (2017) 2:635–8. doi: 10.3329/ajmbr.v2i4.31008
104. Dougherty RW. Bloat in Ruminants. *Nutr Rev.* (2009) 16:300–1. doi: 10.1111/j.1753-4887.1958.tb00631.x
105. Hernández J, Benedito JL, Abuelo A, Castillo C. Ruminal acidosis in feedlot: from aetiology to prevention. *Sci World J.* (2014) 2014:702572. doi: 10.1155/2014/702572
106. Nagaraja TG, Titgemeyer EC. Ruminal acidosis in beef cattle: the current microbiological and nutritional outlook. *J Dairy Sci.* (2007) 90:E17–38. doi: 10.3168/jds.2006-478
107. Abdela N. Sub-acute Ruminal Acidosis (SARA) and its consequence in dairy cattle: a review of past and recent research at global prospective. *Achiev Life Sci.* (2016) 10:187–96. doi: 10.1016/j.als.2016.11.006
108. Jaramillo-López E, Itza-Ortiz MF, Peraza-Mercado G, Carrera-Chávez JM. Ruminal acidosis: strategies for its control. *Austral J Vet Sci.* (2017) 49:139–48. doi: 10.4067/S0719-81322017000300139
109. Krause KM, Oetzel GR. Inducing subacute ruminal acidosis in lactating dairy cows. *J Dairy Sci.* (2005) 88:3633–9. doi: 10.3168/jds.S0022-0302(05)73048-4
110. Plaizier JC, Krause DO, Gozho GN, McBride BW. Subacute ruminal acidosis in dairy cows: The physiological causes, incidence and consequences. *Vet J.* (2008) 176:21–31. doi: 10.1016/j.tvjl.2007.12.016
111. Kleen JL, Hooijer GA, Rehage J, Noordhuizen JPTM. Subacute ruminal acidosis (sara): a review. *J Vet Med Ser A.* (2003) 50:406–14. doi: 10.1046/j.1439-0442.2003.00569.x
112. Klein KA, Clark C, Allen AL. Hypoglycemia in sick and moribund farmed elk calves. *Can Vet J = La Rev Vet Can.* (2002) 43:778–781. Available at: https://pubmed.ncbi.nlm.nih.gov/123\penalty-\@M95760
113. Kronfeld DS. Hypoglycemia in ketotic cows. *J Dairy Sci.* (1971) 54:949–61. doi: 10.3168/jds.S0022-0302(71)85951-9
114. Trefz FM, Lorenz I, Lorch A, Constable PD. Clinical signs, profound acidemia, hypoglycemia, and hypernatremia are predictive of mortality in 1,400 critically ill neonatal calves with diarrhea. *PLoS ONE.* (2017) 12:1–27. doi: 10.1371/journal.pone.0182938
115. Qaid MM, Abdelrahman MM. Role of insulin and other related hormones in energy metabolism: A review. *Cogent Food Agric.* (2016) 2. doi: 10.1080/23311932.2016.1267691
116. Aschenbach JR, Kristensen NB, Donkin SS, Hammon HM, Penner GB. Gluconeogenesis in dairy cows: The secret of making sweet milk from sour dough. *IUBMB Life.* (2010) 62:869–77. doi: 10.1002/iub.400
117. Wu G. "Management of metabolic disorders (including metabolic diseases) in ruminant and nonruminant animals," in *Animal Agriculture* (Elsevier), 471–491.
118. Yuan L, Hensley C, Mahsoub HM, Ramesh AK, Zhou P. *Microbiota in viral infection and disease in humans and farm animals. 1st ed Elsevier Inc.* (2020). doi: 10.1016/bs.pmbts.2020.04.005
119. Sanz-Fernandez MV, Daniel J-B, Seymour DJ, Kvidera SK, Bester Z, Doelman J, et al. Targeting the Hindgut to Improve Health and Performance in Cattle. *Animals.* (2020) 10:1817. doi: 10.3390/ani10101817
120. Peek SF, Mcguirk SM, Sweeney RW, Cummings KJ. "6 - Infectious Diseases of the Gastrointestinal Tract," in, eds. S. F. Peek, T. J. B. T.-R. D. of D. C. Third E. Divers. Elsevier. p 249–356. doi: 10.1016/B978-0-323-39055-2.00006-1

121. Belknap EB, Navarre CB. Differentiation of gastrointestinal diseases in adult cattle. *Vet Clin North Am Food Anim Pract.* (2000) 16:59–86. doi: 10.1016/S0749-0720(15)30137-7
122. Fecteau M-E, Whitlock RH. "Abomasal Ulcers," in *Food Animal Practice*, eds. D. E. Anderson, D. M. B. T.-F. A. P. Fifth E. Rings. Saint Louis: Elsevier. p. 29–34. doi: 10.1016/B978-141603591-6.10010-7
123. El-Ashker M, Salama M, El-Boshy M. Traumatic reticuloperitonitis in water buffalo (*Bubalus bubalis*): clinical findings and the associated inflammatory response. *J Vet Med.* (2013) 2013:808656. doi: 10.1155/2013/808656
124. Braun U, Gerspach C, Ohlerth S, Warislohner S, Nuss K. Aetiology, diagnosis, treatment and outcome of traumatic reticuloperitonitis in cattle. *Vet J.* (2020) 255:105424. doi: 10.1016/j.tvjl.2020.105424
125. Braun U, Warislohner S, Gerspach C, Ohlerth S, Nuss K. Treatment of 503 cattle with traumatic reticuloperitonitis. *Acta Vet Scand.* (2018) 60:55. doi: 10.1186/s13028-018-0410-8
126. Bhattacharjya R, Chatterjee A, Pandey T. Diarrhoeain ruminantsand its control. A Review. *IOSR J Agric Vet Sci.* (2018) 11:19–22.
127. Mulder IE, Schmidt B, Lewis M, Delday M, Stokes CR, Bailey M, et al. Restricting microbial exposure in early life negates the immune benefits associated with gut colonization in environments of high microbial diversity. *PLoS ONE.* (2011) 6:e28279. doi: 10.1371/journal.pone.0028279
128. Li RW, Connor EE Li C, Baldwin VI RL, Sparks ME. Characterization of the rumen microbiota of pre-ruminant calves using metagenomic tools. *Environ Microbiol.* (2012) 14:129–39. doi: 10.1111/j.1462-2920.2011.02543.x
129. Li F, Hitch TCA, Chen Y, Creevey CJ, Guan LL. Comparative metagenomic and metatranscriptomic analyses reveal the breed effect on the rumen microbiome and its associations with feed efficiency in beef cattle 06 Biological Sciences 0604 Genetics 06 Biological Sciences 0605 Microbiology. *Microbiome.* (2019) 7:1–21. doi: 10.1186/s40168-019-0618-5
130. Bi Y, Tu Y, Zhang N, Wang S, Zhang F, Suen G, Shao D, Li S, Diao Q. Multiomics analysis reveals the presence of a microbiome in the gut of fetal lambs. *Gut* (2020) 70:853–64. doi: 10.1136/gutjnl-2020-320951

Conflict of Interest: The authors declare that the research was conducted in the absence of any commercial or financial relationships that could be construed as a potential conflict of interest.

Publisher's Note: All claims expressed in this article are solely those of the authors and do not necessarily represent those of their affiliated organizations, or those of the publisher, the editors and the reviewers. Any product that may be evaluated in this article, or claim that may be made by its manufacturer, is not guaranteed or endorsed by the publisher.

frontiers in Nutrition

ORIGINAL RESEARCH
published: 09 August 2021
doi: 10.3389/fnut.2021.716723

Dietary Inulin Regulated Gut Microbiota and Improved Neonatal Health in a Pregnant Sow Model

*Hao Li†, Longteng Ma†, Longlin Zhang, Nian Liu, Zhiqing Li, Fan Zhang, Xiang Liu and Xiaokang Ma**

College of Animal Science and Technology, Hunan Agricultural University, Changsha, China

This study aimed to investigate the relationship between maternal dietary fiber intake and piglet health. Multiparous sows were randomly assigned to two groups and fed diets without inulin (control group, $n = 20$) or 1.6% inulin (1.6IN group, $n = 20$). The results indicate that 1.6IN prevented the prolonged farrowing duration of sows ($P < 0.05$) and shortened the average piglet birth interval ($P < 0.1$). In addition, 1.6IN decreased the percentage of the piglet born weak and the percentage of the piglet with hyperthermia after birth ($P < 0.01$). Compared with the control group, the 1.6IN group had a lower concentration of urea nitrogen in the colostrum, and also prevented diarrhea, increased litter gain, survival rate, and average daily gain for suckling piglets ($P < 0.05$). Furthermore, 1.6IN decreased the relative abundance of Firmicutes, *Cyanobacteria*, and *Streptococcus*; increased the relative abundance of Bacteroidetes, *Desulfovibrio*, *Paludibacter*, *CF231*, and *Prevotella*. Overall, this study showed that maternal fiber nutrition during pregnancy regulated the health of offspring, and the response of the maternal intestinal microbes played an important role in intervening in the phenotype of sows and neonatal piglets.

Keywords: inulin, sow, piglet, health, gut microbiota

OPEN ACCESS

Edited by:
Hui Han, Chinese Academy of Sciences (CAS), China

Reviewed by:
Tongxing Song, Huazhong Agricultural University, China
Yehui Duan, Institute of Subtropical Agriculture, Chinese Academy of Sciences, China

***Correspondence:**
Xiaokang Ma
maxiaokang@hunau.edu.cn

†These authors have contributed equally to this work

Specialty section:
This article was submitted to Nutrition and Microbes, a section of the journal Frontiers in Nutrition

Received: *29 May 2021*
Accepted: *29 June 2021*
Published: *09 August 2021*

Citation:
Li H, Ma L, Zhang L, Liu N, Li Z, Zhang F, Liu X and Ma X (2021) Dietary Inulin Regulated Gut Microbiota and Improved Neonatal Health in a Pregnant Sow Model. Front. Nutr. 8:716723. doi: 10.3389/fnut.2021.716723

INTRODUCTION

In the intensive pig industry, sows suffered from both endogenous oxidative stress and exogenous stress induced by environmental and management factors, which led to serious adverse reactions on their offspring, such as prolonged birth intervals, low birth weight, and diarrhea (1). These adverse reactions dramatically increased the risk of non-infectious death in neonatal piglets (2). Fortunately, intestinal microbiota has become an important window for regulating the health of sows and their neonatal piglets because of its close relationship with immunity, metabolism, nutrient digestion, and hormones (3–5).

Feeding functional dietary fiber during pregnancy, especially soluble dietary fiber (SDF), has become a key nutritional strategy for improving reproductive performance in sows, based on its significant regulatory effect on intestinal microbiota (1, 6). As a typical SDF, inulin-type fructans are a mixture of polymers and oligomers, which are composed of fructosyl units linked by β (2 → 1) glycosidic bonds (7). In previous studies, inulin has been proven to increase the abundance of probiotics, such as *Bifidobacterium* and *Lactobacillus,* in the intestine in human or mouse experiments (8–10). Zhou et al. (11) confirmed that inulin inhibited the weight gain of pregnant sows caused by high-fat diets and improved the BMI distribution of newborn piglets (11). The previous study also confirmed that sows fed with inulin increased birth weight and pre-weaning survival for piglets (12); however, it is still necessary to understand the relationship between maternal dietary fiber intake and piglet health.

Therefore, this study aimed to investigate the relationship between maternal dietary fiber intake during late pregnancy and piglet health. Phenotypes of sows and piglets, as well as serum markers and intestinal flora of sows, were analyzed to provide some microbial mechanistic insights into the application of inulin to a typical gestation diet of sows for improving neonatal health and performance.

TABLE 1 | Feedstuff ingredients and nutrient composition of experimental diets.

Items	Control	1.6IN	Lactation diet
Ingredients, %			
Corn	56.00	56.00	65.00
Soybean meal	8.00	8.00	20.00
Fermented soybean meal	5.00	5.00	5.00
Soybean oil	1.00	1.00	2.00
DDGS[a]	2.00	2.00	0.00
Soybean hull	16.00	15.20	0.00
Rice bran	8.00	7.20	3.60
Inulin[b]	0.00	1.60	0.00
Salt	0.45	0.45	0.50
L-Lys	0.00	0.00	0.20
D-Met	0.00	0.00	0.10
Dicalcium phosphate	1.18	1.18	1.20
Calcium carbonate	1.37	1.37	1.40
Mineral-vitamin pre-mix[c]	1.00	1.00	1.00
Total	100.00	100.00	100.00
Nutrient composition			
ME of DM, MJ/kg	11.97	11.93	12.94
Crude protein, %	13.98	13.95	17.23
Crude fiber, %	8.18	8.09	2.63
Calcium, %	0.92	0.92	0.88
Phosphorus, %	0.54	0.51	0.58
Total dietary fiber, %	26.61	27.51	16.46

[a] *DDGS, distillers dried grains with soluble.*
[b] *Inulin contains 94% DM, 89.8% inulin, 3.2% monosaccharide, <0.2% crude protein and ash, average monomeric units = 13.*
[c] *Provided per kg of diet: Cu, 10 mg (as $CuSO_4 \cdot 5H_2O$); Fe, 110 mg as ferrous sulfate; Mn, 35 mg (as MnO_2); Zn, 65 mg as zinc sulfate; I, 0.6 mg as potassium iodide; Se, 0.3 mg as selenium selenite; vitamin A, 7,200 IU; vitamin D3, 1,500 IU; vitamin E, 30 mg; vitamin K, 1.2 mg; 1 mg, thiamin; 2 mg, riboflavin; 1 mg, pyridoxine; and 0.015 mg, cobalamin.*

MATERIALS AND METHODS

Ethics Statement

The protocol of this study was approved by the Institutional Animal Care and Use Committee of College of Animal Science and Technology, Hunan Agricultural University (Changsha, China) and was conducted in accordance with the National Institutes of Health (Changsha, China) guidelines for the care and use of experimental animals (No. 43321809). The inulin was provided by Sensus (RG Roosendaal, The Netherlands) with 90% purity.

Experimental Animals, Diets, and Sample Collection

A total of 40 Landrace × Yorkshire second parity sows were selected for this experiment. All the sows were fed with the same standard diet from mating to gestation d80. Then, they were allocated to one of two treatments randomly as a single factorial experimental design after balancing their backfat thickness and body weight. The sows were fed with two different diets: a basic diet based on corn and soybean meal (control group, $n = 20$), and a diet that included 1.6% inulin (1.6IN group, $n = 20$). During gestation from d80 to d109, the sows in each group were fed a daily ration of 3.3 kg dry matter (DM) with their respective diets containing 11.94 ± 0.03 MJ ME/kg. Then, the sows were moved from the gestation pens to the farrowing rooms on day 109 ± 1 of gestation and kept in individual stalls (2.2 × 0.75 m). The sows were offered 3 kg DM of the same lactation diet containing 13.7 MJ ME/kg DM (**Table 1**) and were fed two times a day before farrowing. From the 1st day postpartum until weaning, the sows of both treatments were fed *ad libitum* with the same standard lactation diet (**Table 1**). All the sows had free access to water during the whole experimental period. The experimental design of this study was shown in **Figure 1**.

Colostrum samples (30 ml) were collected from the third, fourth, and fifth pairs of mammary glands of sows (eight sows per diet group) on the farrowing day. Then, the colostrum samples were immediately frozen at −20°C until further analysis. Fresh fecal samples were collected from the sows (eight sows per group) on day 109 ± 1 of gestation and day 18 of lactation. Then, the fecal samples were stored at −80°C until further analysis.

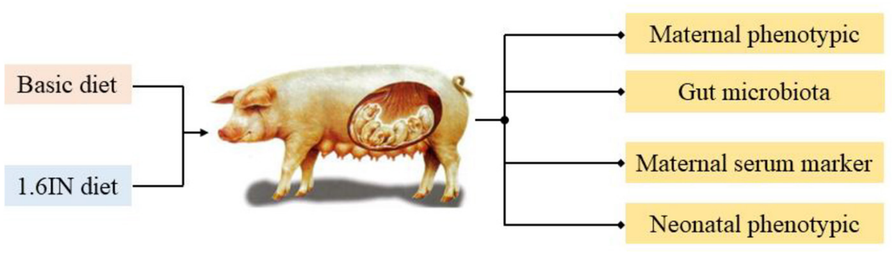

FIGURE 1 | Experimental design of this study.

Performance Measurement

The birth time of each piglet was recorded, which was used to calculate farrowing duration and average piglet birth interval (APBI). After farrowing, the rectal temperature of each piglet was recorded with a digital thermometer (Xiaomi Co. Ltd, Beijing, China, with a display resolution of 0.01 and ± 0.1°C accuracy) and weighed before suckling. Piglets weighing <800 g were recorded as born intrauterine growth retardation (IUGR); otherwise, they were regarded as born effective.

Cross-fostering was kept within diet treatments to adjust litter size to about 12.86 ± 1.2 piglets per sow and average body weight to about 1.8 ± 0.7 kg per litter within 48 h after parturition. During lactation, mortality of each piglet was recorded, and the occurrence of diarrhea was visually assessed and evaluated by individual scoring of the consistency of the feces from 9.00 a.m. to 4.00 p.m. each day by trained observers blind to the treatments according to the method of Marquardt et al. (13). The diarrhea rate (%) was calculated as [(the total number of piglets with diarrhea within a treatment)/(total number of

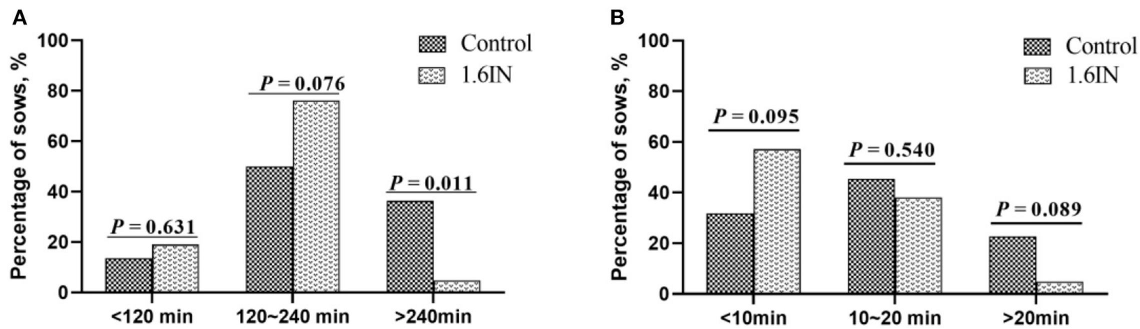

FIGURE 2 | Distribution of **(A)** farrowing duration and **(B)** average piglet birth interval of sows. $N = 20$ for the control group and 1.6IN group. Significance was analyzed by chi-squared test.

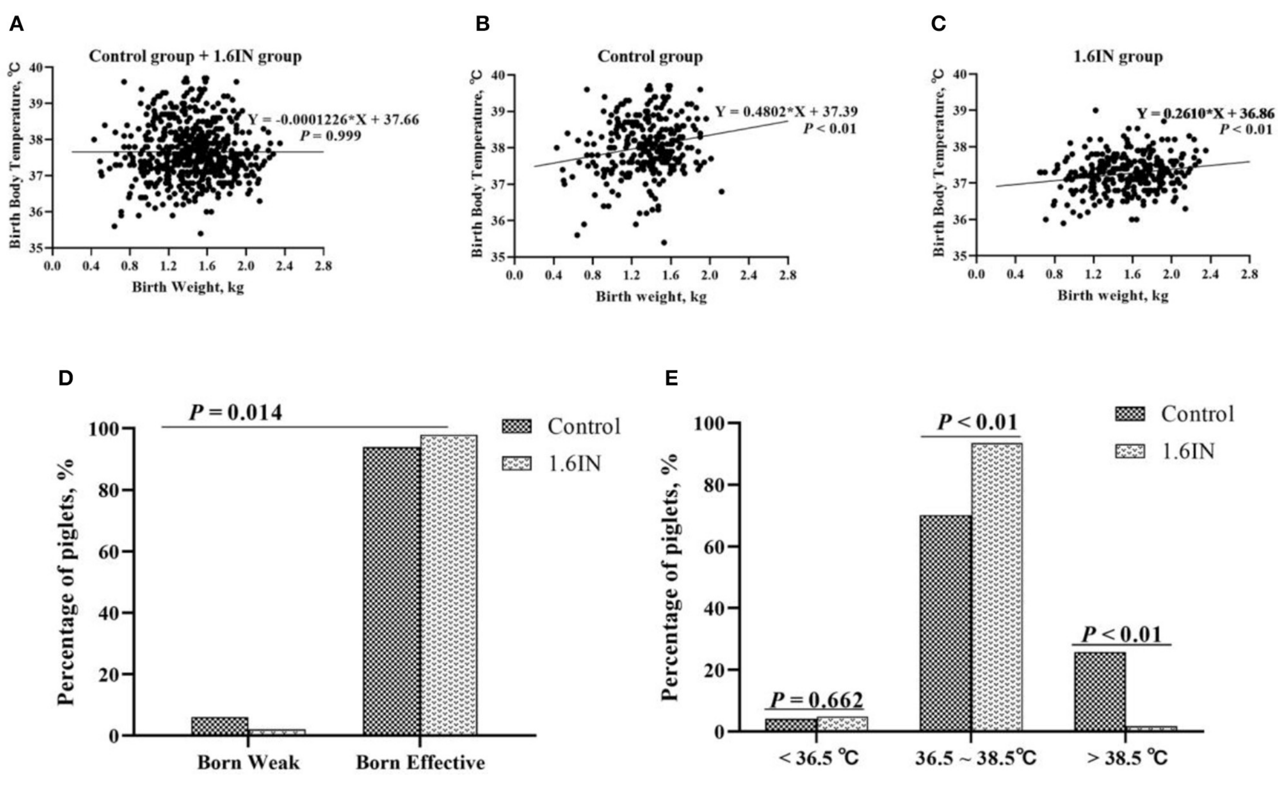

FIGURE 3 | (A–C) Relationship between birth weight and birth body temperature of piglets and **(D,E)** effects of dietary inulin on the birth weight and birth body temperature of newborn piglets. $N = 295$ and 291 for the control group and 1.6IN group, respectively. A Chi-square test was conducted to judge whether **(D)** low birth weight improved or **(E)** distribution of birth body temperature of newborn piglets changed.

experimental piglets × total observational days)] × 100. At weaning (lactation d18), the number of piglets was recorded to calculate the weaning survival rate, and the litter weight was also recorded to calculate the litter gain and the average daily gain (ADG).

Analysis of Colostrum Composition

The colostrum samples of sows in each group were separately analyzed for the concentrations of fat, protein, lactose, urea nitrogen (UN), and total DM using Milko-Scan FT 120 (Foss Electric, Hillerford, Denmark). Somatic cell count (SCC) was measured using FOSS MATIC 5000 (Foss Analytical A/S, Hillerod, Denmark).

DNA Extraction, PCR Amplification, Library Preparation, and Sequencing

DNA was extracted from fecal samples of sows using a Stool DNA Isolation Kit (Tiangen Biotech Co., Ltd., Beijing, China). The V4 hypervariable region of the bacterial 16S rRNA gene was amplified by PCR, where the forward primer was 550F: 5′-GTGCCAGCMGCCGCGGTAA-3′ and the reverse primer was 806R: 5′-GGACTACHVGGGTWTCTAAT-3′. For each fecal sample, a 10-digit barcode sequence was added to the 5′ end of the forward and reverse primers. The sequences were clustered into operational taxonomic units (OTUs) at a similarity level of 97% to generate rarefaction curves and to calculate the richness and diversity indices. OTUs representing <0.005% of the population were removed, and taxonomy was assigned using the Ribosomal Database Project (RDP) classifier. The relative abundance of each OTU was counted at different taxonomic levels. OTU-level alpha diversity indices were calculated using the OTU table in QIIME. β-diversity was assessed by principal component analysis (PCoA) based on the Bray–Curtis distance. Bioinformatics analysis was mainly performed using QIIME (v1.7.0) and R packages (v3.2.0).

Analysis of Fecal Short-Chain Fatty Acids

The concentration of SCFAs in feces was analyzed using a gas chromatographic method, as described by Bosch et al. (14). Briefly, approximately 1.5 g of feces was first homogenized in 1.5 ml of deionized water. The samples were centrifuged at 15,000 × g at 4°C for 10 min. Supernatants (1 ml each) were then acidified with 25% metaphosphoric acid at a 1:5 ratio (1 volume of acid for 5 volumes of the sample) for 30 min on ice. The sample was injected into a GC 2010 series gas chromatograph (Shimadzu, Kyoto, Japan) equipped with a CP-Wax 52 CB column 30 m × 0.53 mm i.d. (Chrompack, Rotterdam, Netherlands). The injector and detector temperatures were 75 and 280°C, respectively. Total SCFAs were determined as the sum of analyzed acetate, propionate, and butyrate. All procedures were performed in triplicate.

Analysis of Serum Marker in Sows

Venous blood from the ear margin of the sow on the day of parturition was used to separate serum. Serum markers, such as malondialdehyde (MDA), total antioxidant capacity (TAOC), superoxide dismutase (SOD), glutathione peroxidase (GSH-Px), lipopolysaccharide (LPS), and lactate were determined using commercial kits by following the instructions of the manufacturer (Nanjing Jiancheng Co. Ltd., Nanjing, China).

Statistical Analysis

Litter gain, survival rate, piglet ADG, diarrhea rate, serum marker, SCFA composition, α-diversities index, and relative abundance were tested for normality and were then analyzed by an unpaired t-test (SPSS 21.0, IBM, Armonk, NY, United States), using each sow as an experimental unit. Data were presented as means ± SEM except that confidence limits were given in brackets instead of SEM values for data of relative abundance at phylum. A chi-square test was performed to analyze the percentage of sows that had a prolonged farrowing duration or prolonged average piglet birth interval and to analyze the percentage of piglets born weak or with hyperthermia after birth. Statistical significance was declared when $P < 0.05$.

RESULTS

Farrowing Duration of Sows and Average Piglet Birth Interval

The results of dietary inulin on farrowing duration and APBI are shown in **Figure 2**. Compared to the control group, 1.6IN

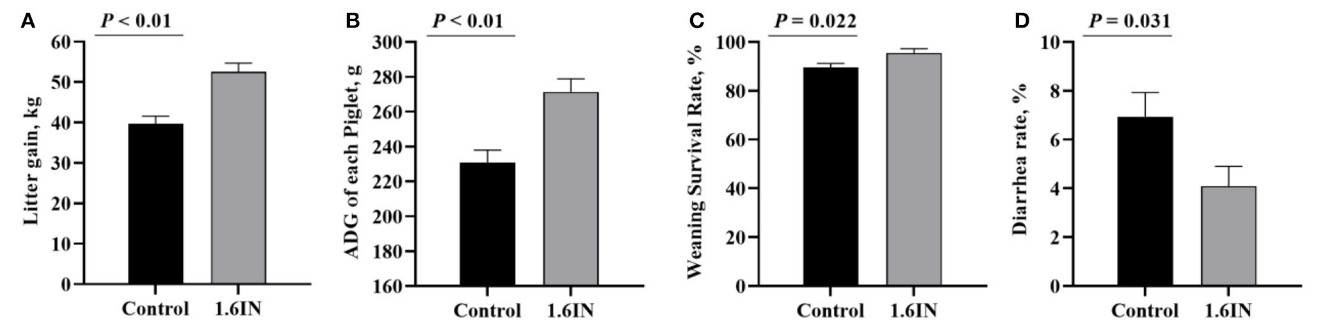

FIGURE 4 | Effects of dietary inulin on the piglet performance during lactation. **(A)** litter gain at weaning; **(B)** average daily gain (ADG) of each piglet; **(C)** survival rate at weaning; **(D)** diarrhea rate during lactation. Significance was analyzed by an unpaired t-test.

decreased the percentage of sows whose farrowing duration was longer than 240 min ($P = 0.011$) and trend to decreased percentage of sows whose APBI was longer than 20 min ($P = 0.089$). In addition, 1.6IN also increased the percentage of sows whose APBI was shorter than 10 min on a trend ($P = 0.095$).

Performance of the Piglet

As shown in **Figure 3**, the birth weight and birth body temperature of a total of 586 piglets from two groups were recorded. When the two groups were analyzed together, there was no significant relationship between the body temperature and weight of newborn piglets; however, when the two groups were analyzed separately, there was a significant linear relationship between piglet body temperature and weight. The control group has a higher slope and intercept, which suggests that the piglets of the control group may have a higher average body temperature, which is more pronounced in high birth weight piglets. In addition, it could be observed that the birth body temperature of piglets was mainly enriched at 36.5–38.5°C. Therefore, piglets with body temperatures lower than 36.5°C and higher than 38.5°C are judged as hyperthermia and hypothermia, respectively. A Chi-square test was conducted to confirm whether dietary inulin improved IUGR or prevented hyperthermia or hypothermia in newborn piglets (**Figure 3**). The results show that 1.6IN decreased the percentage of the piglet in IUGR ($P < 0.05$) and the percentage of the piglet in hyperthermia ($P < 0.01$).

The piglet performance from cross-fostering to weaning is presented in **Figure 4**. Compared with those in the control group, the piglets in the 1.6IN group had higher litter gain and survival rate at weaning ($P < 0.01$), and 1.6IN also increased piglet ADG and decreased diarrhea rate during lactation ($P < 0.05$).

TABLE 2 | The effect of dietary inulin on colostrum composition of sows.

Items	Control	1.6IN	*P*-value
Fat, %	5.35 ± 1.01	4.48 ± 0.43	0.448
Protein, %	17.55 ± 1.08	17.72 ± 0.78	0.901
Lactose, %	4.24 ± 0.19	4.13 ± 0.16	0.667
DM, %	35.31 ± 1.00	34.49 ± 0.91	0.556
UN, mmol/L	66.60 ± 5.69	51.9 ± 2.87	0.042
SCC, L	3,997.00 ± 2,581.00	795.00 ± 259.00	0.271

Colostrum Composition

The results of dietary inulin on colostrum composition are shown in **Table 2**. The colostrum from the 1.6IN group had a lower concentration of UN compared with the control group ($P < 0.05$); however, there was no difference in fat, protein, lactose, DM, and SCC between the two groups ($P > 0.05$).

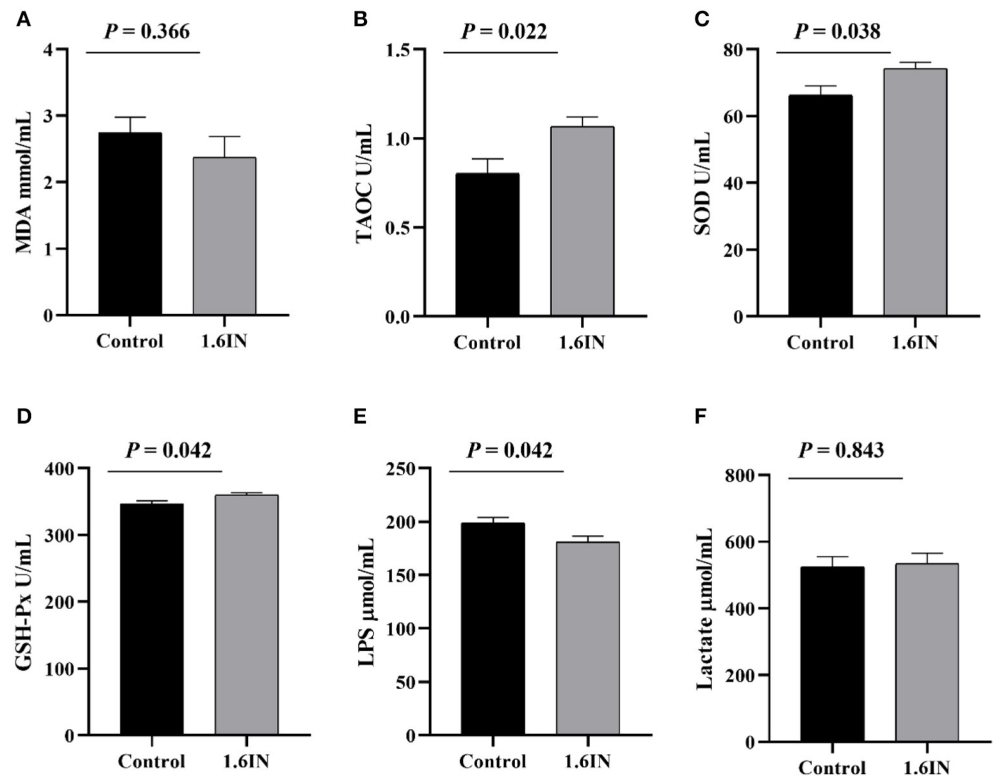

FIGURE 5 | Effects of dietary inulin on the serum markers of sows **(A)** malondialdehyde, MDA; **(B)** total antioxidant capacity, TAOC; **(C)** superoxide dismutase, SOD; **(D)** glutathione peroxidase, GSH-Px; **(E)** lipopolysaccharide, LPS; **(F)** lactate. Significance was analyzed by an unpaired *t*-test.

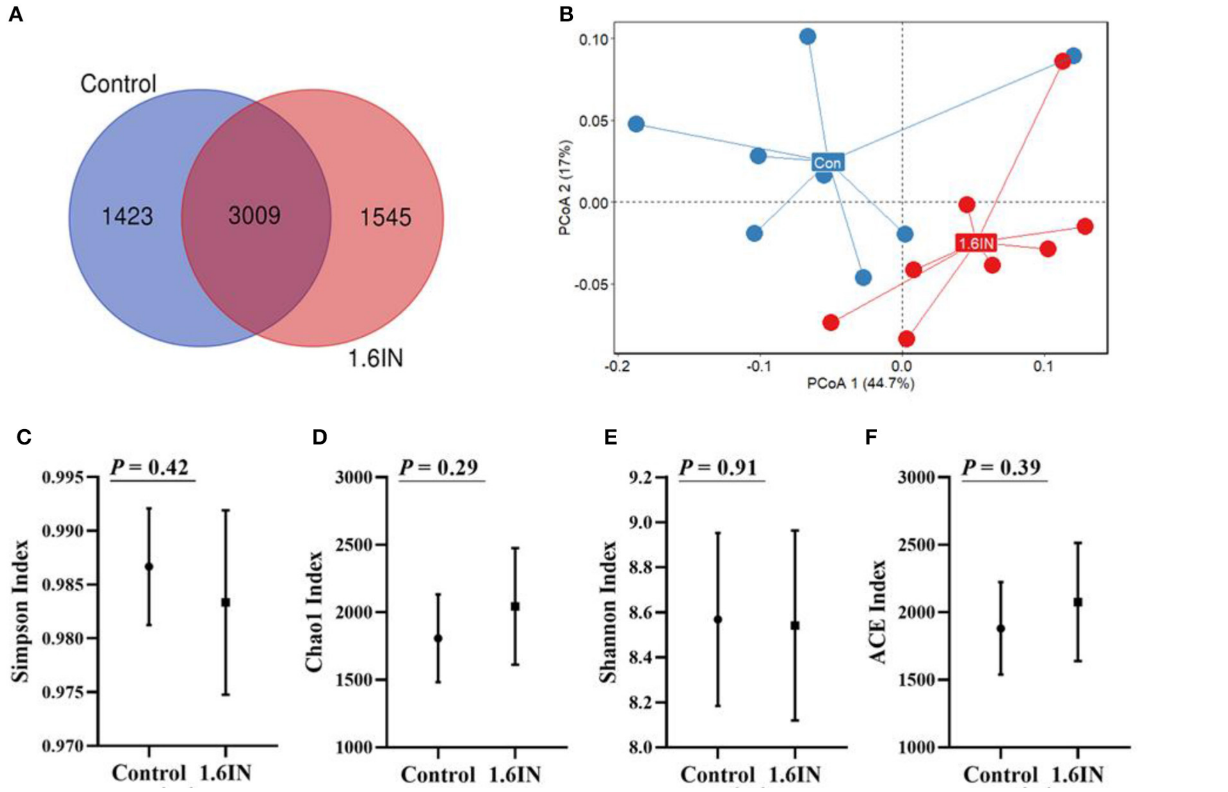

FIGURE 6 | (A) Venn diagram exhibits the shared and unique operational taxonomic units (OTUs) between two groups and **(B)** principal component analysis (PCoA) based on genus level, each point represented one sample, blue points from the control group and red points from the 1.6IN group. **(C)** Simpson index; **(D)** Chao1 index; **(E)** Shannon; **(F)** ACE index. Significance was analyzed by an unpaired *t*-test.

Serum Marker of Sows

The results of dietary inulin on a serum marker of sows are shown in **Figure 5**. The colostrum from the 1.6IN group had higher levels of TAOC, SOD, and GSH-Px compared with the control group ($P < 0.05$); however, there was no difference in MDA and lactate between the two groups ($P > 0.05$).

OTU Partition and Microbial Diversity Analysis

There were means of 4,432 and 4,554 OTUs from the control group and the 1.6IN group, respectively, and there were 3,009 common OTUs between the two groups (**Figure 6A**). There was no difference in α-diversity, such as Shannon index, Chao1 index, Simpson index, and ACE index between the two groups (**Figure 6**), indicating that bacterial richness was not affected by dietary inulin. The microbial communities in all the samples were analyzed and compared by the PCoA (**Figure 6B**). The first two components accounted for 61.7% variation; however, no great variation could be observed between the control group and the 1.6IN group ($P = 0.09$).

Taxonomic Composition Analysis

The results of phylum distribution are shown in **Figure 7**. Taxonomic assignment of the OTU identified 15 phyla in the fecal samples of sows in this study. Nine phyla (average relative abundances >0.1% in at least one group) were chosen for significance analyses, suggesting that the top two phyla, Firmicutes and Bacteroidetes, were dominant in the fecal samples of sows with >90% total relative abundance. Compared with the control group, 1.6IN decreased the relative abundance of Firmicutes, *Cyanobacteria,* and the ratio of Firmicutes/Bacteroidetes ($P < 0.05$) and increased the relative abundance of Bacteroidetes ($P < 0.05$). At the family level, 1.6IN increased the relative abundance of *Prevotellaceae* ($P < 0.01$) but increased the relative abundance of *Ruminococcaceae* ($P < 0.05$).

To identify the specific bacterial taxa among the groups, we compared the fecal microbiota by using LEFSE analysis. The results showed 25 different OTUs between the two groups, 10 OTUs were highly abundant in the 1.6IN group and 15 OTUs in the control group (**Figure 8**). At the family level, a great abundance of *Ruminococcaceae*, *BS11*, *YS02*, *Streptococcaceae*, *Mogibacteriaceae* in the control group, and a great abundance of *Desulfovibrionaceae* and *Paraprevotellaceae* in the 1.6IN group was found. At the genus level, a great abundance of *CF231*, *Paludibacter*, *Prevotella*, and *Desulfovibrio* in the 1.6IN group and *Streptococcus* in the control group was observed.

Fecal SCFA Composition

The results of microbial metabolite SCFAs are shown in **Table 3**. There was no difference in the concentration of acetate,

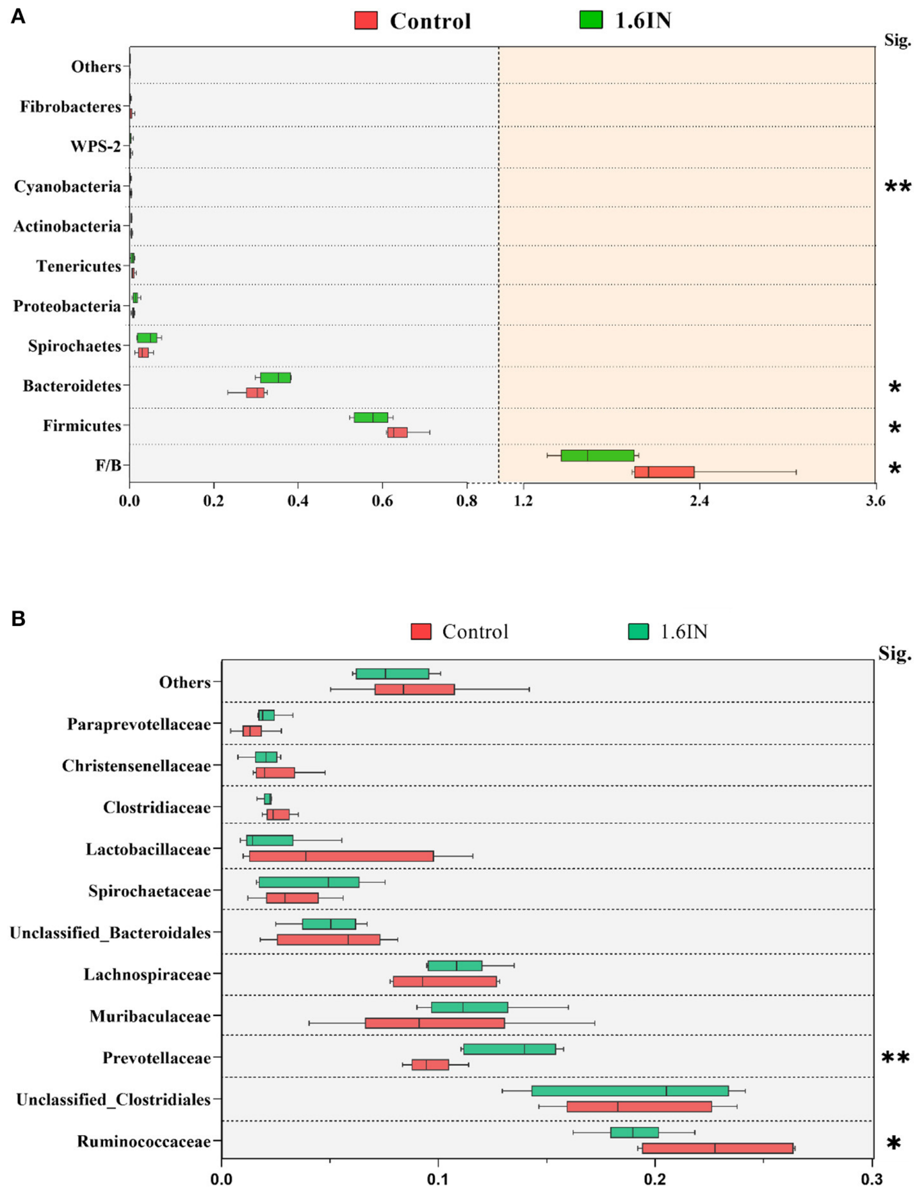

FIGURE 7 | Taxonomy composition of the bacterial communities at **(A)** the phylum level and **(B)** the family level (average relative abundance >0.001 at least one group). Significance was analyzed by an unpaired *t*-test. *$P < 0.05$; ** $P < 0.01$.

propionate, butyrate, and total SCFAs ($P > 0.05$); however, 1.6IN increased the ratio of acetate in the total SCFAs significantly compared with the control group ($P < 0.05$).

Correlations Between Gut Microbiota and Colostrum Composition, Newborn Body Index of Piglets, and Serum Marker of Sows

A Spearman correlation analysis was performed to evaluate the potential link between alterations in gut microbiota composition and colostrum composition, newborn body index of piglets, and serum marker of sows (**Figure 9**). The concentration of fat, DM, and UN was negatively correlated with the phylum Bacteroidetes ($P < 0.05$). In addition, the UN concentration was also negatively correlated with the genus *Prevotella* and *CF231* ($P < 0.05$), and the concentration of UN and SCC was positively correlated with the genus *Streptococcus* ($P < 0.05$). Firmicutes and Bacteroidetes were negatively and positively correlated with the median body weight (MBW) of newborn piglets ($P < 0.05$). Furthermore, lipopolysaccharide (LPS) was negatively correlated with *Cyanobacteria* and positively correlated with *Proteobacteria* and *Desulfovibrio* ($P < 0.05$), respectively, and *Cyanobacteria* also was negatively correlated with TAOC, SOD, and GSH-Px ($P < 0.05$).

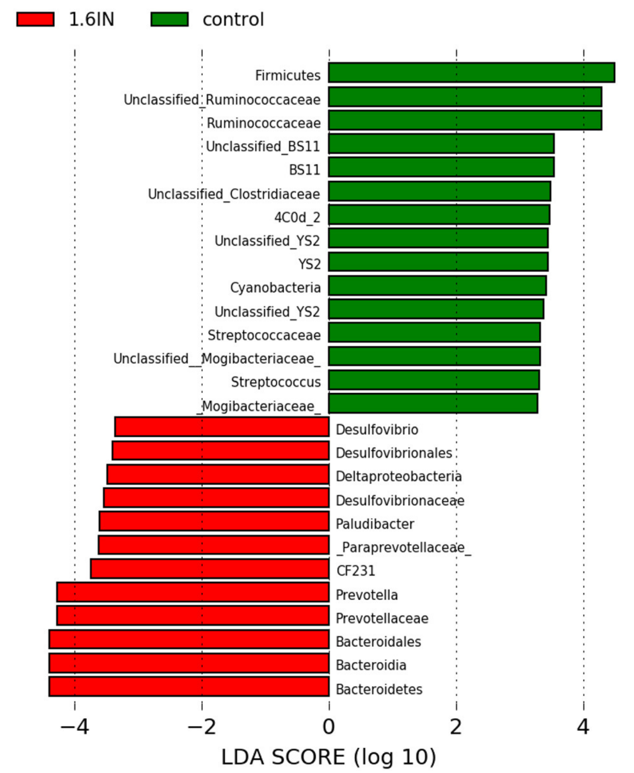

FIGURE 8 | LefSE analysis of colonic microbiota between two dietary groups. LDA scores are calculated for characteristics at the OTU level, and if the value for the LDA score is >3, it means there is a significant difference.

TABLE 3 | The effect of dietary inulin on SCFA composition in the feces of sows.

Items	Control	1.6IN	*P*-value
Concentration, umol/g			
Acetate	93.54 ± 5.38	99.76 ± 2.38	0.315
Propionate	31.31 ± 1.76	29.97 ± 1.35	0.561
Butyrate	14.12 ± 1.51	13.14 ± 0.83	0.585
Total SCFAs	138.96 ± 6.94	142.88 ± 3.55	0.627
Ratio, %			
Acetate	67.2 ± 0.86	69.84 ± 0.70	0.038
Propionate	22.73 ± 1.42	20.97 ± 0.75	0.299
Butyrate	10.07 ± 0.76	9.18 ± 0.48	0.349

DISCUSSION

Because of specific physiological conditions and feeding procedures, pregnant sows are exposed to a series of inevitable problems, such as weight gain during pregnancy, constipation, and prolonged farrowing duration (15). Affected by the above physiological problems from their mothers, newborn piglets often die of low birth weight and poor viability before weaning (2, 15). Birth weight depends on nutritional status and placental transport function during late gestation, while viability is closely related to birth weight and farrowing duration, and may be reflected in the body temperature (16, 17).

Previous studies have suggested that dietary fiber was conducive to shortening the farrowing duration and improved piglet birth weight (12, 18, 19). In this study, 1.6%, the dose with the best improvement effect, was selected as the inulin dosage from the previous study (12). The results of this study showed that 1.6IN reduced the percentage of sows whose farrowing duration was >240 min and that APBI was >20 min. 1.6IN also reduced the percentage of IUGR in the piglet and improved the survival rate before weaning. The reason for these results may be that inulin improved the antioxidant capacity and energy metabolism for sows, which were consistent with the results of previous studies (5, 12, 20).

The body temperature of the piglet during birth and the diarrhea rate before weaning were selected as indicators for judging the health of the piglet. It has been reported that body temperature during birth as an indicator affects survival and growth performance due to which unnormal body temperature is considered to be associated with increased mortality (21, 22). Hypothermia indicated lack of suckling capacity and subsequent growth retardation, whereas hyperthermia may be caused by inflammation, and it means that piglets consume too much-stored energy and oxygen to provide heat, and it may lead to decreased digestive enzyme activity, and cause diarrhea and reduced growth rate (23, 24). In this study, there was no difference between the two groups in the percentage of piglets whose body temperature was lower than 36.5°C, whereas the percentage of piglets with body temperature higher than 38.5°C was significantly reduced in the 1.6IN group. In addition, 1.6IN also reduced the rate of diarrhea and increased the ADG of the piglets, indicating that the preventive effect of 1.6IN on hyperthermia helped to relieve diarrhea of suckling piglets. It was reported that an improvement in intake of the maternal SDF on the antioxidant capacity and the inflammation in the colon of piglets were observed via regulation of the community of gut microbiota, which could explain the results of body temperature in piglets reasonably (12).

Breast milk is the most important source of nutrients, energy, and immunologically active substances for piglets before weaning. In previous studies, dietary fiber in the late gestation could affect the colostrum composition for sows, so this study determined the concentration of fat, protein, lactose, DM, UN, and SCC in colostrum (18, 25). The results showed that 1.6IN did not affect fat, protein, lactose, and DM in colostrum, which meant that there was no difference in the nutritional content of colostrum between the two groups; however, six samples from the control group had elevated UN ($P < 0.05$) and SCC concentrations ($P > 0.05$), which are important indexes for judging milk quality or mastitis (26, 27). The diarrhea rate of piglets in the control group was also significantly higher than that in the 1.6IN group, which also may be caused by low-quality milk from the inflamed breast.

Increasing research focuses on the interactions among diet, gut microbiota, and the host (4, 28). The results of this study have shown that Firmicutes and Bacteroides dominate at the phylum level, which can reach more than 90% relative abundance

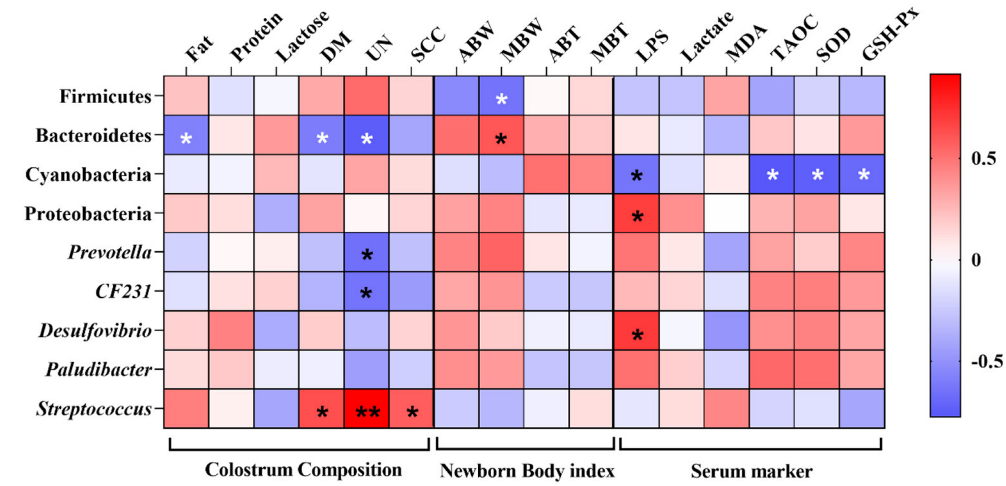

FIGURE 9 | Heatmap of the Spearman's *r* correlations between the gut microbiota significantly modified by different diets treatment and colostrum composition, newborn body index of piglets, and serum marker of sows. ABW, average body weight; MBW, median body weight; ABT, average body temperature; MBT, median body temperature. Significance and correlation coefficient was analyzed by Spearman's correlation analysis. $^*P < 0.05$; $^{**}P < 0.01$.

of the total gut microbiota of sow. The ratio of Firmicutes to Bacteroides (F/B) has been judged to be an important index for affecting the energy metabolism of mammals, which was usually related to energy deposition in humans, mice, and pigs (29, 30). 1.6IN reduced the F/B ratio, affecting the median body weight (MBW) of newborn piglets from correlation results, indicating that the sows fed diet with dietary inulin deposited less energy under the same calorie intake, and the undeposited part may be allocated to the development of the fetus, which was potentially causal with the reduction in the rate of low birth weight (11).

Furthermore, the control group also had a higher relative abundance of *Streptococcaceae* and *Mogibacteriaceae*, which contained lots of common conditional pathogens (31, 32). In particular, *Streptococcus*, one of the core strains in milk, and parasitizing in the breast potentially, was identified as a higher relative abundant species in the control group (33). In previous studies, *Streptococcus* has usually shown a high correlation with mastitis of cows (34). In this study, the relative abundance of *Streptococcus* also showed a positive correlation with the concentration of UN and SCC in colostrum, which suggested the potential connection between *Streptococcus* and sow mastitis. Therefore, the reduction of *Streptococcus* may be the key reason for 1.6IN to reduce UN and SCC in colostrum; however, the results did not confirm whether the *Streptococcus* translocated into the sow breast from the intestines, which required further research.

The physiological status of sows largely determined the health of offspring piglets. Six blood markers that reflect the health status of sows were tested in this study, wherein MDA, SOD, TAOC, and GSH-Px reflected antioxidant capacity (12), LPS reflected intestinal barrier function (35), and lactate reflected the degree of anaerobic respiration of sows during farrowing (36). The results showed that inulin increased the concentrations of SOD, TAOC, and GSH-Px in the serum of sows, suggesting an improvement in antioxidant capacity, which was consistent with previous studies; however, inulin also increased the concentration of LPS, suggesting a reduction in intestinal barrier function of sows.

Two phyla, closely related to serum markers, deserved our attention. Proteobacteria include many common opportunistic pathogens, such as *Escherichia coli* and *Desulfovibrio* (37). *Desulfovibrio* was increased in the 1.6IN group. It can reduce the sulfur-containing substance to produce hydrogen sulfide that irritates mucosa, causing decreased barrier function, and increased serum LPS concentration (38, 39); however, the tolerance of pig immune cells to LPS stimulation has been previously reported (40), and we have not identified a significant stress response in sows and their offspring. Therefore, we have reservations about the negative effects of LPS in sows. *Cyanobacteria*, containing bacteria that produced natural toxins, were found to be significantly higher in the control group (41). A characteristic increase in intestinal *Cyanobacteria* on progeroid mice has been reported by previous studies (42). The results of correlation analysis also showed that *Cyanobacteria* were negatively correlated with TAOC, SOD, and glutathione peroxidase (GSH-Px). Therefore, we speculated that dietary inulin may improve the antioxidant capacity of sows by downregulating the relative abundance of *Cyanobacteria* in the gut microbiota.

In research on dietary fiber, SCFAs were thought of as a "bridge" in the diet–gut microbiome-host metabolism axis (43). Acetate (C2), propionate (C3), and butyrate (C4) are the most abundant, representing more than 90% of the SCFAs present in the colon. The majority of SCFAs are absorbed by colonic epithelial cells, and only 5–10% is excreted in the feces. SCFAs can regulate fat synthesis and cholesterol in the liver, and stabilize blood glucose by triggering glucagon secretion and increasing satiety (44). SCFAs regulate intestinal inflammation in sows and inhibit fat deposition in sows, which has the potential to be a beneficial intervention for positive pregnancy outcomes (5). Results align with those obtained by Marquardt et al. (13) and Zhou et al. (11) who did not detect any significant effects of inulin inclusion on the concentration of SCFA and its constituents in feces of sows during late gestation; however, the feces sample from 1.6IN had a higher acetate ratio in total SCFAs. The relative abundance of acetate-producing bacterium *Prevotella* and *CF231* was also higher in the 1.6IN group, which provided a reasonable explanation for the results of acetate ratio (29, 45).

CONCLUSION

This study verified the beneficial effect of inulin as a functional fiber in the nutrition of sows in late pregnancy, not only in the reproductive performance of sows but also in the survival of newborn piglets. Overall, this study showed that maternal fiber nutrition during pregnancy regulated the health of offspring, and the response of the maternal intestinal microbes played an important role in intervening in the phenotype of sows and neonatal piglets.

DATA AVAILABILITY STATEMENT

The datasets presented in this study can be found in online repositories. The names of the repository/repositories and accession number(s) can be found at: https://www.ncbi.nlm.nih.gov/sra/?term=PRJNA736251.

ETHICS STATEMENT

The animal study was reviewed and approved by Institution Animal Care and Use Committee of college of Animal Science and Technology, Hunan Agricultural University (No.43321809) (Changsha, China).

AUTHOR CONTRIBUTIONS

HL and XM designed the research. XM provided the funding. HL, LM, and XL conducted the research. HL and NL analyzed the data. HL mainly wrote the manuscript. LZ, ZL, and FZ edited the manuscript. All authors contributed to the article and approved the submitted version.

FUNDING

This study was supported by the Scientific Research Fund of Hunan Provincial Education Department (19B267) and the National Natural Science Foundation of China (U20A2054).

REFERENCES

1. Cheng C, Wei H, Yu H, Xu C, Jiang S, Peng J. Metabolic syndrome during perinatal period in sows and the link with gut microbiota and metabolites. *Front Microbiol.* (2018) 9:1989. doi: 10.3389/fmicb.2018.01989
2. Feyera T, Højgaard CK, Vinther J, Bruun TS, Theil PK. Dietary supplement rich in fiber fed to late gestating sows during transition reduces rate of stillborn piglets. *J Anim Sci.* (2017) 95:5430–8. doi: 10.2527/jas2017.2110
3. Cani PD, Everard A, Duparc T. Gut microbiota, enteroendocrine functions and metabolism. *Curr Opin Pharmacol.* (2013) 13:935–40. doi: 10.1016/j.coph.2013.09.008
4. Paul HA, Bomhof MR, Vogel HJ, Reimer RA. Diet-induced changes in maternal gut microbiota and metabolomic profiles influence programming of offspring obesity risk in rats. *Sci Rep.* (2016) 6:20683. doi: 10.1038/srep20683
5. Tan C, Wei H, Ao J, Long G, Peng J. Inclusion of konjac flour in the gestation diet changes the gut microbiota, alleviates oxidative stress, and improves insulin sensitivity in sows. *Appl Environ Microbiol.* (2016) 82:5899–909. doi: 10.1128/AEM.01374-16
6. Zhou H, Chen D, Mao X, He J, Yu J, Zheng P, et al. Evaluation of standardized ileal digestible lysine requirement for 8–20 kg pigs fed low crude protein diets. *Anim Sci J.* (2019) 90:237–46. doi: 10.1111/asj.13142
7. Roberfroid MB. Inulin-type fructans: functional food ingredients. *J Nutr.* (2007) 137:2493–502. doi: 10.1093/jn/137.11.2493S
8. Femia A Pietro, Luceri C, Dolara P, Giannini A, Biggeri A, Salvadori M, et al. Antitumorigenic activity of the prebiotic inulin enriched with oligofructose in combination with the probiotics *Lactobacillus rhamnosus* and *Bifidobacterium lactis* on azoxymethane-induced colon carcinogenesis in rats. *Carcinogenesis.* (2002) 23:1953–60. doi: 10.1093/carcin/23.11.1953
9. Salazar N, Dewulf EM, Neyrinck AM, Bindels LB, Cani PD, Mahillon J, et al. Inulin-type fructans modulate intestinal *Bifidobacterium species* populations and decrease fecal short-chain fatty acids in obese women. *Clin Nutr.* (2015) 34:501–7. doi: 10.1016/j.clnu.2014.06.001
10. Catry E, Bindels LB, Tailleux A, Lestavel S, Neyrinck AM, Goossens JF, et al. Targeting the gut microbiota with inulin-type fructans: preclinical demonstration of a novel approach in the management of endothelial dysfunction. *Gut.* (2018) 67:271–83. doi: 10.1136/gutjnl-2016-313316
11. Zhou P, Zhao Y, Zhang P, Li Y, Gui T, Wang J, et al. Microbial mechanistic insight into the role of inulin in improving maternal health in a pregnant sow model. *Front Microbiol.* (2017) 8:2242. doi: 10.3389/fmicb.2017.02242
12. Li H, Liu Z, Lyu H, Gu X, Song Z, He X, et al. Effects of dietary inulin during late gestation on sow physiology, farrowing duration and piglet performance. *Anim Reprod Sci.* (2020) 219:106531. doi: 10.1016/j.anireprosci.2020.106531
13. Marquardt RR, Jin LZ, Kim JW, Fang L, Frohlich AA, Baidoo SK. Passive protective effect of egg-yolk antibodies against enterotoxigenic *Escherichia coli* K88+ infection in neonatal and early-weaned piglets. *FEMS Immunol Med Microbiol.* (1999) 23:283–8. doi: 10.1016/S0928-8244(98)00147-3
14. Bosch G, Pellikaan WF, Rutten PGP, Van Der Poel AFB, Verstegen MWA, Hendriks WH. Comparative *in vitro* fermentation activity in the canine distal gastrointestinal tract and fermentation kinetics of fiber sources. *J Anim Sci.* (2008) 86:2979–89. doi: 10.2527/jas.2007-0819
15. Daigle C. Parallels between postpartum disorders in humans and preweaning piglet mortality in sows. *Animals.* (2018) 8:22. doi: 10.3390/ani8020022
16. Oliviero C, Heinonen M, Valros A, Peltoniemi O. Environmental and sow-related factors affecting the duration of farrowing. *Anim Reprod Sci.* (2010) 119:85–91. doi: 10.1016/j.anireprosci.2009.12.009
17. Berchieri-Ronchi CB, Kim SW, Zhao Y, Correa CR, Yeum KJ, Ferreira ALA. Oxidative stress status of highly prolific sows during gestation and lactation. *Animal.* (2011) 5:1774–9. doi: 10.1017/S1751731111000772
18. Loisel F, Farmer C, Ramaekers P, Quesnel H. Effects of high fiber intake during late pregnancy on sow physiology, colostrum production, and piglet performance. *J Anim Sci.* (2013) 91:5269–79. doi: 10.2527/jas.2013-6526
19. Gu XL, Li H, Song ZH, Ding YN, He X, Fan ZY. Effects of isomaltooligosaccharide and bacillus supplementation on sow performance,

serum metabolites, and serum and placental oxidative status. *Anim Reprod Sci.* (2019) 207:52–60. doi: 10.1016/j.anireprosci.2019.05.015
20. Xie C, Wu X, Long C, Wang Q, Fan Z, Li S, et al. Chitosan oligosaccharide affects antioxidant defense capacity and placental amino acids transport of sows. *BMC Vet Res.* (2016) 12:243. doi: 10.1186/s12917-016-0872-8
21. Pedersen LJ, Berg P, Jørgensen G, Andersen IL. Neonatal piglet traits of importance for survival in crates and indoor pens. *J Anim Sci.* (2011) 89:1207–18. doi: 10.2527/jas.2010-3248
22. Panzardi A, Bernardi ML, Mellagi AP, Bierhals T, Bortolozzo FP, Wentz I. Newborn piglet traits associated with survival and growth performance until weaning. *Prev Vet Med.* (2013) 110:206–13. doi: 10.1016/j.prevetmed.2012.11.016
23. Akizuki H, Yoshie H, Morita Y, Takahashi K, Hara A, Watanabe T, et al. Nuclear transition of heat shock protein in guinea pig cochlea after hyperthermia. *Hear Res.* (1995) 92:126–30. doi: 10.1016/0378-5955(95)00210-3
24. Keller VA, Melancon JK, Thomas T V., Pigott JD, Flint LM, Lefer DJ, et al. Mild preischemia hypothermia adversely affects postischemic myocardial function in the neonatal piglet heart. *J Surg Res.* (1997) 73:54–8. doi: 10.1006/jsre.1997.5205
25. Krogh U, Bruun TS, Amdi C, Flummer C, Poulsen J, Theil PK. La production de colostrum chez les truies nourries de différentes sources de fibres et de gras pendant les stades tardifs de gestation. *Can J Anim Sci.* (2015) 95:211–23. doi: 10.4141/cjas-2014-060
26. Jashari R, Piepers S, De Vliegher S. Evaluation of the composite milk somatic cell count as a predictor of intramammary infection in dairy cattle. *J Dairy Sci.* (2016) 99:9271–86. doi: 10.3168/jds.2015-10753
27. Song D, Li X, Cheng Y, Wu G, Xiao X, Wang F, et al. Effects of supplementing sow diets with *Saccharomyces cerevisiae* refermented sorghum dried distiller's grains with solubles from late gestation to weaning on the performance of sows and progeny1. *J Anim Sci.* (2017) 95:2025–31. doi: 10.2527/jas.2017.1438
28. Nyangahu DD, Lennard KS, Brown BP, Darby MG, Wendoh JM, Havyarimana E, et al. Disruption of maternal gut microbiota during gestation alters offspring microbiota and immunity. *Microbiome.* (2018) 6:124. doi: 10.1186/s40168-018-0511-7
29. Fernandes J, Su W, Rahat-Rozenbloom S, Wolever TMS, Comelli EM. Adiposity, gut microbiota and faecal short chain fatty acids are linked in adult humans. *Nutr Diabetes.* (2014) 4:e121. doi: 10.1038/nutd.2014.23
30. Lin S, Wang Z, Lam KL, Zeng S, Tan BK, Hu J. Role of intestinal microecology in the regulation of energy metabolism by dietary polyphenols and their metabolites. *Food Nutr Res.* (2019) 63:1–12. doi: 10.29219/fnr.v63.1518
31. Kasuya K, Yoshida E, Harada R, Hasegawa M, Osaka H, Kato M, et al. Systemic *Streptococcus dysgalactiae* subspecies equisimilis infection in a yorkshire pig with severe disseminated suppurative meningoencephalomyelitis. *J Vet Med Sci.* (2014) 76:715–8. doi: 10.1292/jvms.13-0526
32. Louren¸co TGB, Spencer SJ, Alm EJ, Colombo APV. Defining the gut microbiota in individuals with periodontal diseases: an exploratory study. *J Oral Microbiol.* (2018) 10:1487741. doi: 10.1080/20002297.2018.1487741
33. Cheng C, Wei H, Xu C, Xie X, Jiang S, Peng J. Maternal soluble fiber diet during pregnancy changes the intestinal microbiota, improves growth performance, and reduces intestinal permeability in piglets. *Appl Environ Microbiol.* (2018) 84:e01047–18. doi: 10.1128/AEM.01047-18
34. Marshall VM, Bramley AJ. Stimulation of *Streptococcus thermophilus* growth in mastitic milk. *J Dairy Res.* (1984) 51:17–22. doi: 10.1017/S002202990002327X
35. Zhu QA, Gong M, Zhang C, Yong G bing, Xiang S. Preparation of Sb2S3 nanomaterials with different morphologies via a refluxing approach. *J Cryst Growth.* (2009) 311:3651–5. doi: 10.1016/j.jcrysgro.2009.04.024
36. Gladden LB. Lactate metabolism: a new paradigm for the third millennium. *J Physiol.* (2004) 558:5–30. doi: 10.1113/jphysiol.2003.058701
37. Moulin L, Munive A, Dreyfus B, Boivin-masson C. Nodulation of legumes by members of the β-subclass of proteobacteria. *Nature.* (2001) 411:948–50. doi: 10.1038/35082070
38. Montassier E, Al-Ghalith GA, Ward T, Corvec S, Gastinne T, Potel G, et al. Pretreatment gut microbiome predicts chemotherapy-related bloodstream infection. *Genome Med.* (2016) 8:61. doi: 10.1186/s13073-016-0321-0
39. Figliuolo VR, dos Santos LM, Abalo A, Nanini H, Santos A, Brittes NM, et al. Sulfate-reducing bacteria stimulate gut immune responses and contribute to inflammation in experimental colitis. *Life Sci.* (2017) 189:29–38. doi: 10.1016/j.lfs.2017.09.014
40. Cagiola M, Giulio S, Miriam M, Katia F, Paola P, Macrì A, et al. *In vitro* down regulation of proinflammatory cytokines induced by LPS tolerance in pig CD14+ cells. *Vet Immunol Immunopathol.* (2006) 112:316–20. doi: 10.1016/j.vetimm.2006.04.002
41. Chorus I, Falconer IR, Salas HJ, Bartram J. Health risks caused by freshwater cyanobacteria in recreational waters. *J Toxicol Environ Health B Crit Rev.* (2000) 3:323–47. doi: 10.1080/109374000436364
42. Bárcena C, Valdés-Mas R, Mayoral P, Garabaya C, Durand S, Rodríguez F, et al. Healthspan and lifespan extension by fecal microbiota transplantation into progeroid mice. *Nat Med.* (2019) 25:1234–42. doi: 10.1038/s41591-019-0504-5
43. Wu W, Xie J, Zhang H. Dietary fibers influence the intestinal SCFAs and plasma metabolites profiling in growing pigs. *Food Funct.* (2016) 7:4644–54. doi: 10.1039/C6FO01406B
44. den Besten G, Lange K, Havinga R, van Dijk TH, Gerding A, van Eunen K, et al. Gut-derived short-chain fatty acids are vividly assimilated into host carbohydrates and lipids. *Am J Physiol Gastrointest Liver Physiol.* (2013) 305:900–11. doi: 10.1152/ajpgi.00265.2013
45. Marounek M, Dušková D. Metabolism of pectin in rumen bacteria *Butyrivibrio fibrisolvens* and *Prevotella ruminicola*. *Lett Appl Microbiol.* (1999) 29:429–33. doi: 10.1046/j.1472-765X.1999.00671.x

Conflict of Interest: The authors declare that the research was conducted in the absence of any commercial or financial relationships that could be construed as a potential conflict of interest.

Publisher's Note: All claims expressed in this article are solely those of the authors and do not necessarily represent those of their affiliated organizations, or those of the publisher, the editors and the reviewers. Any product that may be evaluated in this article, or claim that may be made by its manufacturer, is not guaranteed or endorsed by the publisher.

frontiers in Nutrition

ORIGINAL RESEARCH
published: 10 August 2021
doi: 10.3389/fnut.2021.701644

Lactobacillus paracasei S16 Alleviates Lumbar Disc Herniation by Modulating Inflammation Response and Gut Microbiota

Zhanchao Wang†, Huiqiao Wu†, Yu Chen, Huajiang Chen, Xinwei Wang and Wen Yuan*

Department of Orthopaedics, Changzheng Hospital, Naval Medical University, Shanghai, China

Lumbar disc herniation (LDH) is a common cause for low back pain. In this study, we aimed to explore the effects of a specific *Lactobacillus paracasei* (*L. paracasei*), *L. paracasei S16*, on the symptoms of LDH using a mouse model of LDH. The results showed that *L. paracasei S16* treatment improved the behavior, increased the cell proliferation, and decreased the apoptosis in LDH mice. Moreover, *L. paracasei S16* treatment alleviated the aberrant inflammation response in the LDH mice, which is characterized by the decreased anti-inflammatory cytokines, increased pro-inflammatory cytokines, and decreased percentage of Th1 and Th2 cells and Th17/Treg ratio. 16S rRNA sequencing results showed that the LDH mice treated with *L. paracasei S16* have higher relative abundance of *Lachnospiraceae* and *Ruminococcaceae* and lower abundance of *Lactobacillaceae* than mice in the LDH group. Additionally, the serum metabolites involved in the linoleic acid metabolism, alanine. aspartate, and glutamate, glycerophospholipid, and TCA cycle were significantly decreased and the metabolite involved in purine metabolism was significantly increased after the *L. paracasei S16* treatment in the LDH mice. These results showed that administration of *L. paracasei S16* can improve inflammation response, alter gut microbiota, and modulate serum metabolomics in a mouse model of LDH.

Keywords: lumbar disc herniation, *Lactobacillus paracasei*, inflammation, gut microbiota, serum metabolomics

OPEN ACCESS

Edited by:
Yong Su,
Nanjing Agricultural University, China

Reviewed by:
David Rios-Covian,
University of California, San Diego, United States
Valeriy Poroyko,
Covance, United States

****Correspondence:***
Xinwei Wang
wangxw_cz@163.com

†These authors share first authorship

Specialty section:
This article was submitted to Nutrition and Microbes, a section of the journal Frontiers in Nutrition

Received: *28 April 2021*
Accepted: *02 July 2021*
Published: *10 August 2021*

Citation:
Wang Z, Wu H, Chen Y, Chen H, Wang X and Yuan W (2021) Lactobacillus paracasei S16 Alleviates Lumbar Disc Herniation by Modulating Inflammation Response and Gut Microbiota. Front. Nutr. 8:701644. doi: 10.3389/fnut.2021.701644

INTRODUCTION

lumbar disc herniation (LDH) is one of the common spinal diseases and affects around 9% population worldwide (1). It has been well established that LDH is highly associated with the inflammation (2). For example, herniated disc tissue has increased levels of proinflammatory and regulatory cytokines, such as interleukin 1β (IL-1β), IL-4, IL-6, IL-12, tumor necrosis factor α (TNF-α), and interferon-γ (IFN-γ) (3–5). Further, these cytokines can activate the differentiation of lymphocyte. T helper 1 (Th1), Th2, and Th 17 lymphocytes plays an important role in activating inflammation, while Treg cell involves in preventing inflammation (6, 7). It has been demonstrated that patients with LDH have increased levels of circulating and disc Th17 and IL-17, which may contribute to pain (8).

Recent studies have shown that the *Lactobacillus paracasei* (*L. paracasei*) treatment can alleviate inflammation-related disorders by modulating the production of anti- and pro-inflammatory cytokines (9, 10). Furthermore, clinical studies also revealed the important role of *L. paracasei* supplementation in ameliorating inflammation in humans (11, 12). Mechanically, *L. paracasei* can act as a probiotic to improve gut microbial composition (13, 14). Increasing evidence has demonstrated that the gut microbiota is highly associated with the host inflammatory response. For example, the gut microbiota can influence the development of chronic inflammatory disorders by regulating the T cells function (15). However, whether the *L. paracasei* can alleviate aberrant inflammation in LDH mice by modulating the gut microbiota is unclear.

In this study, we investigated whether *L. paracasei* exert anti-inflammatory effects via modulating T cell function and gut microbiota in the mice with LDH. To test this hypothesis, we examined the effects of specific strain of *L. paracasei*, *L. paracasei S16*, on the behavior and the production of inflammatory cytokines in LDH mice. In addition, we also analyzed the gut microbiota and serum metabolomics to further explored the mechanism.

MATERIALS AND METHODS

Reagents, Mice, and Ethics

The *Lactobacillus paracasei S16* was purchased from Hangzhou Hongsai biopharmaceutical Co., Ltd. (Zhejiang, China). The male Balb/C mice (20–15 g) were purchased from the Envigo (Indianapolis, USA). Mice were maintained in a 12 h-light/dark cycle and free access to diet and water. All procedures used in this experiment were approved by Changzheng Hospital Ethics Committee (No. 2020-0073).

Mice and Surgery

The mice were divided into 4 groups ($n = 12$/group). The mice in the Sham and LDH groups were received 0.1 mL PBS, and the mice in the Sham + Probiotic and LDH + Probiotic groups were received 0.1 mL of 10^9 CFU/ml *L. paracasei S16* via oral gavage for 4 weeks starting 1 week before the establishment of LDH. A LDH model was established as a previous study (16). Briefly, the mice were anesthetized with intraperitoneal injection of ketamine/xylazine. The lumbar 4-L (L4-L5) disc of mice in the Sham and Sham + Probiotic group were only exposed without puncturing laterally, while the L4-L5 dic of mice in the LDH and LDH +Probiotic groups were punctured laterally. At the post-operation day (POD) 28, blood samples were collected by orbital blooding. Serum was obtained by centrifugation of the blood samples at 1,000 g for 15 min under 4°C and stored in aliquots at −80°C.

Measurement of Mechanical Allodynia and Thermal Hyperalgesia

The mechanical allodynia and thermal hyperalgesia were tested as reported previously (17). Briefly, the mechanical allodynia was measured by the incidence of foot withdrawal responding to non-noxious mechanical indentation of each hind paw using a probe with an 0.5 mm^2 polypropylene tip. The thermal hyperalgesia was defined by the foot withdraw latency to heat stimulation.

Immunohistochemistry

Dorsal root ganglia (DRG) samples were fixed in 4% paraformaldehyde overnight at 4°C. After embedding in paraffin, serial sections of 4 μm thickness were cut and treated with periodic acid to blocked the endogenous peroxidase. After incubated with the primary antibodies (Cyclin, Proteintech, USA; Ki67, Abcam, UK; PCNA, Proteintech, USA) at 4°C overnight, the sections were incubated with secondary antibodies for 30 min at 37°C. The images of the stained sections were captured by fluorescence microscope.

Western Blot Analysis

The protein expression of Cyclin, Ki67, PCNA, Foxp3, IFN-γ, IL-2, IL-4, IL-5, IL-12, IL-17A, TGF-β, and IL-10 in the L4-L5 DRG were determined by Western blot (WB) analysis. Briefly, the samples were lysed in 0.1 mL lysis buffer and the lysate were centrifuged at 12,000 rpm for 15 min at 4°C. The proteins were transferred onto polyvinylidene difluoride membranes and blocked with 5% non-fat milk in tris-Tween-buffered saline buffer (20 mM tris, pH 7.5, 150 mM NaCl, and 0.1% Tween 20) for 1.5 hour and then incubated with the primary antibodies (Proteintech, USA; Abcam, UK) at 4°C overnight, followed by incubation with a goat anti-mouse IgG or a goat anti-rabbit IgG (Proteintech, USA) for 1 h at room temperature. Western blot bands were scanned and analyzed with Alpha Imager 2200 software (Alpha Innotech Corporation, CA, USA). Protein expression was normalized against β-actin.

Terminal Deoxynucleotidyl Transferase Dutp Nick end Labeling (TUNEL) Assay

Cellular apoptosis was measured using the TUNEL assay kit according to the manufactures' instruction (Shanghai Yeasen biotech Co., Ltd., China).

Flow Cytometric Analysis of T Cell Subsets

To determine the Th1, Th2, Th17, and Treg cells in mice, flow cytometric analysis was performed on isolated DRG cells using CD4, Foxp3, IL-17A, TGF-β, and IL-4 antibodies as reported previously (18). Briefly, the cells suspension was transferred into 1 mL phosphate buffer saline (PBS) and centrifuged at 350 g for 5 min. After centrifugation, the supernatant was removed and the cells were resuspended with 500 μL fixation/permeabilization then centrifuged at 350 g for 5 mice after standing at room temperature for 30 min. The resuspension was repeated for twice. The cells were then incubated with monoclonal antibodies, including CD4-FITC, FOXP3-PE, IL-17A-PE, IL-4-PE, and IFN-γ-PE antibodies (eBiosciences, San Diego, California, USA) at dark for 30 min. After washing with PBS, the cells were resuspended in 150 μL PBS and then tested by using Beckman counter flow cytometer (USA). The data were analyzed using FlowjoX software. The lymphocytes were gated by FSC and SSC. $CD4^+IL\text{-}17A^+$, $CD4^+IL\text{-}4^+$, $CD4^+$ $IFN\text{-}\gamma^+$, and $CD4^+$ $FOXP3^+$ lymphocytes were identified as Th17, Th2, Th1, and Treg respectively.

Measurement of Serum Inflammatory Cytokines Levels

The levels of Foxp3, IFN-γ, IL-2, IL-4, IL-5, IL-12, IL-17A, TGF-β, and IL-10 in serum were measured by applying a manual enzyme-linked immunosorbent assay (ELISA)-based spectrophotometric approach involving the use of corresponding assay kits (Wuhan Huamei Bioengineering Co., Ltd, Wuhan, China).

16S rRNA Gene Sequencing

Fecal DNA was extracted using the QIAamp DNA Stool Mini Kit (Qiagen, Hilden, Germany) according to the manufacturer's instructions. DNA concentration and purity were monitored on 1% agarose gels. The V3-V4 region of the bacterial 16S ribosomal RNA gene was amplified using a specific primer (314F, 5′-CCTACGGGNGGCWGCAG-3′; 805R, 5′-GACTACHVGGGTATCTAATCC-3′). Amplicons were detected using 2% agarose gels electrophoresis and purified using the AxyPrep DNA gel extraction kit (Axygen Bioscience, CA, USA). After quantified and purified, paired-end sequencing was performed using an Illumina MiSeq instrument (Illumina, San Diego, CA, USA) at Shanghai Weihuan Bio-Pharm Technology Co. Ltd. (Shanghai, China) according to standard protocols. Raw sequencing data were deposited into the NCBI Sequence Read Archive (SRA) database associated with BioProject ID PRJNA729635. The sequences were analyzed and assigned to operational taxonomic units (OTUs; 97% identity), and chimeric sequences were identified and removed using UCHIME. Taxonomy was assigned to OTUs using the naïve Bayes classifier and q2-feature-classifier plugin against the SILVA-132-99 gene database, with a confidence threshold of 70%. Alpha diversity was analyzed using QIIME 2 (version 2.4), which included the calculation of observe, Chao1, ACE, Shannon, and Simpson indices. Beta diversity was estimated by computing the Bray-Curits distance among samples and visualized using Principal Co-ordinates Analysis (PCoA). The "VeenDiagram" package of R software and jvenn were used to produce Veen diagrams.

Metabolomics Profiling of Serum Samples

The metabolomic process including sample preparation, metabolites extraction and detection, data processing and analysis. Briefly, 80 μL cold methanol was added to 20 μL serum. The mixture was vortexed for 1 min and then incubated at 4°C for 20 min. After centrifuging at 12,000 rpm for 10 min, the supernatant was collected, dried, and then resuspended for further analysis. A ACQUITY ultra-high-performance liquid chromatography system coupled to ABSciex Triple TOF 5600 (ABSciex, Franmingham, MA, USA) and an electrospray ionization source was used to tested the metabolomics profiling. Raw LC-MS data were analyzed using MarkerView and PeakView software for peak detection, identification, and alignment. Kyoto Encylopedia of Genes and Genomes (KEGG) database was used to identify the exact metabolites.

Statistical Analysis

All statistical analyses were analyzed by one-way ANOVA followed by the Ducan test (SPSS 21 software). Data are expressed as the mean ± SEM. $P < 0.05$ was considered statically significant.

RESULTS

L. paracasei S16 Alleviated the Behavior in LDH Mice

The mechanical allodynia and thermal hyperalgesia were tested to explore the effects of *L. paracasei S16* on behavior in LDH mice. The results showed that, in the LDH group, the mechanical and thermal withdraw were significantly decreased from the POD 1 to 28 compared with the Sham group ($P < 0.05$) (**Figures 1A,B**). However, the mechanical withdrawal at the POD 3, 14, and 28 and thermal withdraw from the POD 3 to 28 were significantly higher in the LDH + Probiotic group than the LDH group ($P < 0.05$) (**Figures 1A,B**), suggesting that *L. paracasei S16* treatment significantly alleviated the behavior of LDH mice.

L. paracasei S16 Elevated the Expression of Cell Proliferation Markers in LDH Mice

We further examined the expressions of cell proliferation markers, Cyclin, Ki67, and PCNA in the DRG samples using IHC and WB. The IHC results showed that LDH mice have significantly lower expression of Cyclin and PCNA than the Sham mice, which was significantly reversed by the *L. paracasei S16* treatment ($P < 0.05$) (**Figure 2A**).

Similarly, the WB results showed that the LDH mice have significantly lower relative protein expression of Cyclin, Ki67, and PCNA ($P < 0.05$) (**Figure 2B**), suggesting that LDH mice have inhibited cell proliferation. However, *L. paracasei S16* treatment markedly increased the cell proliferation by enhancing the relative protein expressions of Cyclin, Ki67, and PCNA in LDH mice ($P < 0.05$) (**Figure 2B**).

The cellular apoptosis in DRG was measured by TUNEL assay. The results showed that the percentage of apoptotic to total cells was significantly higher in the LDH group than the Sham group, which was significantly reversed by the *L. paracasei S16* treatment ($P < 0.05$) (**Figure 2C**).

L. paracasei S16 Alleviated the Aberrant Inflammation in LDH Mice

The comparisons of T cell subsets in the DRG were shown in **Figure 3A**. The percentage of Th1 and Th2 and the Th17/Treg ratio were significantly higher in the LDH group than the control group ($P < 0.05$). However, *L. paracasei S16* treatment significantly decreased the percentage of Th1 and Th2 and the Th17/Treg ratio in the LDH mice ($P < 0.05$).

Similarly, in the DRG, the relative protein expression levels of IFN-γ, IL-2, IL-4, IL-5, IL-12, IL-17A were significantly higher in the LDH group than the Sham group, which were significantly reversed by the *L. paracasei S16* treatment ($P < 0.05$) (**Figure 3B**). In addition, the relative protein expression levels of Foxp3, TGF-β and IL-10 were significantly lower in the LDH group than the Sham group, which were significantly reversed by the *L. paracasei S16* treatment ($P < 0.05$) (**Figure 3B**).

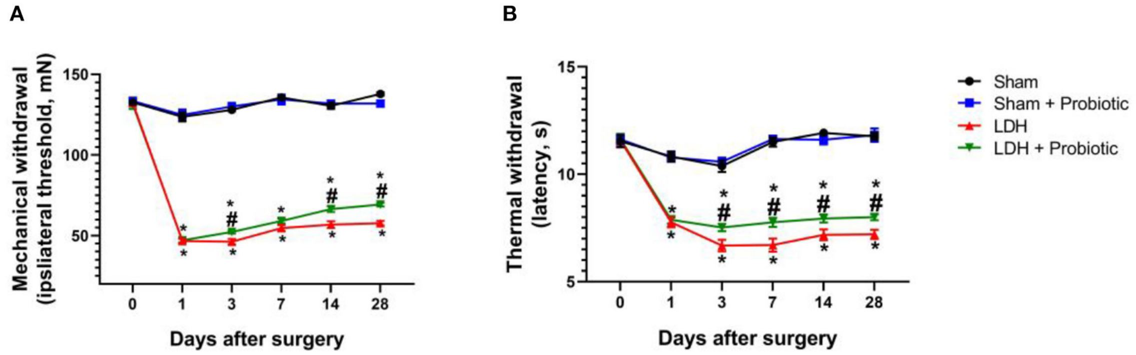

FIGURE 1 | *L. paracasei S16* alleviated the behavior in LDH mice. **(A)** Mechanical withdrawal; **(B)** Thermal withdrawal. Data were expressed as the mean ± SEM. **P* < 0.05 vs. Sham; #*P* < 0.05 vs. LDH.

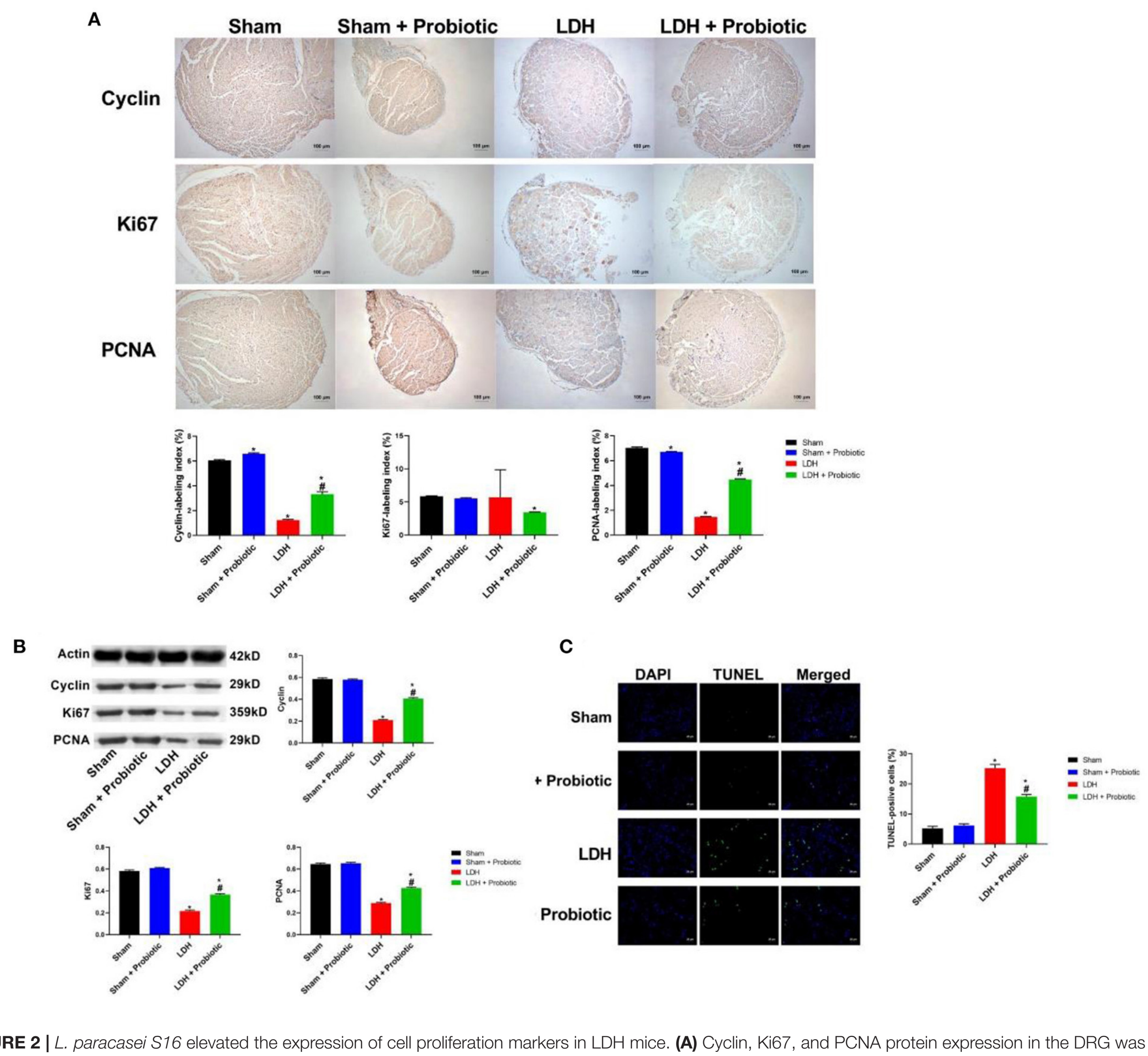

FIGURE 2 | *L. paracasei S16* elevated the expression of cell proliferation markers in LDH mice. **(A)** Cyclin, Ki67, and PCNA protein expression in the DRG was examined by immunohistochemical staining; **(B)** Western blot analysis of cyclin, Ki67, and PCNA in DRG; **(C)** TUNEL analysis of DRG. Data were expressed as the mean ± SEM. **P* < 0.05 vs. Sham; #*P* < 0.05 vs. LDH.

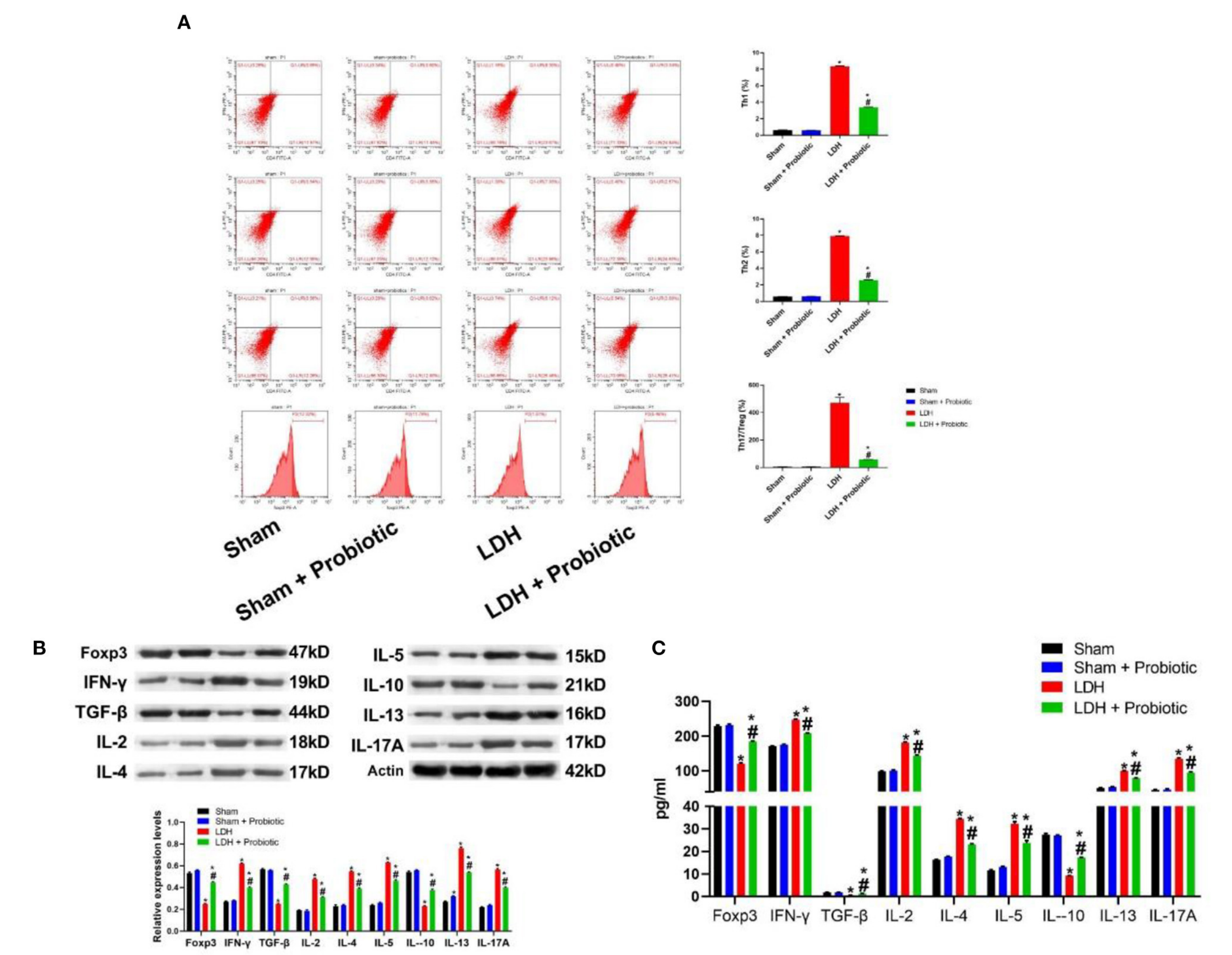

FIGURE 3 | *L. paracasei S16* alleviated the aberrant inflammation in LDH mice. **(A)** Flow cytometric analysis of DRG; **(B)** Western blot analysis of inflammatory cytokines levels in the DRG; **(C)** ELISA of inflammatory cytokines in the serum. Data were expressed as the mean ± SEM. *$P < 0.05$ vs. Sham; #$P < 0.05$ vs. LDH.

The serum levels of Foxp3, IFN-γ, IL-2, IL-4, IL-5, IL-12, IL-17A, TGF-β, and IL-10 were also measured using ELISA. The results showed that LDH mice have significantly higher levels of IFN-γ, IL-2, IL-4, IL-5, IL-12, and IL-17A, which were significantly reversed by the *L. paracasei S16* treatment ($P < 0.05$) (**Figure 3C**). In addition, the serum levels of Foxp3, TGF-β, and IL-10 were significantly lower in the LDH group than the Sham group, which were significantly reversed by the *L. paracasei S16* treatment ($P < 0.05$) (**Figure 3C**).

L. paracasei S16 Altered the Fecal Microbiota in LDH Mice

The fecal microflora was analyzed by sequencing V3+V4 regions of 16S rRNA genes. To identify the microbial α-diversity, Observe, Chao1, ACE, Shannon, Simpson, and J indexes were examined. As shown in **Figure 4A**, LDH mice had significantly lower α-diversity than the Sham mice, which is characterized by the decreased Observe, Chao1, ACE, Shannon, Simpson, and J indexes ($P < 0.05$) (**Figure 4A**). However, *L. paracasei S16* treatment significantly increased the α-diversity in the LDH mice by increasing the Observe, Chao1, ACE, Shannon, Simpson, and J indexes ($P < 0.05$) (**Figure 4A**). The Venn diagram showed that there are 37 common OTUs between the four groups. Meantime, the Sham, Sham + Probiotic, LDH, LDH + Probiotic mice contained individual 119, 33, 91, and 78 OTUs, respectively (**Figure 4B**). To further understand the microbial composition between the two groups, we evaluated beta-diversity using PCoA based on Bray-Curtis distance. The results showed that the microbial community structure in the four groups were significantly different (**Figure 4C**).

We further analyzed the microbial compositions at the phylum and family levels. As shown in **Figure 5A**, at the phylum level, Sham mice had significantly higher relative abundance

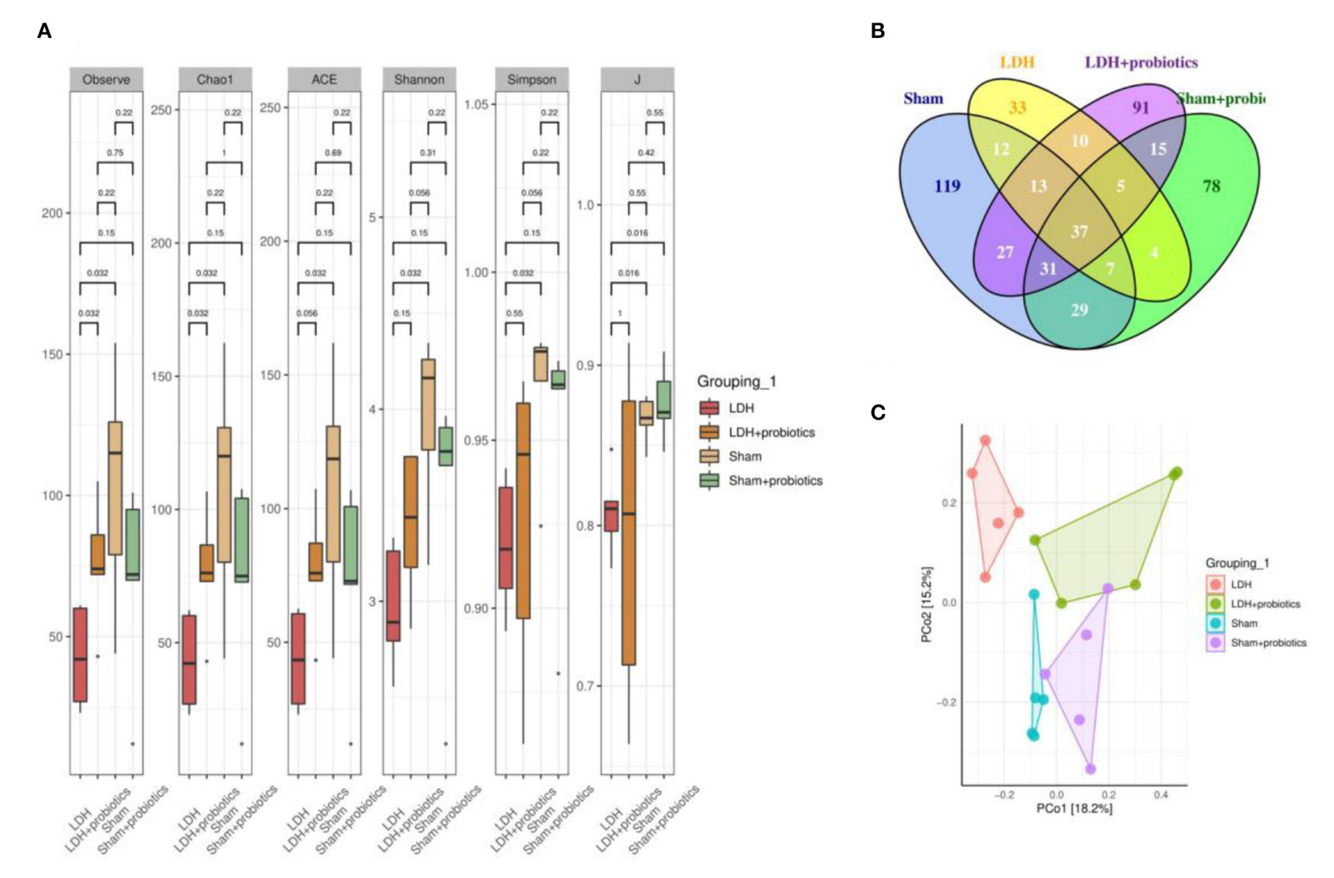

FIGURE 4 | *L. paracasei S16* altered gut microbiota. **(A)** α-diversity; **(B)** Venn diagram; **(C)** PCoA. Data were expressed as the mean ± SEM.

of *Spirochaetes* than the other three groups ($P < 0.05$). At the family level, the LDH mice had significantly higher relative abundance of *Lactobacillaceae* than the Sham mice, which was significantly reversed by the *L. paracasei S16* treatment ($P < 0.05$) (**Figure 5B**). Meantime, the relative abundance of *Lachnospiraceae* and *Ruminococcaceae* are significantly lower in the LDH group than the Sham group ($P < 0.05$) (**Figure 5B**). However, *L. paracasei S16* treatment significantly increased the relative abundance of *Lachnospiraceae* and *Ruminococcaceae* in the LDH mice ($P < 0.05$) (**Figure 5C**). At the genus level, LDH mice have significantly higher relative abundance of *Lactobacillus* and lower relative abundance of *Lachnospiraceae_NK4A136_group* than the control mice ($P < 0.05$) (**Figure 5C**). Interestingly, *L. paracasei S16* supplementation significantly decreased the relative abundance of *Lactobacillus* in mice with LDH ($P < 0.05$) (**Figure 5C**). Additionally, *L. paracasei S16* significantly enhanced the relative abundance of *Lachnospiraceae_NK4A136_group* in the sham mice ($P < 0.05$) (**Figure 5C**).

L. paracasei S16 Altered the Serum Metabolomics in LDH Mice

Serum metabolomics were examined to explore the metabolites altered by *L. paracasei* S16 treatment. The results showed that, there were 32 differential metabolites in the four groups (**Figure 6A**). The potential metabolic pathways of the differential metabolites were analyzed using MetaboAnalyst 5.0 software. The results showed that the differential metabolites involved in linoleic acid metabolism, Retinol metabolism, Alanine, aspartate and glutamate metabolism, Glycerophospholipid metabolism, citrate cycle (TCA cycle), and purine metabolism (**Figure 6B**).

DISCUSSION

LDH is one of the most common cause of low back pain. In this study, we investigated the effects of *L. paracasei S16* administration on the symptoms of LDH in a mouse model. Our results demonstrated that the supplementation with a specific *L. paracasei* strain, *L. paracasei S16*, could ameliorate the symptoms of LDH through improving inflammation, modulating gut microbiota, and altering serum metabolites.

The results of behavior test showed that *L. paracasei S16* treatment had alleviating action on LDH mice, which is characterized by the increased mechanical withdrawal and thermal withdraw. It has been reported that LDH exhibited increased cell apoptosis and decreased cell proliferation (19, 20). Thus, in this study, we examined the effects of *L. paracasei S16* treatment on the expressions of cell proliferation-related

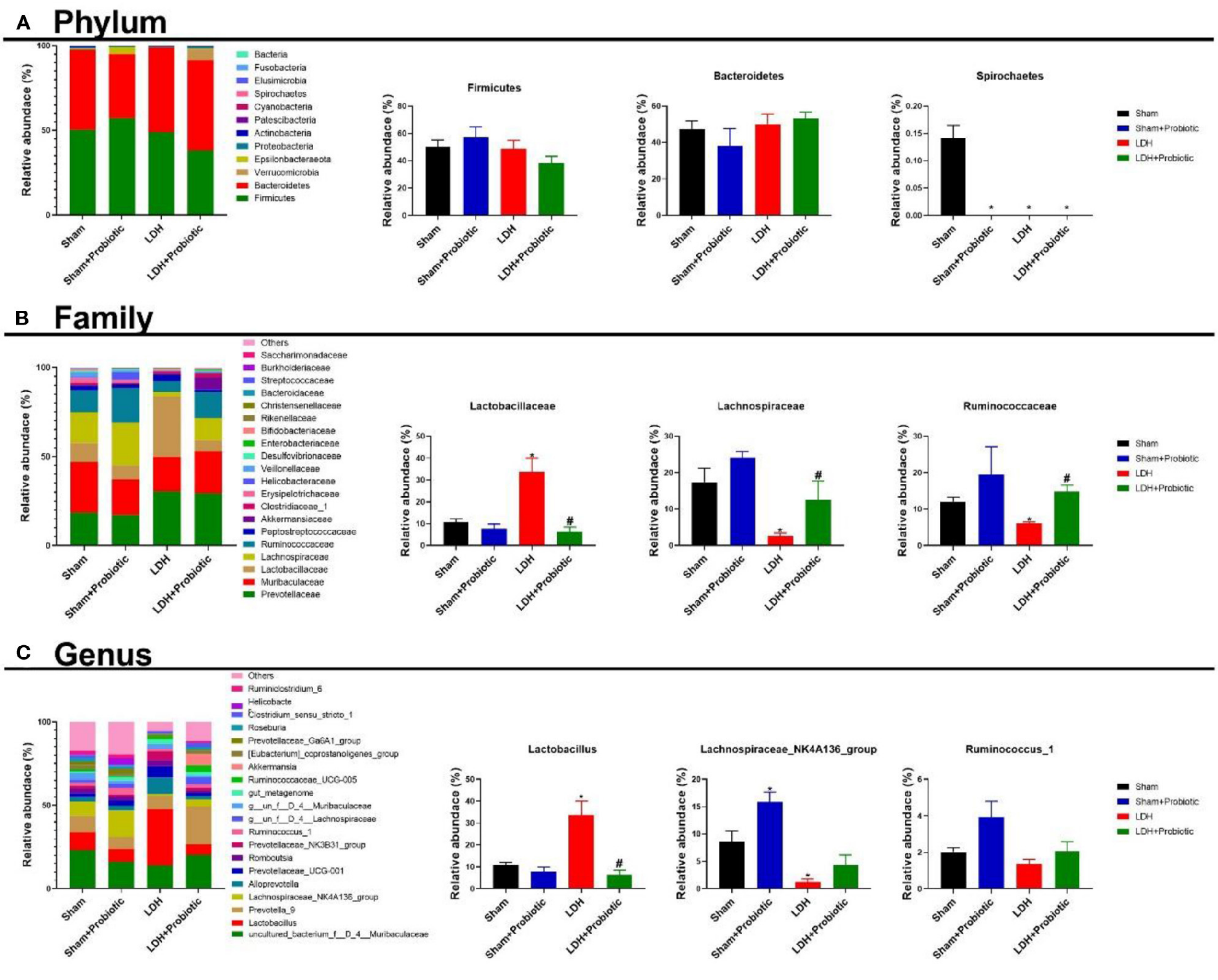

FIGURE 5 | Fecal microbial composition. **(A)** Phylum level; **(B)** Family level; **(C)** Genus level. Data were expressed as the mean ± SEM. **P* < 0.05 vs. Sham; #*P* < 0.05 vs. LDH.

markers. The results showed that *L. paracasei S16* treatment increased the relative protein expressions of Cyclin, Ki67, and PCNA in LDH mice and decreased the apoptosis, suggesting that *L. paracasei S16* may alleviate LDH by inhibiting apoptosis and promote cell proliferation in DRG tissue.

Numerous studies have shown that LDH is accompanied by disordered inflammatory responses, such as increased production of pro-inflammatory cytokines and decreased anti-inflammatory cytokines (3–5). Consistently, in this study, we found that LDH mice have higher levels of pro-inflammation cytokines (IFN-γ, IL-2, IL-4, IL-5, IL-12, and IL-17A) and lower levels of anti-inflammatory cytokines (Foxp3, TGF-β, and IL-10) in the serum and DRG tissue. However, *L. paracasei S16* treatment decreased the production of pro-inflammatory cytokines and increased the production of anti-inflammatory cytokines in the mice with LDH. Similarly, previous studies also found that *L. paracasei* can modulate inflammation by decreasing the production of proinflammatory cytokines (IL-1, IL-2, and TNF-α) and increasing the production of anti-inflammatory cytokines (IL-10 and TGF-β) production and inhibiting inflammatory activation (9, 10). These data showed that *L. paracasei S16* treatment may alleviate LDH by improve inflammation in mice.

Activated T cells can differentiate into different subsets, including Th1, Th2, Th17, and Treg cells, that contribute to immune response. Th1 and Th2 cells can produce IFN-γ and IL-4, IL-13, and IL-5, respectively. Th17 has been shown to play an important role in inducing inflammation and autoimmune diseases (including LDH) by secreting its effector cytokine, IL-17 (6). Contrarily, Treg cells can prevent autoimmunity. TGF-β and Foxp3 are involved in the differentiation Th17 cells and Treg cells, respectively (7). Furthermore, the imbalance of Th17/Treg ratio can cause autoimmune disorders (7, 21). In this study, the data on T cell subsets showed that LDH is associated with higher levels of Th1, Th2, and Th17/Treg ration, which were alleviated by the *L. paracasei s16* treatment. Collectively, these data suggested that *L. paracasei s16* treatment can alleviate inflammation by influencing the

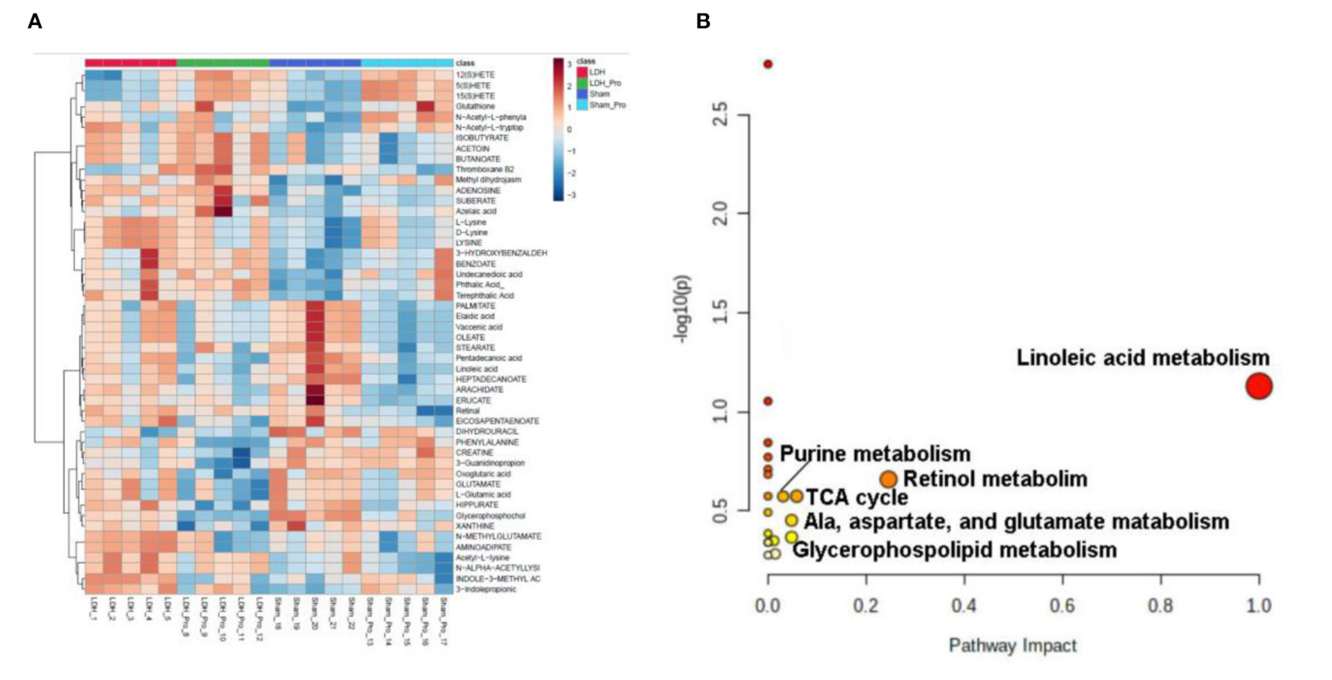

FIGURE 6 | *L. paracasei S16* changed serum metabolomics changes. **(A)** Heat-map of the intensity of 32 significantly different metabolites showing significantly different metabolic profiles between the Sham, Sham + Probiotic, LDH, LDH + Probiotic groups. **(B)** The disturbed metabolic pathways showed differential metabolites by MetaboAnalyst 5.0 software. Node radius was based on pathway impact values. Node color was based on *P* value.

production of inflammatory cytokines and the differentiation of T cells.

Amounting studies have demonstrated that gut microbiota plays an important role in modulating inflammatory response. We found that, compared to the sham mice, the LDH mice have decreased relative abundance of *Spirochaetes*, which is the most neurotropic bacteria (22). However, it has been proved that *Spirochaetes* can induce the production of pro-inflammatory cytokines and cause chronic inflammation (23, 24). Furthermore, animal and clinical studies showed that *L. paracasei* can improve inflammation by modulating gut microbiota (25, 26). Contrarily, in this study LDH mice had higher abundance of *Lactobacillaceae* than the Sham mice. Administration with *L. paracasei s16* decreased the abundance of *Lactobacillaceae* in mice with LDH. Similarly, at the genus level, *L. paracasei s16* decreased the relative abundance of *Lactobacillus*. These conflicting results need further investigation. Additionally, *L. paracasei s16* administration increased the relative abundance of *Lachnospiraceae* and *Ruminococcaceae* in mice with LDH. It has been reported that the short chain fatty acids, such as butyrate and propionate, produced by *Lachnospiraceae* involved in activating Treg cells, reducing pro-inflammatory cytokines, and increasing anti-inflammatory cytokines, which collectively alleviate inflammation (27–29). Similarly, *Ruminococcaceae*, which increased after *L. paracasei s16* administration in mice with LDH, can ameliorate chronic inflammation by producing butyrate (29). Thus, in this study, we speculated that *L. paracasei s16* treatment regulated the T cells populations by modulating gut microbiota, which contribute to alleviating aberrant inflammatory response.

In addition, we also examined the serum metabolomics to explore whether *L. paracasei s16* supplementation improve inflammation through changing serum metabolites in LDH mice. The data showed that the metabolites involved in the linoleic acid metabolism (linoleate), alanine. aspartate, and glutamate (oxoglutaric acid), glycerophospholipid (glycerophosphocholine), and TCA cycle (oxoglutaric acid) were significantly decreased and the metabolite involved in purine metabolism (adenosine) was significantly increased after the *L. paracasei S16* treatment in LDH mice. Similarly, previous studies also found that linoleic acid plays an important role in promoting inflammation (30). A recent clinical study analyzing the relationship between serum metabolites and inflammation showed that the serum oxoglutaric acid has a negative correlation with the inflammation severity. However, in this study, we found that *L. paracasei S16* treatment decreased the serum level of oxoglutaric acid, which may be because the different animal models. Thus, although the specific mechanism is unclear, it is reasonable to hypothesize that *L. paracasei S16* treatment may improve inflammation by modulating the serum metabolites.

Taken together, the current study demonstrated that *L. paracasei S16* treatment can alleviate inflammation by modulating serum metabolites and gut microbiota in LDH mice. However, the casual role of altered gut microbiota in the suppressed inflammation and changes in serum metabolites need further confirmation.

DATA AVAILABILITY STATEMENT

The datasets presented in this study can be found in online repositories. The names of the repository/repositories and accession number(s) can be found here: https://www.ncbi.nlm.nih.gov/Traces/study/?acc=PRJNA729635.

ETHICS STATEMENT

The animal study was reviewed and approved by Changzheng Hospital Ethics Committee (No. 2020-0073).

AUTHOR CONTRIBUTIONS

ZW, HC, and XW designed this study. ZW, HW, and YC participated in the experiment. ZW, HC, and WY analyzed the experiment data. HW and YC wrote and revised this manuscript. All the authors read the final manuscript and agreed to publish it.

FUNDING

This study was supported by Changzheng Hospital.

REFERENCES

1. Cunha C, Silva AJ, Pereira P, Vaz R, Gonçalves RM, Barbosa MA. The inflammatory response in the regression of lumbar disc herniation. *Arthritis Res Ther*. (2018) 20:251. doi: 10.1186/s13075-018-1743-4
2. Wu J, Sun Y, Xiong Z, Liu J, Li H, Liu Y, et al. Association of GSDMC polymorphisms with lumbar disc herniation among Chinese Han population. *Int J Immunogenet*. (2020) 47:546–53. doi: 10.1111/iji.12488
3. Shamji MF, Setton LA, Jarvis W, So S, Chen J, Jing L, et al. Proinflammatory cytokine expression profile in degenerated and herniated human intervertebral disc tissues. *Arthritis Rheum*. (2010) 62:1974–82. doi: 10.1002/art.27444
4. Takada T, Nishida K, Doita M, Miyamoto H, Kurosaka M. Interleukin-6 production is upregulated by interaction between disc tissue and macrophages. *Spine*. (2004) 29:1089–92. doi: 10.1097/00007632-200405150-00007
5. Takada T, Nishida K, Maeno K, Kakutani K, Yurube T, Doita M, et al. Intervertebral disc and macrophage interaction induces mechanical hyperalgesia and cytokine production in a herniated disc model in rats. *Arthritis Rheum*. (2012) 64:2601–10. doi: 10.1002/art.34456
6. Zhang W, Nie L, Guo YJ, Han LX, Wang X, Zhao H, et al. Th17 cell frequency and IL-17 concentration correlate with pre- and postoperative pain sensation in patients with intervertebral disk degeneration. *Orthopedics*. (2014) 37:e685–91. doi: 10.3928/01477447-20140626-62
7. Moaaz M, Youssry S, Elfatatry A, Abd El Rahman M. Th17/Treg cells imbalance and their related cytokines (IL-17, IL-10 and TGF-β) in children with autism spectrum disorder. *J Neuroimmunol*. (2019) 337:577071. doi: 10.1016/j.jneuroim.2019.577071
8. Cheng L, Fan W, Liu B, Wang X, Nie L. Th17 lymphocyte levels are higher in patients with ruptured than non-ruptured lumbar discs, and are correlated with pain intensity. *Injury*. (2013) 44:1805–10. doi: 10.1016/j.injury.2013.04.010
9. Choi JH, Moon CM, Shin TS, Kim EK, McDowell A, Jo MK, et al. Lactobacillus paracasei-derived extracellular vesicles attenuate the intestinal inflammatory response by augmenting the endoplasmic reticulum stress pathway. *Exp Mol Med*. (2020) 52:423–37. doi: 10.1038/s12276-019-0359-3
10. Suzuki H, Yamazaki T, Ohshio K, Sugamata M, Yoshikawa M, Kanauchi O, et al. A Specific Strain of Lactic Acid Bacteria, Lactobacillus paracasei, Inhibits Inflammasome Activation In Vitro and Prevents Inflammation-Related Disorders. *J Immunol*. (2020) 205:811–21. doi: 10.4049/jimmunol.1900657
11. Wang IJ, Wang JY. Children with atopic dermatitis show clinical improvement after Lactobacillus exposure. *Clin Exp Allergy*. (2015) 45:779–87. doi: 10.1111/cea.12489
12. Yoon JY, Cha JM, Hong SS, Kim HK, Kwak MS, Jeon JW, et al. Fermented milk containing Lactobacillus paracasei and Glycyrrhiza glabra has a beneficial effect in patients with Helicobacter pylori infection: A randomized, double-blind, placebo-controlled study. *Medicine (Baltimore)*. (2019) 98:e16601. doi: 10.1097/MD.0000000000016601
13. Kim WK, Jang YJ, Han DH, Jeon K, Lee C, Han HS, et al. Lactobacillus paracasei KBL382 administration attenuates atopic dermatitis by modulating immune response and gut microbiota. *Gut Microbes*. (2020) 12:1–14. doi: 10.1080/19490976.2020.1819156
14. Kim WK, Jang YJ, Han DH, Jeon K, Lee C, Han HS, et al. Lactobacillus paracasei Jlus66 extenuate oxidative stress and inflammation via regulation of intestinal flora in rats with non alcoholic fatty liver disease. *Food Sci Nutr*. (2019) 7:2636–46. doi: 10.1002/fsn3.1118
15. Brown EM, Kenny DJ, Xavier RJ. Gut microbiota regulation of T cells during inflammation and autoimmunity. *Annu Rev Immunol*. (2019) 37:599–624. doi: 10.1146/annurev-immunol-042718-041841
16. Xiao L, Ding M, Fernandez A, Zhao P, Jin L, Li X. Curcumin alleviates lumbar radiculopathy by reducing neuroinflammation, oxidative stress and nociceptive factors. *Eur Cell Mater*. (2017) 33:279–93. doi: 10.22203/eCM.v033a21
17. Zhang A, Wang K, Ding L, Bao X, Wang X, Qiu X, et al. Bay11-7082 attenuates neuropathic pain via inhibition of nuclear factor-kappa B and nucleotide-binding domain-like receptor protein 3 inflammasome activation in dorsal root ganglions in a rat model of lumbar disc herniation. *J Pain Res*. (2017) 10:375–82. doi: 10.2147/JPR.S119820
18. Liu J, Mori M, Sugimoto K, Uzawa A, Masuda H, Uchida T, et al. Peripheral blood helper T cell profiles and their clinical relevance in MOG-IgG-associated and AQP4-IgG-associated disorders and MS. *J Neurol Neurosurg Psychiatry*. (2020) 91:132–9. doi: 10.1136/jnnp-2019-321988
19. Zhao CQ, Liu D, Li H, Jiang LS, Dai LY. Expression of leptin and its functional receptor on disc cells: contribution to cell proliferation. *Spine*. (2008) 33:E858–64. doi: 10.1097/BRS.0b013e31818338e5
20. Tang N, Dong Y, Xiao T, Zhao H. LncRNA TUG1 promotes the intervertebral disc degeneration and nucleus pulposus cell apoptosis though modulating miR-26a/HMGB1 axis and regulating NF-κB activation. *Am J Transl Res*. (2020) 12:5449–64. doi: 10.2139/ssrn.3493212
21. Noack M, Miossec P. Th17 and regulatory T cell balance in autoimmune and inflammatory diseases. *Autoimmun Rev*. (2014) 13:668–77. doi: 10.1016/j.autrev.2013.12.004
22. Ashraf GM, Tarasov VV, Makhmutova A, Chubarev VN, Avila-Rodriguez M, Bachurin SO, et al. The possibility of an infectious etiology of alzheimer disease. *Mol Neurobiol*. (2019) 56:4479–91. doi: 10.1007/s12035-018-1388-y
23. Miklossy J. Chronic inflammation and amyloidogenesis in Alzheimer's disease – role of Spirochetes. *J Alzheimers Dis*. (2008) 13:381–91. doi: 10.3233/JAD-2008-13404
24. Bibi F, Yasir M. S Sohrab S, I Azhar E, H Al-Qahtani M, M Abuzenadah A, et al. Link between chronic bacterial inflammation and Alzheimer disease. *CNS Neurol Disord Drug Targets*. (2014) 13:1140–7. doi: 10.2174/1871527313666140917115741
25. Lai HH, Chiu CH, Kong MS, Chang CJ, Chen CC. Probiotic lactobacillus casei: effective for managing childhood diarrhea by altering gut microbiota and attenuating fecal inflammatory markers. *Nutrients*. (2019) 11:1150. doi: 10.3390/nu11051150
26. Ganji-Arjenaki M, Rafieian-Kopaei M. Probiotics are a good choice in remission of inflammatory bowel diseases: a meta analysis and systematic review. *J Cell Physiol*. (2018) 233:2091–103. doi: 10.1002/jcp.25911
27. Guo H, Chou WC, Lai Y, Liang K, Tam JW, Brickey WJ, et al. Multi-omics analyses of radiation survivors identify radioprotective microbes and metabolites. *Science*. (2020) 370:eaay9097. doi: 10.1126/science.aay9097

28. Arpaia N, Campbell C, Fan X, Dikiy S, Van Der Veeken J, deRoos P, et al. Metabolites produced by commensal bacteria promote peripheral regulatory T-cell generation. *Nature*. (2013) 504:451–5. doi: 10.1038/nature12726
29. Kang C, Wang B, Kaliannan K, Wang X, Lang H, Hui S, et al. Gut microbiota mediates the protective effects of dietary capsaicin against chronic low-grade inflammation and associated obesity induced by high-fat diet. *MBio*. (2017) 8:e00470–17. doi: 10.1128/mBio.00900-17
30. Innes JK. Calder PC. Omega-6 fatty acids and inflammation. *Prostaglandins Leukot Essent Fatty Acids*. (2018) 132:41–8. doi: 10.1016/j.plefa.2018.03.004

Conflict of Interest: The authors declare that the research was conducted in the absence of any commercial or financial relationships that could be construed as a potential conflict of interest.

Publisher's Note: All claims expressed in this article are solely those of the authors and do not necessarily represent those of their affiliated organizations, or those of the publisher, the editors and the reviewers. Any product that may be evaluated in this article, or claim that may be made by its manufacturer, is not guaranteed or endorsed by the publisher.

ORIGINAL RESEARCH
published: 11 August 2021
doi: 10.3389/fnut.2021.712327

The Gut Microbiota Activates AhR Through the Tryptophan Metabolite Kyn to Mediate Renal Cell Carcinoma Metastasis

*Guoyu Dai, Xiang Chen and Yao He**

Department of Urology, Xiangya Hospital, Central South University, Changsha, China

Background: The incidence of renal cell carcinoma (RCC) is increasing year by year. It is difficult to have complete treatment so far. Studies have shown that tryptophan metabolite Kynurenine (Kyn) affects cell proliferation, migration, apoptosis, adhesion, and differentiation. Our aim is to explore whether Kyn activates aromatic hydrocarbon receptor (AhR) to mediate RCC metastasis.

Methods: We collected RCC tissues and feces from RCC patients. 16S rRNA technology was performed to analyze the gut microbial composition of RCC patients. LC-MS/MS was used to analyze the gut microbial metabolites. The AhR was inhibited and treated with Kyn. Immunofluorescence was used to measure the degree of AhR activation. The migration and invasion ability of 786-O cells was tested by Transwell assay. Flow cytometry and cell cycle assay were utilized to observe the apoptosis and cycle of 786-O cells. CCK-8 assay was used to detect 786-O cells proliferation. qRT-PCR and Western blot were used to detect AhR and EMT-related genes expression level.

Results: AhR expression was up-regulated in RCC tissues. RCC gut microbiota was disordered. The proportion of Kyn was increased in RCC. After being treated with Kyn, the migration, invasion, and proliferation ability of 786-O cells were decreased. Furthermore, the expression of EMT-related protein E-cadherin decreased, and the expression of N-cadherin and Vimentin increased. The proportion of 786-O cells in the S phase increased. The apoptosis rate of 786-O cells was inhibited.

Conclusion: The tryptophan metabolite Kyn could activate AhR. Kyn could promote 786-O cells migration and invasion. Gut microbiota could activate AhR through its tryptophan metabolite Kyn to mediate RCC metastasis.

Keywords: rcc, AhR, KYN, EMT, gut microbiota

Edited by:
Jie Yin,
Hunan Agricultural University, China

Reviewed by:
Shusong Wu,
Hunan Agricultural University, China
Zheng Chen,
University of British Columbia, Canada

****Correspondence:***
Yao He
heyao1984@163.com

Specialty section:
This article was submitted to Nutrition and Microbes, a section of the journal Frontiers in Nutrition

Received: *20 May 2021*
Accepted: *20 July 2021*
Published: *11 August 2021*

Citation:
Dai G, Chen X and He Y (2021) The Gut Microbiota Activates AhR Through the Tryptophan Metabolite Kyn to Mediate Renal Cell Carcinoma Metastasis. Front. Nutr. 8:712327. doi: 10.3389/fnut.2021.712327

INTRODUCTION

Renal cell carcinoma (RCC) is still an elusive cancer in lack of biomarkers. It was the eighth most common malignant tumor in the United States (1). In addition to the increase in newly diagnosed cases, RCC patients' prevalence and overall survival rate have also increased significantly (2). Studies have shown a link between the gut microbiota and metastatic RCC (mRCC). Evidence showed that RCC patients have a lower abundance of *bifidobacteria*, compared with healthy adults

(3). However, it needs experimental verification about whether there is a connection between the gut microbiota and RCC needs to.

Many life activities are mediated by metabolites of gut microbiota. Tryptophan is an essential aromatic amino acid, and it is considered necessary in many metabolites between gut microbiota and the host (4, 5). Many tryptophan metabolites derived from abundant microbiota exhibit the activation potential of aromatic hydrocarbon receptor (AhR) (6). Some endogenous tryptophan metabolites are recognized as AhR ligands, including tryptamine (TRA), indole, 5-hydroxyindole-3-acetic acid (5-HIAA), Kynurenine (Kyn), kynurenic acid (KA), and xanthine acid (XA) (7, 8). Tryptophan metabolites as ligands can activate AhR signals in many diseases, such as inflammation, oxidative stress damage, cancer, aging-related diseases, cardiovascular disease (CVD), and chronic kidney disease (CKD) (4). We screened tryptophan metabolites to verify the regulatory relationship between tryptophan metabolites and AhR.

AhR is a cytoplasmic ligand-activated transcription factor involved in various cellular processes. It can mediate the toxicity (including carcinogenicity) of polycyclic aromatic hydrocarbons and induce many enzymes expression. It can participate in critical biological processes, such as signal transduction, cell differentiation, and cell apoptosis (9). Recent studies have shown that AhR is related to CVD, CKD, and RCC (10). Tryptophan catabolites can activate AhR to enhance tumor malignancy and inhibit anti-tumor immunity (11, 12). More studies revealed AhR can be activated by many endogenous ligands. Different ligands bind and activate AhR, which can translocate AhR to the nucleus and induce a series of genes expression (8).

Epithelial-mesenchymal transition (EMT) is a process in which epithelial cells lose their polarized structure and gain the migration and invasion ability. It is believed to be the cause of cancer metastasis (13). EMT biomarkers such as Vimentin, N-cadherin, and MMP9 are overexpressed in cancer and are involved in promoting cancer cells metastasis (14). Many studies have shown that AhR activity leads to loss of cell contact inhibition and changes in extracellular matrix remodeling (15). This study intends to explore the internal relationship between metastatic RCC and the gut microbiota and its metabolism (tryptophan metabolism) and verify whether the tryptophan metabolite Kyn promotes EMT and RCC pathological process by activating AhR.

RESULTS

High Expression of AhR in RCC Tissues

The clinical characteristics of all subjects were presented in **Table 1**. To study whether AhR expression in RCC was abnormal, we used qRT-PCR and Western blot to detect AhR expression. Compared with the Control tissues group, the AhR mRNA expression in the RCC tissues group was significantly increased (**Figure 1A**). AhR protein expression was increased in both the cytoplasm and the nucleus (**Figure 1B**). It showed that AhR expression was abnormally increased in RCC. RCC was often accompanied by EMT conversion (16). We next detected the expression of E-cadherin, N-cadherin, and Vimentin related to EMT. Compared with the Control tissues group, E-cadherin expression in the RCC tissues group was inhibited, but N-cadherin and Vimentin expressions were significantly up-regulated (**Figures 1C,D**). It showed that EMT accompanied the RCC patients, and AhR expression was abnormal.

TABLE 1 | Characteristics of patients with RCC.

Characteristics	Total (n = 10)
Sex, *n*	
Men	6
Women	4
Age at enrollment, years, *n*	
<60	8
≥60	2
Smoking history, *n*	
Yes	4
No	6
Cancer stage, *n*	
T1N0M0	10
Other	0

The Diversity of Gut Microbiota in RCC Changed

Next, we aim to explore whether RCC affected the gut microbiota of RCC patients. PCA analysis showed that the microbial community similarity of the clinical samples of the Control tissues group and the RCC tissues group was low (**Figure 2A**). Anosim analysis further helped obtain an R-value of 0.266, showing that the difference between groups was more significant than the difference within groups (**Figure 2B**). The OUT Venn diagram showed that the Control tissues group had 155 unique OUT numbers, the RCC tissues group had 819 unique OUT numbers, and the two groups had 134 OUT numbers in total (**Figure 2C**). Chao1, Shannon, and Simpson's indexes showed the difference between the two groups was significant (**Figure 2D**) (P < 0.05). The Rank-abundance curve indicated that the RCC tissues group curve had a larger range on the horizontal axis, and the species richness was higher (**Figure 2E**). The abundance bar graph showed a significant difference in species composition between the Control tissues group and RCC tissue group (**Figure 2F**). The heat map showed that compared with the Control tissues group, the abundance of *Bacteroides* and *Akkermansia* was increased significantly in RCC tissues group, while the abundance of *Blautia, Bifidobacterium*, and *Megamonas* was decreased significantly (**Figure 2G**). As shown above, the gut microbiota of RCC patients was imbalanced.

Tryptophan Metabolites From Gut Microbiota Was Related to RCC

The above experiments indicated that RCC could lead to gut microbiota disturbance. We detected tryptophan metabolites. First, we uploaded the metabolic data on the online website

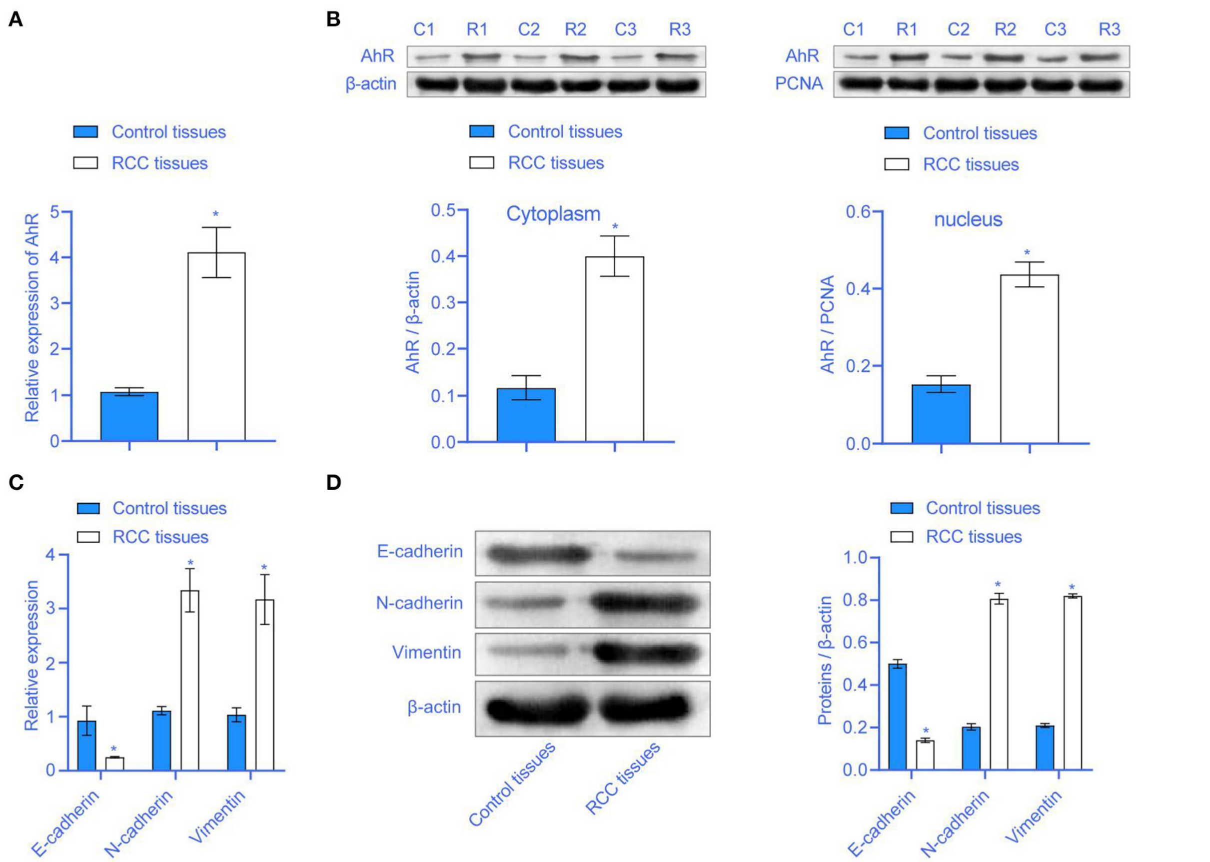

FIGURE 1 | The expression of AhR was higher in RCC. **(A)** The mRNA expression of AhR was higher in the RCC tissues group. **(B)** The expression of AhR protein in the cytoplasm and nucleus. **(C,D)** E-cadherin, N-cadherin, and Vimentin were abnormally expressed in RCC tissues group * compared with Control tissues group, $P < 0.05$.

(https://www.metaboanalyst.ca/MetaboAnalyst/ModuleView.xhtml) to get the heat map (**Figure 3A**). The heat map showed our nine tryptophan metabolites (L-Kynurenine, Tryptamine, Indole, 3-Methylindole, Indoxyl Sulfate potassium, salt, Indole-3-acetic acid, 3-Indolepropionic acid, and 3-Indoleacrylicacid Kynurenic acid) in different groups were different. Percentage of the distribution ratio of tryptophan metabolites in the Control tissues group and the RCC tissues group indicated meaningful differences (**Figure 3B**). Then, original data were concluded. 3-Indoleacrylicacid, Indoxyl Sulfate potassium salt, and 3-Methylindole were significantly reduced (**Figure 3C**). The Spearman's rank correlation was performed to analyze the correlation between the top 20 gut microbiota and nine tryptophan metabolites. The results showed that L-Kynurenine was negatively correlated with *Agathobacter*. Tryptamine was negatively correlated with *Escherichia-Shigella*. Indole was positively correlated with *Tyzzerella_3*. 3-Methylindole was positively correlated with *Romboutsia, Bifidobacterium*, and *[Ruminococcus]_torques_group*. Indoxyl Sulfate potassium salt was positively correlated with Subdoligranulum and *[Ruminococcus]_torques_groups.* Indole-3-acetic acid was positively correlated with *Romboutsia, Blautia, Bifidobacterium*, and *[Ruminococcus]_torques_group*. Indole-3-acetic acid was negatively correlated with *Bacteroides* and *Akkermansia*. 3-Indolepropionic acid was negatively correlated with *Roseburia*, *Prevotella_9, and Megamonas*. 3-Indoleacrylicacid was positively correlated with *Blautia*. 3-Indoleacrylicacid was negatively correlated with *Akkermansia*. *Kynurenic acid* was negatively correlated with *Prevotella_9* and *Akkermansia*. The above results indicated that gut microbiota imbalance in RCC patients might lead to tryptophan metabolites disorders (**Figure 3D**). Next, we analyzed the correlation between the tryptophan metabolites and AhR, E-cadherin, N-cadherin, and Vimentin. The results revealed AhR was significantly negatively correlated with L-Kynurenine. E-cadherin was significantly positively correlated with 3-Indolepropionic acid (**Figure 3E**). The above indicated that the disturbance of tryptophan metabolites from gut microbiota was related to the abnormal expression of EMT and AhR in RCC.

Kyn Could Activate AhR to Inhibit 786-O Cells Apoptosis

To further explore the effect of tryptophan metabolites on RCC, we inhibited AhR. We treated 786-O cells with different

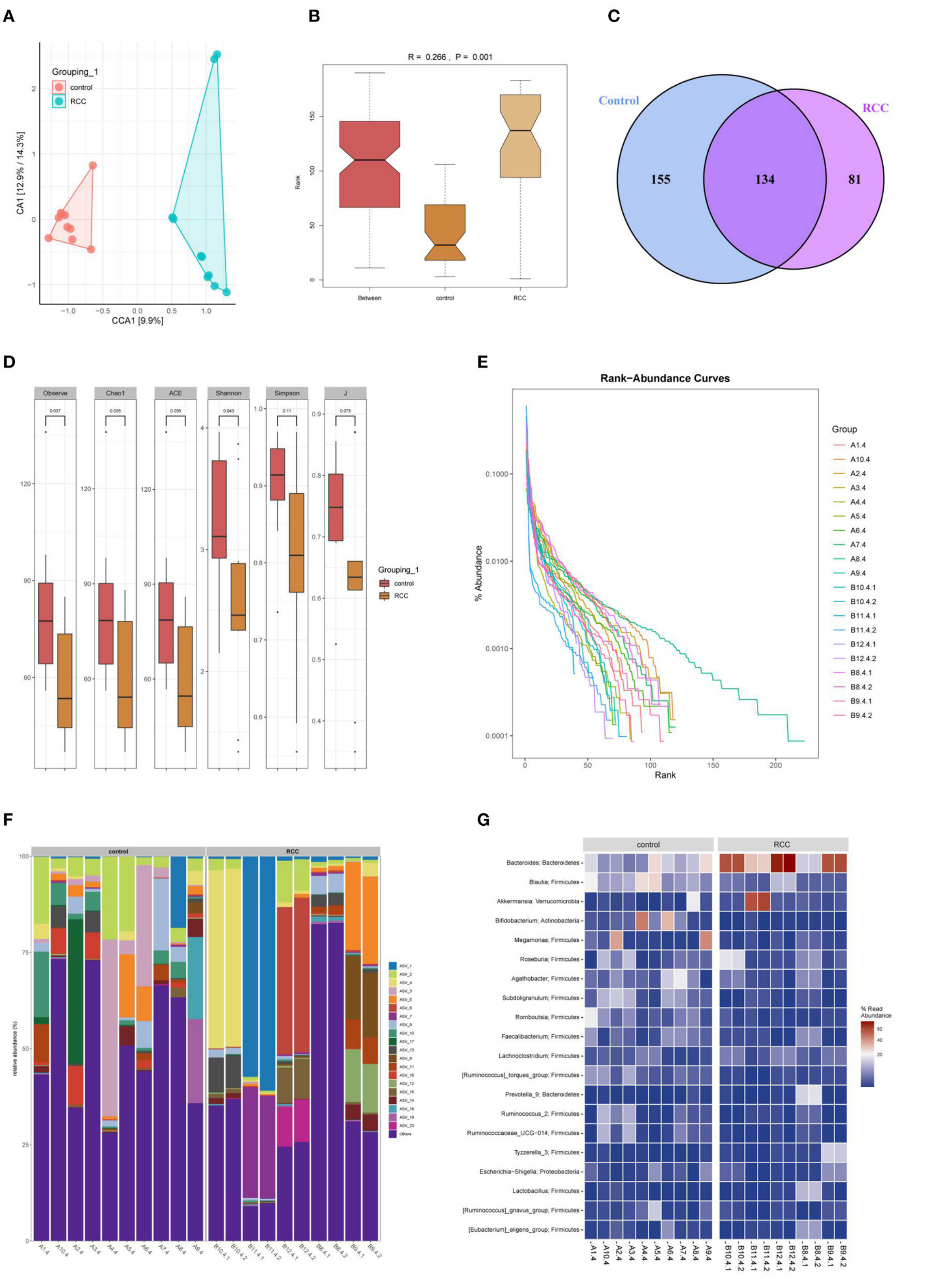

FIGURE 2 | Gut microbiota imbalance caused by RCC. **(A)** The similarity between the Control tissues and RCC tissues groups. **(B)** The difference between the two groups. **(C)** OUT Venn diagram. **(D)** Box chart. **(E)** Rank-abundance curve. **(F)** Histogram of the distribution of phylum species. **(G)** Heat map of phylum-species distribution.

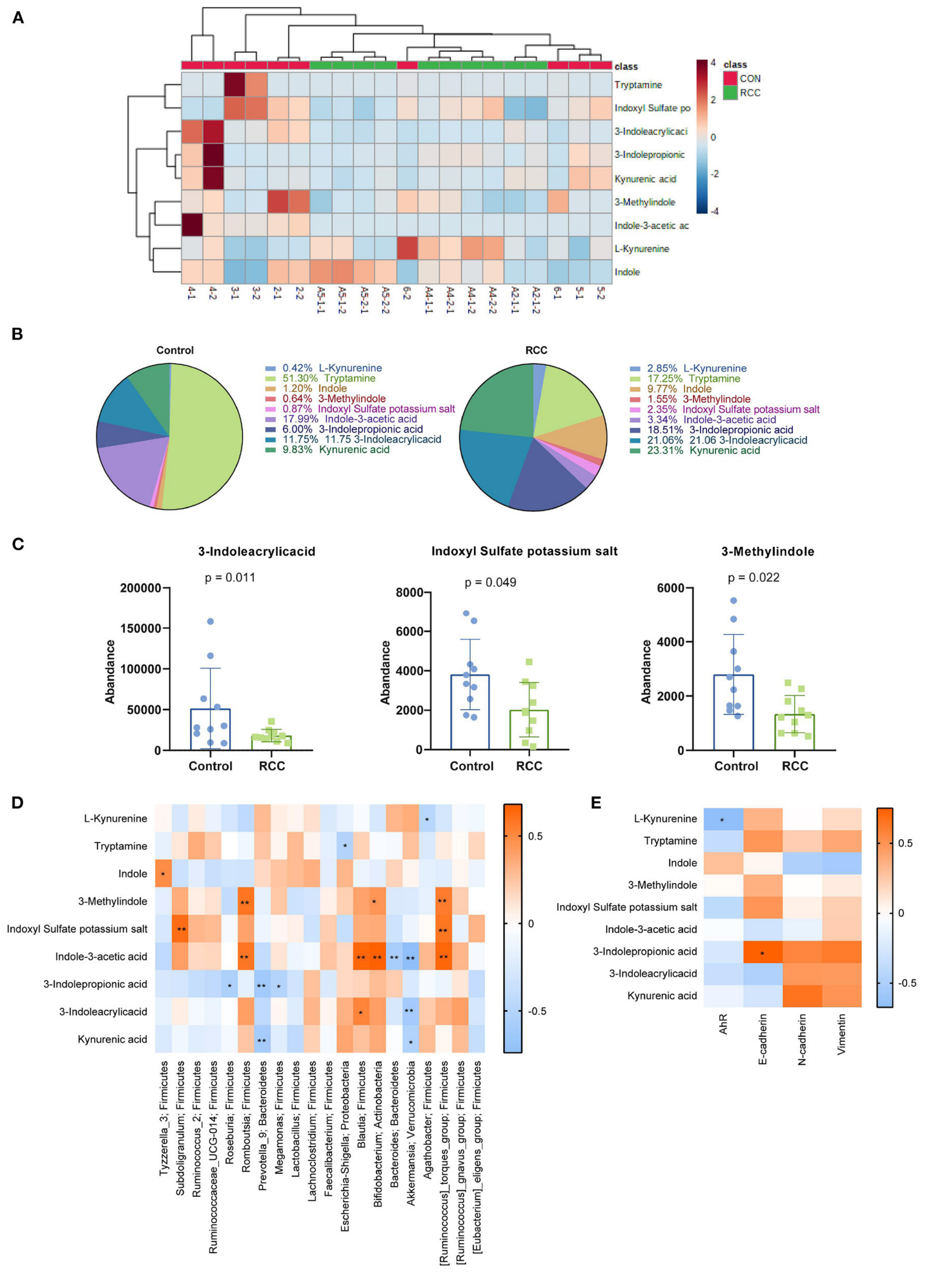

FIGURE 3 | The content of Kyn was high in RCC. **(A)** Heat map of metabolites (2-1, 2-2, 3-1, 3-2, 4-1, 4-2.5-1, 5-2, 6-1, and 6-2 belong to control group, A2-1-1, A2-1-2, A4-1-1, A4-1-2, A4-2-1, A4-2-2, A5-1-1, A5-1-2, A5-2-1, and A5-2-2 belong to RCC group). **(B)** Percentage of nine tryptophan metabolites. **(C)** Three metabolites with reduced content in RCC. **(D)** The relationship between 9 tryptophan metabolites and the top 20 gut microbiota. **(E)** The correlation between the tryptophan metabolites and AhR, E-cadherin, N-cadherin, and Vimentin.

concentrations of Kyn. The immunofluorescence results showed that Kyn could activate AhR in 786-O cells (**Figure 4A**). Cell viability assay showed that 786-O cells viability was increased in Low-Kyn and High-Kyn groups compared with the Control group. Compared with the AhR antagonist group, the 786-O cells viability in the Low-Kyn + AhR antagonist and High-Kyn + AhR antagonist groups was increased (**Figure 4B**). Then, we checked the cell cycle and cell apoptosis. Kyn was added to treat 786-O cells, and the results suggested that the cells number arrested in the G1/G2 phase decreased, and the cells number in the S phase increased. The AhR of 786-O cells was inhibited. Then Kyn was added to treat 786-O cells. The cells number arrested in the G1/G2 phase was also significantly reduced, and cells number in the S phase was increased substantially (**Figure 4C**). It indicated that Kyn could regulate the normal life cycle of 786-O cells. Flow cytometry was used to measure the 786-O cells apoptosis (**Figure 4D**). The results suggested that Kyn could effectively inhibit 786-O cells apoptosis. In summary, Kyn could activate AhR to inhibit 786-O cells apoptosis.

Kyn Could Promote 786-O Cells Migration and Invasion by Activating AhR

The above experimental results indicated that Kyn could inhibit the 786-O cells apoptosis. Next, we tested whether Kyn could affect the invasion and EMT process of 786-O cells. Compared with the Control group, 786-O cells migration and invasion ability in the Low-Kyn and High-Kyn groups was increased. Compared with the AhR antagonist group, 786-O cells migration and invasion ability in the Low-Kyn + AhR antagonist and High-Kyn + AhR antagonist groups were increased. It suggested that Kyn could promote the 786-O cells migration and invasion (**Figures 5A,B**). Finally, qRT-PCR and Western blot were used to detect the expression of E-cadherin, N-cadherin, and Vimentin related to EMT genes. Kyn was added to treat 786-O cells. The E-cadherin expression in 786-O cells was inhibited, but N-cadherin and Vimentin expressions were significantly up-regulated (**Figure 5C**). In short, Kyn could activate AhR to promote the migration, invasion, and EMT process of 786-O cells.

MATERIALS AND METHODS

Clinical Sample Collection

We collected 10 RCC tissues samples and Control tissues (at least 5 cm from the tumor tissues) from the Xiangya hospital central south university. We also collected patient feces. These samples came from RCC patients after surgery. None of these patients received chemotherapy or radiotherapy before surgery. Patients with infectious diseases, autoimmune diseases, or multiple primary cancers were excluded. We also collected 10 normal human feces. Before the sample collection, all subjects did not receive antibiotics or similar drugs. The research was approved by the Ethics Association and related hospitals.

Cell Culture

Human RCC 786-O cells were cultured in a T25 cell culture flask (690175, Greiner Bio-One Vilvoorde, Belgium) supplemented with 100 U/ml penicillin. The cells were cultured in a 5% CO_2 medium containing 10% fetal bovine serum (FBS) (Gibco). The medium was replaced with a serum-free medium. 786-O cells were inoculated into a six-well culture plate and incubated for at least 12. The cells were grouped as the Control tissues group (786-O cells), the Low-Kyn group (786-O cells were cultured in 0.2 mmol/L Kyn for 24 h), the High-Kyn group (786-O cells were cultured in 2 mmol/L Kyn for 24 h), the AhR antagonist group (786-O cells were pretreated with DMF (3′, 4′-dimethoxyflavone) for 12 h), the Low-Kyn + AhR antagonist group (786-O cells were pretreated with DMF and cultured at 0.2 mmol/L Kyn), and the High-Kyn + AhR antagonist group (786-O cells were pretreated with DMF and cultured under two mmol/L Kyn) (17).

Bacterial 16S rRNA Data Processing and Analysis

We de-joined and filtered the raw data with low-quality. The representative sequence of each out was annotated. We have separated and filtered the low-quality raw data. We have annotated the representative sequence of each OTU. The random sampling method was adopted, and the OTU analysis was performed with the number of effective sequences drawn. The alpha diversity indexes were calculated. A dilution curve was constructed. We obtained the R-value by analyzing the distance matrix between samples. Finally, the composition and abundance of the gut microbiota were identified.

Liquid Chromatography-Tandem Mass Spectrometry (LC-MS/MS)

Fecal samples from all subjects were centrifuged at 1,150 g and 4°C for 10 min. Then the supernatant was further divided into 100 μl, put into the labeled tube and stored at −80°C before preparing for metabonomics analysis. Each bisection sample was separated from 300 μl cold acetonitrile, mixed and then swirled for 30 s before analysis. The mixture was deproteinized by centrifugation at 4°C (21,130 g, 30 min), and 1 μl of supernatant was injected into UPLC. The ion source parameters and scanning parameters were optimized.

Quantitative Real-Time PCR

About 0.02 g tissues in Trizol were put into a 1.5 ml centrifuge tube, and 1 ml of Trizol was added to the homogenizer to grind and homogenize thoroughly. About 500 μl of the cells in Trizol were placed in a 1.5 ml centrifuge tube. Fluorescence quantitative PCR (quantstudio1, Thermo, USA) was performed on a fluorescence quantitative PCR machine. The reaction conditions were pre-denaturation at 95°C for 10 min, denaturation at 94°C for 15 s, and annealing at 60°C for 30 s, a total of 40 cycles. The internal reference primer was β-actin, and the primer sequence was shown in **Table 2**.

Western Blot

We cut 0.025 g tissues, and then washed the tissues with ice-cold PBS. We added 300 μl RIPA lysate and ground the tissues repeatedly in the biological sample homogenizer until no tissue masses were visible. For primary antibodies,

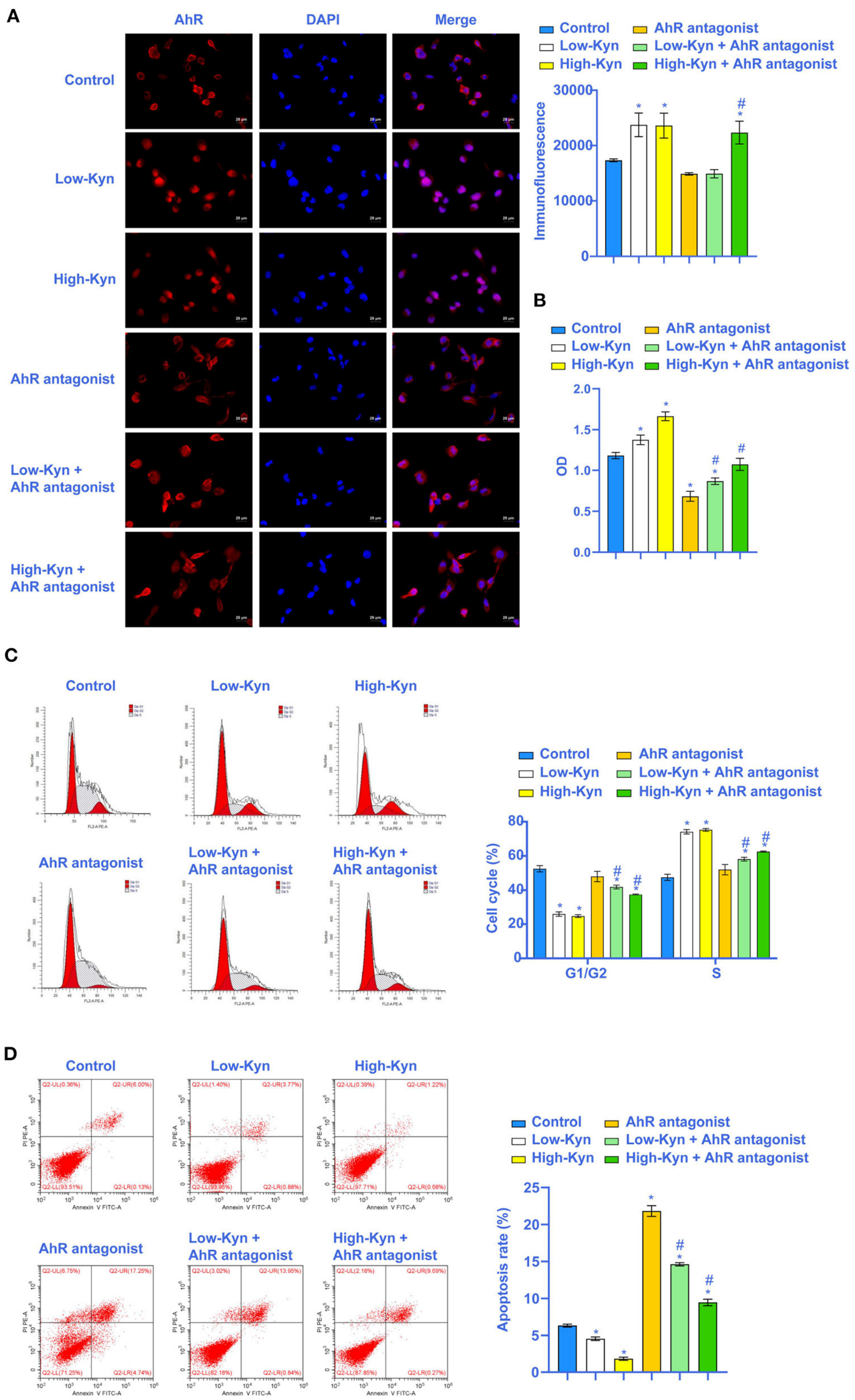

FIGURE 4 | Kyn could inhibit 786-O cells apoptosis. **(A)** AhR was activated by Kyn. **(B)** CCK-8 assay was used to measure the cell vitality. **(C)** Kyn could stabilize the 786-O cells cycle (×200, Scale bar = 50 μm). **(D)** Flow cytometry was used to measure the apoptosis rate of 786-O cells. * Compared with the Control group, $P < 0.05$. # Compared with the AhR antagonist group, $P < 0.05$.

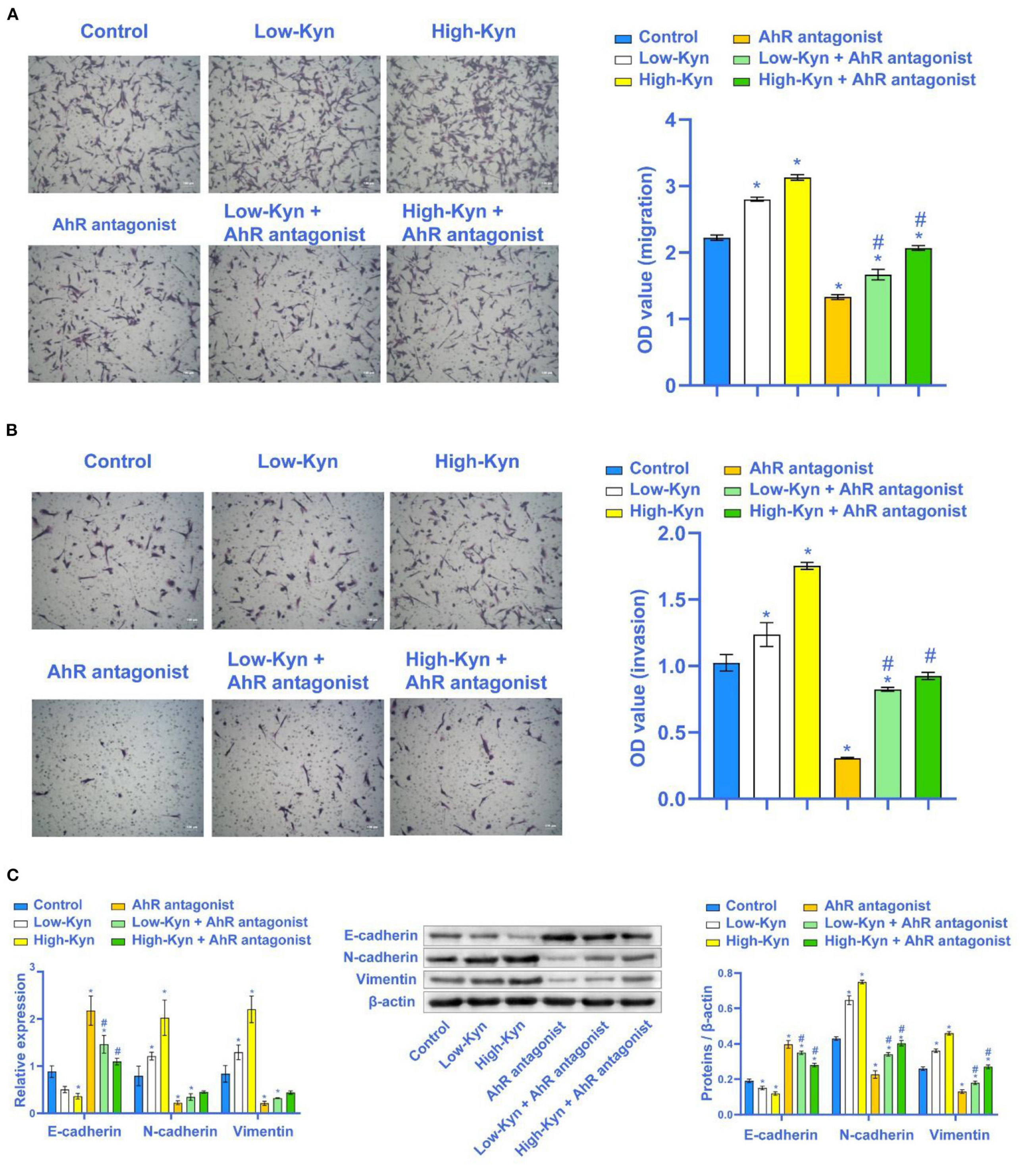

FIGURE 5 | Kyn could promote the migration and invasion of 786-O cells. **(A)** and **(B)** Transwell was used to detect the migration and invasion ability of 786-O cells (×100, Scale bar = 100 μm). **(C)** E-cadherin was inhibited by Kyn. N-cadherin and Vimentin were activated by Kyn. * Compared with the Control group, $P < 0.05$. # Compared with the AhR antagonist group, $P < 0.05$.

we used rabbit anti-AhR (1:1,000, #83200, CST), rabbit anti-E-cadherin (1:5,000, 20874-1-AP, Proteintech), mouse anti-N-cadherin (1:6,000, 66219-1-Ig, Proteintech), rabbit anti-Vimentin (1:5,000, ab92547, Abcam), rabbit anti-PCNA (1:5,000, 10205-2-AP, Proteintech) and mouse anti-β-actin (1:5,000, 60008-1-Ig, Proteintech). We rinsed the membrane three times with TBST for

TABLE 2 | Primer sequences.

Gene	Genbank number	Sequences (5′–3′)
E-cadherin	NG_008021	F: ATTTTTCCCTCGACACCCGAT
		R: TCCCAGGCGTAGACCAAGA
N-cadherin	NC_000018	F: GGGAAATGGAAACTTGATGGCA
		R: TGGAAAGCTTCTCACGGCAT
Vimentin	NG_012413	F: CCCTTGACATTGAGATTGCCACC
		R: ACCGTCTTAATCAGAAGTGTCCT
AhR	NC_000007	F: CAACAGCAACAGTCCTTGGC
		R: GTTGCTGTGGCTCCACTACT
β-actin	NG_007992	F: ACCCTGAAGTACCCCATCGAG
		R: AGCACAGCCTGGATAGCAAC

10 min each time. Then we incubated secondary antibodies HRP-conjugated Affinipure Goat Anti-Mouse IgG (H + L) (1:5,000, SA00001-1, Proteintech) and HRP-conjugated Affinipure Goat Anti-Rabbit IgG (H+L) (1:6,000, SA00001-2, Proteintech). The film was immersed in SuperECL Plus (K-12045-D50, Advansta, USA) for luminescence development.

Cell Counting Kit-8 Assay

We used the CCK-8 kit (NU679, Dojindo Molecular Technologies, Inc., Japan) to analyze the cell viability. The cells were taken in a logarithmic growth phase and were digested with trypsin. At the density of 5×10^3 cells/well, the cells were inoculated into a 96-well plate with 100 μl/well. Ten microliter CCK8 solution of complete culture medium was co-cultured with cells in each well. The absorbance (OD) value at 450 nm was analyzed by a Bio-Tek microplate reader after incubation with 5 % CO_2 at 37°C for 4 h.

Transwell Assay

We diluted Matrigel with 100 μl cold, serum-free DMEM medium per well. Then we placed 500 μl complete medium containing 10% FBS in the lower chamber. The cells were digested with trypsin to form a single cell. We put the upper chamber into a new hole with PBS. We used 0.1% crystal violet for 5 min.

Flow Cytometry

Cells were collected with trypsin digestion solution (c0201, Beyotime, China) without EDTA. We collected about 2×10^5 cells. Five hundred microliter of binding buffer was added to the cell suspension. We added 5 μl annexin V-FITC (kga108, keygen, China) and mixed well. Finally, we added 5 μl Propidium Iodide (PI) (mb2920, Meilunbio, China) into the mixture and mixed them well. Flow cytometry was used to observe the changes within 1 h.

Immunofluorescence

The slices were cleaned 2∼3 times with PBS. Then the slices were fixed with 4% paraformaldehyde for 30 min. The primary antibody AhR was dripped onto the slices at 4°C overnight. The second antibody was incubated by dropping 50–100 μl anti-rabbit IgG labeled fluorescent antibody. Then the slices were incubated at 37°C for 90 min. Finally, the slices were washed with PBS 3 times, 5 min each. DAPI solution was used to stain the nucleus at 37°C for 10 min. Then PBS was washed 3 times, 5 min each. The slices were placed under a fluorescent microscope for observation.

Cell Cycle Assay

We took out the fixed sample. One microliter of pre-cooled PBS was added to the sample for cell suspension. We added 150 μl PI working solution into the cell solution and stained it at 4°C for 30 min. PI was excited by 488 nm argon ion laser and received by 630 nm pass filter. 1×10^4 cells were collected by FSC/SSC scatterplot. Adhesion cells and fragments were excluded by gating technique. The percentage of cell cycle on PI fluorescence histogram was analyzed.

Statistical Analysis

All experimental data were analyzed by GraphPad 8.0 software. Measurement data were expressed as mean ± standard deviation. The unpaired *T*-test was used between the two groups conforming to the normal distribution. One-way analysis of variance (ANOVA) was used for comparison between multiple groups. $P < 0.05$ was considered statistically significant.

DISCUSSION

This study found that RCC has a certain internal relationship with gut microbiota and tryptophan metabolite. Through cell experiments, we found that Kyn may promote EMT by activating AhR, further promote RCC cells migration and invasion and inhibit RCC cells apoptosis.

The gut microbiota is closely related to cancer (18). We found that the composition of gut microbiota in RCC patients was changed significantly. *Bacteroides* and *Akkermansia* were increased significantly, while *Blautia*, *Bifidobacterium*, and *Megamonas* were decreased significantly. Recent studies have shown that gut microbiota composition affects the success of immune checkpoint blocking therapy for RCC (19). Clinical studies have shown that patients treated with vascular endothelial growth factor tyrosine kinase inhibitor (VEGF-TKIs) combined with mRCC have higher *Bacteroides* and lower *Prevotella* (20). These results indicated that the gut microbiota composition changes were related to the occurrence and development of RCC.

Tryptophan catabolism has become a critical metabolic regulation factor for tumor progression (21). Different cancers prognosis showed that an essential indicator of tryptophan metabolism is serum KTR. When the serum KTR increased, tryptophan was metabolizing through indoleamine 2,3-dioxygenase 1 (IDO1) or tryptophan 2,3 -Dioxygenase (TDO) through the Kyn pathway. At the same time, other researchers have reported higher KTR in the serum of patients with advanced RCC or resistance to immune checkpoint inhibitor (22, 23). The composition of the gut microbiota determines several tryptophan metabolites because they are catabolism products of gut microbiota. These tryptophan-derived microbial catabolites are important signaling molecules in the host and the microorganisms (24, 25). Targeted metabolomics studies have shown that RCC patients have elevated Kyn pathway metabolites (26). Our experiment revealed that the distribution of tryptophan metabolites in gut microbiota changed significantly in RCC. Through correlation analysis, it was found that the tryptophan metabolites were correlated considerably with *Agathobacter*, *Escherichia-Shigella*, *Romboutsia*, and *Akkermansia*, etc. Studies have shown that microorganisms mediate gut Trp metabolism changes and participate in the occurrence of cancer (27). This was consistent with our research. Through correlation analysis, we also found that tryptophan metabolites of gut microbiota were significantly correlated with AhR and E-cadherin expressions in RCC. These results indicated that the Kyn metabolic pathway of the gut microbiota might be involved in the pathogenetic progress of RCC. This experiment assessed that the Kyn pathway was operable and could be used as a therapeutic target for RCC.

Kyn is the main product of the tryptophan metabolic pathway catalyzed by TDO2 and IDO in tumor cells. Kyn proved that AhR could be activated. AhR in an autocrine/paracrine manner can inhibit the anti-tumor immune response and promote tumor cell survival and movement (28). AhR was identified as a ligand-activated transcription factor of the basic helix-loop-helix (bHLH) Per-Arnt-Sim (PAS) family, and it played an important role in a wide range of physiological and pathological conditions (29–31). AhR participates in the induction of Slug expression, and this process inhibits E-cadherin expression. MMPs expression is also a target of the AhR pathway. Odibenzo-p-dioxin (TCDD) exposure up-regulated the expression and activity of MMP9 in a variety of malignant tumors, including melanoma cells, urothelial cancer cells, prostate cancer cells, and gastric cancer cells (32). AhR is involved in the induction of EMT by PCBs in HCC cells (33). In this study, we aimed to study the influence of AhR on the progress of EMT in RCC. Our results showed that AhR was highly expressed in RCC. In addition, Kyn could promote 786-O cells migration and invasion and inhibit 786-O cells apoptosis by activating AhR.

Fecal microorganisms and metabolites are often affected by diet (34). In this study, the subjects were not given a standardized diet like other studies (3) but kept the original eating habits, which is the limitation of this study. However, non-invasive research can be overcome by expanding the sample size. In addition, the effect of tryptophan metabolites of gut microbiota on the AhR activation pathway of the host itself was complex, which may require more evidence to prove its specific regulatory mechanism. Based on these factors, we will expand the sample size in future research and explore the influence of tryptophan metabolites of gut microbiota on RCC in combination with clinical and animal experiments.

In conclusion, through the research of this subject, we have verified that the RCC gut microbiota metabolism is disordered, and the Kyn metabolism is increased. *In vitro* experiments further confirmed that Kyn could promote 786-O cells migration and invasion and the progress of EMT and inhibit 786-O cells apoptosis by activating AhR. Our design clarified that the gut microbiota could activate AhR through its tryptophan metabolism to mediate the metastasis of RCC.

DATA AVAILABILITY STATEMENT

The original contributions presented in the study are publicly available. This data can be found here: https://www.ncbi.nlm.nih.gov/sra/PRJNA735071.

ETHICS STATEMENT

All experiments were performed according to the guidelines set by the Medical Ethics Committee of Xiangya Hospital of Central South University (202105187), Changsha, Hunan, China. Written informed consent was obtained from all participates. The patients/participants provided their written informed consent to participate in this study.

AUTHOR CONTRIBUTIONS

GD, XC, and YH designed the study, performed the research, analyzed data, and wrote the paper. All authors contributed to the article and approved the submitted version.

FUNDING

This work was supported by the National Natural Science Foundation of Hunan (2020JJ5895).

REFERENCES

1. Siegel RL, Miller KD. Cancer Statistics, 2017. *CA Cancer J Clin.* (2017) 67:7–30. doi: 10.3322/caac.21387
2. Adashek JJ, Salgia MM, Posadas EM, Figlin RA, Gong J. Role of biomarkers in prediction of response to therapeutics in metastatic renal-cell carcinoma. *Clin Genitourin Cancer.* (2019) 17:e454–60. doi: 10.1016/j.clgc.2019.01.004
3. Dizman N, Hsu J, Bergerot PG, Gillece JD, Folkerts M, Reining L, et al. Randomized trial assessing impact of probiotic supplementation on gut microbiome and clinical outcome from targeted therapy in metastatic renal cell carcinoma. *Cancer Med.* (2021) 10:79–86. doi: 10.1002/cam4.3569
4. Liu J-R, Miao H. Gut microbiota-derived tryptophan metabolism mediates renal fibrosis by aryl hydrocarbon receptor signaling activation. *Cell Mol Life Sci.* (2021) 78:909–22. doi: 10.1007/s00018-020-03645-1
5. Trott JF, Kim J. Inhibiting tryptophan metabolism enhances interferon therapy in kidney cancer. *Oncotarget.* (2016) 7:66540–57. doi: 10.18632/oncotarget.11658
6. Dong F, Hao F, Murray IA, Smith PB, Koo I, Tindall AM, et al. Intestinal microbiota-derived tryptophan metabolites are predictive of Ah receptor activity. *Gut Microbes.* (2020) 12:1–24. doi: 10.1080/19490976.2020.1788899
7. Dong F, Perdew GH. The aryl hydrocarbon receptor as a mediator of host-microbiota interplay. *Gut Microbes.* (2020) 12:1859812. doi: 10.1080/19490976.2020.1859812
8. Gao J, Xu K, Liu H, Liu G, Bai M, Peng C, et al. Impact of the gut microbiota on intestinal immunity mediated by tryptophan metabolism. *Front Cell Infect Microbiol.* (2018) 8:13. doi: 10.3389/fcimb.2018.00013

9. Rothhammer V. Type I interferons and microbial metabolites of tryptophan modulate astrocyte activity and CNS inflammation via the aryl hydrocarbon receptor. *Nat Med.* (2016) 22:586–97. doi: 10.1038/nm.4106
10. Zhao H, Lin Chen, Yang T, Feng Y-L, Vaziri ND, Liu B-L, et al. Aryl hydrocarbon receptor activation mediates kidney disease and renal cell carcinoma. *J Transl Med.* (2019) 17:302. doi: 10.1186/s12967-019-2054-5
11. Sadik A, Somarribas Patterson LF, Öztürk S, Mohapatra SR, Panitz V, Secker PF, et al. IL4I1 Is a metabolic immune checkpoint that activates the AHR and promotes tumor progression. *Cell.* (2020) 182:1252–70.e34. doi: 10.1016/j.cell.2020.07.038
12. Labadie BW, Bao R. Reimagining IDO pathway inhibition in cancer immunotherapy via downstream focus on the tryptophan-kynurenine-aryl hydrocarbon axis. *Clin Cancer Res.* (2019) 25:1462–71. doi: 10.1158/1078-0432.CCR-18-2882
13. Giannelli G. Role of epithelial to mesenchymal transition in hepatocellular carcinoma. *J Hepatol.* (2016) 64:798–808. doi: 10.1016/j.jhep.2016.05.007
14. Yang S, Liu Y. FOXP3 promotes tumor growth and metastasis by activating Wnt/β-catenin signaling pathway and EMT in non-small cell lung cancer. *Mol Cancer.* (2017) 16:124. doi: 10.1186/s12943-017-0700-1
15. Feng S. Role of aryl hydrocarbon receptor in cancer. *Biochim Biophys Acta.* (2013) 1836:197–210. doi: 10.1016/j.bbcan.2013.05.001
16. Liu H, Hu G. circPTCH1 promotes invasion and metastasis in renal cell carcinoma via regulating miR-485-5p/MMP14 axis. *Theranostics.* (2020) 10:10791–807. doi: 10.7150/thno.47239
17. Eisa NH, Reddy SV. Kynurenine promotes RANKL-induced osteoclastogenesis in vitro by activating the aryl hydrocarbon receptor pathway. *Int J Mol Sci.* (2020) 21:7931. doi: 10.3390/ijms21217931
18. Baffy G. Gut microbiota and cancer of the host: colliding interests. *Adv Exp Med Biol.* (2020) 1219:93–107. doi: 10.1007/978-3-030-34025-4_5
19. Derosa L, Routy B, Fidelle M, Iebba V, Alla L, Pasolli E, et al. Gut bacteria composition drives primary resistance to cancer immunotherapy in renal cell carcinoma patients. *Eur Urol.* (2020) 78:195–206. doi: 10.1016/j.eururo.2020.04.044
20. Pal SK, Li SM, Wu X, Qin H, Kortylewski M, Hsu J, et al. Stool bacteriomic profiling in patients with metastatic renal cell carcinoma receiving vascular endothelial growth factor-tyrosine kinase inhibitors. *Clin Cancer Res.* (2015) 21:5286–93. doi: 10.1158/1078-0432.CCR-15-0724
21. Opitz CA, Somarribas Patterson LF, Mohapatra SR, Dewi DL, Sadik A, Platten M, et al. The therapeutic potential of targeting tryptophan catabolism in cancer. *Br J Cancer.* (2020) 122:30–44. doi: 10.1038/s41416-019-0664-6
22. Lucarelli G, Rutigliano M. Activation of the kynurenine pathway predicts poor outcome in patients with clear cell renal cell carcinoma. *Urol Oncol.* (2017) 35:461.e15–461.e27. doi: 10.1016/j.urolonc.2017.02.011
23. Li H, Bullock K, Gurjao C, Braun D, Shukla SA, Bossé D, et al. Metabolomic adaptations and correlates of survival to immune checkpoint blockade. *Nat Commun.* (2019) 10:4346. doi: 10.1038/s41467-019-12361-9
24. Hsu C-N, Tain YL. Developmental programming and reprogramming of hypertension and kidney disease: impact of tryptophan metabolism. *Int J Mol Sci.* (2020) 21:8705. doi: 10.3390/ijms21228705
25. Sumitomo M, Takahara K. Tryptophan 2,3-dioxygenase in tumor cells is associated with resistance to immunotherapy in renal cell carcinoma. *Cancer Sci.* (2021) 112:1038–47. doi: 10.1111/cas.14797
26. Kim K. Urine metabolomic analysis identifies potential biomarkers and pathogenic pathways in kidney cancer. *OMICS.* (2011) 15:293–303. doi: 10.1089/omi.2010.0094
27. Sun XZ, Zhao D-Y, Zhou Y-C, Wang Q-Q, Qin G, Yao S-K. Alteration of fecal tryptophan metabolism correlates with shifted microbiota and may be involved in pathogenesis of colorectal cancer. *World J Gastroenterol.* (2020) 26:7173–90. doi: 10.3748/wjg.v26.i45.7173
28. Opitz CA. An endogenous tumour-promoting ligand of the human aryl hydrocarbon receptor. *Nature.* (2011) 478:197–203. doi: 10.1038/nature10491
29. Zhou L. AHR Function in lymphocytes: emerging concepts. *Trends Immunol.* (2016) 37:17–31. doi: 10.1016/j.it.2015.11.007
30. Pilotte L. Reversal of tumoral immune resistance by inhibition of tryptophan 2,3-dioxygenase. *Proc Natl Acad Sci USA.* (2012) 109:2497–502. doi: 10.1073/pnas.1113873109
31. Song L, Guo L. Molecular mechanisms of 3,3'4,4',5-pentachlorobiphenyl-induced epithelial-mesenchymal transition in human hepatocellular carcinoma cells. *Toxicol Appl Pharmacol.* (2017) 322:75–88. doi: 10.1016/j.taap.2017.03.003
32. Li L, Wang T. TDO2 promotes the EMT of hepatocellular carcinoma through Kyn-AhR pathway. *Front Oncol.* (2020) 10:562823. doi: 10.3389/fonc.2020.562823
33. Venkateswaran N. MYC promotes tryptophan uptake and metabolism by the kynurenine pathway in colon cancer. *Genes.* (2019) 33:1236–51. doi: 10.1101/gad.327056.119
34. De Filippis F, Pellegrini N, Vannini L, Jeffery IB, La Storia A, Laghi L, et al. High-level adherence to a Mediterranean diet beneficially impacts the gut microbiota and associated metabolome. *Gut.* (2016) 65:1812–21. doi: 10.1136/gutjnl-2015-309957

Conflict of Interest: The authors declare that the research was conducted in the absence of any commercial or financial relationships that could be construed as a potential conflict of interest.

Publisher's Note: All claims expressed in this article are solely those of the authors and do not necessarily represent those of their affiliated organizations, or those of the publisher, the editors and the reviewers. Any product that may be evaluated in this article, or claim that may be made by its manufacturer, is not guaranteed or endorsed by the publisher.

frontiers in Nutrition

ORIGINAL RESEARCH
published: 19 August 2021
doi: 10.3389/fnut.2021.713256

Effects of *Lactococcus lactis* on the Intestinal Functions in Weaning Piglets

Dongming Yu[1,2], Yaoyao Xia[1], Liangpeng Ge[2]*, Bie Tan[1,3,4,5]* and Shuai Chen[1,3,4,5]*

[1] Guangdong Laboratory of Lingnan Modern Agriculture, College of Animal Science, South China Agricultural University, Guangzhou, China, [2] Chongqing Academy of Animal Sciences, Chongqing, China, [3] Laboratory of Animal Nutritional Physiology and Metabolic Process, Key Laboratory of Agro-Ecological Processes in Subtropical Region, Changsha, China, [4] National Engineering Laboratory for Pollution Control and Waste Utilization in Livestock and Poultry Production, Changsha, China, [5] Institute of Subtropical Agriculture, Chinese Academy of Sciences, Changsha, China

Post-weaning diarrhea of piglets is associated with gut microbiota dysbiosis and intestinal pathogen infection. Recent studies have shown that *Lactococcus lactis* (*L.lactis*) could help suppress pathogen infection. This study aimed to investigate the effects of *L.lactis* on various factors related to growth and immunity in weaning piglets. The results showed that *L.lactis* improved the growth performance, regulated the amino acid profile (for example, increasing serum tryptophan and ileal mucosal cystine) and the intestinal GABAergic system (including inhibiting ileal gene expression of SLC6A13, GABAAρ1, π, θ, and γ1, and promoting ileal GABAAα5 expression). *L.lactis* also modulated intestinal immunity by promoting jejunal interleukin 17, 18, 22, ileal toll-like receptor 2, 5, 6, and myeloid differentiation primary response protein 88 gene expression while inhibiting jejunal interferon-γ and ileal interleukin 22 expressions. *L.lactis* highly affected the intestinal microbiota by improving the beta diversity of gut microbiota and the relative abundance of *Halomonas* and *Shewanella*. In conclusion, *L.lactis* improved the growth performance and regulated amino acid profiles, intestinal immunity and microbiota in weaning piglets.

Keywords: *Lactococcus lactis*, amino acid, weaning piglet, intestinal immunity, gut microbiota

OPEN ACCESS

Edited by:
Yong Su,
Nanjing Agricultural University, China

Reviewed by:
Mingliang Jin,
Northwestern Polytechnical University, China
Shusong Wu,
Hunan Agricultural University, China

Correspondence:
Liangpeng Ge
geliangpeng1982@163.com
Bie Tan
bietan@isa.ac.cn
Shuai Chen
chenshuai@mail.com

Specialty section:
This article was submitted to Nutrition and Microbes, a section of the journal Frontiers in Nutrition

Received: *22 May 2021*
Accepted: *19 July 2021*
Published: *19 August 2021*

Citation:
Yu D, Xia Y, Ge L, Tan B and Chen S (2021) Effects of Lactococcus lactis on the Intestinal Functions in Weaning Piglets. Front. Nutr. 8:713256. doi: 10.3389/fnut.2021.713256

INTRODUCTION

Weaning is the most critical phase in pig production and is generally associated with intestinal infections and diarrhea (1). The biggest challenge for weaning piglets is diarrhea caused by weaning stress and pathogen infection such as enterotoxigenic *Escherichia coli* (ETEC). As an active player in host physiological activities, the gut microbiota plays a vital role in modulating pathogen infection and diarrhea in piglets (2). Weaning changes the gut microbiota in humans, piglets, and cows (3–5), which can result in immune system less development, insufficiency of physiological function (6), and increased risk of pathogen infection (7). Thus, appropriate strategies in microbiology could be used to relieve the stress of weaning and prevent infections.

In the past, antibiotics were wildly used as feed additives to promote growth and prevent pathogens in animal production and disease treatment (8–10). However, the overuse of antibiotics resulted in serious public health problems, such as antibiotic resistance gene transfer and an increase in antibiotic-resistance bacteria. Thus, animal producers in many countries have reduced or eliminated the use of antibiotics in feed (11).

There is a great opportunity to develop new strategies for preventing intestinal pathogen infection in weaning piglets. Probiotics can prevent infections caused by pathogens such as *Clostridium difficile* (12, 13). However, the ability of probiotics to prevent infection varies (14). *Lactococcus lactis* (*L.lactis*) was recently reported to prevent cholera (15, 16). Our previous research showed that *L.lactis* regulated the intestinal immune reaction via gamma-aminobutyric acid (GABA) production and prevented pathogen infections in piglets (17, 18). These findings suggest that *L.lactis* has great potential to prevent intestinal infections in piglets.

The current study aimed to evaluate the modulatory role of *L.lactis* in growth performance, amino acid profile, intestinal immunity, and gut microbiota in piglets.

MATERIALS AND METHODS

Animals and Experiment Design

Fifteen healthy piglets (Duroc × Landrace × Landrace, aged 21 days) were purchased from Hunan New Wellful Co., Ltd (Changsha, China). After an adaption period of 3 days, piglets were randomly assigned to the control group ($n = 7$) and the *L.lactis* group ($n = 8$). This study shared the data of the control group with our previous research (19). The piglets in the *L.lactis* group were orally dosed with *L.lactis* ($2.0*10^9$ CFU/ml, 20 ml) on days 1 and 8. All piglets were fed a corn-and soybean meal-based diet (**Supplementary Table 1**), and other feedings and environmental control conditions were the same as in our previous study (19). Body weight and feed intake were monitored weekly throughout the experiment, and average daily gain (ADG), average daily feed intake (ADFI), and feed conversion ratio (FCR) were calculated. At the end of week 3, piglets were sacrificed after anesthesia.

The blood, jejunum, jejunal mucosa, ileum, ileal mucosa, colon and luminal content were collected immediately, snap-frozen in liquid nitrogen, and stored at −80°C until further processing. All animal experiment procedures were approved by the Animal Welfare Committee of the Institute of Subtropical Agriculture, Chinese Academy of Sciences (2016-4B).

Culture of *L.lactis*

L.lactis (ATCC 19435) was grown overnight in 5 ml of M17 medium (Thermo Fisher Scientific, Waltham, MA USA) broth at 37°C with gentle agitation (180 rpm/min). The next day, 3 ml of M17 medium was inoculated with 100 µl of the overnight culture for further amplification and culture.

Diarrhea Index and Counting of *E.coli*

The diarrhea index and diarrhea rate data of piglets were recorded daily according to the criterion of feces score (**Supplementary Table 2**). The *E.coli* loads in the jejunal mucosa, ileal mucosa, and colonic content were quantified by Maconkey Agar (Sigma-Aldrich, Burlington, United States) according to the previous work (17).

Free Amino Acids Analysis

According to our previous report (19), the ileal mucosa and serum amino acid levels were measured using high-performance liquid chromatography. Authentic standards (Sigma-Aldrich, Burlington, United States) were used to quantify the amino acids in the samples.

Gene Expression Analysis

Expression of the GABAergic system and immune-associated genes was analyzed by reverse transcriptase-polymerase chain reaction (RT-PCR), and primers (**Supplementary Table 3**) were selected according to our previous study (19). The samples were individually normalized to the housekeeping genes, β-actin (ACTB) and glyceraldehyde-3 phosphate dehydrogenase (GAPDH). The relative gene expression was calculated by formula $2^{-(\Delta\Delta CT)}$.

16S rDNA Sequencing With Illumina MiSeq Sequencing

We used 16S rDNA gene sequencing to analyze the V3–V4 region of ileal microbiota according to our previous study (19). The QIAGEN QIAamp DNA Stool Mini Kit (Qiagen, Hilden, NRW, Germany) was used to extract DNA from the ileal contents and Agarose gel electrophoresis was used to quantify the DNA. Sequencing libraries were then generated using the Ion Plus Fragment Library Kit (Thermo Fisher Scientific, Waltham, MA, USA), assessed on the Qubit® 2.0 Fluorometer (Thermo Fisher Scientific, Waltham, MA, USA), and sequenced on the Illumina MiSeq Sequencer. Under specific filtering conditions, the raw data were filtered to obtain high-quality clean reads according to the Cutadapt quality control process. Uparse software (Uparse v7.0.1001) was used for sequence analysis and operational taxonomic unit (OTU) clustering and the identity threshold was set to 97%. The species annotation was performed with the RDP Classifier (V2.2, Michigan State 14 University Board of Trustees, East Lansing MI) based on the GreenGene database. MUSCLE software (Version 3.8.31) was used for phylogenetic relationship analysis. Subsequently, we used R and QIIME software (V 1.7) on the normalized output data to analyze the alpha diversity, beta diversity, and environmental factor correlation (Spearman analysis). The FAPROTAX database was used for function prediction. Illumina MiSeq sequencing, processing of sequencing data, and bioinformatics analysis were performed by Beijing Novogene Bioinformatics Technology Co., Ltd. (Beijing, China).

Environmental Factor Correlation Analysis

According to the relative abundance at the phylum level, the top 28 taxa were used for correlation analysis with growth performance indicators, amino acid profiles, and intestinal immune factors.

Abbreviations: *L.lactis*, *Lactococcus lactis*; MyD88, myeloid differentiation primary response protein 88; ADFI, average daily feed intake; ADG, average daily weight gain; *E.coli*, *Escherichia coli*; ETEC, Enterotoxigenic *E.coli*; GABA, gamma-aminobutyric acid; GAD, glutamic acid decarboxylase; GAT, GABA transporter; SLC, solute carriers; IFN-γ, interferences-gamma; IL, interleukin; AHR, aryl hydrocarbon receptor; OTU, operational taxonomic unit; RT-PCR, reverse transcription-polymerase chain reaction; SEM, standard error of the mean; TNF-α, tumor necrosis factor-alpha; DSS, dextran sulfate sodium.

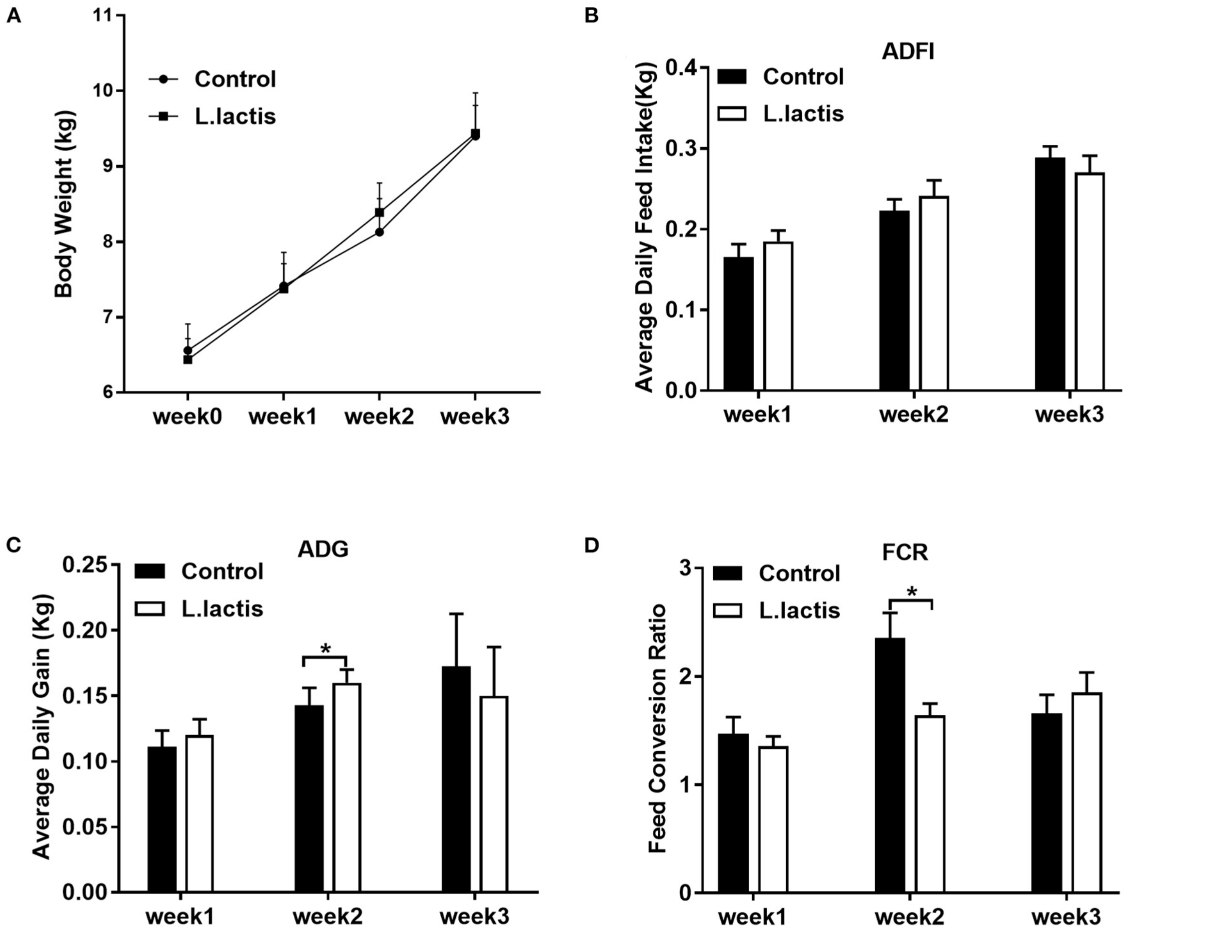

FIGURE 1 | Effects of *L.lactis* on piglet growth performance. **(A)** Body weight; **(B)** average daily feed intake; **(C)** average daily gain; **(D)** feed conversion ratio (FCR). An unpaired *t*-test was used for analyzing the data (mean ± SEM). *$P < 0.05$.

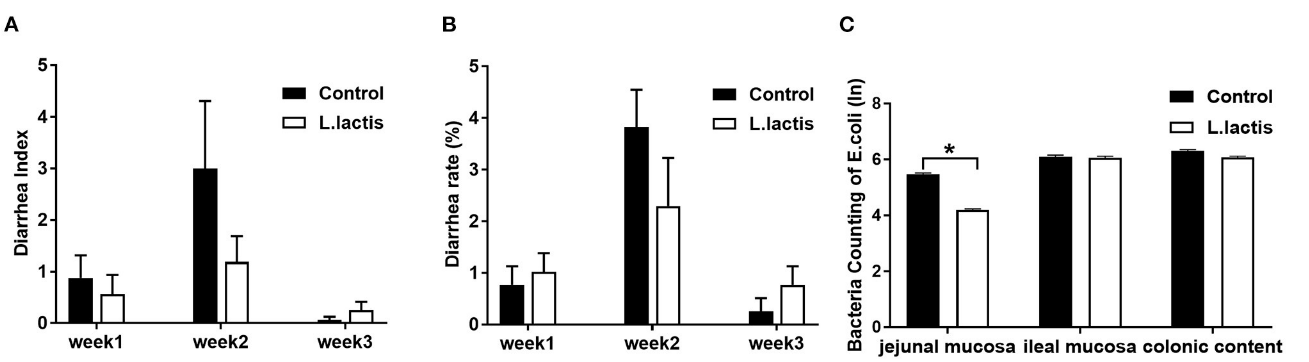

FIGURE 2 | Effects of *L.lactis* on diarrhea and counting of *E.coli*. **(A)** Diarrhea index; **(B)** diarrhea rate; **(C)** *E.coli* count. Wilcoxon rank-sum test was used to analyze the data (mean ± SEM). *$P < 0.05$.

Statistical Analyses

The results were expressed as the mean ± standard error of the mean (SEM). All data were pre-processed with Excel 2019 (Microsoft, Redmond, Washington, USA). Word 2019 software (Microsoft, Redmond, Washington, USA) was used to prepare tables, and GraphPad Prism 8.0 (GraphPad Software, Inc., La Jolla, CA, USA) was used to analyze statistics and generate figures. If the data followed a normal distribution, an unpaired *t*-test was used for the statistical analysis between the two groups; otherwise, the Wilcoxon signed-rank test was used for analysis. A *P*-value < 0.05 was considered statistically significant.

RESULTS

L.lactis Partly Improved the Growth Performance of Weaning Piglets

The body weight and average daily feed intake of piglets were similar between the control and *L.lactis* groups (**Figures 1A,B**). *L.lactis* increased average daily weight gain and reduced FCR in the 2nd week ($P < 0.05$), while did not affect them in the other 2 weeks (**Figures 1C,D**).

L.lactis Reduced Intestinal *E.coli* Load

Results of diarrhea index and diarrhea rate showed that *L.lactis* did not affect the diarrhea of piglets (**Figures 2A,B**). And *L.lactis* reduced *E.coli* load ($P < 0.05$) in jejunal mucosa but not ileal mucosa and colonic content (**Figure 2C**).

L.lactis Regulated the Amino Acid Profiles

L.lactis significantly increased ($P < 0.05$) the concentrations of L-cystine and decreased ($P < 0.05$) the level of L-glutamic acid in ileal mucosa (**Table 1**). In peripheral circulation, the serum level of L-tryptophan (Trp) was improved ($P < 0.05$) due to *L.lactis* administration (**Table 1**).

L.lactis Affected Intestinal Immunity

To examine the effect of *L.lactis* on intestinal immunity, we used RT-PCR to measure the mRNA expression of jejunal and ileal immunity-related factors, including toll-like receptors (TLR)-2, 4, 5, and 6, myeloid differentiation primary response protein-88 (MyD88), tumor necrosis factor-alpha (TNF-α), interferon-gamma (IFN-γ), and interleukin (IL)-1, 2, 4, 6, 10, 17, 18, and 22. In the *L.lactis* group, jejunal IFN-γ ($P < 0.01$) and ileal IL-22 ($P < 0.05$) were reduced, and jejunal IL-17 ($P < 0.05$), 18 ($P < 0.05$), and 22 ($P < 0.05$), ileal TLR-2, 5, 6 ($P < 0.01$), and MyD88 ($P < 0.05$) were increased, while other factors was not changed, comparing with the controls (**Figure 3**).

L.lactis Regulated the Intestinal GABAergic System

The mRNA expression of the gut GABAergic system was analyzed using RT-PCR. The results showed that the expression of SLC6A13 was inhibited ($P < 0.05$) due to *L.lactis* treatment (**Table 2**). Analysis of the gene expressions of GABA receptors (GABAB1-2, GABAAα1-5, β2, γ1-2, δ, ε, π, θ, and ρ1) showed that *L.lactis* inhibited the expression of GABAAρ1, π, θ, and γ1 ($P < 0.05$), while it increased GABAAα5 expression ($P < 0.05$) (**Table 2**).

L.lactis Shifted the Gut Microbiota

The ileal microbiota was analyzed by 16S rDNA sequencing. According to the Venn diagram, 988 OTUs were clustered, in which 199 and 357 OTUs were unique in the control and *L.lactis* group, separately (**Figure 4A**). The Beta diversity analysis showed a remarkable difference between control and *L.lactis* groups (**Figure 4B**), while the Alpha diversity analysis showed no difference (**Supplementary Table 4**). At the phylum, family, genus, and species level, *Firmicutes*, *Clostridiaceae_1*, *Clostridium_sensu_stricto_1*, and *Veillonella parvula* were by far the dominative populations (**Figures 4C–F**). According to Linear discriminant analysis effect size (LEfSe) results, *Oceanospirillales*, *Halomonas*, and *Halomonadaceae* were enriched in the *L.lactis* group, while *Burkholderiaceae* and *Clostridiales*

TABLE 1 | Effects of *L.lactis* on the ileal mucosa (μg/g) and serum (μg/mL) the amino acid profiles.

	Control	*L.lactis*	*P*-value
Ileal mucosa			
L-Alanine	283.96 ± 5.83	280.49 ± 5.53	0.71
L-Valine	92.78 ± 8.77	98.29 ± 2.58	0.60
L-Leucine	224.37 ± 14.95	214.48 ± 3.48	0.61
L-Isoleucine	108.68 ± 7.88	101.49 ± 4.84	0.47
L-Phenylalanine	132.41 ± 8.30	134.52 ± 1.23	0.84
L-Tryptophan	21.46 ± 1.57	20.54 ± 0.67	0.64
L-Methionine	88.81 ± 7.49	85.77 ± 1.54	0.75
L-Proline	136.35 ± 10.11	135.88 ± 2.66	0.96
Glycine	509.36 ± 44.67	446.92 ± 12.5	0.26
L-Serine	179.35 ± 11.26	187.20 ± 6.51	0.58
L-Threonine	97.75 ± 10.06	92.06 ± 4.17	0.63
L-Cystine	24.24 ± 1.93	37.32 ± 1.69*	0.01
L-Tyrosine	125.17 ± 9.13	128.06 ± 5.54	0.80
L-Aspartic acid	242.80 ± 14.60	214.95 ± 14.17	0.22
L-Glutamic acid	1183.57 ± 52.8	997.92 ± 30.01*	0.01
L-Lysine	148.06 ± 11.61	150.80 ± 2.56	0.84
L-Arginine	131.12 ± 11.43	134.16 ± 2.29	0.82
L-Histidine	45.74 ± 1.93	47.87 ± 1.15	0.40
Serum			
L-Histidine	7.00 ± 0.53	8.57 ± 0.56	0.09
L-Serine	16.87 ± 0.18	18.00 ± 1.85	0.60
L-Arginine	20.92 ± 0.65	18.34 ± 2.22	0.34
Glycine	42.92 ± 4.10	48.72 ± 6.79	0.50
L-Aspartic acid	4.29 ± 0.48	4.53 ± 0.57	0.76
L-Glutamic acid	42.33 ± 1.63	48.21 ± 3.47	0.17
L-Threonine	5.40 ± 0.10	5.27 ± 0.38	0.78
L-Alanine	42.84 ± 1.97	43.62 ± 5.86	0.90
L-Proline	30.17 ± 1.18	30.79 ± 3.40	0.87
L-Cystine	2.01 ± 0.35	2.31 ± 0.26	0.55
L-Lysine	42.92 ± 3.12	38.49 ± 2.34	0.30
L-Tyrosine	19.55 ± 1.44	18.48 ± 0.70	0.54
L-Methionine	9.49 ± 0.79	7.46 ± 0.75	0.10
L-Valine	19.41 ± 1.24	20.51 ± 1.92	0.67
L-Isoleucine	12.11 ± 0.57	11.59 ± 0.39	0.51
L-Leucine	18.00 ± 0.71	19.04 ± 2.33	0.71
L-Phenylalanine	12.71 ± 0.94	14.28 ± 1.32	0.38
L-Tryptophan	4.75 ± 0.18	6.56 ± 0.62*	0.02

*Amino acid profiles of the ileal mucosa and serum were detected by HPLC. Piglets from control group (n = 7) and L.lactis group (n = 8). Unpaired t-test was used to analyze data (mean ± SEM). *P < 0.05.*

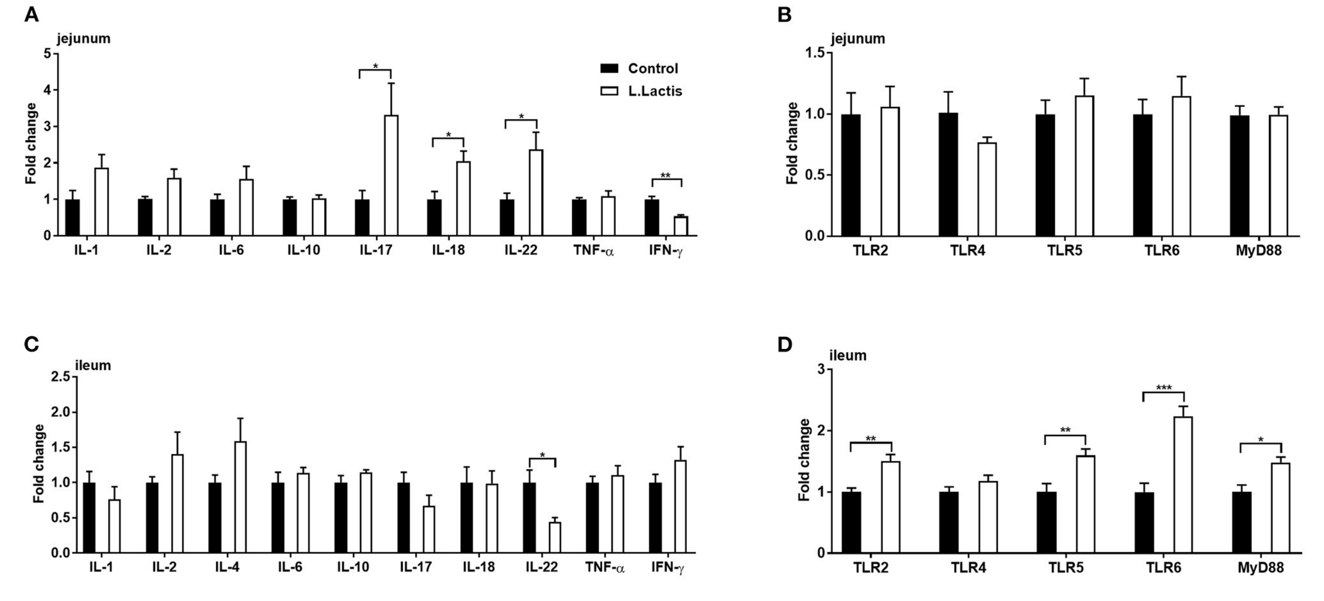

FIGURE 3 | Jejunal and ileal mRNA expression of immune-related factors. Relative gene expression of **(A,C)** IL-1, 2, 4, 6, 8, 10, 17, 18, 22, TNF-α, and IFN-γ, and **(B,D)** TLR-2, 4, 5, 6, and MyD88 were analyzed by RT-PCR (jejunal IL-4 was undetected). An unpaired *t*-test was used for analyzing the data (mean ± SEM). $^*P < 0.05$; $^{**}P < 0.01$; $^{***}P < 0.001$.

TABLE 2 | Expression of GABAergic system in the ilea of piglets.

	Control	*L.lactis*	*P*-value
SLC6A1	1.00 ± 0.18	1.21 ± 0.09	0.66
SLC6A11	1.00 ± 0.09	0.68 ± 0.14	0.09
SLC6A12	1.00 ± 0.04	0.88 ± 0.11	0.79
SLC6A13	1.00 ± 0.12	0.61 ± 0.05*	0.01
GABAB1	1.00 ± 0.10	0.88 ± 0.07	0.27
GABAB2	1.00 ± 0.17	0.95 ± 0.20	0.98
GABAAβ2	1.00 ± 0.12	1.09 ± 0.29	0.69
GABAAδ	1.00 ± 0.12	0.89 ± 0.12	0.38
GABAAε	1.00 ± 0.25	0.79 ± 0.11	0.20
GABAAρ1	1.00 ± 0.25	0.55 ± 0.06*	0.04
GABAAπ	1.00 ± 0.13	0.24 ± 0.03*	0.01
GABAAθ	1.00 ± 0.13	0.30 ± 0.04*	0.01
GABAAγ1	1.00 ± 0.16	0.46 ± 0.05*	0.01
GABAAγ2	1.00 ± 0.12	0.93 ± 0.16	0.57
GABAAα1	1.00 ± 0.02	0.92 ± 0.09	0.48
GABAAα2	1.00 ± 0.39	1.60 ± 0.52	0.79
GABAAα3	1.00 ± 0.13	0.80 ± 0.06	0.15
GABAAα4	1.00 ± 0.17	1.44 ± 0.12	0.18
GABAAα5	1.00 ± 0.08	1.64 ± 0.12*	0.01

*Ileal gene expression of GAT, GABA receptors, and GAD (undetected) were analyzed by RT-PCR. Piglets from control group (n = 7) and L.lactis group (n = 8). Unpaired t-test was used to analyze the data (mean ± SEM). *P < 0.05.*

bacterium_canine_oral_taxon_219 were enriched in the controls (**Figures 5A,B**). *L.lactis* increased the relative abundance of *Oceanospirillales*, *Halomonadaceae*, *Shewanellaceae*, *Halomonas*, *Shewanella*, and *Shewanella_algae* (**Figure 5C**), and reduced the relative abundance of *Burkholderiaceae* (**Figure 5D**). Spearman correlation analysis indicated that ADG of the 2nd week was positively correlated with the relative abundance of *Fusobacteria* (**Figure 5E**). Ileal TLR-5 mRNA expression and the level of Trp in serum were positively correlated with the relative abundance of *Thaumarchaeota*. The serum level of Trp also was positively correlated with the relative abundance of *Proteobacteria* (**Figure 5F**).

DISCUSSION

The biggest challenge that weaning piglets faced is diarrhea caused by weaning stress and pathogen infection. During weaning, the gut microbiota of piglets is maladjusted due to diet and environmental changes (1), often leading to infection (2). Previous studies showed that the administration of probiotics could reduce weaning stress and pathogen infection by regulating the gut microbiota (20, 21). Our study showed that *L.lactis* improved growth performance and modulated intestinal immunity, ileal microbiota, and amino acid profiles of ileal mucosal and serum in weaning piglets.

Weaning stress impairs the feed intake and growth performance of the weaned piglets. Our previous research (18) showed that *L.lactis* promoted intestinal GABA production, and GABA was reported to enhance the growth performance (19) and inhibit the expression of cholecystokinin-related genes (22). We found that *L.lactis* partly increased the ADG and reduced the FCR in the 2nd week. The mechanism might be that GABA produced by *L.lactis* increased the secretion of hormones closely related to growth performance. The ADG and FCR of

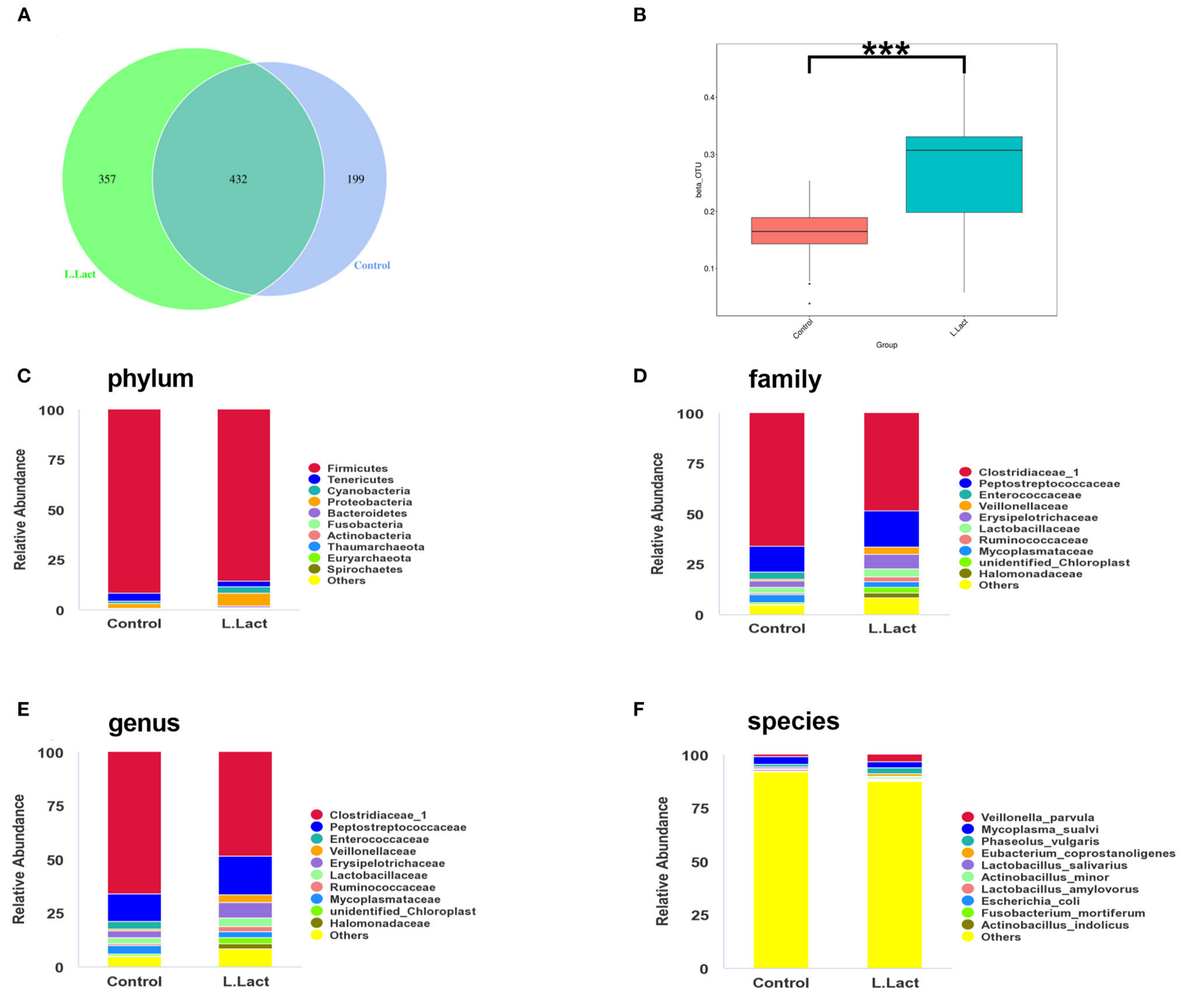

FIGURE 4 | Effects of *L.lactis* on ileal microbiota of the piglets. **(A)** The Venn diagram shows the common and unique OTUs of the control and *L.lactis* groups. **(B)** Rank abundance curves of beta diversity in the control and *L.lactis* groups. **(C–F)** Relative abundance of top 10 phyla **(C)**, families **(D)**, genera **(E)**, and species **(F)** in the control and *L.lactis* groups. ***$P < 0.001$.

week 3 were similar between the control and *L.lactis* groups. The possible reason is that the *L.lactis* transplantation has a time-limited effect on piglets. Our results contradicted a previous finding that the administration of *L.lactis* reduced body weight (23). The difference may be explained by different animal models or different dosages of *L.lactis*. However, the mechanism under the improvement of growth performance driven by *L.lactis* needs to be further studied.

The weaning stress of piglets usually causes diarrhea, slowing down the growth of piglets. Weaning piglets are susceptible to diarrhea caused by pathogenic *E.coli* (e.g., ETEC) infection. Growing studies indicate that probiotics prevent pathogenic bacteria colonization and proliferation (12, 13). Manuela et al. (24) showed that probiotics inhibited pathogenic bacteria by producing antimicrobial metabolites and competing for energy substances. *Lactic acid bacteria* have been found to produce various antimicrobial substances (e.g., lactic acid, bacteriocins, and hydrogen peroxide) to inhibit pathogenic bacteria colonization (25–27). Similarly, we found that *L.lactis* reduced the jejunal mucosal *E.coli* load, which helps prevent diarrhea caused by harmful *E.coli* colonization.

The GABAergic system plays vital role in intestinal health and disease, partly relying on hormone secretion and intestinal immunity (28, 29). Therefore, we analyzed the effect of *L.lactis* on the intestinal GABAergic system. An increasing number of studies have illustrated the critical roles of GABA transporters (GAT) on health and diseases. Xia et al. (30) showed that GAT2 (SLC6A13) sustained IL-1β production

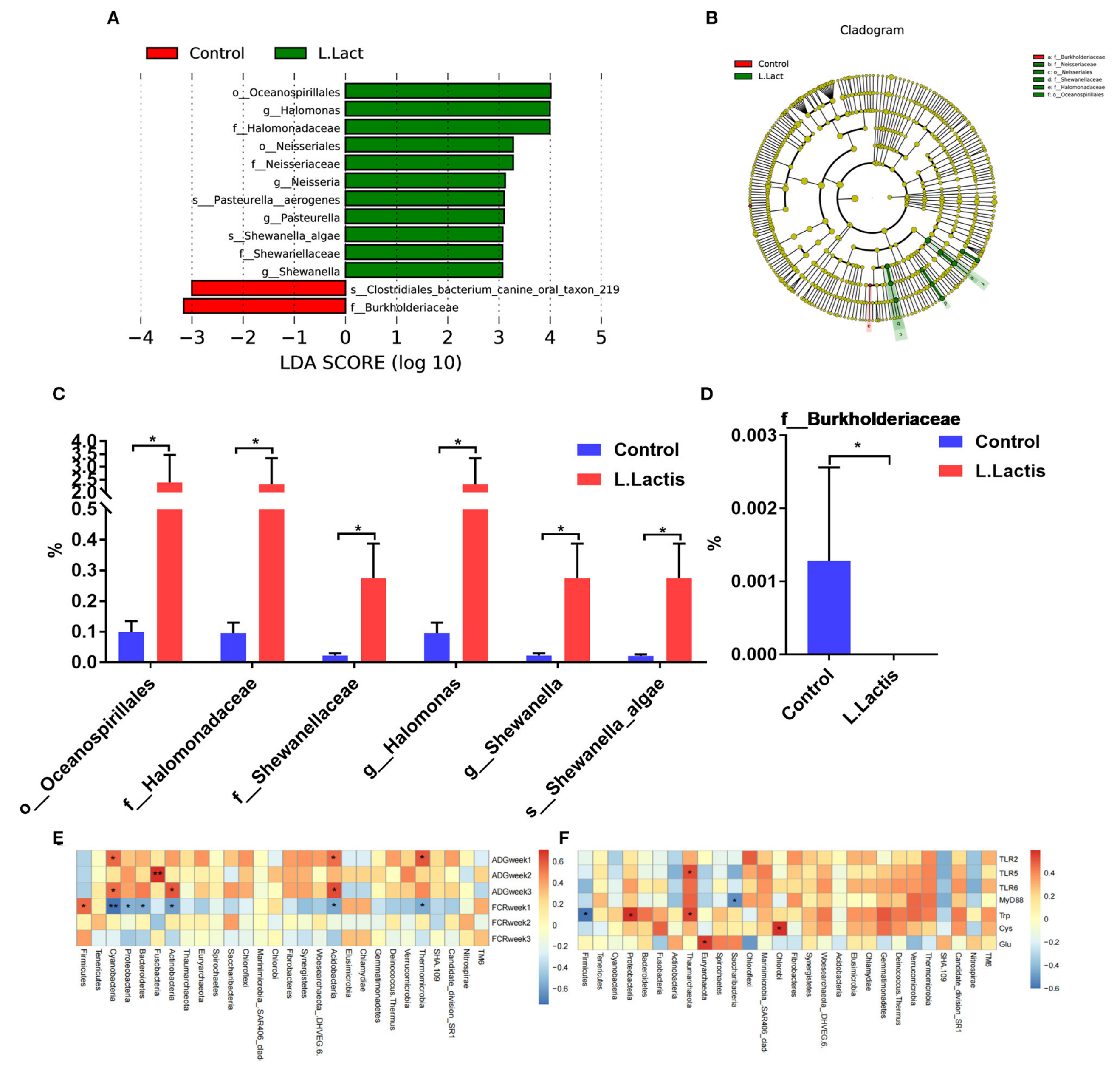

FIGURE 5 | *L.lactis* regulated the ileal microbiota of the piglets. **(A–D)** LEfSe analysis demonstrated the significant members in the control and *L.lactis* groups. **(E)** Environmental factor correlation analysis indicated that ADG of week 2 was positively correlated with Fusobacteria. **(F)** Ileal TLR-5 mRNA expression and serum tryptophan (Trp) level were positively correlated with the relative abundance of *Thaumarchaeota*; serum Trp level was also positively correlated with the relative abundance of *Proteobacteria*. *$P < 0.05$; **$P < 0.01$.

in macrophages, and Ren et al. (18) identified the role of GAT2 in the defense against pathogen infection. This study found that *L.lactis* reduced GAT2 expression and regulated GABA receptors. Thus, *L.lactis* transplantation caused significant regulation of the intestinal GABAergic system. *L.lactis* can regulate the function of immune cells by regulating the intestinal GABAergic system, thus maintaining intestinal homeostasis. However, these results are limited in clarifying the relationship between *L.lactis*, intestinal GABAergic system and intestinal immune responses.

Amino acids play an essential role as reactive substances in peptide and protein biosynthesis. Moreover, recent studies have shown that amino acids (e.g., tryptophan, cysteine) contribute to the metabolic reprogramming of immune cells such as T cells and macrophages (31). For example, tryptophan is required for T cell proliferation and activation, and tryptophan metabolism is enhanced in activated immune cells. Our study showed that *L.lactis* transplantation increased the tryptophan level of serum, which might subsequently activate immune cells to resist pathogenic infection. Cysteine, by facilitating glutathione synthesis, plays a vital role in maintaining redox balance to support the function of immune cells (32). In this study, the improved level of ileal mucosal cysteine facilitated by *L.lactis* might further generate glutathione to counter the production of reactive oxygen species that can cause cell death at high concentrations. Many amino acids such as tryptophan, cysteine and glutamic acid are regulators of growth performance, intestinal immunity, and gut microbiota, indicating that *L.lactis* promotes growth performance and regulates intestinal immunity might partly by affecting amino acids.

The intestinal tract is the primary organ for food digestion and nutrient absorption and is also the largest immune organ. The intestinal immune system is essential to resisting pathogen infection (33). Our study showed that *L.lactis* promoted the ileal expression of TLR-2, 5, and 6, as well as MyD88, in weaning piglets. These TLRs recognize different pathogenic components and activate immune cells to kill pathogens (34). Therefore, *L.lactis* could activate immune cells by activating TLRs signaling pathways, thus resisting intestinal infection. According to our previous research, ETEC-infection increased the abundance of *L.lactis*, promoting the T helper cell 17 (Th17) immune response via GABA production (18). Indeed, *L.lactis*-promoted jejunal IL-17 gene expression was also observed in this study. Our previous study showed that GABA supplementation could increase the expression of intestinal SLC6A13 during ETEC infection (35). Thus, the glutamate in the intestine might be used for GABA production in this study. It was reported that the glutamine-glutamate-GABA metabolic pathway supports the Th17 immune reaction to IL-17 production (36). According to these results, the intestinal GABA derived from host glutamate metabolism and *L.lactis* might support the Th17 immune reaction. Our study also found that *L.lactis* increased the jejunal gene expression of IL-18 and IL-22 and reduced the ileal gene expression of IL-22. IL-18 can induce the intestinal epithelium to produce antimicrobial proteins (37), while, intestinal IL-22 signaling was positively correlated with the differentiation and antimicrobial effect of Paneth cells (38), and IL-22 has been reported to promote intestinal stem cell-mediated epithelial regeneration (39). Thus, *L.lactis* transplantation regulates intestinal immune response, which would help maintain intestinal immune homeostasis. For example, *Lactobacillus* could mitigate colitis by producing aryl hydrocarbon receptor agonists (AHR) (40).

The gut microbiota affects many physiological functions of the host and is linked to the pathogenesis of various diseases such as inflammatory bowel disease (41), cancer (42), and obesity (43). Numerous studies have reported that health and disease markers highly correlate with the gut microbiome (44), and the occurrence of various diseases is associated with the decrease of intestinal microbial diversity (45). Recent studies demonstrated that many probiotics regulated gut microbiota and inhibited intestinal diseases (46). As a promising non-colonizing probiotic, it is reasonable that *L.lacatis* was undetectable after short-term and low dosage administration. Although it did not change the relative abundance of intestinal *L.lactis* after treatment for 2 weeks, *L.lactis* was found sifted and regulated the gut microbiota, such as enriching some beneficial bacteria and suppressing potential pathogenic bacteria. *L.lactis* treatment reduced the relative abundance of *Burkholderia*, which is highly related to inflammatory bowel disease and intestinal infection (47, 48). And *L.lactis* transplantation increased the relative abundance of *Shewanella* which benefits pancreatic beta cell expansion and insulin production (49). Li et al. (50) showed that transplantation of fecal bacteria from healthy pigs improved the growth status of the recipient pigs, although the overall composition of intestinal bacteria could not be changed, some potential probiotics were significantly enriched. Derrien et al. (51) showed that probiotics do not significantly alter the composition of fecal microbiota in healthy adults but can help maintain the dynamic balance of gut microbiota and reduce the adverse effects of intestinal microbial disorders. Therefore, the function of *L.lactis* may be more dependent on maintaining the dynamic balance of gut microbiota and microbial metabolic activities. For example, tryptophan metabolites of gut microbiota can improve intestinal barrier function and alleviate dextran sulfate sodium (DSS)-induced colitis in mice (52). Spearman correlation analysis of our data indicated that the effect of *L.lactis* on the gut microbiota was closely related to amino acid profiles, growth performance, and intestinal immunity. Thus, *L.lactis* may influence the intestinal microbiota to help regulate these factors in weaning piglets.

CONCLUSION

L.lactis improved the growth performance, regulated amino acid profiles and intestinal immunity in weaning piglets, which might be associated with changing the intestinal microbiota. These results would help evaluate the feasibility of *L.lactis* in pig production to reduce the negative health effects of weaning.

DATA AVAILABILITY STATEMENT

The datasets presented in this study can be found in online repositories. The names of the repository/repositories and accession number(s) can be found below: 16S rDNA gene profiling data were available in the NCBI database under BioProject PRJNA745933.

ETHICS STATEMENT

The animal study was reviewed and approved by the Animal Welfare Committee of the Institute of Subtropical Agriculture, Chinese Academy of Sciences.

AUTHOR CONTRIBUTIONS

SC, BT, and LG designed the experiment and reviewed and revised the manuscript. DY, SC, and YX conducted the experiment. DY and SC analyzed the data. DY and LG prepared tables and figures. DY prepared the manuscript. All authors contributed to the article and approved the submitted version.

FUNDING

This research was supported by the National Key Research and Development Program of China (2017YFD0500503) and the Innovation Province Project (Grant: 2019RS3021).

SUPPLEMENTARY MATERIAL

The Supplementary Material for this article can be found online at: https://www.frontiersin.org/articles/10.3389/fnut.2021.713256/full#supplementary-material

REFERENCES

1. Gresse R, Chaucheyras-Durand F, Fleury MA, Van de Wiele T, Forano E, Blanquet-Diot S. Gut microbiota dysbiosis in postweaning piglets: understanding the Keys to Health. *Trends Microbiol.* (2017) 25:851–73. doi: 10.1016/j.tim.2017.05.004
2. Bin P, Tang Z, Liu S, Chen S, Xia Y, Liu J, et al. Intestinal microbiota mediates enterotoxigenic *Escherichia coli*-induced diarrhea in piglets. *BMC Vet Res.* (2018) 14:385. doi: 10.1186/s12917-018-1704-9
3. Khine WWT, Rahayu ES, See TY, Kuah S, Salminen S, Nakayama J, et al. Indonesian children fecal microbiome from birth until weaning was different from microbiomes of their mothers. *Gut Microbes.* (2020) 12:e1761240. doi: 10.1080/19490976.2020.1761240
4. Hu J, Nie Y, Chen J, Zhang Y, Wang Z, Fan Q, et al. Gradual changes of gut microbiota in weaned miniature piglets. *Front Microbiol.* (2016) 7:1727. doi: 10.3389/fmicb.2016.01727
5. Meale SJ, Li SC, Azevedo P, Derakhshani H, DeVries TJ, Plaizier JC, et al. Weaning age influences the severity of gastrointestinal microbiome shifts in dairy calves. *Sci Rep.* (2017) 7:198. doi: 10.1038/s41598-017-00223-7
6. Al Nabhani Z, Dulauroy S, Marques R, Cousu C, Al Bounny S, Déjardin F, et al. A weaning reaction to microbiota is required for resistance to immunopathologies in the adult. *Immunity.* (2019) 50:1276–88. doi: 10.1016/j.immuni.2019.02.014
7. Jayaraman B, Nyachoti CM. Husbandry practices and gut health outcomes in weaned piglets: a review. *Anim Nutr.* (2017) 3:205–11. doi: 10.1016/j.aninu.2017.06.002
8. Chatterjee A, Modarai M, Naylor NR, Boyd SE, Atun R, Barlow J, et al. Quantifying drivers of antibiotic resistance in humans: a systematic review. *Lancet Infect Dis.* (2018) 18:e368–78. doi: 10.1016/S1473-3099(18)30296-2
9. Van den Bergh B, Michiels JE, Wenseleers T, Windels EM, Boer PV, Kestemont D, et al. Frequency of antibiotic application drives rapid evolutionary adaptation of *Escherichia coli* persistence. *Nat Microbiol.* (2016) 1:16020. doi: 10.1038/nmicrobiol.2016.20
10. Van Boeckel TP, Pires J, Silvester R, Zhao C, Song J, Criscuolo NG, et al. Global trends in antimicrobial resistance in animals in low- and middle-income countries. *Science.* (2019) 365:eaaw1944. doi: 10.1126/science.aaw1944
11. Laxminarayan R, Sridhar D, Blaser M, Wang M, Woolhouse M. Achieving global targets for antimicrobial resistance. *Science.* (2016) 353:874–5. doi: 10.1126/science.aaf9286
12. Goldenberg JZ, Mertz D, Johnston BC. Probiotics to prevent clostridium difficile infection in patients receiving antibiotics. *Jama.* (2018) 320:499–500. doi: 10.1001/jama.2018.9064
13. Mullish BH, Marchesi JR, McDonald JAK, Pass DA, Masetti G, Michael DR, et al. Probiotics reduce self-reported symptoms of upper respiratory tract infection in overweight and obese adults: should we be considering probiotics during viral pandemics? *Gut Microbes.* (2021) 13:1–9. doi: 10.1080/19490976.2021.1900997
14. Kandasamy S, Vlasova AN, Fischer DD, Chattha KS, Shao L, Kumar A, et al. Unraveling the differences between gram-positive and gram-negative probiotics in modulating protective immunity to enteric infections. *Front Immunol.* (2017) 8:334. doi: 10.3389/fimmu.2017.00334
15. Satchell KJF. Engineered bacteria for cholera prophylaxis. *Cell Host Microbe.* (2018) 24:192–4. doi: 10.1016/j.chom.2018.07.013
16. Mao N, Cubillos-Ruiz A, Cameron DE, Collins JJ. Probiotic strains detect and suppress cholera in mice. *Sci Transl Med.* (2018) 10:eaao2586. doi: 10.1126/scitranslmed.aao2586
17. Liu G, Ren W, Fang J, Hu CA, Guan G, Al-Dhabi NA, et al. L-Glutamine and L-arginine protect against enterotoxigenic *Escherichia coli* infection via intestinal innate immunity in mice. *Amino Acids.* (2017) 49:1945–54. doi: 10.1007/s00726-017-2410-9
18. Ren W, Yin J, Xiao H, Chen S, Liu G, Tan B, et al. Intestinal microbiota-derived GABA mediates interleukin-17 expression during enterotoxigenic *Escherichia coli* infection. *Front Immunol.* (2016) 7:685. doi: 10.3389/fimmu.2016.00685
19. Chen S, Tan B, Xia Y, Liao S, Wang M, Yin J, et al. Effects of dietary gamma-aminobutyric acid supplementation on the intestinal functions in weaning piglets. *Food Funct.* (2019) 10:366–78. doi: 10.1039/C8FO02161A
20. Zhang W, Zhu YH, Yang GY, Liu X, Xia B, Hu X, et al. *Lactobacillus rhamnosus* GG affects microbiota and suppresses autophagy in the intestines of pigs challenged with *Salmonella* infantis. *Front Microbiol.* (2017) 8:2705. doi: 10.3389/fmicb.2017.02705
21. Barba-Vidal E, Castillejos L, Roll VFB, Cifuentes-Orjuela G, Moreno Muñoz JA, Martín-Orúe SM. The probiotic combination of *Bifidobacterium longum* subsp. infantis CECT 7210 and *Bifidobacterium animalis subsp. lactis* BPL6 reduces pathogen loads and improves gut health of weaned piglets orally challenged with *Salmonella typhimurium*. *Front Microbiol.* (2017) 8:1570. doi: 10.3389/fmicb.2017.01570
22. Wang DM, Chacher B, Liu HY, Wang JK, Lin J, Liu JX. Effects of γ-aminobutyric acid on feed intake, growth performance and expression of related genes in growing lambs. *Animal.* (2015) 9:445–8. doi: 10.1017/S1751731114002651
23. Naudin CR, Maner-Smith K, Owens JA, Wynn GM, Robinson BS, Matthews JD, et al. *Lactococcus lactis* subspecies cremoris elicits protection against metabolic changes induced by a western-style diet. *Gastroenterology.* (2020) 159:639–51. doi: 10.1053/j.gastro.2020.03.010
24. Raffatellu M. Learning from bacterial competition in the host to develop antimicrobials. *Nat Med.* (2018) 24:1097–103. doi: 10.1038/s41591-018-0145-0
25. Zamfir M, Callewaert R, Cornea PC, De Vuyst L. Production kinetics of acidophilin 801, a bacteriocin produced by *Lactobacillus acidophilus* IBB 801. *FEMS Microbiol Lett.* (2000) 190:305–8. doi: 10.1111/j.1574-6968.2000.tb09303.x
26. Mahrous H, Mohamed A, El-Mongy MA, El-Batal AI, Hamza HAJF. Study bacteriocin production and optimization using new isolates of *Lactobacillus* spp. isolated from some dairy products under different culture conditions. *Food Nutr Sci.* (2013) 4:342–56. doi: 10.4236/fns.2013.43045
27. Abo-Amer AE. Optimization of bacteriocin production by *Lactobacillus acidophilus* AA11, a strain isolated from Egyptian cheese. *Ann Microbiol.* (2011) 61:445–52. doi: 10.1007/s13213-010-0157-6
28. Auteri M, Zizzo MG, Serio R. GABA and GABA receptors in the gastrointestinal tract: from motility to inflammation. *Pharmacol Res.* (2015) 93:11–21. doi: 10.1016/j.phrs.2014.12.001
29. Vlainić JV, Šuran J, Vlainić T, Vukorep AL. Probiotics as an adjuvant therapy in major depressive disorder. *Curr Neuropharmacol.* (2016) 14:952–8. doi: 10.2174/1570159X14666160526120928
30. Xia Y, He F, Wu X, Tan B, Chen S, Liao Y, et al. GABA transporter sustains IL-1β production in macrophages. *Sci Adv.* (2021) 7:eabe9274. doi: 10.1126/sciadv.abe9274
31. Kelly B, Pearce EL. Amino Assets: how amino acids support immunity. *Cell Metab.* (2020) 32:154–75. doi: 10.1016/j.cmet.2020.06.010
32. Vene R, Delfino L, Castellani P, Balza E, Bertolotti M, Sitia R, et al. Redox remodeling allows and controls B-cell activation and differentiation. *Antioxid Redox Sign.* (2010) 13:1145–55. doi: 10.1089/ars.2009.3078
33. Ren W, Chen S, Zhang L, Liu G, Hussain T, Hao X, et al. Interferon tau affects mouse intestinal microbiota and expression of IL-17. *Mediat Inflamm.* (2016) 2016:2839232. doi: 10.1155/2016/2839232
34. Akira S, Uematsu S, Takeuchi O. Pathogen recognition and innate immunity. *Cell.* (2006) 124:783–801. doi: 10.1016/j.cell.2006.02.015

35. Chen S, Wu X, Xia Y, Wang M, Liao S, Li F, et al. Effects of dietary gamma-aminobutyric acid supplementation on amino acid profile, intestinal immunity, and microbiota in ETEC-challenged piglets. *Food Funct.* (2020) 11:9067–74. doi: 10.1039/D0FO01729A
36. Yang G, Xia Y, Ren W. Glutamine metabolism in Th17/Treg cell fate: applications in Th17 cell-associated diseases. *Sci China Life Sci.* (2021) 64:221–33. doi: 10.1007/s11427-020-1703-2
37. Jarret A, Jackson R, Duizer C, Healy ME, Zhao J, Rone JM, et al. Enteric nervous system-derived IL-18 orchestrates mucosal barrier immunity. *Cell.* (2020) 180:50–63. doi: 10.1016/j.cell.2019.12.016
38. Gaudino SJ, Beaupre M, Lin X, Joshi P, Rathi S, McLaughlin PA, et al. IL-22 receptor signaling in Paneth cells is critical for their maturation, microbiota colonization, Th17-related immune responses, and anti-Salmonella immunity. *Mucosal Immunol.* (2021) 14:389–401. doi: 10.1038/s41385-020-00348-5
39. Lindemans CA, Calafiore M, Mertelsmann AM, O'Connor MH, Dudakov JA, Jenq RR, et al. Interleukin-22 promotes intestinal-stem-cell-mediated epithelial regeneration. *Nature.* (2015) 528:560–4. doi: 10.1038/nature16460
40. Lamas B, Richard ML, Leducq V, Pham HP, Michel ML, Da Costa G, et al. CARD9 impacts colitis by altering gut microbiota metabolism of tryptophan into aryl hydrocarbon receptor ligands. *Nat Med.* (2016) 22:598–605. doi: 10.1038/nm.4102
41. Roager HM, Licht TR. Microbial tryptophan catabolites in health and disease. *Nat Commun.* (2018) 9:3294. doi: 10.1038/s41467-018-05470-4
42. Louis P, Hold GL, Flint HJ. The gut microbiota, bacterial metabolites and colorectal cancer. *Nat Rev Microbiol.* (2014) 12:661–72. doi: 10.1038/nrmicro3344
43. Anhe FF, Roy D, Pilon G, Dudonne S, Matamoros S, Varin TV, et al. A polyphenol-rich cranberry extract protects from diet-induced obesity, insulin resistance and intestinal inflammation in association with increased *Akkermansia* spp. population in the gut microbiota of mice. *Gut.* (2015) 64:872–83. doi: 10.1136/gutjnl-2014-307142
44. Manor O, Dai CL, Kornilov SA, Smith B, Price ND, Lovejoy JC, et al. Health and disease markers correlate with gut microbiome composition across thousands of people. *Nat Commun.* (2020) 11:5206. doi: 10.1038/s41467-020-18871-1
45. Kriss M, Hazleton KZ, Nusbacher NM, Martin CG, Lozupone CA. Low diversity gut microbiota dysbiosis: drivers, functional implications and recovery. *Curr Opin Microbiol.* (2018) 44:34–40. doi: 10.1016/j.mib.2018.07.003
46. Sanders ME, Merenstein DJ, Reid G, Gibson GR, Rastall RA. Probiotics and prebiotics in intestinal health and disease: from biology to the clinic. *Nat Rev Gastro Hepat.* (2019) 16:605–16. doi: 10.1038/s41575-019-0173-3
47. Ananthakrishnan AN, Luo C, Yajnik V, Khalili H, Garber JJ, Stevens BW, et al. Gut microbiome function predicts response to anti-integrin biologic therapy in inflammatory bowel diseases. *Cell Host Microbe.* (2017) 21:603–10. doi: 10.1016/j.chom.2017.04.010
48. Schieber AM, Lee YM, Chang MW, Leblanc M, Collins B, Downes M, et al. Disease tolerance mediated by microbiome *E. coli* involves inflammasome and IGF-1 signaling. *Science.* (2015) 350:558–63. doi: 10.1126/science.aac6468
49. Hill JH, Franzosa EA, Huttenhower C, Guillemin K. A conserved bacterial protein induces pancreatic beta cell expansion during zebrafish development. *eLife.* (2016) 5:e20145. doi: 10.7554/eLife.20145
50. Li Y, Wang X, Wang XQ, Wang J, Zhao J. Life-long dynamics of the swine gut microbiome and their implications in probiotics development and food safety. *Gut microbes.* (2020) 11:1824–32. doi: 10.1080/19490976.2020.1773748
51. Derrien M, van Hylckama Vlieg JE. Fate, activity, and impact of ingested bacteria within the human gut microbiota. *Trends Microbiol.* (2015) 23:354–66. doi: 10.1016/j.tim.2015.03.002
52. Scott SA, Fu J, Chang PV. Microbial tryptophan metabolites regulate gut barrier function via the aryl hydrocarbon receptor. *Proc Natl Acad Sci USA.* (2020) 117:19376–87. doi: 10.1073/pnas.2000047117

Conflict of Interest: The authors declare that the research was conducted in the absence of any commercial or financial relationships that could be construed as a potential conflict of interest.

Publisher's Note: All claims expressed in this article are solely those of the authors and do not necessarily represent those of their affiliated organizations, or those of the publisher, the editors and the reviewers. Any product that may be evaluated in this article, or claim that may be made by its manufacturer, is not guaranteed or endorsed by the publisher.

frontiers in Nutrition

ORIGINAL RESEARCH
published: 23 August 2021
doi: 10.3389/fnut.2021.702085

Changes in Intestinal Flora Structure and Metabolites Are Associated With Myocardial Fibrosis in Patients With Persistent Atrial Fibrillation

Langsha Liu[1], *Juan Su*[2], *Rui Li*[3] *and Fanyan Luo*[1]*

[1] Department of Cardiac Surgery, Xiangya Hospital, Central South University, Changsha, China, [2] Department of Medical Administration, Zhuzhou Central Hospital, Zhuzhou, China, [3] Operating Theatre, Zhuzhou Central Hospital, Zhuzhou, China

Background: The occurrence of atrial fibrillation is often accompanied by myocardial fibrosis. An increasing number of studies have shown that intestinal flora is involved in the occurrence and development of a variety of cardiovascular diseases. This study explores the relationship between changes in the structure and function of intestinal flora and the progression of myocardial fibrosis in patients with persistent atrial fibrillation.

Methods: Serum and stool samples were collected from 10 healthy people and 10 patients with persistent atrial fibrillation (PeAF), and statistical analyses were performed on the subjects' clinical baseline conditions. ELISA was used to measure the levels of carboxy-terminal telopeptide of type I collagen (CTX-I), propeptide of type I procollagen (PICP), procollagen III N-terminal propeptide (PIIINP), fibroblast growth factor-23 (FGF-23), and transforming growth factor-beta 1 (TGF-β1) in serum. Through 16S rRNA sequencing technology, the structural composition of the intestinal flora was detected and analyzed. In addition, metabolomics data were analyzed to determine the differences in the metabolites produced by the intestinal flora of the subjects.

Results: By comparing the baseline data of the subjects, it was found that compared with those of the control group, the levels of creatinine (CRE) and serum uric acid (SUA) in the serum of PeAF patients were significantly increased. In addition, we found that the levels of CTX-I, PICP, PIIINP, and TGF-β1 in the serum of PeAF patients were significantly higher than those of the control group subjects. Although the control and PeAF groups exhibited no significant differences in the α diversity index, there were significant differences in the β diversity indexes (Bray-Curtis, weighted UniFrac and Anosim). At the phylum, family and species levels, the community structure and composition of the intestinal flora of the control group and those of the PeAF group showed significant differences. In addition, the compositions of the intestinal metabolites in the two different groups of people were significantly different. They were correlated considerably with PIIINP and specific communities in the intestinal flora.

Conclusion: Pathologically, PeAF patients may have a higher risk of myocardial fibrosis. Systematically, abnormal changes in the structure and composition of the intestinal flora in PeAF patients may lead to differences in intestinal metabolites, which are involved in the process of myocardial fibrosis through metabolite pathways.

Keywords: persistent atrial fibrillation, intestinal flora, metabolism, myocardial fibrosis, gut-heart

OPEN ACCESS

Edited by:
Hui Han,
Chinese Academy of Sciences (CAS), China

Reviewed by:
Séverine Zirah,
Muséum National d'Histoire Naturelle, France
Huan Li,
Lanzhou University, China

Correspondence:
Fanyan Luo
xyyylfy@163.com

Specialty section:
This article was submitted to Nutrition and Microbes, a section of the journal Frontiers in Nutrition

Received: *29 April 2021*
Accepted: *13 July 2021*
Published: *23 August 2021*

Citation:
Liu L, Su J, Li R and Luo F (2021) Changes in Intestinal Flora Structure and Metabolites Are Associated With Myocardial Fibrosis in Patients With Persistent Atrial Fibrillation. Front. Nutr. 8:702085. doi: 10.3389/fnut.2021.702085

INTRODUCTION

Atrial fibrillation (AF) is one of the most common arrhythmias, and persistent atrial fibrillation (PeAF) is often associated with a higher risk of stroke (1). Atrial fibrosis is considered a potential key factor and biomarker in the treatment of atrial fibrillation (2). Atrial fibrosis plays an essential role in the occurrence and continuation of atrial fibrillation through structural and electrical remodeling (3). In animal models, this heterogeneity can affect electrical conduction and signal transmission between cells, thereby providing a basis for the occurrence and development of atrial fibrillation (4). Myocardial fibrosis in atrial fibrillation is mediated by various factors, but the specific mechanism of atrial fibrosis-atrial fibrillation is still not fully understood.

Imbalance in collagen synthesis and its decomposition and metabolism are the causes of the occurrence and development of myocardial fibrosis (5). It is well-known that the extracellular matrix of the heart is mainly composed of fibrous type I collagen and type III collagen. Many circulating biomarkers related to collagen synthesis have been proposed to assess myocardial fibrosis, such as CTX-I, PICP, and PIIINP. They are considered functional factors that directly reflect the degree of fibrosis (6). In addition, FGF-23 directly participates in the development of myocardial fibrosis by activating fibroblast growth factor receptor (FGFR) (7). Studies have also shown that FGF-23 induces atrial fibrosis in patients with atrial fibrillation by increasing reactive oxygen species (ROS) production and subsequently activating signal transducer and activator of transcription 3 (STAT3) and SMAD3 signaling (8). Therefore, FGF-23 can also be used as a marker of myocardial fibrosis. Besides, TGF-β1, as an essential fibrosis mediator, promotes the synthesis of collagen fibers through typical Smad-dependent and non-classical Smad-independent pathways and can also be used as an indirect marker of myocardial fibrosis (9, 10).

As the concept of the "gut-heart" axis has gradually attracted attention, increasing evidence has confirmed the connection between the gut microbiota and cardiovascular diseases (CVDs), such as hypertension, atherosclerosis, myocardial infarction, heart failure, and arrhythmia (11, 12). Atrial fibrillation has also been determined to be related to an imbalanced intestinal flora (13). For example, Zuo et al. found that the duration of persistent atrial fibrillation is related to changes in human intestinal flora and metabolic phenotypes (14). In addition, studies have found that specific intestinal microbial changes (such as changes in the abundances of Nitrosomonadaceae and Lentisphaeraceae) are associated with the risk of atrial fibrillation recurrence (15). Therefore, we reasonably speculate that the intestinal flora may be involved in atrial fibrillation myocardial fibrosis development. Intestinal microbial-derived metabolites, such as trimethylamine N-oxide (TMAO), short-chain fatty acids (SCFAs), and secondary bile acids (BAs), have been proposed to be markers of major cardiac adverse events (16). A recent study showed that TMAO synthesized by the gut microbiota is enriched in patients with atrial fibrillation (17). The underlying mechanism of the intestinal flora is generally thought to involve immune regulation, host energy metabolism, and oxidative stress. These findings indicate that the function of the gut microbiome is similar to that of an endocrine organ, which can directly or indirectly affect the physiology of the host by producing biologically active metabolites (18). Therefore, we speculate that the abnormal changes in the intestinal flora in PeAF patients may lead to disordered or imbalanced host-related metabolic function, which may be one of the crucial mechanisms of the intestinal flora in the mediation of myocardial fibrosis.

In this study, based on 16S rRNA sequencing and metabonomic techniques, we investigated the correlation between atrial fibrosis and gut microbiota and their derived metabolites in PeAF patients. The mechanism of atrial fibrosis in PeAF patients was preliminarily explored from the perspective of "gut-heart." This study may provide new ideas for the prevention and treatment of persistent atrial fibrillation.

MATERIALS AND METHODS

Subjects

Ten PeAF patients admitted to the Cardiac Surgery Department of Xiangya Hospital were selected as the PeAF group. Ten volunteers with a healthy physical examination in the same period were selected as the control group. There were no statistically significant differences in sex or age between the two groups of people ($P > 0.05$). The selection criteria for PeAF patients were based on the guidelines for atrial fibrillation recommended by the European Society of Cardiology (ESC) (19). The exclusion criteria were as follows: (1) patients with gastrointestinal diseases or recent diarrhea and (2) patients who had recently taken antibiotics, hormone drugs, or microecological preparations. Clinical baseline condition for all subjects was obtained by checking hospital or medical records. After standing for 2 h, all the collected blood from subjects was centrifuged at 4,000 rpm for 15 min to obtain serum. Architect CI8200 integrated system (Abbott, IL, USA) was used to determine concentrations of CRE and SUA in all collected volunteer serum (20). This study was approved by the Ethic Committee of Xiangya Hospital Central South University (202004176), and the patients and family members consented to their inclusion in the study.

Sample Selection

All participants used a sterile stool collection kit to collect stool samples. After the sample was collected, it was quickly placed in a freezing tube, placed in liquid nitrogen for quick freezing, and then transferred to a −20°C refrigerator for storage. Five ml of fasting venous blood was collected from each subject, maintained at room temperature for 2 h, and then centrifuged at 2–8°C at 1,000 g for 15 min. The supernatant was then collected for subsequent experiments.

ELISA

According to the manufacturer's instructions, ELISA was performed using the following kits: CTX-I (CSB-E11224h, CUSABIO BIOTECH, Wuhan), PICP (CSB-E08079h, CUSABIO BIOTECH, Wuhan), PIIINP (JL19037, Jianglai, China), FGF-23 (CSB-E10113h, CUSABIO BIOTECH, Wuhan), and TGF-β1 (CSB-E04725h, CUSABIO BIOTECH, Wuhan). After the reactions were terminated, the optical density (OD value) of each sample was sequentially measured at 450 nm wavelength with a microplate reader.

16S rRNA Sequencing

Illumina NovaSeq PE250 was used for 16S amplicon sequencing to obtain raw data. The raw data were subjected to joint removal, filtering, deduplication, base correction, and removal of chimera sequences to obtain clean data for subsequent analyses. The QIIME 2 analysis process was adopted, and DADA2 was used to denoise the raw data, equivalent to clustering with 100% similarity. Only low-quality sequences were removed and corrected, and algorithms were identified and de-embedded. The denoised sequences were de-redundant. Additionally, feature [including Amplifier sequencing variation (ASV)] information was obtained. Each ASV sequence was annotated to obtain corresponding species information, including abundance distribution. QIIME 2 software was used to calculate the alpha diversity index (Chao1, ACE, Shannon, Simpson) of each sample. The ANOSIM analysis method was used to test the significance of differences in the community structures of the grouped samples. R software was used to draw a PCoA dimensionality reduction analysis diagram based on Bray-Curtis, unweighted UniFrac, and weighted UniFrac distances (phyloseq/vegan package).

Metabolomics

After freezing and grinding each stool sample, ∼50 mg was weighed and placed in a centrifuge tube. Four hundred microliter precooled (4°C) extraction solution (Methanol: Acetonitrile (v/v) = 1:1) was added to the sample tube, followed by vortexing and mixing, and then the mixed solution was incubated on ice for 10–15 min. Subsequently, the mixture was centrifuged at 16,000 g at 4°C for 10 min, and the supernatant was collected, transferred to a new centrifuge tube, and dried with nitrogen. The LC-MS analysis system consisted of an ultrahigh-performance liquid chromatograph (Agilent 7890B-5977B) paired with a Q Exactive Orbitrap high-resolution mass spectrometer (Thermo Fisher Scientific). The flow rate was set at 0.3 ml/min; the temperature of the sample tray was 4°C, and the column temperature was 40°C. A Waters HSS T3 column (100 × 2.1 mm, 1.7 µm) was used with (A) H_2O (0.1% formic acid) and (B) acetonitrile, with an injection volume of 3 µl. Mass conditions were as follow: Time of Flight is 60–100 dm/z, Ion source Gas1is 55psi, Ion source Gas2 is 55psi, Curtain Gas is 35psi, Temperature is set to 550°C, Declustering potential is 80 V, Collision Energy is 10 V, IonSpray Voltage is 5500 V (POS) or −4500 V (NEG). According to the plain peak area obtained by detection from the detection and AB SCIEX (AB Sciex Pte Ltd.) commercial and self-built databases, relative quantification of metabolites was carried out. The signal correction of the LC-MS metabolomics raw data was performed by using the R language package Stattarget. Then, we use MetaboAnalyst 5.0 (https://www.metaboanalyst.ca/faces/home.xhtml) website online analysis for a series of subsequent analyses, including Principal Component Analysis (PCA), partial least-squares discrimination analysis (PLS-DA), orthogonal partial least-squares discrimination analysis (OPLS-DA), and Sparse PLS discriminant analysis (sPLS-DA). Kyoto Encyclopedia of Genes and Genomes (KEGG, https://www.genome.jp/kegg/pathway.html) database was used for metabolic pathway analysis.

Data Analyses

GraphPad (GraphPad Software, San Diego, California, USA) statistical software was used for the analyses. Variables conforming to a normal distribution are expressed as the mean ± standard deviation (SD). Comparisons between two groups were performed using *t*-tests or one-way analysis of variance (ANOVA). The measurement data that did not conform to a normal distribution were analyzed using the Wilcoxon rank-sum test. The Spearman correlation analysis method was used for correlation analysis. A $p < 0.05$ was considered significantly different.

RESULTS

Baseline Characteristics of the Subjects

First, we analyzed and compared the baseline characteristics of the 10 healthy people and the 10 PeAF patients included in this study. As shown in **Table 1**, there were no significant differences between the two groups in terms of age, body mass index (BMI), systolic blood pressure (SBP), diastolic blood pressure (DBP), fasting blood glucose (FBG), albumin (ALB), total cholesterol (TC), triacylglycerol (TG), high-density lipoprotein cholesterol (HDL-c), low-density lipoprotein cholesterol (LDL-c), white blood cells (WBC) or neutrophil (N). However, we noticed that the levels of CRE and SUA in the serum of the PeAF patients were significantly higher than that of the healthy individuals.

Expression of Cardiac Fibrosis Markers

We first detected the expression of cardiac fibrosis markers in the serum of all the subjects. As shown in **Figure 1A**, compared with healthy people, the level of CTX-I was increased in the serum of the PeAF patients. Similarly, the levels of PICP and PIIINP were also high in the serum of the PeAF patients (**Figures 1B,C**). In addition, we observed that the level of FGF-23 in the serum of the PeAF patients was significantly higher than that of the healthy people (**Figure 1D**). Similarly, the content of TGF-β1 in serum of PeAF patients was much higher than that of healthy people, as shown in **Figure 1E**.

Alterations in Intestinal Flora Diversity

To further explore the differences between the diversity of intestinal flora in the PeAF patients and healthy people, we performed 16S rRNA sequencing on all subjects. As shown in **Figure 2A**, a Venn diagram was drawn based on the common and unique ASVs of the two groups of people. There were 342 unique ASVs in the control group, 200 unique ASVs in the PeAF group, and 310 ASVs were shared between the control and PeAF groups. The Wilcoxon rank-sum test was performed to analyze the differences in the alpha diversity index between the two groups. The results showed that the Chao1 index, ACE index, Shannon index and Simpson index showed no significant differences between the PeAF group and the control group ($p > 0.05$) (**Figures 2B–E**). Therefore, there

TABLE 1 | Baseline characteristics of subjects.

	Control	PeAF	Difference	*P*-value
Age	40.5 ± 8.7[a]	71.4 ± 10.2	ns	0.673
Female/Male	6/4	6/4		
BMI/(kg/m^2)	22.24 ± 2.30	22.118 ± 3.00	ns	>0.9999
SBP/mmHg	124 ± 11.08	128 ± 24.47	ns	>0.9999
DBP/mmHg	72 ± 7.28	84.2 ± 13.57	ns	>0.9999
NYHA				
II		3		
III		4		
IV		3		
CRE/(μmol/L)	68.9 ± 9.22	144.2 ± 153.20	***	0.0003
SUA/(μmol/L)	293 ± 70.85	413.51 ± 111.97	****	<0.0001
FBG/(μmol/L)	5.039 ± 0.49	6.769 ± 2.30	ns	>0.9999
ALB/(g/L)	48.41 ± 3.64	35.35 ± 3.84	ns	0.9998
TC/(μmol/L)	4.942 ± 0.96	3.77 ± 0.86	ns	>0.9999
TG/(μmol/L)	1.048 ± 0.41	1.149 ± 0.43	ns	>0.9999
HDL-c/(μmol/L)	1.329 ± 0.32	1.01 ± 0.48	ns	>0.9999
LDL-c/(μmol/L)	3.164 ± 1.01	2.182 ± 0.63	ns	>0.9999
WBC/(×10^9/L)	5.776 ± 1.10	6.151 ± 2.87	ns	>0.9999
N/(×10^9/L)	3.063 ± 0.51	4.795 ± 2.73	ns	>0.9999

*[a]represented mean ± standard deviation, ns indicated no statistical difference, ***compared with the control group, P < 0.001, ****compared with the control group, P < 0.0001. BMI, Body Mass Index; SBP, Systolic Blood Pressure; DBP, Diastolic Blood Pressure; NYHA, New York Heart Association class; CRE, Creatinine; SUA, Serumuric Acid; FBG, Fasting Blood Glucose; ALB, Albumin; TC, Total cholesterol; TG, Triacylglycerol; HDL-c, high-density lipoprotein cholesterol; LDL-c, low-density lipoprotein cholesterol; WBC, White Blood Cells; N, Neutrophil.*

were no significant differences between the intestinal flora of PeAF patients and healthy people in terms of alpha diversity. Next, we analyzed the differences in Bray-Curtis, unweighted UniFrac, and weighted UniFrac between the two groups using the Wilcoxon rank-sum test. The results showed that Bray-Curtis and weighted UniFrac index were significantly different between the two groups (**Figures 2F,H**). The unweighted UniFrac index was slightly different between the groups ($0.05 < p < 0.1$) (**Figure 2G**). These results show significant differences in the β diversity of the intestinal flora between the PeAF patients and healthy people.

Changes in the Intestinal Microbial Community Structure

As shown in **Figure 3A**, we used the Anosim analysis method to conduct similarity analysis on the community structures of the grouped samples and found that the community structures between the control group and the PeAF group were significantly different ($P = 0.001$) (**Figure 3A**). Further analysis of the community structure differences of different samples and groups at the phylum and species levels showed that at the phylum level, the relative abundances of Firmicutes and Actinobacteria showed a downward trend in the PeAF patients compared to the healthy people. At the same time, Bacteroidetes, Verrucomicrobia, and Proteobacteria followed an opposite trend (**Figures 3B,C**). At the species level, we noticed that the healthy people had more abundant intestinal flora than the PeAF patients in terms of community structure (**Figures 3D,E**). Therefore, compared with healthy people, the structural composition of the intestinal flora in PeAF patients is changed.

Abundance Analysis of Differential Bacteria and Their Correlation With Myocardial Fibrosis

We further analyzed the differences in the relative abundances in the flora at different levels. As shown in **Figure 4A**, we first conducted a heat map analysis of the relative abundances of different bacterial groups at the family level. The abundances of different bacterial genera in the two groups of people were quite different. Among these differences, the relative abundances of *Dorea* (**Figure 4B**), *Fusicatenibacter* (**Figure 4C**), *[Eubacterium]_hallii_group* (**Figure 4D**) and *[Ruminococcus]_torques_group* (**Figure 4E**) were significantly reduced in the PeAF patients. Coincidentally, these four taxa belong to the Firmicutes phylum.

As shown in **Figure 5A**, at the species level, the relative abundances of some bacterial taxa were quite different between the control group and the PeAF group. Further analysis revealed that compared with the control group, the abundances of *g_Fusicatenibacter_ASV_26* (*Fusicatenibacter* genus) and *g_Blautia_ASV_5* (*Blautia* genus) were significantly reduced in the PeAF group (**Figures 5B,C**). The abundances of *g__Faecalibacterium_ASV_20* (*Faecalibacterium* genus), *g__Blautia_ASV_21* (*Blautia* genus), and *Bacteroides_uniformis* (*Bacteroides*) in the PeAF group were significantly increased (**Figures 5D–F**). In addition, through Spearman's

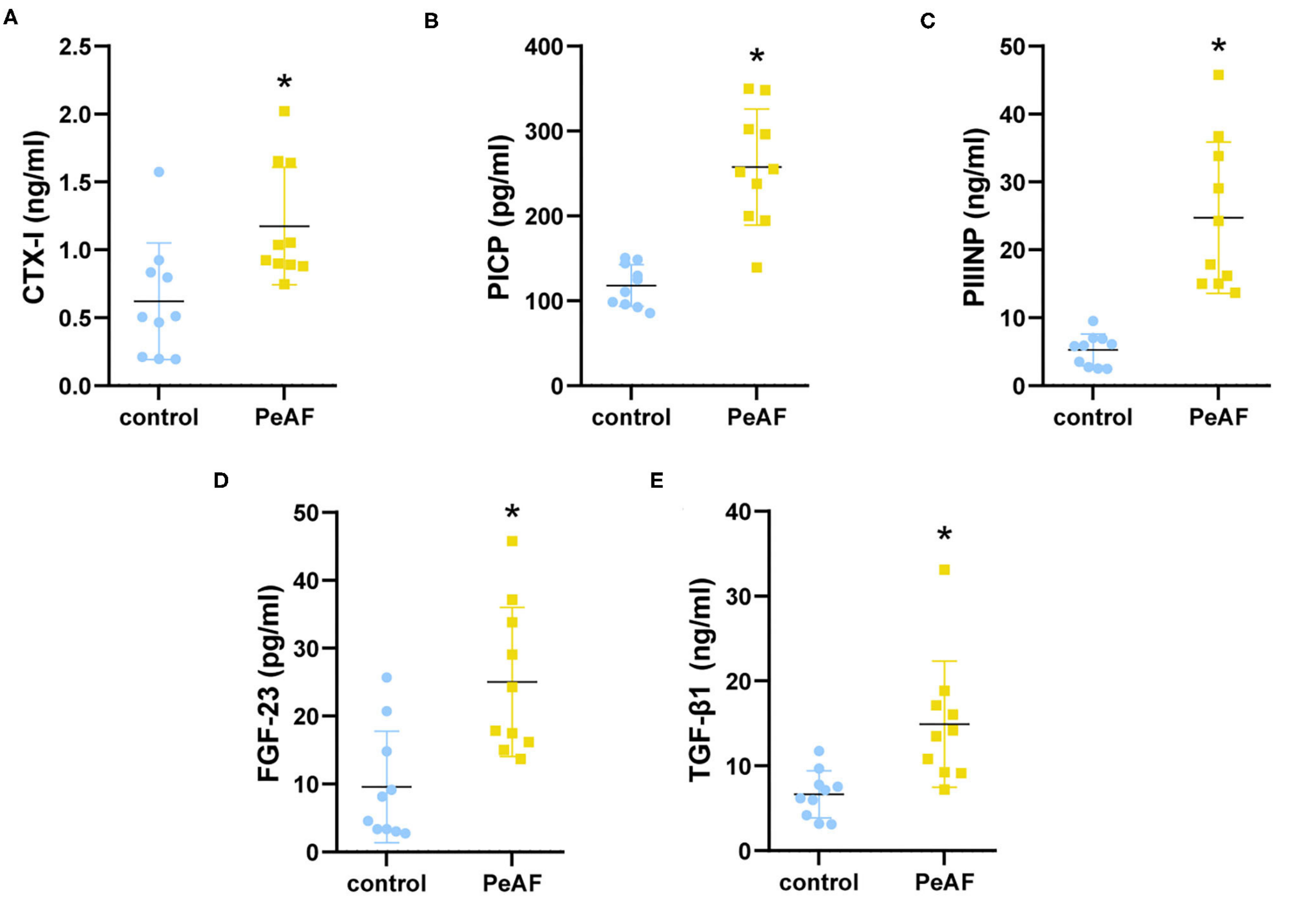

FIGURE 1 | Serum levels of myocardial fibrosis markers. **(A)** Levels of CTX-I in serum. **(B)** Levels of PICP in serum. **(C)** Levels of PIIINP in serum. **(D)** Levels of FGF-23 in serum. **(E)** Levels of TGF-β1 in serum. **(F)** Levels of PIIINP in serum. $^{*}p < 0.05$ vs. control group. CTX-I, carboxy-terminal telopeptide of type I collagen; PICP, propeptide of type I procollagen; PIIINP, procollagen III N-terminal propeptide; FGF-23, fibroblast growth factor-23; TGF-β1, transforming growth factor-beta 1.

correlation analysis, we found that, at the species level, *g__Faecalibacterium_ASV_20* (*Faecalibacterium* genus) had a significant positive correlation with the CTX-I, PICP, PIIINP and FGF-23 level ($p < 0.05$). *g__Blautia_ASV_21* (*Blautia* genus) was also significantly positively correlated with PICP, PIIINP and FGF-23 levels ($p < 0.05$). *Bacteroides uniformis* (*Bacteroides* genus) was positively correlated with the level of the myocardial fibrosis marker FGF-23 ($p < 0.05$), while *g__Blautia_ASV_5* (*Blautia* genus) was significantly negatively correlated with FGF-23 and PIIINP level ($p < 0.05$) (**Figure 5G**).

Difference Analysis of Intestinal Metabolites

It is known that an essential way for the intestinal flora to exert positive and/or negative effects on the host is achieved through the metabolites produced by the flora. Therefore, we detected and analyzed the intestinal metabolites in the subjects in this study. As shown in **Figure 6**, the PCA score obtained by LC-MS metabonomics showed some degree of aggregation between the two groups (**Figure 6A**). Further analysis using PLS-DA (**Figure 6B**), OPLS-DA (**Figure 6C**), and SPLS-DA (**Figure 6D**) revealed that the control group samples were wholly separated from the PeAF group samples. We tested the abundances of 281 metabolites in total and analyzed the abundances of 70 different metabolites to generate an intestinal metabolite abundance heat map (**Figure 6E**). According to the multiple metabolite changes, we found that 48 metabolites were significantly increased, and 46 metabolites were significantly decreased in the PeAF group (**Figure 6F**).

Functional Analysis of Differential Metabolite Abundances and Their Correlations With Myocardial Fibrosis

Based on the differences in the abundances of intestinal metabolites that we found, we performed *t*-tests to analyze the changes in metabolites in the control group and the PeAF group. The top 5 differential metabolites that decreased and increased the most in the two groups were shown in **Figure 7A**, which were 2-hydroxy-2-methylbutyric acid, Glycochenodeoxycholate, Glycocholate, 1,3-dimethyluric acid, 1,9-Dimmethyluric acid, Urate, Erucate, Heptadecanoate, Canrenone, and Furosemide.

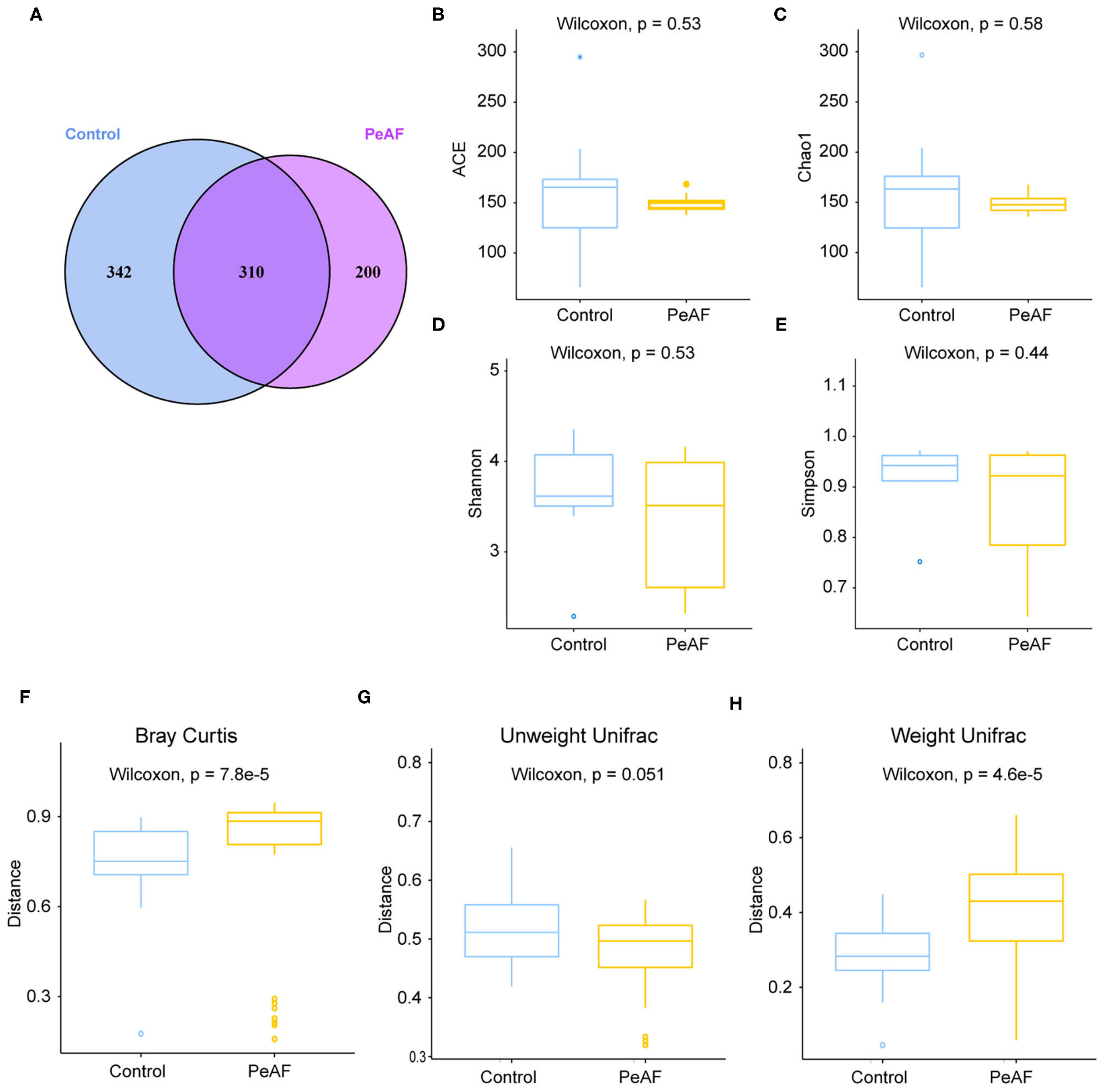

FIGURE 2 | Alterations in intestinal flora diversity. **(A)** Venn diagram of shared ASVs and ASVs unique to different populations. **(B)** ACE index. **(C)** Chao1 index. **(D)** Shannon index. **(E)** Simpson index. **(F)** Bray-Curtis analysis. **(G)** Unweighted UniFrac analysis. **(H)** Weighted UniFrac analysis. Wilcoxon rank sum test; $p < 0.05$ was considered statistically significant. When $0.05 < p < 0.1$, there was a relevant changing trend.

Among these, Glycochenodeoxycholate, 1,3-dimethyluric acid and 1,9-dimethyluric acid were significantly reduced in the PeAF group compared to the control group. The levels of Urate and Heptadecanoate were elevated considerably. Then, through KEGG pathway analysis, the top 16 signal pathways of the control group and the PeAF group were obtained (**Figure 7B**). The analysis performed using the KEGG pathway database (https://www.genome.jp/kegg/pathway.html), the functional metabolic pathways at the L1 level intestines PeAF patients changed significantly. In addition, 8 intestinal metabolites in the "valine, leucine, and isoleucine biosynthesis" pathway (L3 level) belonging to "amino acid metabolism" category (L2 level) were enriched in the PeAF patients ($p = 1.07E-02$); of these metabolites, C00671 [(S)-3-Methyl—2-oxopentanoic acid] and C00233 (4-Methyl-2-oxopentanoate) were significantly enriched in the intestines of the PeAF patients

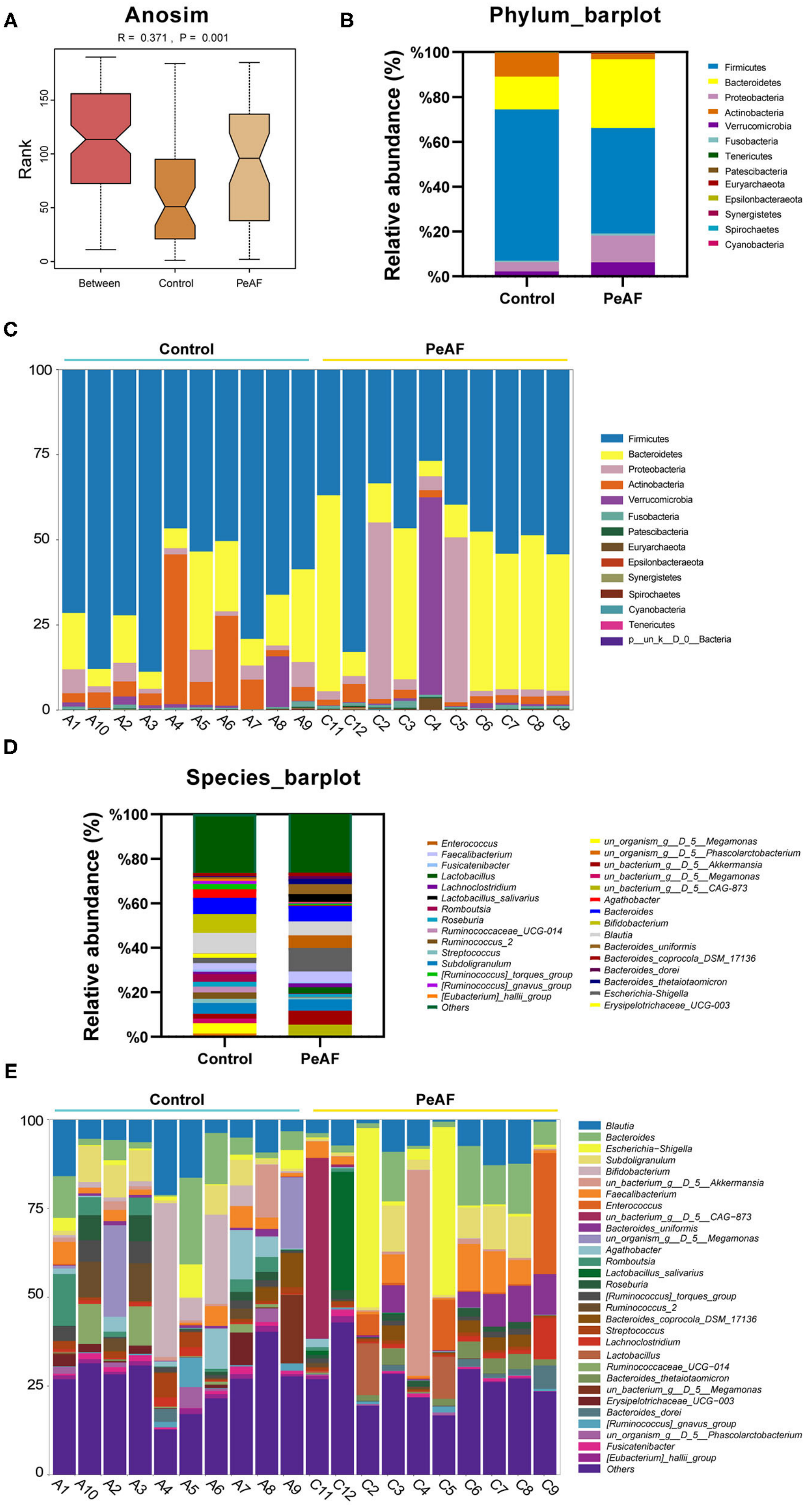

FIGURE 3 | Changes in the intestinal microbial community structure. **(A)** Anosim analysis; $p < 0.05$ was regarded as statistically significant. **(B,C)**. Histogram of the relative abundances in the intestinal flora of different populations at the phylum level. **(D,E)** Species-level analysis of the relative abundances in the intestinal flora of different populations.

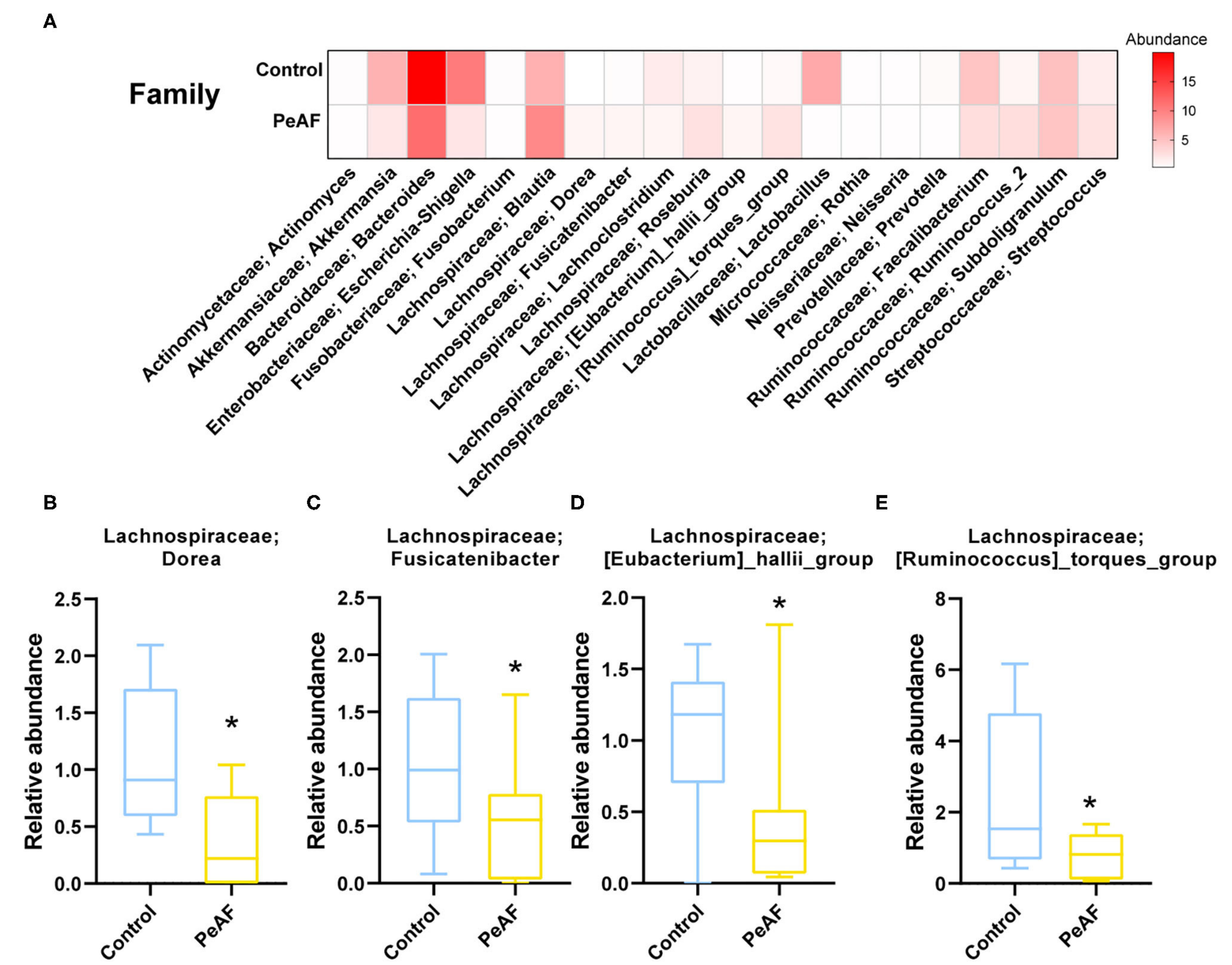

FIGURE 4 | Variations in the abundances in the intestinal flora at the family level. **(A)** Abundance heat map of the top 20 families; the darker the color is, the higher the abundance level. **(B)** The relative abundance of Lachnospiraceae; *Dorea*. **(C)** The relative abundance of Lachnospiraceae; *Fusicatenibacter*. **(D)** The relative abundance of Lachnospiraceae; *[Eubacterium]_hallii_group*. **(E)** The relative abundance of Lachnospiraceae; *[Ruminococcus]_torques_group*. *Compared to the control group, $p < 0.05$.

(**Figure 7B**). Meanwhile, a total of 42 plasma metabolites in the "tyrosine metabolism" pathway (L3 level) belonging to the "amino acid metabolism" category (L2 level) were enriched in the PeAF patients ($P = 5.32E\text{-}02$), of which metabolites C00628 (2,5-dihydroxybenzoate), C00642 (4-hydroxyphenylacetate), and C05582 (homovanillate) were significantly enriched in the intestines of patients in the PeAF group (**Figure 7B**). In addition, 46 intestinal metabolites in the "Primary bile acid biosynthesis" pathway (L3 level) belonging to the "Lipid metabolism" category (L2 level) were enriched ($P = 6.66E\text{-}02$), including C01921 (Glycocholate), C05466 (glycochenodeoxycholate), and C05122 (Taurocholate; Taurocholic acid), which were significantly enriched in the intestines of the PeAF patients (**Figure 7B**). These results indicate that the significantly enriched metabolites in the intestines of PeAF patients are related to the functional metabolic trends in amino acid metabolism and lipid metabolism pathways. Spearman's correlation analysis indicated that PIIINP significantly correlates with Urate, Erucate, Canrenone, and Furosemide ($p < 0.05$). In contrast, PIIINP has a significant negative correlation with 1,3-dimethyluric acid, 1,9-dimethyluric acid, Glycocholate, and glycochenodeoxycholate. FGF-23 is also significantly and negatively correlated with 1,3-dimethyluric acid and 1,9-dimethyluric acid. TGF-β1 was positively correlated with Urate and Erucate and negatively correlated with 2-hydroxy−2-methylbutyric acid. In addition, CTX-I, and PICP were positively correlated with Furosemide and Urate, respectively (**Figure 7C**). These results indicate that there may be a correlation between intestinal metabolism and myocardial fibrosis in PeAF patients.

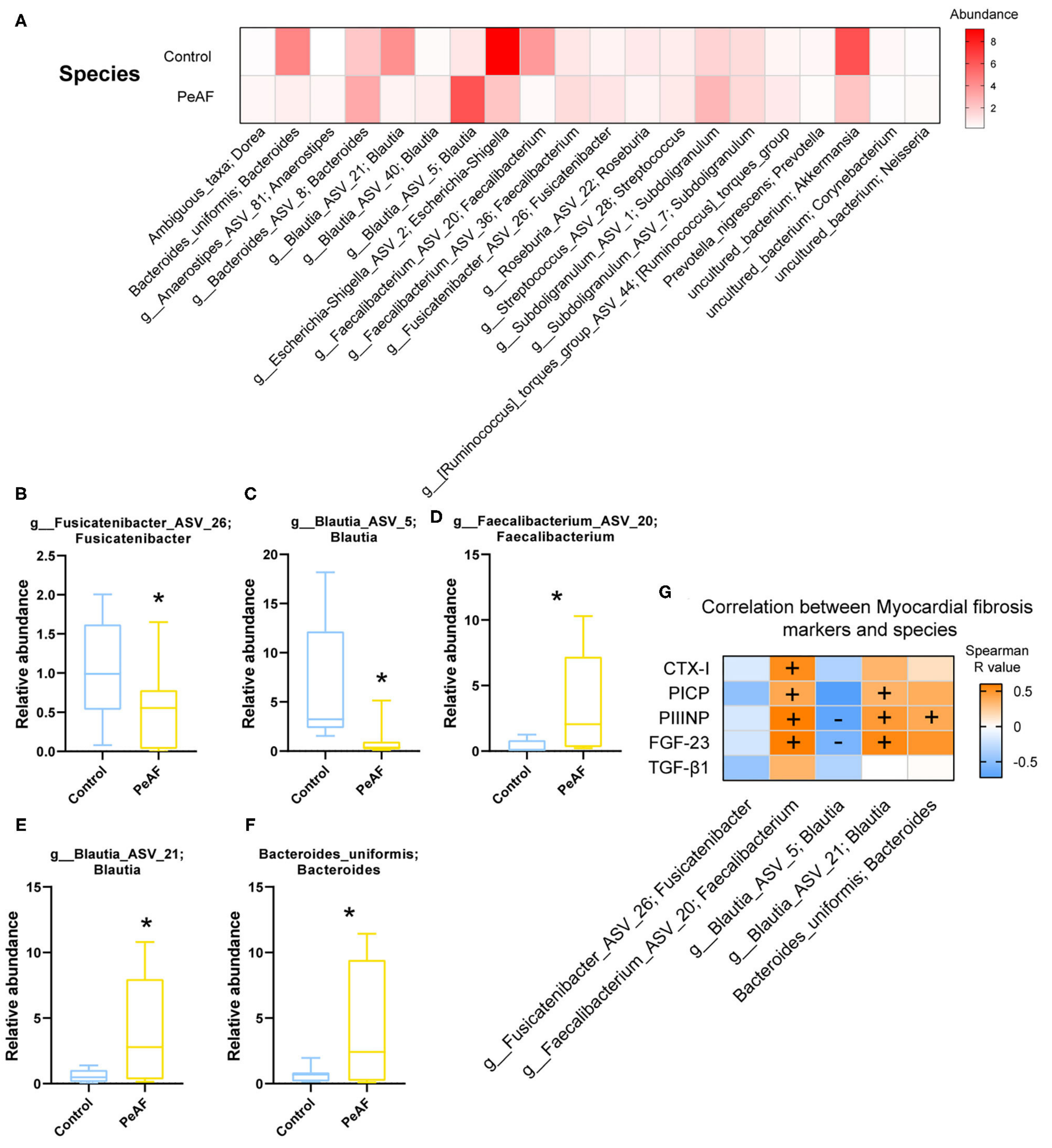

FIGURE 5 | Variations in the abundances in the intestinal flora at the species level. **(A)** Abundance heat map of the top 20 species; the darker the color is, the higher the abundance level. **(B)** Relative abundance of *g_Fusicatenibacter ASV 26; Fusicatenibacter.* **(C)** The relative abundance of *g_Blautia_ASV_5; Blautia.* **(D)** The relative abundance of *g_Faecalibacterium_ASV_20; Faecalibacterium.* **(E)** The relative abundance of *g_Blautia_ASV_21; Blautia.* **(F)** The relative abundance of *Bacteroides uniformis; Bacteroides.* *Compared to the control group, $p < 0.05$. **(G)**. Correlation analysis between myocardial fibrosis markers and different flora. "+" indicates positive correlation (orange), $p < 0.05$. "-" indicates negative correlation (blue), $p < 0.05$.

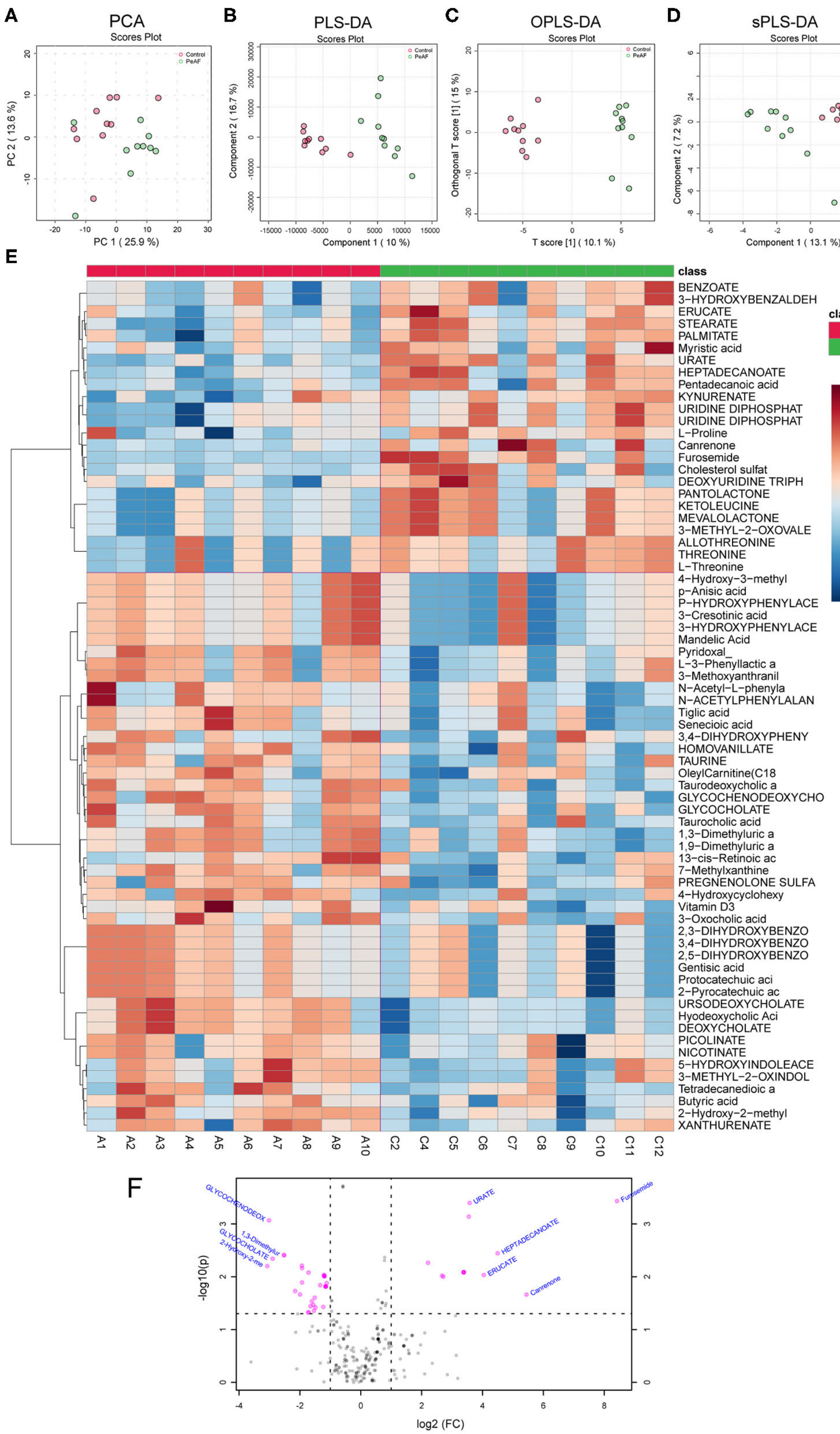

FIGURE 6 | Differences in metabolites produced by the intestinal flora. **(A)** Principal component analysis (PCA). **(B)** Partial least squares discriminant analysis (PLS-DA). **(C)** Orthogonal partial least squares discriminant analysis (OPLS-DA). **(D)** Sparse partial least squares-discriminant analysis (SPLS-DA). **(E)** Cluster analysis of 70 different types of metabolites. **(F)** Volcanic plot of differential metabolites (|log2(FC)|>1, PeAF/control).

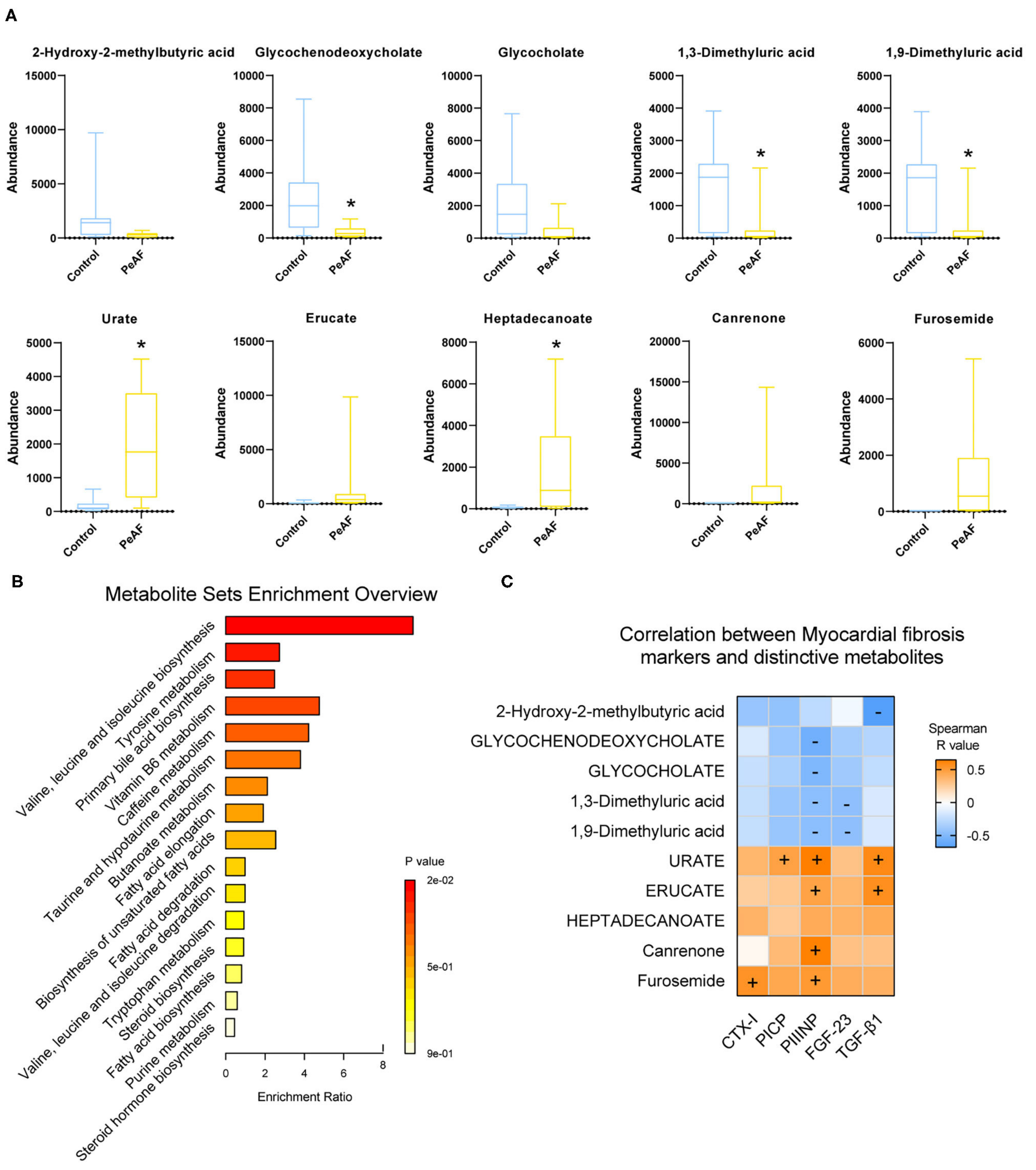

FIGURE 7 | Functional analysis of differential metabolites and their correlation with myocardial fibrosis. **(A)** The top 5 differential metabolites that decreased and increased the most between control group and PeAF group. *Compared to the control group, $p < 0.05$. **(B)** Analysis of KEGG pathways of differential metabolites. **(C)** Correlation analysis of myocardial fibrosis markers and differential metabolites. "+" indicates positive correlation (orange), $p < 0.05$. "–" indicates negative correlation (blue), $p < 0.05$.

DISCUSSION

In this study, the relationship between myocardial fibrosis and the composition of the intestinal flora and metabolic function in patients with PeAF was preliminarily explored. Atrial fibrillation (AF) is mediated by oxidative stress, neurohormonal activation, and inflammatory activation. Serum uric acid (SUA) is a surrogate indicator of oxidative stress (21). The reduction in the urinary albumin/creatinine ratio caused by high creatinine levels has also been associated with an increased risk of atrial fibrillation (22). In this study, similar results were obtained, and the levels of SUA and creatinine in the PeAF patients were significantly higher than those in the healthy population. Atrial fibrosis is a sign of the remodeling of the heart structure in patients with atrial fibrillation, and it is the basis for the development of atrial fibrillation. In addition, atrial fibrillation can aggravate atrial fibrosis. We found high levels of the cardiac fibrosis markers CIXT, PICP, PIIICP, FGF-23, and TGF-β1 in PeAF patients. Similar to CRE, FGF-23 levels have been previously reported to increase with decreased renal function in patients with atrial fibrillation (23). The health and normal functioning of the cardiovascular system and the renal system mainly depend on the crosstalk of the gut-kidney-cardiovascular system (24). It was also reflected in our research.

In recent years, the role of intestinal flora in cardiovascular disease has gradually attracted attention. Researchers have found that in many diseases, including atrial fibrillation, the structure and composition of the intestinal flora change to a certain extent. In this study, although the alpha diversity of the intestinal flora between healthy people and PeAF patients was no apparent difference, we observed significant differences in the relative indexes in terms of beta diversity, such as Bray-Curtis, weighted UniFrac and Anosim. It implies that the steady state of the intestinal microbial community structure of the PeAF population had been altered. Similarly, in a previous investigation, researchers found that the abundance of gut microbes in AF patients was lower than that of people without atrial fibrillation. However, they found no differences in gut microbial diversity between the two groups (25). This result may have been due to the limited number of samples. Firmicute has been identified as a beneficial bacterial phylum. In this study, at the phylum level, the abundance of Firmicutes was decreased sharply in the PeAF patients. In contrast, the abundance of Actinobacteria was significantly increased in the PeAF patients. Notably, the abundance of *Blautia* (Firmicutes phylum) has also been previously found to be significantly reduced in patients with chronic heart failure (26). *Rothia* (Actinobacteria phylum) has been found that was over-enriched in patients with certain diseases, such as pancreatic cancer and primary sclerosing cholangitis (27, 28). Previous studies have also indicated that a reduction in *Faecalibacterium prausnitzii* abundance is one of the fundamental characteristics of patients with chronic heart failure (29). However, at the species level, we observed an increase in the abundance of *g_Faecalibacterium_ASV_20* (*Faecalibacterium* genus) in the PeAF patients, which may be related to differences in the pathological development of different diseases. Kaburova et al. found that both PICP and PIIINP were significantly and negatively correlated with beneficial intestinal bacteria and significantly positively correlated with several potentially harmful bacteria in the intestine (30). We found that at the species level, *g_Faecalibacterium_ASV_20* (*Faecalibacterium* genus) and *g__Blautia_ASV_21* (*Blautia* genus) were significantly and positively correlated with PICP, PIIINP, and FGF-23 level, while *g__Blautia_ASV_5* (*Blautia* genus) was significantly and negatively correlated with PIIINP and FGF-23 level. This finding suggests that the specific intestinal flora of PeAF patients may be involved in the process of myocardial fibrosis.

The evidence obtained to date suggests that one of the potential mechanisms by which the intestinal flora has an impact on the host is by directly affecting the host through host-derived metabolites. For example, SCFAs produced through the metabolism of the intestinal flora can maintain the host's sugar, lipid and protein metabolism balance and reduce the occurrence and development of cardiovascular diseases (31). The metabolism of intestinal microorganisms determines the developmental direction of the host's health and illness to a certain extent. This study found that the intestinal metabolites Urate (i.e., Uric acid) and Heptadecanoate were increased significantly in the PeAF patients. Among them, uric acid is the end product of purine metabolism in humans. Studies have shown that Urate acts as a pro-oxidant at high concentrations, which induces AF to activate apoptosis and the immune system (32, 33). Kuo et al. found that in AF patients, the variation trend of some metabolites in feces and serum was consistent (13). Coincidentally, we also found a synchronous increase of uric acid in feces and serum in PeAF patients in this study. Thus, we hypothesize that gut microbial dysfunction at least partly affected the development of AF through internal circulation. In contrast, we found that the levels of 1,3/1,9-Dimethyluric acid and Glycochenodeoxycholate (i.e., Glycochenodeoxycholic acid) in the PeAF patients were significantly decreased. Glycochenodeoxycholate is a kind of conjugated primary bile acid. Although the abundance of Glycocholate (i.e., Glycocholic acid) did not differ significantly between the two groups, we observed a decreasing trend in the PEAF group. Interestingly, Glycochenodeoxycholate and Glycocholate belong to primary bile acids and secondary acids, respectively.

There is evidence that excessive lipid accumulation can lead to apoptosis and mitochondrial dysfunction and increase cardiac fibrosis (34, 35). In this study, we found through a KEGG pathway analysis that some enriched metabolites in PeAF patients are related to amino acid metabolism (valine, leucine, and isoleucine biosynthesis and tyrosine metabolism) and lipid metabolism (primary bile acid biosynthesis) pathways. Therefore, reducing amino acid metabolism and lipid metabolism damage may be an essential way to improve myocardial fibrosis patients with atrial fibrillation. In this study, Spearman's correlation analysis revealed that some metabolites were significantly related to myocardial fibrosis markers, especially PIIINP. Therefore, we speculate that the changes in the composition and structure of the specific flora of PeAF patients may trigger certain metabolic changes, and the resulting disruption in intestinal homeostasis may be a strong promoter that accelerates the process of myocardial fibrosis in PeAF patients.

We must admit that our study also has some limitations. On the one hand, the sample size included in this study was limited. It resulted in some changes that were not significantly different between the two groups (although some trends were observed). On the other hand, there was age bias between the two groups. Some of the differences in gut microbiota between individuals may be caused by age (36). Although we cannot completely rule out age bias in this study, we are collecting more clinical samples. We will validate our findings in larger cohorts and try to minimize any possible differences between groups due to age.

CONCLUSION

In summary, our research shows that the occurrence of atrial fibrillation is accompanied by a certain degree of intestinal flora disorder. In addition, the degree of cardiac fibrosis in patients with atrial fibrillation is closely related to the abundance and metabolic function of particular intestinal flora. These microbes may directly or indirectly participate in cardiac fibrosis through metabolic pathways in patients with atrial fibrillation. The results provide new insights into the relationship between atrial fibrillation-myocardial fibrosis and intestinal flora.

DATA AVAILABILITY STATEMENT

The datasets presented in this study can be found in online repositories. The names of the repository/repositories and accession number(s) can be found at: https://www.ncbi.nlm.nih.gov/sra/PRJNA728204.

ETHICS STATEMENT

The studies involving human participants were reviewed and approved by the Ethic Committee of Xiangya Hospital Central South University (202004176). The patients/participants provided their written informed consent to participate in this study.

AUTHOR CONTRIBUTIONS

FL and LL designed the research and performed the research. JS and RL analyzed the data. All authors contributed to the writing and revisions and reviewed the manuscript.

FUNDING

This study was supported by the National Natural Science Foundation of China (to FL; no. 82070352).

REFERENCES

1. Zuo K, Yin X, Li K, Zhang J, Wang P, Jiao J, et al. Different types of atrial fibrillation share patterns of gut microbiota dysbiosis[J]. *mSphere.* (2020) 5:e00071-20. doi: 10.1128/mSphere.00071-20
2. Sohns C, Marrouche NF. Atrial fibrillation and cardiac fibrosis. *Eur Heart J.* (2020) 41:1123–31. doi: 10.1093/eurheartj/ehz786
3. Xintarakou A, Tzeis S, Psarras S, Asvestas D, Vardas P. Atrial fibrosis as a dominant factor for the development of atrial fibrillation: facts and gaps. *Europace*. (2020) 22:342–51. doi: 10.1093/europace/euaa009
4. Begg GA, Holden AV, Lip GY, Plein S, Tayebjee MH. Assessment of atrial fibrosis for the rhythm control of atrial fibrillation. *Int J Cardiol.* (2016) 220:155–61. doi: 10.1016/j.ijcard.2016.06.144
5. Ding Y, Wang Y, Zhang W, Jia Q, Wang X, Li Y, et al. Roles of biomarkers in myocardial fibrosis. *Aging Dis.* (2020) 11:1157–74. doi: 10.14336/AD.2020.0604
6. Bi X, Yang C, Song Y, Yuan J, Cui J, Hu F, et al. Matrix metalloproteinases increase because of hypoperfusion in obstructive hypertrophic cardiomyopathy. *Ann Thorac Surg.* (2021) 111:915–22. doi: 10.1016/j.athoracsur.2020.05.156
7. Vázquez-Sánchez S, Poveda J, Navarro-García JA, González-Lafuente L, Rodríguez-Sánchez E, Ruilope LM, et al. An overview of FGF-23 as a novel candidate biomarker of cardiovascular risk. *Front Physiol.* (2021) 12:632260. doi: 10.3389/fphys.2021.632260
8. Dong Q, Li S, Wang W, Han L, Xia Z, Wu Y, et al. FGF23 regulates atrial fibrosis in atrial fibrillation by mediating the STAT3 and SMAD3 pathways. *J Cell Physiol.* (2019) 234:19502–10. doi: 10.1002/jcp.28548
9. Manfrini O, Cenko E, Ricci B, Bugiardini R. Post cardiovascular surgery atrial fibrillation. biomarkers determining prognosis. *Curr Med Chem.* (2019) 26:916–24. doi: 10.2174/0929867324666170727104930
10. Li CY, Zhang JR, Hu WN, Li SN. Atrial fibrosis underlying atrial fibrillation (Review). *Int J Mol Med.* (2021) 47:1. doi: 10.3892/ijmm.2020.4842
11. Zhou W, Cheng Y, Zhu P, Nasser MI, Zhang X, Zhao M. Implication of gut microbiota in cardiovascular diseases. *Oxid Med Cell Longev*. (2020) 2020:5394096. doi: 10.1155/2020/5394096
12. Tang WHW, Bäckhed F, Landmesser U, Hazen SL. Intestinal microbiota in cardiovascular health and disease: JACC state-of-the-Art review. *J Am Coll Cardiol.* (2019) 73:2089–105. doi: 10.1016/j.jacc.2019.03.024
13. Zuo K, Li J, Li K, Hu C, Gao Y, Chen M, et al. Disordered gut microbiota and alterations in metabolic patterns are associated with atrial fibrillation. *GigaScience*. (2019) 8:giz058. doi: 10.1093/gigascience/giz058
14. Zuo K, Li J, Wang P, Liu Y, Liu Z, Yin X, et al. Duration of persistent atrial fibrillation is associated with alterations in human gut microbiota and metabolic phenotypes. *mSystems.* (2019) 4:e00422-19. doi: 10.1128/mSystems.00422-19
15. Li J, Zuo K, Zhang J, Hu C, Wang P, Jiao J, et al. Shifts in gut microbiome and metabolome are associated with risk of recurrent atrial fibrillation. *J Cell Mol Med.* (2020) 24:13356–69. doi: 10.1111/jcmm.15959
16. Jia J, Dou P, Gao M, Kong X, Li C, Liu Z, et al. Assessment of causal direction between gut microbiota-dependent metabolites and cardiometabolic health: a bidirectional mendelian randomization analysis. *Diabetes.* (2019) 68:1747–55. doi: 10.2337/db19-0153
17. Zuo K, Liu X, Wang P, Jiao J, Han C, Liu Z, et al. Metagenomic data-mining reveals enrichment of trimethylamine-N-oxide synthesis in gut microbiome in atrial fibrillation patients. *BMC Genomics.* (2020) 21:526. doi: 10.1186/s12864-020-06944-w
18. Tang WHW, Li DY, Hazen SL. Dietary metabolism, the gut microbiome, and heart failure. *Nat Rev Cardiol.* (2019) 16:137–54. doi: 10.1038/s41569-018-0108-7
19. Agewall S, Camm J. New ESC/ EACTS Guidelines for the management of atrial fibrillation[J]. *Eur Heart J Cardiovas Pharmacother.* (2017) 3:71.
20. Tamariz L, Hernandez F, Bush A, Palacio A, Hare JM. Association between serum uric acid and atrial fibrillation: a systematic review and meta-analysis. *Heart Rhythm.* (2014) 11:1102–8. doi: 10.1016/j.hrthm.2014.04.003
21. Laukkanen JA, Zaccardi F, Karppi J, Ronkainen K, Kurl S. Reduced kidney function is a risk factor for atrial fibrillation. *Nephrology.* (2016) 21:717–20. doi: 10.1111/nep.12727
22. Carrero JJ, Trevisan M, Sood MM, Bárány P, Xu H, Evans M, et al. Incident atrial fibrillation and the risk of stroke in adults with chronic kidney disease:

the Stockholm CREAtinine Measurements (SCREAM) project. *Clin J Am Soc Nephrol.* (2018) 13:1314–20. doi: 10.2215/CJN.04060318
23. Onal EM, Afsar B, Covic A, Vaziri ND, Kanbay M. Gut microbiota and inflammation in chronic kidney disease and their roles in the development of cardiovascular disease. *Hypertens Res.* (2019) 42:123–40. doi: 10.1038/s41440-018-0144-z
24. Tabata T, Yamashita T, Hosomi K, Park J, Hayashi T, Yoshida N, et al. Gut microbial composition in patients with atrial fibrillation: effects of diet and drugs. *Heart Vessels.* (2020) 36:105–14. doi: 10.1007/s00380-020-01669-y
25. Luedde M, Winkler T, Heinsen FA, Rühlemann MC, Spehlmann ME, Bajrovic A, et al. Heart failure is associated with depletion of core intestinal microbiota. *ESC Heart Fail.* (2017) 4:282–90. doi: 10.1002/ehf2.12155
26. Bajer L, Kverka M, Kostovcik M, Macinga P, Dvorak J, Stehlikova Z, et al. Distinct gut microbiota profiles in patients with primary sclerosing cholangitis and ulcerative colitis. *World J Gastroenterol.* (2017) 23:4548–58. doi: 10.3748/wjg.v23.i25.4548
27. Kohi S, Macgregor-Das A, Dbouk M, Yoshida T, Chuidian M, Abe T, et al. Alterations in the duodenal fluid microbiome of patients with pancreatic cancer[J]. *Clin Gastroenterol Hepatol.* (2020). doi: 10.1016/j.cgh.2020.11.006. [Epub ahead of print].
28. Cui X, Ye L, Li J, Jin L, Wang W, Li S, et al. Metagenomic and metabolomic analyses unveil dysbiosis of gut microbiota in chronic heart failure patients. *Sci Rep.* (2018) 8:635. doi: 10.1038/s41598-017-18756-2
29. Kaburova AN, Drapkina OM, Uydin SM, Pokrovskaya MS, Koretsky SN, Efimova IA, et al. The relationship between the key markers of myocardial fibrosis and gut microbiota composition in patients with heart failure and preserved ejection fraction. *Eur Heart J.* (2020) 41(Suppl. 2). doi: 10.1093/ehjci/ehaa946.0861
30. Zhu Y, Shui X, Liang Z, Huang Z, Qi Y, He Y, et al. Gut microbiota metabolites as integral mediators in cardiovascular diseases (Review). *Int J Mol Med.* (2020) 46:936–48. doi: 10.3892/ijmm.2020.4674
31. Bachhawat AK, Yadav S, Jainarayanan AK, Dubey P. Heart failure and the glutathione cycle: an integrated view. *Biochem J.* (2020) 477:3123–30. doi: 10.1042/BCJ20200429
32. van der Pol A, Gil A, Tromp J, Silljé HHW, van Veldhuisen DJ, Voors AA, et al. OPLAH ablation leads to accumulation of 5-oxoproline, oxidative stress, fibrosis, and elevated fillings pressures: a murine model for heart failure with a preserved ejection fraction. *Cardiovasc Res.* (2018) 114:1871–82. doi: 10.1093/cvr/cvy187
33. Wei SG, Yu Y, Weiss RM, Felder RB. Endoplasmic reticulum stress increases brain MAPK signaling, inflammation and renin-angiotensin system activity and sympathetic nerve activity in heart failure. *Am J Physiol Heart Circ Physiol.* (2016) 311:H871–h80. doi: 10.1152/ajpheart.00362.2016
34. Groenendyk J, Lee D, Jung J, Dyck JR, Lopaschuk GD, Agellon LB, et al. Inhibition of the unfolded protein response mechanism prevents cardiac fibrosis. *PLoS ONE.* (2016) 11:e0159682. doi: 10.1371/journal.pone.0159682
35. Lee HC, Lin YH. The pathogenic role of very low density lipoprotein on atrial remodeling in the metabolic syndrome. *Int J Mol Sci.* (2020) 21:891. doi: 10.3390/ijms21030891
36. Schulze PC, Drosatos K, Goldberg IJ. Lipid use and misuse by the heart. *Circul Res.* (2016) 118:1736–51. doi: 10.1161/CIRCRESAHA.116.306842

Conflict of Interest: The authors declare that the research was conducted in the absence of any commercial or financial relationships that could be construed as a potential conflict of interest.

frontiers in Nutrition

ORIGINAL RESEARCH
published: 13 September 2021
doi: 10.3389/fnut.2021.702659

Gut Microbiota Disorders Promote Inflammation and Aggravate Spinal Cord Injury Through the TLR4/MyD88 Signaling Pathway

Zijie Rong[1,2], *Yuliang Huang*[2,3], *Honghua Cai*[1,2], *Min Chen*[1,2], *Hao Wang*[1,2], *Guihua Liu*[1,2], *Zhiwen Zhang*[2,3] *and Jiawen Wu*[4]*

[1] *Department of Spine Surgery, Huizhou Municipal Central Hospital, Huizhou, China,* [2] *Orthopaedic Institute, Huizhou Municipal Central Hospital, Huizhou, China,* [3] *Department of Orthopaedics, Huizhou Municipal Central Hospital, Huizhou, China,* [4] *Department of Spine Surgery, The People's Hospital of Longhua, Shenzhen Longhua Clinical Medical College of Guangdong Medical University, Shenzhen, China*

OPEN ACCESS

Edited by:
Jie YIN,
Hunan Agricultural University, China

Reviewed by:
Sachchida Nand Rai,
University of Allahabad, India
Yong Cao,
Central South University, China
Alexis M. Ziemba,
Smith College, United States

***Correspondence:**
Jiawen Wu
78141350@qq.com

Specialty section:
This article was submitted to Nutrition and Microbes, a section of the journal Frontiers in Nutrition

Received: *29 April 2021*
Accepted: *23 August 2021*
Published: *13 September 2021*

Citation:
Rong Z, Huang Y, Cai H, Chen M, Wang H, Liu G, Zhang Z and Wu J (2021) Gut Microbiota Disorders Promote Inflammation and Aggravate Spinal Cord Injury Through the TLR4/MyD88 Signaling Pathway. Front. Nutr. 8:702659. doi: 10.3389/fnut.2021.702659

Background: In spinal cord injury (SCI), systemic inflammation and the death of nerve cells in the spinal cord are life threatening. The connection between gut microbiota and signaling pathways has been a hot research topic in recent years. The Toll-like receptor 4/Myeloid differentiation factor 88 (TLR4/MyD88) signaling pathway is closely related to the inflammatory response. This study explored whether the gut microbiota imbalance could affect the TLR4/MyD88 signaling pathway to regulate SCI to provide a new basis for SCI research and treatment.

Methods: An SCI model was constructed to study the influence on the injury of gut microbiota. 16S amplicon sequencing was used to identify the diversity and abundance of gut microbes. Fecal microbiota transplantation was performed in mice with SCI. ELISA was used to detect the serum levels of pro-inflammatory and anti-inflammatory factors in mice. Hematoxylin and eosin staining was used to observe SCI in mice. Immunofluorescence was used to detect the rates of loss glial fibrillary acidic protein (GFAP), neuronal nuclear protein (NeuN), and ionized calcium-binding adapter molecule 1 (IBA1) in the spinal cord as indicators of apoptosis. The expression of the TLR4/MyD88 signaling pathway was detected by qRT-PCR and western blotting.

Results: Significant differences were observed in the gut microbiota of SCI mice and normal mice. The gut microbiota of SCI mice was imbalanced. The levels of pro-inflammatory cytokines tumor necrosis factor-α, interleukin (IL)-1β, and IL-6 in SCI mice were increased, as was the level of the toxic induced nitric oxide synthase. The levels of anti-inflammatory factors IL-4, transforming growth factor-β, and IL-10 were decreased, as was the level of arginase-1. The apoptosis rates of GFAP, NeuN, and IBA1 were increased. The TLR4/MyD88 signaling pathway was activated. In the SCI group, inflammation increased after fecal transplantation, apoptosis of GFAP, NeuN, and IBA1 increased, and SCI was more serious.

Conclusion: The TLR4/MyD88 signaling pathway promotes the death of nerve cells by inducing inflammation. Gut microbiota dysregulation can lead to aggravated SCI by activating the TLR4/MyD88 signaling pathway.

Keywords: SCI, gut microbiota, TLR4, MyD88, GFAP, inflammation

INTRODUCTION

SCI has a significant socio-economic impact on society reflecting the considerable life-long health care expenditures (1). In SCI, synaptic connection loss, demyelination, and axonal injury destroy signal propagation, and neurons undergo mechanically induced cell death (2). Excessive inflammation may hinder nerve repair and regeneration. Many studies have been conducted to improve the treatment of SCI by reducing secondary inflammation (3). However, SCI treatment remains a medical concern worldwide.

Oral broad-spectrum antibiotics produce an imbalance in the gut microbiota due to the perturbation of the gut microbiota. This alteration in the gut microbiota can exacerbate neurological damage and spinal cord pathology after SCI. Dysbiosis develops when the composition of the gut microbiota is altered such that beneficial non-pathogenic gut bacteria (i.e., probionts) are depleted or become overwhelmed by pathogenic inflammatory bacteria (i.e., pathobionts). Autoimmune diseases (e.g., multiple sclerosis, type I diabetes, and rheumatoid arthritis), allergies, and metabolic disorders have been linked to gut dysbiosis (4–7). Recent data in humans and rodent models suggest that changes in the gut microbiota are disease-mitigating factors that could affect system physiology and pathophysiology. The exact mechanism remains unclear.

Changes in the composition of the gut microbiota and its metabolites will transfer from the intestine to the intestinal wall and cross the ruptured intestinal barrier, intensifying inflammation and affecting various organs (8). Fecal microbiota transplantation (FMT) protects Parkinson's disease model mice by inhibiting neuroinflammation and reducing Toll-like receptor 4/Tumor necrosis factor-alpha (TLR4/TNF-α) signaling (9). Studies show that SCI-induced gut dysbiosis is involved in the development of anxiety-like behavior following SCI, since both gut dysbiosis and anxiety-like behaviors were significantly reduced following treatment with an FMT. TLR4 is expressed on the cell membranes of microglia, the principal immune cells of the central nervous system (CNS). It was postulated that microglial activation participates in I/R injury through the release of growth factors, chemokines, regulatory cytokines, and other toxic mediators (10). Changes in the gut microbiota lead to neuroinflammation and intestinal damage through intestinal leakage and TLR4 activation (11). TLR4 promotes microglial apoptosis by activating the phosphoinositide 3-kinase (PI3K)/AKT pathway after SCI (12). Following SCI, necrotic astrocytes induce high inflammatory response genes encoding TLR4 and myeloid differentiation primary response gene 88 (MyD88) (13). Overexpression of the TLR4 receptor leads to enhanced astrocyte proliferation/microglial cell response and exacerbates SCI (14). However, it has not yet been reported that the gut microbiota exacerbates SCI through the TLR4/MyD88 signaling pathway. We used FMT to explore whether the gut microbiota of SCI mice could exacerbate SCI and systemic inflammation in mice.

TLR4 is activated by lipopolysaccharide (LPS), a component of the cell envelope of gram-negative bacteria. Activated TLR4 induces the production of pro-inflammatory mediators to destroy the bacteria (15). Dysregulation of the host response to LPS can lead to a systemic inflammation called sepsis (16). Typically, before TLR4 is activated, it binds to CD14 proteins anchored in cholesterol and sphingolipid-rich microdomain (termed a raft) in the plasma membrane (17). MyD88 is mainly responsible for directing intracellular signal transduction, which is essential for innate immune regulation (18). MyD88 is an anchoring adaptor protein that integrates and transduces intracellular signals generated by the TLR and interleukin (IL)-1 receptor (TLR/IL-1R) superfamily (19). We are interested in exploring whether activation of the TLR4/MyD88 signaling pathway could aggravate SCI and systemic inflammation in mice.

Although previous research results support that activation of the TLR4/MyD88 signaling pathway may trigger spinal cord cell inflammation and apoptosis, there has been no relevant research on whether the SCI gut microbiota could aggravate SCI through the TLR4/MyD88 signaling pathway.

MATERIALS AND METHODS

Cell Culture

Mouse microglia BV2 cells and LPS (1 μg/mL) were used to establish like a microglial model of inflammation. The number of cells in each well was normalized to the average number of cells in the control condition (100%). Then cultured for 7 days. The Control group comprised BV2 cells and the LPS group comprised LPS-treated BV2 cells for 24 h.

Animals

Thirty-two, 6-week-old C57BL/6 mice weighing 25 ± 2 g were purchased from Hunan Slack Jingda Experimental Animal Co., Ltd. The handling of animals during the experiment complied with the *Guiding Opinions on the Good Treatment of Laboratory Animals*, published by the Ministry of Science and Technology in 2006. 10 mice were selected as the Sham group, and the remaining 22 were used to construct the SCI model.

SCI Model

After anesthetizing the mouse, laminectomy was performed to expose the spinal cord at T10. A spinal cord impactor (68,097, RWD, CA, USA) was used to create injuries by dropping a 5-g rod onto the spinal cord from a height of 6.5 cm. Immediately afterward, the overlying muscle was sutured and the skin were sutured. The animal's bladder was emptied three times a day until reflex control of bladder function was restored. The procedure in the Sham operation group was similar to that in the SCI group, except that no substantial injury was caused to the spinal cord. Twenty-two animals were used for modeling. Two died, representing a modeling success rate was 90.91%. On the 1st day after operation, hind limb paralysis and motor deficits appeared in mice. 20 successfully modeled animals were divided into four groups ($n = 5$): SCI (spinal cord injury mice), SCI+PBS (spinal cord injury mice have received the enema with PBS), SCI + Sham-FMT group (spinal cord injury transplanted with Sham mouse feces transplanted), and SCI + SCI-FMT group (spinal cord injury transplanted with SCI mouse feces). 10 mice of Sham were divided into two groups ($n = 5$): Sham (A laminectomy without SCI damage), Sham+PBS (Mice without SCI damage have received the enema with PBS). Seven days after operation, locomotor behavior was monitored Subsequently, mice were euthanized with an overdose of barbiturate (150 mg/kg) and spinal cord tissues at the injury epicenter were isolated for quantitative real-time PCR (qRT-PCR) and western blot.

Analysis of rRNA Amplicons

After collecting fecal samples from normal and SCI mice, three qualified Control groups (10.1, 8.1, and 9.1) and seven SCI DNA samples from the SCI group (1.1, 2.1, 3.1, 3.2, 4.1, 4.2, and 4.3) were detected. The qualified library was sequenced using an Illumina pe150 device. The raw data were used for later information analysis. The representative sequences of each operational taxonomic unit (OUT) were annotated to obtain the corresponding species and species abundance distributions. At the same time, OTU abundance and alpha diversity were calculated to obtain species richness and evenness information in samples and common and unique OTU information among different samples or groups. Multi-sequence alignment of OTUs was performed and a phylogenetic tree was constructed. To further explore the differences in community structure among grouped samples, *t*-test, metastat, lefse, analysis of similarities, and multiple response permutation procedures were used to test the significance of species composition and community structure of grouped samples.

ELISA

Concentrations of stimulating follicle hormone, progesterone, luteinizing hormone, and testosterone in serum samples were determined using an ELISA kit (CSB-E04634m, CSB-E08054m, CSB-E08326m, CSB-E04639m, CSB-E04594m, CSB-E04741m, CSB-E04726m, CusaBio, Wuhan, China) according to the manufacturer's instructions, and were repeated three times. The liquid was discarded and the wells dried without washing. Biotin-labeled antibody working solution (100 μL) was added to each well, covered with a new plate, and incubated at 37°C for 1 h. Horseradish peroxidase-labeled avidin solution (100 μL) was added to each well, covered with a new plate, and incubated at 37°C for 1 h. Substrate solution (90 μL) was added to each well to develop the color at 37°C in darkness for 15–30 min. Within 5 min after the termination of the reaction, the optical density of each well was measured using a microplate reader at 450 nm.

Hematoxylin-Eosin Staining

Sections were heated at 60°C for 1–2 h. Each section was immersed in solutions of 100, 95, 85, and 75% ethanol for 5 min each. Hematoxylin was applied for 5–10 min, the section was washed with distilled water, and PBS back to blue. Eosin was applied for 3–5 min followed by rinsing with distilled water. Each section was dehydrated using a graded series of ethanol solutions gradient alcohol (95–100%) for 5 min each. The final solution was removed and replaced by xylene for 10 min. The sections on a slide were sealed with neutral gum and examined by microscopy. Each group of three mice were selected and a cross section was selected on each mouse.

Quantitative Real-Time PCR

Total RNA from colon and spinal cord cells was extracted using TRIzol (15596026, Thermo Fisher Scientific, Waltham, MA, USA). The sample RNA was reverse transcribed to cDNA according to the instructions of the reverse transcription kit (cw2569, Kangwei Century Company, China). Subsequently, real-time PCR was performed on a fluorescence quantitative RCP instrument (QuantStudio1, Thermo, USA) using a UltraSYBR Mixture (CW2601, CWBIO, China). The reaction system is 20 μL. Fluorescence quantitative PCR was performed in a fluorescence quantitative RCP instrument (QuantStudio1, Thermo, USA). The reaction conditions were denaturation at 95°C for 10 min, denaturation at 94°C for 15 s, annealing at 60°C for 30 s, for 40 cycles. The primer internal reference was β-actin. The primer sequences are shown in **Table 1**. With 2 μg cDNA as template, the relative quantitative method ($2^{-\Delta\Delta Ct}$ method) was used to calculate the relative transcription level of the target gene: $\Delta\Delta Ct = \Delta$ experimental group $-\Delta$ Control group, $\Delta Ct = Ct$ (target gene)-Ct (β-actin). The experiment was repeated three times.

TABLE 1 | Primer sequences.

Gene	Sequences (5′-3′)
TLR4	F: AGACACTTTATTCAGAGCCGTTG
	R: AAGGCGATACAATTCCACC
MyD88	F: TCCCCAAGAAAGTGAGTCTCC
	R: AAAGTACAAACACGAGCCCTT
IκBa	F: AGCATCTCCACTCCGTCCTG
	R: ACATCAGCACCCAAAGTCACC
p65	F: TAGCCAGCGAATCCAGACCAACA
	R: TGGGTCCCGCACTGTCACCT
β-actin	F: ACATCCGTAAAGACCTCTATGCC
	R: TACTCCTGCTTGCTGATCCAC

Western Blot

Total protein was extracted from colon and spinal cord cells using the Ripa Kit (r0010, Solarbio, China). The protein concentration was determined using the BCA method. Quantitative analysis was performed in accordance with the different concentrations. Protein were resolved was by 10% SDS-PAGE and transferred to a nitrocellulose membrane by electroporation. The membrane was incubated with 5% skim milk for 2 h at room temperature to bind with nonspecific protein, and then incubated at 4°C. Primary antibodies, rabbit anti-TLR4 (1:500 dilution, ab13867, Abcam, Cambridge, UK), rabbit anti-MyD88 (1:1000, 23230-1-AP, Proteintech, Rockford, IL, USA), rabbit anti-p-IkBα (1:2000, ab133462, Abcam), rabbit anti-IκBα (1:2000, 10268-1-AP, Proteintech), rabbit anti-p-p65 (1:1000, #3033, Cell Signaling Technology, Danvers, MA, USA), rabbit anti-p65 (1:1000, ab32536, Abcam), followed by rinsing three times for 10 min each time using Tris-buffered saline-Tween. This was followed by exposure to horseradish peroxidase-conjugated goat anti-mouse IgG (1:5000, sa00001-1, Proteintech). The membrane was immersed in Supernal Plus (k-12045-d50, Advansta, USA) for luminescence development. β-actin was used as an internal reference. Protein bands were scanned using Scion image software.

Immunofluorescence Double-Staining

The sections were deparaffinized with water. Sections were stained to detect apoptosis using a terminal deoxynucleotidyl transferase-mediated digoxigenin-dUTP nick end-labeling (TUNEL) assay. The sections were placed in three xylene solutions for 20 min each time. They were then treated with 100, 95, 85, and 75% ethanol for 5 min each. The sections were then soaked in distilled water for 5 min and then placed in citrate buffer solution (pH 6.0) and boiled by continuous microwaving for 23 min, and cooled to room temperature. Each section was then placed in sodium borohydride solution at room temperature for 30 min and rinsed with water for 5 min. This was followed by exposure to Sudan black dye solution at room temperature for 5 min and rinsing with water for 3 min. Following addition of normal serum (10%) and bovine serum albumin (5%) for 60 min, each section was exposed to terminal deoxynucleotidyl transferase (TDT) buffer, 34 uL deionized distilled water, 10 μL 5× equilibration buffer, 5 μL fluorescein isothiocyanate-12-Dutp Labeling Mix, and 1 uL recombinant TDT. The primary antibodies incubated overnight at 4°C were anti-GFAP (1:100, 16825-1-AP, Proteintech), anti-IBA1 (1:100, 10904-1-AP, Proteintech), and anti-NeuN (1:100, AB177487, Abcam). The sections were rinsed with PBS three times, 5 min each time, and then treated with 50 to 100 uL of anti-rabbit, rabbit, and rabbit-IgG-labeled fluorescent antibody at 37 °C for 90 min. Following rinsing with PBS three times for 5 min each time, cell nuclei were stained by 4', 6-diamidino-2-phenylindole (DAPI) at 37 °C for 10 min. Each section was rinsed three times with PBS for 5 min each 3 time, sealed with buffered glycerin, and examined by fluorescence microscopy. The confocal images of cells were sequentially acquired with Zeiss AIM software on a Zeiss LSM 510 confocal microscope system. Each group of three mice was selected and a cross section was selected on each mouse.

Statistical Analyses

All data were analyzed using GraphPad Prism 8.0 software (GraphPad Software, La Jolla, CA, USA). The results were expressed as mean ± standard deviation (SD). Unpaired t-test was used to compare the two groups with a normal distribution. Comparisons among multiple groups were conducted using one-way analysis of variance (ANOVA), followed by Tukey's *post hoc* test. Differences were considered statistically significant at $P < 0.05$.

RESULTS

LPS Induces Inflammation in BV2 Cells and Promotes Apoptosis

We constructed an *in vitro* microglial model of inflammation in mice using BV2 cells to evaluate the inflammatory response and survival of BV2 cells. ELISA was used to identify the levels of pro-inflammatory and anti-inflammatory factors released by BV2 cells. Compared with the Control group, LPS-treated cells released more pro-inflammatory factors (IL-1β, TNF-α, and IL-6), induced nitric oxide synthase (iNOS) was significantly increased ($p < 0.001$). Anti-inflammatory factors (TGF-β, IL-4, IL-10) and arginase 1 (Arg-1) were significantly decreased ($p < 0.001$). These data indicate that the LPS-induced inflammatory response in BV2 cells was exacerbated (**Figures 1A,B**). Compared with the Control group, the fluorescence intensity of TUNEL increased in the LPS group. Apoptosis in the spinal cord of mice was examined in more detail ($p < 0.001$) (**Figure 1C**). The collective findings indicate the LPS-induced inflammation in BV2 cells.

LPS Activates the TLR4/MyD88 Signaling Pathway in Microglia

The initial results indicated that LPS could induce apoptosis of BV2 cells. We next explored whether LPS could affect the viability of BV2 cells by activating the TLR4/MyD88 signaling pathway. qRT-PCR was used to detect the expression of TLR4/MyD8. In LPS stimulated BV2 cells, the mRNA expression of TLR4, MyD88, p65, and IκBα increased ($p < 0.001$) (**Figure 2A**). The findings indicated that LPS might affect the TLR4/MyD88 signaling pathway. LPS stimulation of BV2 also significantly increased the protein expression levels of TLR4, MyD88, p-p65, and p-IκBα ($p < 0.001$), with no significant change in p65 and IκBα ($p > 0.05$) (**Figure 2B**). The findings indicate that LPS may promote the activation of the TLR4/MyD88 signaling pathway in microglia.

Inflammatory Response Is Enhanced in SCI Mice, and SCI Is Aggravated

The above experiments showed that the inflammatory response in the SCI model *in vitro* was enhanced, and that the apoptosis of BV2 cells was intensified. Next, an SCI mouse model was constructed. The results of ELISA experiments in **Figures 3A,B**

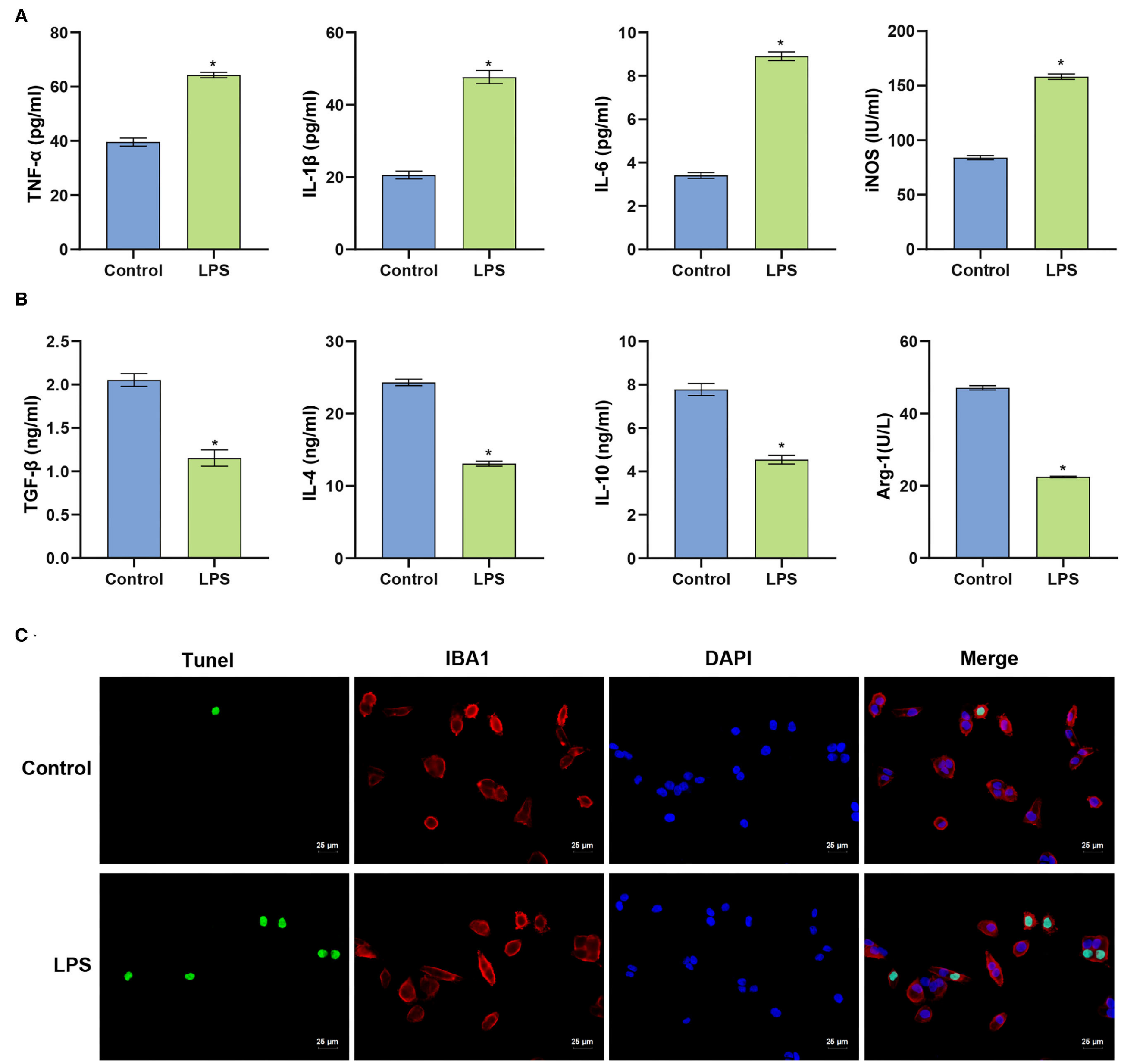

FIGURE 1 | LPS induces apoptosis of BV2 cells. **(A)** Level of the measured pro-inflammatory factors in BV2 cells. **(B)** ELISA determination of the levels of anti-inflammatory factors in BV2 cells. **(C)** TUNEL assay (Scale bar = 25 μm). The unpaired *t*-test was used to analyze comparisons between two groups. $^*P < 0.05$ compared with the control group.

demonstrated that compared with the Sham group, serum pro-inflammatory factors (TNF-α, IL-1β, IL-6) and nitric oxide synthase (iNOS) in SCI mice were significantly higher ($p < 0.001$). Increased, anti-inflammatory factors (TGF-β, IL-4, IL-10) and arginase 1 (Arg-1) decreased significantly. The findings indicated the successful construction of the SCI model ($p < 0.001$). The TUNEL and immunofluorescence co-localization experiment was performed on spinal cord sections of Sham and SCI mice to determine the survival and apoptotic cells in the spinal cord. Compared with the Sham group, the fluorescence intensity of the neuron marker (NeuN), microglia marker (IBA1) and astrocyte marker (GFAP) increased in the spinal cord tissue in SCI group. The results suggested that the body may activate neuron, microglia and astrocyte cells to repair the damage when the spinal cord was injured. The amount of apoptotic neurons, microglia and astrocyte also increased, suggesting that spinal cord injury could cause apoptosis at a certain degree ($p < 0.001$) (**Figure 3C**).

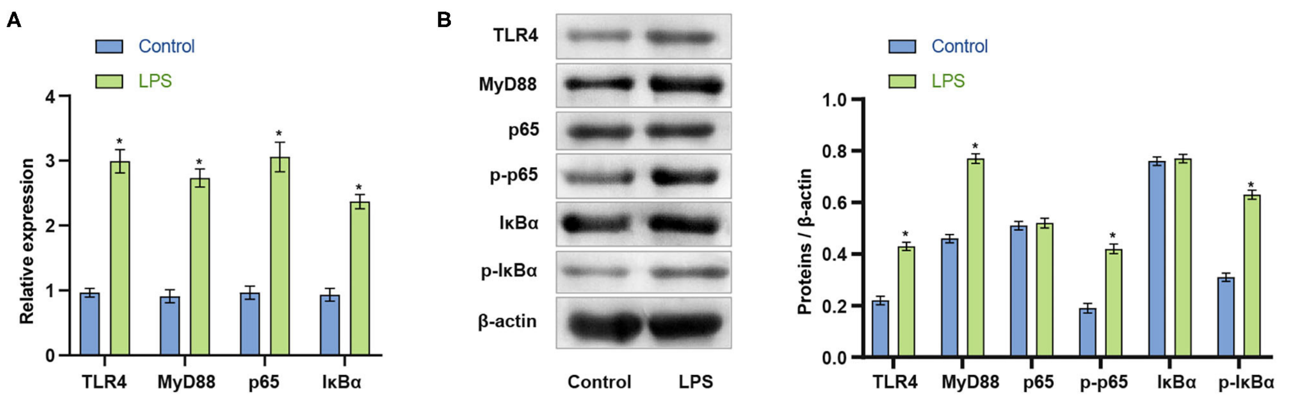

FIGURE 2 | LPS activates the TLR4/MyD88 signaling pathway in microglia. **(A)** The expression of TLR4, MyD88, p65, and IκBα increased after LPS stimulation of BV2 cells. **(B)** Western blot measurement of the expression of MyD88, TLR4, p65, p-p65, IκBα, and p-IκBα protein in BV2 cells. $^*P < 0.05$ compared with the Control group. The unpaired *t*-test was used to analyze comparisons between two groups.

In fact, the amounts of both survival and apoptotic neuron, microglia and astrocyte increased based on the fluorescence images from the co-localization experiments of TUNEL and immunofluorescence.

Activation of the TLR4/MyD88 Signaling Pathway in the Spinal Cord and Colon of SCI Mice

To further investigate whether the TLR4/MyD88 signaling pathway was activated *in vivo*, we removed spinal cord and colon tissues from the SCI mice for qRT-PCR and western blot analyses. Compared with the Sham group, the mRNA expression of TLR4, MyD88, p65, and IκBα in the spinal cord and colon tissues of the SCI group was considerably increased ($p < 0.001$) (**Figure 4A**). The data indicated that the TLR4/MyD88 signaling pathway was activated. Western blot examination was used to detect the TLR4/MyD88 signaling pathway in the spinal cord and colon tissue. The expression of TLR4, MyD88, p-p65, and p-IκBα increased dramatically ($p < 0.001$), while the expression of non-phosphorylated p65 and IκBα did not increase significantly ($p < 0.001$) (**Figure 4B**). The collective findings indicate that the TLR4/MyD88 signaling pathway was activated in SCI mice.

Gut Microbiota Imbalance in SCI Mice

The above experimental results indicated that the inflammatory response of the SCI model *in vivo* was increased, and the TLR4/MyD88 signaling pathway was activated. We speculated that these physiological phenomena might reflect changes in the gut microbiota of SCI mice. Rank-abundance curve analysis revealed that the SCI group curve had a smaller range on the horizontal axis, indicating that the species abundance was the lowest (**Figure 5A**). The distance matrix between the samples was analyzed ($R = -0.008$) (**Figure 5B**). Although the difference between the Control and SCI groups was not noticeable, the principal component analysis revealed differences in microbial communities in the two samples (**Figure 5C**). The farther the distance, the lower was the similarity. The species distribution map and operational taxonomic unit (out) abundance clustering heat map indicated a difference in bacterial population distribution between the control and SCI groups (**Figures 5D,E**). The collective findings were indicative of gut microbiota deregulation in SCI mice.

Gut Microbiota Imbalance Activates the TLR4/MyD88 Signaling Pathway

We speculated that activation of the mouse TLR4/MyD88 signaling pathway is related to an imbalance in the gut microbiota. To assess this, we performed FMT in mice to detect the expression of the TLR4/MyD88 signaling pathway in the spinal cord and colon. Compared with the SCI + Sham-FMT group, the mRNA expression of TLR4, MyD88, p65, and IκBα in the SCI + SCI-FMT group increased sharply and was more significant than that in the SCI + phosphate-buffered saline (PBS) group ($p < 0.001$). The data indicated that the imbalance of gut microbiota could promote the activation of the TLR4/MyD88 signaling pathway (**Figure 6A**). Next, we used western blot to detect the expression of proteins in the TLR4/MyD88 signaling pathway in spinal cord tissue and colon tissue. Compared with the SCI + Sham-FMT group, the data of the SCI + SCI-FMT group showed that the expression of TLR4, MyD88, p-p65, and p-IκBα increased dramatically ($p < 0.001$), while the levels of non-phosphorylated p65 and IκBα were not significantly different ($p < 0.001$) (**Figure 6B**). The collective findings supported the view that the gut microbiota imbalance in SCI mice could activate the TLR4/MyD88 signaling pathway.

The data in **Figure 6** indicated that an imbalance of the gut microbiota could activate the TLR4/MyD88 signaling pathway, promote inflammation, and exacerbate SCI. To study this further, we analyzed explored mice following FMT. Compared to Sham + PBS mice, the visible damage to SCI + PBS mice was more serious. The SCI + SCI + FMT group displayed the most severe SCI ($p < 0.001$) (**Figure 7A**). The results showed that the imbalance of gut microbiota exacerbated SCI. ELISA determined the levels of pro-inflammatory cytokines and anti-inflammatory

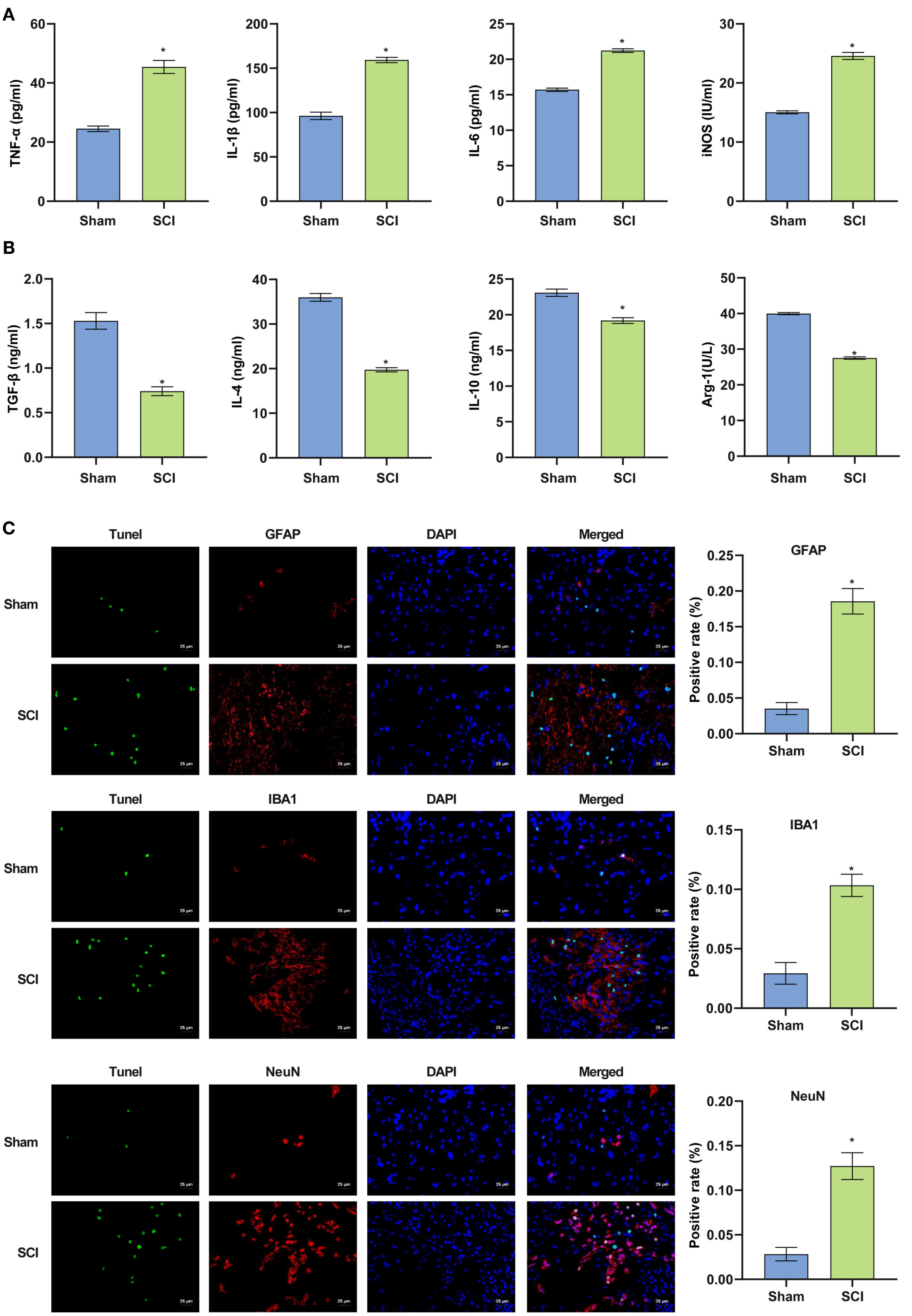

FIGURE 3 | The successful construction of the SCI mouse model. **(A,B)** Pro-inflammatory factors were increased in SCI mice and anti-inflammatory factors were decreased. **(C)** Terminal deoxynucleotidyl transferase dUTP nick end labeling assay was used to detect cell apoptosis in the spinal cord of mice (Scale bar = 25μm). *$P < 0.05$ compared with Sham group. The unpaired t-test was used to analyze comparisons between two groups $n = 5$.

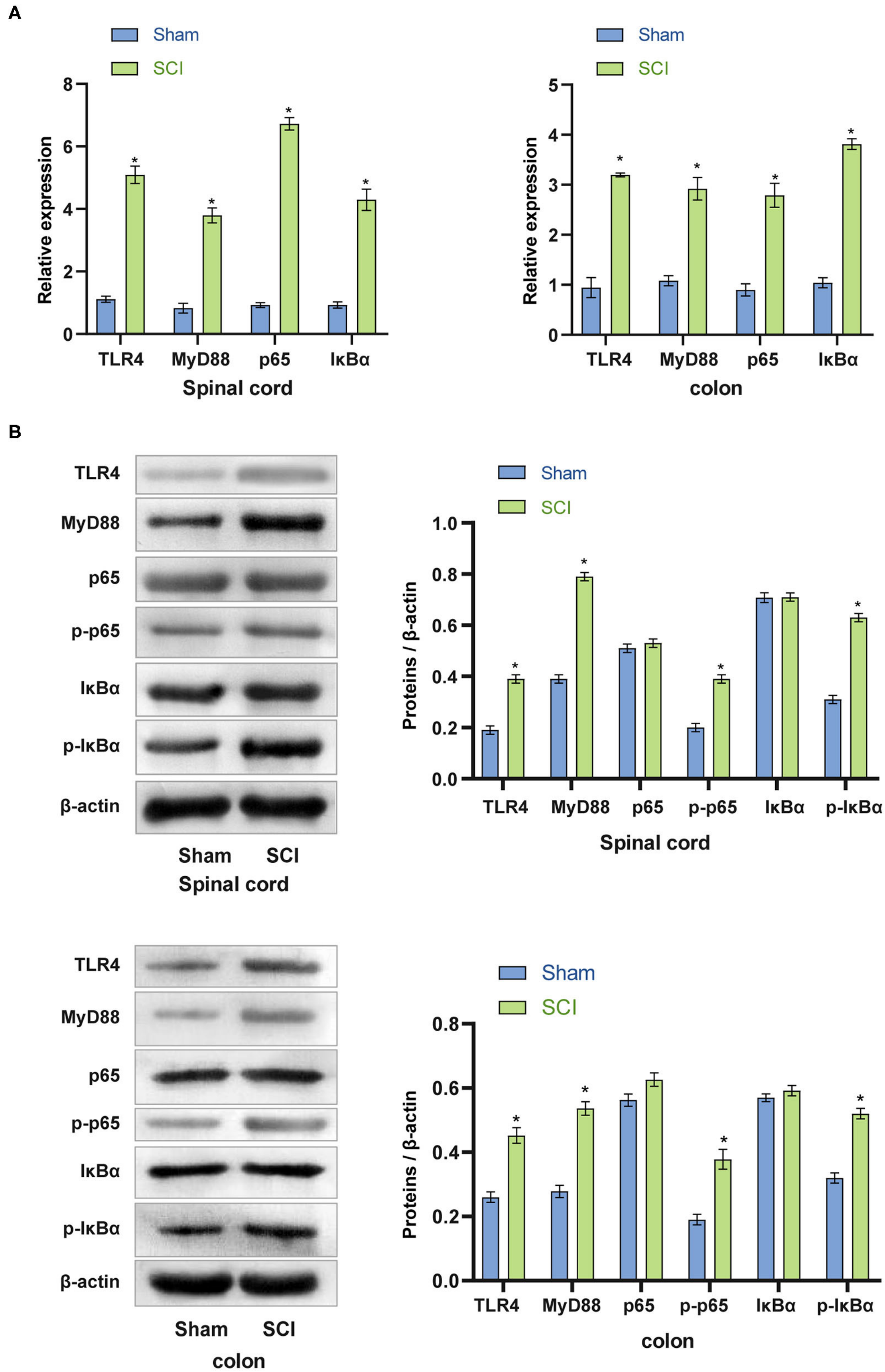

FIGURE 4 | Activation of the TLR4/MyD88 signaling pathway in the spinal cord and colon of SCI mice. **(A)** qRT-PCR was used to analyze the expression of TLR4, MyD88, p65, IκBα in the spinal cord and colon tissues. **(B)** The protein expression of TLR4, MyD88, p-p65, and p-IκBα increased significantly in SCI mice. *$P < 0.05$ compared with the Sham group. The unpaired *t*-test was used to analyze comparisons between two groups $n = 5$.

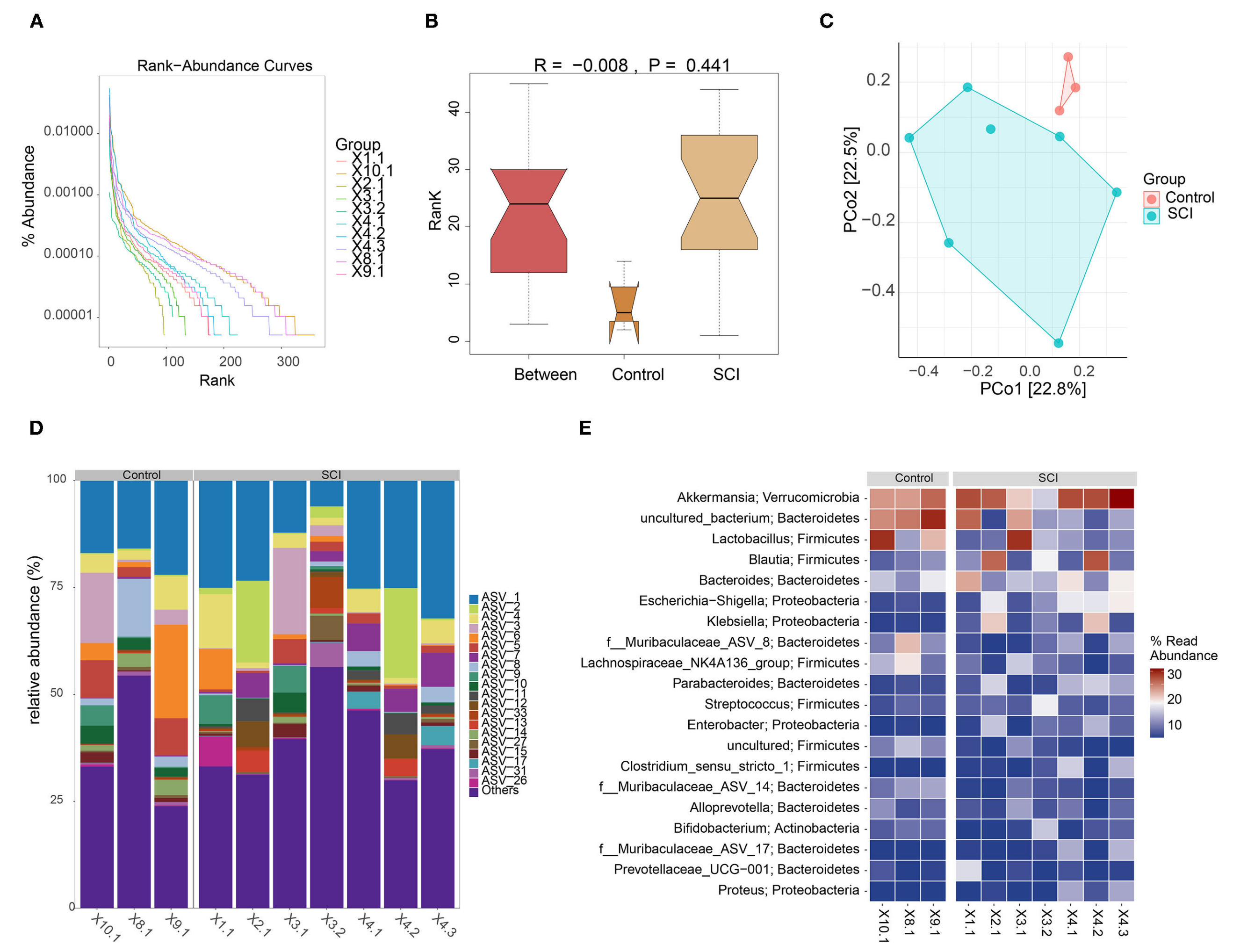

FIGURE 5 | Gut microbiota analyses. **(A)** Rank-abundance curve. **(B)** Box plot of diversity differences between the analyses of similarities groups. **(C)** Principal component analysis plot. **(D)** Histogram of species distribution. **(E)** Operational taxonomic unit abundance clustering heat map.

cytokines in the serum. The increase in pro-inflammatory cytokines (TNF-α, IL-1β, and IL-6) in the SCI + SCI + FMT group was the most obvious, and the anti-inflammatory cell factors (TGF-β, IL-4, and IL-10) were most severely inhibited ($p < 0.001$) (**Figures 7B,C**). Finally, the fluorescence intensity of GFAP, NeuN and IBA1 was the highest in SCI + SCI + FMT. It showed that fecal transplantation could increase the amount of survival neuron, microglia and astrocyte cells at the site of spinal cord injury ($p < 0.001$) (**Figure 7D**). The collective results showed that an imbalance in gut microbiota could promote inflammation and exacerbate SCI.

DISCUSSION

The gut microbiota of mice with SCI was disordered, which caused systemic inflammation. After FMT in mice with SCI, the injury aggravated systemic inflammation. *In vitro*, LPS activated the TLR4/MyD88 signaling pathway in microglia, inducing the production of inflammatory cytokines and increasing microglial apoptosis. The findings indicate that TLR4/MyD88 pathway signal transduction may be related to the aggravation of SCI caused by the imbalanced gut microbiota.

SCI refers to the direct or indirect external damage to normal spinal and spinal cord tissues, which can affect spinal cord function. Recent data from rodents indicate that SCI causes gut dysbiosis, which exacerbates intraspinal inflammation and lesion pathology leading to impaired recovery of motor function. Postinjury delivery of probiotics containing various types of "good" bacteria can partially overcome the pathophysiologic effects of gut dysbiosis. Immune function, locomotor recovery, and spinal cord integrity are partially restored by a sustained regimen of oral probiotics (5). Firmicutes and Bacteroides spp. are the most predominant phylum in the gut. They ferment non-digestible polysaccharides and generate metabolites that can be used for energy by the host. Acetate, propionate and butyrate are among the most well characterized single chain fatty acid metabolites that are produced following carbohydrate fermentation in the gut. Short chain fatty acids, butyrate in

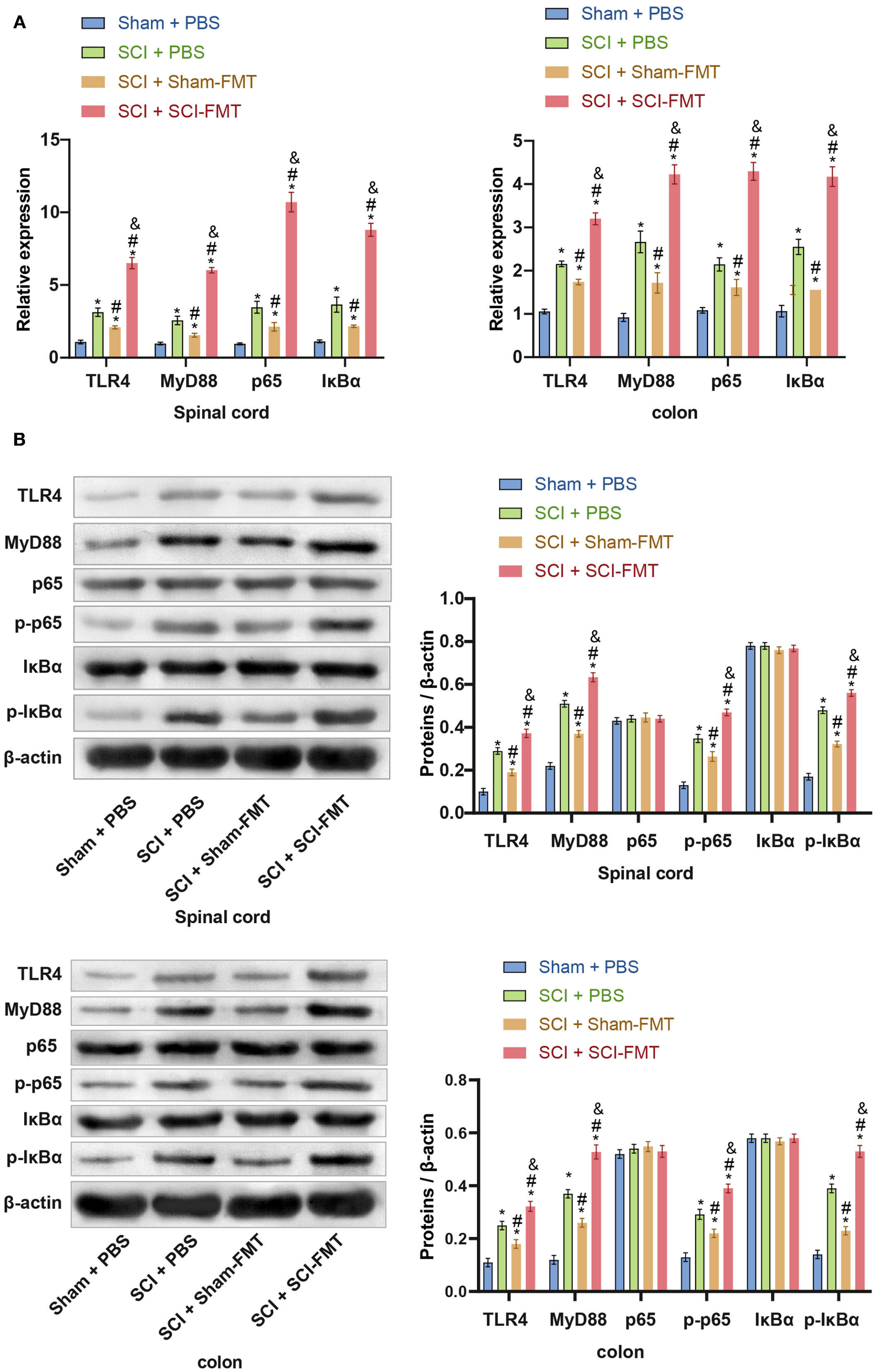

FIGURE 6 | The imbalance of the gut microbiota in SCI mice could activate the TLR4/MyD88 signaling pathway. **(A)** The expression of TLR4, MyD88, p65, and IκBα in the spinal cord and colon tissues. **(B)** Imbalance of the gut microbiota of SCI mice could promote the protein expression of TLR4, MyD88, p-p65, and p-IκBα. *, $P < 0.05$ compared with the Sham + PBS group. #, $P < 0.05$ compared with the SCI + PBS group. &, $P < 0.05$ compared with the SCI + Sham-FMT group. Multiple comparisons in groups were evaluated by one-way analysis of variance $n = 5$.

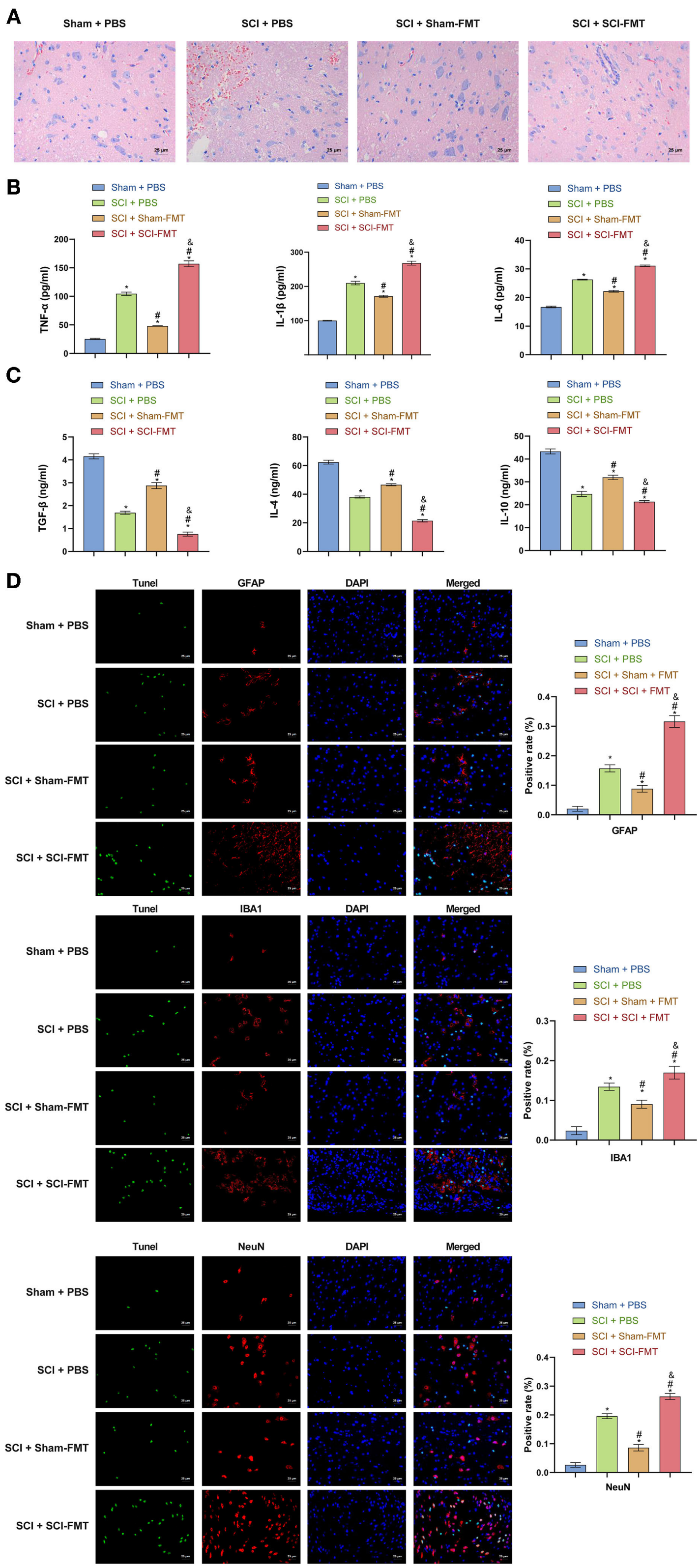

FIGURE 7 | Imbalance of gut microbiota exacerbates SCI. **(A)** Hematoxylin and eosin staining was used to detect SCI in each group. **(B, C)** ELISA was used to observe the content of inflammatory factors in the serum of mice in each group. **(D)** TUNEL assay and immunofluorescence detection of spinal cord cell apoptosis in each group of mice (Scale bar = 25 μm). *, $P < 0.05$ compared with the Sham + PBS group. #, $P < 0.05$ compared with the SCI + PBS group. &, $P < 0.05$ compared with the SCI +Sham-FMT group. Multiple comparisons in groups were evaluated by one-way analysis of variance $n = 5$.

particular, have potent anti-inflammatory effects on macrophages and can suppress ongoing inflammation in the Central nervous system (20). Gut microbiota is a key and potential target for SCI (4, 7), although its crosstalk with the TLR4/MyD88 signaling pathway during SCI is still unclear (21). The gut microbiota relies on the TLR4 pathogen recognition receptor, which interacts with the host. TLR4 recognizes LPS in gram-negative bacteria and activates downstream pro-inflammatory signaling, including the TLR4/MyD88/p38 mitogen-activated protein kinase pathway, which is also thought to be involved in the regulation of TJPs and intestinal permeability (22, 23). Compared with wild-type mice, TLR4-/- mice reportedly show less pancreatic damage and inflammation in pancreatitis, which supports the importance of TLR4 in the pathogenesis of pancreatitis. TLR4 has also been shown to cause intestinal damage. TLR4 signal transduction increased the immunopathology of the ileum in TLR4-/- mice (24). Neuroinflammation plays a crucial role in the secondary phase of SCI, and is initiated following the activation of TLR4. Pyroptosis is a form of inflammatory programmed cell death, which is closely involved in neuroinflammation, and it can be regulated by TLR4 according to a recent research (12). BMSCs-derived exosomes could inhibit apoptosis and inflammation response induced by spinal cord injury and promote motor function recovery by inhibiting the TLR4/MyD88/NF-κB signaling pathway (25). In the present study, FMT led to the activation of the TLR4/MyD88 signaling pathway in the transplanted mice and aggravation of SCI was. The data verified that the gut microbiota may be a key target of SCI and may target TLR4.

Activation of the TLR4/MyD88 pathway and upregulation of the TNF-α, IL-12, and IL-6 inflammatory cytokines are involved in the development of SCI, which are closely related to neuroinflammatory injury and can be used as a reference index to evaluate the prognosis of SCI patients (26). TLR4/MyD88 was shown to activate the nuclear factor-kappa B (NF-κB) inflammatory pathway in enteritis (27), promote myocardial infarction (28) and induce acute pneumonia (29). As a key component of the inflammatory microenvironment, inflammatory factors also play a key role in the repair of nerve damage after SCI. This involves pro-inflammatory factors, including IL-1β, TNF-αIL-6, and β, IL-4, IL-10 and IL-13 (30). Most TLRs perform their functions through the MyD88 pathway (31). GFAP and IBA1, which are the assigned markers for the activated astrocytes and microglia, were significantly upregulated in the treated group. The inhibition of TLR4 further inhibited the expression of its downstream effectors (IBA1) in the microglial cells (32). Studies hypothesized that suppressed MyD88 adaptor protein in the spinal cord could alleviate peripheral nerve injury-induced neuropathic pain. MyD88 adaptor protein involved in the neuropathic pain and may provide potential therapeutic strategies for treatment of neuropathic pain (33). Previous studies revealed that GFAP and IBA1 labeled astrocyte and microglia increased and NeuN labeled neuron decreased in SCI spinal cord injury (34). Our results showed that GFAP, NeuN and IBA1 labeled cells increased. However, the co-localization results of TUNEL showed that the amount of apoptotic neurons also increased. There may exist several reasons. Firstly, apoptotic cells associated with spinal cord injury cannot be avoided. It is possible that rapid self-repair happened in SCI mice. In a previous study, neurons of spinal cord injury also increased at 8 days after SCI modeling (35). Moreover, endogenous neural stem cells and ependymal stem cells could differentiate into neurons after spinal cord injury (36, 37). Lineage tracing experiments have shown that it is solely the ependymal cell population that is capable of generating neurospheres *in vitro*, and this hallmark of NSC potential remains restricted to the ependymal population following SCI (38). This may also be one of the reasons for the increase in neuron. We are very interested in the emergence of these different results. We plan to study the reasons for the increase in NeuN under spinal cord injury in the future. The results of the present study showed that the activation of the TLR4/MyD88 pathway could trigger the overexpression of pro-inflammatory factors, promote cell apoptosis, and further aggravate nerve damage.

In conclusion, LPS-induced microglia have an inflammatory response, TLR4/MyD88 is activated, and the rate of microglial apoptosis increases. *In vivo*, the disturbance of the gut microbiota in mice with SCI confirmed that gut microbiota disorders can aggravate SCI by activating the TLR4/MyD88 signaling pathway in mice and has potential value as a treatment for SCI and other neuroinflammation-related diseases.

DATA AVAILABILITY STATEMENT

The datasets presented in this study can be found in online repositories. The names of the repository/repositories and accession number(s) can be found below: https://www.ncbi.nlm.nih.gov/, PRJNA726026.

ETHICS STATEMENT

The animal study was reviewed and approved by the Ethics Committee of Huizhou Municipal Central Hospital.

AUTHOR CONTRIBUTIONS

ZR, YH, HC, and JW performed the experiment and analyzed the data. ZR, MC, HW, GL, and ZZ performed the experiment. ZR and JW guided the experiment and edited the manuscript. YH, HC, MC, GL, and HW revised the manuscript. All authors read and approved the final manuscript.

FUNDING

This work was partially supported by the funds from the Science and Technology Program of Huizhou (2021WC0106362).

ACKNOWLEDGMENTS

We would like to thank the Huizhou Municipal Central Hospital, People's Hospital of Longhua, Shenzhen Longhua Clinical Medical College of Guangdong Medical University for their support.

REFERENCES

1. Martirosyan NL, Turner GH. Manganese-enhanced MRI Offers Correlation with Severity of Spinal Cord Injury in Experimental Models. *Open Neuroimag J.* (2016) 10:139–47. doi: 10.2174/1874440001610010139
2. Orr MB, Gensel JC. Spinal cord injury scarring and inflammation: therapies targeting glial and inflammatory responses. *Neurotherapeutics*. (2018) 15:541–53. doi: 10.1007/s13311-018-0631-6
3. Meng XL, Hai Y, Zhang XN, Wang YS, Liu XH, Ma LL, et al. Hyperbaric oxygen improves functional recovery of rats after spinal cord injury via activating stromal cell-derived factor-1/CXC chemokine receptor 4 axis and promoting brain-derived neurothrophic factor expression. *Chin Med J.* (2019) 132:699–706. doi: 10.1097/CM9.0000000000000115
4. Kigerl KA, Hall JC, Wang L, Mo X, Yu Z, Popovich PG. Gut dysbiosis impairs recovery after spinal cord injury. *J Exp Med.* (2016) 213:2603–20. doi: 10.1084/jem.20151345
5. Kigerl KA, Mostacada K, Popovich PG. Gut microbiota are disease-modifying factors after traumatic spinal cord injury. *Neurotherapeutics.* (2018) 15:60–7. doi: 10.1007/s13311-017-0583-2
6. Jing Y, Yang D, Bai F, Zhang C, Qin C, Li D, et al. Melatonin treatment alleviates spinal cord injury-induced gut dysbiosis in mice. *J Neurotrauma.* (2019) 36:2646–64. doi: 10.1089/neu.2018.6012
7. O'Connor G, Jeffrey E, Madorma D, Marcillo A, Abreu MT, Deo SK, et al. Investigation of microbiota alterations and intestinal inflammation post-spinal cord injury in rat model. *J Neurotrauma.* (2018) 35:2159–66. doi: 10.1089/neu.2017.5349
8. Tilg H, Zmora N, Adolph TE, Elinav E. The intestinal microbiota fuelling metabolic inflammation. *Nat Rev Immunol.* (2020) 20:40–54. doi: 10.1038/s41577-019-0198-4
9. Sun MF, Zhu YL, Zhou ZL, Jia XB, Xu YD, Yang Q, et al. Neuroprotective effects of fecal microbiota transplantation on MPTP-induced Parkinson's disease mice: gut microbiota, glial reaction and TLR4/TNF-α signaling pathway. *Brain Behav Immun.* (2018) 70:48–60. doi: 10.1016/j.bbi.2018.02.005
10. Sun Z, Zhao T. Dexmedetomidine attenuates spinal cord ischemia–reperfusion injury through both anti-inflammation and anti-apoptosis mechanisms in rabbits. *J Transl Med*. (2018) 16:1–11. doi: 10.1186/s12967-018-1583-7
11. Alhasson F, Das S, Seth R, Dattaroy D, Chandrashekaran V, Ryan CN, et al. Altered gut microbiome in a mouse model of Gulf War Illness causes neuroinflammation and intestinal injury via leaky gut and TLR4 activation. *PLoS ONE.* (2017) 12:e0172914. doi: 10.1371/journal.pone.0172914
12. Xu S, Wang J, Jiang J, Song J, Zhu W, Zhang F, et al. TLR4 promotes microglial pyroptosis via lncRNA-F630028O10Rik by activating PI3K/AKT pathway after spinal cord injury. *Cell Death Dis.* (2020) 11:693. doi: 10.1038/s41419-020-02824-z
13. Mi S, Wu Y, Hong Z, Wang Z, Feng X, Zheng G. Expression of TLR4/MyD88/NF-κB pathway genes and its related inflammatory factors in secondary spinal cord injury. *Zhejiang Da Xue Xue Bao Yi Xue Ban.* (2019) 48:609–16.
14. Ribeiro P, Castro MV, Perez M, Cartarozzi LP, Spejo AB, Chiarotto GB, et al. Toll-like receptor 4 (TLR4) influences the glial reaction in the spinal cord and the neural response to injury following peripheral nerve crush. *Brain Res Bull.* (2020) 155:67–80. doi: 10.1016/j.brainresbull.2019.11.008
15. Xu J, Lu C, Liu Z, Zhang P, Guo H, Wang T. Schizandrin B protects LPS-induced sepsis via TLR4/NF-κB/MyD88 signaling pathway. *Am J Transl Res.* (2018) 10:1155–63.
16. Ryu J-K, Kim SJ. Reconstruction of LPS transfer cascade reveals structural determinants within LBP, CD14, and TLR4-MD2 for efficient LPS recognition and transfer. *Immunity.* (2017) 46:38–50. doi: 10.1016/j.immuni.2016.11.007
17. Yu F-Z, Wen X. L6H21 prolonged rats survival after limb allotransplantation by inhibiting acute rejection. *Eur Rev Med Pharmacol Sci.* (2017) 21:1891–903.
18. Saikh KU. MyD88 and beyond: a perspective on MyD88-targeted therapeutic approach for modulation of host immunity. *Immunol Res.* (2021) 69:117–28. doi: 10.1007/s12026-021-09188-2
19. Hu N, Wang C. Phillygenin inhibits LPS-induced activation and inflammation of LX2 cells by TLR4/MyD88/NF-κB signaling pathway. J Ethnopharmacol. (2020) 248:112361. doi: 10.1016/j.jep.2019.112361
20. Gungor B, Adiguzel E. Intestinal microbiota in patients with spinal cord injury. *PLoS ONE*. (2016) 11:e0145878. doi: 10.1371/journal.pone.0145878
21. Zheng J, Lou L. Commensal escherichia coli aggravates acute necrotizing pancreatitis through targeting of intestinal epithelial cells. *Appl Environ Microbiol.* (2019) 85:e00059–19. doi: 10.1128/AEM.00059-19
22. Ouyang J. Up-regulation of tight-junction proteins by p38 mitogen-activated protein kinase/p53 inhibition leads to a reduction of injury to the intestinal mucosal barrier in severe acute pancreatitis. *Pancreas.* (2016) 45:1136–44. doi: 10.1097/MPA.0000000000000656
23. Liu L, Jiang Y. Toll-like receptor 4 regulates occludin and zonula occludens 1 to reduce retinal permeability both *in vitro* and *in vivo*. *J Vasc Res.* (2018) 54:367–75. doi: 10.1159/000480455
24. Kløve S, Genger C. Toll-like receptor-4 is involved in mediating intestinal and extra-intestinal inflammation in campylobacter coli-infected secondary abiotic il-10 -/- mice. *Microorganisms*. (2020) 8:1882. doi: 10.3390/microorganisms8121882
25. Fan L, Dong J. Bone marrow mesenchymal stem cells-derived exosomes reduce apoptosis and inflammatory response during spinal cord injury by inhibiting the TLR4/MyD88/NF-κB signaling pathway. *Hum Exp Toxicol*. (2021) 29:09603271211003311. doi: 10.1177/09603271211003311
26. Mi S, Wu Y. Expression of TLR4/MyD88/NF-κB pathway genes and its related inflammatory factors in secondary spinal cord injury. *Zhejiang Da Xue Xue Bao Yi Xue Ban.* (2019) 48:609–16.
27. Zhou M, Xu W. Boosting mTOR-dependent autophagy via upstream TLR4-MyD88-MAPK signalling and downstream NF-κB pathway quenches intestinal inflammation and oxidative stress injury. *EBioMedicine.* (2018) 35:345–60. doi: 10.1016/j.ebiom.2018.08.035
28. Xu G-R, Zhang C. Modified citrus pectin ameliorates myocardial fibrosis and inflammation via suppressing galectin-3 and TLR4/MyD88/NF-κB signaling pathway. *Biomed Pharmacother*. (2020) 126:110071. doi: 10.1016/j.biopha.2020.110071
29. Liu G, Lu Y. TLR4-MyD88 signaling pathway is responsible for acute lung inflammation induced by reclaimed water. *J Hazard Mater*. (2020) 396:122586. doi: 10.1016/j.jhazmat.2020.122586
30. Bank M, Stein A. Elevated circulating levels of the pro-inflammatory cytokine macrophage migration inhibitory factor in individuals with acute spinal cord injury. *Arch Phys Med Rehabil.* (2015) 96:633–44. doi: 10.1016/j.apmr.2014.10.021
31. Zhu X, Liu J. Neuroprotective and anti-inflammatory effects of isoliquiritigenin in kainic acid-induced epileptic rats via the TLR4/MYD88 signaling pathway. *Inflammopharmacology.* (2019) 27:1143–53. doi: 10.1007/s10787-019-00592-7
32. Ikram M, Saeed K. Natural dietary supplementation of curcumin protects mice brains against ethanol-induced oxidative stress-mediated neurodegeneration and memory impairment via Nrf2/TLR4/RAGE signaling. *Nutrients.* (2019) 11:1082. doi: 10.3390/nu11051082
33. Liu F, Wang Z. Suppression of MyD88-dependent signaling alleviates neuropathic pain induced by peripheral nerve injury in the rat. *J Neuroinflammation*. (2017) 14:1–12. doi: 10.1186/s12974-017-0822-9
34. Qian J, Zhu W, Lu M, Ni B, Yang J. D-β-hydroxybutyrate promotes functional recovery and relieves pain hypersensitivity in mice with spinal cord injury. *Br J Pharmacol.* (2017) 174:1961–71. doi: 10.1111/bph.13788
35. Torres BB, Caldeira FM, Gomes MG, Serakides R, de Marco Viott A, Bertagnolli AC, et al. Effects of dantrolene on apoptosis and immunohistochemical expression of NeuN in the spinal cord after traumatic injury in rats. *Int J Exp Pathol.* (2010) 91:530–6. doi: 10.1111/j.1365-2613.2010.00738.x
36. Zhang L, Fan C, Hao W, Zhuang Y, Liu X, Zhao Y, et al. NSCs migration promoted and drug delivered exosomes-collagen scaffold via a bio-specific

peptide for one-step spinal cord injury repair. *Adv Healthc Mater*. (2021) 10:e2001896. doi: 10.1002/adhm.202001896

37. Grégoire CA, Goldenstein BL, Floriddia EM, Barnabé-Heider F, Fernandes KJ. Endogenous neural stem cell responses to stroke and spinal cord injury. *Glia*. (2015) 63:1469–82. doi: 10.1002/glia.22851
38. Barnabé-Heider F, Göritz C, Sabelström H, Takebayashi H, Pfrieger FW, Meletis K, et al. Origin of new glial cells in intact and injured adult spinal cord. *Cell Stem Cell*. (2010) 7:470–82. doi: 10.1016/j.stem.2010.07.014

Conflict of Interest: The authors declare that the research was conducted in the absence of any commercial or financial relationships that could be construed as a potential conflict of interest.

frontiers in Nutrition

ORIGINAL RESEARCH
published: 14 October 2021
doi: 10.3389/fnut.2021.706148

Dietary Supplementation With *Lactobacillus plantarum* Ameliorates Compromise of Growth Performance by Modulating Short-Chain Fatty Acids and Intestinal Dysbiosis in Broilers Under *Clostridium perfringens* Challenge

Baikui Wang [1†], Yuanhao Zhou [1], Yulong Mao [1], Li Gong [1,2], Xiang Li [1], Shujie Xu [1], Fei Wang [1], Qianpeng Guo [1], Huihua Zhang [2*] and Weifen Li [1*†]

[1] Key Laboratory of Molecular Animal Nutrition of the Ministry of Education, Key Laboratory of Animal Nutrition and Feed Science (Eastern of China) of the Ministry of Agriculture, Key Laboratory of Animal Feed and Nutrition of Zhejiang, College of Animal Sciences, Institute of Animal Nutrition and Feed Sciences, Zhejiang University, Hangzhou, China, [2] School of Life Science and Engineering, Foshan University, Foshan, China

OPEN ACCESS

Edited by:
Hui Han,
Chinese Academy of Sciences (CAS), China

Reviewed by:
Yuan Gao,
Zhejiang Academy of Agricultural Sciences, China
Séverine Zirah,
Muséum National d'Histoire Naturelle, France
Xianyong Ma,
Guangdong Academy of Agricultural Sciences (GDAAS), China

***Correspondence:**
Weifen Li
wfli@zju.edu.cn
Huihua Zhang
hhzhang2@163.com

†ORCID:
Baikui Wang
orcid.org/0000-0001-5283-7337
Weifen Li
orcid.org/0000-0001-8159-9876

Specialty section:
This article was submitted to Nutrition and Microbes, a section of the journal Frontiers in Nutrition

Received: 06 May 2021
Accepted: 17 September 2021
Published: 14 October 2021

Citation:
Wang B, Zhou Y, Mao Y, Gong L, Li X, Xu S, Wang F, Guo Q, Zhang H and Li W (2021) Dietary Supplementation With Lactobacillus plantarum Ameliorates Compromise of Growth Performance by Modulating Short-Chain Fatty Acids and Intestinal Dysbiosis in Broilers Under Clostridium perfringens Challenge. Front. Nutr. 8:706148. doi: 10.3389/fnut.2021.706148

Clostridium perfringens is an important zoonotic pathogen associated with food contamination and poisoning, gas gangrene, necrotizing enterocolitis or necrotic enteritis in humans and animals. Dysbacteriosis is supposedly associated with the development of *C. perfringens* infection induced necrotic enteritis, but the detailed relationship between intestinal health, microbiome, and *C. perfringens* infection-induced necrotic enteritis remains poorly understood. This research investigated the effect of probiotics on the growth performance and intestinal health of broilers, and the involved roles of intestinal microbiota and microbial metabolic functions under *C. perfringens* infection. Results showed that subclinical necrotic enteritis was successfully induced as evidenced by the significant lower body weight (BW), suppressed feed conversion ratio (FCR), decreased ileal villus height and mucosal barrier function, and increased ileal histopathological score and bursal weight index. *Lactobacillus plantarum* or *Paenibacillus polymyxa* significantly attenuated *C. perfringens*-induced compromise of growth performance (BW, FCR) and ileal mucosa damage as illustrated by the increased ileal villus height and villus/crypt ratio, the decreased ileal histopathological score and the enhanced ileal mucosal barrier function. *L. plantarum* also significantly alleviated *C. perfringens*-induced enlarged bursa of fabricius and the decreased levels of ileal total SCFAs, acetate, lactate, and butyrate. Furthermore, dietary *L. plantarum* improved *C. perfringens* infection-induced intestinal dysbiosis as evidenced by significantly enriched short-chain fatty acids-producing bacteria (*Lachnospiraceae*, *Ruminococcaceae*, *Oscillospira*, *Faecalibacterium*, *Blautia*), reduced drug-resistant bacteria (*Bacteroides*, *Alistipes*) and enteric pathogens (*Escherichia coli*, *Bacteroides fragilis*) and bacterial metabolic dysfunctions as illustrated by significantly increased bacterial fatty acid biosynthesis, decreased bacterial lipopolysaccharide biosynthesis, and antibiotic biosynthesis (streptomycin and vancomycin). Additionally, the BW and intestinal SCFAs were the principal factors affecting the bacterial communities and microbial metabolic functions. The above findings indicate that dietary with *L. plantarum* attenuates *C. perfringens*-induced compromise of growth performance and intestinal dysbiosis by increasing SCFAs and improving intestinal health in broilers.

Keywords: ***Lactobacillus plantarum*, *Paenibacillus polymyxa*, *Clostridium perfringens*, necrotic enteritis, growth performance, short-chain fatty acids, intestinal health, intestinal dysbiosis**

INTRODUCTION

Clostridium perfringens (*C. perfringens*) is a widely distributed anaerobic spore-forming zoonotic pathogen, which causes foodborne illnesses in humans and necrotic enteritis in animals (1, 2). Foodborne illness caused by *C. perfringens*-contaminated food in the United States is estimated to be nearly 1 million cases per year (2). Necrotic enteritis induced by *C. perfringens* is a widespread avian intestinal necrotic disease, which is estimated to cause the total global economic loss in poultry industry to be over US$6 billion annually (3). Clinical form of necrotic enteritis is characterized by sudden death and increased mortality of chickens, with a mortality rate from 2 to 50% (4). Subclinical infection leads to disrupted villus-crypt micro-architecture and reduced nutrient digestion and absorption, which adversely decreases feed conversion and impairs growth performance (4, 5). Infeed antibiotics used to be the main strategy for preventing or controlling necrotic enteritis in poultry production. However, with the increasing public concerns about antimicrobial resistance and antibiotic residues in food animal products, infeed antimicrobial growth promoters have been widely removed from the animal feed by increasing global countries (6, 7). Subsequently, outbreaks of necrotic enteritis have become a significant economic concern for poultry farmers, especially in subclinical form, which shows unobvious pathological symptoms and thereby compromises the growth performance (8). The withdrawal of infeed prophylactic antibiotics and outbreaks of necrotic enteritis in the commercial poultry industry inspires an interest in seeking effective alternative antimicrobial strategies to prevent or control necrotic enteritis outbreaks. In recent years, multiple dietary alternatives to prophylactic antibiotics, such as probiotics, prebiotics, plant extracts, enzymes, and organic acids, have been proved to be effective in reducing or abolishing *C. perfringens*-induced necrotic enteritis (5, 9).

Intestinal microbes play crucial roles in the development of the intestinal defense system (immune function and barrier function) and in regulating the processes of inflammation and maintaining homeostasis (10–12). It is reported that the anomalous intestinal microbiota is associated with the development of necrotic enteritis in animals or necrotizing enterocolitis in humans, but interactive roles of intestinal microbes in this relationship remain poorly understood (13, 14). As a potential advanced alternative to antibiotic growth promoters, many studies have shown that probiotics and commensal microbes exert beneficial effects on inhibiting growth and toxin secretion of pathogens, modulating gastrointestinal immune systems against adhesion and invasion of pathogens, restoring altered intestinal microbes, maintaining gastrointestinal homeostasis, and promoting tissue healing (15–17). Many studies have proved that *L. plantarum* exerts antibacterial activities by secreting lactic acid (18) and plantaricin (19, 20), and *P. polymyxa* exerts antibacterial activities by secreting polymyxin and lantibiotic (21, 22). Although numerous studies have demonstrated that probiotics, such as *lactobacillus*, *bacillus*, and yeast, could alleviate or abolish *C. perfringens* infection-induced necrotic enteritis (23–26), the involved interactive roles of intestinal microbiota, microbial metabolic functions, and short-chain fatty acids (SCFAs) under *C. perfringens* infection-induced necrotic enteritis remain poorly understood. Our previous works found that two probiotics, *Lactobacillus plantarum* (Lac16) and *Paenibacillus polymyxa* (BSC10), had *in vitro* anti-*C. perfringens* activities and Lac16 protected-*Caenorhabditis elegans* against *C. perfringens* infection (**Supplementary Figure 1**). The present study further evaluated the effect of the two probiotics on growth performance and intestinal health of broilers challenged with *C. perfringens*, and the interactive roles of intestinal microbial communities, bacterial metabolic functions, and SCFAs under *C. perfringens* infection condition.

EXPERIMENTAL PROCEDURES

Bacteria Preparation

L. plantarum (Lac16) deposited in China Center for Type Culture Collection (CCTCC M2016259) was isolated from fermented vegetables, and *P. polymyxa* (BSC10) was purchased from China General Microbiological Culture Collection Center (CGMCC1.10711). The Lac16 and BSC10 were separately cultured in DeMan-Rogosa-Sharpe and Luria-Bertani broth at 37°C for overnight under aerobic conditions. *Clostridium perfringens* type A (ATCC13124, Cp) was cultured in reinforced clostridium medium at 37°C for 20 h in anaerobic gas-generating packs (Mitsubishi Gas Chemical Company Inc., Tokyo, Japan). After centrifugation at 3,500 × *g* for 10 min at 4°C, the BSC10, Lac16, and Cp pellets were collected and then washed three times with sterile phosphate-buffered saline (PBS, pH 7.2), respectively. Finally, the concentration of the bacteria was constantly checked by spreading the plate method (27).

Chicken Experiment

Seven hundred and twenty hatched 1-day-old Cobb 500 broilers with similar body weight were randomly allocated into four treatments with six pens per group and 30 birds per pen: (1) Control group: birds were fed a basal diet (**Supplementary Table 1**) formulated to meet the nutritional requirements of broilers (28), (2) Cp group: birds were fed a basal diet and then orally challenged with *C. perfringens* type A cultures [1. × 10^8 colony-forming units (CFU)/bird] on day 1 and during day 14–20 of age, (3) BSC10+Cp group: birds were fed a basal diet supplemented with *P. polymyxa* (1. × 10^8 CFU/kg feed) and orally challenged with *C. perfringens* A cultures (1. × 10^8 CFU/bird) on day 1 and during day 14–20 of age, (4) Lac16 + Cp group: birds were fed a basal diet supplemented with *L. plantarum* (1. × 10^8 CFU/kg feed) and orally challenged with *C. perfringens* A cultures (1. × 10^8 CFU/bird) on day 1 and during day 14–20 of age. The animal experiment lasted for 21 days. Birds were allowed *ad libitum* access to mashed diets and fresh water. Feed consumption and body weight were recorded every week. Mortality was recorded every day, and dead birds were weighed to adjust estimates of body weight gain, feed intake, and feed conversion ratio.

Sample Collection

At day 21 of age, six birds from each group were randomly selected, weighed, and euthanized by electrical stun after deprivation of feed for 6 h (05:00–11:00 A.M.). After being removed and weighed, spleen and bursa of fabricius indexes were calculated as a percentage relative to body weight. The ileal segments were fixed in 4% paraformaldehyde for hematoxylin and eosin (H&E) staining or in 2.5% buffered glutaraldehyde for transmission electron microscopy (TEM). The ileal contents and whole caecum of birds were sampled, snap frozen in liquid nitrogen, and stored at −80°C for short-chain fatty acids (SCFAs) and microbial analysis.

Ileal Morphological Analysis

After being fixed in 4% paraformaldehyde, ileal samples were embedded in paraffin, sliced, dehydrated, and stained with hematoxylin and eosin. Images were observed by Olympus microsystem (Tokyo, Japan). Histopathological scores of the ileal samples were examined by three independent observers as previously described (29).

For TEM observation, after being fixed in 2.5% buffered glutaraldehyde, ileal segments were washed three times by a cold 100-mM phosphate buffer, and then postfixed in cold 0.1% buffered osmium tetroxide (OsO_4) for 2 h. After being washed by a phosphate buffer, the ileal segments were rapidly dehydrated in ascending grades of ethanol (30, 50, 70, 95, and 100%), and then transferred into a 1:1 mixture of propylene oxide and epoxy araldite. The ultrathin ileal sections were embedded and cut by an LKB Nova ultramicrotome (Leica Microsystems, Buffalo Grove, IL) and then stained with uranyl acetate. Transmission electron micrographs of the ileal samples were then observed and captured by the transmission electron microscope (JEOL, Tokyo, Japan).

Lactate and SCFAs Analysis

Lactate levels in ileal digesta were determined by the Lactic Acid assay kit (NanJingJianCheng Bioengineering Institute, Nanjing, China) according to the instructions of the manufacturer. SCFAs contents in ileal digesta were measured as follows: 1 g of digesta was mixed with 2. ml of distilled water. After being homogenized and centrifuged at 5,000 × g for 10 min at 4°C, 500 µl of the supernatant were mixed with 0.2 ml 25% (w/v) phosphoric acid and then stored at −20°C for overnight. After thawing, the mixtures were centrifuged (15,000 × g for 10 min at 4°C), filtered by 0.22-µm membrane filter and then analyzed by gas chromatography (Varian CP-3800, USA). Quantification of SCFAs was carried out by using the external calibration standard curves method and expressed as µmol/g of wet ileal digesta.

Microbial Analysis

The bacterial genomic DNA from cecal contents was extracted under sterile conditions using the TIANamp Stool DNA Kit (Tiangen, Beijing, China) and was stored at −80°C for PCR amplification and sequencing. The V3-V4 hypervariable region of the 16S rRNA gene was amplified by using the 341F/805R primer pairs, and the amplicon sequencing was performed on an Illumina MiSeq platform (Illumina Inc., San Diego, CA, USA). The Quantitative Insights into Microbial Ecology (QIIME) software (version 1.9.1) was used for the quality filter of raw sequences and a cluster of filtered sequences into operational taxonomic unit (OTU) at 97% similarity (30). Bacterial OTU representative sequences were assigned to a taxonomic lineage by a Ribosomal Database Project (RDP) classifier based on the Greengenes 13.8 database.

Alpha and beta diversities of the microbial community were analyzed based on a subsample of a minimum number of sequences (12981) by QIIME software. Significant differences in microbial beta diversity and metagenome predicational functions among different groups (based on the Bray-Curtis distance matrices) were calculated by ANOSIM (analysis of similarities), PERMANOVA (permutational multivariate analysis of variance), and MRPP (multi-response permutation procedure) analyses using a "vegan" package and were visualized by Principal coordinates analysis (PCoA) using the "ggplot2" package of R software (v4.1.0). Canonical correspondence analysis (CCA) and variation partitioning analysis (VPA) were performed using the R package "vegan." The linear discriminant analysis (LDA) effect size (LEfSe) analysis (https://huttenhower.sph.harvard.edu/galaxy/) was performed to analyze and characterize the bacterial differences and microbial predicted pathway functions among different groups.

The metagenome functional predictions based on 16S rRNA gene sequencing of bacterial communities were analyzed by the Phylogenetic Investigation of Communities by the Reconstruction of Unobserved States 1 (PICRUSt 1) method (31). The OTU table and representative sequences subsampled at a minimum number of sequences (12981) were selected for the functional annotation to KEGG ortholog groups (KO) based on KEGG databases. Significant differential predicted pathway abundances were then analyzed and visualized by statistical analysis of taxonomic and functional profiles (STAMP) software with a two-sided Welch's *t*-test (32). Pearson correlation between phenotypic variables was analyzed and visualized by R software (v4.1.0) using the "corrplot" package. Mantel test was performed to examine the linkage between phenotypic variables and microbial communities or microbial predicted pathways (33).

The co-occurrence patterns were constructed to visualize the correlations between bacterial communities and microbial predicted pathways. Firstly, only those bacterial OTUs and microbial predicted KOs pathways with an average relative abundance >0.1% across all samples were retained according to Hartman et al. (34). We then normalized the filtered bacterial OTUs and microbial predicted KOs pathways separately by the "trimmed means of M" (TMM) method, and the normalized counts were expressed as relative abundance counts per million (CPM) using the R package "edgeR." The indicator species of the filtered bacterial OTUs and microbial predicted KOs pathways were analyzed using the R package "indicspecies." Differential OTUs and KOs abundances among all the groups were also analyzed by likelihood ratio tests (LRT) using the R package "edgeR." The differential OTUs and KOs at a value of $p < 0.05$ were defined as OTUs and KOs responsive. Treatment-sensitive OTUs and KOs (hereafter: tsNodes) were then confirmed by both indicator species analysis and LRT. The TMM-normalized CPM counts of bacterial OTUs and microbial-predicted KOs pathways were then combined and further calculated the Spearman rank correlations by the R package "Hmisc." Significant correlations ($\rho > 0.7$ and FDR-adjusted $p < 0.01$) were kept as the edges of the co-occurrence networks. Then, the co-occurrence networks were visualized using the *Fruchterman-Reingold* layout by the R package "igraph." The network topological properties and modules were also calculated and identified to describe the complex patterns of the interrelationships. Keystone OTUs and KOs were identified as those nodes within top 1% of node degree values in the networks.

Statistical Analysis

Data on growth performance and ileal histomorphology analysis were assessed using SPSS^{TM} software (SPSS Inc., Chicago, IL, USA) by one-way ANOVA, and the contrast of means was evaluated by Tukey's multiple range tests. The data on SCFAs analysis were analyzed by two-tailed Student's *T*-test using SPSS^{TM} software.

RESULTS

Growth Performance

Performance results showed that, compared with the control group, *C. perfringens* infection significantly ($p < 0.05$) decreased the body weight and feed conversion and significantly ($p < 0.05$) increased bursal weight index of broilers, whereas dietary with *P. polymyxa* or *L. plantarum* significantly ($p < 0.05$) ameliorated *C. perfringens*-induced side effects of growth performance (body weight and feed conversion) (**Table 1**). Additionally, *L. plantarum* treatment also attenuated *C. perfringens*-induced enlarged bursa of fabricius ($p < 0.05$).

TABLE 1 | Effect of probiotics on growth performance and immune organ indexes of broilers infected with *C. perfringens*.

Items	Control	Cp	BSC10+Cp	Lac16+Cp	SEM	*P*-value
Body weight (g)						
Day 1	48.03	48.13	47.43	48.16	0.42	0.67
Day 21	637.88^{a}	615.15^{b}	648.48^{a}	636.97^{a}	8.33	0.016
Day 1–21						
BWG (g/d)	29.49^{ab}	28.35^{b}	30.05^{a}	29.44^{ab}	0.40	0.011
FI (g/d)	52.82	55.11	54.18	52.68	0.87	0.18
FCR	1.79^{b}	1.94^{a}	1.80^{b}	1.79^{b}	0.04	0.01
Immune organ indexes						
Spleen	0.85	1.02	0.9	1.11	0.096	0.22
Bursa of fabricius	1.87^{b}	2.55^{a}	2.3^{a}	1.62^{b}	0.25	<0.001

^{a,b}*Mean values within a row with no common superscript differ significantly (p < 0.05). SEM, standard error of mean; BWG, body weight gain; FI, feed intake; FCR, feed conversion ratio. n = 6 samples.*

TABLE 2 | The ileal histomorphology of broilers infected with *C. perfringens*.

Items	Control	Cp	BSC10+Cp	Lac16+Cp	SEM	*P*-value
Villus height (μm)	444.50^{c}	382.85^{d}	529.27^{b}	627.77^{a}	38.11	<0.001
Crypt depth (μm)	118.01^{a}	121.31^{a}	118.29^{a}	96.24^{b}	6.22	0.009
Villus/crypt ratio	3.79^{bc}	3.19^{c}	4.50^{b}	6.59^{a}	0.55	<0.001
Histopathological score	0.17^{c}	3.00^{a}	1.33^{b}	1.17^{b}	0.46	<0.001

^{a,b,c,d}*Mean values within a row with no common superscript differ significantly (p < 0.05). SEM, standard error of mean. n = six samples.*

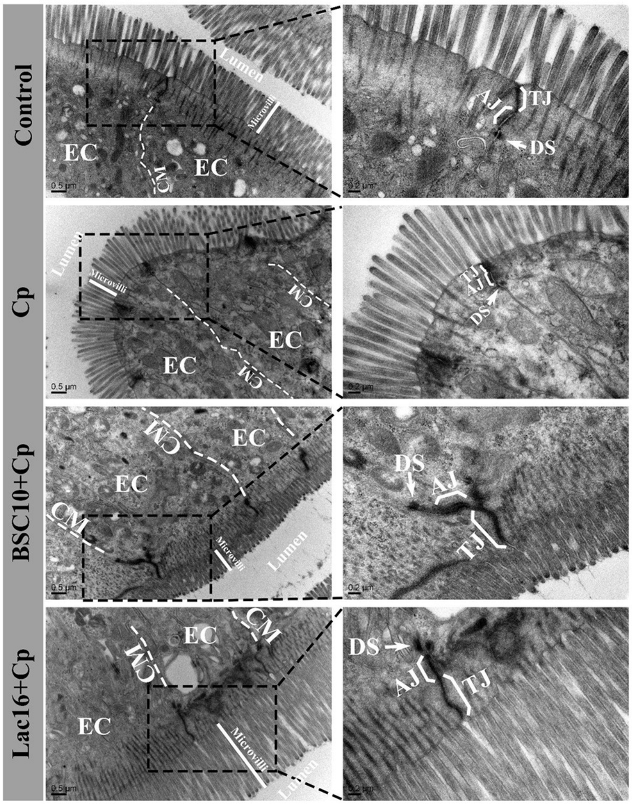

FIGURE 1 | Transmission electron micrographs of the ileal microvilli in broilers at day 21 of age. EC, epithelial cell; CM, cell membrane; TJ, tight junction; AJ, adherens junction. The white arrow indicates desmosomes (DS).

Morphological Observation

As presented in **Table 2**, *C. perfringens* infection significantly ($p < 0.05$) decreased the villus height and significantly ($p < 0.05$) increased the histopathological score of the ileum compared with those of the uninfected birds. Dietary with *P. polymyxa* or *L. plantarum* significantly ($p < 0.05$) ameliorated *C. perfringens*-induced ileal mucosa injury, as evidenced by the significantly ($p < 0.05$) increased villus height and villus height to crypt depth ratio, and decreased crypt depth and the histopathological score of the ileum.

TEM results showed that, compared with the control group, the ileum of the *C. perfringens*-infected birds showed sparse microvilli, disrupted and shorter tight junction, adherens junction, and desmosomes (**Figure 1**). Compared with the *C. perfringens*-infected group, the improved ileal intercellular junctional complexes of broilers in BSC10+Cp and Lac16+Cp groups were observed as evidenced by higher and ordered microvillus, longer tight junction and adherens junction, and darker desmosomes.

SCFAs in Ileal Digesta

The levels of total SCFAs, acetate, lactate, and butyrate in ileal digesta of the *C. perfringens*-infected broilers were significantly ($p < 0.01$) decreased compared with the uninfected broilers (**Figure 2**). Compared with the *C. perfringens*-infected group, *P. polymyxa* treatment increased the concentrations of total SCFAs, acetate, lactate, and butyrate in ileal digesta of the *C. perfringens*-infected broilers but had no significant differences ($p > 0.05$). Dietary with *L. plantarum* significantly ($p < 0.05$) increased the contents of total SCFAs, acetate, lactate, and butyrate in ileal digesta of the *C. perfringens*-infected broilers.

Microbial Composition

Alpha diversity analysis showed that no significant difference was observed among the four groups ($p > 0.05$, **Figure 3A**). PCoA based on Bray-Curtis distance showed that the microbial communities were clustered into two different types of communities (**Figure 3B**). The microbial communities of broilers in control and Lac16+Cp groups formed a cluster and formed another cluster in the Cp and BSC10+Cp groups. Significant differences in beta diversity of microbial communities among all treatments were further confirmed by ANOSIM, PERMANOVA, and MRPP analyses (**Table 3**).

LEfSe analysis was employed to explore the specific microbial features among the four groups (**Figure 4**). It was found that 36 taxa biomarkers in four groups were identified with LDA score >3, which mainly belong to the phyla of *Firmicutes*, *Bacteroidetes*, *Proteobacteria*, *Tenericutes*, and *Cyanobacteria*. Differential analysis results (**Figure 5**) further showed that, compared with the uninfected group, *C. perfringens* infection significantly ($p < 0.05$ or $p < 0.01$) reduced the relative abundances of *Firmicutes*, *Clostridia*, *Clostridiales*, *Lachnospiraceae*, *Ruminococcaceae*, [*Ruminococcus*], *Oscillospira*, *Blautia*, and *Clostridium citroniae* in the cecum, while markedly ($p < 0.05$ or $p < 0.01$) increased the relative abundances of *Bacteroidetes*, *Rikenellaceae*, *Alistipes*, *Alistipesmassiliensis*, *Clostridium*, and *Clostridium methylpentosum*. Compared with the *C. perfringens*-infected birds, the significantly ($p < 0.05$ or $p < 0.01$) increased *Oscillospira* abundance and decreased relative abundances of *Faecalibacterium*, and *Escherichia coli* were observed in the broilers of the BSC10+Cp group. Furthermore, *L. plantarum* significantly ($p < 0.05$ or $p < 0.01$) improved the anomalous microbial composition induced by *C. perfringens* infection, as evidenced by the increased relative abundances of *Firmicutes*, *Clostridia*, *Clostridiales*, *Lachnospiraceae*, *Ruminococcaceae*, [*Ruminococcus*], *Oscillospira*, *Faecalibacterium*, and *Blautia* and the reduced relative abundances of *Bacteroidetes*, *Rikenellaceae*, *Bacteroides*, *Alistipes*, *Alistipesmassiliensis*, *Clostridium*, *Escherichia coli*, *Bacteroides fragilis*, *Bacteroides acidifaciens*, *Clostridium methylpentosum* (**Figure 5**).

Metagenome Functional Predictions

PICRUSt analysis was performed to explore the metagenome functions based on 16S rRNA marker gene sequences. PCoA results based on Bray-Curtis distance showed that the microbial metabolic functions were significantly distinct among the groups (**Figure 6**). Consisted with PCoA results for microbial communities, *C. perfringens* infection also altered the bacterial metabolic functions, whereas dietary with *L. plantarum* significantly ($R^2 = 0.781$, $P = 0.009$) ameliorated the shifts of bacterial metabolic functions induced by *C. perfringens*

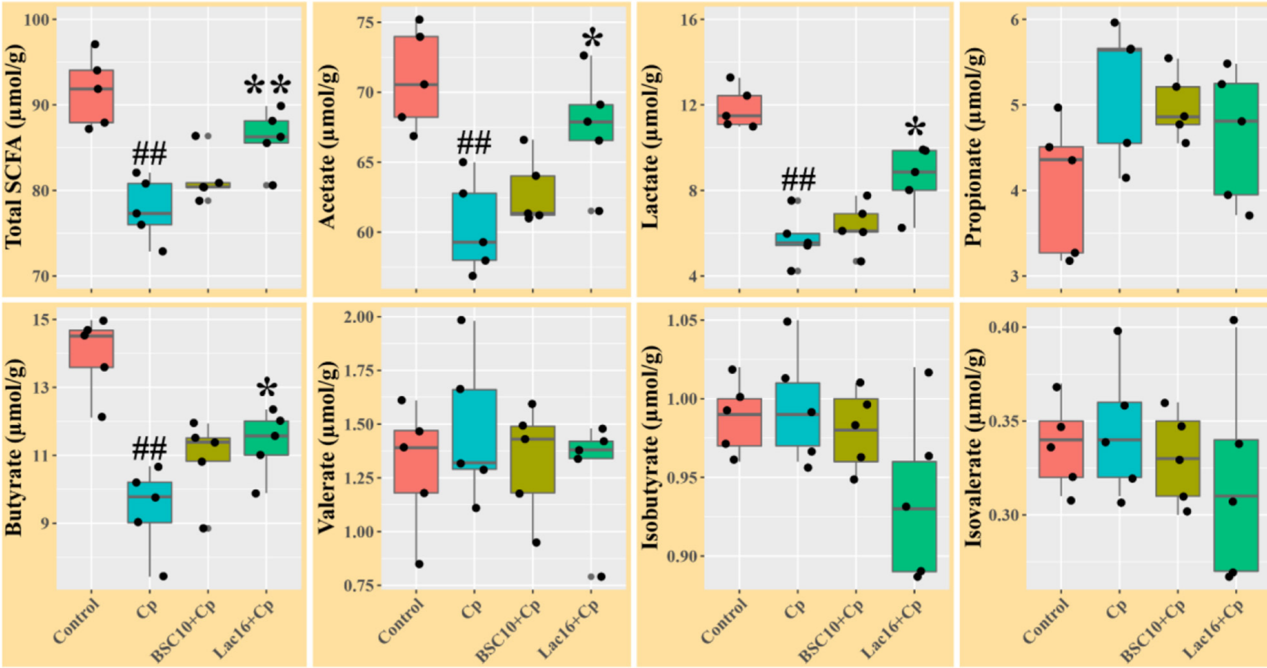

FIGURE 2 | Short chain fatty acids levels in ileal digesta of broilers at day 21 of age. Significant differences vs. the control group: $^{\#\#}p < 0.01$. Significant differences vs. the Cp group: $^{*}p < 0.05$; $^{**}p < 0.01$. n = five samples.

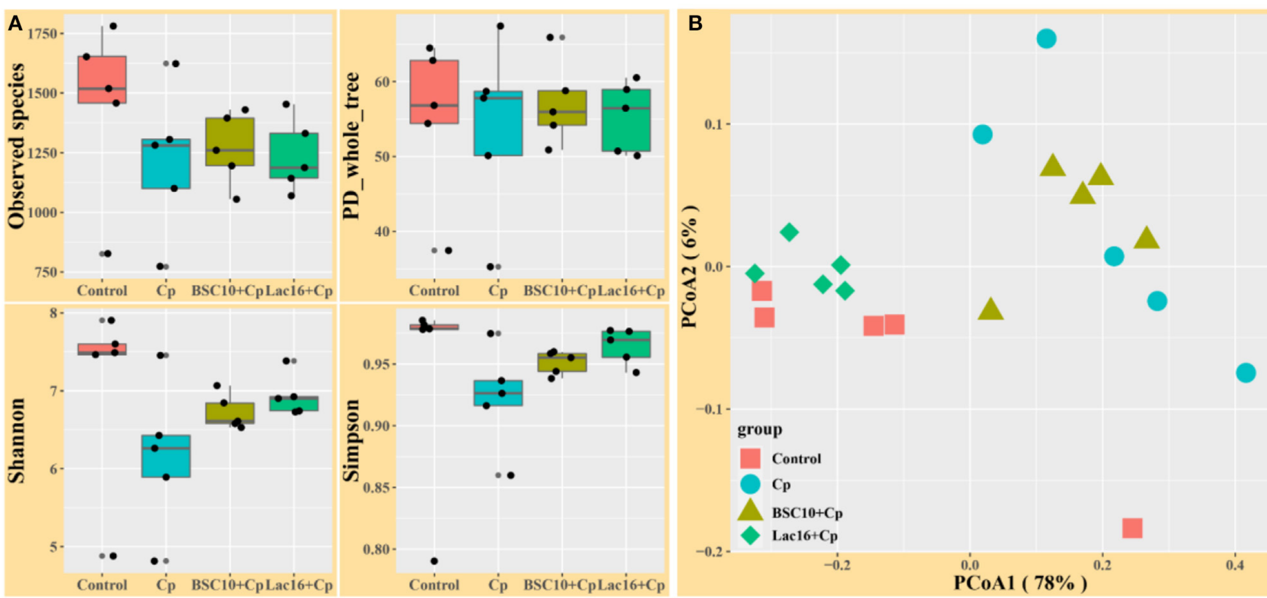

FIGURE 3 | Diversity analyses of microbial communities among groups. **(A)** Alpha diversity analysis **(B)** Principal coordinates analysis (PCoA) based on Bray-Curtis distance. n = five samples.

infection. The STAMP and LEfSe analysis based on level 1 and level 3 of the microbial-predicted pathway functions further verified the differences in metabolic functions (**Figures 7, 8** and **Supplementary Figure 2**). Specifically, *L. plantarum* treatment significantly ($p < 0.05$) inversed the shifts of bacterial metabolic functions induced by *C. perfringens* infection, such as metabolism, lipopolysaccharide (LPS) biosynthesis, LPS biosynthesis proteins, fatty acid biosynthesis, streptomycin biosynthesis, biosynthesis of vancomycin group antibiotics, cysteine and methionine metabolism, lysine biosynthesis,

TABLE 3 | ANOSIM, PERMANOVA, and MRPP analysis of microbial diversity among different treatments.

	Anosim		Permanova		Mrpp	
	R	***P***	R^2	***P***	***A***	***P***
Treatment	0.561	0.001	0.597	0.002	0.327	0.001
Control vs. Cp	0.492	0.020	0.439	0.034	0.217	0.022
Cp vs. BSC10+Cp	0.084	0.232	0.109	0.376	0.018	0.275
Cp vs. Lac16+Cp	0.928	0.005	0.720	0.007	0.425	0.007

ANOSIM, analysis of similarities; PERMANOVA, permutational multivariate analysis of variance; MRPP, multi-response permutation procedure. n = five samples.

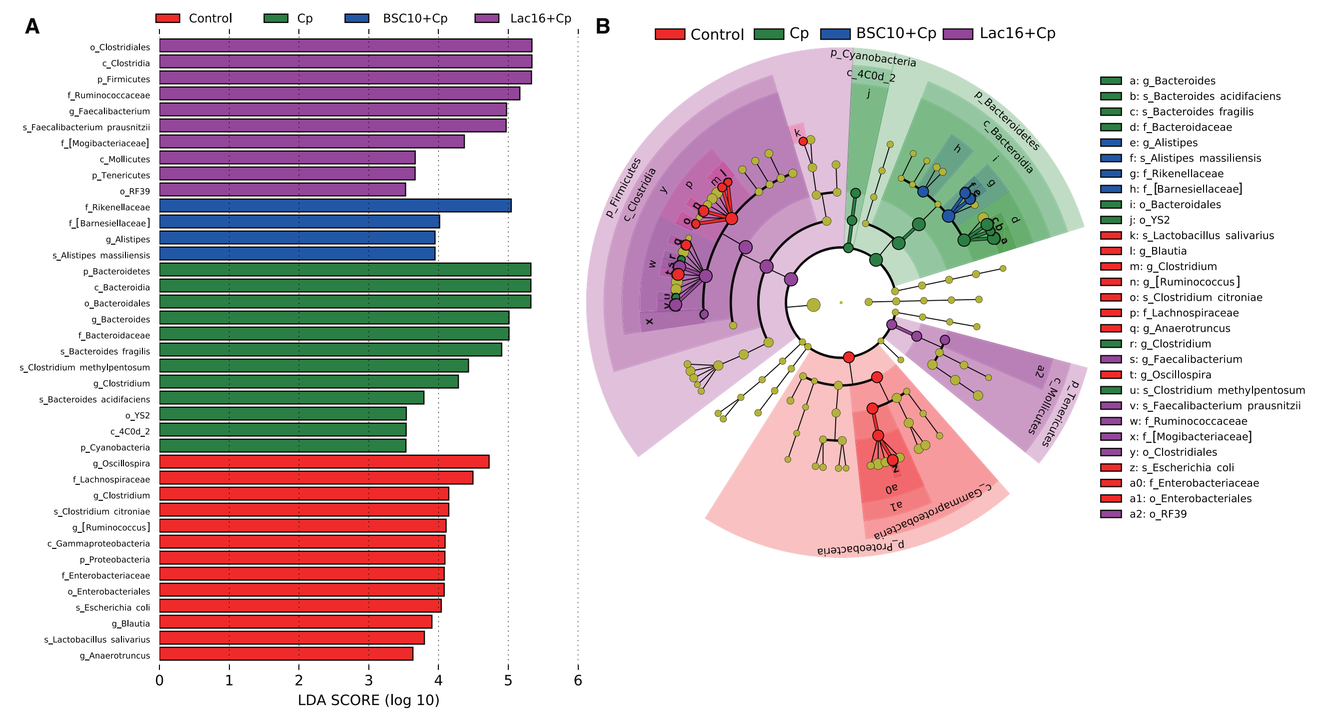

FIGURE 4 | Linear discriminant analysis (LDA) effect size (LEfSe) analysis (LDA > 3., p <0.05) of the intestinal microbes. Histogram **(A)** and cladogram **(B)** of LEfSe analysis among the four groups. The prefixes "p_," "c_," "o_," "f_," "g_," and "s_" represent the annotated levels of phylum, class, order, family, genus, and species.

thiamine metabolism, histidine metabolism, and cell division (**Figure 8** and **Supplementary Figure 2**). Dietary with *P. polymyxa* had less effects on microbial metabolic functions than *L. plantarum* in *C. perfringens*-infected broilers (**Figure 8** and **Supplementary Figure 2**).

Relationships Between Phenotypic Variables, Bacterial Communities and Microbial Metabolic Functions

The shifts in microbial community and metabolic functional composition induced by *C. perfringens* infection and dietary with probiotics were tightly linked to phenotypic variables and ileal SCFAs as revealed by the Mantel test (**Figure 9**), CCA and VPA analyses (**Supplementary Figure 3**). Pearson correlation analysis (**Figure 9**) showed that the ileal SCFAs (including total SCFAs, acetate, lactate and butyrate) were positively ($p < 0.001$) correlated with the final body weight, whereas were negatively ($p < 0.05$ or $p < 0.01$) correlated with immune organ indexes (spleen and bursa of Fabricius). The bursa of Fabricius index was positively ($p < 0.05$) correlated with propionate and isobutyrate. Additionally, the spleen index was negatively ($p < 0.05$) correlated with valerate, isobutyrate, and isovalerate. Mantel correlation analysis (**Figure 9**) showed that taxonomic composition was significantly correlated with bursa of Fabricius index ($0.25 < r < 0.5$, $0.001 < p < 0.01$), total SCFAs ($0.25 < r < 0.5$, $0.01 < p < 0.05$), acetate ($r < 0.25$, $0.01 < p < 0.05$), lactate ($r < 0.25$, $0.01 < p < 0.05$), and butyrate ($r < 0.25$, $0.01 < p < 0.05$). The microbial functional compositions were significantly correlated with the final body weight ($r < 0.25$, $0.01 < p < 0.05$), bursa of Fabricius index ($r > 0.5$, $0.001 < p < 0.01$), total SCFAs ($r > 0.5$, $0.001 < p < 0.01$), acetate ($r > 0.5$, $0.001 < p < 0.01$), lactate ($r > 0.5$, $0.001 < p < 0.01$), and butyrate ($0.25 < r < 0.5$, $0.001 < p$ <0.01). CCA analysis showed that bursa of Fabricius

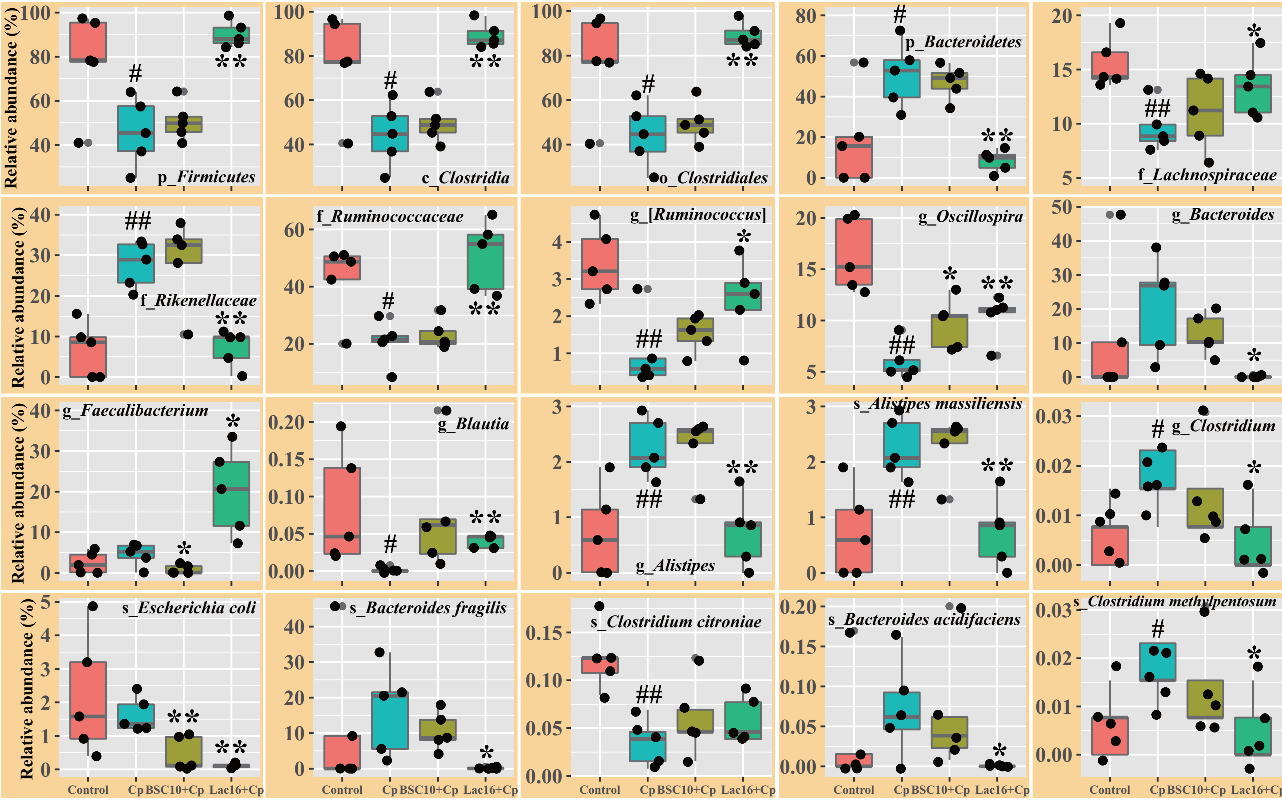

FIGURE 5 | Comparison of the intestinal microbiota among the groups. Significant differences vs. the control group: $^{\#}p < 0.05$; $^{\#\#}p < 0.01$. Significant differences vs. the Cp group: $^{*}p < 0.05$; $^{**}p < 0.01$. The prefixes "p_," "c_," "o_," "f_," "g_," and "s_" represent the annotated level of phylum, class, order, family, genus, and species. n = five samples.

index ($R^2 = 0.56$, $P = 0.004$; $R^2 = 0.55$, $P = 0.004$), ileal total SCFAs ($R^2 = 0.58$, $P = 0.002$; $R^2 = 0.68$, $P = 0.001$), acetate ($R^2 = 0.53$, $P = 0.002$; $R^2 = 0.67$, $P = 0.001$), lactate ($R^2 = 0.66$, $P = 0.002$; $R^2 = 0.65$, $P = 0.001$), and butyrate ($R^2 = 0.51$, $P = 0.005$; $R^2 = 0.72$, $P = 0.001$) were significantly correlated with the bacterial (**Supplementary Figure 3A**) and microbial functional (**Supplementary Figure 3B**) community structures. The final body weight ($R^2 = 0.36$, $P = 0.026$) and isobutyrate ($R^2 = 0.48$, $P = 0.002$) were also significantly correlated with the microbial functional community structure (**Supplementary Figure 3B**). The VPA analysis showed that the phenotypic variables and ileal SCFAs explained 27.21 and 28.73% of the variations in the bacterial communities, and their interaction explained 10.72% of the variation (**Supplementary Figure 3C**). For the microbial predicted pathway functions, phenotypic variables and ileal SCFAs explained 17.07 and 25.26% of the variations, respectively, and the interaction explained 24.00% of the variation (**Supplementary Figure 3D**).

To further investigate the specific relationships between phenotypic variables and the microbial community or microbial metabolic functional composition, Pearson's correlation analysis was performed (**Figure 10**). As shown in **Figure 10A**, we found that the final body weight was positively ($p < 0.05$, $p < 0.01$, or $p < 0.001$) correlated with cecal *Firmicutes*, *Blautia*, *Dorea*, *Oscillospira*, cc_115, *Lactobacillus*, *Lactobacillus salivarius*, and *Butyricicoccus pullicaecorum* but negatively correlated with *Bacteroides* and *Citrobacter*. The bursa of Fabricius index was positively ($p < 0.05$, $p < 0.01$, or $p < 0.001$) correlated with cecal *Cyanobacteria*, *Bacteroidetes*, *Alistipes*, *Alistipes massiliensis*, and *Clostridium methylpentosum*, whereas negatively correlated with *Firmicutes*, *Dehalobacterium*, [*Ruminococcus*], *Oscillospira*, and *Ruminococcus*. The ileal SCFAs (such as total SCFAs, acetate, lactate, and butyrate) were positively ($p < 0.05$, $p < 0.01$, or $p < 0.001$) correlated with cecal *Firmicutes*, *Blautia*, [*Ruminococcus*], *Anaerotruncus*, *Oscillospira*, *Ruminococcus*, *Coprobacillus*, cc_115, *Lactobacillus*, *Butyricicoccus*, *Clostridium citroniae*, *Lactobacillus salivarius*, and *Butyricicoccus pullicaecorum*, whereas negatively ($p < 0.05$, $p < 0.01$, or $p < 0.001$) correlated with *Bacteroidetes*, *Alistipes*, *Citrobacter*, and *Alistipes massiliensis*. The ileal propionate and valerate were positively ($p < 0.05$, $p < 0.01$, or $p < 0.001$) correlated with cecal *Proteobacteria*, *Escherichia*, *Shigella*, *Escherichia coli*, and *Shigella sonnei*. As shown in **Figure 10B**, the results showed that the final body weight and ileal SCFAs (including total SCFAs, acetate, lactate, and butyrate) were positively ($p < 0.05$, $p < 0.01$, or $p < 0.001$) correlated with cecal microbial carbohydrate metabolism, amino acid metabolism, peptidoglycan biosynthesis, fatty acid biosynthesis,

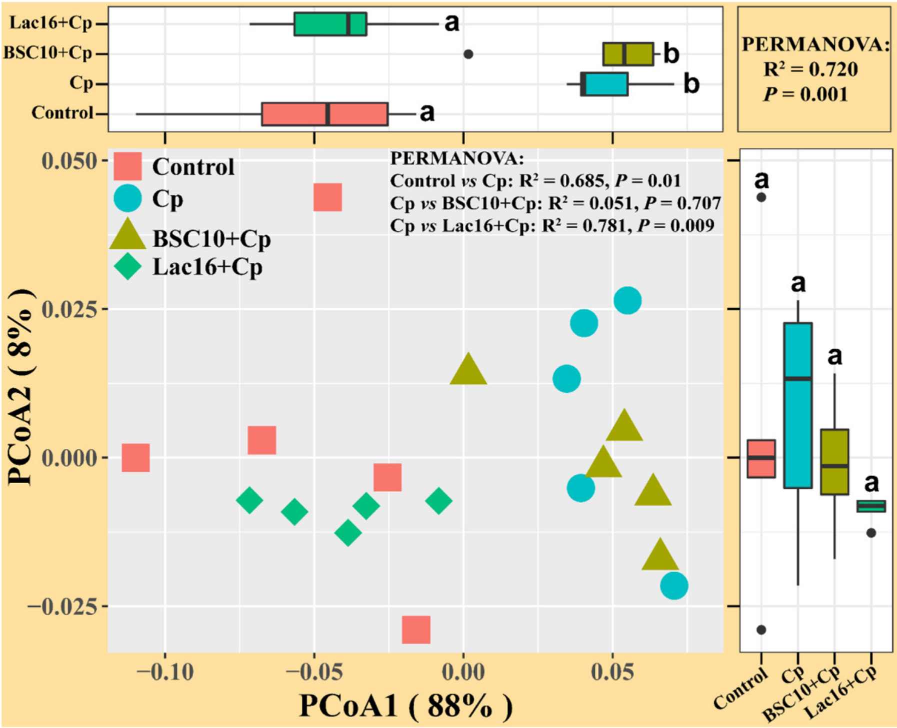

FIGURE 6 | Principal coordinates analysis (**PCoA**) of predicated metabolic functions among groups based on Bray-Curtis distance. [a,b]indicate a significant difference ($p < 0.05$).

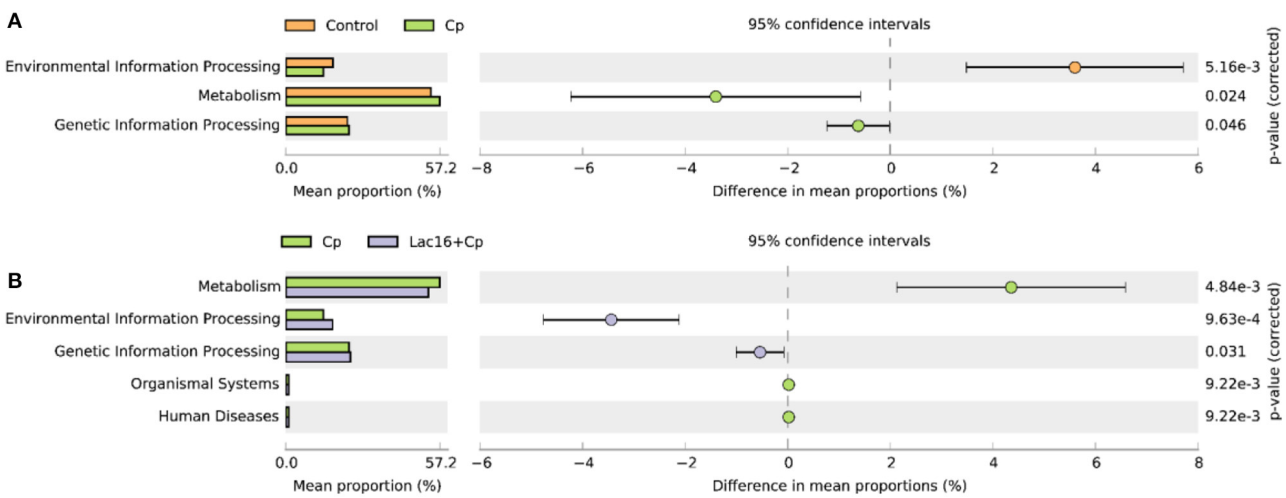

FIGURE 7 | Comparison of predicted metabolic pathway abundances between the groups by statistical analysis of taxonomic and functional profiles (**STAMP**) at Level 1. **(A)** Control vs. Cp; **(B)** Cp vs. Lac16+Cp.

and tetracycline biosynthesis, whereas negatively ($p < 0.05$, $p < 0.01$, or $p < 0.001$) correlated with glycan biosynthesis and metabolism (such as LPS biosynthesis and LPS biosynthesis proteins) and antibiotic biosynthesis (streptomycin biosynthesis and biosynthesis of vancomycin group antibiotics). The bursa of Fabricius index exerts opposite effect on the correlation with the cecal microbial metabolic functions compared with that of final body weight.

Microbial Co-occurrence Patterns

Next, we explored the distribution patterns of sensitive OTUs and KOs in the co-occurrence patterns of bacterial communities

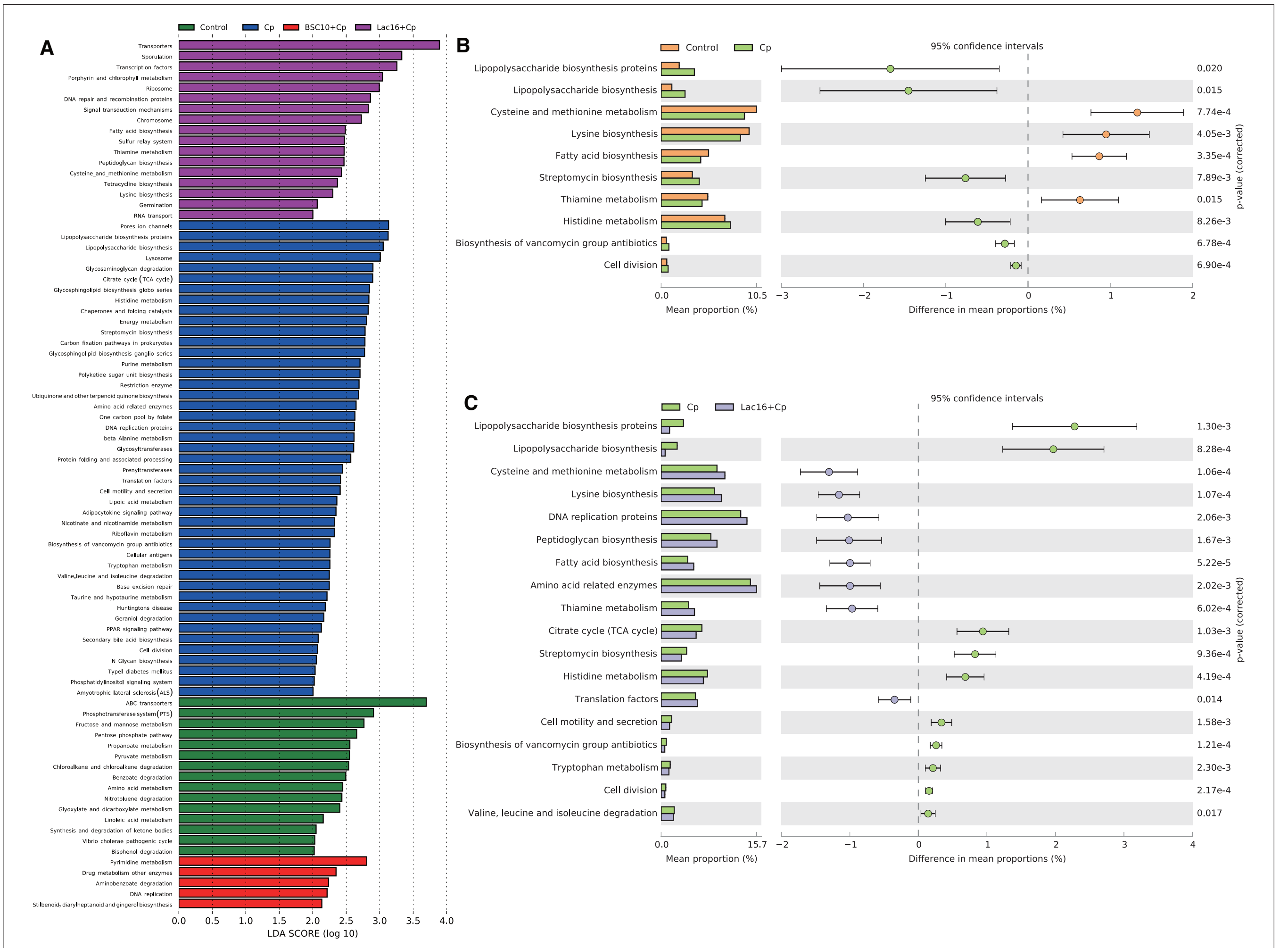

FIGURE 8 | (A) LEfSe analysis (LDA > 2., $p < 0.01$) of the microbial-predicted metabolic pathway functions at Level 3. **(B,C)** Comparison of predicted pathway abundances between the groups by statistical analysis of taxonomic and functional profiles (**STAMP**) at Level 3. **(B)** Control vs. Cp; **(C)** Cp vs. Lac16+Cp.

and microbial metabolic functions in four groups (**Figure 11** and **Table 4**). The co-occurrence network consisted of 1,633 nodes and 7,309 edges (with a mean of 8.95 edges per node) (**Figure 11A**). In the network, the bacteria shared 1,368 nodes with 2,204 edges (with a mean of 3.22 edges per node), and the microbial metabolic functions shared 265 nodes with 4,027 edges (with a mean of 30.39 edges per node). Among the 1,633 nodes, 387 nodes (235 tsOTUs and 150 tsKOs) were identified as treatment-sensitive nodes, and 17 nodes (three OTUs and 14 KOs) were defined as keystones (**Table 4** and **Supplementary Tables 2, 3**). Consistent with the results showed in **Figures 5**, **8**, compared with the uninfected group, *C. perfringens* infection significantly ($p < 0.05$ or $p < 0.01$) increased the relative abundance of 15 keystones, such as *Rikenellaceae* and microbial metabolisms (LPS biosynthesis, LPS biosynthesis proteins, streptomycin biosynthesis, etc.) (**Figure 4**). Compared with the *C. perfringens*-infected group, dietary with *L. plantarum* significantly ($p < 0.05$ or $p < 0.01$) decreased *C. perfringens*-induced relative abundance of 17 keystones.

In addition, we noticed that the distribution patterns of microbial and microbial functional associations also responded to treatments. Six modules with relatively high proportions in the network were identified and visualized (**Figures 11A,B**). We found that the type of sensitivity of these modules to the specific-treated groups (**Figures 11A,B**), and their distribution in the network partially reflected the community similarity showed in **Figures 3B**, **6**. For example, the effect of *C. perfringens* infection in the cecal microbial and functional communities was apparent with discrete modules (Modules 2 and 6) in the network (**Figure 11B**). Module 2 and Module 6 were separated from other modules that primarily contained sensitive OTUs and KOs specific to the control (Modules 7 and 8) and Lac16+Cp (Module 3 and Module 4) groups. The cumulative-relative abundances of the sensitive nodes of Module 2 in the BSC10+Cp and Lac16+Cp groups were significantly ($p < 0.05$) lower than those in the *C. perfringens*-infected group. The cumulative-relative abundances of the sensitive nodes of three modules (Modules 3, 4, and 8) in the Lac16+Cp group and Module 6 in the BSC10+Cp group

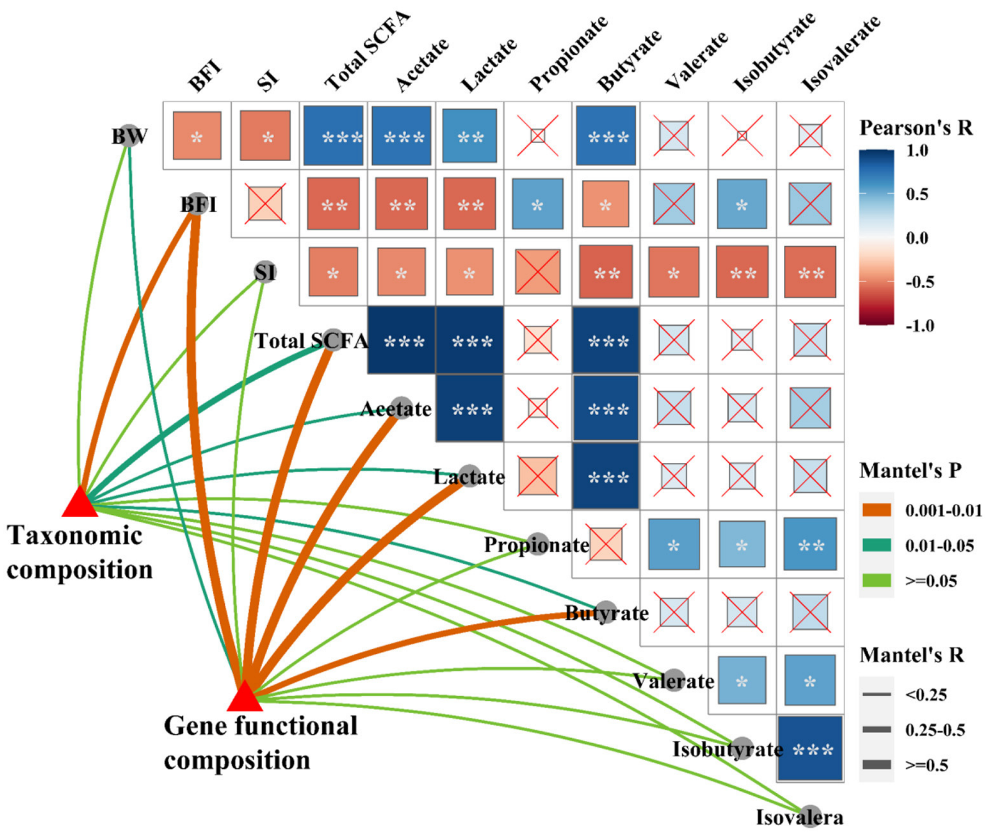

FIGURE 9 | Relationships among phenotypic variables, the microbial community, and metabolic functional composition. Pairwise comparisons of phenotypic variables with a color gradient denoting Pearson correlation coefficient. Taxonomic and functional community structures were related to each phenotypic variable by Mantel correlation (based on Bray-Curtis dissimilarity). The edge width represents the Mantel's r statistic for the corresponding distance correlations, and edge color denotes the statistical significance. *$p < 0.05$; **$p < 0.01$; ***$p < 0.001$.

were significantly ($p < 0.05$ or $p < 0.01$) higher than those in the *C. perfringens*-infected group. Furthermore, we found that the six responsive modules comprised a broad set of bacteria and microbial metabolic functions (**Figure 11C**), indicating that the different treatments may be not target-specific microbial lineages.

DISCUSSION

Necrotic enteritis caused by *C. perfringens* in poultry exists in two forms: clinical (acute) or subclinical (chronic) infections. Subclinical necrotic enteritis infection accompanies with continuously chronic damage of the gastrointestinal mucosa, which leads to poor growth performance (decreased digestion and absorption, reduced body weight and the feed-conversion ratio) of broilers with or without mortality (9, 35). Subclinical necrotic enteritis without mortality in the present study was successfully induced by *C. perfringens* infection as observed by decreased body weight and feed conversion, and increased bursal weight index of broilers. The result was consistent with previous studies that subclinical necrotic enteritis infection impaired broiler growth performance with no mortality (36, 37).

Our previous study reported that *Saccharomyces boulardii* attenuates *C. perfringens*-induced inflammatory response *via* the TLR4/TLR15-MyD88-signaling pathway in HD11 avian macrophages (23). *Bacillus amyloliquefaciens* could alleviate necrotic enteritis-induced undesirable effects by modulation of genes related to gut integrity, apoptosis, and immunity, hence further improve performance (38). Although many studies have reported that *Lactobacillus* or *Bacillus* could attenuate *C. perfringens*-induced necrotic enteritis (24–26), but the potential protective mechanism of probiotics against *C. perfringens* infection remains poorly understood, which needs to be further investigated. This study shows that dietary with *L. plantarum* or *P. polymyxa* significantly attenuates *C. perfringens* infection-induced compromise of growth performance. Previous studies showed that *C. perfringens* infection compromised the growth performance of broilers by impairing intestinal health and inducing intestinal dysbacteriosis (24, 39). The ameliorated growth performance of *C. perfringens*-infected broilers in *L. plantarum* or *P. polymyxa*-fed groups in this study may be related to the improved intestinal health and intestinal microbiota.

Healthy intestinal morphology and balance of intestinal microbes are important indicators of gastrointestinal tract

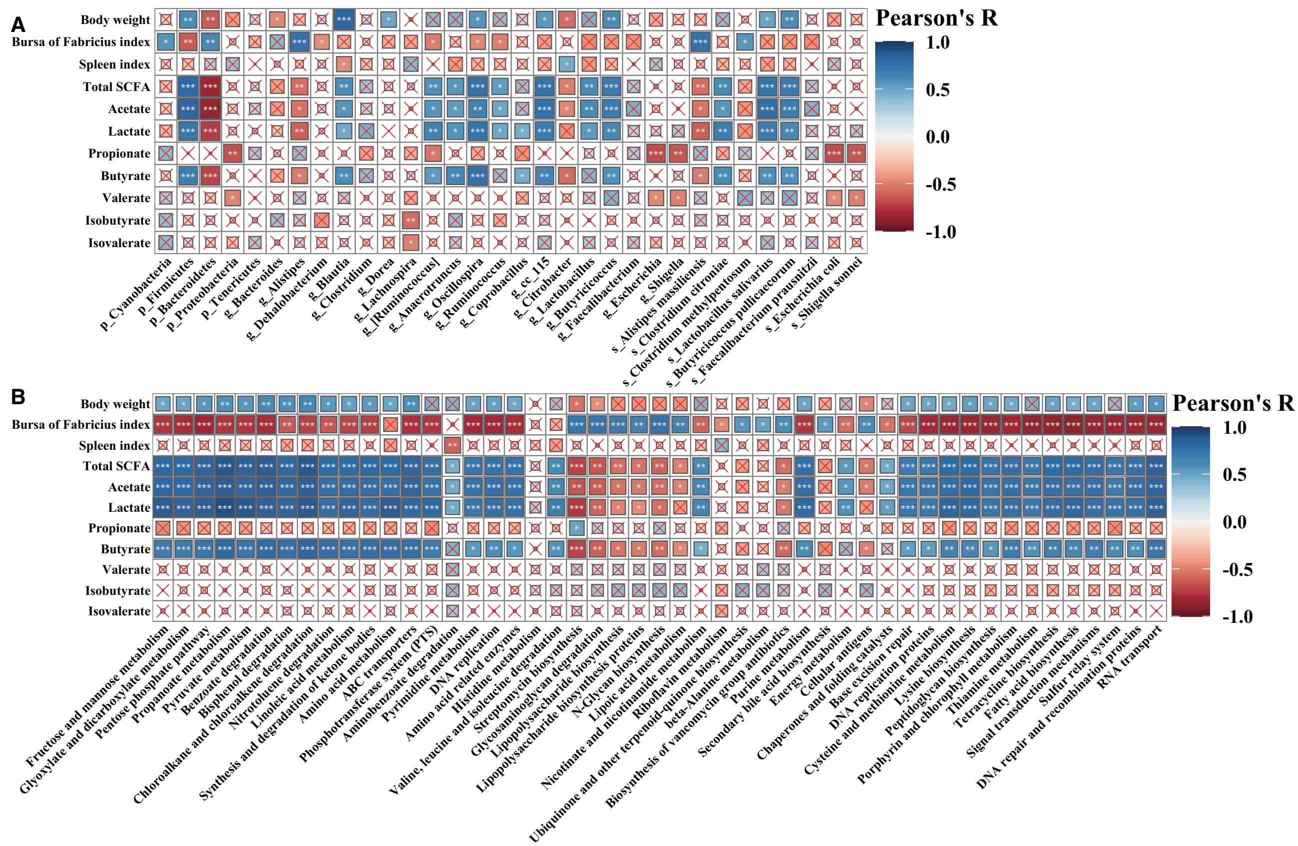

FIGURE 10 | Pearson's correlation analysis. Correlation of phenotypic variables and microbial communities **(A)** and microbial-predicted metabolic pathway functions **(B)**. The color and the dot size represent the correlation coefficient. **p* < 0.05; ***p* < 0.01; ****p* < 0.001.

homeostasis (40, 41). Due to the continuously chronic intestinal mucosa damage with low or no mortality, subclinical necrotic enteritis imposes a huge economic burden on global poultry industry (9). In this study, the increased ileal crypt depth and the histopathological score and the decreased ileal villus height and villus height to the crypt-depth ratio were observed in *C. perfringens*-infected broilers, which was the main reason to impair the growth performance mentioned above and also indicated that subclinical necrotic enteritis was successfully induced (35). It was found that *C. perfringens*-induced ileal mucosa damage was alleviated by dietary with *P. polymyxa* or *L. plantarum*, as illustrated by increased ileal villus height and villus height to the crypt-depth ratio and decreased ileal crypt depth and the histopathological score. Previous studies also reported that dietary with probiotics had positive effects on reducing subclinical necrotic enteritis occurrence by ameliorating *C. perfringens*-induced damage of intestinal mucosa (24, 42). The intact intestinal epithelium serves as a physical intestinal mucosal barrier function against invasion of zoonotic enteric pathogens and is responsible for proper nutrient absorption and utilization and waste secretion (43). This physical mucosal barrier is composed of junctional complexes, which provide different types of intercellular connections (44). It is reported that the junctional complexes are binding sites of *C. perfringens* toxins and enterotoxins (45, 46). In the present study, *C. perfringens*-infected broilers showed shorter and sparse ileal microvilli, disrupted and shorter tight junction, adherens junction, and desmosomes, consistent with previous studies (47, 48). The intestinal epithelial junction was enhanced in the increased ileal villus of broilers in BSC10+Cp and Lac16+Cp groups, as observed by higher and ordered microvillus, longer tight junction, enhanced adherens junction, and darker desmosomes. The improved intestinal morphology and mucosal barrier function in probiotics treatments may contribute to greater nutrient absorption and utilization from the intestinal digesta (25) and thereby attenuates impairment of growth performance in *C. perfringens*-infected broilers mentioned above.

SCFAs (mainly including acetate, propionate, and butyrate) are fermentative products metabolized by the gastrointestinal commensal microbiota from dietary carbohydrates (49, 50). As one of the major microbial metabolites, SCFAs play critical roles in maintaining or improving the integrity of intestinal epithelium and tissue repair after mucosal damage (50, 51). *C. perfringens* infection in this study decreased the levels of ileal total SCFAs, acetate, lactate, and butyrate of broilers, which might impair the energy supply for intestinal enterocytes to repair mucosal

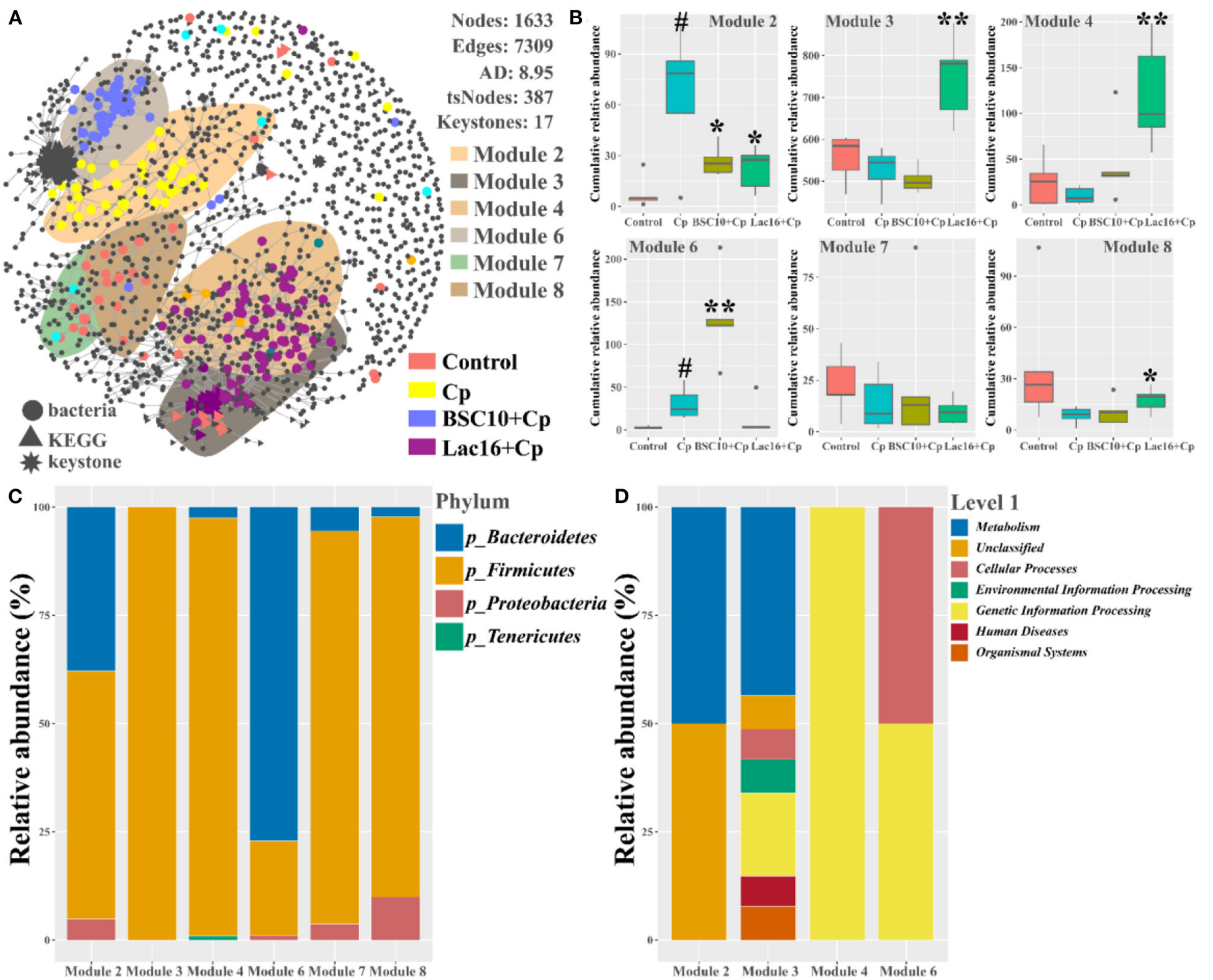

FIGURE 11 | Co-occurrence network of bacterial and metabolic functional communities. **(A)** Significant and close (|ρ| >0.8, $p < 0.05$) correlations among bacterial OTUs and metabolic KOs are visualized in the network with gray lines. The bacterial, metabolic functional, and keystone nodes are indicated by circles, triangles, and stars, respectively. Sensitive nodes are colored by their association with the treatments, and gray nodes are insensitive to the treatments. Shaded areas represent the top six modules with high proportions. **(B)** Cumulative-relative abundance (as counts per million, CPM; y-axis in ×1,000) of the bacterial OTUs metabolic KOs belonging to the responsive modules. **(C)** The bacterial phyla and metabolic functional compositions for each module. Significant differences versus Control group: $^{\#}p < 0.05$. Significant differences versus Cp group: $^{*}p < 0.05$; $^{**}p < 0.01$.

damage. Partially consistent with our findings, a previous study reported that subclinical necrotic enteritis infection decreased concentrations of cecal acetate and butyrate of broilers, but increased levels of cecal lactate and propionate partly because of the increased relative abundance of *Lactobacillus* (52). SCFAs exert not only as an energy source for the host but also as main regulators of the physiological function of intestinal epithelial cells and immune cells (50, 53). SCFAs, especially butyrate and lactate, are also important bacterial metabolites that exert antibacterial and anti-inflammatory activities (53–55). The altered concentrations of the ileal SCFAs (total SCFAs, acetate, lactate, and butyrate) induced by *C. perfringens* infection were significantly reversed in the Lac16+Cp group, but not significantly reversed in the BSC10+Cp group, indicating that the improved intestinal morphology and mucosal barrier function of *C. perfringens*-infected broilers in the *L. plantarum*-treated group may be partly due to the increased intestinal SCFAs levels.

The enteric pathogen infection-induced intestinal dysbiosis could aggravate the gastrointestinal mucosal injury and then compromise the intestinal health and growth performance (56). Many studies reported that dysbiosis is allegedly correlated with *C. perfringens* infection (14, 57, 58), but it remains unclear about the causal relationship between the intestinal dysbiosis and gastrointestinal infectious diseases (59). In this study, *L. plantarum* supplementation significantly improved *C.*

TABLE 4 | Topological properties of the co-occurrence network.

Community	Bacteria	KEGG
Nodes	1,368	265
Edges	2,204	4,027
Interactive edges	1,078	
Average degree	3.22	30.39
sNodes	235	152
Keystones	3	14

perfringens infection-induced intestinal dysbiosis and bacterial metabolic dysfunctions. PCoA results clearly indicated that dietary *L. plantarum* significantly reversed *C. perfringens* infection induced shifts of structures of microbial communities (**Figure 3B** and **Table 3**) and bacterial metabolic functions (**Figure 6**), which is consistent with previous studies (60, 61). *C. perfringens* infection significantly induced a shift of broiler intestinal microbiota structure (61), which could be reversed by dietary *Bacillus* direct-fed microbial (DFM) in feed (60). The structural shifts may be related with the changes of microbial and microbial metabolic compositions. Dietary *L. plantarum* improved *C. perfringens* infection-induced anomalous microbial composition as evidenced by enriched *Firmicutes*, *Ruminococcaceae*, SCFAs-producing bacteria (*Lachnospiraceae*, *Ruminococcaceae*, *Oscillospira*, *Faecalibacterium*, and *Blautia*) (62–65), which may be partly related to the increase of bacterial fatty acid biosynthesis and intestinal SCFAs levels observed in this study. *L. plantarum* supplementation significantly reduced *Bacteroidetes*, drug-resistant bacteria (*Bacteroides*, *Alistipes*) (66, 67), and enteric pathogens (*Escherichia coli*, *Bacteroides fragilis*) (66), which may partly contribute to the inhibition of bacterial LPS biosynthesis and antibiotic biosynthesis (streptomycin and vancomycin). These findings indicated that *L. plantarum*-mediated-ameliorated compromise of growth performance in *C. perfringens*-infected broilers may be related to the restored gut microbial communities and bacterial metabolic functions, which should be further confirmed by whole shotgun metagenomic sequencing because of the limited taxonomical and functional attributes offered by 16S rRNA gene sequencing.

Strong correlations among the final body weight, ileal SCFAs (including total SCFAs, acetate, lactate, and butyrate), microbial communities, and microbial metabolic functions were observed. Consistent with previous reports (68, 69), the final body weight had a strong positive correlation with the ileal SCFAs (including total SCFAs, acetate, lactate, and butyrate), further indicating that the increased intestinal SCFAs levels were beneficial for ameliorating *C. perfringens* infection-induced compromise of broiler growth performance. Furthermore, the final body weight and ileal SCFAs (including total SCFAs, acetate, lactate, and butyrate) were positively correlated with SCFAs-producing bacteria (*Blautia*, *Oscillospira*, *Lactobacillus*, *Lactobacillus salivarius*, and *Butyricicoccus pullicaecorum*) and bacterial fatty acid biosynthesis, whereas negatively correlated with drug-resistant bacteria (*Bacteroides* and *Citrobacter*), which was partly consistent with previous findings (70–72). These results indicated that the body weight and intestinal SCFAs might be principal factors affecting the bacterial communities and microbial metabolic functions.

Co-occurrence patterns of gut microbiota were further performed to investigate the treatment-sensitive species, keystones, and the microbial interactions. The results found that 235 bacteria and 150 microbial metabolic functions were sensitive to the four treatments, and most of the tsNodes significantly grouped in six distinct modules that reflected the different treatments. The uninfected treatment-sensitive nodes grouped in Modules 7 and 8; *C. perfringens*-infected-treatment-sensitive nodes grouped in Modules 2 and 6; *P. polymyxa* pretreatment-sensitive nodes grouped in Module 6; *L. plantarum* pretreatment-sensitive nodes grouped in Modules 3 and 4, indicating that dietary *L. plantarum* significantly modulated the co-occurrence interactions of intestinal microbes. By frequently interacting with many other microbes, keystone species are thought to play crucial roles in modulating microbial communities and functions (34, 73). The present study found that three bacteria (*Rikenellaceae*, *Bacteroides*, *Bacteroides*_unidentified) and 14 bacterial metabolic functions (LPS biosynthesis, LPS biosynthesis proteins, streptomycin biosynthesis etc.) were defined as keystones, in which dietary *L. plantarum* significantly decreased *C. perfringens* infection induced all the 17 keystones. *Bacteroides* species are multiple drug-resistant and significant clinical anaerobic pathogenic bacteria that can cause life-threatening infection with mortality of more than 19% (66). As the major component of the outer membrane of gram-negative microbes, LPS acts as a key pathogenic stimulator for the dysfunctions and plays major role in pathogens-mediated toxicity and pathogenicity (74). These results indicate that the shifts of these keystones maybe the driving factors involved in *L. plantarum*-mediated-ameliorated growth performance and improved mucosal damage of the *C. perfringens*-infected broilers.

CONCLUSION

The current results indicate that dietary *L. plantarum*-mediated amelioration of growth performance and improvement of intestinal mucosal damage of broilers under subclinical NE condition are associated with the increased intestinal SCFAs levels, enhanced intestinal epithelial barriers, and improved intestinal dysbiosis. Dietary *P. polymyxa*-mediated amelioration of broiler growth performance under subclinical NE condition may partly be due to the improved mucosal structure and intestinal epithelial barriers. These findings provide a potential preventive approach against avian necrotic enteritis caused by *C. perfringens* infection. However, the detailed preventive mechanism of *L. plantarum* against subclinical necrotic enteritis should be further investigated.

DATA AVAILABILITY STATEMENT

Raw sequences have been deposited in the Genome Sequence Archive (GSA) of the BIG Data Center (https://bigd.big.ac.cn/gsa/) under accession number PRJCA004271/CRA003760.

ETHICS STATEMENT

All the procedures of this project were conducted according to the Chinese guidelines for animal welfare and were approved by the Zhejiang University Institutional Animal Care and Use Committee (Permission number: ZJU20160416).

AUTHOR CONTRIBUTIONS

WL and HZ conceptualization and supervision. BW, YM, and YZ data curation, microbial analysis, writing—original draft, review, and editing. BW, QG, and YZ conducted the animal experiments. LG, XL, SX, and FW assisted with the experiments. XL and SX assisted in the manuscript preparation. All authors contributed to the article and approved the submitted version.

FUNDING

This study was supported by the National Natural Science Foundation of China (Grant Nos. 31472128 and 31672460), the Natural Science Foundation of Zhejiang province (Grants Nos. LZ20C170002 and 2006C12086), and National High-Tech R&D Program (863) of China (Grant No. 2013AA102803D).

SUPPLEMENTARY MATERIAL

The Supplementary Material for this article can be found online at: https://www.frontiersin.org/articles/10.3389/fnut.2021.706148/full#supplementary-material

Figure S1 | Probiotics exerts anti-*C. perfringens* activity. **(A)** Fermented supernatant of *P. polymyxa* (BSC10) and *L. plantarum* (Lac16) significantly inhibited the expression of virulence genes (α and β toxins) of *C. perfringens*. Significant differences versus control group: $^{*}p < 0.05$. **(B)** BSC10 and Lac16 cultures significantly inhibited *C. perfringens* growth. **(C)** Live Lac16 significantly protect *C. elegans* against *C. perfringens* infection.

Figure S2 | Comparison of predicted pathway abundances between the groups by statistical analysis of taxonomic and functional profiles (STAMP). **(A)** Control versus Cp; **(A)** Cp versus BSC10+Cp; **(B)** Cp versus Lac16+Cp.

Figure S3 | Canonical correspondence analysis and variation partitioning analysis of the phenotypic variables (including body weight, bursa of fabricius index and spleen index) and ileal SCFAs for the bacterial community **(A,C)** and microbial predicted pathway functions **(B,D)**.

Figure S4 | Relative abundances of the keystone species. Significant differences versus Control group: $^{\#}p < 0.05$; $^{\#\#}p < 0.01$. Significant differences versus Cp group: $^{*}p < 0.05$; $^{**}p < 0.01$. The prefixes "b_" and "k_" represent the bacteria and KEGG. $n = 5$ samples.

REFERENCES

1. Prescott JF, Parreira VR, Gohari IM, Lepp D, Gong J. The pathogenesis of necrotic enteritis in chickens: what we know and what we need to know: a review. *Avian Pathol.* (2016) 45:288–94. doi: 10.1080/03079457.2016.1139688
2. Grass JE, Gould LH, Mahon BE. Epidemiology of foodborne disease outbreaks caused by clostridium perfringens, United States, 1998-2010. *Foodborne Pathog Dis.* (2013) 10:131–6. doi: 10.1089/fpd.2012.1316
3. Wade B, Keyburn A. The true cost of necrotic enteritis. *World Poult.* (2015) 31:16–7. Available online at: https://www.poultryworld.net/Meat/Articles/2015/10/The-true-cost-of-necrotic-enteritis-2699819W/
4. Lee KW, Lillehoj HS, Jeong W, Jeoung HY, An DJ. Avian necrotic enteritis: Experimental models, host immunity, pathogenesis, risk factors, vaccine development. *Poultry Sci.* (2011) 90:1381–90. doi: 10.3382/ps.2010-01319
5. Caly DL, D'Inca R, Auclair E, Drider D. Alternatives to antibiotics to prevent necrotic enteritis in broiler chickens: a microbiologist's perspective. *Front Microbiol.* (2015) 6:1336. doi: 10.3389/fmicb.2015.01336
6. Castanon JIR. History of the use of antibiotic as growth promoters in European poultry feeds. *Poultry Sci.* (2007) 86:2466–71. doi: 10.3382/ps.2007-00249
7. China. *Announcement of the Ministry of Agriculture and Rural People's Republic of China*. (2019). Available online at: http://www.moa.gov.cn/nybgb/2017/dqq/201801/t20180103_6133925.htm (accessed July 20, 2017).
8. Hofacre CL, Smith JA, Mathis GF. An optimist's view on limiting necrotic enteritis and maintaining broiler gut health and performance in today's marketing, food safety, regulatory climate. *Poult Sci.* (2018) 97:1929–33. doi: 10.3382/ps/pey082
9. M'Sadeq SA, Wu S, Swick RA, Choct M. Towards the control of necrotic enteritis in broiler chickens with in-feed antibiotics phasing-out worldwide. *Anim Nutr.* (2015) 1:1–11. doi: 10.1016/j.aninu.2015.02.004
10. Caballero S, Pamer EG. Microbiota-mediated inflammation and antimicrobial defense in the intestine. *Annu Rev Immunol.* (2015) 33:227–56. doi: 10.1146/annurev-immunol-032713-120238
11. Hooper LV, Littman DR, Macpherson AJ. Interactions between the microbiota and the immune system. *Science.* (2012) 336:1268–73. doi: 10.1126/science.1223490
12. Kurashima Y, Kiyono H. Mucosal ecological network of epithelium and immune cells for gut homeostasis and tissue healing. *Ann Rev Immunol.* (2017) 35:119–47. doi: 10.1146/annurev-immunol-051116-052424
13. Heida FH, van Zoonen AGJF, Hulscher JBF, te Kiefte BJC, Wessels R, Kooi EMW, et al. A necrotizing enterocolitis-associated gut microbiota is present in the meconium: results of a prospective study. *Clin Infect Dis.* (2016) 62:863–70. doi: 10.1093/cid/ciw016
14. Bortoluzzi C, Vieira BS, Hofacre C, Applegate TJ. Effect of different challenge models to induce necrotic enteritis on the growth performance and intestinal microbiota of broiler chickens. *Poultry Sci.* (2019) 98:2800–12. doi: 10.3382/ps/pez084
15. Yeoman CJ, White BA. Gastrointestinal tract microbiota and probiotics in production animals. *Ann Rev Animal Biosci.* (2014) 2:469–86. doi: 10.1146/annurev-animal-022513-114149
16. Buntyn JO, Schmidt TB, Nisbet DJ, Callaway TR. The role of direct-fed microbials in conventional livestock production. *Annu Rev Anim Biosci.* (2016) 4:335–55. doi: 10.1146/annurev-animal-022114-111123
17. Sanchez B, Delgado S, Blanco-Miguez A, Lourenco A, Gueimonde M, Margolles A. Probiotics, gut microbiota, and their influence on host health and disease. *Mol Nutr Food Res.* (2017) 61:1600240. doi: 10.1002/mnfr.201600240
18. Todorov SD, Franco BDGD. *Lactobacillus plantarum*: characterization of the species and application in food production. *Food Rev Int.* (2010) 26:205–29. doi: 10.1080/87559129.2010.484113
19. Kareem RA, Razavi SH. Plantaricin bacteriocins: As safe alternative antimicrobial peptides in food preservation-A review. *J Food Safety.* (2020) 40:12735. doi: 10.1111/jfs.12735
20. Sabo SD, Vitolo M, Gonzalez JMD, Oliveira RPD. Overview of *Lactobacillus plantarum* as a promising bacteriocin producer among lactic acid bacteria. *Food Res Int.* (2014) 64:527–36. doi: 10.1016/j.foodres.2014.07.041
21. He ZG, Kisla D, Zhang LW, Yuan CH, Green-Church KB, Yousef AE. Isolation and identification of a Paenibacillus polymyxa strain that coproduces a novel lantibiotic and polymyxin. *Appl Environ Microb.* (2007) 73:168–78. doi: 10.1128/Aem.02023-06
22. Ma MC, Wang CC, Ding YQ, Li L, Shen DL, Jiang X, et al. Complete genome sequence of paenibacillus polymyxa SC2, a strain of plant growth-promoting rhizobacterium with broad-spectrum antimicrobial activity. *J Bacteriol.* (2011) 193:311–2. doi: 10.1128/Jb.01234-10
23. Wang B, Hussain A, Zhou Y, Zeng Z, Wang Q, Zou P, et al. Saccharomyces boulardii attenuates inflammatory response induced by Clostridium perfringens via TLR4/TLR15-MyD8 pathway in HD11 avian macrophages. *Poult Sci.* (2020) 99:5356–65. doi: 10.1016/j.psj.2020.07.045

24. Li Z, Wang W, Liu D, Guo Y. Effects of Lactobacillus acidophilus on the growth performance and intestinal health of broilers challenged with Clostridium perfringens. *J Anim Sci Biotechnol.* (2018) 9:25. doi: 10.1186/s40104-018-0243-3
25. Ramlucken U, Ramchuran SO, Moonsamy G, Lalloo R, Thantsha MS, van Rensburg CJ. A novel Bacillus based multi-strain probiotic improves growth performance and intestinal properties of Clostridium perfringens challenged broilers. *Poultry Sci.* (2020) 99:331–41. doi: 10.3382/ps/pez496
26. Guo SS, Xi Y, Xia Y, Wu T, Zhao D, Zhang ZF, et al. Dietary *Lactobacillus fermentum* and *Bacillus coagulans* supplementation modulates intestinal immunity and microbiota of broiler chickens challenged by *Clostridium perfringens*. *Front Vet Sci.* (2021) 8:e680742. doi: 10.3389/fvets.2021.680742
27. Wang B, Zhou Y, Tang L, Zeng Z, Gong L, Wu Y, et al. Effects of Bacillus amyloliquefaciens instead of antibiotics on growth performance, intestinal health and intestinal microbiota of broilers. *Front Vet Sci.* (2021) 8:679368. doi: 10.3389/fvets.2021.679368
28. Council NN. *Nutrient Requirements of Poultry (9th rev. ed.)*. Washington, DC: National Academies Press (1994).
29. Jerzsele A, Szeker K, Csizinszky R, Gere E, Jakab C, Mallo JJ, et al. Efficacy of protected sodium butyrate, a protected blend of essential oils, their combination, and Bacillus amyloliquefaciens spore suspension against artificially induced necrotic enteritis in broilers. *Poultry Sci.* (2012) 91:837–43. doi: 10.3382/ps.2011-01853
30. Caporaso JG, Kuczynski J, Stombaugh J, Bittinger K, Bushman FD, Costello EK, et al. QIIME allows analysis of high-throughput community sequencing data. *Nat Methods.* (2010) 7:335–6. doi: 10.1038/nmeth.f.303
31. Langille MGI, Zaneveld J, Caporaso JG, McDonald D, Knights D, Reyes JA, et al. Predictive functional profiling of microbial communities using 16S rRNA marker gene sequences. *Nat Biotechnol.* (2013) 31:814–21. doi: 10.1038/nbt.2676
32. Parks DH, Tyson GW, Hugenholtz P, Beiko RG. STAMP: statistical analysis of taxonomic and functional profiles. *Bioinformatics.* (2014) 30:3123–4. doi: 10.1093/bioinformatics/btu494
33. Guo X, Gao Q, Yuan MT, Wang GS, Zhou XS, Feng JJ, et al. Gene-informed decomposition model predicts lower soil carbon loss due to persistent microbial adaptation to warming. *Nat Commun.* (2020) 11:1. doi: 10.1038/s41467-020-18706-z
34. Hartman K, van der Heijden MGA, Wittwer RA, Banerjee S, Walser JC, Schlaeppi K. Cropping practices manipulate abundance patterns of root and soil microbiome members paving the way to smart farming. *Microbiome.* (2018) 6:1–14. doi: 10.1186/s40168-017-0389-9
35. Van Immerseel F, Rood JI, Moore RJ, Titball RW. Rethinking our understanding of the pathogenesis of necrotic enteritis in chickens. *Trends Microbiol.* (2009) 17:32–6. doi: 10.1016/j.tim.2008.09.005
36. Bansal M, Fu Y, Alrubaye B, Abraha M, Almansour A, Gupta A, et al. A secondary bile acid from microbiota metabolism attenuates ileitis and bile acid reduction in subclinical necrotic enteritis in chickens. *J Anim Sci Biotechno.* (2020) 11:1–10. doi: 10.1186/s40104-020-00441-6
37. Xue GD, Wu SB, Choct M, Swick RA. The role of supplemental glycine in establishing a subclinical necrotic enteritis challenge model in broiler chickens. *Anim Nutr.* (2017) 3:266–70. doi: 10.1016/j.aninu.2017.05.004
38. Gharib-Naseri K, de Paula Dorigam JC, Doranalli K, Kheravii S, Swick RA, Choct M, et al. Modulations of genes related to gut integrity, apoptosis, and immunity underlie the beneficial effects of Bacillus amyloliquefaciens CECT 5940 in broilers fed diets with different protein levels in a necrotic enteritis challenge model. *J Anim Sci Biotechnol.* (2020) 11:104. doi: 10.1186/s40104-020-00508-4
39. Kheravii SK, Swick RA, Choct M, Wu SB. Effect of oat hulls as a free choice feeding on broiler performance, short chain fatty acids and microflora under a mild necrotic enteritis challenge. *Anim Nutr.* (2018) 4:65–72. doi: 10.1016/j.aninu.2017.11.003
40. Ohland CL, Jobin C. Microbial activities and intestinal homeostasis: a delicate balance between health and disease. *Cell Mol Gastroenter.* (2015) 1:28–40. doi: 10.1016/j.jcmgh.2014.11.004
41. Pham VH, Kan LG, Huang JY, Geng YQ, Zhen WR, Guo YM, et al. Dietary encapsulated essential oils and organic acids mixture improves gut health in broiler chickens challenged with necrotic enteritis. *J Anim Sci Biotechno.* (2020) 11:1–18. doi: 10.1186/s40104-019-0421-y
42. Wu YY, Shao YJ, Song BC, Zhen WR, Wang Z, Guo YM, et al. Effects of Bacillus coagulans supplementation on the growth performance and gut health of broiler chickens with Clostridium perfringens-induced necrotic enteritis. *J Anim Sci Biotechno.* (2018) 9:1–14. doi: 10.1186/s40104-017-0220-2
43. Turner JR. Intestinal mucosal barrier function in health and disease. *Nat Rev Immunol.* (2009) 9:799–809. doi: 10.1038/nri2653
44. Shen L, Weber CR, Raleigh DR, Yu D, Tumer JR. Tight, junction pore and leak pathways: a dynamic duo. *Annu Rev Physiol.* (2011) 73:283–309. doi: 10.1146/annurev-physiol-012110-142150
45. Eichner M, Protze J, Piontek A, Krause G, Piontek J. Targeting and alteration of tight junctions by bacteria and their virulence factors such as Clostridium perfringens enterotoxin. *Pflug Arch Eur J Phy.* (2017) 469:77–90. doi: 10.1007/s00424-016-1902-x
46. Petit L, Gibert M, Popoff MR. Clostridium perfringens: toxinotype and genotype. *Trends Microbiol.* (1999) 7:104–10. doi: 10.1016/S0966-842x(98)01430-9
47. Cao L, Wu XH, Bai YL, Wu XY, Gu SB. Anti-inflammatory and antioxidant activities of probiotic powder containing *Lactobacillus plantarum* 1.2567 in necrotic enteritis model of broiler chickens. *Livest Sci.* (2019) 223:157–63. doi: 10.1016/j.livsci.2019.03.009
48. Olkowski AA, Wojnarowicz C, Chirino-Trejo M, Laarveld B, Sawicki G. Sub-clinical necrotic enteritis in broiler chickens: Novel etiological consideration based on ultra-structural and molecular changes in the intestinal tissue. *Res Vet Sci.* (2008) 85:543–53. doi: 10.1016/j.rvsc.2008.02.007
49. Dalile B, Van Oudenhove L, Vervliet B, Verbeke K. The role of short-chain fatty acids in microbiota-gut-brain communication. *Nat Rev Gastro Hepat.* (2019) 16:461–78. doi: 10.1038/s41575-019-0157-3
50. Kayama H, Okumura R, Takeda K. Interaction between the microbiota, epithelia, and immune cells in the intestine. *Ann Rev Immunol.* (2020) 38:23–48. doi: 10.1146/annurev-immunol-070119-115104
51. Goncalves P, Araujo JR, Di Santo JP. A cross-talk between microbiota-derived short-chain fatty acids and the host mucosal immune system regulates intestinal homeostasis and inflammatory bowel disease. *Inflamm Bowel Dis.* (2018) 24:558–72. doi: 10.1093/ibd/izx029
52. Gharib-Naseri K, Kheravii SK, Keerqin C, Morgan N, Swick RA, Choct M, et al. Two different Clostridium perfringens strains produce different levels of necrotic enteritis in broiler chickens. *Poultry Sci.* (2019) 98:6422–32. doi: 10.3382/ps/pez480
53. McCarville JL, Chen GY, Cuevas VD, Troha K, Ayres JS. Microbiota metabolites in health and disease. *Ann Rev Immunol.* (2020) 38:147–70. doi: 10.1146/annurev-immunol-071219-125715
54. Koh A, De Vadder F, Kovatcheva-Datchary P, Backhed F. From dietary fiber to host physiology: short-chain fatty acids as key bacterial metabolites. *Cell.* (2016) 165:1332–45. doi: 10.1016/j.cell.2016.05.041
55. Lamas A, Regal P, Vazquez B, Cepeda A, Franco CM. Short chain fatty acids commonly produced by gut microbiota influence salmonella enterica motility, biofilm formation, gene expression. *Antibiotics-Basel.* (2019) 8:265. doi: 10.3390/antibiotics8040265
56. Wang C, Li Q, Ren J. Microbiota-immune interaction in the pathogenesis of gut-derived infection. *Front Immunol.* (2019) 10:1873. doi: 10.3389/fimmu.2019.01873
57. Minamoto Y, Dhanani N, Markel ME, Steiner JM, Suchodolski JS. Prevalence of Clostridium perfringens, Clostridium perfringens enterotoxin and dysbiosis in fecal samples of dogs with diarrhea. *Vet Microbiol.* (2014) 174:463–73. doi: 10.1016/j.vetmic.2014.10.005
58. Lacey JA, Stanley D, Keyburn AL, Ford M, Chen H, Johanesen P, et al. Clostridium perfringens-mediated necrotic enteritis is not influenced by the pre-existing microbiota but is promoted by large changes in the post-challenge microbiota. *Vet Microbiol.* (2018) 227:119–26. doi: 10.1016/j.vetmic.2018.10.022
59. Bien J, Palagani V, Bozko P. The intestinal microbiota dysbiosis and Clostridium difficile infection: is there a relationship with inflammatory bowel disease? *Ther Adv Gastroenter.* (2013) 6:53–68. doi: 10.1177/1756283x12454590
60. Hernandez-Patlan D, Solis-Cruz B, Pontin KP, Hernandez-Velasco X, Merino-Guzman R, Adhikari B, et al. Impact of a bacillus direct-fed microbial on growth performance, intestinal barrier integrity, necrotic enteritis lesions, and ileal microbiota in broiler chickens using a laboratory

challenge model. *Front Vet Sci.* (2019) 6:108–19. doi: 10.3389/fvets.2019.00108
61. Latorre JD, Adhikari B, Park SH, Teague KD, Graham LE, Mahaffey BD, et al. Evaluation of the epithelial barrier function and ileal microbiome in an established necrotic enteritis challenge model in broiler chickens. *Front Vet Sci.* (2018) 5:199. doi: 10.3389/fvets.2018.00199
62. Bai S, Wang W, Wang T, Li J, Zhang S, Chen Z, et al. CD36 deficiency affects depressive-like behaviors possibly by modifying gut microbiota and the inflammasome pathway in mice. *Transl Psychiatry.* (2021) 11:16. doi: 10.1038/s41398-020-01130-8
63. Konikoff T, Gophna U. Oscillospira: a central, enigmatic component of the human gut microbiota. *Trends Microbiol.* (2016) 24:523–4. doi: 10.1016/j.tim.2016.02.015
64. Ozato N, Saito S, Yamaguchi T, Katashima M, Tokuda I, Sawada K, et al. Blautia genus associated with visceral fat accumulation in adults 20-76 years of age. *Npj Biofilms Microbi.* (2019) 5:1–9. doi: 10.1038/s41522-019-0101-x
65. Reichardt N, Duncan SH, Young P, Belenguer A, Leitch CM, Scott KP, et al. Phylogenetic distribution of three pathways for propionate production within the human gut microbiota. *Isme J.* (2014) 8:1323–35. doi: 10.1038/ismej.2014.14
66. Wexler HM. Bacteroides: the good, the bad, the nitty-gritty. *Clin Microbiol Rev.* (2007) 20:593–621. doi: 10.1128/Cmr.00008-07
67. Parker BJ, Wearsch PA, Veloo ACM, Rodriguez-Palacios A. The genus alistipes: gut bacteria with emerging implications to inflammation, cancer, mental health. *Front Immunol.* (2020) 11:906. doi: 10.3389/fimmu.2020.00906
68. Kumar A, Toghyani M, Kheravii SK, Pineda L, Han Y, Swick RA, et al. Potential of blended organic acids to improve performance and health of broilers infected with necrotic enteritis. *Anim Nutr.* (2021) 7:440–9. doi: 10.1016/j.aninu.2020.11.006
69. Yu M, Li ZM, Chen WD, Wang G, Cui YY, Ma XY. Dietary supplementation with citrus extract altered the intestinal microbiota and microbial metabolite profiles and enhanced the mucosal immune homeostasis in yellow-feathered broilers. *Front Microbiol.* (2019) 10:2662. doi: 10.3389/fmicb.2019.02662
70. Guo F, Wang F, Ma H, Ren Z, Yang X, Yang X. Study on the interactive effect of deoxynivalenol and Clostridium perfringens on the jejunal health of broiler chickens. *Poultry Sci.* (2020) 100:1–13. doi: 10.1016/j.psj.2020.10.061
71. Liao XD, Shao YX, Sun GM, Yang YF, Zhang LY, Guo YL, et al. The relationship among gut microbiota, short-chain fatty acids, and intestinal morphology of growing and healthy broilers. *Poultry Sci.* (2020) 99:5883–95. doi: 10.1016/j.psj.2020.08.033
72. Liu J, Stewart SN, Robinson K, Yang Q, Lyu W, Whitmore MA, et al. Linkage between the intestinal microbiota and residual feed intake in broiler chickens. *J Anim Sci Biotechno.* (2021) 12:22. doi: 10.1186/s40104-020-00542-2
73. Zhang XP, Bian FY, Zhong ZK, Gai X, Yang CB. Deciphering the rhizosphere microbiome of a bamboo plant in response to different chromium contamination levels. *J Hazard Mater.* (2020) 399:123107. doi: 10.1016/j.jhazmat.2020.123107
74. Raetz CRH, Whitfield C. Lipopolysaccharide endotoxins. *Annu Rev Biochem.* (2002) 71:635–700. doi: 10.1146/annurev.biochem.71.110601.135414

Conflict of Interest: The authors declare that the research was conducted in the absence of any commercial or financial relationships that could be construed as a potential conflict of interest.

Publisher's Note: All claims expressed in this article are solely those of the authors and do not necessarily represent those of their affiliated organizations, or those of the publisher, the editors and the reviewers. Any product that may be evaluated in this article, or claim that may be made by its manufacturer, is not guaranteed or endorsed by the publisher.

Advantages of publishing in Frontiers

OPEN ACCESS
Articles are free to read for greatest visibility and readership

FAST PUBLICATION
Around 90 days from submission to decision

HIGH QUALITY PEER-REVIEW
Rigorous, collaborative, and constructive peer-review

TRANSPARENT PEER-REVIEW
Editors and reviewers acknowledged by name on published articles

Frontiers
Avenue du Tribunal-Fédéral 34
1005 Lausanne | Switzerland

Visit us: www.frontiersin.org
Contact us: frontiersin.org/about/contact

REPRODUCIBILITY OF RESEARCH
Support open data and methods to enhance research reproducibility

DIGITAL PUBLISHING
Articles designed for optimal readership across devices

FOLLOW US
@frontiersin

IMPACT METRICS
Advanced article metrics track visibility across digital media

EXTENSIVE PROMOTION
Marketing and promotion of impactful research

LOOP RESEARCH NETWORK
Our network increases your article's readership